UNIVERSITÀ DELLA CALABRIA

Istituto per la Tecnologia delle Membrane
Consiglio Nazionale delle Ricerche

UNIVERSITAT POLITÈCNICA DE VALÈNCIA

CHARACTERIZATION AND RECOVERY OF BIOACTIVE COMPOUNDS FROM NATURAL SOURCES AND BY-PRODUCTS

Doctor of philosophy by
Martina Gaglianò

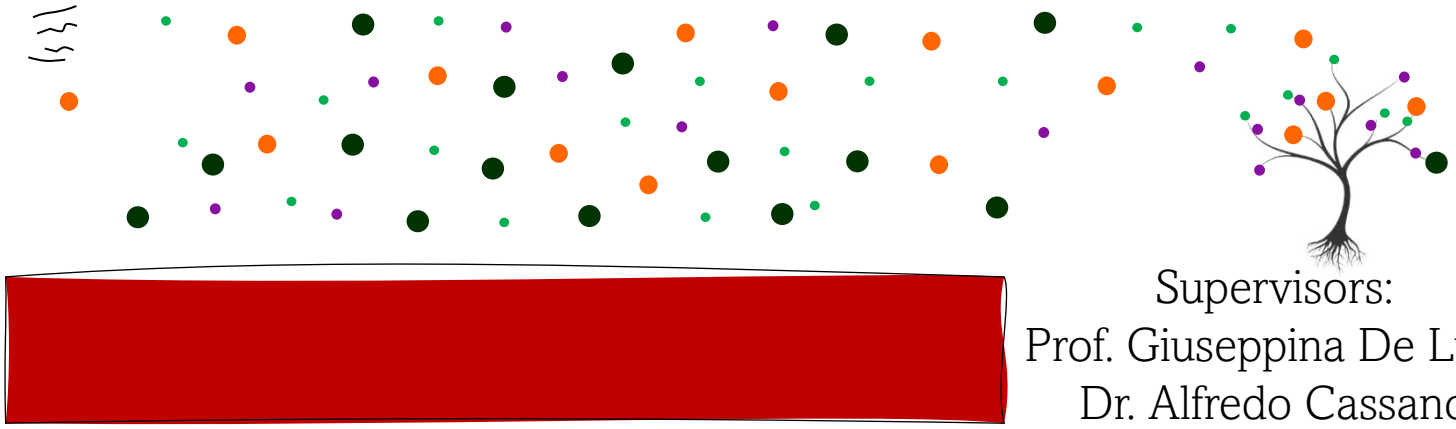

Supervisors:
Prof. Giuseppina De Luca
Dr. Alfredo Cassano

Doctorate in Physical, Chemical and Materials Sciences and Technologies
Departments of Chemistry and Chemical Technologies (CTC)

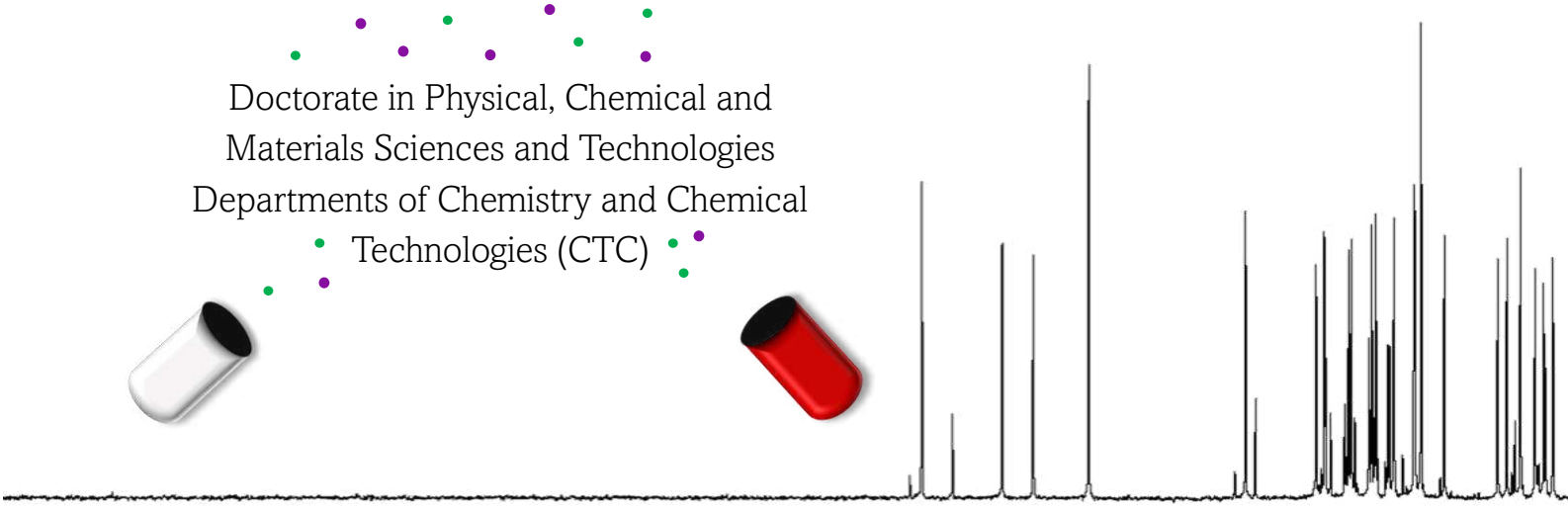

UNIVERSITÀ DELLA CALABRIA

UNIVERSITA' DELLA CALABRIA

Dipartimento di Fisica

Dottorato di Ricerca in

Scienze e Tecnologie Fisiche, Chimiche e dei Materiali

CICLO

XXVI

TITOLO TESI

CHARACTERIZATION AND RECOVERY OF BIOACTIVE COMPOUNDS FROM NATURAL SOURCES AND BY-PRODUCTS

Settore Scientifico Disciplinare

Coordinatore: Ch.ma Prof.ssa Gabriella Cipparrone

Firma Cipparrone Gabriella 24.05.2024 10:18:36 GMT+01:00

Supervisore/Tutor: Prof.ssa Giuseppina De Luca

Firma

Supervisore/Tutor: Dott. Alfredo Cassano

Firma

Dottorando: Dott.ssa Martina Gaglianò

Firma

“La borsa di dottorato è stata cofinanziata con risorse del Programma Operativo Regionale Calabria FSE/FESR 2014-2020 (CCI 2014IT16M2OP006)”

Abstract

The work presented in this PhD thesis aims to chemically characterize natural sources and by-products to properly design integrated systems to recover and fractionate bioactive compounds, such as polyphenols. Various analytical techniques, including UV-visible spectrophotometry, High-Performance Liquid Chromatography (HPLC), Mass Spectrometry (MS), and especially Nuclear Magnetic Resonance (NMR) coupled with chemometric methods, were employed to study the metabolomic profile of the investigated matrices. On the other hand, membrane technologies such as ultrafiltration (UF) and nanofiltration (NF) as well as polymeric resins were applied over conventional technologies for extracting and separating valuable molecules. The work, supported by the University of Calabria and POR Calabria — FSE/FESR 2014–2020, was developed within the Department of Chemical and Chemical Technologies (CTC) of the University of Calabria (Italy). Part of the experimental work was carried out at the Institute on Membrane Technology (ITM) of Italian National Research Council (CNR), located in Rende (CS, Italy). An almost six-months stage was also performed at the Institute of Food Engineering for Development (IIAD) of the Universitat Politècnica de València (UPV).

Chapter 1 of this thesis briefly introduces theoretical concepts about characterisation and separation techniques, while the following Chapters show the experimental results of the conducted research. The first work, presented in Chapter 2, deals with the characterization of Calabrian apple juices from different cultivars (Pink Lady,Golden Delicious, Fuji, and Royal Gala) by NMR and HPLC-UV-ESI-MS/MS methodologies. Specifically, the combined use of ^{1}H-NMR spectra and the multivariate analysis, particularly PrincipComponent Analysis (PCA) was tested to evaluate the possibility of distinguishing juices depending on the variety. Moreover, a nanofiltration (NF) process was applied to the Golden Delicious juice to produce enriched fractions in phenolic compounds. However, the composition of apple juice is complex, with valuable compounds having similar molecular masses to sugars, resulting in insufficient NF membrane selectivity. Therefore, in a subsequent work, NF membranes with a molecular weight cut-off (MWCO) ranging from 200 to 600 Da were tested to reduce the sugar content in apple juice through a combination of diafiltration and batch concentration processes.

Membrane technologies such as UF and NF were also applied for the recovery of bioactive compounds from citrus tacle juice. In this third study, spectrophotometric assays and ^{1}H-NMR spectra of fractions coming from membrane operations coupled with the Principal

Component Analysis (PCA), were used to explore the impact of UF and NF processes on the metabolic profile of the juice.

In the fourth work NMR spectroscopy was applied to analyze extracts from the seeds and inflorescences of different varieties of Cannabis sativa grown in Calabria. Finally, the last study focuses on the recovery and purification of bioactive compounds from white wine lees, a by-product of the wine processing industry, through the use of different commercial non-ionic resins.

List of Abbreviations

ABTS – 2,2'-azino-bis(3-ethylbenzthiazoline-6-sulfonic acid)

APE – Average Percentage Error

AR – Adsorption Ratio

BV – Bed volume

CAT – Chemometric Agile Tools

CAT – Chemometric Agile Tools

CBD – Cannabidiol

CBDA – Cannabidiolic Acid

CBG – Cannabigerol

CF – Concentration Factor

CID – Collision-Induced Dissociation

COLMAR –Complex Mixture Analysis by NMR

Da – Dalton

DF – Diafiltration

DFP – Diafiltration Permeate

DFR – Diafiltration Retentate

DMP – Dimethylproline

DOE – Design of Experiments

DR – desorption ratio

DSS – Trimethylsilylpropanesulfonic acid sodium salt

DV – Diafiltration Volume

ED – Electrodialysis

ESI – Electrospray Ionisation

FC – Folin–Ciocalteu

FID – Free Induction Decay

FTIR – Fourier-transform infrared spectroscopy

FUF – Feed Ultrafiltration

GABA – γ-aminobutyric acid

GAE – Gallic Acid Equivalents

GC – Gas Chromatography

Gly – Glycerol

GRAS – Generally Recognized As Safe

HAT – Hydrogen Atom Transfer

HFA – High Field Approximation

HHPE – High Hydrostatic Pressure Extraction

HMDB – Human Metabolome Database

HOMO – Highest Energy Occupied Molecular Orbital

HPLC – High-performance Liquid Chromatography

J-Res – J-Resolved spectroscopy

LA – Linoleic Acid

LC – Liquid Chromatography

LLE – Liquid-Liquid Extraction

LUMO – Lowest Energy Unoccupied Molecular Orbital

MAE – Microwave-Assisted Extraction

MC – Membrane Crystallization

MD – Membrane Distillation

MF – Microfiltration

MW– Molecular Weight

MWCO – Molecular Weight Cut-Off

NF – Nanofiltration

NMR – Nuclear Magnetic Resonance

NS – Number of Scans

PCA – Principal Component Analysis

PCs – Principal Components

PDF – Permeate Diafiltration

PDVB – Polydivinylbenzene

PEG – Polyethylene glycol

PES – Polyethersulphone

PLE – Pressurised Liquid Extraction

PS-DVB – Polystyrene crosslinked with divinylbenzene

PUF – Permeate Ultrafiltration

PUFAs – Polyunsaturated Fatty Acids

PVP – Poly(Vinyl)Pyrrolidone

qNMR – quantitative NMR

RDF – Retentate Diafiltration

RO – Reverse Osmosis

RP – Reverse Phase

RUF – Retentate Ultrafiltration

SD – Standard Deviation

SET – Single Electron Transfer

SLE – Solid-Liquid Extraction

SNR – Signal-to-Noise Ratio

SW – Spectral Width

TAA – Total Antioxidant Activity

TAGs – Triacylglycerols

TFC – Thin-Film Composite

TFMs – Thin film membranes

TMP – Transmembrane pressure

TMS – Tetramethylsilane

TMS – Trimethylsilylpropanoic acid sodium salt

TPC – Total phenolic compounds

TPI – Total phenolic index

TPs – Total Phenolics

TSS – Total Soluble Solids

UAE – Ultrasound-Assisted Extraction

UF – Ultrafiltration

UV – Ultraviolet

VIS – Visible

VRF– Volume Reduction Factor

WHO – World Health Organization

Δ^9-THC – Δ^9-trans-tetrahydrocannabinol

αLA – α-Linolenic Acid

List of Figures

List of Tables

Contents

Chapter 1: Background and motivation

1.1 Background and motivation

In today's world, where consumers are constantly seeking new and healthier products, and waste almost surpasses raw resources, it is crucial to develop progressively greener and more efficient technologies to analyse and extract nutraceutical compounds from foods, natural stuff and industrial production wastes (da Silva et al. 2016). Nutraceuticals are highly beneficial organic molecules that positively impact human health, exhibiting anti-oxidant, anti-carcinogenic, and anti-inflammatory effects, thus assisting in preventing and treating diseases like diabetes, inflammatory disorders, cancer, cardiovascular and neurodegenerative diseases (Roy et al. 2019; Rudrapal et al. 2022). Secondary metabolites, such as terpenoids, vitamins, alkaloids, phytosterols and low-molecular-weight polyphenols, are examples of nutraceutical compounds (Ruiz-Rodriguez et al. 2010; Wahyuni et al. 2013; Wolfender et al. 2019) and object of study of metabolomics. Metabolomics is the ultimate -*omic* science level in a living system, preceded by genomics, proteomics, and transcriptomics, and studies the complete set of metabolites, small molecules weighing below 1500 Da, called the metabolome. In metabolomics, there are two main approaches: "untargeted methods", which aim at performing a comprehensive analysis of all detectable analytes without any *a priori* on their structure and "targeted strategies", which aim at providing more accurate quantification of a small number of well-defined analytes.

Fruits and vegetables, including agricultural waste, contain primary metabolites, such as sugars and acids, and secondary metabolites, which, as mentioned, are characterized by health-promoting properties. Among them polyphenols have been recognized for their wide range of biological activities and promising applications in many fields, mainly in the medical, cosmetics, dietary supplement and food industries (Rajha et al. 2022). These compounds are typically characterized by an aromatic ring bearing hydroxyl substituents and range from simple phenolic acids, including derivatives of benzoic and cinnamic acids, to more complex compounds, such as stilbenes, lignans, or the ubiquitous and well-studied flavonoids, which are present in many fruits (Pott et al. 2019). The typical structure of flavonoids and their subclasses are shown in Figure 1.1.

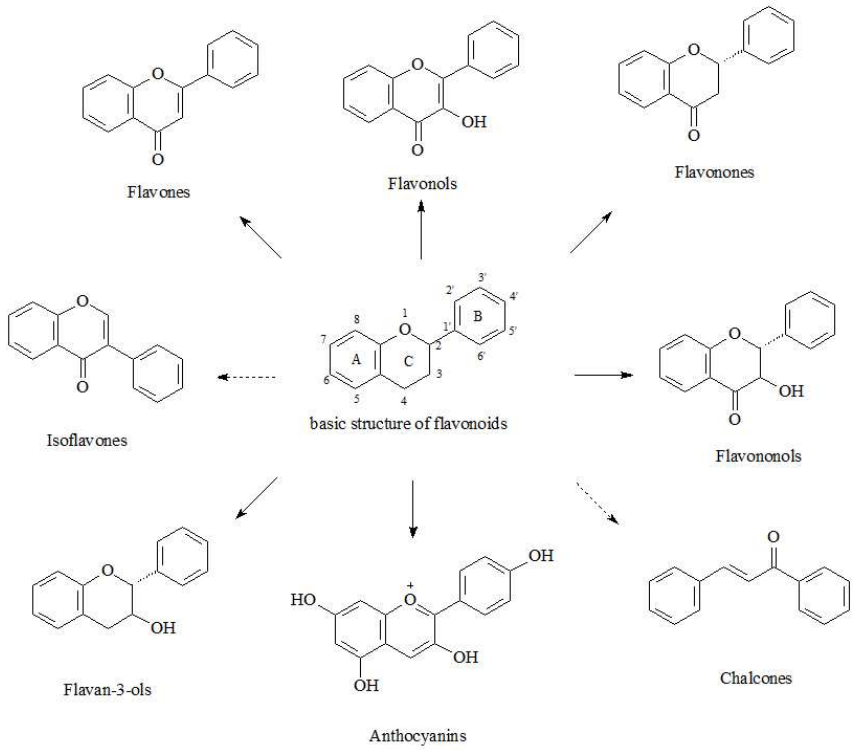

Figure 1.1 Structures of flavonoid subgroups.

Most flavonoids appear in nature in their glycoside forms (O-glycosidic or C-glycosidic) and a few in their aglycone form. Phenolic compounds (ArOH) benefit health as they are antioxidants and, as such scavenge reactive radicals ($R^{\bullet}$), potentially harmful and highly reactive waste products, which can attack many biomolecules and be very dangerous for the human body. Polyphenols can directly react with radicals, converting them into more stable products by donating a hydrogen atom (HAT) or a single-electron (SET) (Gutiérrez-Del-río et al. 2021). In the HAT mechanism, the products of the reaction are the inactive RH species and the oxidised $ArO^{\bullet}$ radical, which is much more stable than $R^{\bullet}$ since the antioxidant radical is stabilised by delocalisation of the unpaired electron along the phenolic ring to generate regular resonance hybrids. The SET mechanism can also stabilise the free radical via electron donation to the R radical, which results in an energetically stable R^{-} anion and a radical cation $ArOH^{\bullet+}$, which is then deprotonated by interacting with water. Moreover, polyphenols can act as secondary antioxidants, decreasing the oxidation rate by chelating prooxidant metals.

There are various assays for measuring the total antioxidant capacity of antioxidants in food constituents or natural extracts (Munteanu and Apetrei 2021). One of these is the ABTS•+ (2,2′-azino-bis(3-ethylbenzothiazoline-6-sulfonate)) radical scavenging assay, an electron

transfer-based assay in which the radical cation ABTS•+, which has a dark blue colour, is reduced by an antioxidant into colourless ABTS, which is measured spectrophotometrically (Ilyasov et al. 2020). UV/Vis spectrophotometric methods can also evaluate the total content of phenols, flavonoids, and anthocyanins. The Folin–Ciocalteu (FC) assay is one of the most popular assays for quantifying total phenolics and is based on the transfer of electrons from a phenolic compound to Folin–Ciocalteu reagent (a mixture of phosphomolybdate and phosphotungstate that contains molybdotungstophosphate heteropolyanion) under alkaline conditions (Ivanova et al. 2020). At the same time, phenolic compounds can be individually detected by using high-throughput methods such as *High-Performance Liquid Chromatography* (HPLC) analysis interfaced with a UV detector or Mass Spectrometer as well as the Nuclear Magnetic Resonance technique, which also allows the simultaneous analysis of all the metabolites most present in the sample under investigation without any separation of the individual compounds upstream. The advantage of NMR in detecting and characterising molecules that are less tractable to LC-MS analysis, such as sugars, organic acids, alcohol, polyols and other compounds, is simultaneously a disadvantage for NMR polyphenol profiling and identification. For example, in NMR spectra of natural matrices, polyphenols can be hindered because of other signals prevailing, like carbohydrate ones, causing spectral overlap and compromising dynamic range. In this case, a pre-extraction before analysis by NMR spectroscopy can significantly aid both the number of detectable compounds and their identification by reduction of spectral overlap and selective removal of heavily dominating compounds (Savage et al. 2011). For the specific analysis of individual phenolic compounds, the use of LC-MS can therefore be advantageous, also for its higher sensitivity (it allows the study of metabolites with a concentration higher than 10 nM, while NMR has a lower sensitivity and allows the identification of metabolites with a concentration higher than 1 μM) (Emwas et al. 2019). However, NMR still possesses indisputable advantages, including high level of reproducibility, simplicity in sample preparation, capacity to handle diverse sample types (liquids, solids, gels), and quantitative and non-destructive nature. Obtaining a metabolic profile *v*ia NMR provides a snapshot of the organism's metabolic state: metabolites vary depending on genetic, processing or environmental changes (Pedrosa et al. 2021) and thus represent indices of differentiation in samples whose traceability, wholesomeness, origin or nutraceutical properties are to be verified. Moreover, the utilization of chemometrics, particularly multivariate statistical analysis, can help rationalize numerous NMR spectra and a broad chemical data set in general. This opens the door to using NMR-based metabolomics in industrial, clinical, food production, and food safety applications.

Once the nutraceutical compounds have been identified, extraction and purification methods to create exciting marketable products are the next challenging steps due to the sensitivity of biological components to extremes of heat, pH and shear and because of the contemporary need for clean and cost-effective procedures. Methods to recover polyphenols from natural stuff and by-products could be classified into mild and conventional approaches (Ebrahimi and Lante 2022). Conventional extraction methods involve using a large volume of solvents and manual procedures that rely heavily on the investigator and are labour-intensive. As a result, these techniques are inconsistent. These methods include Solid-Liquid Extraction (SLE) or Soxhlet extraction, Liquid-Liquid Extraction (LLE), and maceration. Mild techniques offer several benefits over conventional methods, including automation, enhanced selectivity, higher extraction efficiency, and reduced consumption of extraction solvents. Unconventional methods include pressurised liquid extraction (PLE), supercritical fluid extraction (SFE), microwave-assisted extraction (MAE), ultrasound-assisted extraction (UAE), high hydrostatic pressure extraction (HHPE), membrane technologies and adsorption-desorption operations with resins among the others (Alara et al. 2021).

Membrane separation techniques have been extensively utilised in the food and pharmacy industries to effectively isolate and enhance the concentration of biologically active compounds. Compared to other separation and concentration methods, such as distillation and vacuum drying, membrane technology provides several advantages, such as simplicity in equipment, ambient operating temperature, high selectivity, low energy consumption, and no phase transition or chemical changes. Typical membrane operations include microfiltration (MF), ultrafiltration (UF), nanofiltration (NF), reverse osmosis (RO), membrane distillation (MD), separation of gases and vapours, dialysis, membrane crystallization (MC), electrodialysis (ED), etc. (Baker 2010).

Macroporous adsorption resins have also demonstrated high efficiency in the concentration and purification of polyphenols in natural products on a large scale through the employment of van der Waals forces and other interactions. This technique is attractive due to its ease of use, low energy consumption, and simple regeneration (He et al. 2017).

Permeate and retentate samples produced by membrane operations, as well as eluants and eluates in the case of treatment with resins can be further studied from a metabolomic perspective using the already mentioned characterisation techniques and chemometric tools. Indeed, combining metabolomics-based data with multivariate statistical analysis allows for a direct correlation with food and natural extracts' quality, safety, processing, storage, and authenticity. As a result, recovering and characterising these compounds provide the scientific basis to evaluate the possible use of nutritional and health claims associated with

the investigated matrices. This can increase the value of natural products and by-products, providing new services on industrial scale in pharmaceutical applications, cosmetics, food supplements, and phytosanitary products (Vidal-Casanella et al. 2021).

This thesis fits into this scenario and focuses on the following topics:

a) use of analytical and chemical-physical techniques for studying and identifying chemical compounds in natural and food matrices. Among the characterisation techniques, a particular focus is on High-Resolution NMR, coupled with the Principal Component Analysis (PCA), a chemometric tool handy to rationalise information on samples' composition and its variations relating to multiple factors;

b) use of cutting-edge techniques, particularly pressure-driven membrane operations (i.e. UF and NF) and polymeric resins processes, to recover biologically active substances from natural sources, specifically food items from the Calabrian area. This approach has aimed to acquire valuable products, even employing starting waste materials to reduce environmental impact and foster growth in the local market and the region.

The following subparagraphs delve deeper into the fundamental principles of detecting and extracting metabolites from natural matrices. The discussed techniques include UV-VIS spectroscopy, HPLC, MS, and NMR, as well as chemometric methods for analysis and concepts related to membrane technologies and resins as extracting and separative techniques.

1.1.1 UV-Visible spectroscopy

Ultraviolet and visible light have sufficient energy to induce electronic transitions in molecules, that is, the promotion of an electron from one molecular orbital to another with higher energy. Depending on the energy required for the electronic transition, a molecule absorbs ultraviolet (a UV spectrum is obtained) or visible light (a Visible spectrum is acquired) (Fleming and Williams 2020). However, ultraviolet and visible radiation have sufficient energy only to induce the two electronic transitions shown in Figure 1.2:

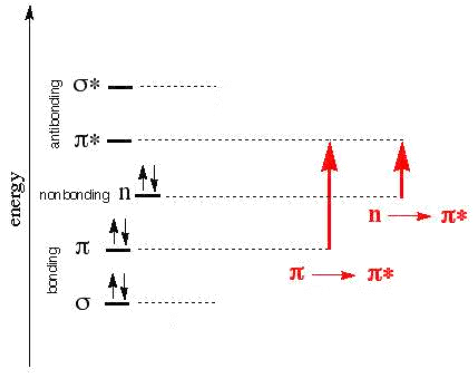

Figure 1.2 Molecular orbitals energy diagram.

The electronic transition that requires less energy relates to promoting a non-bonding electron (n) to a molecular orbital of antibonding π* (n → π* transition). The highest energy electronic transition, π → π* transition, regards the promotion of an electron from a π-bonding molecular orbital to a π* antibonding molecular orbital. Since both transitions promote an electron into a π* antibonding molecular orbital, only organic compounds with π-electrons can give UV/Vis spectra (Bruice 2011). Thus, ultraviolet and visible (UV/Vis) spectroscopy provides information on unsaturated compounds. Polyphenols are π-conjugated compounds. Therefore, they absorb in the UV/Vis range, showing adsorption bands (Anouar et al. 2012; Kaeswurm et al. 2021). The absorption bands are wide because each electronic state has vibrational sublevels, and electronic transitions can occur between different vibrational sublevels. As a result, electronic transitions span a range of wavelengths. The chromophore is that part of the molecule that absorbs UV or visible radiation. Compounds containing identical chromophores are characterised by a maximum wavelength of approximately the same.

Polyphenols sub-classes show different absorption maxima, i.e. 280 nm for flavanol monomers and polymers and some phenolic acids, 320 nm for hydroxycinnamic acids, 360 nm for flavonols and 520 nm for anthocyanins (Aleixandre-Tudo and Du Toit, 2019). The more double bonds a compound has, the longer the wavelength at which the n → π* and π → π* transitions occur. Conjugation increases the energy of the HOMO (highest energy occupied molecular orbital), simultaneously decreasing the energy of the LUMO (lowest energy unoccupied molecular orbital) so that less energy is required for an electronic transition to occur in a system conjugated compared to a non-conjugated (Bruice 2011; Fleming and Williams 2020). If a compound has a sufficient number of conjugated double bonds, it absorbs in the visible region (λ_{max} > 400 nm) and, therefore, is coloured. For example, β-carotene, a precursor of vitamin A with a λ_{max} = 455 nm, is an orange-coloured substance found in carrots and many fruits. Lycopene with λ_{max} = 474 nm is a red-coloured compound found in tomatoes, watermelons and pink grapefruits. Therefore, the UV-vis spectroscopy technique can identify molecules by their characteristic spectrum. However, the most common application of the UV-Vis technique is quantitatively determining a substance or a class of substances in solution.

Wilhelm Beer and Johann Lambert, independently of each other, proposed that the absorbance of a sample at a given wavelength depends on the amount of substance that absorbs the radiation when it passes through a solution of the sample. In other words, absorbance depends on the sample's concentration and the optical path length through the

sample (Swinehart 1962). The relationship between absorbance, concentration and optical path length is known as the Lambert-Beer Law and is given by:

$$A = \varepsilon \cdot c \cdot l \quad (1.1)$$

where:

- A is the sample absorbance and is equal to log I_0/I; where I_0 is the intensity of the light incident on the sample, and I is the intensity of the light emerging from the sample;
- c is the sample concentration (mol/L);
- l is the length of the optical path through the sample (cm): for instance, in a cuvette (the cell where the sample is placed to measure its UV-Vis absorbance), the path is standardised to 1 cm;
- ε is the extinction coefficient ($L \cdot M^{-1} \cdot cm^{-1}$). The extinction coefficient is a unique property of a substance that depends on various factors, including wavelength, solvent, and temperature. However, the instrument used can also influence the measured extinction coefficient. As a result, predetermined extinction coefficient values are generally not used for quantitative analysis. Instead, a calibration curve is developed for the substance under investigation using one or more standard solutions with known analyte concentrations (Owen 1996).

  In studying phenolic compounds, UV-Vis spectrophotometric assays are cheap and fast but lack specificity as they identify compound categories, such as total phenolic, total flavonoid, total anthocyanin, or total tannin content, rather than individual molecules (Aleixandre-Tudo and Du Toit 2019).

1.1.2 High-Performance Liquid Chromatography

High-performance liquid chromatography (HPLC) analysis can be carried out to identify and quantify individual phenolic compounds (Anticona et al. 2022; Brito et al. 2014; López-Fernández et al.2020; Zhang et al. 2023). Chromatography is the science of separating the components of a mixture. HPLC is a widely used technique for separating non-volatile and thermally labile compounds (Toldrá and Nollet 2017). Like all chromatographic techniques, liquid chromatography separates two or more compounds in a solution by exploiting the affinity balance between a "stationary phase" placed inside the chromatographic column and a "mobile phase" that flows through it (Lough and Wainer 1995). A substance more similar to the stationary phase than the mobile phase takes longer to travel through the chromatographic column (retention time, t_R) compared to a sense with low affinity for the stationary phase and high affinity for the mobile phase. Thus, separating a mixture into its

components depends on different degrees of retention of each component in the column. The mobile step is a low-viscosity liquid, and the stationary phase comprises porous particles possibly coated by a liquid phase.

The stationary phase is packed in columns whose lengths normally range from 10 to 30 cm. Since columns are filled with tiny particles ranging from 3 to 5 μm, the eluent flow can only be obtained by exerting a relatively high pressure using unique pumps (Abdu Hussen 2022). Based on the polarity of the phases, it is possible to distinguish direct-phase chromatographic techniques, in which the stationary phase is polar and the mobile phase apolar, and reversed-phase chromatographic techniques, in which the stationary phase is apolar and the mobile phase opposite (Engelhardt 1979). For the chromatographic separation of polyphenols, before spectrometric analysis, reverse phase chromatography (RP-LC) using the stationary phases C18 and C8 is the most commonly used (Chiriac et al. 2021). Mixtures of ultrapure water acidified with formic acid or acetic acid 0.05–0.5% and methanol or acetonitrile as organic solvents (often acidified with formic acid or acetic acid) are usually used as mobile phases (Sánchez Maldonado et al. 2014; Yang and Chen 2022). The addition of 0.1% trifluoroacetic acid can result in improved peak separation, tailing reduction and superior peak symmetry (López-Fernández et al. 2020). HPLC analysis instrumentation can take on different configurations, primarily based on the column elution mode; the latter can be eluted isocratically, i.e. with an eluent of constant composition, or with gradient elution, in which the nature of the eluent varies during the analysis (Engelhardt 1979). The analyte signal can be recorded using an extensive series of detectors. Still, all of them must satisfy precise characteristics, including sensitivity suited to the analyst's needs and the type of sample, good stability and reproducibility, linear response for more orders of magnitude, short response time, and uniformity. Common detectors are (Swartz 2010):

 UV-Vis detector, which, as seen in the previous paragraph, allows to analyse samples capable of absorbing in the wavelength range between 190 and 800 nm: it is, therefore, a very versatile detector. However, this detector is non-specific since a given signal is not necessarily attributed only to the analyte. Furthermore, it is not very sensitive: it can reach tens of ppm (5-10 ppm). For these reasons, other types of detectors are often used.

 The fluorescence detector is very sensitive; typically, there is a sensitivity of 0.01 ppb (1000 times higher than UV-visible absorption). A detector is limited to determining fluorescent compounds, but derivatisation is possible.

 The refractive index is a non-specific detector based on the variations in the refractive index of the solvent caused by the analyte molecules. It is mainly used on compounds that do not absorb specific wavelengths.

 The Mass Spectrometer cannot equal the sensitivity of fluorescence-based detectors but boasts of being a universal detector, as it is possible to analyse almost everything that elutes. More details about mass spectrometry are shown in the subsequent paragraph.

1.1.3 Mass spectrometry

Mass spectrometry is a highly sensitive technique used for structural analysis. It involves ionizing the chemical substance under investigation and then separating the resulting ions based on their mass-to-charge ratio. The mass spectrum, which shows the abundance of ions relative to their mass-to-charge ratio, is unique to each compound and is a characteristic fingerprint for identification purposes. The principle components of a mass spectrometer are schematized in Figure 1.3.

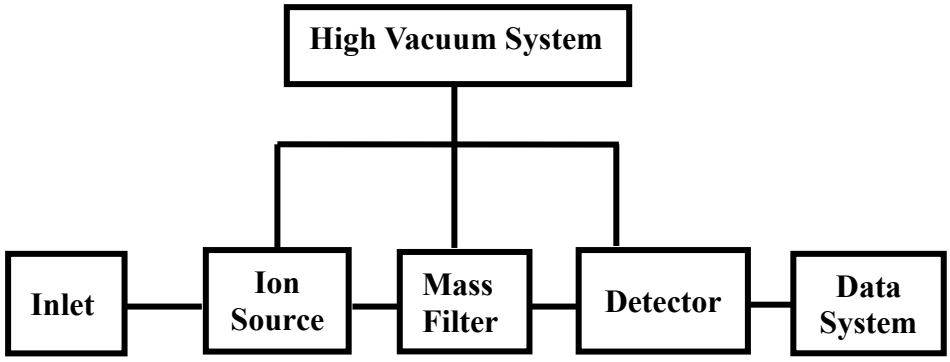

Figure 1.3 Main components of a mass spectrometer.

The function of an inlet system is to introduce a small amount of sample into the ion source with minimal loss of vacuum. The sample can be introduced directly or come from a separation system such as a gas chromatograph, HPLC, etc. The ionization source has the task of producing the analyte ions in the gaseous phase, while the mass analyzer separates the ions produced in the source based on their m/z ratio. The detector receives the ionic current generated by the ions coming from the analyzer. Finally, a data processing and management system, deals with the transformation of the analog signal coming from the analyzer into a digital signal and the generation and storage of the mass spectrum and data relating to the analysis. Furthermore, this part is able to manage all parts of the instrument, allowing the control and modification of the analysis parameters. Moreover, it is important to ensure by means of a pumping system a high vacuum inside the instrument in order to allow effective transmission of the ions (Nakorchevsky and Yates, 2012). Ions are, in fact, very reactive species and if they collide with neutral species, they lose energy and charge.

Precisely for this reason the analyzer must be under high vacuum; the source, however, can be either vacuum or at ambient pressure.

The most common ionisation source in the LC-MS analysis of polyphenols is electrospray ionisation (ESI) (Chiriac et al. 2021). Electrospray is an ionization source on the liquid phase (polar) at atmospheric pressure. This is a soft ionization technique since fragmentation is minimal. The ionisable molecules must have a medium-high polarity, while there are no limits relating to the molecular weight. With this source, it is possible to ionise compounds with a low molecular weight and a high molecular weight (up to 150,000 Da). This technique is incompatible with using non-volatile buffers and non-polar organic solvents, which inhibit the formation of surface charges on the analyte droplets. Furthermore, ionisation can be inhibited by high salt concentrations. The sample is passed through a capillary tube under tension. A potential atomizes the solution into myriad "charged droplets" containing the sample. Depending on the applied potential, positively or negatively charged ions are generated. The MS analysis of polyphenols through an ESI source usually operates in the negative mode, providing the deprotonated molecules $[M-H]^-$ (Sun et al., 2007). As the solvent evaporates, the charge concentration on the droplet's surface increases until it exceeds the surface tension, causing a "coulomb explosion". Solvent-free analyte ions are thus formed. The charges are statistically distributed among the available sites of the analyte, often leading to the formation of multiply charged ions. The generated ions are then directed towards the analyser using a series of lenses at different potentials. The triple quadrupole is generally the analyser of choice for the detection of phenolic compounds (Chiriac et al. 2021). It consists of three quadrupoles in series: Q1, Q2, and Q3. A triple-quadrupole instrument can be operated in a number of different ways, the simpler one being to resemble a single-quadrupole instrument by using either Q1 or Q3 as pass-all filter (*full scan*) to detect ions molecular mass (Polettini 2006). However, a triple-quadrupole allows tandem mass spectrometry (MS/MS). One of the most typical MS/MS scanning modes is the so-called *product-ion scan*, in which the first quadrupole is used as a mass filter, which transmits only ions with a preselected m/z ratio (precursor ion). The second "quadrupole" is not a mass analyzer, but is a reaction chamber containing an inert gas such as argon. The precursor ions, selected by the first quadrupole, enter the reaction chamber and collide with molecules of the inert gas. These low-energy collisions induce fragmentation of the precursor ions giving rise to a spectrum of lower mass product ions. This process is known as collision-induced dissociation (CID). The distribution of the product ions is obtained by scanning the third quadrupole (Ahuja 2011). Full scan and product-ion scan are powerful scanning mode for structural analysis of compounds, providing direct information on their ions' weight and

fragmentation pathways. For the study and identification of phenolic compounds, the comparative study of the theoretical mass and fragmentation patterns of the reference standards vs. target compounds is used to unequivocally confirm the identity of polyphenolic compounds in "targeted" analysis (Chiriac et al. 2021).

1.1.4 Nuclear Magnetic Resonance

Nuclear Magnetic Resonance (NMR) is one of the most powerful and versatile techniques to identify molecular structures, monitor reactions, and study metabolism in bio-systems, but it also finds applications in medicine, biochemistry, physics, industry, and almost every imaginable branch of science (Berthault et al. 2023; Cheng 2023; Flügge et al. 2023; Smith et al. 2015). The founding fathers of NMR were Felix Bloch and Edward M. Purcell, two physicists who, working independently in the United States, first succeeded in observing the phenomenon of NMR, respectively, in liquid (water) and solid (paraffin wax). They set the starting point for discoveries and Nobel Prizes in this field (Günther 2013).

NMR spectroscopy studies the interaction between radio waves and the spins of atomic nuclei in a static magnetic field. "External" and "internal" physical interactions occur when a nuclear spin system is placed in an NMR spectrometer. These interactions are described by the nuclear spin Hamiltonian, the only one that contributes to the Schrödinger equation for the purpose of NMR (*spin Hamiltonian hypothesis).* External interactions are the *Zeeman Interaction* and the *Spin-Radio Frequency Field Interaction:* they concern the interaction between nuclear spins and the two external fields supplied by the spectrophotometer. Moreover, the nuclei experience magnetic and electric fields originating from the sample. These interactions are the so-called "internal interactions". In diamagnetic substances, the internal spin Hamiltonian contains the following terms: *Shielding interaction, Indirect spin-spin coupling, Dipolar coupling, and Quadrupolar Interaction* (for nuclei with spin moment higher than ½).

Delving into the details of these interactions, it's possible to understand better nuclear magnetic phenomena and the information this technique yields.

NMR external interactions

Zeeman interaction

An isotope is observable by NMR only if its ground state nuclear spin is non-zero ($I \neq 0$). Nuclei with odd mass number have a half-integer spin (i.e. I = 1/2, 3/2, 5/2, 7/2, 9/2), for

example ^{1}H, ^{13}C, ^{15}N, ^{19}F. On the other hand, nuclei with even mass number have an integer spin, which is different from zero if the atomic number is odd, as for ^{2}H, ^{6}Li, ^{10}B, ^{14}N; while, nuclei with a even atomic number have no spin and are not NMR-active, for example ^{2}He, ^{12}C, ^{16}O, ^{32}S.

Nuclei that possess an angular momentum, $\vec{I}$, also have a magnetic moment, $\vec{\mu}$, defined as (Palmer III et al. 2006):

$$\vec{\mu}=\gamma\vec{I} \tag{1.2}$$

where γ (in rad T^{-1} s^{-1}), the magnetogyric ratio, is a constant characteristic of the particular nucleus. Angular momentum and nuclear magnetic moment are quantized, as they don't vary continuously but only take discreet values. The allowed values for the angular momentum in the z-direction of an arbitrarily chosen Cartesian coordinate system are measured in units of ħ (h/2π) and are defined by the relation:

$$I_z = \hbar m_I \tag{1.3}$$

being m_I the magnetic quantum number and according to the quantum condition it can take only the following values

$$m_I = I, I-1, I-2, \ldots, -I \tag{1.4}$$

for a total of $2I+1$ values called spin states. These spin states are degenerate, or they have the same energy. Still, in a static magnetic field B_0, this degeneracy is lifted due to the interaction of the nuclear magnetic moment μ with B_0, called *Zeeman interaction*, and spin states have different energy. The values of these energies are the eigenvalues of Zeeman Hamiltonian, which is so defined (Canet 1996):

$$\hat{H}_Z = -\sum_i \mu_i B_0 = -\hbar \sum_i \gamma_i B_0 \hat{I}_{i,Z} \tag{1.5}$$

where *i* runs over all nuclei of the sample. Since the static magnetic field B_0 is aligned with Z-axis in the laboratory frame, the only remaining component of the spin angular momentum will be $\hat{I}_{i,Z}$.

For spin-1/2 nuclei, the eigenvalues of Zeeman Hamiltonian are $E_\alpha = -\frac{1}{2}\hbar\gamma B_0$ (for spin state α with $m_I = +1/2$) and $E_\beta = \frac{1}{2}\hbar\gamma B_0$ (for spin state β with $m_I = -1/2$), thus $\Delta E_{\alpha \rightarrow \beta} = \hbar\gamma B_0$ (Palmer III et al. 2006). $\gamma B_0 = \omega_0$ is the Larmor frequency, that is the resonance frequency; nuclear Larmor frequencies are in the range of radiofrequencies and differs between isotopes. The irradiation of a spin -1/2 nuclei sample with photons of energy $\Delta E = |E(\beta) - E(\alpha)| = \hbar\omega_0$ can flip protons from state α to β state.

At equilibrium there is a slight excess of $|\alpha\rangle$ over $|\beta\rangle$ nuclei ($N\alpha/N\beta$ = approx. 1.0001/1), thus the population difference between spin states is small and hence NMR sensitivity is low.

Spins-radio frequency field interaction

As mentioned, the nuclei can be excited by sending them an appropriate radio wave, which is actually a radio frequency (rf) pulse centered on the Larmour frequency.

The rf field is applied perpendicular to the static field. Usually, it is chosen parallel to the x axis (Haeberlen 2012):

$B_{rf} = (B_1(t) \cos[\omega t + \varphi(t)], 0, 0)$ (1.6)

This form of B_{rf} implies an rf irradiation that may be modulated in both its amplitude and phase, but that has a constant carrier frequency $\omega/2\pi$. Consequently:

$\hat{H}_{rf} = -\hbar B_1(t) \cos[\omega t + \varphi(t)] \sum_i \gamma_i \hat{I}_{i,x}$ (1.7)

In a semi-classical description, the collective behavior of spins is given by the vector sum of the individual magnetic vectors, known as the bulk, or net magnetization vector, M_0. When immersed in the magnetic field, the projection of the M_0 vector along the x and y axes (M_x=M_y=0) is zero, and the enhanced population in one orientation over the other leads to a net vector in one direction ($M_z = M_0$), which is parallel to B_0. The rf pulses excite the system by rotating the net magnetization vector of a "flip angle", θ, defined as (Rule and Hitchens 2005):

$\theta = \gamma B_1 \tau_p$ (1.8)

where γB_1 is the intensity of the applied pulse (field strength), and τ_p its duration. The intensity and duration of the pulse are experimental variables set by the spectroscopist. A 90° flip angle (or 90° pulse), the most commonly used pulse in NMR experiments, rotates magnetization through 90°, thus switch the magnetization vector of the Z axis in the XY plane. This is a non-equilibrium state, and the system relaxes back towards equilibrium where $M_z = M_0$ and $M_x = M_y = 0$. The absorbed energy or the energy released on relaxation back to equilibrium is measured. Energy can be released from the nuclei with two different relaxation processes: a) the nuclei exchange energy with the surrounding environment represented by the instrument (this process is regulated by the spin-lattice or T_1 relaxation time); b) the nuclei exchange energy with each other (process regulated by the transverse time T_2). As the nuclei relax, an instrument device records a time domain emission signal, called FID (Free Induction Decay). This signal, which depends on time, is turned into the well-known NMR spectrum using the Fourier transformation, a mathematical operation (Günther 2013).

NMR internal interactions

So far, it has been seen the Zeeman Hamiltonian describes the interaction between nuclear spins and the external static magnetic field B_0, whose eigenvalues are E_α and E_β, and $\Delta E_{\alpha \rightarrow \beta} = \hbar\gamma B_0$ (Palmer III et al. 2006). This result would be valid only if the nucleus were "naked" or "isolated", i.e. if it was only affected by the interaction with B_0. If this were the case, NMR would be practically useless because all the nuclei of the same species would give rise to the same spectral frequencies. On the contrary, nuclei are surrounded by particles (electrons and other nuclei), generating local magnetic fields that add to (or subtract from) B_0. The nucleus, therefore, interacts not only with the external magnetic field B_0 but also with these local fields. These latter interactions are called "internal", as the magnetic fields are generated internally to the matter (Levitt 2008). For diamagnetic systems (the vast majority of those present in nature) there are four most important internal interactions: *Shielding interaction, Indirect spin-spin coupling, Dipolar coupling, and Quadrupolar Interaction*.

The various internal Hamiltonians can be described as the coupling between two vectors (generically *U* and *V*) through a generic second-rank tensor (Canet 1996):

$$\widehat{H_\lambda} = \widehat{U_\lambda} \cdot \overleftrightarrow{T_\lambda} \cdot \widehat{V_\lambda} \tag{1.9}$$

$\overleftrightarrow{T_\lambda}$ is the second rank tensor describing the λ-th interaction, $\widehat{U_\lambda}$ and $\widehat{V_\lambda}$ are the vector operators of two interacting physical quantities.

Since vectors have three components each, any tensor $\overleftrightarrow{T_\lambda}$ may be represented by a 3 × 3 matrix with 9 components (Palmer III et al. 2006).

$$\overleftrightarrow{T}_\lambda^{LAB} = \begin{pmatrix} T_{XX} & T_{XY} & T_{XZ} \\ T_{YX} & T_{YY} & T_{YZ} \\ T_{ZX} & T_{ZY} & T_{ZZ} \end{pmatrix} \tag{1.10}$$

All the components of the $\overleftrightarrow{T_\lambda}$ tensor can be considered negligible with respect to the component in the Z direction (T_{ZZ}). This is due to an approximation, called *Secular* or *High Field Approximation* (HFA), which consider Zeeman interaction as the predominant one having a higher magnitude direction that causes the quantisation along the z-axis of the laboratory reference frame and treats internal interactions as a perturbative correction to the energy. Therefore, the only part of the spin Hamiltonian relevant for the various internal interactions is the one commuting with Zeeman Hamiltonian, which in the cartesian representation corresponds with taking only T_{ZZ}. This component is made up as follows (Diehl et al. 2011; Emsley and Lindon 1975):

$$T_{ZZ} = \frac{1}{3}Tr(T) + \frac{2}{3}\sum_{\alpha\beta}\frac{1}{2}\left(3\cos\theta_{\alpha z}\cos\theta_{\beta z} - \delta_{\alpha\beta}\right)T_{\alpha\beta} \tag{1.11}$$

where, $Tr(T)$ is the trace of the tensor $\tilde{T}_{\lambda}$. $\theta_{\alpha z}$ and $\theta_{\beta z}$ are the angles between the Z axis of the laboratory system and the molecular axis α and β. $T_{\alpha\beta}$ represents the components of the interaction tensor $\tilde{T}_{\lambda}$ expressed in the molecular reference frame (α, β, γ). $\delta_{\alpha\beta}$ is the Kronecker delta.

As molecules move rapidly, their α, β, and γ axes constantly change direction about the fixed laboratory axes. This behaviour leads to variations in values over time, resulting in a motionally averaged measurement of the interaction. Therefore, the previous equation can be expressed as:

$$\langle T_{ZZ}\rangle = \frac{1}{3}Tr(T) + \frac{2}{3}\sum_{\alpha\beta}\frac{1}{2}\langle\left(3\cos\theta_{\alpha z}\cos\theta_{\beta z} - \delta_{\alpha\beta}\right)T_{\alpha\beta}\rangle \quad (1.12)$$

in which the brackets, $\langle\ldots\rangle$, indicate the average over the molecular motions. $\frac{1}{2}\left(3\cos\theta_{\alpha z}\cos\theta_{\beta z} - \delta_{\alpha\beta}\right) = S_{\alpha\beta}$ are the elements of the Saupe ordering matrix and represent the average orientation of the laboratory Z axis in the chosen molecular system. For the properties of the director cosines, the Saupe ordering matrix is a 3×3 real, symmetric, traceless tensor. Therefore it is necessary to know five components in order to express the orientation of a molecule with respect to the laboratory system. But, if the Principal Axis System (PAS) is chosen, the Saupe order matrix is a diagonal matrix, so the elements off the diagonal are zero and only two elements must be determined.

The 1.12 relation can be re-written as:

$$\langle T_{ZZ}\rangle = T^{iso} + T^{aniso} \quad (1.13)$$

In isotropic systems, such as the natural extracts studied in this thesis, the elements of the Saupe order matrix are averaged to zero by molecular motion since all orientations have the same probability of occurring. Therefore, T^{aniso} is zero, and consequently, the only contribution that influences the spectrum is the T^{iso}. The *Direct dipolar interaction tensor* and the *Quadrupolar interaction tensor* having zero traces will not influence the spectra in the isotropic phase (Levitt 2008). Thus, the only information that can be obtained from the isotropic spectra are the values of the *Chemical shifts* and the *J-coupling constants.* Therefore, in the following, attention will not focus on the *Direct dipolar coupling term*, which describes the direct interaction between the nuclear spins, nor on the *Quadrupolar interaction*, which applies to nuclei with a spin moment higher than ½. Instead, we will see the chemical *Shielding* and the *Indirect spin-spin coupling* interactions in detail.

Shielding interaction

The external magnetic field, B_0, induces an electronic current in the bonds surrounding the nucleus. The circulating electrons generate an induced magnetic field, $B_{induced}$, which modifies B_0 and the resonance frequency of the nucleus. The $B_{induced}$ direction is, generally, opposite to B_0, hence the term chemical "shielding". The induced magnetic field is, in a good approximation, linearly dependent on B_0 and can be expressed as $B_{\text{induced}} = \check{\sigma}_i \cdot \mathrm{B}_0$ where $\check{\sigma}$ is the shielding tensor. The nuclear spins interact with this induced field and the associated Hamiltonian is given by (Canet 1996):

$$\widehat{H}_S = -\hbar \sum_i \gamma_i B_0 \, \sigma_{i,zz} \hat{I}_{i,z} = -\sum_i \omega_{i,0} \, \sigma_{i,zz} \hat{I}_{i,z} \tag{1.14}$$

In NMR spectra, the shielding interaction causes different resonant frequencies for nuclei with varying electronic environments. This effect is called the *chemical shift*. In isotropic liquid,

$$B_{\text{induced}} = \sigma^{iso} \cdot \mathrm{B}_0 \tag{1.15}$$

where, $\sigma^{iso} \approx 10^{-4}$ is the isotropic chemical shift.

The chemical shift modifies the resonance frequency, but absolute chemical shifts are difficult to determine. Therefore, it's common practice to define the chemical shift in terms of the difference in resonance frequencies between the nucleus of interest (ν) and a reference nucleus (ν_{ref}), by means of a dimensionless parameter δ (Canet 1996):

$$\delta = 10^6 \, \frac{(\nu - \nu_{ref})}{(\nu_{ref})} \tag{1.16}$$

The 10^6 is pre-factor: as the chemical shifts are small, they are often quoted as in 'parts per million' (ppm) in order to make the numbers more convenient. For ^{1}H and ^{13}C, reference signals (ν_{ref}) are usually those of *TMS (tetramethylsilane)* for organic solvents, or *DSS (trimethylsilylpropanesulfonic acid sodium salt)* and *TMSP* (*Trimethylsilylpropanoic acid sodium salt)* for aqueous samples.

Since, as said, the circulation of the electron cloud around the nucleus shields it from B_0, nuclei in an electron-rich environment resonate at low chemical shifts. In contrast, nuclei in an electron-poor environment resonate at high chemical shifts. Thus chemical shift indicates the local electronic environment. Chemically equivalent nuclei have the same chemical shift.

Indirect spin-spin coupling

Another important interaction which provides a direct spectral manifestation of the *chemical bond*s in molecules is the indirect spin-spin coupling interaction. This one results from a

magnetic interaction between individual nuclei that is not transmitted through space but rather by the bonding electrons through which the nuclei are indirectly connected. Therefore, in this case the interacting quantities are two spins $\widehat{I_A}$ and $\widehat{I_X}$. The type of interaction is expressed by the $\check{J}_{AX}$ tensor and the general form of the Hamiltonian is the following (Canet 1996; Haeberlen 2012):

$$\widehat{H_J} = \hbar \sum_{A<X} \widehat{I_A} \cdot \check{J}_{AX} \cdot \widehat{I_X} \tag{1.17}$$

The magnetic moment of nucleus A causes a weak magnetic polarization of the bonding electrons. This polarization is then transmitted to nucleus X via overlapping orbitals while observing the Pauli principle. The external field at nucleus X could either be increased or decreased depending on the spin state of nucleus A. This variation in magnetic field magnitude is responsible for the resonance frequency of nucleus X, which results in splitting the NMR signal into a doublet. The same is also true for nucleus A. Since both spin states of A are almost equally probable, the doublet lines have equal intensity (Günther 2013).

The frequency splitting is called the J-coupling constant. The J-coupling does not depend on B_0 since the electron-nucleus and electron-electron couplings are independent of B_0. The J-coupling provides a direct spectral manifestation of the chemical bonds: two nucleus have a measurable J-coupling only if they linked together by a small number of chemical bonds, including hydrogen bond (Levitt 2008).

The magnitude of the J-coupling constant depend on several factor, including the gyromagnetic ratio of the nuclei, the number of bonds between the nuclei, and the geometry of the bonds. When coupling occurs between identical nuclei (^{1}H-^{1}H), it is called homonuclear J-coupling. In contrast, heteronuclear J-coupling is the coupling between distinct nuclei (^{1}H-^{13}C, ^{1}H-^{19}F, ^{1}H-^{31}P...). The J-coupling constant between two nuclei separated by N bonds is ^{N}J. Both ^{3}J and ^{4}J can give detectable effect in a spectrum, but couplings over a larger number of bonds can generally be ignored.

Chemically equivalent nuclei that also show identical couplings to all nuclei in the molecule are said to be magnetically equivalent. J-coupling between magnetically equivalent nuclei has no effect on the NMR spectrum. The signal of a proton-coupled to N magnetically equivalent protons is split into N+1 peaks, their relative intensities being in accord with Pascal's triangle (Günther 2013).

In general, a collection of nuclei that interact with one another through spin-spin interactions are denoted as “spin system”. To describe a spin system, capital letters with subscripts to different nuclei, such as AX_2 or A_3X_2, are assigned to indicate their number. The relative chemical shift is then represented by letters that are either close neighbours in the alphabet

or more distant, like ABC or AMX. So long as the chemical shift difference Δν between the multiplets is much larger than the coupling constant J, normal multiplets are observed (first order spectra) and what we have seen so far applies. These are referred to as AX spin systems. However, as the signals get closer (Δν ≈ J, AB spin system), spectra of greater complexity may occur due to second order effects. In such non-first order spectra, multiplets may be highly distorted and very difficult to analyze, as additional peaks of various intensities appear and complicate the signal.

1.1.4.1 NMR Experiments in Metabolomics

In metabolomics applications, choosing suitable experiments to acquire NMR profiles is critical for obtaining well-resolved patterns to detect the most significant possible number of metabolites (Keun 2018). Proton NMR is a powerful tool for determining organic structures, as most organic compounds, and thus almost all known metabolites, contain many hydrogen atoms. Furthermore, the ^{1}H isotope has a natural abundance of approximately 99%, so high-resolution spectra are generated. The pulse sequence generally used in recording one-dimensional proton spectra is the simple ***zg***, characterized by a 90° pulse and the acquisition of the FID when the pulse is blocked. However, food matrices like fruit juices have a high-water content. As a flared singlet signal, water protons are visible in the ^{1}H–NMR spectrum. This singlet can cover other signals that fall at the same chemical shift value and, at the same time, alter the baseline of the spectrum. Therefore, its suppression is essential. Many methods of solvent suppression exist (Zheng and Price 2010). ***noesypr1d*** pulse sequence with water presaturation is the most popular acquisition scheme for collecting metabolite fingerprints from aqueous samples (Keun 2018). The ***noesypr1d*** pulse sequence (Figure 1.4) begin with a long, very lower power (i.e., 80 Hz γB_1 has been recommended) period (Mckay 2011).

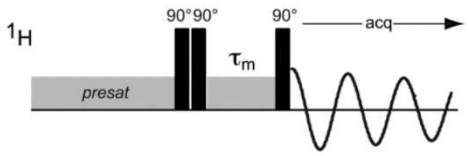

Figure 1.4 *noesypr1d* pulse sequence (Keun 2018).

This low, long radio frequency pulse serves to presaturate, to suppress most intensity of the water signal or rather to align the magnetization of the water protons on the xy plane. After the *presat* pulse two 90° pulses invert all magnetizations (solute and residual solvent) to the –z axis in a vector presentation. When metabolites (solutes) relax toward the +z axis

(equilibrium state) during a specific delay (termed as mixing time, τ_m), the residual water signal relaxes slower as water has longer T_1 relaxation time than metabolites (Teng 2012). Moreover, water suppression is also maintained by irradiation of the water frequency during the mixing time (Lindon et al. 2007). To measure the relaxed or partially relaxed solute signal, a final 90° excitation pulse is applied, which brings it back into the xy plane. Meanwhile, the solvent, lacking any phase coherence, is unperturbed by the final pulse and contributes little or no measurable signal in the receiver circuitry (Mckay 2011).

However, while solving the solvent signal problem, in metabolomic studies, ^{1}H–NMR spectra are complicated by numerous resonances in a narrow frequency range (0-11 ppm) (Schleif et al. 2011; Serkova and Niemann 2006; Ward et al. 2010). By definition, all organic molecules contain carbon atoms. Carbon NMR is also possible and has become one of the most important analytical tools available to chemists in combination with ^{1}H–NMR. The ^{13}C–NMR spectrum is more resolved than the proton spectrum as the spectral window is wider (0-200 ppm); however, the sensitivity is much lower due to the low ^{13}C isotopic abundance (1.1%), low magnetogyric ratio and longer relaxation times. ^{13}C resonances of small metabolites are narrow singlets with ^{1}H decoupling (that means selectively irradiating ^{1}H nuclei to send them to the higher energy state for the whole time of the experiment).^{13}C–{^{1}H} NMR spectra represent an alternative and complementary route in the identification of metabolites (Clendinen et al. 2014). In this thesis, ^{13}C spectra are recordered using the inverse-gated pulse sequence ***zgig*** which allows to obtain quantitative ^{13}C information from the ^{13}C–{^{1}H} NMR spectrum (Salvino et al. 2021). In some instances, the identification of metabolites' molecular structure cannot be achieved through one-dimensional (1D) spectra alone. To overcome this limitation, two-dimensional (2D) NMR spectra are used (Cultivars et al. 2023; Mahrous and Farag 2015; Miricioiu et al. 2023). Conventional 1D spectra are plots of intensity vs frequency. In 2D NMR, intensity is plotted as a function of two different frequencies. This allows a new resolution of the spectrum in the second dimension. There are various ways of representing 2D spectra, but the most practical and commonly used is a flat square or rectangle with the 2 frequency coordinates F1 (X axis) and F2 (Y axis). Peaks are contour plots in which the intensity is represented by contour lines (in the same way as topographical maps). Each line of the contour plot is an «altitude level», with the signal intensity in the Z axis. The contour plots blotches (or pseudo-3D peaks) represent coupling interactions between different nuclei, which are correlation signals. There are various types of 2D NMR experiments, each of which gives a different kind of structural information. Homonuclear 2D NMR experiments identify correlations between nuclei of the same type (most commonly ^{1}H–^{1}H clarifies the couplings between protons). Heteronuclear 2D NMR

experiments (usually $^{13}C-^{1}H$ or $^{15}N-^{1}H$) give additional information on the connectivity of the molecule. In this thesis work, $^{1}H-^{1}H$ COSY (COrrelation SpectroscopY), ^{1}H Homonuclear 2D J-Resolved spectroscopy and $^{1}H-^{13}C$ HMQC (Heteronuclear Multiple Quantum Coherence) experiments have been used.

The COSY experiment detects through-bond ^{2}J geminal and ^{3}J vicinal scalar couplings (Silverstein et al. 2014). Long range couplings are usually to small to be seen. Both the X and Y axis are projections of the $^{1}H-$NMR spectrum. In a 2D NMR spectrum, the diagonal represents the 1D ^{1}H spectrum viewed from above. Any dots above or below the diagonal indicate pairs of protons that are correlated with each other. These dots are known as cross peaks. The symmetry of the spectrum is observed concerning the diagonal: each coupling correlation appears on both sides. COSY is an effective method for tracing coupling networks in molecules. This 2D experiment is instrumental in resolving crowded regions in the $^{1}H-$NMR spectrum of a given molecule. Furthermore, it can aid in identifying coupling partners in complex second-order spectra, which may be challenging to determine in 1D NMR (Günther 2013). Additional assistance in this regard can be obtained from ^{1}H J-Resolved (J-RES) experiments. This approach separates chemical shifts and *J*-couplings in two spectral dimensions. Chemical shifts are along F2 axis, while coupling constants are along F1. This offers a powerful procedure for unraveling complex overlapping multiplets (Rehman and Choudhary 1996).

The HMQC experiment correlates a proton (X-axis) with the carbon directly attached (Y-axis). In this case, the spectrum does not show any symmetry. The HMQC method helps determine a molecule's connectivity and assign carbon peaks. It can also help resolve a complicated proton spectrum, where overlapping signals are dispersed in the second dimension. Additionally, it provides a convenient way of identifying diastereotopic protons as they produce two correlations at the same carbon (Silverstein et al. 2014).

Therefore, 1D and 2D NMR experiments are essentials in metabolomics studies and very broad is the variety of NMR metabolomics applications (Cesare et al. 2023; Cuny et al. 2008; Girelli et al. 2020; Palama et al. 2016), as shown in Figure 1.5:

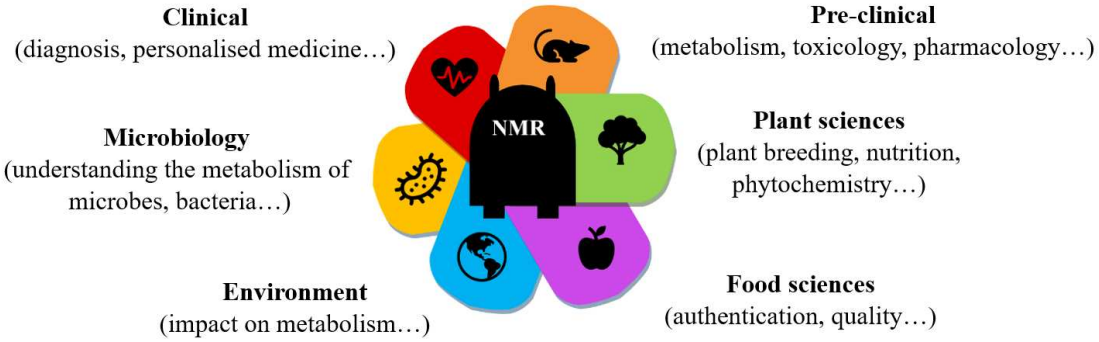

Figure 1.5 Applications of NMR metabolomics.

Generally, the structural information obtained from NMR spectra is combined with library data and public and commercial databases, such as Human Metabolome Database (HMDB), Complex Mixture Analysis by NMR (COLMAR) or Chenomx (Edmonton, Canada) (Abreu and Fernández 2020) to recognise metabolites properly. Moreover, metabolomic studies often involve analysing multiple samples to identify trends, jumps, clusters, outliers, and the variables responsible for that. However, when dealing with many samples and signals, it becomes necessary to use advanced calculations such as *multivariate statistical analysis*, a branch of *chemometrics*. This approach is generally employed when dealing with extensive data sets from analytical and chemical-physical studies. In fact, as the number of dimensions of data increases, it becomes more and more difficult to process, and multivariate analysis helps to simplify multivariate problems.

1.1.5 Chemometrics

The term *chemometrics* was coined in 1972 by the Swedish chemist Svante Wold. Chemometrics is the chemical discipline that uses mathematical and statistical methods for two key purposes. Firstly, to design or select optimal procedures and experiments (known as *Experimental Design*) and, secondly, to analyse a multitude of chemical data by performing a compression of high-dimensional datasets to get over the maximum chemical information (*Multivariate Statistical Analysis or Pattern Recognition*) (Varmuza and Filzmoser 2009). In this thesis, chemometrics is used for pattern recognition, especially to extrapolate information from NMR data and, as shown in Chapter 5, also from UV-Vis data. However, chemometrics can be applied to any type of measurement and to quantitative continuous or discrete variables. The principal steps of pattern recognition are shown in Figure 1.6:

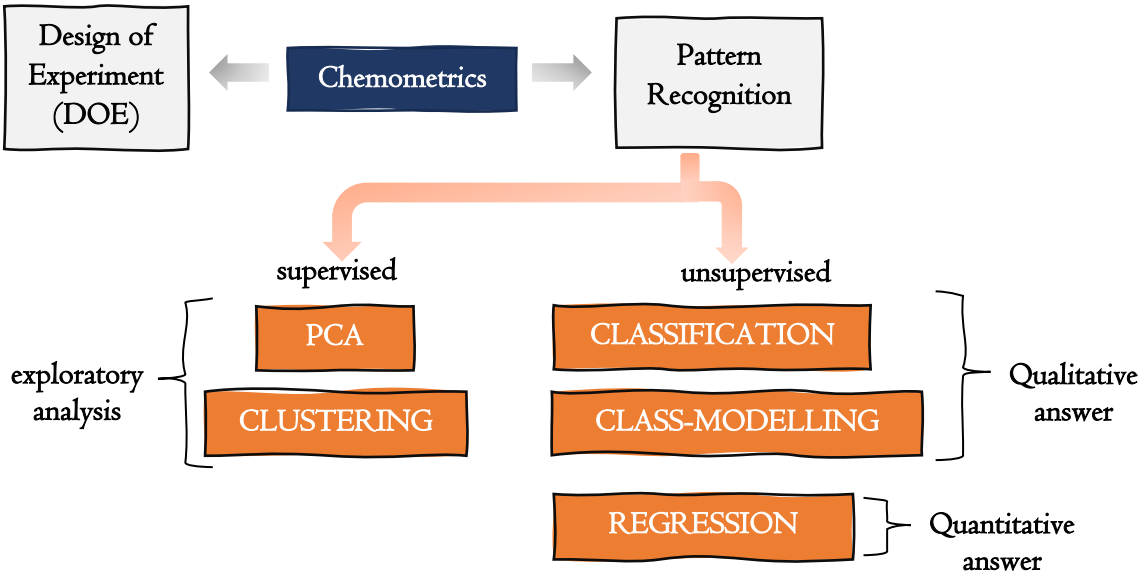

Figure 1.6 Branches of chemometrics and fundamental stages involved in multivariate statistical analysis.

The Principal Component Analysis (PCA) represents the foundations of multivariate statistical analysis. Like clustering, PCA is used to conduct an exploratory study on a very large number of samples and variables. This method reduces the dimensionality of the original data size, increases the interpretability of data while preserving the maximum amount of information, and enables the visualisation of multidimensional data. PCA does not require a priori information on the data (Oliveri, Malegori, Mustorgi, et al. 2020). On the contrary, additional information on the analysed samples is necessary for supervised methods, in which mathematical models are developed, validated, and used to predict a qualitative or quantitative response on unknown samples. This thesis used only unsupervised PCA analysis, so this technique is now diving deeper.

1.1.5.1 Principal Component Analysis (PCA)

Principal component analysis (PCA) is a handy tool which helps manage high-dimensional datasets. It allows an understanding of the interrelations among samples, between samples and measured variables, and the inter-correlations among the variables. The idea behind PCA is to extrapolate the maximum amount of data information by constructing some principal components (PCs) that explain most of the data's variability. Variability describes how far apart data points lie from each other and from the distribution centre and can be considered synonymous with information. For example, a high variability in a quality control approach

indicates that the sample moves away from the standard. This means that the process/product is out of control, and the system has to be revised, thus, in this case, variability is a problem. Instead, when the goal is to understand a phenomenon, such as understanding if some samples have the same or different composition, variability is regarded as an opportunity to capture the information retained in the samples. The first principal component constructed in PCA is the component that explains the variability of the data the most, followed by PC2, PC3 and so on, until the last components, which contain only noise, are reached. The first components are, therefore, those that contain the most information on the system and are sufficient to completely explain the phenomenon under examination, simplifying the interpretation of the data. Now, let's see better how these main components are generated, starting by saying that variability is mathematically quantified by variance, expressed as follows (Varmuza and Filzmoser 2009):

$$Var(x) = s_x^2 = \frac{\sum_{i=1}^{n}(x_i - \bar{x})^2}{n-1} \tag{1.18}$$

where x_i refers to a variable, $\bar{x}$ is the mean of the sample data set, and n is the total number of observations. The square root of the variance is the standard deviation, s_x.

In a multidimensional space of original data, PCA algorithms seek the direction of the maximum variance.

Usually, chemical data are organised in a matrix, X_{NV}, in which, conventionally, each row is an N object (sample, molecule, individual…) described by many V variables, one for each column (Krull 2012). In the case of instrumental data (e.g. spectra), each signal profile is an object, and each measured quantity is variable.

For discerning the correct directions of maximum variance in PCA, the data matrix has to be at least mean-centred column-wise (Oliveri, Malegori, Mustorgi, et al. 2020), which corresponds in formulas and graphically as follows:

$$(x_{iv})_{centered} = x_{iv} - \bar{x}_v \tag{1.19}$$

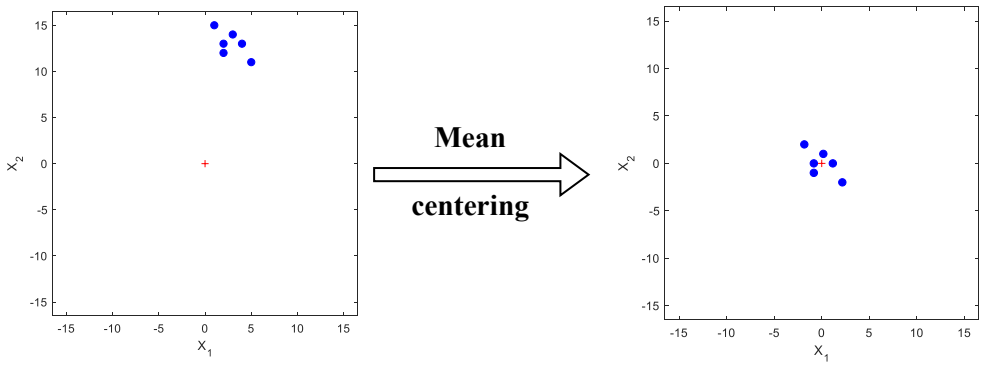

Figure 1.7 Visualization of mean-centering transformation.

Thus, the average of the values that make up that column is subtracted from each value in a column. However, for variables of different nature, this column pretreatment is not sufficient, so scaling is added, i.e. the centred values are divided by the standard deviation, and thus differences in location and dispersion among the original variables are eliminated (Oliveri et al. 2020a). Centering plus scaling is called column autoscaling, shown in formulas and graphically as follows:

$$(x_{iv})_{autoscaled} = \frac{x_{iv} - \bar{x}_v}{s_v} \quad (1.20)$$

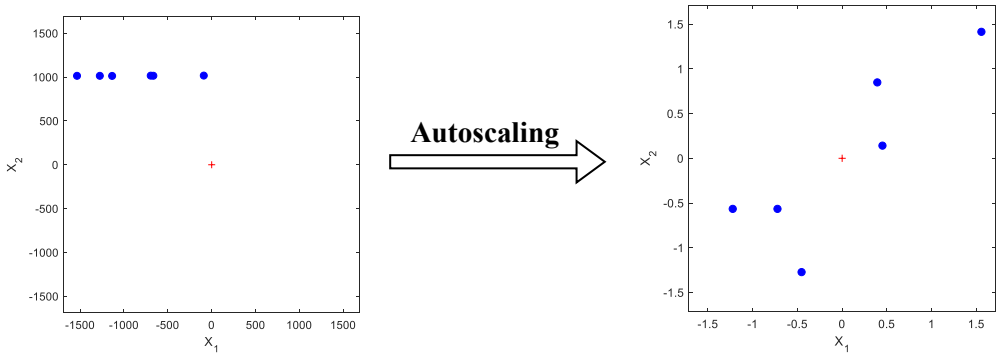

Figure 1.8 Visualization of mean-centering transformation.

These pre-treatments ensure that when searching for maximum variance, new axes, different from those to which the original data refer, rotate about the data centroid until the direction of maximum variance is found (Krull 2012). The maximum variance direction represents the first principal component (PC). The second PC is the direction, which keeps the maximum variance among all directions orthogonal to the first PC. It follows that the second PC explains the maximum information not explained by the first one or, in other words, these two new variables are uncorrelated. The process allows the identification of a maximum number of PCs equal to the rank of the matrix: the lower between the number of rows minus one and the number of columns. The PCs are expressible as linear combinations of the original variables: the coefficients that multiply each variable are called loadings. They represent the cosine values (director cosines) of the angles between the PCs and the original (Oliveri, Malegori, Mustorgi, et al. 2020). In terms of matrix algebra, the data matrix X_{NV} is decomposed into two orthogonal matrices: S_{NV} (score matrix) and L_{VV} (loading matrix). The loadings, as said, represent weights for each original variable when calculating the principal components, and that's what comes out mathematically. On the other hand, the score matrix contains the original objects in a rotated coordinate system and is obtained by multiplying the loadings matrix by the original data matrix (Oliveri, Malegori, and Casale 2020):

$S_{NV} = X_{NV} \cdot L_{VV}$ (1.21)

Different software programs are available to perform PCA on a dataset (Manly and Navarro Alberto 2016). The most well-known software is R (Cornea-Cipcigan et al. 2023; Feng et al. 2023; Kimwemwe et al. 2023; Narvaez-Montoya et al. 2023), characterised by a graphical user interface (GUI) that is adequate to input code and to get numerical results displayed in a console (Manly and Navarro Alberto 2016). This rudimentary functionality of the standard R GUI makes R a little tricky to use. In this thesis work CAT (Chemometric Agile Tools) software was used to perform the PCA. It is always an R-based software but with a friendlier interface (Alberti et al. 2023).

PCA is implemented through software by executing the following steps from a mathematical perspective (Krull 2012; Leardi 2002; Varmuza and Filzmoser 2009):

1) The original data matrix file is loaded into the software.
2) Autoscaling or other column transformations are performed using the appropriate commands.
3) The *variance-covariance matrix* of the original data is calculated. This matrix has as many rows and columns as variables in the data set. Assuming to have only two variables, the *variance-covariance matrix* is:

$$C = \begin{bmatrix} s_1^2 & s_{12} \\ s_{12} & s_2^2 \end{bmatrix} \quad (1.22)$$

where s_{12} is the covariance. Covariance allows to understand the correlation between two variables in term of importance and direction, and is expressed as:

$$Cov(x) = s_{x1x2} = \frac{\sum_{i=1}^{n}(x_{1,i}-\bar{x}_1)(x_{2,i}-\bar{x}_2)}{n-1} \quad (1.23)$$

On the diagonal of the *variance-covariance matrix* there are the variances respectively of the first (s_1^2) and the second (s_2^2) columns of the data matrix, since the covariance of a variable with itself coincides with the variance.

4) The *variance-covariance matrix* is diagonalised. Diagonalising means transforming a square matrix into a diagonal matrix with non-zero elements only along its diagonal. This refers to making the correlation between different variables equal to zero, thus creating new uncorrelated, orthogonal principal components. The percentage of variance explained by the principal components is described by the *eigenvalues*, or rather the numbers on the diagonal of the diagonalized *variance-covariance matrix*. These numbers decrease along the diagonal, because as mentioned before, the information they contain is less and less. From the diagonalization of the *variance-covariance matrix*, the *eigenvectors*, i.e. the loadings, are also obtained.

5) In the end, simple graphs are obtained from the PCA analysis: a 'score plot' and a 'loadings plot'. The score plot, representing the matrix S_{NV}, reports the samples in the new space defined by the principal components. On the other hand, the loading plot, in the form of a scatter plot or line plot, reports the variables in the PCs space, allowing to understand the relative importance of the original variables in constructing the principal components. Since scores and loadings actually derive from the same data matrix, X_{NV}, it is essential to look at the two graphs together; they can also be depicted in a single graph called a 'biplot'.

1.1.4.2 PCA on NMR data

The most commonly used experiments for statistical treatment in NMR are 1D ^{1}H spectra. However, before performing appropriate chemometric analysis, the raw NMR data must undergo preprocessing to minimize any undesired variability caused by line shape and chemical shift changes, noise, baseline shift, signal referencing, and signal intensity. Data preprocessing is necessary to ensure reliable analysis and involves the following steps (Craig et al. 2006; Hatzakis 2019; Pacholczyk-Sienicka et al. 2021; Simon and Köstler 2019):

1. *Apodization and Zero filling* – before the Fourier Transform, a mathematical function multiplies the FIDs to increase the sensitivity, i.e. the Signal-to-Noise Ratio (SNR) of the spectra and data points are added to the end of the FIDs of each 1D ^{1}H NMR spectra.
2. *Baseline correction* −The influence of the baseline components can be eliminated by using polynomial baseline correction.
3. *Chemical shift alignment* − To compare the spectra with each other, spectra are aligned by calibrating a known resonance of a reference signal.
4. *Binning* – All spectra are divided into small regions named bins or buckets, large enough to include little chemical shift variations and each bucket's integral is then calculated. Binning (or bucketing) can be performed with constant (e.g. 0.05 ppm) or variable width. It can be executed manually from Bruker TopSpin or using programs such as AMIX, KnowItAll Metabolomics or NMRProcFLow package (Abreu and Fernández 2020). If certain regions in the ^{1}H NMR spectra have a very low signal-to-noise ratio, they can be excluded from binning to reduce errors.
5. *Normalization* − Normalization procedures must be applied to minimise the imperfection caused by differences in the pulse length, relaxation times, and dilution of samples. The

normalisation relies on eliminating systematic bias by scaling the signal elements to a constant factor. In practice, the spectral intensities for each sample are scaled to a constant, which may derive from an internal standard or the sum of the areas in the spectrum. In the works reported in this PhD thesis, the data have been normalised with respect to the total area by setting the sum of the bins' areas in each spectrum equal to 100. As a consequence of normalisation, the data derived from all samples can be directly compared.

6. *Data extrapolation* − 1D NMR data (samples and the bin integrals variables) are transformed into a matrix containing samples in the rows and variables in the columns.

   Once obtained, the data matrix is loaded onto the CAT software and subjected to column transformations (mean-centering or autoscaling), as described in the previous paragraph, to perform PCA. After completing the task, the console displays the variance for each calculated principal component explains. The explained variance as a function of the number of PCs can be displayed graphically as a scree plot, which takes the form of a broken line with an always negative slope. By analyzing this graph, it is possible to identify the point at which the slope changes abruptly. This point indicates the number of PCs to be considered. Once determined the number of principal components significant enough to explain the data, attention turns towards examining the scores and loadings graphs.

   Moreover, to improve the metabolome coverage and obtain further information about samples, NMR data can be statistically combined with others analytical and chemical-physical methods (data fusion). When executing PCA in multiblock data sets auto-scaling might be not sufficient as column pre-treatment, in particular when there is a highly different number of variables in each block. In this case, as in the work of Chapter 5, block-scaling pretreatment is required, otherwise, the inferences from the data analysis would be biased by the dominance of the variation contained in the largest blocks. Block scaling can be carried out using either *hard* or *soft* scaling methods. In the *soft* block scaling approach, the variables of each block are scaled such that the sum of their variances equals the square root of the number of variables in that block. On the other hand, in the *hard* block scaling approach, the blocks' variables are scaled so that the sum of their variances is equal to one (Eriksson et al. 2006).

1.1.6 Membrane operations

Membranes are selective barriers that allow specific components of a mixture to pass through while retaining others under the influence of an appropriate driving force (Liu et al. 2018). This force can be generated by a difference in pressure, concentration, temperature, or electric potential between the two sides of the membrane. However, the separation process is not solely based on the driving force but also considers the chemical-physical and morphological properties of the membrane and the substances being separated, such as the size and chemical nature of compounds in the mixture to treat, the material the membrane is made of, its configuration, its structure, etc. A membrane separates a feed solution into two fractions (streams): the permeate/filtrate and the retentate/concentrate (Figure 1.9). The permeate contains the solvent and solutes that pass through the membrane, while the retentate contains the particles and compounds that have not been transported through the membrane.

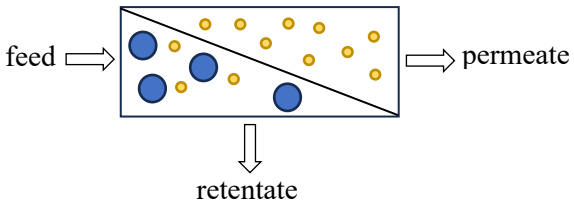

Figure 1.9 General scheme of a membrane system.

Membranes' separation abilities have been known since 1748 when Abbé Nolet experimented with separating water from solutes through a semi-permeable membrane, coining the word *osmosis* to describe the process (Tamime 2013). Throughout the 18th and 19th centuries, membranes were used exclusively for laboratory applications and often were animal-based (membranes consisted of sausage casing made from animal intestines or the bladders of pigs, cattle or fish). The first synthetic membranes were produced by Fick in 1855 and were made of nitrocellulose. During the following years, membrane technology was expanded to other polymers, notably cellulose acetate. Membranes found their first significant application at the end of the Second World War to filter water and obtain drinking water without micro-organisms. By 1960, the elements of modern membrane science had been developed. However, membranes were still not so widespread as they suffered four problems: they were too unreliable, too slow, too unselective, and too expensive. Over the years, solutions to these problems have been developed, and membrane-based separation processes are now commonplace (Baker 2012).

Over 200 materials have been commercially utilised for making membranes (Cheryan 1998). Most membranes used commercially are synthetic organic polymer-based. However, inorganic membranes are also common. Moreover, in recent times, there has been an increasing use of natural polymers (biopolymers) in the preparation of membranes, which helps reduce environmental impact (De Bartolo et al. 2017).

Biopolymers derived from animal (polylactic acid, polyhydroxyalkanoates, polybutylene succinate) or vegetable sources (cellulose-based polymers, alginate, polyisoprene, starch), as well as from bacterial fermentation products (chitin, chitosan, collagen, sericin) (Galiano et al. 2018). Some of the most commonly used membrane materials are shown in Table 1.1.

Table 1.1 Organic (natural and synthetic) and inorganic membrane materials.

Synthetic polymers membranes	Biopolymers-based membranes	Inorganic membranes
Polyvinylidene	Cellulose Acetate	Alumina
Polyacrylonitrile	Polylactic acid	Carbon
Polyamide	Alginate	Nickel
Polycarbonate	Starch	Silicon
Polypropylene	Chitin	Stainless
Polysulfone	Chitosan	Titania
Polyethersulfone	Collagen	Zirconia
Polysulfone sulfonate	Cellulose esters	
Polyvinyl alcohol	Polybutylene	
Polyethylene	Polyhydroxyalkanoate	
Polystyrene	Polyisoprene	
Polytetrafluoroethylene	Sericin	

The efficiency of membrane separation is assessed by flux and rejection. Flux is the amount of permeate produced in a given time period, and the term generally is provided as a volume or mass per unit membrane per unit time. It determines the capacity (throughput) and cost of a membrane system. On the other hand, rejection measures the membrane's separation capabilities for a particular solute. It is expressed in terms of solute concentration in the permeate (C_P) and the retentate (C_R) (Liu et al. 2018):

$$R = \frac{1-C_P}{C_R} \tag{1.24}$$

To perform effectively, a membrane must meet specific requirements, including high permeability, good retention capacity based on the particular application, excellent mechanical strength, chemical stability and inertness, thermal stability, resistance to cleaning and sanitising agents, resistance to microbial activity, smooth and fouling-resistant surface, compliance with all other food safety requirements, extended service life, and affordability

(Berk and Berk 2009). It is important to note that these characteristics may conflict. For instance, a high retention rate might result in low permeate flux, while high mechanical strength can be achieved by increasing the thickness of the membrane, which in turn reduces the flux. Thin film membranes (TFMs) are used to solve this issue. These membranes consist of multiple layers, each with a different composition or structure, contributing to the assembly of various characteristics.

There are two main methods in membrane filtration: direct flow or dead-end filtration and tangential flow or cross-flow filtration (Murkes 1990). The traditional direct flow filtration involves a vertical sample flow through the membrane, separating small molecules from larger ones. However, this method has a drawback as macromolecules can build up on the membrane surface, leading to reduced filtration efficiency and the need for frequent membrane replacements. Tangential flow filtration, on the other hand, operates with the sample flow moving horizontally across the membrane surface at a tangential angle. The flow is continuously filtered and rinses the membrane surface as it circulates, preventing the accumulation of macromolecules and reducing concentration polarisation caused by reduced flow rates. This ensures a stable flow rate and effectively prolongs the lifespan of the filter membrane. Tangential flow filtration offers additional advantages, simultaneously allowing for concentration and diafiltration. Due to these advantages, most industrial membrane processes rely on tangential filtration operations. The tangential flow filtration method can be applied using various membrane modules. Membrane modules are typically small units in which membranes are packed. Four basic designs, illustrated in Figure 1.10, are available for membrane modules: plate-and-frame, spiral wound, tubular and hollow-fibre configurations (Judd and Jefferson 2003). The membrane geometry is planar in the first two and cylindrical in the others. The module configuration and the arrangement of modules in a system are based on economic considerations, the type of separation, ease of cleaning, maintenance and operation.

Plat-and-frame module comprises rectangular or (pseudo) circular flat sheet membranes with separators and support plates. The surface area-to-volume ratio of plate-and-frame modules is low. Moreover, they are limited to low-pressure operations. Because of their relatively high cost, they have mainly been replaced by spiral-wound and hollow-fibre modules in most applications.

Spiral wound module consists of large membrane sheets wound into a compact spiral configuration around a central permeate collector tube. Their surface area-to-volume ratio is high, but spiral-wound modules are well-compacted and cost-saving. However, they are more susceptible to plugging and may be difficult to clean.

Tubular modules consist of tubular support with the membrane inserted. The feed solution is pumped through the tube, and the permeate passes through the membrane/porous support composite. Tubular configurations are well-suited for applications where the feed stream has a high concentration of suspended solids or requires a high concentration. They allow for maintaining high tangential velocity and have a relatively large diameter, making them easy to clean and inspect. Tubular modules' surface area-to-volume ratio is not high.

Hollow-fibre modules are similar in principle to the tubular setup but with much thinner "tubes" with diameters ranging from 1 mm to capillary size. The primary advantage of hollow-fibre modules is their compactness, which enables them to achieve thousands of square meters of membrane area per cubic meter of module bulk volume. However, they are highly prone to fouling and clogging, which limits their use to relatively low-viscosity clear fluids.

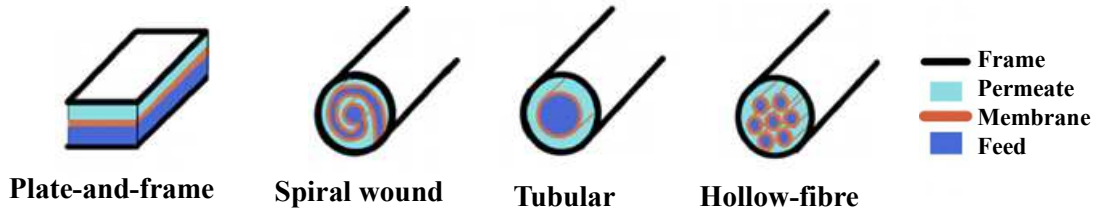

Figure 1.10 Basic designs of membrane modules.

Membrane operations are distinguished not only by different types of modules but also by the type of driving force used to transport specific components through the membrane. There are many different membrane processes and various fields of applications, such as water purification (Ursino et al. 2018), separation of gas mixtures (González-Revuelta et al. 2023), concentration of bioactive substances (Conidi et al. 2011; Mir-Cerdà et al. 2023), and biomedical applications (Radu et al. 2023). The food industry has widely studied membrane processes, and many of them have become established technological innovations, such as in the concentration of whole milk, in the production of cheese, and in the recovery of whey proteins (Brans et al. 2004; Mistry and Maubois 2017). Membrane-based technologies, like microfiltration (MF), ultrafiltration (UF), nanofiltration (NF), and reverse osmosis (RO), are valuable tools for separating, concentrating, and recovering high-added value compounds from agro-food products (Castro-Muñoz et al., 2019; Conidi et al., 2018), thus matching the objective of this PhD thesis. MF, UF, NF and RO are called pressure-driven membrane processes since the driving force for material transport through the membrane is the pressure drop across the membrane or the transmembrane pressure difference (TMP or ΔP_{TM}). The

pressure at the permeate side is practically uniform. The pressure at the retentate's side decreases in the flow's direction. The transmembrane pressure difference is defined as (Berk and Berk 2009):

$$TMP = \frac{P_1 + P_2}{2} - P_3 \quad (1.25)$$

where:

P_1, P_2 = retentate side pressure at the module inlet and outlet, respectively;

P_3 = permeate side pressure, assumed uniform.

Pressure-driven membrane operations are categorised based on the size of their pores, which is expressed using meter submultiples to indicate the diameter. Alternatively, the size of membrane pores is measured using the nominal molecular weight cut-offs (MWCO). MWCO refers to the lowest molecular weight (in Daltons) of a test molecule (non-ionic solutes such as polyethylene glycol (PEG), oligostyrenes, alkanes and dextrans), which the membrane retains at a rate of 90% (Kadel et al. 2019).

Table 1.2 displays the main pressure-driven membrane processes with their corresponding pore sizes, MWCO, and required TMP.

Table 1.2 Pressure-driven membrane operations (Cassano et al. 2018; Tapia-Quirós et al. 2022).

Membrane process	Pore size (nm)	MWCO (Da)	TMP (bar)
Microfiltration (MF)	100 − 10.000	>100.000	0.1 − 2
Ultrafiltration (UF)	2 − 100	1000 −100.000	0.1 −7
Nanofiltration (NF)	0.5 − 2	120 −1.000	3 − 25
Reverse osmosis (RO)	< 0.5	1 − 100	35 − 100

MF membranes reject compounds with a molecular weight larger than 100 kDa, such as suspended solids, bacteria, or large colloids. Since polyphenols have molecular masses between 100 and 30.000 Da, they smoothly pass across the membrane. Moreover, having a high permeability, MF membranes allow a high flux at low pressure.

UF membranes present 2 to 100 nm pores and can retain macromolecules such as suspended solids, proteins and viruses, tannins, and high molecular weight phenolic compounds.

NF membranes can separate low molecular weight (MW) components from each other (e.g. sugar from salts). This technology has been revealed to be promising to fractionate and concentrate low-MW polyphenols. NF is an intermediate process between MF/UF and RO. The separation mechanism is based on particle size, such as for MF and UF, and on the chemical nature of the particles, such as for RO.

RO membranes are characterised by pore sizes less than 0.5 nm and MWCO of 1–100 Da, which are used for concentration and stream reduction. The permeability is slow, and the rejection is not related to the size of the molecules but to a solution-diffusion mechanism.
Therefore, to recover low-MW bioactive streams at room temperature, preserving their functional properties, integrated pressure-driven membrane operations can be adopted.
MF and UF can be primarily used for primary treatment to remove macromolecules that may cause operational issues in subsequent operations, particularly membrane fouling.
Membrane fouling is the undesirable deposition of suspended or dissolved substances on the membrane surface (*external fouling*) and within its pores (*internal fouling,* defined as *pore blocking*) (Liu et al. 2018). In the external fouling, the foulant layer is generally named the "*cake layer*" because the surface layer morphology resembles a cake. However, a thin gel-like layer generally forms between the thick cake layer and membrane surface (Lei et al. 2021). The gel-like layer is reported to result mainly from the gelation of colloids and dissolved matter. This layer, known as the *gel layer*, has a significantly different morphology and physicochemical properties than the cake layer. Another fouling type verifies when solutes and ions accumulate in the thin liquid layer adjacent to the membrane surface; it is called *concentration polarisation.* When fouling occurs, it results in a decrease in permeate flux, an increase in feed pressure, a reduction in productivity, an increase in system downtime, an increase in membrane maintenance and operation costs due to membrane cleaning, and a decrease in the lifespan of the membrane modules (Du et al. 2020). There are two types of membrane fouling: reversible and irreversible fouling. Physical methods like backwashing can remove reversible fouling and refer to contaminants loosely deposited on the surface of the membrane. On the other hand, irreversible fouling requires chemical cleaning. It cannot be removed by physical cleaning, as the blockage of membrane pores and the strong adhesion of contaminants to the surface of the membrane causes it. The most commonly used chemicals for cleaning the membranes are caustic (NaOH), oxidants/sanitisers (NaOCl, H_2O_2), acids (citric acid, nitric acid), chelating agents (citric acid, EDTA), and non-ionic surfactants. The success of a cleaning regimen is determined by how much of the original water flux has been regained (Kale and Cheryarr 2005).
NF and RO serve as final treatments to effectively separate and concentrate phenolic compounds. (Tapia-Quirós et al. 2022).

1.1.7 Polymeric adsorbent resins

Polymeric adsorbent resins are porous solid materials that offer a surface on which atoms or molecules (adsorbate) found in a fluid (feed) in contact with the adsorbent can be attracted and then desorbed (Pourhakkak et al. 2021). This results in a distribution of these atoms and molecules between the adsorbent and the fluid and their selective transfer from the fluid to the surface of the solid adsorbent. According to the second law of thermodynamics, the adsorption of substances on solids takes place to reduce the free surface energy of the solid (Pourhakkak et al. 2021). In adsorption/desorption processes, molecule and resin chemical-physical characteristics must be considered to achieve good application performance. The adsorption of a species depends upon its similarity to a polymeric adsorbent on the basis that "like attracts like". Thus, hydrophobic molecules interact with a hydrophobic resin surface, while ionic molecules are well-adsorbed by ionic functionality adsorbents. The greater the resin's surface area is, the more molecules can be adsorbed. Moreover, it's crucial to consider the size of the molecules that need to be adsorbed and compare them to the porosity of the adsorbent. If the molecules are too large to fit into the pores of the resin, they won't be able to penetrate the pores and will pass through the resin bed. Finally, elution and regeneration steps must be carefully executed to recover the molecules of interest adsorbed onto the resin and restore the adsorbent to its original state. Both processes can be considered the same basic process in which the attractive forces between the solute and the polymer are weakened enough to break up. When a solute is adsorbed on a polymeric adsorbent, it can be removed by changing the solvent. The new solvent will have a higher affinity for the polymer matrix and disrupt the solute/resin interactions by solvating the solute better.

Examples of porous adsorbents from naturally occurring materials are granular carbon, bone char and activated alumina (Pourhakkak et al. 2021). However, in what follows, only synthetic polymeric adsorbents, such as the ones used in a part of the work of this PhD thesis, are considered. The size of the pores (pore diameter) is classified as micropores, mesopores, and macropores, defined as follows:

Micropores < 20 Angstroms

Mesopores 20 – 500 Angstroms

Macropores > 500 Angstroms

Porous synthetic adsorbents were made at the end of the 1950s by Rohm and Haas Company, Bayer and Permutit and produced industrially in the early 1960s by Rohm and Haas Company (Zaganiaris 2011). Mostly, porous synthetic adsorbents come in spherical beads between 0.3−1.2 mm and can be made of aromatic, acrylic or phenolic materials, usually in the form of macroporous copolymers. In principle, aromatic adsorbents come without any

functional groups and are hydrophobic. They interact with dissolved molecules mainly by π-bond interactions. However, aromatic adsorbent-bearing functional groups exist, either sulfonic (cation exchange) or amine (anion exchange) groups, to give some hydrophilicity to the matrix while still keeping the aromatic backbone to favour the adsorption of certain compounds. Acrylic adsorbents are polymethylmethacrylates crosslinked with a diol or a triol. They are hydrophilic and interact with dissolved molecules mainly with van der Waals forces or hydrogen bonds. In 1969, Davankov introduced a second type of adsorption material in addition to the traditional macroporous copolymers, defined as hyper-crosslinked polymers (Fontanals et al. 2015), and commercially called Hypersol-Macronet TM sorbents (Purolite International Ltd.) (Zaganiaris 2011). In these polymer types, porosity was introduced not during polymerisation but during a post-crosslinking step (Ahn et al. 2006). As a result, a rigid hyper-crosslinker structure with a very high surface area (800-1500 m^2/g) and a small average pore diameter in the range of 10-40 Å is formed. Adsorbents having both small and large pores offer more accessible access to the tiny pores and, therefore, a better utilisation of the internal surface. The better compatibility between adsorbate and adsorbent leads the adsorption capacities of hyper-crosslinked copolymers to be more than five times higher than those of macroporous copolymers. Moreover, the hyper-crosslinked resins also show fast adsorption kinetics and good thermal and mechanical stability (Mota and Lyubchik 2008).

Polymeric resin adsorbents have been extensively used for separation processes, pollutant removal, target isolation, gas storage, and sample pretreatment.

Resins can be used in batch stir, inserting a volume of polymeric adsorbent in contact with a particular solution for a certain length of time or as stationary phases in chromatographic columns, especially in those applications where the separation of two or more species is required. Different adsorption isotherms and kinetic models, as illustrated in Chapter 6, can be examined to evaluate the efficiency and characteristics of the adsorbents, such as adsorption and desorption capacity and feasibility (Pourhakkak et al. 2021).

1.2 Thesis Outline

The following chapters show the applications of the concepts previously outlined, and a brief diagram of the experimental part of this thesis is reported in Figure 1.11. In particular, Chapter 2 addresses combining techniques such as HPLC-UV-ESI-MS/MS and NMR for a complete characterisation of metabolites in Calabrian apple juices. These juices were obtained from different apple cultivars, and based on their proton spectra, it was possible to distinguish them in the PCA. The apple juice was also processed via ultrafiltration (UF) followed by nanofiltration (NF), which allowed for a concentration of bioactive compounds in the NF retentate. Chapter 3 continues to explore NF processes applied to apple juice for the concentration of polyphenols with the combined objective of also decreasing the concentration of sugars in the retentate, which is why the NF in this work is conducted in diafiltration (DF) mode, i.e. the concentration process via NF was interspersed with additions of water to the system to enhance the degree of separation of membrane-retained macrosolutes from membrane-permeable microsolutes. UF, DF and NF are still critical topics in Chapter 4. Still, this time, they are used to process the citrus hybrid juice, called tacle and obtained by crossing the Tarocco orange and the Monreal Clementine. Tacle's metabolome was identified using polar and apolar solvent systems with HR-NMR. Furthermore, UV-visible spectroscopy was utilised to analyse its antioxidant capacity, flavonoids, polyphenols, and β-carotene content. The impact of UF and NF processes on the metabolic profile was thoroughly explored using a low-level NMR and UV-Vis Data Fusion. Chapter 5 changes the investigated matrix, moving from fruit juices to *Cannabis sativa.* Hemp seed oil and inflorescence extracts are studied using NMR, which, in this study, is also tested as an alternative to the most common methods in quantifying cannabinoids present in inflorescence extracts. Also, different conventional extraction procedures with common solvents were tested and evaluated by NMR spectroscopy to obtain inflorescence extracts poor in psychotropic agents and rich in medical cannabinoids and triacylglycerols (TAGs), which have an ω-6/ω-3 ratio that is excellent from a nutritional point of view. Finally, Chapter 6 concerns the study of white wine lees, by-products containing phenolic compounds that can be exploited. Consequently, commercial food-grade polymeric resins are tested to recover and purify these compounds from sugars. UV-Vis technique was mainly used to monitor the total polyphenol (TPs) content.

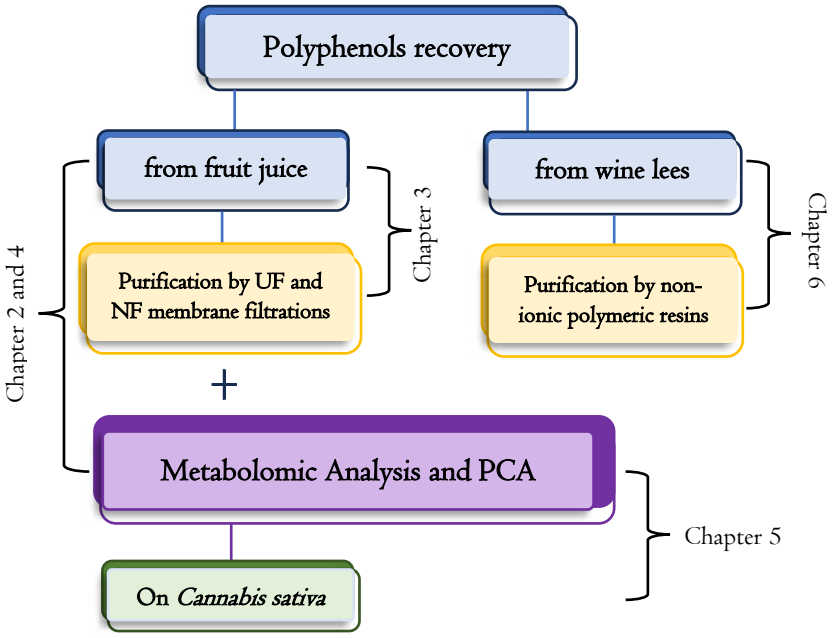

Figure 1.11 The overall scheme that describes the experimental thesis overview.

1.3 References

Abdu Hussen, A. (2022). High-Performance Liquid Chromatography (HPLC): A review. *Annals of Advances in Chemistry*, *6*(1), 010–020. https://doi.org/10.29328/journal.aac.1001026

Abreu, A. C., & Fernández, I. (2020). NMR Metabolomics Applied on the Discrimination of Variables Influencing Tomato (Solanum lycopersicum). *Molecules*, *25*(16). https://doi.org/10.3390/molecules25163738

Ahn, J. H., Jang, J. E., Oh, C. G., Ihm, S. K., Cortez, J., & Sherrington, D. C. (2006). Rapid generation and control of microporosity, bimodal pore size distribution, and surface area in Davankov-type hyper-cross-linked resins. *Macromolecules*, *39*(2), 627–632. https://doi.org/10.1021/ma051152n

Ahuja, S. (2011). *Handbook of Bioseparations*. Academic Press.

Alara, O. R., Abdurahman, N. H., & Ukaegbu, C. I. (2021). Extraction of phenolic compounds: A review. *Current Research in Food Science*, *4*(February), 200–214. https://doi.org/10.1016/j.crfs.2021.03.011

Alberti, G., Magnaghi, L. R., Iurato, M., Zanoni, C., & Biesuz, R. (2023). Colorimetric Paper-Based Analytical Devices (PADs) Backed by Chemometrics for Pd(II) Detection. *Sensors*, *23*(17). https://doi.org/10.3390/s23177425

Aleixandre-Tudo, J. L., & Du Toit, W. (2019). The Role of UV-Visible Spectroscopy for Phenolic Compounds Quantification in Winemaking. *Frontiers and New Trends in the Science of Fermented Food and Beverages*, 1–21.

https://doi.org/10.5772/intechopen.79550

Anouar, E. H., Gierschner, J., Duroux, J. L., & Trouillas, P. (2012). UV/Visible spectra of natural polyphenols: A time-dependent density functional theory study. *Food Chemistry*, *131*(1), 79–89. https://doi.org/10.1016/j.foodchem.2011.08.034

Anticona, M., Lopez-Malo, D., Frigola, A., Esteve, M. J., & Blesa, J. (2022). Comprehensive analysis of polyphenols from hybrid Mandarin peels by SPE and HPLC-UV. *Lwt*, *165*(July), 113770. https://doi.org/10.1016/j.lwt.2022.113770

Baker, R. W. (2012). *Membrane Technology and Applications* (3th ed.). Wiley.

Berk, Z., & Berk, Z. (2009). Chapter 10 – Membrane processes. *Food Process Engineering and Technology*, 233–257. https://doi.org/10.1016/B978-0-12-373660-4.00010-7

Berthault, M., Buzlukov, A., Dubois, L., Bayle, P. A., Porcher, W., Gutel, T., et al. (2023). Lithium isotope tracing in silicon-based electrodes using solid-state MAS NMR: a powerful comprehensive tool for the characterization of lithium batteries. *Physical Chemistry Chemical Physics*, *25*(33), 22145–22154. https://doi.org/10.1039/d3cp02646a

Boussu, K., Vandecasteele, C., & Van der Bruggen, B. (2008). Relation between membrane characteristics and performance in nanofiltration. *Journal of Membrane Science*, *310*(1–2), 51–65. https://doi.org/10.1016/j.memsci.2007.10.030

Brans, G., Schroën, C. G. P. H., Van Der Sman, R. G. M., & Boom, R. M. (2004). Membrane fractionation of milk: State of the art and challenges. *Journal of Membrane Science*, *243*(1–2), 263–272. https://doi.org/10.1016/j.memsci.2004.06.029

Brito, A., Ramirez, J. E., Areche, C., Sepúlveda, B., & Simirgiotis, M. J. (2014). HPLC-UV-MS profiles of phenolic compounds and antioxidant activity of fruits from three citrus species consumed in Northern Chile. *Molecules*, *19*(11), 17400–17421. https://doi.org/10.3390/molecules191117400

Bruice, P. Y. (2011). *Organic Chemistry*. Prentice Hall.

Canet, D. (1996). *Nuclear Magnetic Resonance, Concepts and Methods*. Wiley.

Cassano, A., Conidi, C., Ruby-Figueroa, R., & Castro-Muñoz, R. (2018). Nanofiltration and tight ultrafiltration membranes for the recovery of polyphenols from agro-food by-products. *International Journal of Molecular Sciences*, *19*(2). https://doi.org/10.3390/ijms19020351

Cesare, F. Di, Calgaro, M., Ghini, V., Squarzanti, D. F., Prisco, A. De, Visciglia, A., et al. (2023). Exploring the Effects of Probiotic Treatment on Urinary and Serum Metabolic Profiles in Healthy Individuals. https://doi.org/10.1021/acs.jproteome.3c00548

Cheng, L. L. (2023). High-resolution magic angle spinning NMR for intact biological specimen analysis: Initial discovery, recent developments, and future directions. *NMR in Biomedicine*, *36*(4), 1–22. https://doi.org/10.1002/nbm.4684

Cheryan, M. (1998). *Ultrafiltration and Microfiltration Handbook* (2nd ed.). CRC PRESS.

Chiriac, E. R., Chiţescu, C. L., Geană, E. I., Gird, C. E., Socoteanu, R. P., & Boscencu, R. (2021). Advanced analytical approaches for the analysis of polyphenols in plants matrices—a review. *Separations*, *8*(5). https://doi.org/10.3390/separations8050065

Clendinen, C. S., Lee-McMullen, B., Williams, C. M., Stupp, G. S., Vandenborne, K.,

Hahn, D. A., et al. (2014). 13C NMR metabolomics: Applications at natural abundance. *Analytical Chemistry*, *86*(18), 9242–9250. https://doi.org/10.1021/ac502346h

Conidi, C., Cassano, A., & Drioli, E. (2011). A membrane-based study for the recovery of polyphenols from bergamot juice. *Journal of Membrane Science*, *375*(1–2), 182–190. https://doi.org/10.1016/j.memsci.2011.03.035

Cornea-Cipcigan, M., Pamfil, D., Sisea, C. R., & Margaoan, R. (2023). Characterization of Cyclamen genotypes using morphological descriptors and DNA molecular markers in a multivariate analysis. *Frontiers in Plant Science*, *14*(January), 1–15. https://doi.org/10.3389/fpls.2023.1100099

Craig, A., Cloarec, O., Holmes, E., Nicholson, J. K., & Lindon, J. C. (2006). Scaling and normalization effects in NMR spectroscopic metabonomic data sets. *Analytical Chemistry*, *78*(7), 2262–2267. https://doi.org/10.1021/ac0519312

Cultivars, P., Liu, J., Zhou, X., Chen, D., Guo, J., & Chen, K. (2023). NMR-Based Metabolic Profiling to Follow Changes in.

Cuny, M., Vigneau, E., Le Gall, G., Colquhoun, I., Lees, M., & Rutledge, D. N. (2008). Fruit juice authentication by 1H NMR spectroscopy in combination with different chemometrics tools. *Analytical and Bioanalytical Chemistry*, *390*(1), 419–427. https://doi.org/10.1007/s00216-007-1708-y

da Silva, R. P. F. F., Rocha-Santos, T. A. P., & Duarte, A. C. (2016). Supercritical fluid extraction of bioactive compounds. *TrAC - Trends in Analytical Chemistry*, *76*, 40–51. https://doi.org/10.1016/j.trac.2015.11.013

De Bartolo, L., Curcio, E., & Drioli, E. (2017). *Membrane Systems For Bioartificial Organs and Regenerative Medicine*. De Gruyter.

Diehl, P., Fluck, E., & Kosfeld, R. (2011). *NMR Basic Principles and Progress*. Springer.

Du, X., Shi, Y., Jegatheesan, V., & Ul Haq, I. (2020). *A review on the mechanism, impacts and control methods of membrane fouling in MBR system*. *Membranes* (Vol. 10). https://doi.org/10.3390/membranes10020024

Ebrahimi, P., & Lante, A. (2022). Environmentally Friendly Techniques for the Recovery of Polyphenols from Food By-Products and Their Impact on Polyphenol Oxidase: A Critical Review. *Applied Sciences (Switzerland)*, *12*(4). https://doi.org/10.3390/app12041923

Emsley, J. W., & Lindon, J. C. (1975). *NMR Spectroscopy Using Liquid Crystal Solvents*. Pergamon Press: Oxford.

Emwas, A. H., Roy, R., McKay, R. T., Tenori, L., Saccenti, E., Nagana Gowda, G. A., et al. (2019). Nmr spectroscopy for metabolomics research. *Metabolites*, *9*(7). https://doi.org/10.3390/metabo9070123

Engelhardt, E. (1979). *High Performance Liquid Chromatography Chemical Laboratory Practice*. Springer-Verlag Berlin Heidelberg New York.

Eriksson, L., Byrne, T., Johansson, E., Trygg, J., & Vikström, C. (2006). *Multi- and Megavariate Data Analysis Basic Principles and Applications*. Umetrics Academy.

Feng, D. C., Zhu, W. Z., Shi, X., Xiong, Q., You, J., Wei, Q., & Yang, L. (2023). Identification of senescence-related molecular subtypes and key genes for prostate

cancer. *Asian Journal of Andrology*, *25*(2), 223–229. https://doi.org/10.4103/aja202258

Fleming, I., & Williams, D. (2020). *Spectroscopic Methods in Organic Chemistry* (7th ed.). Springer.

Flügge, F., Kerkow, T., Kowalski, P., Bornhöft, J., Seemann, E., Creydt, M., et al. (2023). Qualitative and quantitative food authentication of oregano using NGS and NMR with chemometrics. *Food Control*, *145*(October 2022). https://doi.org/10.1016/j.foodcont.2022.109497

Fontanals, N., Marcé, R. M., Borrull, F., & Cormack, P. A. G. (2015). Hypercrosslinked Materials. *Polymer Science*, *41*, 258–269.

Galiano, F., Briceño, K., Marino, T., Molino, A., Christensen, K. V., & Figoli, A. (2018). Advances in biopolymer-based membrane preparation and applications. *Journal of Membrane Science*, *564*(May), 562–586. https://doi.org/10.1016/j.memsci.2018.07.059

Girelli, C. R., Calò, F., Angilè, F., Mazzi, L., Barbini, D., & Fanizzi, F. P. (2020). 1H Nmr Spectroscopy To Characterize Italian Extra Virgin Olive Oil Blends, Using Statistical Models and Databases Based on Monocultivar Reference Oils. *Foods*, *9*(12). https://doi.org/10.3390/foods9121797

González-Revuelta, D., Fallanza, M., Ortiz, A., & Gorri, D. (2023). Thin-Film Composite Matrimid-Based Hollow Fiber Membranes for Oxygen/Nitrogen Separation by Gas Permeation. *Membranes*, *13*(2). https://doi.org/10.3390/membranes13020218

Günther, H. (2013). *NMR Spectroscopy: Basic Principles, Concepts, and Applications in Chemistry* (3rd ed.). Wiley-VCH.

Gutiérrez-Del-río, I., López-Ibáñez, S., Magadán-Corpas, P., Fernández-Calleja, L., Pérez-Valero, Á., Tuñón-Granda, M., et al. (2021). Terpenoids and polyphenols as natural antioxidant agents in food preservation. *Antioxidants*, *10*(8). https://doi.org/10.3390/antiox10081264

Haeberlen, U. (2012). *High Resolution NMR in Solids Selective Averaging: Supplement 1 Advances in Magnetic Resonance*. Academic Press.

Hatzakis, E. (2019). Nuclear Magnetic Resonance (NMR) Spectroscopy in Food Science: A Comprehensive Review. *Comprehensive Reviews in Food Science and Food Safety*, *18*(1), 189–220. https://doi.org/10.1111/1541-4337.12408

He, S., Lou, Q., Shi, J., Sun, H., Zhang, M., & Li, Q. (2017). Water Extraction of Anthocyanins from Black Rice and Purification Using Membrane Separation and Resin Adsorption. *Journal of Food Processing and Preservation*, *41*(4), 1–8. https://doi.org/10.1111/jfpp.13091

Ilyasov, I. R., Beloborodov, V. L., Selivanova, I. A., & Terekhov, R. P. (2020). ABTS/PP decolorization assay of antioxidant capacity reaction pathways. *International Journal of Molecular Sciences*, *21*(3). https://doi.org/10.3390/ijms21031131

Ivanova, A., Gerasimova, E., & Gazizullina, E. (2020). Study of Antioxidant Properties of Agents from the Perspective of Their Action Mechanisms. *Molecules*, *25*(18). https://doi.org/10.3390/molecules25184251

Judd, S., & Jefferson, B. (2003). *Membranes for Industrial Wastewater Recovery and Re-use*. Elsevier.

Kadel, S., Pellerin, G., Thibodeau, J., Perreault, V., Lainé, C., & Bazinet, L. (2019). How molecular weight cut-offs and physicochemical properties of polyether sulfone membranes affect peptide migration and selectivity during electrodialysis with filtration membranes. *Membranes*, *9*(11). https://doi.org/10.3390/membranes9110153

Kaeswurm, J. A. H., Scharinger, A., Teipel, J., & Buchweitz, M. (2021). Absorption coefficients of phenolic structures in different solvents routinely used for experiments. *Molecules*, *26*(15), 1–15. https://doi.org/10.3390/molecules26154656

Kale, A. V, & Cheryarr, M. (2005). Membranes , Chromatography and Membrane Chromatography . Separation Technologies for the Biopharm and Nutraceutical Era, *2005*(March), 59–86.

Keun, H. C. (2018). *NMR-based Metabolomics* (1st ed.). Royal Society of Chemistry.

Kimwemwe, P. K., Bukomarhe, C. B., Mamati, E. G., Githiri, S. M., Civava, R. M., Mignouna, J., et al. (2023). Population Structure and Genetic Diversity of Rice (Oryza sativa L.) Germplasm from the Democratic Republic of Congo (DRC) Using DArTseq-Derived Single Nucleotide Polymorphism (SNP). *Agronomy*, *13*(7), 1906. https://doi.org/10.3390/agronomy13071906

Krull, I. S. S. (2012). *Analytical Chemistry*. IntechOpen.

Leardi, R. (2002). Chemometrics: From classical to genetic algorithms. *Grasas y Aceites*, *53*(1), 115–127. https://doi.org/10.3989/gya.2002.v53.i1.294

Lei, Z., Wang, J., Leng, L., Yang, S., Dzakpasu, M., Li, Q., et al. (2021). New insight into the membrane fouling of anaerobic membrane bioreactors treating sewage: Physicochemical and biological characterization of cake and gel layers. *Journal of Membrane Science*, *632*(13), 119383. https://doi.org/10.1016/j.memsci.2021.119383

Levitt, M. H. (2008). *Spin Dynamics: Basics of Nuclear Magnetic Resonance* (2nd ed.). Wiley.

Lindon, J. C., Nicholson, J. K., & Holmes, E. (2007). *The Handbook of Metabonomics and Metabolomics* (1st ed.). Elsevier Science.

Liu, L., Luo, X. B., Ding, L., & Luo, S. L. (2018). *Application of Nanotechnology in the Removal of Heavy Metal From Water*. *Nanomaterials for the Removal of Pollutants and Resource Reutilization*. Elsevier Inc. https://doi.org/10.1016/B978-0-12-814837-2.00004-4

López-fernández, O., Domínguez, R., Pateiro, M., Munekata, P. E. S., Rocchetti, G., & Lorenzo, J. M. (2020). Determination of polyphenols using liquid chromatography–tandem mass spectrometry technique (LC–MS/MS): A review. *Antioxidants*, *9*(6), 1–27. https://doi.org/10.3390/antiox9060479

Lough, W. J., & Wainer, I. W. (1995). *High Performance Liquid Chromatography Fundamental Principles and Practice*. Taylor & Francis.

Mahrous, E. A., & Farag, M. A. (2015). Two dimensional NMR spectroscopic approaches for exploring plant metabolome: A review. *Journal of Advanced Research*, *6*(1), 3–15. https://doi.org/10.1016/j.jare.2014.10.003

Manly, B. F. J., & Navarro Alberto, J. A. (2016). *Multivariate Statistical Methods: A Primer* (4th ed.). Chapman and Hall/CRC.

Mckay, R. T. (2011). How the 1D-NOESY suppresses solvent signal in metabonomics

NMR spectroscopy: An examination of the pulse sequence components and evolution. *Concepts in Magnetic Resonance Part A: Bridging Education and Research*, *38 A*(5), 197–220. https://doi.org/10.1002/cmr.a.20223

Mir-Cerdà, A., Carretero, I., Coves, J. R., Pedrouso, A., Castro-Barros, C. M., Alvarino, T., et al. (2023). Recovery of phenolic compounds from wine lees using green processing: Identifying target molecules and assessing membrane ultrafiltration performance. *Science of the Total Environment*, *857*(July 2022), 1–7. https://doi.org/10.1016/j.scitotenv.2022.159623

Miricioiu, M. G., Ionete, R. E., Simova, S., Gerginova, D., & Botoran, O. R. (2023). Metabolite Profiling of Conifer Needles : Tracing Pollution and Climate Effects.

Mistry, V. V., & Maubois, J. L. (2017). *Application of Membrane Separation Technology to Cheese Production*. *Cheese: Chemistry, Physics and Microbiology: Fourth Edition* (Fourth Edi., Vol. 1). Elsevier Ltd. https://doi.org/10.1016/B978-0-12-417012-4.00027-2

Mota, J. P., & Lyubchik, S. (2008). *Recent Advances in Adsorption Processes for Environmental Protection and Security*. (Springer Netherlands, Ed.).

Munteanu, I. G., & Apetrei, C. (2021). Analytical methods used in determining antioxidant activity: A review. *International Journal of Molecular Sciences*, *22*(7). https://doi.org/10.3390/ijms22073380

Murkes, J. (1990). Fundamentals of crossflow filtration. *Separation & Purification Reviews*, *19*(1), 1–29. https://doi.org/10.1080/03602549008050928

Nakorchevsky, A., & Yates, J. R. (2012). *Mass spectrometry*. *Comprehensive Biophysics* (Vol. 1). https://doi.org/10.1016/B978-0-12-374920-8.00121-1

Narvaez-Montoya, C., Mahlknecht, J., Torres-Martínez, J. A., Mora, A., & Bertrand, G. (2023). Seawater intrusion pattern recognition supported by unsupervised learning: A systematic review and application. *Science of the Total Environment*, *864*(September 2022). https://doi.org/10.1016/j.scitotenv.2022.160933

Oliveri, P., Malegori, C., & Casale, M. (2020). *Chemometrics: multivariate analysis of chemical data*. *Chemical Analysis of Food*. https://doi.org/10.1016/b978-0-12-813266-1.00002-4

Oliveri, P., Malegori, C., Mustorgi, E., & Casale, M. (2020). *4.05 - Application of Chemometrics in the Food Sciences*. *Comprehensive Chemometrics: Chemical and Biochemical Data Analysis, Second Edition: Four Volume Set* (Second Edi., Vol. 4). Elsevier. https://doi.org/10.1016/B978-0-12-409547-2.14748-1

Owen, T. (1996). *Fundamentals of Modern UV-Visible Spectroscopy : A Primer*. Hewlett-Packard.

Pacholczyk-Sienicka, B., Ciepielowski, G., & Albrecht, Ł. (2021). The application of nmr spectroscopy and chemometrics in authentication of spices. *Molecules*, *26*(2). https://doi.org/10.3390/molecules26020382

Palama, T. L., Canard, I., Rautureau, G. J. P., Mirande, C., Chatellier, S., & Elena-Herrmann, B. (2016). Identification of bacterial species by untargeted NMR spectroscopy of the: Exo -metabolome. *Analyst*, *141*(15), 4558–4561. https://doi.org/10.1039/c6an00393a

Palmer III, A. ., Fairbrother, W. J., Cavanagh, J., Skelton, N. J., & Rance, M. (2006).

Protein NMR Spectroscopy: Principles and Practice. Academic Press.

Pedrosa, M. C., Lima, L., Heleno, S., Carocho, M., Ferreira, I. C. F. R., & Barros, L. (2021). Food metabolites as tools for authentication, processing, and nutritive value assessment. *Foods*, *10*(9). https://doi.org/10.3390/foods10092213

Peiris, R. H., Hallé, C., Budman, H., Moresoli, C., Peldszus, S., Huck, P. M., & Legge, R. L. (2010). Identifying fouling events in a membrane-based drinking water treatment process using principal component analysis of fluorescence excitation-emission matrices. *Water Research*, *44*(1), 185–194. https://doi.org/10.1016/j.watres.2009.09.036

Polettini, A. (2006). *Applications of LC-MS in Toxicology*. Pharmaceutical Press.

Pott, D. M., Osorio, S., & Vallarino, J. G. (2019). From central to specialized metabolism: An overview of some secondary compounds derived from the primary metabolism for their role in conferring nutritional and organoleptic characteristics to fruit. *Frontiers in Plant Science*, *10*(June). https://doi.org/10.3389/fpls.2019.00835

Pourhakkak, P., Taghizadeh, M., Taghizadeh, A., & Ghaedi, M. (2021). Chapter 2 - Adsorption. In Elsevier (Ed.), *Adsorption: Fundamental Processes and Applications* (pp. 71–210). https://doi.org/https://doi.org/10.1016/B978-0-12-818805-7.00009-6

Radu, E. R., Voicu, S. I., & Thakur, V. K. (2023). Polymeric Membranes for Biomedical Applications. *Polymers*, *15*(3). https://doi.org/10.3390/polym15030619

Rajha, H. N., Paule, A., Aragonès, G., Barbosa, M., Caddeo, C., Debs, E., et al. (2022). Recent Advances in Research on Polyphenols: Effects on Microbiota, Metabolism, and Health. *Molecular Nutrition and Food Research*, *66*(1), 1–11. https://doi.org/10.1002/mnfr.202100670

Rehman, A., & Choudhary, M. . (1996). *Solving Problems with NMR Spectroscopy* (1st ed.). Academic Press.

Richard W. Baker. (2010). Membrnae Technology. *Encyclopedia Of Polymer Science and Technology*, *3*, 121–153. http://www.sciencedirect.com/science/article/pii/B9781856176323000070

Roy, A., Chatterjee, S., Nandi, S., Sarkar, T., & Chakraborty, R. (2019). Nutrition Open Science Publications Nutraceuticals in Human Diseases: Therapeutic and Prophylactic Potentials Review Article. *Indian Journal of Nutrition*, *6*(2), 1–11.

Rudrapal, M., Khairnar, S. J., Khan, J., Dukhyil, A. Bin, Ansari, M. A., Alomary, M. N., et al. (2022). Dietary Polyphenols and Their Role in Oxidative Stress-Induced Human Diseases: Insights Into Protective Effects, Antioxidant Potentials and Mechanism(s) of Action. *Frontiers in Pharmacology*, *13*(February), 1–15. https://doi.org/10.3389/fphar.2022.806470

Ruiz-Rodriguez, A., Reglero, G., & Ibañez, E. (2010). Recent trends in the advanced analysis of bioactive fatty acids. *Journal of Pharmaceutical and Biomedical Analysis*, *51*(2), 305–326. https://doi.org/10.1016/j.jpba.2009.05.012

Rule, G. S., & Hitchens, T. K. (2005). *Fundamentals of Protein NMR Spectroscopy*. Springer.

Salvino, R. A., Celebre, G., & De Luca, G. (2021). Molecular characterization of the organic fraction of municipal solid waste and compositional evolution during oxidative processes assessed by hr-mas13c nmr spectroscopy. *Applied Sciences*

(Switzerland), *11*(5), 1–11. https://doi.org/10.3390/app11052267

Sánchez Maldonado, A. F., Mudge, E., Gänzle, M. G., & Schieber, A. (2014). Extraction and fractionation of phenolic acids and glycoalkaloids from potato peels using acidified water/ethanol-based solvents. *Food Research International*, *65*(PA), 27–34. https://doi.org/10.1016/j.foodres.2014.06.018

Savage, A. K., Van Duynhoven, J. P. M., Tucker, G., & Daykin, C. A. (2011). Enhanced NMR-based profiling of polyphenols in commercially available grape juices using solid-phase extraction. *Magnetic Resonance in Chemistry*, *49*(SUPPL. 1). https://doi.org/10.1002/mrc.2846

Schleif, F. M., Riemer, T., Börner, U., Schnapka-Hille, L., & Cross, M. (2011). Genetic algorithm for shift-uncertainty correction in 1-D NMR-based metabolite identifications and quantifications. *Bioinformatics*, *27*(4), 524–533. https://doi.org/10.1093/bioinformatics/btq661

Serkova, N. J., & Niemann, C. U. (2006). Pattern recognition and biomarker H-NMR-based metabolomics. *Expert Review of Molecular Diagnostics*, 717–731.

Silverstein, R. M., Webster, F. X., Kiemle, D. J., & Bryce, D. L. (2014). *Spectrometric Identification of Organic Compounds* (8th ed.). Wiley.

Simon, B., & Köstler, H. (2019). Improving the sensitivity of FT-NMR spectroscopy by apodization weighted sampling. *Journal of Biomolecular NMR*, *73*(3–4), 155–165. https://doi.org/10.1007/s10858-019-00243-7

Smith, M. J., Marshall, C. B., Theillet, F. X., Binolfi, A., Selenko, P., & Ikura, M. (2015). Real-time NMR monitoring of biological activities in complex physiological environments. *Current Opinion in Structural Biology*, *32*, 39–47. https://doi.org/10.1016/j.sbi.2015.02.003

Sun, J., Liang, F., Bin, Y., Li, P., & Duan, C. (2007). Screening non-colored phenolics in red wines using liquid chromatography/ultraviolet and mass spectrometry/mass spectrometry libraries. *Molecules*, *12*(3), 679–693. https://doi.org/10.3390/12030679

Swartz, M. (2010). HPLC detectors: A brief review. *Journal of Liquid Chromatography and Related Technologies*, *33*(9–12), 1130–1150. https://doi.org/10.1080/10826076.2010.484356

Swinehart, D. F. (1962). The Beer-Lambert law. *Journal of Chemical Education*, *39*(7), 333–335. https://doi.org/10.1021/ed039p333

Tamime, A. Y. (2013). *Membrane Processing: Dairy and Beverage Applications*. Wiley.

Tapia-Quirós, P., Montenegro-Landívar, M. F., Reig, M., Vecino, X., Saurina, J., Granados, M., & Cortina, J. L. (2022). Integration of Nanofiltration and Reverse Osmosis Technologies in Polyphenols Recovery Schemes from Winery and Olive Mill Wastes by Aqueous-Based Processing. *Membranes*, *12*(3). https://doi.org/10.3390/membranes12030339

Teng, Q. (2012). *Structural Biology: Practical NMR Applications* (2nd ed.). Springer.

Toldrá, F. ., & Nollet, L. (2017). *Advances in Food Diagnostics*. Wiley.

Ursino, C., Castro-Muñoz, R., Drioli, E., Gzara, L., Albeirutty, M. H., & Figoli, A. (2018). Progress of nanocomposite membranes for water treatment. *Membranes*, *8*(2), 1–40. https://doi.org/10.3390/membranes8020018

Varmuza, K., & Filzmoser, P. (2009). *Introduction to Multivariate Statistical Analysis in Chemometrics*. CRC PRESS.

Vidal-Casanella, O., Núñez, O., Granados, M., Saurina, J., & Sentellas, S. (2021). Analytical methods for exploring nutraceuticals based on phenolic acids and polyphenols. *Applied Sciences (Switzerland)*, *11*(18). https://doi.org/10.3390/app11188276

Wahyuni, Y., Ballester, A. R., Sudarmonowati, E., Bino, R. J., & Bovy, A. G. (2013). Secondary metabolites of Capsicum species and their importance in the human diet. *Journal of Natural Products*, *76*(4), 783–793. https://doi.org/10.1021/np300898z

Ward, J. L., Baker, J. M., Miller, S. J., Deborde, C., Maucourt, M., Biais, B., et al. (2010). An inter-laboratory comparison demonstrates that [1H]-NMR metabolite fingerprinting is a robust technique for collaborative plant metabolomic data collection. *Metabolomics*, *6*(2), 263–273. https://doi.org/10.1007/s11306-010-0200-4

Wolfender, J. L., Nuzillard, J. M., Van Der Hooft, J. J. J., Renault, J. H., & Bertrand, S. (2019). Accelerating Metabolite Identification in Natural Product Research: Toward an Ideal Combination of Liquid Chromatography-High-Resolution Tandem Mass Spectrometry and NMR Profiling, in Silico Databases, and Chemometrics. *Analytical Chemistry*, *91*(1), 704–742. https://doi.org/10.1021/acs.analchem.8b05112

Yang, L., & Chen, S. (2022). QuEChERS and biphenyl-UHPLC tandem, *30*(3).

Zaganiaris, E. J. (2011). *Ion Exchange Resins and Synthetic Adsorbents in Food Processing*. (Books on Demand, Ed.) (2nd ed.).

Zdarta, J., Thygesen, A., Holm, M. S., Meyer, A. S., & Pinelo, M. (2020). Direct separation of acetate and furfural from xylose by nanofiltration of birch pretreated liquor: Effect of process conditions and separation mechanism. *Separation and Purification Technology*, *239*(January). https://doi.org/10.1016/j.seppur.2020.116546

Zhang, Y., Cao, C., Yang, Z., Jia, G., Liu, X., Li, X., et al. (2023). Simultaneous determination of 20 phenolic compounds in propolis by HPLC-UV and HPLC-MS/MS. *Journal of Food Composition and Analysis*, *115*(1), 104877. https://doi.org/10.1016/j.jfca.2022.104877

Zheng, G., & Price, W. S. (2010). Solvent signal suppression in NMR. *Progress in Nuclear Magnetic Resonance Spectroscopy*, *56*(3), 267–288. https://doi.org/10.1016/j.pnmrs.2010.01.001

Chapter 2: An Integrated Approach Based on NMR and HPLC–UV-ESI–MS/MS to Characterize Apple Juices and Their Nanofiltration (NF) Bioactive Extracts

Part of this work was published as: Martina Gaglianò, Carmela Conidi, Lucia Bartella, · Rosachiara A. Salvino, Leonardo Di Donna, Alfredo Cassano, Giuseppina De Luca, "An Integrated Approach Based on NMR and HPLC–UV-ESI–MS/MS to Characterize Apple Juices and Their Nanofiltration (NF) Bioactive Extracts", Food and Bioprocess Technology (2021) 14:2273–2285.

The PhD candidate was involved in planning and performing the experiments, as well as in the discussion and interpretation of the results and manuscript preparation.

2.1 Introduction

Apple is one of the most commonly consumed fruits worldwide as well as its juice (Gunathilake & Considine 2018). Apples and apple juice are appreciated for their nutritional value, aroma, firmness, and health-promoting effects (Harker et al. 2003; Ting et al. 2013). All these qualities are ultimately based on the given fruit's metabolic composition (primary and secondary metabolites) (Cuthbertson et al. 2012). In fact, while amino acids, sugars, and organic acids, respectively, determine taste, sweetness, and acidity, the polyphenolic compounds, mostly located in apple skins, are potential disease-preventing agents (Boyer & Liu 2004; Francini & Sebastiani 2013; Gerhauser 2008; Koutsos et al. 2015; Pirlak et al. 2017); indeed, they reduce risk of chronic pathologies such as cardiovascular disease, specific cancers, and diabetes (Koutsos et al. 2015). The major structural classes of phenolics in apples are flavonoids and phenolic acids, as reported in Figure 2.1.

Polyphenol Class		
Flavonoids		
	Anthocyanins	
		Cyanidin 3-O-arabinoside
		Cyanidin 3-O-galactoside
		Cyanidin 3-O-xyloside
	Dihydrochalcones	
		3- Hydroxyphloretin 2′-O-glucoside
		Phloridzin
		Phloretin
		Phloretin-2-xyloglucoside
	Flavanols	
		Catechin
		Epicatechin
		Procyanidin B1
		Procyanidin B2
		Procyanidin C1
		Procyanidin-tetramer
		Procyanidin-pentamer
	Flavonols	
		Quercetin-3-arabinopyranoside
		Quercetin-3-arabinofuranoside
		Quercetin 3-O-glactoside
		Quercetin 3-O-glucoside
		Quercetin 3-O-rhamnoside
		Quercetin 3-O-rutinoside
		Quercetin 3-O-xyloside
		Quercetin (aglycone)
Phenolic acids	Hydroxy benzoic acid	
		Syringic acid
	Hydroxy cinnamic acid	
		Caffeic acid
		4-p-Coumaroylquinic acid
		4-Caffeoylquinic acid
		Ferulic acid
		p-Coumaric acid

Figure 2.1 Major structural classes of phenolics present in apples (Rana & Bhushan 2016).

Many factors affect the metabolomic composition of plant-based foods. The metabolome varies with genetic species, environment, cultivation, geographical location, growing season, storage conditions, and when dealing with a transforming product such as a juice, also the industrial treatments (Duda-Chodak et al. 2010; Kumar et al. 2012; Jeong et al. 2015). Even the smallest variation of one of these factors can cause a variation on the concentration of some metabolites or cause the appearance of new ones usually not present (Salvino et al. 2021), making the metabolome a potential marker for determining quality, origin, and authenticity of fruit and fruit-derived foods (Sobolev et al. 2015). In literature, many analytical methodologies have been applied to identify specific fruit metabolites (Tallapally et al. 2020; Mamat et al. 2020; Lima et al. 2020; Seger & Sturm 2007). However, as previously mentioned in Chapter 1 of this PhD thesis, nuclear magnetic resonance (NMR) spectroscopy and mass spectrometry (MS), usually hyphenated to chromatographic separation techniques like liquid (LC) or gas (GC) chromatography, are the two most widely used techniques for structural identification of compounds in complex mixtures. (Bingol 2018; Abreu & Fernandez 2020; Olennikov et al. 2020), and thus ideal for fruit juice analysis.

It is known that processing steps for producing ready-to-drink apple juices, including juice extraction and clarification, hurt the health-promoting compounds of apples. Typically, the content of polyphenols and vitamin C is reduced during processing and juicing, and fibres are almost entirely removed during clarification (Vallée Marcotte et al. 2022). To attain a juice with a greater nutritional the application of membrane operations is an effective solution. Membrane processes represents a promising technology for recovering biologically active compounds from foods and their by-products. (Castro-Muñoz et al. 2018) and might be integrated in the production cycle to separate and concentrate polyphenols. Among these processes, nanofiltration (NF) is particularly adequate for (i) the purification, fractionation, and concentration of several food products and by-products and (ii) the recovery of value-added compounds and solvents from food wastes (Nath et al. 2018).

The present study was undertaken for a twofold purpose: (a) to perform an NMR-metabolic analysis of four different varieties of Calabrian apple juices, namely, Golden Delicious, Royal Gala, Pink Lady, and Fuji, grown in the same Calabrian orchard, and harvested in the same period of the year, i.e., February 2020, and (b) to determine the polyphenolic component *via* HPLC–ESI–MS/MS and probe its concentration by NF.

2.2 Materials and Methods

2.2.1 Materials

Gioia Succhi Srl (San Ferdinando, Reggio Calabria, Italy) which generally produces juices industrially in large quantities supplied the apple juices used in this work. The fruits used for the preparation of the juices came from the same Calabrian geographical area, i.e., grown in the same Calabrian orchard, and were harvested in the same period of the year, February 2020, therefore with the same degree of ripeness. For our purposes, following the industrial process, five samples were prepared for each apple variety in small quantities, about 500 mL, by combining the material coming from six fruits for each of them. From these initial batches 20 NMR samples, i.e., five NMR samples for each cultivar, were prepared. For the Golden Delicious variety alone, about another 20 L of juice have been prepared, from the same fruits, since these quantities are necessary for the subsequent membrane concentration treatment. Each apple variety, one at a time, was ground entirely (peel, flesh, and seeds) through a small-scale mill. Then, each sample was pasteurized to inhibit the tyrosinase action. Successively, potassium metabisulfite ($K_2S_2O_5$) was added as preservative followed

by the addition of a pectolytic enzyme to degrade pectin and to reduce the viscosity of the juice so that it can be handled easily. Finally, the liquid part was separated from the pulp by filtration. Only the liquid part was transferred to aseptic bags and stored in the cold room at −18 °C to be thawed for subsequent processes and analysis. All chemicals and reagents were of commercial origin: 3-(trimethylsilyl) propionic-2,2,3,3-d4 acid sodium salt (98 atom % D), deuterium oxide (99.9 atom % D), and sodium azide were purchased from Sigma-Aldrich as well as chlorogenic, caffeic acids, and the Folin-Ciocalteu reagent. Formic acid, methanol of LC–MS grade (Sigma-Aldrich), and ultrapure water of Milli-Q gradient were used for chromatography.

2.2.2 Concentration of Apple Juice by NF

Apple juice of the Golden Delicious variety was concentrated by NF. In particular, the depectinized juice was previously clarified by UF using a laboratory plant equipped with a 500 kDa polyethersulfone hollow fiber (HF) membrane module (FB-02-FC from Microdyn Nadir, Wiesbaden, Germany) in selected conditions of transmembrane pressure (about 0.40 bar), axial feed flow rate (460 L/h), and temperature (20 ± 2 °C). The clarified juice was then submitted to a NF process performed by using a bench plant manufactured by DeltaE s.r.l. (Cosenza, Italy) and equipped with a stainless steel housing able to accommodate a spiral-wound membrane module featuring an effective membrane area of 0.32 m^2. The equipment consists of a feed tank with a capacity of 5 L, a high-pressure pump, a digital flowmeter, and a control panel. The feed temperature was adjusted by circulating tap water in the two-layered feed tank. Pressure was monitored at the entrance and exit of the membrane module; it was controlled by a back-pressure control valve located after the membrane module and by setting the pump speed on the control panel. The plant was equipped with a NF membrane module in polyamide supplied by GE Osmonics (Desal DK, Minnetonka, MN) with a MWCO of 150–300 Da. Experiments were performed according to a batch concentration configuration in which the permeate is collected separately while the retentate is recycled back to the feed reservoir. The NF process was performed at a temperature of 25 ± 2 °C, a transmembrane pressure of 20 bar, and an axial feed flow rate of 420 L/h up to a volume reduction factor (VRF) of 3.3. VRF is defined as the ratio of feed volume to residual retentate volume according to the following equation (Garcia-Castello et al. 2011):

$$VRF = \frac{V_f}{V_r} = 1 + \frac{V_p}{V_r} \quad (2.1)$$

where V_f, V_p and V_r are the volume of the feed, permeate and retentate, respectively. The clarified juice with a total soluble solids (TSS) content of about 7° Brix was concentrated up to a final value of 22° Brix. As expected, a decrease in permeate flux was observed throughout the time due to concentration polarization and fouling of the NF membrane. The measured permeate flux was in the range of 0.50-28.12 L/m^{2}h, while the average permeate flux was equal to 5.72 L/m^{2}h. After the NF treatment, the membrane module was cleaned according to the manufacturer's instructions. The selectivity of the NF membrane towards bioactive compounds was evaluated at different VRF values. In particular, the analysed samples through NMR and HPLC-UV were picked up at VRF 2, 2.5, 3 and 3.3, therefore at increased concentration of soluble solids. The observed rejection for a specific compound was calculated according to the following equation:

$$R_i = \left(1 - \frac{C_{ip}}{C_{if}}\right) \cdot 100 \quad (2.2)$$

where R_i is the observed retention of compound i (%), and C_{ip} and C_{if} are the concentrations of compound i in permeate and feed (mg/L), respectively.

2.2.3 Sample NMR preparation and spectral acquisition

The samples for NMR isotropic analysis were prepared following the procedure reported in literature (Belton et al. 1997; Iaccarino et al. 2019). Apple juices from the four varieties were first thawed at room temperature and a small volume, about 8 mL, of each batch was centrifuged (4000 rpm for 20 minutes) to remove suspended substances. To have chemical shifts values comparable to each other and to those reported in the literature, it was necessary to operate at similar pH values. Then, for each centrifuged sample analyzed, the pH has been adjusted to a value of 3.25–3.38 by adding microliter amounts of 1M HCl solution. In addition, an aqueous solution of NaN_3 was added to minimize the alteration in the composition of the juice during the time of sample preparation and acquisition of NMR spectra. Sodium azide acts as a preservative, avoiding the formation and/or degeneration of metabolites by bacteria. TMSP-d_4 (i.e. 3-(Trimethylsilyl)propionic-2,2,3,3-d_4 acid sodium salt) was used as internal standard. The samples were then prepared by transferring about 0.5 g of the supernatant at the right pH value in 5-mm o.d. NMR tube together with about 0.03 g of the solution of TMSP-d_4 (100mM) and NaN_3 (2mM) in D_2O. A further amount of D_2O was added to this solution and used as the field frequency lock signal. The same

preparation was carried out on the samples arising from the membrane processes. All the NMR spectra have been acquired at 298 K on a high-resolution Bruker Avance 500 MHz spectrometer (11.74 T) (Bruker, Fällanden, Switzerland) equipped with a 5-mm TBO probe and a standard variable-temperature unit BVT-3000. The 1D ^{1}H and ^{13}C-{^{1}H} NMR experiments and 2D homo and heteronuclear correlation NMR spectra , ^{1}H-^{1}H COSY and ^{1}H-^{13}C HMQC, were performed on each sample. The latter have been very useful, together with the data present in the literature (Belton et al. 1997; Vermathen et al. 2011, 2012), in assigning the frequencies of the various metabolites. To suppress the residual water signal, the *noesypr1d* sequence has been used for recording the 1H NMR spectra by acquiring, for each spectrum, 256 FID and using a spectral width of 11.26 ppm. Proton broad-band decoupling has been used to record the 1D ^{13}C-{^{1}H} NMR spectra collecting 500 FIDs and using a spectral width of 266.80 ppm and a relaxation delay of 10 s. The COSY experiments were acquired using a SW of 11.26 ppm on both dimensions, 2 K data points, 28 scans, and 512 increments, while the ^{1}H-^{13}C HMQC spectra were recorded using a SW of 11.26 ppm (^{1}H) and 266.80 ppm (^{13}C), 2 K data points, 256 scans, and 32 experiments.

2.2.4 Data Processing and Pre-treatment

The ^{1}H-NMR spectra were phased, baseline-corrected, and the chemical shifts referenced to the TMSP signal. The ^{13}C-{^{1}H} NMR spectra were filtered with 1-Hz line broadening before Fourier-transformed. Each ^{1}H-NMR spectrum was segmented into identical intervals ("buckets") of fixed 0.05 ppm in the range from 1.10 to 5.60 ppm. The bucketing procedure was performed defining the integration range on the first spectrum, the integration regions were saved, and the other spectra were bucketed automatically using this saved list. The integrals were normalized and compose the data matrix that exported to an excel file was subjected to statistical analysis. A dataset of 20 samples, 5 for each variety, and 51 variables has been obtained. All the data processing steps were carried out using TopSpin 3.6 software (Bruker BioSpin, Rheinstetten, Germany) (TopSpin, 2018). NMR data matrix was mean-centered and scaled and PCA was performed with R software (R Core Team, 2019).

2.2.5 Sample preparation for LC-UV-ESI-MS/MS and analysis

HPLC-UV-ESI-MS/MS analysis was carried out on the juice of the Golden Delicious variety only. The juice was initially thawed at room temperature and centrifuged. Then, the supernatant (20 ml) was filtered and passed through C_{18} cartridge (Supelco, USA). The loaded stationary phase was initially washed with water (12 × 20 ml) to remove the sugars and water soluble fraction, and then eluted with 10 ml of methanol. The methanol was evaporated using the rotavapor and sample was redissolved in 3 ml of a solution H_2O:MeOH (50:50 v/v). The purified and concentrated sample was then injected into the HPLC. HPLC-UV analysis was performed using a Fractionlynx instrument (Waters, Milford, MA) equipped with an autosampler/collector Waters 2767 Sample Manager, a 600E pump working in analytical mode, a 2486 nm UV detector. The HPLC separation was achieved using a 250 × 4.6 mm, 5 μm reversed phase C_{18} Luna-Phenomenex column at a flow rate of 1 ml/ min. The run time was 70 min and the mobile phase was composed by 0.1% formic acid in water (solvent A) and methanol (solvent B). The chromatographic run (70 min) consisted of the following steps: isocratic at 80% A for 7 min; linear gradient from 80% A to 40% A in 33 min; isocratic at 40% A for 5 min; linear gradient from 40% A to 20% A in 5 min; isocratic at 20% A for 7 min; linear gradient from 20% A to 80% A in 5 min; equilibration of the column for 8 min. The UV detector was set at 280 nm and at 340 nm. Afterwards, the different UV fractions were collected at the wavelength of 340 nm. ESI MS and MS/MS spectra were acquired by direct infusion of the UV fractions into a Thermo Scientific TSQ Quantum Vantage triple-stage quadrupole mass spectrometer (Thermo Fisher Scientific, San José, CA). Since polyphenols are easily deprotonable compounds, spectra were acquired in negative ion mode. Tandem mass spectra were acquired using a collision energy (CE) of 15 and 20 eV. The samples deriving from the membrane processes were not purified and concentrated by SPE, but were simply centrifuged and the supernatant was subjected to the HPLC-UV analysis only, in order to verify variations in the chromatographic profiles.

The quantitative analysis was carried out using a different HPLC-system (Agilent 1100 series, Agilent Technologies, Waldbronn, Germany) but it was always equipped with a Luna C_{18} column (250 mm × 4.6 mm, 5 μm, Phenomenex, Torrance) and an UV detector. Peaks were quantified at λ=340 nm using also the same mobile phase and the same gradient than that used for the identification.

2.3 Results and Discussion

2.3.1 NMR characterization of apple juice varieties

Figure 2.2 shows the ^{1}H NMR spectrum of the Golden Delicious juice obtained with *noesypr1d* sequence.

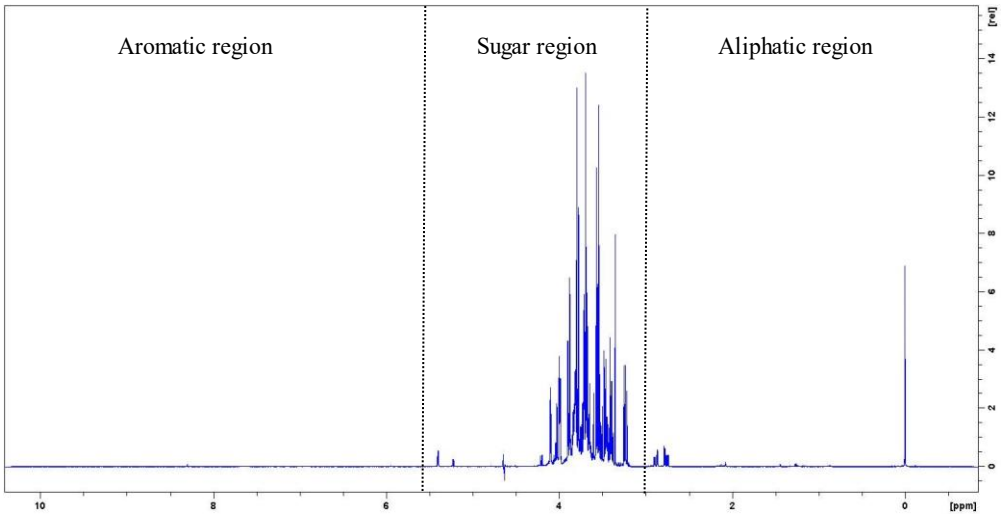

Figure 2.2 500 MHz ^{1}H NMR spectrum of Golden Delicious apple juice.

The spectrum of Golden Delicious apple juice can be divided into three regions: the first which goes from 0 to 3 ppm contains the frequencies of aliphatic substances which are mostly amino-acids and organic acids; the resonances appeared in the region between 3 and 5.6 ppm include the signals of α-glucose, β-glucose, sucrose and fructose; while the third region, from 5.6 to 10 ppm, is the aromatic region relating to phenolic metabolites. As is evident from the spectrum in Figure 2.2, the main constituents in apple juice are sugar compounds. Another prominent compound is malic acid with resonances around 2.7 and 4.4 ppm. The signals assignment of the various metabolites was carried out using not only one-dimensional ^{1}H but also ^{13}C-{^{1}H} NMR spectrum, 2D correlation experiments ^{1}H-^{1}H COSY and ^{1}H-^{13}C HMQC, reported respectively in Figure 2.3, Figure 2.4, and Figure 2.5.

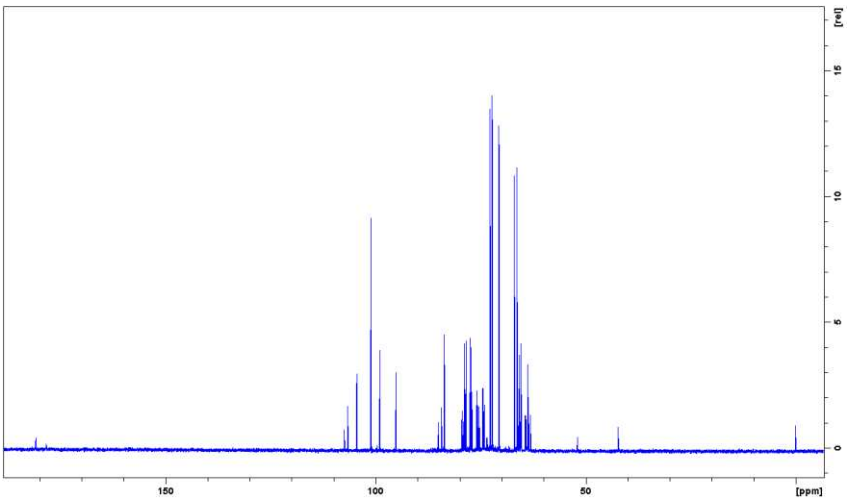

Figure 2.3 1D ^{13}C-{^{1}H} NMR spectrum (Bruker pulse sequence: *zgdc*) recorded on Golden Delicious juice in D_2O (field strength of 11.74 T).

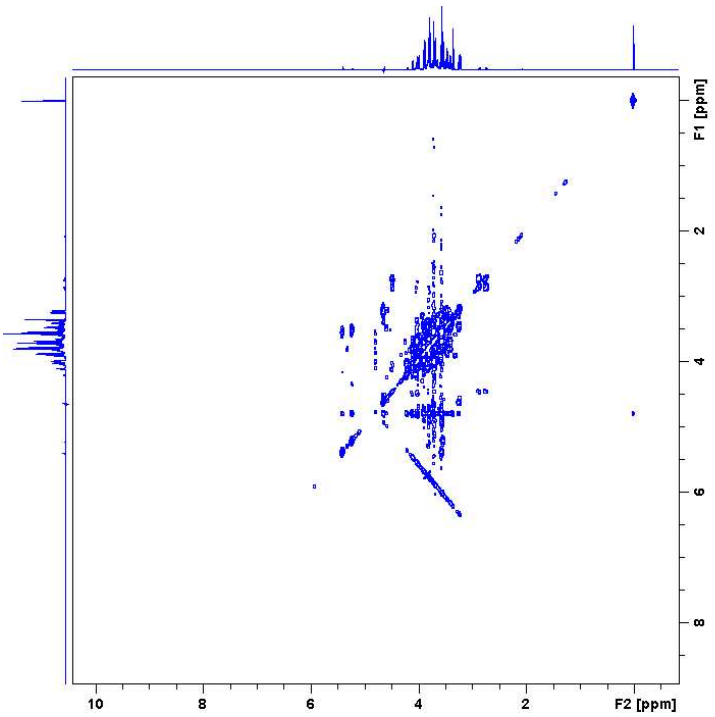

Figure 2.4 2D ^{1}H COSY spectrum (Bruker pulse sequence: *cosygpprqf*) recorded on Golden Delicious juice in D_2O (field strength of 11.74 T).

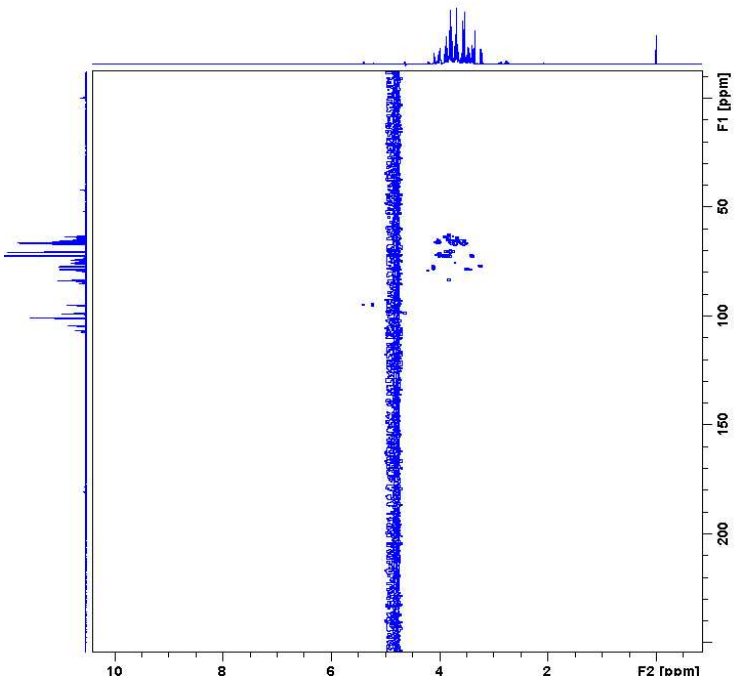

Figure 2.5 2D ^{1}H-^{13}C HMQC spectrum (Bruker pulse sequence: *hmqcgpqf*) recorded on Golden Delicious juice in D_2O (field strength of 11.74 T).

The compounds were identified by evaluating the experimental information obtained from NMR spectra and using works from the literature. (Vermathen et al. 2011; Tomita et al. 2015; Belton et al. 1997; Vermathen et al. 2012).

The procedure for assigning each individual metabolite was rather laborious, and the method of operation is described below, using malic acid assignment as an example. Malic acid, present mainly in the peel of apples, is an alpha-hydroxylated organic acid whose structure is shown in Figure 2.6.

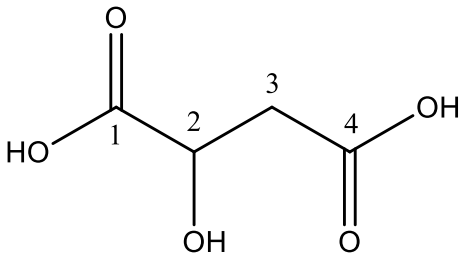

Figure 2.6 Chemical structure of malic acid and numbering used in the text.

Malic acid has four types of protons. Hydrogens bonded to oxygen atoms are not visible in the ^{1}H-NMR spectrum as they are broad and weak signals that probably end up in the baseline. The hydrogens bonded to C3 are diasterotopic, falling at slightly different chemical shift values (spin system AB) (3a = 2.69 ppm and 3b = 2.84 ppm) as reported in the literature (Vermathen et al. 2011), while the hydrogen bonded to C2 falls at 4.44 ppm. Protons 3a and 3b, being magnetically non-equivalent, have different coupling constants and generate doublets of doublets by coupling with each other and with the proton H2. These doublets of doublets are clearly visible in the one-dimensional spectrum. Since the chemical shifts of these signals are close, the doublets are distorted, with the innermost branches more intense, as visible in Figure 2.7.

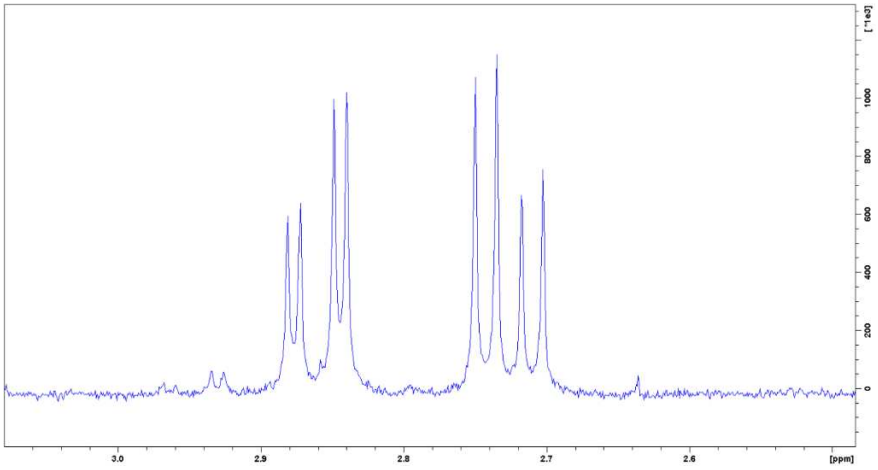

Figure 2.7 Enlargement of the ^{1}H-NMR spectrum in the malic acid region from which the roof effect generated by protons 3a and 3b is clearly seen.

On the other hand, the H2 proton signal is not recognisable in 1D spectrum due to overlap with other signals. However, it is possible to understand its exact chemical shift value through the 2D ^{1}H-^{1}H COSY spectrum, as it possible to visualize the correlations between protons H3a and H3b with H2 (Figure 2.8).

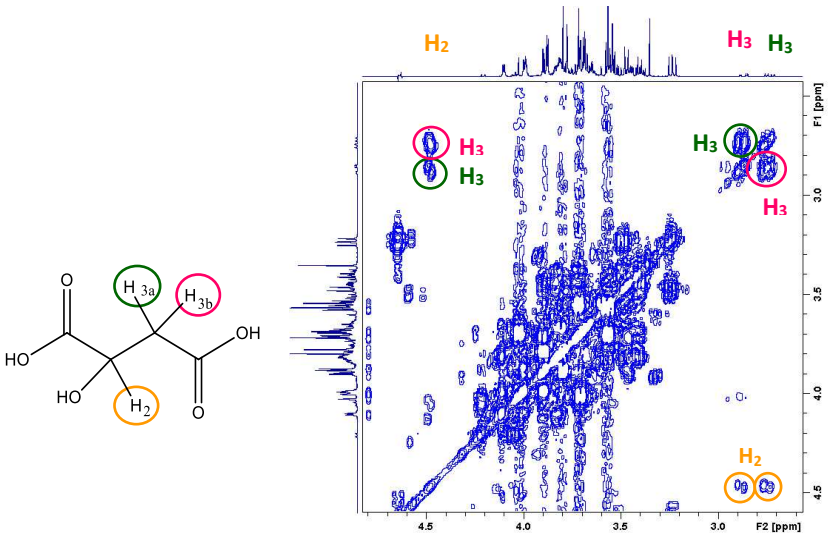

Figure 2.8 ^{1}H-^{1}H COSY spectrum of the Golden Delicious juice sample showing the correlations between protons 3a, 3b, and 2.

Once the chemical shifts of the protons are known, it is possible to assign, *via* the 2D HMQC spectrum, the signals generated by the carbon atoms to which the protons are bound (Figures 2.9 and 2.10).

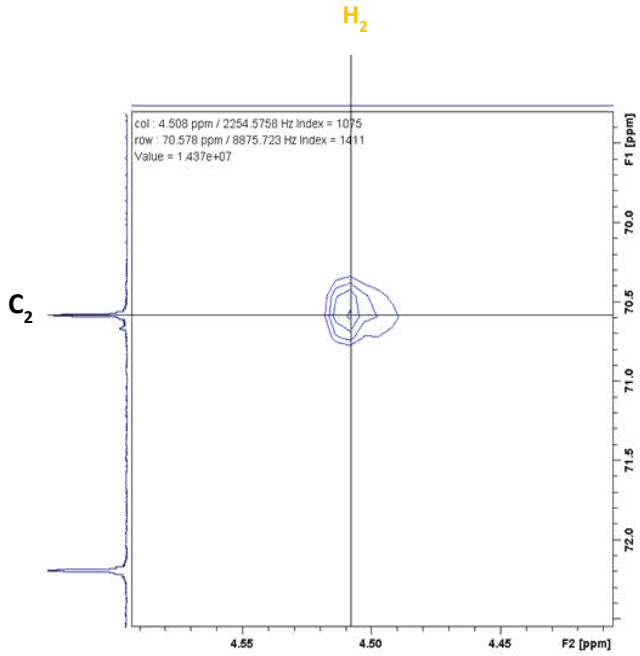

Figure 2.9 Enlargement of the HMQC spectrum showing the correlations between proton 2 of malic acid with its respective carbon.

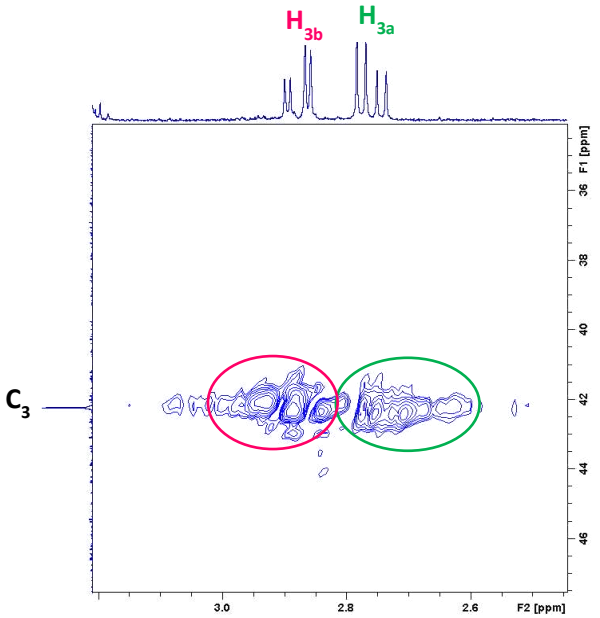

Figure 2.10 Enlargement of the HMQC spectrum showing the correlations between protons 3 of malic acid with their respective carbon.

The other visible correlations in HMQC spectrum are those between the protons and carbons of the sugars. Consider, for example, fructose, particularly in the form of α-D-fructofuranose.

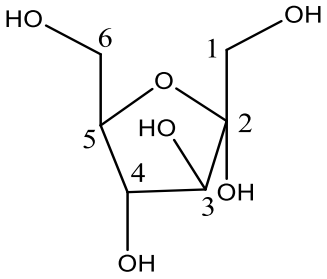

Figure 2.11 Chemical structure of α-D-fructofuranose and numbering used in the text.

From the literature (Filhoa et al. 2020) the proton bound to carbon 3 and the proton bound to carbon 4 fall at the same chemical shift value (4.10 ppm). The HMQC experiment, which in this case shows the heteronuclear correlations well, confirms what has just been said and the chemical shifts of the carbon atoms match those present in the literature (Filhoa et al. 2020).

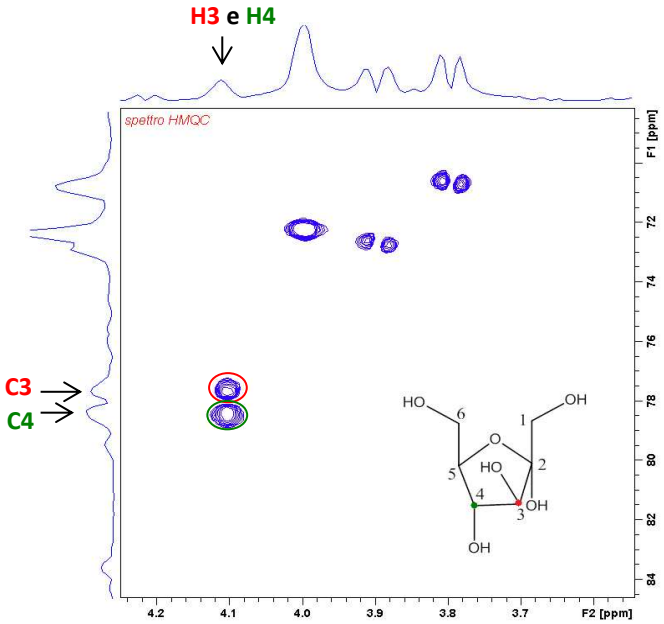

Figure 2.12 Enlargement of the HMQC spectrum showing the correlations between protons 3 and 4 of α-D-fructofuranose with their respective carbons.

Following the same procedure, it was possible to identify the other metabolite signals. The assignments are shown in Table 2.1, where the twelve metabolites assigned with all the experimental information obtained from the NMR spectra relating to Golden Delicious apple juice are reported.

Table 2.1 ^{1}H and ^{13}C chemical shifts and multiplicity of compounds in apple juice of Golden Delicious.

Compound	δ ^{1}H (ppm)	Multiplicity J [Hz]	δ ^{13}C (ppm)	Group
Amino acid and organic acid region (0-3 ppm)				
ethanol	1.17	t [7.09]		CH_3
L-rhamnitol	1.27	d [6.40]		CH_3
citramalic acid	1.42	s		CH_3
quinic acid	1.89 – 2.12			CH_2 – CH
chlorogenic acid	2.01 – 2.08			CH_2 – CH
malic acid	2.73	dd [16.20, 7.51]	42.19	β-CH_2
	2.86	dd [16.20, 4.67]		β-CH_2
	4.47		70.58	CH
			180.85	α-COOH
			178.31	δ-COOH
Sugar region (3-5.6 ppm)				

β-glucose 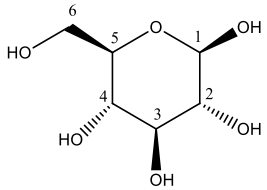	3.23	dd [9.99,8.06]	77.18	H– C(2)
	3.40	m		H– C(5)
	3.46	m	78.78	H– C(3)
	3.46	m	78.85	H– C(5)
	3.46	m		H (6a)– C(6)
	3.73	m		H (6b)– C(6)
	4.63	d	98.87	H– C(1)
α-glucose 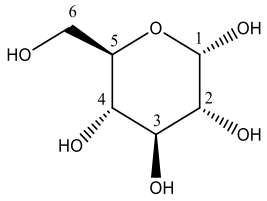	3.40	m		H– C(4)
	3.52	dd [9.80, 3.67]	74.50	H– C(2)
	3.73	m		H– C(3)
	3.73	m		H (6a)– C(6)
	3.82	m	74.35	H– C(5)
	3.82	m		H (6b)– C(6)
	5.22	d [3.10]	95.06	H– C(1)
Sucrose 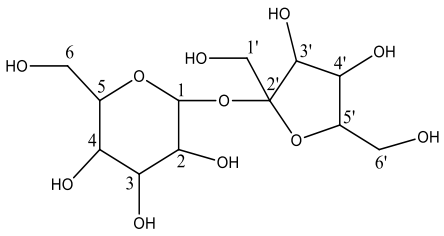	3.46	t		H– C(4)
	3.55	dd		H– C(2)
	3.67	s		H– C'(1)
	3.75	t		H– C(3)
	3.82	m		H – C(6)
	3.86	dd		H– C(5)
	4.20	d	79.40	H– C'(3)
	5.40	d [3.82]	95.06	H– C(1)
			106.55	C'(2)
α-D-fructofuranose 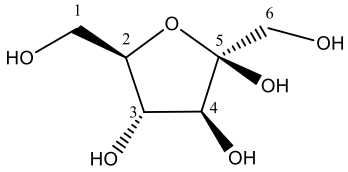	3.54	m		H (6b)– C(6)
	3.59	m		H (6a)– C(6)
	3.67	m		H (1b)– C(1)
	3.80	m		H (1a)– C(1)
	3.82	m	83.58	H– C(2)
	4.10	m	77.44	H– C(3)
	4.10	m	78.40	H– C(4)
			104.44	C(5)
β-D-fructofuranose 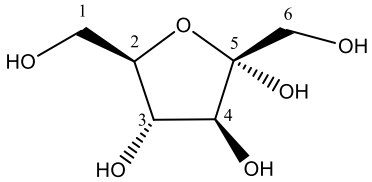	3.55	m	66.90	H (6b)– C(6)
	3.69	m	66.90	H (6a)– C(6)
	3.69	m	66.27	H (1b)– C(1)
	3.78	m	70.58	H– C(4)
	3.88	dd		H– C(3)
	3.98	m	72.18	H– C(2)
	4.01		66.27	H (1a)– C(1)
			101.02	C(5)
Aromatic region (5.6-10 ppm)				
Formic acid	8.32	s		H

These attributions are reported directly in the enlarged regions of Golden Delicious juice's proton spectrum, as seen in Figure 2.13.

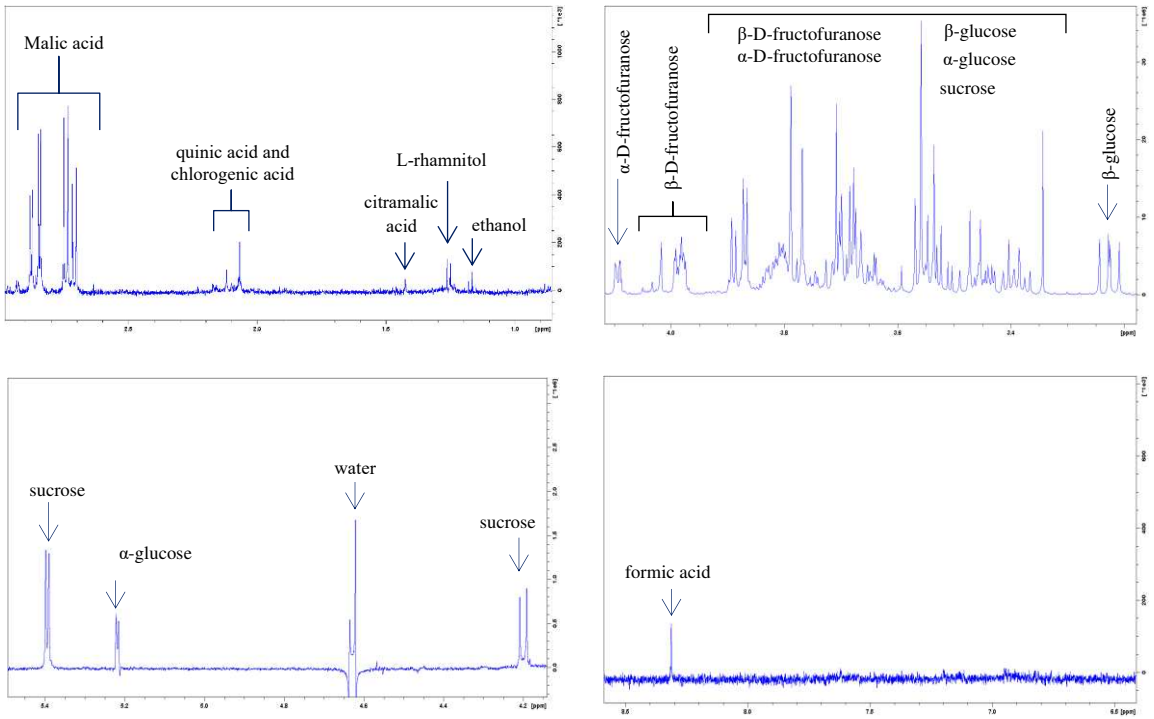

Figure 2.13 Expanded ^{1}H NMR spectrum of Golden Delicious juice and signals assignment.

Once the metabolic profile for the Golden Delicious was determined, a comparison between the NMR spectra of the samples relating to the other apple varieties was possible.

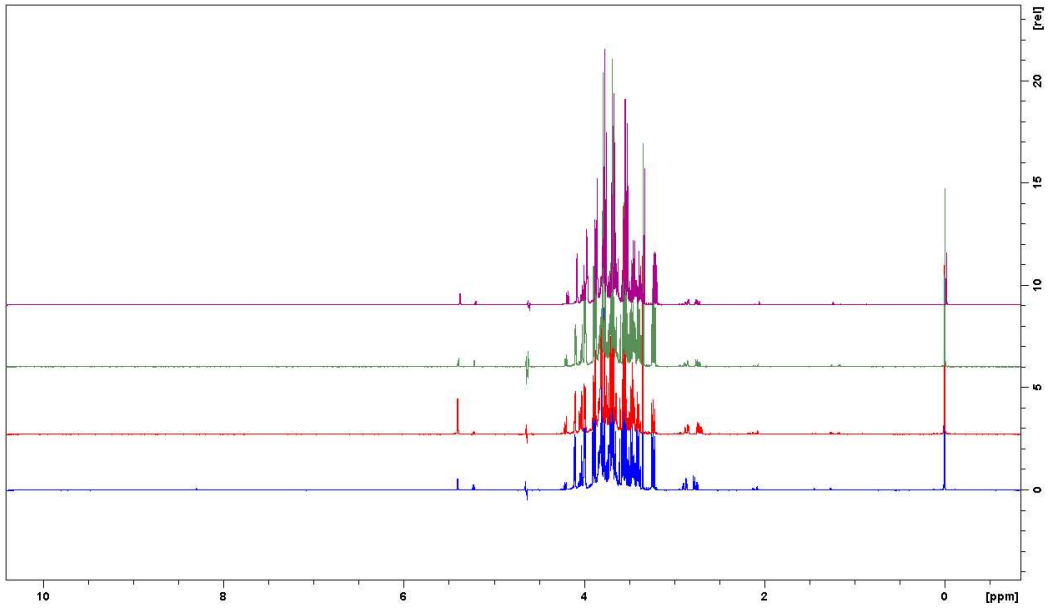

Figure 2.14 Comparison of ^{1}H NMR spectra of Golden Delicious (in blue), Pink Lady (in red), Fuji (in green) and Royal Gala (in violet).

Figure 2.14 shows that the metabolic profile is the same for all four varieties of apples; in particular, the metabolites recognised for the Golden Delicious variety are recognisable also in the other apple varieties, which show no other signals than those already identified, except the different relative intensity of the signals and small variations in chemical shift. However, to obtain more information and to evaluate any relationships and variations in composition in the four different juices, the Principal Component Analysis (PCA) method was used.

2.3.2 PCA Analysis on NMR data from apple juice varieties

To perform a PCA, a variable selection is necessary. The NMR regions choose by manual selection is the aliphatic region that contains most abundant compounds as sugar and organic acids. In particular, the integration of the proton spectrum (binning procedure) was made considering chemical shift intervals of 0.05 ppm belonging to the following spectral windows: from 1.1 to 1.5 ppm that is the region of the ethanol, L-rhamnitol and citramalic acid methyl protons signals; from 1.9 to 2.25 ppm that is the region of quinic and chlorogenic acid aliphatic ring signals; from 2.6 to 3.0 ppm which includes the doublets of doublets related to the methylenic and methynic protons of malic acid; and finally from 3.15 to 4.25 ppm which is the sugar region. Instead, some regions have been excluded from the bucketing process: the interval from 4.30 to 5.10 ppm because of the residual water signal and the interval from 5.6 to 10 ppm in which, due to the too low S/N (Signal to Noise) ratio. A dataset of 20 samples (5 for each variety) and 51 variables has been obtained. The 3D score plot obtained is reported in Figure 2.13, where a cumulative percentage of explained data variance of 81.6% (52.3%, 22.2% and 7.1% for PC1, PC2 and PC3 respectively) summarises the relationship between samples. As can be seen from the score plot (Figure 2.15), there is a clear separation between the four varieties of apples. Specifically, the Pink Lady variety has negative values of PC2 while Royal Gala, Golden Delicious and Fuji have positive value of this component. This trend highlights that samples belonging to the Golden Delicious,

Fuji and Royal Gala varieties have a more similar metabolic composition than the juices from the Pink Lady variety.

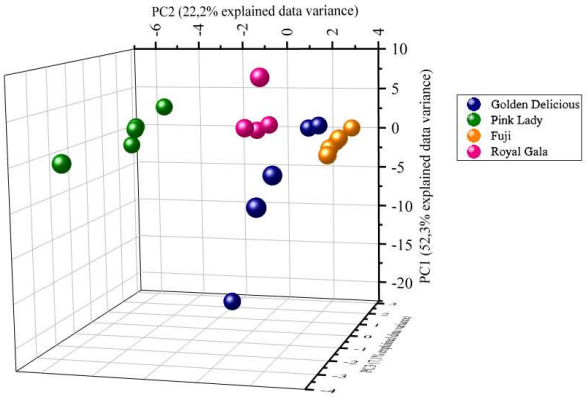

Figure 2.15 Principal Component Analysis (PCA) of Golden Delicious, Pink Lady, Fuji and Royal Gala juices. The score plot showing the first three PCs: PC1, PC2 and PC3 with their respective variation. R^2 X(PC1) = 52.3%, R^2 X(PC2) = 22.2%. R^2 X(PC3) =7.1%.

In order to understand how the metabolites contribute to the varieties separation, the biplot need to be examined. The biplot is a two dimensional scattered plot which links the score plot and the loading plot information in a single chart. Due to the low information content of PC3 and since a good separation in varieties is obtained from the first two PCs, the biplot reported in Figure 2.16 is a 2D plot where only the PC1 and PC2 are considered.

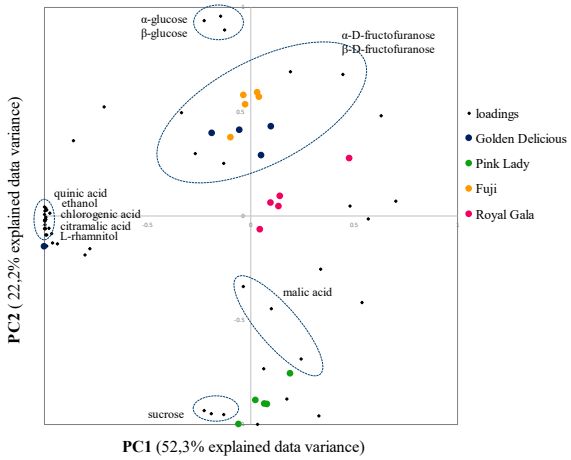

Figure 2.16 Biplot of the first two PCs, PC1 and PC2, taking into account the loadings and the scores obtained from the PCA carried out on NMR spectra of the Golden Delicious, Pink Lady, Fuji and Royal Gala juices.

From the biplot emerged that Pink Lady variety is characterized by a major sucrose and malic acid content respect to other ones, while Golden Delicious and Fuji are richer in α-glucose, β-glucose, α-D-fructofuranose and β-D-fructofuranose. Royal Gala seems to have an intermediate composition between Pink Lady variety and Golden Delicious and Fuji varieties even if it is closer to the last two. Minor compounds such as ethanol, quinic acid, chlorogenic acid, L-rhamitol and citramalic acid, have null values of PC2, i.e. the dimension in which the apple varieties are better separated. This means that these 5 metabolites do not affect the separation and can be neglected as marker of variety separation.

2.3.3 NMR Characterization of UF and NF membrane fractions

^{1}H NMR spectra were also recorded on fractions of Golden Delicious juice treated by means of membrane processes, shown in Figures 2.17, 2.18 and 2.19.

Figure 2.17 compares ^{1}H NMR spectra of Golden Delicious juice and UF permeate of the same juice. It can be seen that there are no relevant differences between the spectral profile of the original juice and the UF permeate, neither in terms of signals nor intensity.

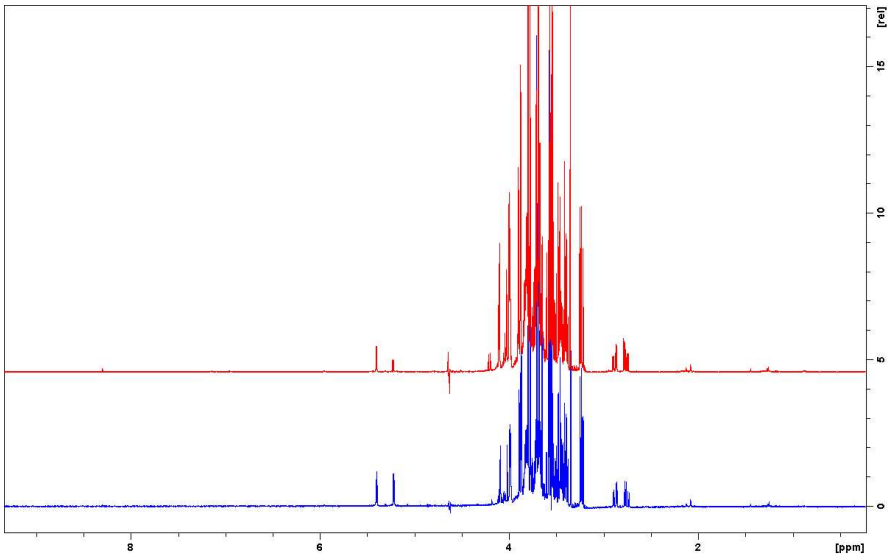

Figure 2.17 Comparison of ^{1}H NMR spectra of Golden Delicious juice (in blue) and UF permeate of the same juice.

On the other hand, as shown in Figures 2.18 and 2.19, malic acid signals are missing from the spectra of the NF permeates and NF retentates, which, therefore, may have remained adsorbed in the used NF membrane.

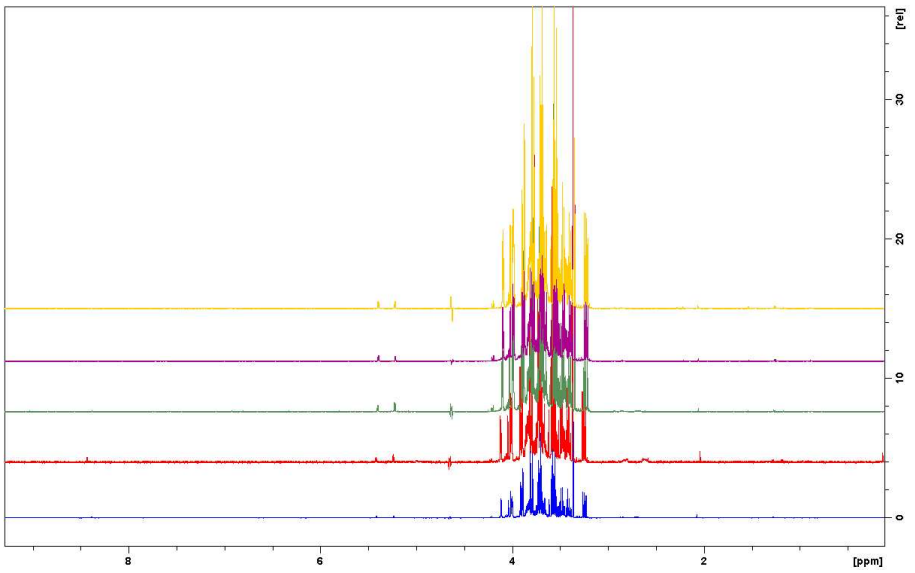

Figure 2.18 Comparison of ^{1}H NMR spectra of NF Golden Delicious permeates at different VRFs values. The spectrum in blue is referred to total permeate, while from red to yellow are reported spectra related to permeates from VRF 2 to VRF 3.3.

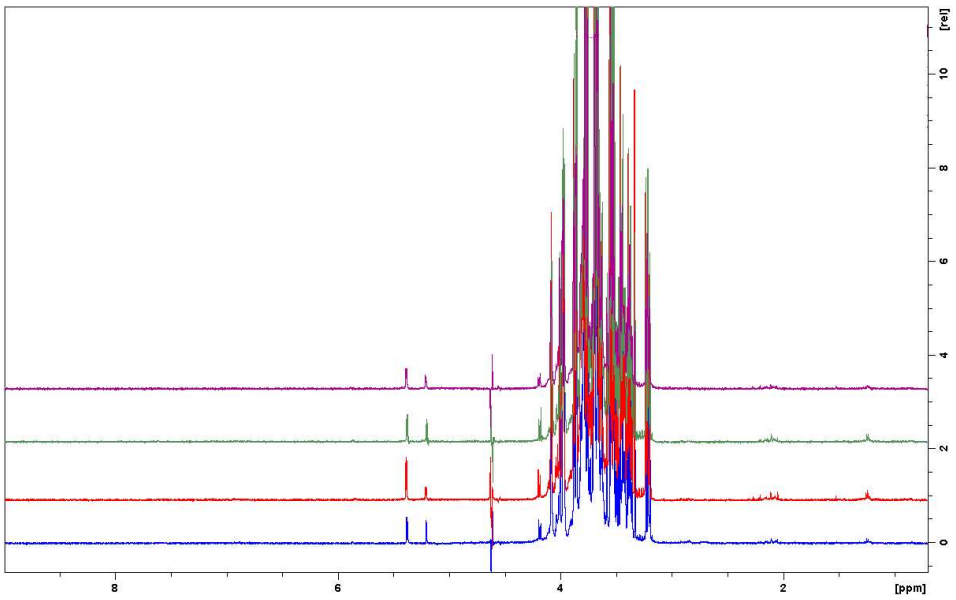

Figure 2.19 Comparison of ^{1}H NMR spectra of NF Golden Delicious retentates at different VRFs values: VRF 2 (in blue), VRF 2.5 (in red), VRF 3 (in green) and VRF 3.3 (in violet).

2.3.4 NMR analysis of apple juice after SPE extraction

In all the recorded spectra, both of the juices from different varieties and in the fractions of Golden Delicious juice processed with membranes, no detectable signals appear in the aromatic region of the ^{1}H NMR spectra attributable to phenolic compounds, which as mentioned in the literature reported in the introduction, should be found in apples and also in its juice. For this reason, an SPE extraction was carried out on the supernatant of the Golden Delicious juice with a C_{18} cartridge to remove the most present sugar fraction and recover and concentrate the phenolic fraction of the juice, if present. Therefore, the original Golden Delicious juice was centrifuged, and its supernatant was loaded onto the C_{18} cartridge. Water was first added to further remove polar compounds, such as sugars, and then methanol was used as eluent to recover the remaining juice compounds adsorbed on the cartridge. The solvent was then removed with the rotavapor and the sample solubilized in deuterated water to be analyzed, together with the sodium azide and the TMSP-d_4 standard. The ^{1}H NMR profile of the eluate is shown in the Figure 2.20. It is a different profile from those seen previously and above all, signals now appear in the aromatic region of the spectrum. However, their exact attribution via NMR was not simple because of signal overlapping and because most of the various open databases for the metabolites' identification contain information on human metabolites and very few resources for identifying secondary metabolites of plants. Consequently, to carry out a more precise qualitative and quantitative analysis of the phenolic component, the HPLC-UV-MS analysis was carried out.

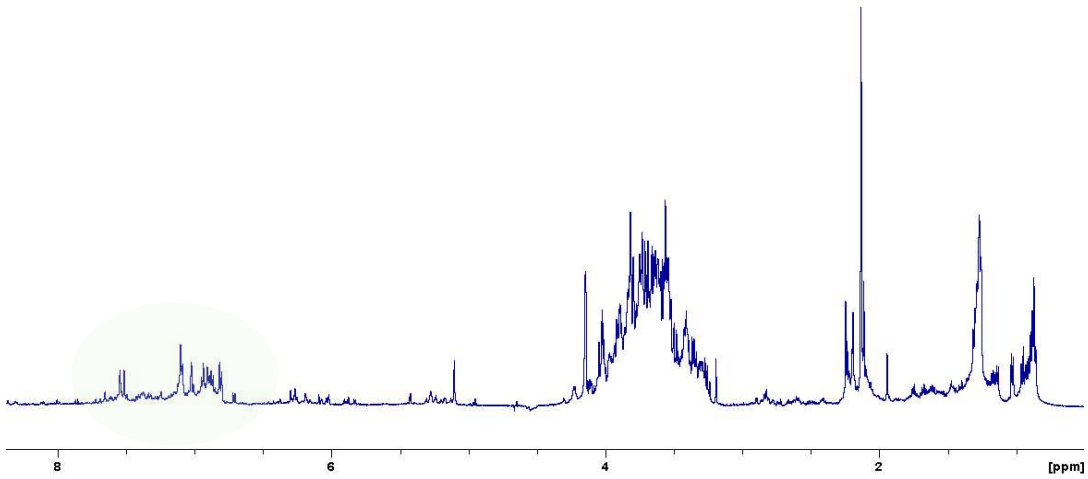

Figure 2.20 ^{1}H-NMR spectrum of eluant of Golden Delicious juice after SPE extraction.

2.3.5 HPLC-UV-ESI-MS/MS

Figure 2.23 shows the HPLC-UV chromatogram and signal attributions of the purified and concentrated supernatant related to Golden Delicious juice after SPE extraction. UV fractions were collected and infused into the mass spectrometer. MS and MS/MS spectra were recorded for each fraction, as reported for example in Figures 2.21 and 2.22 for the fraction with a retention time of 16.72 min. Based on the molecular weight of the $[M-H]^-$ ion, the fragmentations, and the literature (Kahle et al. 2005) 10 phenolic compounds were identified and reported in Table 2.2 as well as directly on HPLC-UV chromatogram in Figure 2.23.

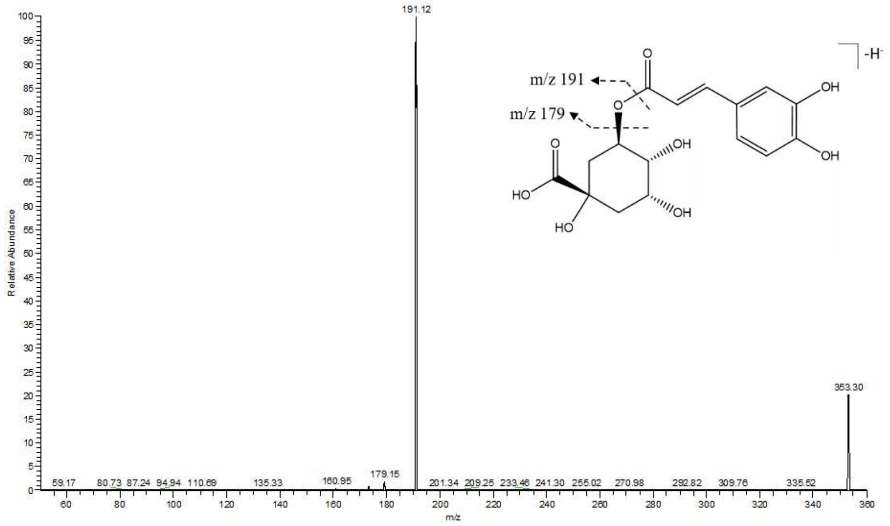

Figure 2.21 ESI-MS spectrum obtained from the UV fraction collected at 16.72 minutes.

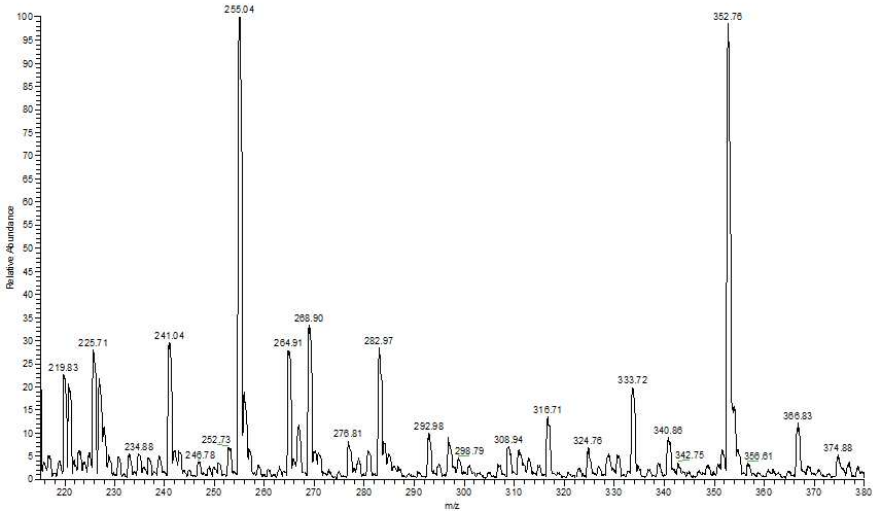

Figure 2.22 ESI-MS/MS spectrum related to ion $[M-H]^-$ at 353 m/z related to chlorogenic acid.

Table 2.2 Polyphenolic compounds in Golden Delicious juice.

Group of polyphenols	Compound	$[M-H]^-$ (m/z)	MS^2
Phenolic acids	chlorogenic acid	353.3	191.1, 179.1
	caffeic acid	179.0	135.0
	4-p-cumaroylquinic acid	337.3	191.3, 173.3, 162.9
Flavon-3-ols	(+)-catechin	289.2	254.3, 205.2, 202.9, 137.0
	(-)-epicatechin	289.2	254.3, 205.2, 202.9, 137.0
Dihydrochalcones	phloretin-2'-O-xyloglucoside	567.3	273.2
Flavonols	quercetin-3-O-glucoside	463.1	299.9, 301.0
	quercetin-3-O-galactoside	463.1	299.9, 301.0
	quercetin-3-O-xyloside	433.5	300.0, 301.0
	quercetin-3-O-arabinoside	433.5	300.0, 301.0

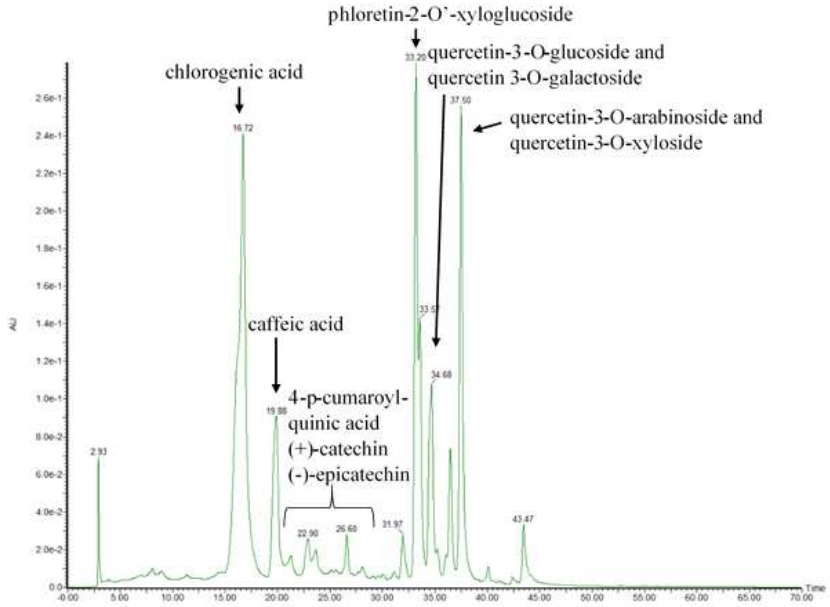

Figure 2.23 HPLC-UV Chromatogram related to Golden Delicious juice purified and concentrated by means of SPE.

2.3.6 HPLC-UV analysis of NF samples

The HPLC–UV analysis was also performed on the clarified juice (UF permeate) and on permeate and retentate samples from the NF process (Figure 2.24a-c).

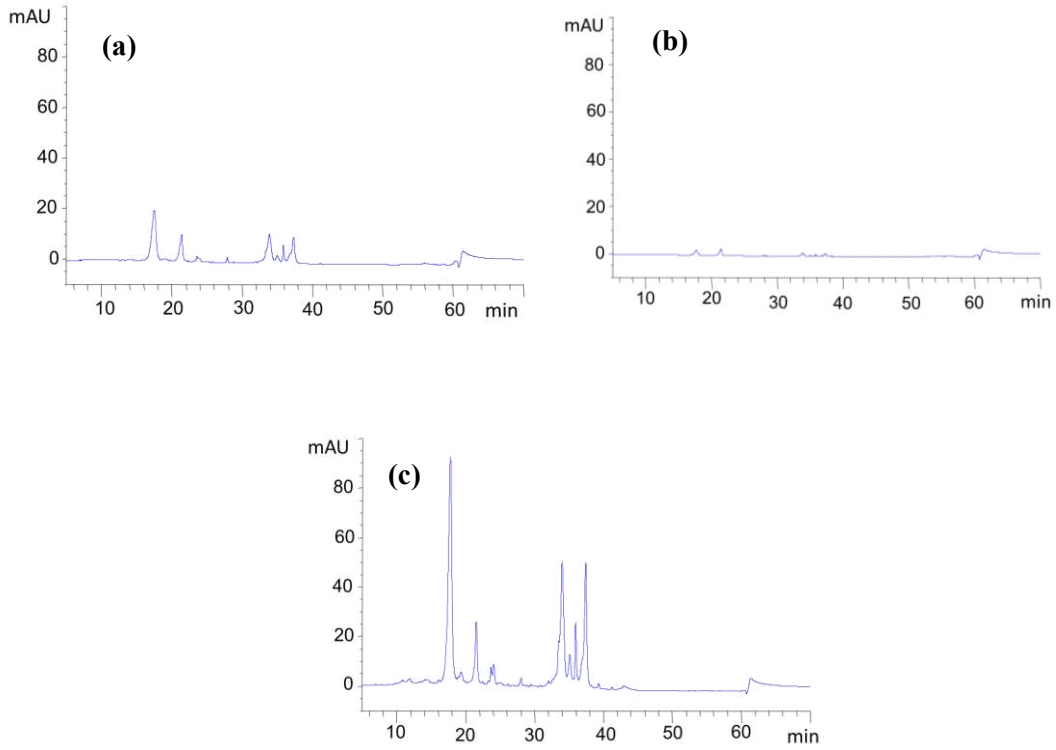

Figure 2.24 HPLC-UV chromatograms of: (a) feed, (b) NF permeate and (c) NF retentate of Golden Delicious juice.

The quantitative data were performed by external calibration curves with standards. Mean values of three replicates for each sample together the SD% values are reported in Table 2.3.

Table 2.3 Phenolic compounds detected in the HPLC analysis of clarified apple juice (feed NF), NF permeate and NF retentate (VRF = 3.3) (Data are mean ± SD, *n* = 3).

Compound	**MW** (g/mol)	**Concentration (mg/L)**		
		Clarified juice	NF permeate	NF retentate
Chlorogenic acid	354.31	16.20 ± 0.04	0.94 ±0.02	60.90 ± 2.70
Caffeic acid	180.16	3.35 ± 0.44	1.02 ± 0.02	7.50 ± 0.46

According to these data, the rejection index of the NF membrane towards chlorogenic acid and caffeic acid, calculated from Eq. (2.2), resulted of 94.2% and 69.6%, respectively. These

results are in agreement with the MWCO of the NF membrane (150–300 Da) and the molecular weight of target compounds (354.31 g/mol for chlorogenic acid and 180.16 g/mol for caffeic acid). However, several factors, which include the reduction of pore size of the membrane, adsorption of solutes, concentration polarization, and fouling, contribute to the retention of these compounds, other than molecular sieving mechanisms (Nghiem & Hawkes 2007). Similar results have been reported in literature in the treatment of different agro-food processing wastewater by using the Desal DK membrane. For example, a chlorogenic acid rejection between 88.2% and 96.7% was measured in the treatment of artichoke brines in a range of operating pressures of 4–12 bar (Cassano et al. 2016). Conidi et al. (2019) reported a rejection of about 60% towards caffeic acid in the treatment of clarified licorice wastewaters at an operating pressure of 25 bar; caffeic acid rejections of 75% have been detected in the treatment of microfiltered olive mill wastewaters at 7 bar (Tundis et al. 2020). In Figure 2.23 the effect of VRF on the concentration of chlorogenic acid and caffeic acid in the retentate fraction is reported. As expected, the concentration of both compounds increases by increasing the VRF. However, according to the measured rejections, the concentration factor observed for the chlorogenic acid is much higher than that measured for the caffeic acid. An increased concentration of chlorogenic acid and caffeoylquinic acid derivatives by increasing the VRF of the NF treatment of artichoke brine with the Desal DK membrane was also reported by Cassano et al. (2016). Other studies are needed to define and optimize the operating and fluid dynamics conditions and to improve the performance of the NF process in terms of productivity and selectivity towards phenolic compounds with respect to sugars. These preliminary studies confirm the potential of the NF process as a promising technique to obtain enriched fractions of bioactive compounds from apple juices.

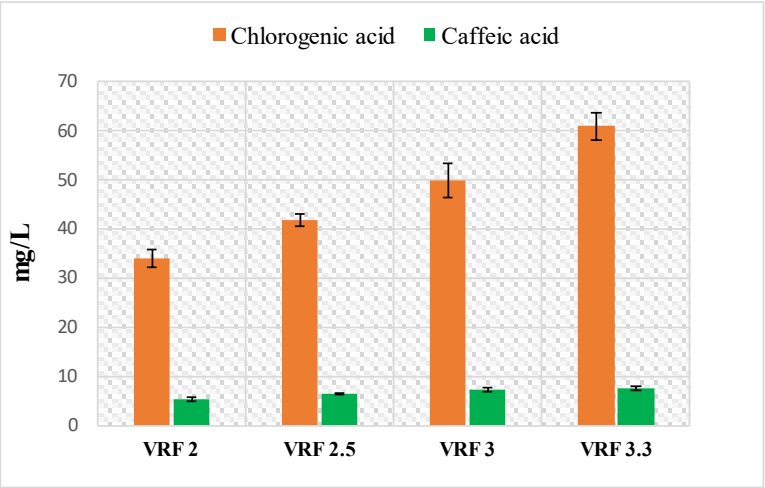

Figure 2.25 Histogram showing the increasing in concentration of chlorogenic acid and caffeic acid at the increasing of VRF values.

2.4 Conclusions

This work was aimed at the metabolic characterization through NMR spectroscopy and HPLC–UV-MS/MS of complex food matrices such as Calabrian apple juices from four different varieties and their bioactive extracts obtained through membrane technologies. By means of high-resolution multinuclear (^{1}H and ^{13}C) 1D and 2D NMR experiments, it was possible to identify 12 metabolites including organic acids and sugars all present in the four varieties. Moreover, the combination of ^{1}H NMR spectra of squeezed juices with multivariate data analysis (PCA) is able to distinguish samples from the four varieties of apples; i.e., each variety is clustered in a defined region. From the PCA score plot it is possible to highlight that Golden Delicious, Fuji, and Royal Gala varieties have a more similar metabolic composition than the juices from the Pink Lady variety. Instead, the PCA biplot shows that the sugars and malic acid contents are responsible of the separation between the four varieties. Since in no variety it has been possible to identify appreciable NMR signals in the aromatic region relating to the polyphenols typically found in apples, HPLC–UV-ESI–MS/MS was alternatively used for this purpose. Due to the higher content of phenolic compounds identified in the Golden Delicious juice, only this variety has been analyzed through mass spectrometry combined with liquid chromatography and 10 polyphenol compounds were identified. The same variety has been subjected to ultrafiltration (UF) and nanofiltration (NF) processes with the aim of producing enriched fractions in phenolic compounds. In addition to characterizing the starting juice, also the UF and the NF permeates as well as the NF retentates at different VRFs were characterized by NMR and by HPLC–UV. The analysis of the ^{1}H NMR spectra of the samples subjected to membrane processes did not show any changes in the metabolic profile of the permeate from the UF compared to the starting juice. The HPLC–UV analysis showed that the chromatographic profile remains the same among the Golden Delicious juice, UF permeate, and sample derived from NF process. This means that the phenolic compounds of interest are both in the permeate and in the retentate of the NF process, but certainly in concentration significantly different. Indeed, NF retentate is much more concentrated in phenolic compounds, even if further studies are needed to understand the separative capacity of the process of NF towards sugars, with respect to the phenolic component. Therefore, up to now, these preliminary results obtained showed that the integrated UF-NF process is able to collect fractions enriched in bioactive compounds from the starting juice of apples.

2.5 References

Abreu, A. C., & Fernández, I. (2020). NMR metabolomics applied on the discrimination of variables influencing tomato (Solanum lycopersicum). Molecules, 25(16), 3738. https://doi.org/10.3390/molecules25163738.

Belton, P. S., Delgadillo, I., Gil, A. M., Roma, P., Casuscelli, F., Colquhoun, I. J., Dennis, M. J., & Spraul, M. (1997). High-field proton studies of apple juices, Magnetic Resonance in Chemistry, 35, S52-S60. https://doi.org/10.1002/(SICI)1097-458X(199712)35:13<S52::AID-OMR212>3.0.CO;2-D.

Bingol, K. (2018). Recent advances in targeted and untargeted metabolomics by NMR and MS/NMR methods. High-Throughput, 7, 9. https://doi.org/10.3390/ht7020009.

Boyer, J., & Liu, R. H. (2004). Apple phytochemicals and their health benefits. Nutrition Journal, 3, 1-15. https://doi.org/10.1186/1475-2891-3-5.

Cassano, A., Cabri, W., Mombelli, G., Peterlongo, F., Giorno, L. (2016). Recovery of bioactive compounds from artichoke brines by nanofiltration. Food and Bioproducts Processing, 98, 257-265. https://doi.org/10.1016/j.fbp.2016.02.004.

Castro-Muñoz, R., Conidi, C., & Cassano, A. (2018). Membrane-based technologies for meeting the recovery of biologically active compounds from foods and their by-products. Critical Reviewes in Food Science and Nutrition, 59(18), 2927-2948. https://doi.org/10.1080/10408398.2018.1478796.

Conidi, C., Fucà, L., Drioli, E. & Cassano, A. (2019). A membrane-based process for the recovery of glycyrrhizin and phenolic compounds from licorice wastewaters. Molecules, 24, 2279. https://doi.org/10.3390/molecules24122279.

Cuthbertson, D., Andrews, P. K., Reganold, J. P., Davies, N. M., & Lange, B. M. (2012). Utility of metabolomics toward assessing the metabolic basis of quality traits in apple fruit with an emphasis on antioxidants. Journal of Agricultural and Food Chemistry, 60(35), 8552−8560. https://doi.org/10.1021/jf3031088.

Duda-Chodak, A., Tarko, T., Satora, P., Sroka, P., & Tuszyńsk, T. (2010). The profile of polyphenols and antioxidant properties of selected apple cultivars grown in Poland. Journal of Fruit and Ornamental Plant Research, 18(2), 39-50.

Filhoa, E.G. A., Silva, L.M.A, Wurlitzerb, N.J., Fernandesc, F.A.N., Fontelesa, T.V., Rodriguesa, S., De Brito, E.S. (2020). An integrated analytical approach based on NMR, LC–MS and GC–MS to evaluate thermal and non-thermal processing of cashew apple juice, Food Chemistry, 1-8. https://doi.org/10.1016/j.foodchem.2019.125761.

Francini, A., & Sebastiani, L. (2013). Phenolic compounds in apple (Malus x domestica Borkh.): compounds characterization and stability during postharvest and after processing. Antioxidants, 2(3), 181-193. https://doi.org/10.3390/antiox2030181.

Gerhauser, C. (2008). Cancer chemopreventive potential of apples, apple Juice, and apple components. Planta Medica, 74(13), 1608-1624. https://doi.org/10.1055/s-0028-1088300.

Gunathilake, C., & Considine, M. (2018). Flavonoids rich apple for healthy life. MOJ Food Processing & Technology, 6(1), 89-91. https://doi.org/10.15406/mojfpt.2018.06.00149.

Harker, F. R., Gunson, F. A., & Jaeger, S. R. (2003). The case for fruit quality: an interpretive review of consumer attitudes, and preferences for apples. Postharvest Biology and Technology, 28(3), 333-347. https://doi.org/10.1016/S0925-5214(02)00215-6.

Iaccarino, N., Varming, Petersen, M. A., Viereck, N., Schütz, B., Toldam-Andersen, T. B., Randazzo, A., & Engelsen, S.B. (2019). Ancient Danish apple cultivars - A comprehensive metabolite and sensory profiling of apple juices. Metabolites, 9(7), 139. https://doi.org/10.3390/metabo9070139.

Jeong, S.W., Kim, G.-S., Lee, W. S., Kim, Y.-H., Kang, N. J., Jin, J. S., Lee, G. M., Kim, S. T., El-Aty, A. M. A., Shim, J.-H., & Shin, S. C. (2015). The effects of different night-time temperatures and cultivation durations on the polyphenolic contents of lettuce: application of principal component analysis. Journal of Advanced Research, 6(3), 493-499. https://doi.org/10.1016/j.jare.2015.01.004.

Kahle, K., Kraus, M., & Richling, E. (2005). Polyphenol profiles of apple juices. Molecular Nutrition & Food Research, 49, 797-806. https://doi.org/10.1002/mnfr.200500064.

Koutsos, A., Tuohy, K. M., & Lovegrove, J. A. (2015). Apples and cardiovascular health—is the gut microbiota a core consideration?. Nutrients, 7(6), 3959-3998. https://doi.org/10.3390/nu7063959.

Kumar, S., Bink, M. C. A. M., Volz, R. K., Bus, V. G. M., & Chagné, D. (2012). Towards genomic selection in apple (Malus × domestica Borkh.) breeding programmes: prospects, challenges and strategies. Tree Genetics and Genomes, 8, 1-14. https://doi.org/10.1007/s11295-011-0425-z.

Lima, L. G. B., Montenegro, J., Pimentel de Abreu, J., Barros Santos, M. C., Pimenta do Nascimento, T., Santos, M., Ferreira, A. G., Cameron, L. C., Ferreira, M. S. L., & Teodoro, A. J. (2020). Metabolite profiling by UPLC-MSE, NMR, and antioxidant properties of Amazonian fruits: Mamey apple (Mammea Americana), Camapu (Physalis Angulata), and Uxi (Endopleura Uchi). Molecules, 25(2), 342. https://doi.org/10.3390/molecules25020342.

Mamat, S. F., Azizan, K. A., Baharum, S. N., Noor, N. M., & Aizat, W. M. (2020). GC-MS and LC-MS analyses reveal the distribution of primary and secondary metabolites in mangosteen (Garcinia mangostana Linn.) fruit during ripening. Scientia Horticulturae, 262, Article 109004. https://doi.org/10.1016/j.scienta.2019.109004.

Nath, K., Dave, H. K., & Patel, T. M. (2018). Revisiting the recent applications of nanofiltration in food processing industries: progress and prognosis. Trends in Food Science & Technology, 73, 12-24. https://doi.org/10.1016/B978-0-12-815866-1.00003-0.

Nghiem, L. D., & Hawkes, S. (2007). Effects of membrane fouling on the nanofiltration of pharmaceutically active compounds (PhACs): mechanisms and role of membrane pore size. Separation and Purification Technology, 57(1), 176-184. https://doi.org/10.1016/j.seppur.2007.04.002

Olennikov, D. N., Vasilieva, A. G., & Chirikova, N. K. (2020). Fragaria viridis fruit metabolites: variation of LC-MS profile and antioxidant potential during ripening and storage. Pharmaceuticals, 13(9), 262. https://doi.org/10.3390/ph13090262.

Pirlak, L., Ünüvar, G., & Ersoy, N. (2017). Determination of antioxidant activities of some apple cultivars. Horticultural Science, 44(3), 120-125.

https://doi.org/10.17221/276/2015-HORTSCI.

Rana, S., & Bhushan, S. (2016). Apple phenolics as nutraceuticals: assessment, analysis and application. Journal of Food Science and Technology, 53(4), 1727-1738. https://doi.org/10.1007/s13197-015-2093-8.

Salvino, R., Colella, M., De Luca, G. (2021). NMR-based metabolomics analysis of Calabrian citrus fruit juices and its application to industrial process quality control. Food Control, 121, Article 107619. https://doi.org/10.1016/j.foodcont.2020.107619.

Seger, C., & Sturm, S. (2007). Analytical aspects of plant metabolite profiling platforms: current standings and future aim. Journal of Proteome Research, 6(2), 480-497. https://doi.org/10.1021/pr0604716.

Sobolev, A. P., Mannina, L., Proietti, N., Carradori, S., Daglia, M., Giusti, A. M., Antiochia, R., & Capitani, D. (2015). Untargeted NMR-based methodology in the study of fruit metabolites, Molecules, 20(3), 4088-4108. https://doi.org/10.3390/molecules20034088.

Tallapally, M., Sadiq, A. S., Mehtab, V., Chilakala, S., Vemula, M., Chenna, S., & Upadhyayula, V. (2020). GC-MS based targeted metabolomics approach for studying the variations of phenolic metabolites in artificially ripened banana fruits. LWT - Food Science and Technology, 130, Article 109622. https://doi.org/10.1016/j.lwt.2020.109622.

Ting, V. J. L., Silcock, P., Bremer, P. J., & Biasioli, F. (2013). X-ray micro-computer tomographic method to visualize the microstructure of different apple cultivars. Journal of Food Science, 78(11), E1735-E1742. https://doi.org/10.1111/1750-3841.12290.

Tomita, S., Nemoto, T., Matsuo, Y., Shoji, T., Tanaka, F., Nakagawa, H., Ono, H., Kikuchi, J., Ohnishi-Kameyama, M., & Sekiyama, Y. (2015). A NMR-based, non-targeted multistep metabolic profiling revealed L-rhamnitol as a metabolite that characterised apples from different geographic origins. Food Chemistry, 174, 163-172. https://doi.org/10.1016/j.foodchem.2014.11.028.

Tundis, R., Conidi, C., Loizzo, M. R., Sicari, V., & Cassano, A. (2020). Olive mill wastewater polyphenol-enriched fractions by integrated membrane process: a promising source of antioxidant, hypolipidemic and hypoglycaemic compounds. Antioxidants, 9(7), 602. https://doi.org/10.3390/antiox9070602.

Vallée Marcotte, B., Verheyde, M., Pomerleau, S., Doyen, A., Couillard, C. (2022). Health Benefits of Apple Juice Consumption: A Review of Interventional Trials on Humans. Nutrients, 14, 821. https://doi.org/10.3390/nu14040821.

Vermathen, M., Marzoratia, M., & Vermathen, P. (2012). Exploring high-resolution magic angle spinning (HR-MAS) NMR spectroscopy for metabonomic analysis of apples. CHIMIA International Journal for Chemistry, 66(10), 747-751. https://doi.org/10.2533/chimia.2012.747.

Chapter 3: Partial Removal of Sugar from Apple Juice by Nanofiltration and Discontinuous Diafiltration

This work was published as: Martina Gaglianò, Carmela Conidi, Giuseppina De Luca, Alfredo Cassano "Partial Removal of Sugar from Apple Juice by Nanofiltration and Discontinuous Diafiltration", Membranes (2022) 12(7):712

The author was involved in planning and performing the experiments, as well as in discussing and interpreting the results and manuscript preparation.

3.1 Introduction

In Chapter 2, it was probed that NF in batch concentration mode is a promising technology for obtaining apple juice concentrated in bioactive compounds. However, the metabolomic composition of apple juice is quite complex. The molecular masses of valuable compounds are close to those of sugars (mono and disaccharides), which means that while the polyphenols are concentrated with NF membranes, the sugars are simultaneously concentrated, and this is undesirable if the goal is a product only with a marked phenolic component. Furthermore, having a drink with a low sugar content is also health-wise attractive. Indeed, New World Health Organization (WHO) guidelines recommend that adults and children reduce their daily intake of free sugars to less than 10% of their total energy intake (WHO 2015). A further reduction to less than 5% of their total caloric intake—equivalent to about 25 g of sugar per day for a person with a healthy body weight—provides additional health benefits (WHO 2018). However, partially removing sugars in fruit juices without compromising their bio-functional properties represents a significant technological challenge. Although chromatographic separations continue to attract extensive interest for the target separation of sugars, these processes are difficult to apply on a large scale. The alternatives may include biochemical transformations of sugars into corresponding compounds such as ethanol, oligosaccharides, or organic acids. Still, these would lead to a significant change in the fruit juice, which does not align with the previous goal. Thus, it is worthwhile to continue investigating and improving the NF process due to its numerous advantages over conventional technologies. To enhance membrane selectivity towards target compounds and achieve a high purity of biomolecules, NF can be operated in diafiltration (DF) mode (Conidi et al. 2022). Diafiltration involves the addition of water or any other solvent or buffer to the feed solution to enhance the degree of separation of membrane-

retained macrosolutes from membrane-permeable microsolutes (Doran 2013). It can be performed in a continuous or discontinuous mode (Loewe et al. 2022). In continuous diafiltration, the solvent is added to the system at the same rate as permeate flux. Discontinuous diafiltration, instead, involves first diluting the sample with water and then concentrating the diluted sample back to its original volume by membrane filtration. Each subsequent dilution should remove more of the small molecules (Schwartz 2003). Typical applications have been studied for the recovery of biochemical products from their fermentation broths (Khunnonkwao et al. 2018; Zhou et al., 2006), the purification of water-soluble nanoparticles (Sweeney et al. 2006), the reduction of alcohol content from alcoholic beverages (Ambrosi et al. 2020), the purification of phycocyanin from Spirulina (Arthrospira maxima) (Nisticò et al. 2022), the separation of sugars from biologically active compounds (Almanasrah et al. 2015; Conidi et al. 2022) among many others. The number of publications dealing with sugar reduction in apple juices (or other natural juices) is very limited. Wei et al. (2007) investigated the separation of polyphenols and sugars in apple juice by a loose NF membrane (MWCO 1 kDa) obtaining a sugar-reduced juice as a permeate stream. The results showed that at four bar, the sugar recovery in permeate was around 72% and the recovery of polyphenols in retentate was around 43%. Ceramic tubular UF membranes, with an MWCO of 15 kDa, have recently been investigated to produce a concentrate fraction from apple−cranberry cloudy juice with the simultaneous removal of some amount of sugars (Barańska et al. 2020). Pruksasri et al. (2020) proposed a combination of mechanical pre-fractionation and NF for the reduction of sugar in cloudy apple juice. In the first step, a fruit flesh juice (stream A) with a low content of polyphenols is produced after peeling and coring a certain amount of apple (45% of raw material). In the second step, the flesh juice is treated by NF/diafiltration with the production of a clarified juice (permeate) with low sugar content. The NF permeate is finally mixed with stream B enriched in phenolic compounds produced by milling, pressing, and centrifugation of the rest of the apples together with peels and cores from stream A. Thus, mechanical fractionation was considered as a separation step to reduce the losses of biofunctional compounds.

Bearing in mind that the reduction of sugar in natural fruit juices is a very challenging separation task and its applicability depends on the rejection and selectivity properties of membranes, we investigated an integrated NF/diafiltration approach without peeling apples, thus avoiding any sort of the previous pretreatment. The diafiltration process may contribute to reducing fouling phenomena with a consequent change in selectivity to promote the diffusion of sugars through the membranes. Furthermore, separation characteristics of NF membranes are not only based on size exclusion and this could play in favor of the rejection

of polyphenols ahead of sugars during the NF/diafiltration process. In the light of these considerations, the present study evaluated the feasibility of phenolic compounds' separation from sugars in apple juice by using three different spiral-wound commercial membranes with an MWCO in the range of 200–500 Da. The performance of selected membranes was assessed in terms of productivity (permeate fluxes) and selectivity towards target compounds.

3.2 Materials and Methods

3.2.1 Chemicals

Folin−Ciocalteu phenol reagent, gallic acid, and sodium hydroxide were purchased from Sigma Aldrich (Milan, Italy), while sodium carbonate anhydrous was purchased from Carlo Erba (Milan, Italy). "Yellow line" enzymatic kits were supplied by Roche Diagnostics (Darmstadt, Germany).

3.2.2 Feed Solution

Apple juice was supplied by Gioia Succhi S.r.l. (San Ferdinando, Reggio Calabria, Italy) and processed according to the procedure reported by Gaglianò et al. (2021). The juice was clarified by using a laboratory plant equipped with hollow-fiber UF membranes made of polyethersulfone with an MWCO of 500 kDa (FB-02-FC from Microdyn Nadir, Wiesbaden, Germany). Then, the clarified juice was submitted to a discontinuous diafiltration, followed by an NF process in batch concentration mode. The clarified apple juice composition is reported in Table 3.1.

Table 3.1 Composition of clarified apple juice subjected to a diafiltration−nanofiltration process.

Parameter	Value
Glucose (g/L)	17.2 ± 1.3
Fructose (g/L)	43.7 ± 2.4
Total phenolic content (mg GAE/L)	241.5 ± 8.1
Total soluble solids (°Brix)	7.0 ± 0.1
pH	3.78 ± 0.02

3.2.3 Diafiltration–Nanofiltration Process: Experimental Set-Up and Procedure

NF-based diafiltration experiments were performed by using a bench plant (DeltaE S.r.l., Cosenza, Italy) equipped with a stainless steel housing able to accommodate a spiral-wound element with a dimension of 1.8" × 1.2" (membrane area of about 0.23 m2). The experimental setup consists of a high-pressure pump (Cat Pumps, Milano, Italy, Model 3CP1221), a 5 L stainless steel feed tank, a digital flowmeter (SM6000, ifm electronic gmbh, Essen, Germany), two pressure gauges (Wika Instrument, Lawrenceville, GA, USA), and a control panel. The feed temperature was adjusted by circulating tap water in the two-layered feed tank. The pressure was monitored at the entrance and exit of the membrane module through a frequency inverter and a needle valve located after the membrane module. NF experiments were performed by using three selected spiral-wound membrane modules supplied by Microdyn-Nadir (Wiesbaden, Germany). Their properties are summarised in Table 3.2.

Table 3.2 Characteristics of selected membranes according to manufacturers unless otherwise stated.

Membrane type	**TS40**	**XN45**	**NP030**
Membrane material	TFC	TFC	PES
Configuration	spiral-wound	spiral-wound	spiral-wound
Max. operating pressure (bar)	41	41	35
Max. operating temperature (°C)	50	50	70
pH	1-12	1-12	0-14
Surface area (m^2)	0.23	0.23	0.23
Nominal MWCO (Da)	200-300	300-500	300-400
Contact angle (°)	30[a]	57[b]	80[c]
Water permeability at 25 °C (kg/m^2hbar)	4.48[d]	6.12[d]	2.99[d]

TFC, thin-film composite, PES, polyethersulphone; [a] data from Zdarta et al. 2020; [b] data from Peiris et al. 2010; [c] data from Boussu et al. 2008; [d] own measurements.

The diafiltration volume (ratio of the solvent volume added per volume of feed solution) was calculated as follows (Mittal et al. 2020):

$$DV = \frac{V_p}{V_0} = \frac{V_w}{V_0} \quad (3.1)$$

where V_p and V_0 are the volumes of permeate and feed solution, respectively, and V_w is the volume of water added during the diafiltration process.

The NF process was operated at a transmembrane pressure (TMP) of 25 bar, an axial feed flowrate (Q_f) of 7 L/min and a temperature (T) of 25±1 °C during the diafiltration step. Then, the juice was concentrated according to a batch concentration configuration, in the same operating conditions, up to a volume reduction factor (VRF) of 4. VRF is defined as the ratio of feed volume to residual retentate volume according to the following equation:

$$VRF = \frac{V_f}{V_r} = 1 + \frac{V_p}{V_r} \quad (3.2)$$

where V_f, V_p and V_r are the volume of the feed, permeate and retentate, respectively. During both diafiltration and batch concentration steps the permeate flux was gravimetrically measured at different time intervals. The flow chart of the experimental set-up is shown in Figure 3.1. The fouled membranes were cleaned with an enzymatic solution (Ultrasil 53, 1.0%, 40 °C, 60 min) followed by an alkaline cleaning (Ultraclean WA, 0.2%, 40 °C, 60 min) and final rinsing with tap water. The cleaning efficiency was evaluated by the flux recovery method (Chen et al., 2006) measuring the water permeability before and after the enzymatic/ chemical cleaning.

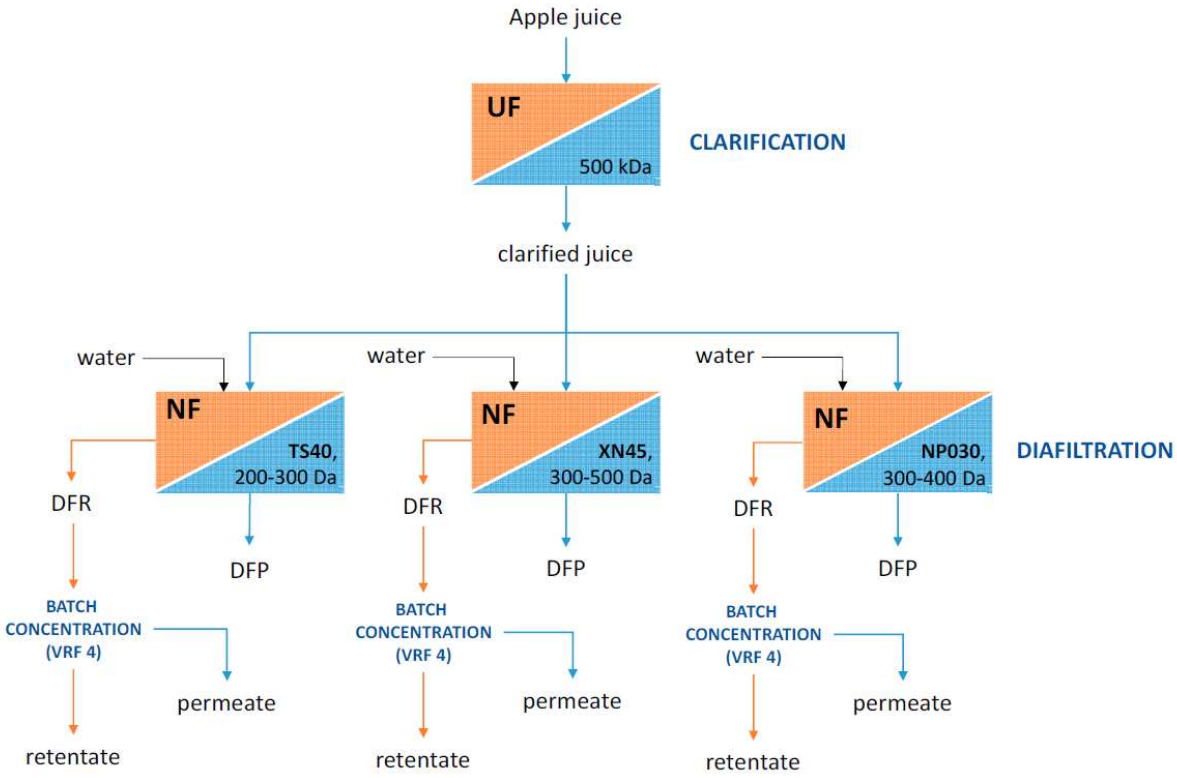

Figure 3.1 Flow chart of the experimental set-up (UF, ultrafiltration; NF, nanofiltration; DFR, diafil- trated retentate; DFP, diafiltrated permeate).

3.2.4 Performance parameters

The membrane performance was measured in terms of permeate flux, J_p, concentration factor, $CF_{i\ (R,P)}$, and recovery rate, $R_{i(R,P)}$ (%), of a certain species.

The volumetric flux of permeate was calculated according to the following equation:

$$J_p = \frac{V_P}{A \cdot t} \quad (3.3)$$

where J_p is the volumetric flux of permeate (L/m^{2}h), V_P is the volume of collected permeate (L), t is the time (h) and A the membrane permeation area (m^2).

The recovery rate (%) of a species i is obtained by its total mass in either permeate or retentate divided by its total mass in feed solution (Sun et al. 2017; Wei et al. 2007):

$$R_{i(R,P)} = \frac{C_{i(R,P)} \cdot V_{i(R,P)}}{C_{i(F)} \cdot V_{i(F)}} \quad (3.4)$$

where $C_{i(R,P)}$ and $V_{i(R,P)}$ are the concentration and the volume of species i in either permeate or retentate solution, while $C_{i(F)}$ and $V_{i(F)}$ are the concentration and the volume of species i in the feed.

The volume $V_{i(R)}$ of species i in retentate solution and the volume of species i in the feed $V_{i(F)}$ are equal when samples are collected at different DV during diafiltration. This implies that volumes can be simplified in Eq. (3.4) and the yield values for specific components throughout the diafiltration process can be calculated as a fraction of the original solute concentration remaining in the feed (Conidi et al. 2022):

$$R_{i(R)} = \frac{C_{i(R)}}{C_{i(F)}} \quad (3.5)$$

The concentration factor (CF) is the concentration of species i in either permeate or retentate solution $C_{i(R,P)}$ divided by its concentration in the feed solution $C_{i(F)}$ (Wei et al. 2007):

$$CF_{i(R,P)} = \frac{C_{i(R,P)}}{C_{i(F)}} \quad (3.6)$$

The adsorbed phenolics and sugars amount Q_{ADS} (mg/m^2) on the membrane surface at different VRF values was determined as follows (Conidi et al. 2014):

$$Q_{ADS} = \frac{C_F V_F - (C_R V_R + C_P V_P)}{A} \quad (3.7)$$

where V_F, V_R and V_P are the feed, retentate and permeate volumes, respectively; C_R and C_P are the concentration of phenolics or sugars in the retentate and permeate streams, respectively, and A the membrane surface area.

3.2.5. Analytical Measurements

The collected samples include: NF feed, NF retentates at different DV values, NF retentate and NF permeate at different VRF values. Total Dissolved Solids (TDS), total phenolic content (TPC), D-Glucose and D-Fructose were measured. The results of the analytical measurements were expressed as mean ± standard deviation (SD) of three independent determinations.

3.2.5.1. Total dissolved solids

Total dissolved solids (TDS) measurements were carried out by using a hand refractometer (Atago Co., Ltd., Tokyo, Japan) with a scale range of 0–32 °Brix.

3.2.5.2. Total phenolic content (TPC)

The total phenolic content (TPC) was determined by the Folin-Ciocalteu method (Singleton et al. 1999). The sample (0.2 mL) was mixed with 1 mL of 10% (*w/v*) Folin-Ciocalteu reagent and 0.8 mL of a 7.5% (*w/v*) sodium carbonate solution. After 30 min of incubation at room temperature, the absorbance of the resulting solution was measured at 765 nm against a blank. Spectrophotometric measurements were performed with Shimadzu UV-160A UV-visible spectroscopy system. The TPC was calculated on the basis of the calibration curve of gallic acid and expressed as mg of gallic acid equivalents per liter (mg GAE/L).

3.2.5.3. D-glucose and D-fructose quantification

D-glucose and D-fructose were determined enzymatically in a specific way. A multi-parametric automatic analyzer (iMagic-M9, Darmstadt, Germany) was used to independently perform all the manual analytical procedures required for enzymatic tests. The system automatically collects and dispenses reagents and samples, and calculates the analytical data. Detailed procedures used for sample preparation, enzymes, and reactions involved in the determinations of the sugars of interest are reported by R-Biopharm AG (Enzytec Liquid D-Glucose, 2017; Enzytec Liquid D-Glucose/D-Fructose, 2017).

3.3 Results and discussion

3.3.1. Permeate flux evaluation

Permeate fluxes and permeate quality are the most important aspects for the selection of a proper membrane (Laorko et al. 2010). Figure 3.2 shows the permeate flux (J_p) as a function of diafiltration volumes for all the investigated membranes in the selected operating conditions. For each membrane, the permeate flux increased by increasing the diafiltration volume. The addition of water during the process reduced the viscosity of the feed solution (Servent et al. 2020) and limited the formation of the concentration polarization layer on the membrane's surface. Therefore, the clogging of membrane pores was reduced and the transport of micro-solutes through the membrane was facilitated (Nguyen et al. 2016). The XN45 membrane exhibited the highest permeate flux with values higher than 60 kg/m^{2}h at a DV of 5.5. On the other hand, the NP030 membrane showed much lower fluxes in comparison with TS40 and XN45 membranes, whose greater hydrophilicity played an important role in water solution transport through the membrane (Lyu et al. 2016; Nicolini et al. 2016).

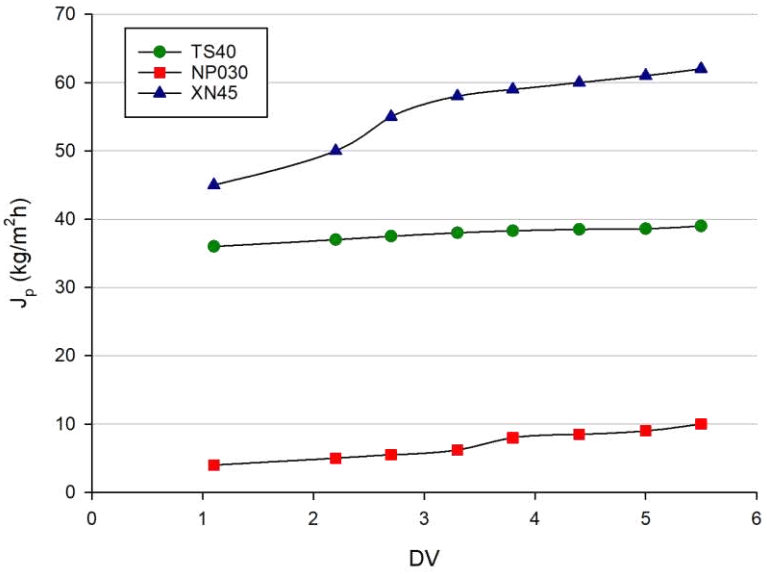

Figure 3.2. Diafiltration of clarified apple juice with selected membranes. Permeate flux as a function of diafiltration volume (Operating conditions: TMP, 25 bar; Q_f, 7 L/min; T, 25±1 °C).

Figure 3.3 shows the permeate flux (J_p) as a function of VRF during the NF process of the diafiltered juice with selected membranes according to the batch concentration configuration and in the same operating conditions of the diafiltration process. For XN45 and TS40 membranes, the build-up of solutes at the upstream interface (concentration polarization)

determined a rapid permeate flux decay, followed by a long and gradual decline towards a steady-state limit value. Fouling mechanisms, such as the adsorption of particles on the membrane pore walls and pore plugging, are additional phenomena (de Oliveira and de Barros 2011). In the selected operating conditions steady-state values for XN45 and TS40 membranes were of the order of 48 kg/m^{2}h and 8 kg/m^{2}h, respectively. For the NP030 membrane, the initial permeate flux was about 10 kg/m^{2}h, much lower than those observed for the other two investigated membranes. In addition, for this membrane, the permeate flux reduction at VRF 4 was only about 20% in relation to the initial value.

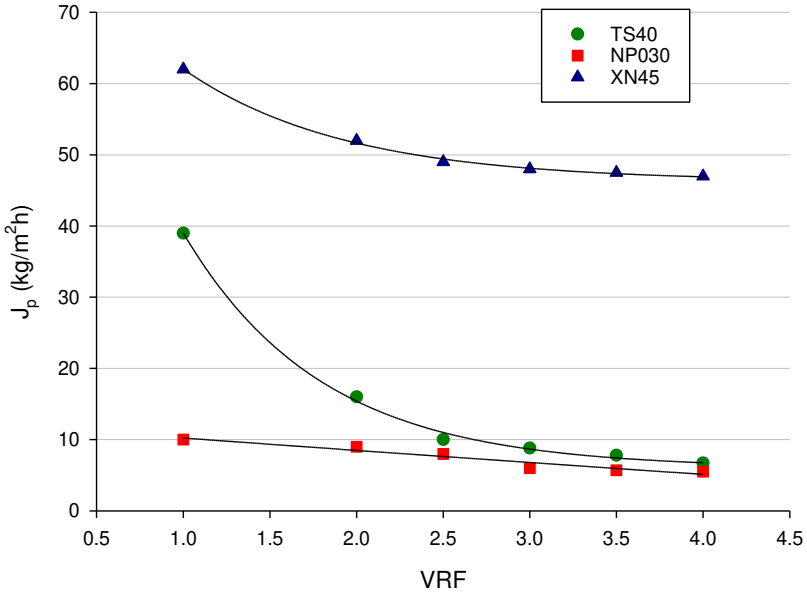

Figure 3.3 Nanofiltration in batch concentration mode of diafiltered apple juice with selected membranes. Permeate flux as a function of volume reduction factor (Operating conditions: TMP, 25 bar; Q_f, 7 L/min; T, 25±1 °C).

Fot all the selected membranes, the cleaning efficiency after the cleaning protocol was higher than 90%.

3.3.2. Recovery rate of D-glucose, D-fructose and TPC during discontinuous diafiltration

The recovery rate of both phenolic compounds and carbohydrates in the retentate stream was plotted as a function of the diafiltration volume, as shown in Figure 3.4. The selected membranes showed a similar behaviour: in particular, the recovery rate of both sugars and TPC decreased in the retentate by increasing the diafiltration volume indicating that the addition of distilled water as washing solvent during the diafiltration process caused the removal of these compounds in the clarified extract. Nevertheless, carbohydrates and TPC were removed at varying degrees for different membranes. Regardless of the diafiltration volume, the separation factor between TPC and sugars remained almost unchanged during the process: in fact the more the number of diavolumes increased, the more the sugars passed into the permeate in the same ratio in which the polyphenols also passed. This has a negative and a positive aspects. The negative aspect is linked to the fact that the separation between the compounds in the selected operating conditions cannot be improved with the addition of water, but this is also an advantage from an economic point of view because the separation reached at DV 5.5 is almost the same obtained at DV 1.1. This implies a lower consumption of fresh water to achieve the same result.

Although the NP030 membrane was characterized by lower permeate fluxes, it allowed for achieving a greater separation factor between TPC and carbohydrates. At DV of 1.1, nearly 36% of D-Glucose and 34% of D-fructose were removed, while 95% of TPC remained in the retentate juice. According to Pruksasri et al. (2020), the degree of sugar reduction of about 30-40% could be an appropriate target. Therefore, a single diananofiltration process accomplished with an appropriate membrane and proper selected operating conditions may be applicable to remove a sufficient amount of sugar and recover efficiently phenolic compounds without losing their activity. In this way, a diafiltered retentate as the high added-value product can be obtained with significant advantages from both nutritional and economical points of view.

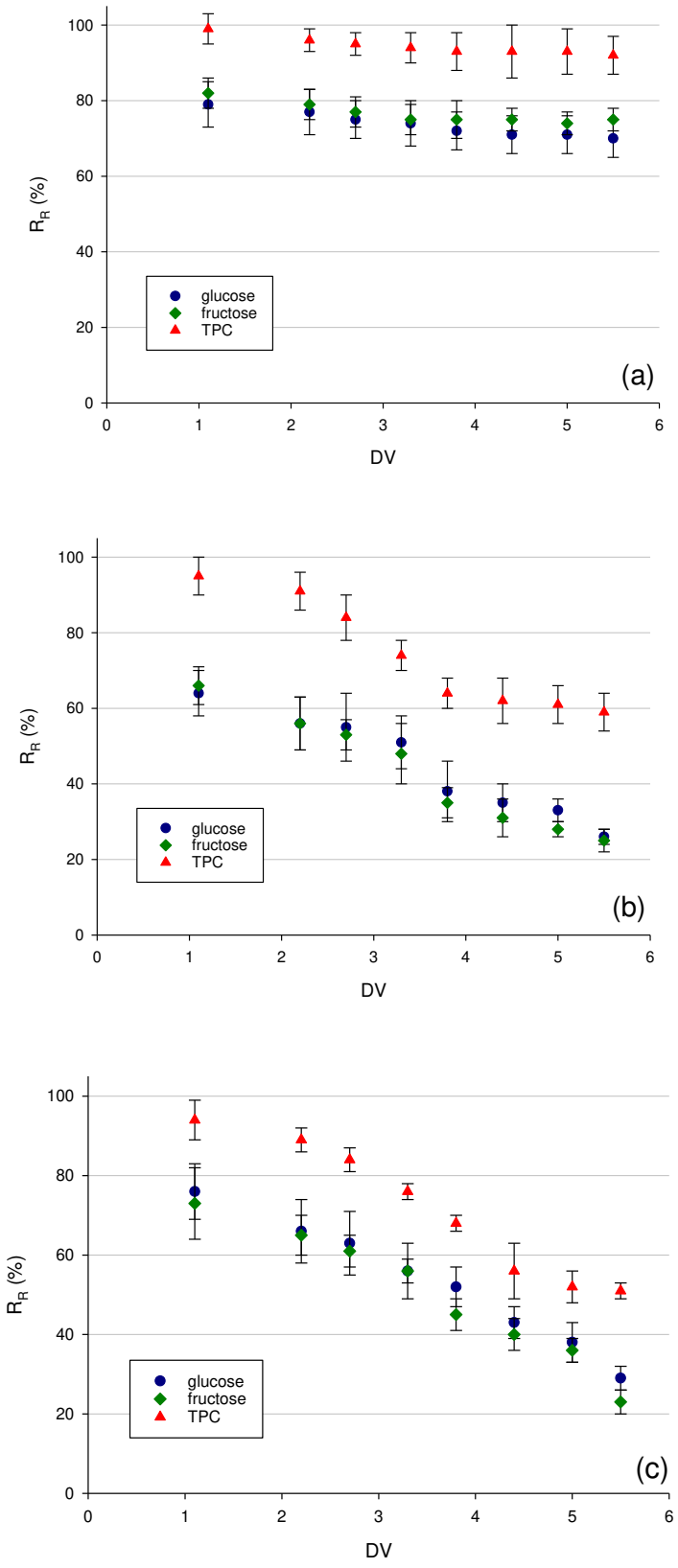

Figure 3.4. Recovery rate of total phenolic compounds, glucose and fructose in the retentate stream during diafiltration with (a) TS40 (b) NP030 and (c) XN45 membranes.

3.3.3. Concentration factor of D-glucose, D-fructose and TPC during nanofiltration in batch concentration mode

After diafiltration, the clarified juice was concentrated up to VRF 4 with each one of the investigated membranes. In this way, it was possible to evaluate the behaviour of each membrane in retaining and separating the compounds of interest in concentration mode. It is known that rejection is controlled by molecular size and interaction force between the membrane and the solute (Suhalim et al. 2022). Among the investigated membranes, the TS40 had a higher rejection for sugars and polyphenols due to its lower MWCO of 200-300: in fact, the concentration factor at VRF 4 was 3.5 for TPC and 2.6 for sugars, respectively (Figure 3.5a). Therefore, only about 12.5% of the polyphenols were lost during the batch concentration process, while about 35% of sugars were further removed. The XN45 membrane showed the same trend: a higher concentration factor for polyphenols was observed concerning glucose and fructose. However, this membrane exhibited a worst separation gap between carbohydrates and TPC and a major removal in the retentate sample for all compounds. The concentration factor at VRF 4 was 2.3 for TPC, 2.0 for fructose, and 1.6 for glucose, respectively (Figure 3.5c). On the contrary, for the NP030 membrane, the concentration factor for glucose and fructose was higher than polyphenols, independently of the VRF value.

For all selected membranes, the retention level was relatively high if compared with the molecular weight of glucose (180.1559 g/mol) and fructose (180.16 g/mol). This behaviour might be explained by assuming that other phenomena, in addition to the steric hindrance, affect the retention coefficients including interactions between the membrane material and the solutes, as well as association of sugars with phenolic compounds (Muñoz et al. 2021). In addition, for all selected membranes, a significant increase in phenolic compounds was observed by increasing the VRF of the process. An increased concentration of phenolic compounds as a function of the VRF of the process was also observed in the treatment of the mate bark aqueous extracts (Prudêncio et al. 2012) and artichoke brine (Cassano et al. 2016), with spiral-wound NF membranes characterized by an approximate MWCO of 150–300 Da (Desal HL and Desal DG from GE Osmonics, respectively). Different factors, including the surface morphology, pore size distribution, and adhesion in the membrane may contribute to this phenomenon (Tsuru et al 2001).

In Figure 3.6, the recovery rate of total phenolic compounds, glucose, and fructose in the retentate stream as a function of VRF for all selected membranes is shown. At VRF 4 more than 70% of phenolic compounds were recovered in the retentate of the TS40 membrane; at the same time, the removal efficiency of glucose and fructose was 59% and 56%, respectively (corresponding to a recovery factor in the retentate of 41% and 44%, respectively).

For membranes NP030 and XN45, the recovery factors of both phenolic compounds and sugars in the retentate stream were significantly lower than those observed for the TS40 membrane. Indeed, for the NP030 membranes, the recovery factors of sugars and phenolic compounds were about 10% and 20%, respectively. Similar values were observed for the recovery of sugar compounds in the retentate of the XN45 membrane while for phenolic compounds the recovery factor at VRF 4 was 26%. Therefore, the global result indicated the TS40 membrane was the best one to preserve phenolic compounds of apple juice through a combination of diafiltration and batch concentration processes while reducing the content of sugars by the order of 60%.

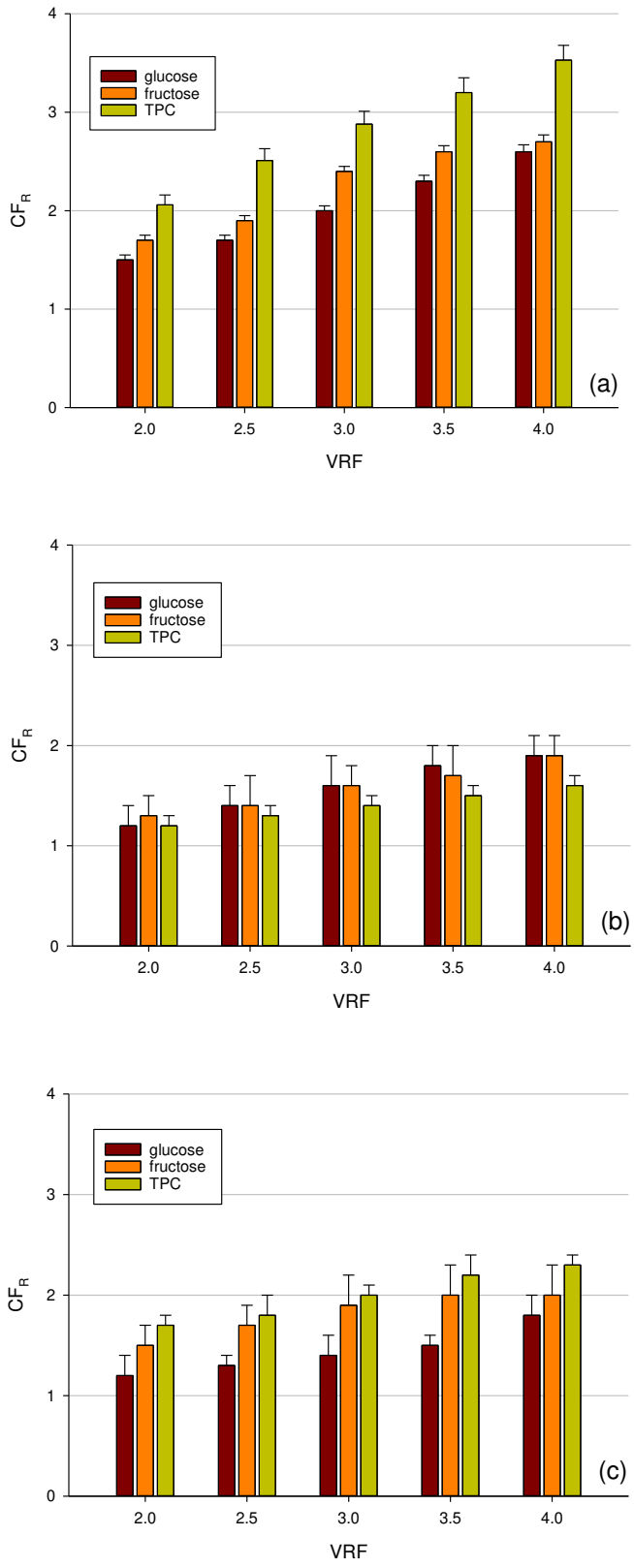

Figure 3.5 Concentration factor of total phenolic compounds, glucose and fructose in the retentate stream during the concentration with (a) TS40 (b) NP030 and (c) XN45 membranes.

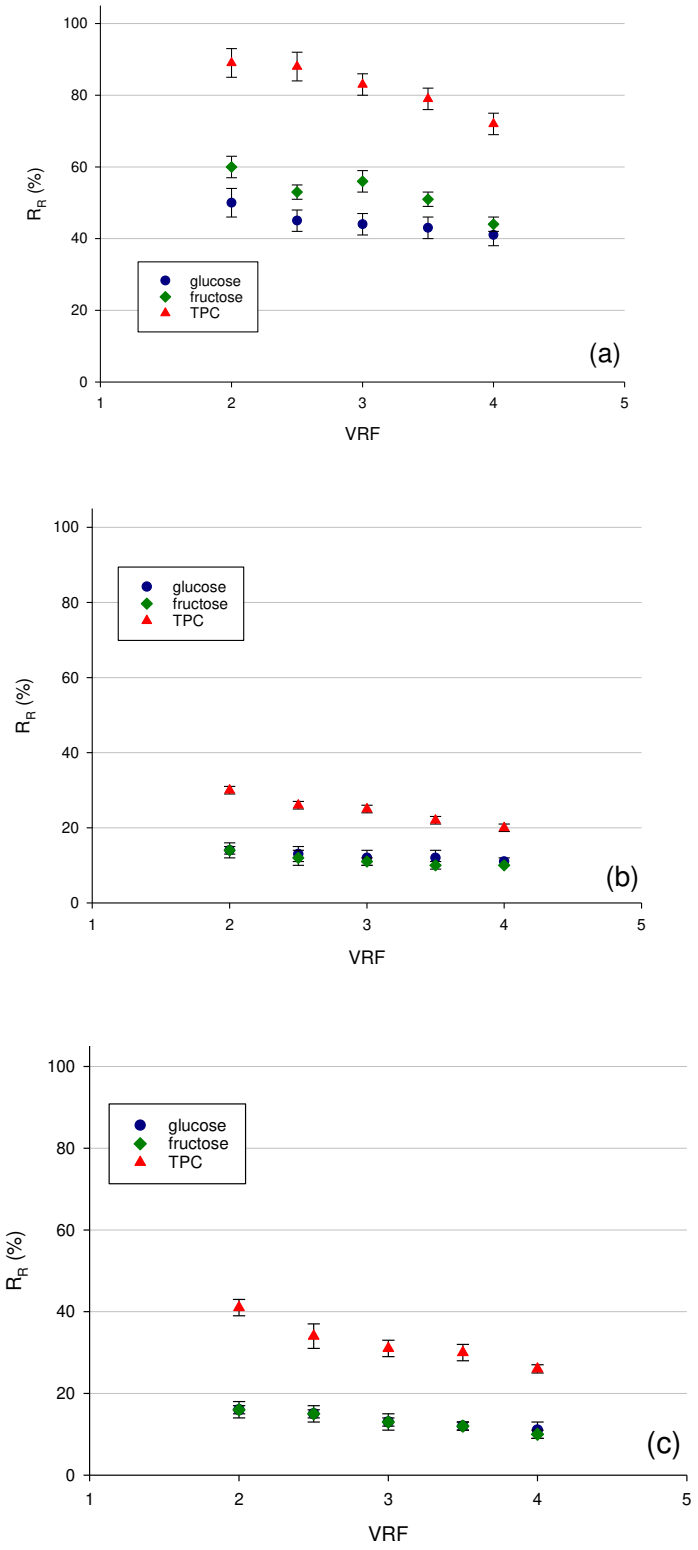

Figure 3.6 Recovery rate of total phenolic compounds, glucose and fructose in the retentate stream during the batch concentration process with (a) TS40 (b) NP030 and (c) XN45 membranes.

3.3.4. Mass balance and adsorption of sugars and TPC

The mass balance of the whole filtration process, which includes the initial feed solution, the diafiltrated solution, the permeate stream, and the remaining retentate can give an insight into deposit formation on the membrane surface and eventual pore blocking. Table 3.3 shows the mass balance related to sugars and TPC in both diafiltration and concentration processes for the selected membranes. As it can be seen, the batch concentration configuration is characterized by a substantial deviation from the mass balance in comparison to diafiltration. These results can be attributed to pore blocking phenomena due to the adsorption of monosaccharides and low molecular weight phenolic compounds on both the outer and the inner membrane surface.

Table 3.3 Mass balance (%) of glucose, fructose and TPC in diafiltration and batch concentration processes for selected membrane.

Membrane type	Process	Component		
		Glucose	**Fructose**	**TPC**
TS40	Diafiltration	94.62	93.56	97.49
	Batch concentration	68.81	68.19	81.51
NP030	Diafiltration	95.83	99.99	90.98
	Batch concentration	59.07	59.63	54.33
XN45	Diafiltration	100.00	99.99	99.99
	Batch concentration	63.13	72.45	58.00

The TS40 membrane showed the lowest deviation from the mass balance of TPC during nanofiltration in concentration mode. This might be due to the smallest MWCO of this membrane which tends to prevent the inner pore blocking of polyphenols. On the other hand, the mass balance of both sugars and TPC is higher than 91% for all selected membranes. Diafiltration ensures more favorable hydrodynamic conditions in the membrane boundary layer, thus controlling the thickness of the concentration polarization layer and pore-clogging. These conditions reduce the amount of sugar adsorbed on the membrane, improving their diffusion. Similar results have been reported recently by Tonova et al. (2022) who evaluated the performance of the NP030 membrane in flat-sheet configuration in the separation of saccharides from phenolics from an aquatic weed hydrolysate.

In Figure 3.7 the adsorbed amount of sugars and TPC on the selected membranes evaluated at the end of the batch concentration process is reported. The amount of adsorbed fructose

for the TS40 membrane, about 217 g/m^2, was much higher in comparison to the other NF membranes. The adsorbed amount of glucose for this membrane (82.39 g/m^2) was also higher than the other two membranes (30.13 and 31.73 g/m^2 for NP030 and XN45 membranes, respectively). On the other hand, the adsorbed amount of phenolic compounds for all selected membranes was much lower than that of sugars in relation to the predominant content of sugars in the original juice. Among the selected membranes, the NP030 exhibited the highest amount of adsorbed phenolics (1.16 g/m^2 against 0.74 and 0.33 g/m^2 for TS40 and XN45 membranes, respectively). Saleh et al. (2006) reported up to 4.3 g of polyphenolics adsorbed per m^2 of the membrane in the treatment of apple juice with a SelRO® spiral-wound membrane of 1 kDa MWCO (MPS-36 from Koch Membrane Systems).

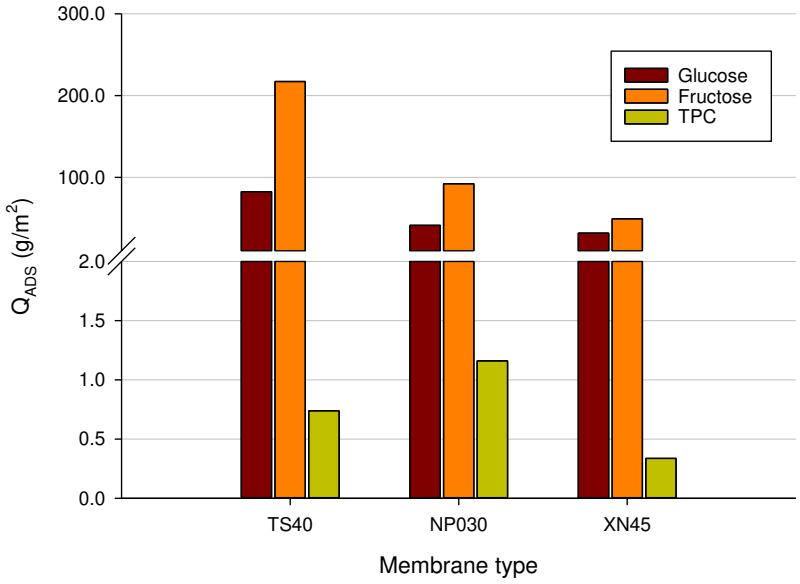

Figure 3.7 Amount of adsorbed glucose, fructose and TPC for selected membranes.

The more hydrophobic character of the NP030 membrane, with a top layer in PES material, enhances the adsorption of phenolic compounds on the membrane surface and the formation of a hydrophobic layer onto the membrane surface which could modify the physicochemical properties of the membrane (Sotto et al. 2013) leading to lower permeate fluxes and modification of the rejection performance. Susanto et al. (2009) supported the existence of benzene ring-benzene ring interactions to justify the adsorption of phenolic compounds on PES membranes. Moreover, the formation of multiple hydrogen bonds between polyphenols and the additive poly(vinyl)pyrrolidone usually used in the manufacturing process in PES membranes is considered an additional contribution to the adsorption phenomena of phenolic

compounds (Cassano et al. 2017). Cai et al. (2017) found that for phenolic compounds, a cake/gel layer as a reversible fouling was the main fouling resistance, while the adsorption played a significant role in the irreversible fouling resistance of polyamide and polypiperazine amide NF membranes with MWCOs of 240 and 150 Da, respectively.

3.4 Conclusions

Nanofiltration membranes with MWCO in the range of 200-600 Da were tested to reduce the sugar content in apple juice through a combination of diafiltration and batch concentration processes. For all selected membranes, the recovery rate of both sugars and phenolic compounds decreased in the retentate by increasing the diafiltration volume; however, the separation factor between phenolic compounds and sugars remained almost unchanged during the diafiltration process.

Among the investigated membranes, the TS40 membrane, a thin-film composite membrane with the lowest MWCO (200-300 Da) showed the highest retention of sugars and phenolic compounds in the selected operating conditions of both diafiltration and concentration processes. More than 70% of phenolic compounds were recovered in the retentate stream of this membrane at a volume reduction factor of 4, while recoveries of glucose and fructose were 41 and 44%, respectively. On the other hand, the other investigated membranes allowed for to recovery of a much lower amount of phenolic compounds in the retentate stream despite a greater removal of sugars on the permeate side. Therefore, the global results indicate that the combination of diafiltration and batch concentration with the TS40 membrane is a good compromise to remove up to 60% of sugars from apple juice with minimal losses of phenolic compounds.

3.5 References

Almanasrah, M., Brazinha, C., Kallioinen, M., Duarte, L. C., Roseiro, L. B., Bogel-Lukasik, R., Carvalheiro, F., Manttari, M., Crespo, J.G. (2015). Nanofiltration and reverse osmosis as a platform for production of natural botanic extracts: the case study of carob by-products. Separation and Purification Technology, 149, 389-397. https://doi.org/10.1016/j.seppur.2015.06.008

Ambrosi, A., Motke, M.B., Souza-Silva, É.A., Zini, C.A., McCutcheon, J.R., Cardozo, N.S. M., Tessaro, I.C. (2020). Beer dealcoholization by forward osmosis diafiltration. Innovative Food Science and Emerging Technologies, 63, 102371. https://doi.org/10.1016/j.ifset.2020.102371

Barańska, A., Kot, A., Samborska, K. (2020). Ultrafiltration as a method to obtain sugar reduced cloudy juices – a research on juice's properties. Zeszyty Problemowe Postępów Nauk Rolniczych, 600, 3-11. https://doi.org/10.22630/ZPPNR.2020.600.1

Boussu, K., Vandecasteele, C., Van der Bruggen, B. (2008). Relation between membrane characteristics and performance in nanofiltration. Journal of Membrane Science, 310(1–2), 51-65. https://doi.org/10.1016/j.memsci.2007.10.030

Cassano, A., Cabri, W., Mombelli, G., Peterlongo, F., Giorno, L. (2016). Recovery of bioactive compounds from artichoke brines by nanofiltration. Food and Bioproducts Processing, 98, 257-265, https://doi:10.1016/j.fbp.2016.02.004

Cassano, A., De Luca, G., Conidi, C., Drioli, E. (2017). Effect of polyphenols-membrane interactions on the performance of membrane-based processes. A review. Coordination Chemistry Reviews, 351, 45-75. https://doi.org/10.1016/j.ccr.2017.06.013

Cai, M.; Hou, W.; Li, Z.; Lv, Y.; Sun, P. (2017) Understanding nanofiltration fouling of phenolic compounds in model juice solution with two membranes. Food and Bioprocess Technology. 10, 2123–2131.

Chen, V., Li, H., Li, D., Tan, S., Petrus, H.B. (2006) Cleaning strategies for membrane fouled with protein mixtures. Desalination, 200, 198–200.

Conidi, C., Cassano, A., & Garcia-Castello, E. (2014). Valorization of artichoke wastewaters by integrated membrane process. Water Research, 48(1), 363-374. https://doi.org/10.1016/j.watres.2013.09.047

Conidi, C., Cassano, A., Drioli, E. (2022). Membrane diafiltration for enhanced purification of biologically active compounds from goji berries extracts. Separation and Purification Technology, 282, 119991. https://doi.org/10.1016/j.seppur.2021.119991

de Oliveira, R.C., de Barros, S.T.D. (2011). Beer clarification with polysulfone membrane and study on fouling mechanism. Brazilian Archives of Biology and Technology, 54(6), 1335-1342. https://doi.org/10.1590/S1516-89132011000600020

Doran, P.M. (2013). Unit operations, In: Bioprocess Engineering Principles, Doran P.M. (Ed.), Elsevier, Amsterdam, pp. 445-595. https://doi.org/10.1016/B978-0-12-220851-5.00011-3

Enzytec Liquid D-Glucose/D-Fructose. (2017). https://food.r-biopharm.com/wp-content/uploads/2017/07/e-liquid_ifu_e8160_glucose-fructose_en.pdf

Enzytec Liquid D-Glucose. (2017). https://food.r-biopharm.com/wp-content/uploads/2017/05/E-Liquid_IFU_E8140_Glucose_EN.pdf

Gaglianò, M., Conidi, C., Bartella, L., Salvino, R.A., Di Donna, L., Cassano, A., De Luca, G. (2021). An integrated approach based on NMR and HPLC–UV-ESI–MS/MS to characterize apple juices and their nanofiltration (NF) bioactive extracts. Food and Bioprocess Technology, 14(12), 2273-2285. https://doi.org/10.1007/s11947-021-02718-8

Khunnonkwao, P., Jantama, K., Kanchanatawee, S., Galier, S., Roux-de Balmann, H. (2018). A two steps membrane process for the recovery of succinic acid from fermentation broth. Separation and Purification Technology, 207, 451-460. https://doi.org/10.1016/j.seppur.2018.06.056

Laorko, A., Li, Z., Tongchitpakdee, S., Chantachum, S., & Youravong, W. (2010). Effect of membrane property and operating conditions on phytochemical properties and permeate flux during clarification of pineapple juice. Journal of Food Engineering, 100(3), 514–521. https://doi.org/10.1016/j.jfoodeng.2010.04.039

Loewe, D., Dieken, H., Grein, T.A., Salzig, D., Czermak, P. (2022). A combined ultrafiltration/diafiltration process for the purification of oncolytic measles virus. Membranes, 12(2), 1-14. https://doi.org/10.3390/membranes12020105

Lyu, H., Fang, Y., Ren, S., Chen, K., Luo, G., Zhang, S., Chen, J. (2016). Monophenols separation from monosaccharides and acids by two-stage nanofiltration and reverse osmosis in hydrothermal liquefaction hydrolysates. Journal of Membrane Science, 504, 141-152. https://doi.org/10.1016/j.memsci.2015.12.048

Mittal, R., Lamdande, A.G., Sharma, R., Raghavarao, K.S.M.S. (2020). Membrane processing for purification of R-Phycoerythrin from marine macro-alga, Gelidium pusillum and process integration. Separation and Purification Technology, 252, 117470. https://doi.org/10.1016/j.seppur.2020.117470

Muñoz, P., Pérez, K., Cassano, A., Ruby-Figueroa, R. (2021). Recovery of anthocyanins and monosaccharides from grape marc extract by nanofiltration membranes. Molecules, 26(7), 1-12. https://doi.org/10.3390/molecules26072003

Nguyen, D.T.N.N., Lameloise, M.L., Guiga, W., Lewandowski, R., Bouix, M., Fargues, C. (2016). Optimization and modeling of diananofiltration process for the detoxification of ligno-cellulosic hydrolysates - Study at pre-industrial scale. Journal of Membrane Science, 512, 111-121. https://doi.org/10.1016/j.memsci.2016.04.008

Nicolini, J.V., Borges, C.P., Ferraz, H.C. (2016). Selective rejection of ions and correlation with surface properties of nanofiltration membranes. Separation and Purification Technology, 171, 238-247. https://doi.org/10.1016/j.seppur.2016.07.042

Nisticò, D.M., Piro, A., Oliva, D., Osso, V., Mazzuca, S., Fagà, F.A., Morelli, R., Conidi, C., Figoli, A., Cassano, A. (2022). A combination of aqueous extraction and ultrafiltration for the purification of phycocyanin from Arthrospira maxima. Microorganisms, 10(2), 308. https://doi.org/10.3390/microorganisms10020308

Peiris, R.H., Hallé, C., Budman, H., Moresoli, C., Peldszus, S., Huck, P.M., Legge, R.L. (2010). Identifying fouling events in a membrane-based drinking water treatment process using principal component analysis of fluorescence excitation-emission matrices. Water Research, 44(1), 185-194. https://doi.org/10.1016/j.watres.2009.09.036

Prudêncio, A.P.A., Prudêncio, E.S., Amboni, R.D.M.C., Murakami, A.N.N., Maraschin, M., Petrus, J.C.C., Ogliari, P.J., Leite, R.S. (2012). Phenolic composition and antioxidant activity of the aqueous extract of bark from residues from mate tree (Ilex paraguariensis St. Hil.) bark harvesting concentrated by nanofiltration. Food and Bioproducts Processing, 90, 399-405. https://doi.org/10.1016/j.fbp.2011.12.003

Pruksasri, S., Lanner, B., Novalin, S. (2020). Nanofiltration as a potential process for the reduction of sugar in apple juices on an industrial scale. LWT-Food Science and Technology, 133, 110118. https://doi.org/10.1016/j.lwt.2020.110118

Saleh, Z.S., Stanley, R., Wibisono, R. (2006). Separation and concentration of health compounds by membrane filtration. International Journal of Food Engineering, 2(3), article 4. https://doi.org/10.2202/1556-3758.1125

Schwartz, L. (2003). Diafiltration: a fast, efficient method for desalting or buffer exchange of biological samples. Pall Scientific & Technical Report, 6. http://www4.pall.com/pdf/02.0629_Buffer_Exchange_STR.pdf

Servent, A., Abreu, F.A.P., Dhuique-Mayer, C., Belleville, M.P., Dornier, M. (2020). Concentration and purification by crossflow microfiltration with diafiltration of carotenoids from a by-product of cashew apple juice processing. Innovative Food Science and Emerging Technologies, 66, 102519. https://doi.org/10.1016/j.ifset.2020.102519

Sotto, A., Arsuaga, J.M., Van der Bruggen, B. (2013). Sorption of phenolic compounds on NF/RO membrane surfaces: Influence on membrane performance. Desalination, 309, 64-73. https://doi.org/10.1016/j.desal.2012.09.023

Suhalim, N.S., Kasim, N., Mahmoudi, E., Shamsudin, I.J., Mohammad, A.W., Zuki, F.M., Jamari, N.L.A. (2022). Rejection mechanism of ionic solute removal by nanofiltration membranes: an overview. Nanomaterials, 12(3), 437. https://doi.org/10.3390/nano12030437

Sun, X., Lu, H., Wang, J. (2017). Recovery of citric acid from fermented liquid by bipolar membrane electrodialysis. Journal of Cleaner Production, 143, 250-256. https://doi.org/10.1016/j.jclepro.2016.12.118

Susanto, H., Feng, Y., Ulbricht, M. (2009). Fouling behavior of aqueous solutions of polyphenolic compounds during ultrafiltration. Journal of Food Engineering, 91, 333-340. https://doi.org/10.1016/j.jfoodeng.2008.09.011

Sweeney, S.F., Woehrle, G.H., Hutchison, J.E. (2006). Rapid purification and size separation of gold nanoparticles via diafiltration. Journal of the American Chemical Society, 128(10), 3190–3197. https://doi.org/10.1021/ja0558241

Tonova, K., Lazarova, M., Dencheva-Zarkova, M., Genova, J. (2022) Nanofiltration of aquatic weed hydrolysate: Diafiltration versus concentration mode for separating saccharides from phenolics. Chemical Engineering Research and Design. 182, 360–370.

Tsuru, T., Sudoh, T., Yoshioka, T., Asaeda, M. (2001). Nanofiltration in non-aqueous solutions by porous silica-zirconia membranes. Journal of Membrane Science, 185, 253-261, https://doi.10.1016/S0376-738800651-7

Wei, D.S., Hossain, M., Saleh ZS. (2007). Separation of polyphenolics and sugar by ultrafiltration : effects of operating conditions on fouling and diafiltration. Proceedings of World Academy of Science, Engineering and Technology, 23, 349-

356.

World Health Organization (2015). Guideline: sugars intake for adults and children, Geneva. https://www.who.int/publications/i/item/9789241549028

World Health Organization (2018). A healthy diet sustainably produced. https://apps.who.int/iris/bitstream/handle/10665/278948/WHO-NMH-NHD-18.12-eng.pdf

Zdarta, J., Thygesen, A., Holm, M. S., Meyer, A. S., Pinelo, M. (2020). Direct separation of acetate and furfural from xylose by nanofiltration of birch pretreated liquor: Effect of process conditions and separation mechanism. Separation and Purification Technology, 239, 116546. https://doi.org/10.1016/j.seppur.2020.116546

Zhou, H., Ni, J., Huang, W., Zhang, J. (2006). Separation of hyaluronic acid from fermentation broth by tangential flow microfiltration and ultrafiltration. Separation and Purification Technology, 52(1), 29-38. https://doi.org/10.1016/j.seppur.2006.03.011

Chapter 4: NMR-based characterization of citrus Tacle juice and low-level NMR and UV-Vis data fusion for monitoring its fractions from membrane-based operations

This work was published as: Martina Gaglianò, Giuseppina De Luca, Carmela Conidi, Alfredo Cassano "NMR-based characterization of citrus Tacle juice and low-level NMR and UV-Vis data fusion for monitoring its fractions from membrane-based operations", Antioxidants (2022) 12(1):2

The author was involved in planning and performing the experiments, as well as in discussing and interpreting the results and manuscript preparation.

4.1 Introduction

Tacle is a new triploid citrus hybrid developed in Sicily using traditional, strictly non-GMO techniques. Both its name and flavour recall the two parents' cultivars: the Tarocco orange (C. sinensis L. Osbeck) and the Monreal Clementine (C. clementina Hort. ex Tan.) (Monreal and Hort 2008).This innovative fruit was mainly studied for its high antioxidant activity (Rapisarda et al. 2009), which confers the citrus extracts' health-promoting effects in preventing chronic heart and vascular diseases and treating metabolic disorders such as obesity and diabetes (Casacchia et al. 2019; Grande et al. 2021). The outbreak of the Covid-19 pandemic has increased the already high consumers' demand for immune-boosting, natural and organic products (Hamulka et al. 2021). The high nutraceutical profile of Tacle perfectly responds to this request. Still, the main bottleneck may lie in its juice's production process, which must allow the obtaining of processed food very close to the raw material. Hence, apart from the sensory attributes, one should minimize the loss of colour, texture, and significantly bioactive compounds. Traditionally, fruit processing techniques include clarification with filter aids and fining agents as well as thermal processes such as pasteurization, sterilization and concentration aimed at improving the shelf-life of the juice by inactivating enzymes, spoilage and pathogenic microorganisms. Unfortunately, these processes lead to a dramatic change in phenolic and carotenoid compounds, vitamins, taste and color of juices as well as to the formation of undesirable substances such as furfural, 5-hydroxymethylfurfural, furan and acrylamide (Kechinski et al. 2010). Consequently, the fruit

juice quality in terms of nutritional, functional, physicochemical and sensorial properties is definitely compromised. To alternatively process the juice, minimising the degradation of functional molecules and promoting the development of high-quality products with considerable shelf stability, pressure-driven membrane operations can be used (Cassano et al. 2006; Conidi et al. 2020; Galaverna et al. 2008). Microfiltration (MF) and ultrafiltration (UF) provide cost-effective alternatives to traditional fining and clarification methodologies, separating the raw juice into a fibrous concentrated pulp (retentate) and a clarified fraction free of spoilage microorganisms (permeate), suspended solids and colloids like proteins (D. Kumar et al. 2022). The combination of these processes with diafiltration (DF) allows the purity of the obtained fractions to be increased. For instance, carotenoid extracts from solid by-products of cashew apple (Anacardium occidentale L.) juice processing as well as from orange juice have been obtained through a combination of crossflow MF and DF (Polidori et al. 2018; Servent et al. 2020). Clarified juices can be further fractionated or concentrated by using nanofiltration (NF) and reverse osmosis (RO) operations (Nath et al. 2018; Zin et al. 2022). The environmental friendliness, economics, and ease of use are further advantages encouraging the application of these technologies (Bera et al. 2022). The evaluation of membrane processes in retaining metabolites which exhibit high nutritional value, shape organoleptic characteristics and hence formulate the fundamental quality properties of the product can be detected by means of several analytical methodologies (Castillejos-Mijangos et al. 2022; Mattoli et al. 2023; Rivera-Pérez et al. 2022; Yao et al. 2006). NMR spectroscopy is emerging as a leading technique in metabolomic studies, being a fast, robust and reliable technique which allows the detection of a wide range of structurally diverse metabolites simultaneously. However, because the richness of information often results in high spectral complexity, it calls for using multivariate analysis to study large numbers of spectra and extract meaningful information and first of all, principal component analysis (PCA) is a widely used. Recently, NMR-based metabolomics coupled with chemometric analysis has been applied to obtain metabolic profiles of various kinds of food, among which honey, olive oil, apple, and pomegranate juice, thus establishing adulteration, variety, geographical origin, quality, and authenticity (Calò et al. 2022; Gaglianò et al. 2021; Pappalardo 2022; Yong et al. 2022). PCA has also been applied very successfully to the study of industrial processing of citrus fruit juices to evaluate for reliable process control, to assess the quality of orange juice, and to identify potential mislabeled samples (Salvino et al. 2021). Furthermore, even though it is still a scientific challenge, NMR measurements can be combined with other techniques' data from a metabolomic and statistical perspective. For example, Tristán et al. (2022) probed the feasibility of using FTIR and NMR data to achieve

through the models developed a fast and accessible tool for evaluating the ripe state of the melon fruits. Additionally, data-fusion of ^{1}H- NMR and chromatographic techniques (gas and liquid chromatography) coupled with mass spectrometry was applied to provide more accurate knowledge about the classification of golden rums (Belmonte-Sánchez et al. 2020). The combined use of multi-technique data in chemometric analysis produced the best results compared to the individual techniques in classifying and distinguishing samples (Gu et al. 2011).

In this work, NMR has been applied to the analysis of Tacle juice with multiple aims. A preliminary chemical characterization of the juice was performed by using deuterium oxide (D_2O) and deuterated chloroform ($CDCl_3$) as solvents in order to capture both polar and non-polar metabolites from the original sample, thus improving the coverage of its metabolome. The juice was treated by UF to obtain a clarified fraction free of suspended solids and with a phenolic composition similar to that of the raw juice. The combination with DF was also studied to improve the retentate fraction's purity. A final NF step was performed in order to obtain a concentrated fraction of bioactive compounds from the clarified juice. NMR experiments and colourimetric assays were carried out on UF/DF and NF fractions to investigate and monitor how membrane processes affect the metabolic profile of the juice. Antioxidant activity and the total content of flavonoids, polyphenols and β-carotene were the variables determined by means of UV-visible spectroscopy and evaluated in combination with NMR measurements for the principal statistical analysis (PCA).

4.2 Materials and Methods

4.2.1. Tacle juice and juice processing

Tacle juice was supplied by Società Agricola Terzeria S.r.l located in Francavilla Marittima (CS), Calabria. The juice was ultrafiltered by using a laboratory plant equipped with a hollow fiber membrane module supplied by Microdyn-Nadir (Wiesbaden, Germany). It featured polyethersulphone hollow fiber membranes with an inner diameter of 0.8 mm and a molecular weight cut-off (MWCO) of 500 kDa. The UF process was operated in selected operating conditions according to the batch concentration configuration in order to clarify the juice up to a volume reduction factor (VRF, defined as the ratio between the initial feed volume and the volume of the resulting retentate) of 4.08. At the end of the UF process two different streams were produced from the original juice (feed UF, abbreviated as FUF): a clarified juice (indicated as PUF) and a retentate juice (indicated as RUF). Then, the retentate

was diafiltered in continuous mode by adding water to the feed tank at the same rate as the permeate flux so as to keep the feed volume constant during the process. Two fractions were collected at the end of the diafiltration process: a retentate stream (named as RDF) and a permeate stream (named as PDF). Both permeates resulting from ultrafiltration and diafiltration operations were, then, merged in the same ratio and the mixed product was submitted to a nanofiltration process by using a laboratory plant equipped with a stainless steel housing able to accommodate a spiral-wound membrane module having an effective membrane area of 0.38 m^2. NF experiments were performed in selected operating conditions by using two different membrane modules both in thin-film composite supplied by Microdyn-Nadir: a membrane module with a MWCO of 200-300 Da (NF1) and a membrane module with a MWCO of 300-500 Da (NF2). The NF processes were operated up to a VRF of 3.5. A schematic layout of the investigated process is depicted in Figure 4.1. UF/DF and NF processes were repeated five times on five batches of Tacle juice. Each batch, previously frozen at a temperature of -18° C, was thawed after about two weeks to be subjected to membrane processes and the resulting fractions were then frozen again to be thawed in view of the analysis of chemical characteristics: all samples collected from juice processing, for a total of 50 samples, were spectroscopically and spectrophotometrically analyzed and statistically processed by PCA.

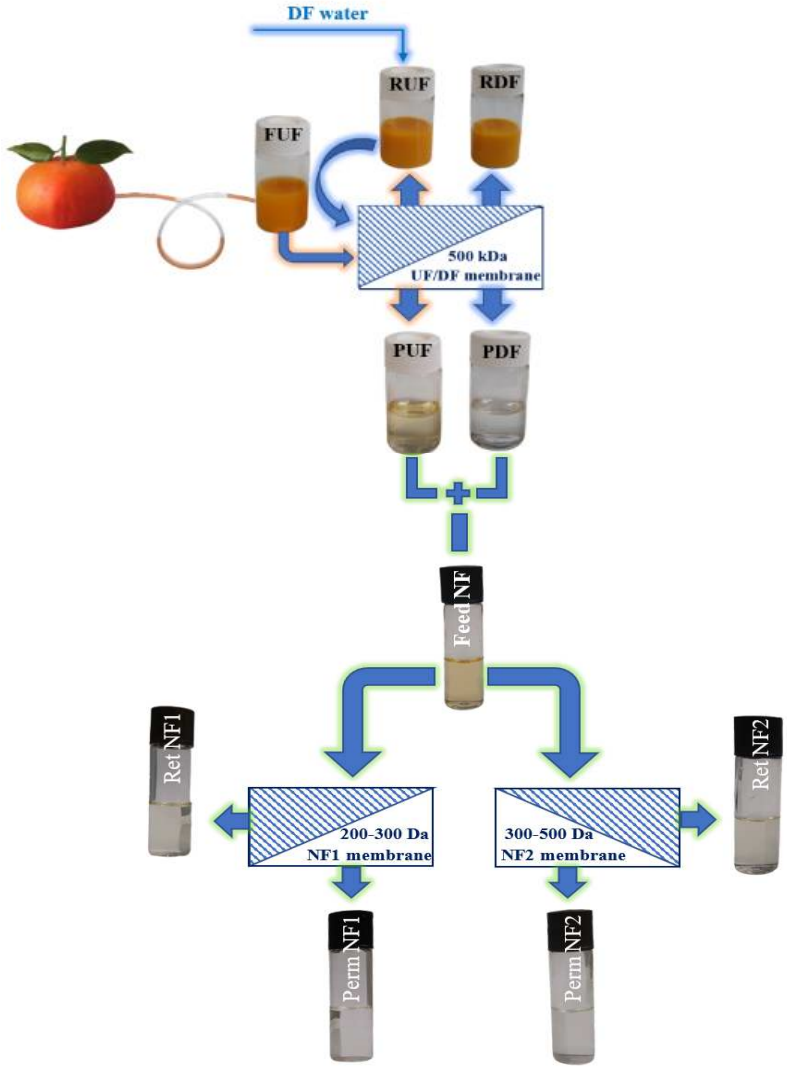

Figure 4.1 Schematic layout of the investigated process (UF, ultrafiltration; DF, diafiltration; NF, nanofiltration; F, feed; R, retentate; P, permeate).

4.2.2. NMR sample preparation

The chemical composition of polar compounds in tacle juice was evaluated on a sample prepared as follows: Tacle juice (FUF) was thawed at room temperature, diluted in a ratio 1:1 with distilled water and centrifuged (6000 rpm x 5 min) to separate the supernatant from the pulp. In addition, the pH of the supernatant was measured as being a crucial parameter to be known before the signals attribution phase to the various metabolites whose resonance frequency is strongly dependent on the pH. In the specific case, the measured pH value of the sample was 3.41. Subsequently, a volume of 500 µL of supernatant was transferred into a 5 mm NMR tube to which 100 µL of D_2O and 20 µL of a 100mM solution of sodium deuterated 3-trimethylsilylpropionate (TMSP-d_4) and 20mM of NaN_3 in D2O were added.

Deuterated water was used for locking the signal, TMSP-d_4 as a reference material for chemical shift referencing and sodium azide (NaN_3) to prevent the onset of bacteria capable of destroying juice metabolites during the recording of mono and bi-dimensional multinuclear NMR experiments. The preparation of the NMR samples used for the multivariate statistical analysis did not require using the internal standard neither the sodium azide, given the much shorter times for recording a single proton spectrum. NMR sample preparation for RUF and RDF was exactly the same of FUF. These samples were diluted and centrifuged and then 500 µL of supernatant were added to 100 µL of D_2O in an NMR tube. PUF and PDF samples were diluted too, but they don't need to be centrifuged, not having suspended solids which might interfere with the homogeneity of the magnetic field. All NF samples were, instead, not diluted, nor centrifuged but directly transferred in the NMR tube with D_2O always in a 5:1 ratio. Before transferring the supernatants or directly samples into the NMR tube, the pH value was evaluated for each sample type. Utilizing NaOH or HCl solutions, the pH value of UF samples was adjusted to be the same, just as for NF samples. A synthetic scheme of the NMR sample preparation in aqueous phase is shown in Figure 4.2.

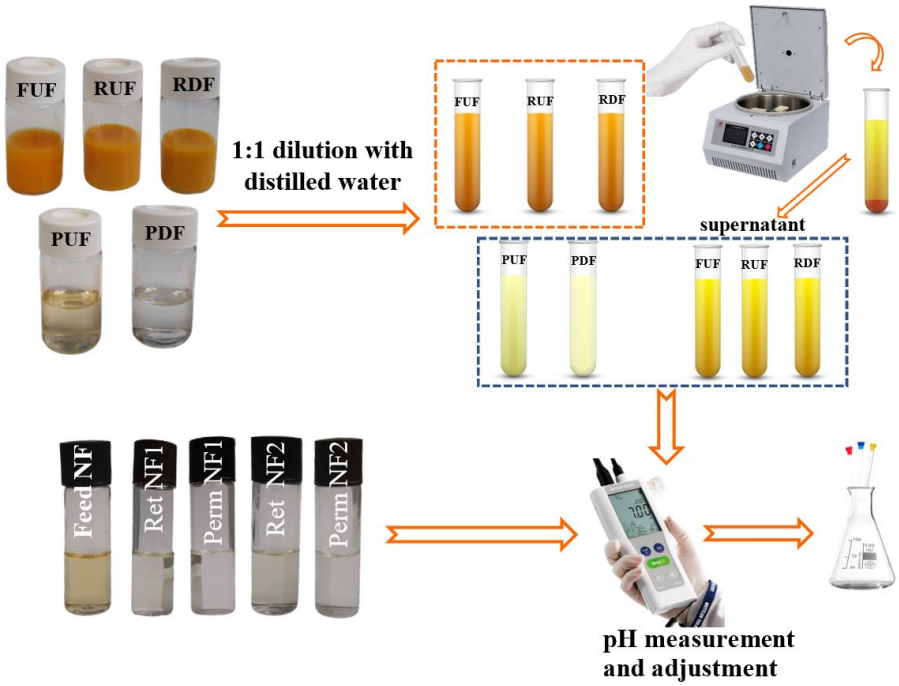

Figure 4.2. Polar phase sample preparation.

On the other hand, to characterize the apolar fraction of tacle juice metabolome, a simple, time-effective, and low-solvent consuming ultrasound-assisted extraction (UAE) method utilizing the deuterated solvent $CDCl_3$ was investigated. 1mL of tacle juice (FUF) was added with 1mL of $CDCl_3$ containing 0.01% TMS and placed in an Ultrasonic bath (UAE; Hielcher UP 100Hz, 100 W pulse, 30 kHz frequency) for 15 min. After the extraction two separate phases were observed: the aqueous phase above, which was removed, and the organic phase below, which was transferred into a 5mm NMR glass tube. A synthetic scheme of the NMR sample preparation in organic phase is shown in Figure 4.3.

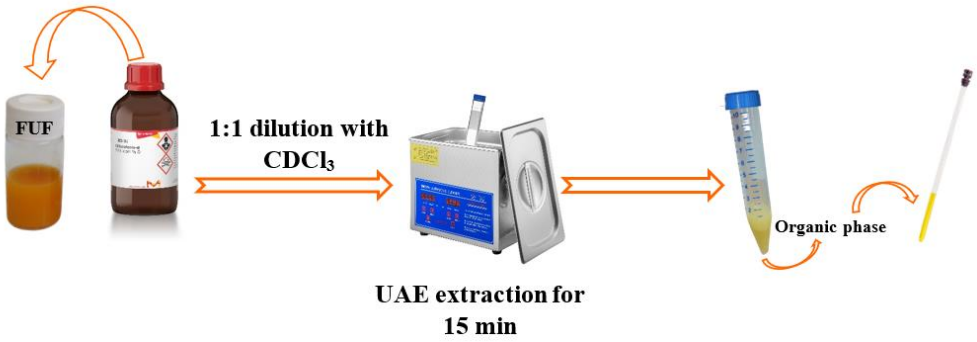

Figure 4.3. Organic phase sample preparation.

4.2.3. NMR data acquisition and processing

All spectra were acquired on a Bruker Avance 500 spectrometer operating at 500.13 MHz, 298 K, and a magnetic field of 11.7 tesla. ^{1}H NMR spectra of polar extracts were acquired using a NOESY presaturation pulse sequence (Bruker sequence denoted as *noesypr1d*) to suppress the residual water signal through selective irradiation at the water frequency during the mixing and recycle delays. For each experiment 512 FIDs were acquired using a spectral width of 11.25 ppm and a relaxation delay of 3 s. ^{1}H NMR spectra for lipophilic extracts were obtained using the Bruker pulse sequence *zg*. The acquisition conditions for $CDCl_3$ extracts were the following: number of scans (NS) = 512; spectral width (SW) = 11.25 ppm, size of FID (TD) = 65536 and relaxation delay (D1) = 3 s. All ^{1}H-NMR spectra were phased and then baseline corrected using the software TopSpin 3.6.2. (Bruker Corporation, Billerica, MA, USA). The obtained spectra were calibrated according to the internal standard. Additionally, the ^{1}H-^{1}H correlation spectroscopy (COSY) and ^{1}H-^{13}C heteronuclear multiple quantum coherence (HMQC) spectra were recorded in the aqueous and organic phase to verify metabolites chemical shift assignments' using the Bruker sequences *cosygpprqf* and *hmqcgpqf*. A sine filter and a qsine filter were applied on both dimensions, F1 and F2, respectively on COSY and HMQC experiments before Fourier-transformed.

4.2.4. UV-Visible analysis of total polyphenols, flavonoids, in vitro total antioxidant activity and β-carotene

Total polyphenols were measured colorimetrically by the Folin–Ciocalteau method, as reported elsewhere (Türkyilmaz et al. 2013). Gallic acid was used as a calibration standard and results were expressed as mg gallic acid equivalent (GAE) per liter of sample (mg GAE/L). The total flavonoid content was determined according to the Davis method (Davis 1947). Quantification was done on the basis of the standard curve of naringin (r^2 = 0.990), with the results expressed as mg naringin equivalents (NE)/L. The total antioxidant activity (TAA) was assessed via the 2,2-azino-bis (ethylbenzothiazoline-6-sulfonic acid) (ABTS) assay by monitoring the reduction of the radical cation as the percentage inhibition of absorbance at 734 nm (Stämpfli et al. 2007). Results of TAA were expressed in terms of mM of 6-hydroxy-2,5,7,8-tetramethylchroman-2-carboxylic acid (Trolox) equivalent. The concentration of β-carotene was, determined using the spectrophotometric method reported by Lime and Griffiths (1953) and results were expressed as μg β-carotene/ml. Total content

of β-carotene was quantified only in UF/DF samples because as being a large and lipophilic compound we expected to find it mostly in the starting juice and in the UF retentate fractions. Since the subsequent steps of the membrane processes (NF) concerned the use and treatment of the clarified juice, the focus was placed on monitoring low molecular weight compounds, which is why β-carotene was not quantified for NF samples. Total phenolics and total flavonoids, having a lower molecular weight, and TAA were, instead, determined for all UF/DF and NF samples. Each analysis on each sample was replicated three times, and the mean value obtained was inserted into the matrix also containing the NMR data and used as variables to be considered for the PCA statistical analysis.

4.2.5. Chemometric analysis and procedure

NMR aqueous phase spectra recorded on membrane samples were aligned, divided into uniform spectral bins (so-called buckets) of 0.05 ppm-width, and the signal area was integrated for each bucket. The water region from δ 4.2–5.1 was excluded from the spectra as well as the region from δ 5.5–5.9 which does not contain any significant signal. For the residual regions (δ 0.6–8.4 for UF/DF samples and δ 0.4–9.1 for NF samples), binning was performed. The buckets were normalized to the whole spectral area and exported in an excel file. A dataset of 25 samples and 127 NMR variables has been obtained for UF/DF processes, while 25 samples and 144 NMR variables were considered for NF processes. On the 50 samples of UF/DF and NF processes, the content of total phenolics, flavonoids and antioxidant activity were quantified. For the 25 samples of UF/DF the total β-carotene was also determined. Adding these variables obtained with the UV-Visible technique, the data matrices used for the chemometric analysis were formed as follows: 25 samples and 131 variables (127 NMR + 4 UV-Vis variables) for UF/DF, and 25 samples and 147 variables (144 NMR + 3 UV-Vis variables) for NF. In this way, a large block of variables (NMR variables) dominated over a smaller block of variables (UV-Visible variable) for purely numeric reasons. To address this problem and give each block the same importance, block-scaling procedure was employed as scaling procedure in the pre-processing phase of multivariate data (Turrini et al. 2021). This corresponds to down-weighting blocks of variables in relation to a selected basis scaling procedure. The basis scaling method is generally scaling to unit variance, mainly when variables differ noticeably in nature and numerical range (Eriksson et al. 2006). In this work, block scaling treatment was previously carried out, and then PCA was performed on the fused matrices, which combined NMR and

UV-Vis data. Multivariate statistical analysis was performed by the Chemometric Agile Tool CAT.

4.3. Results and Discussions

4.3.1. Tacle juice metabolic profiling by NMR

The characterization of the metabolic profile of tacle juice through NMR spectroscopy was performed in both aqueous and lipophilic citrus extracts to obtain as much compositional information as possible about major compounds in the tested samples. Figure 4.4a-c shows three ^{1}H-NMR spectral expansions of an aqueous extract of tacle evidencing the assigned metabolites. Most of them belong to sugars, amino acids, and organic acids. As mentioned before, all assignments were based on the analysis of 1D, and 2D NMR experiments, these last reported in Figures 4.5 and 4.6, and on the use of HMDB database and literature data (Ryu et al. 2016; Sobolev et al. 2015). Additionally, Figure 4.4d provides a typical ^{1}H-NMR spectrum of an organic extract where the main families of metabolites identified were fatty acids and triacylglycerols (TAGs). A numeric nomenclature is used to identify each signal, following a descending field order. The assignment of the different signals was based on previous reports on the ^{1}H-NMR analysis of fats (Alexandri et al. 2017; Castejón et al. 2016; González-Domfnguez et al. 2020; R. Kumar et al. 2011) and is summarized in Table 4.1. On the other hand, Table 4.2 goes into detail about the attributions of the metabolites for the aqueous phase.

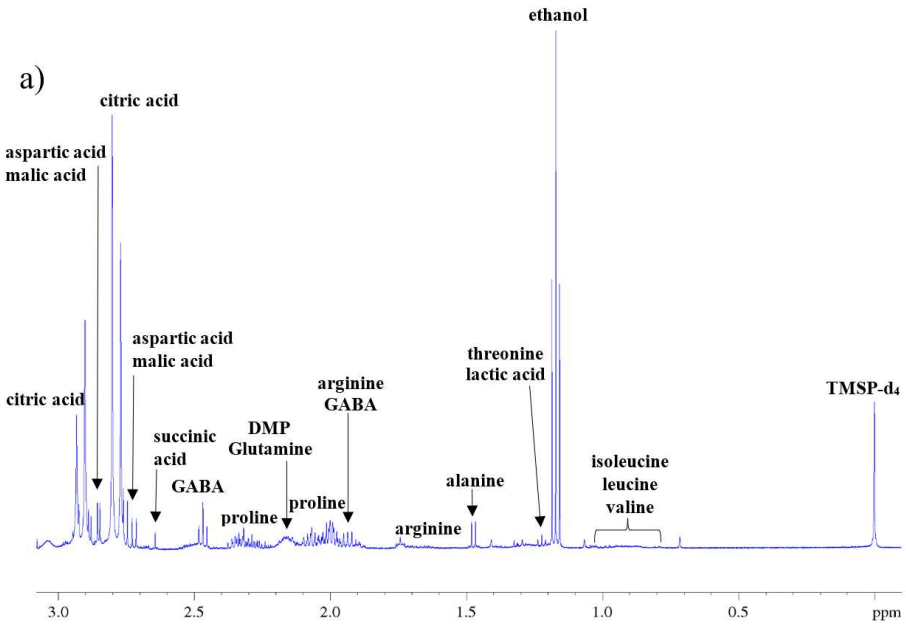

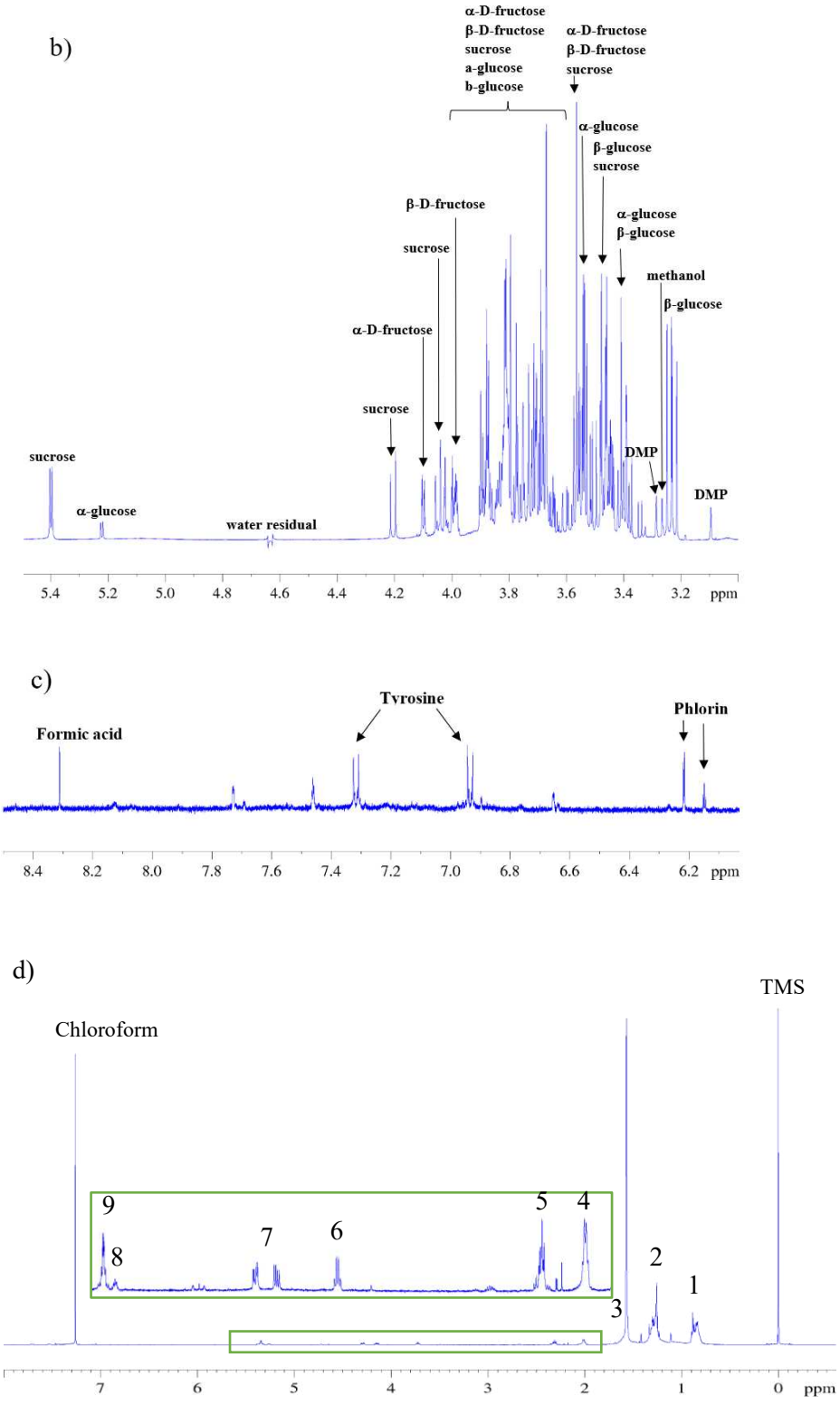

Figure 4.4 ^{1}H-NMR spectra obtained at 500 MHz of (a–c) the aqueous phase of tacle juice divided into three regions (see Table 4.2 for detailed assignment) and (d) lipophilic tacle extract (see Table 4.1 for assignment).

Table 4.1. ^{1}H NMR peak assignment of a typical lipid extract from tacle juice. Peak labels (1 to 9) agree with those given in Figure 4.4d.

Peak	δ ppm	Multiplicity, *J* (Hz)	Assignment
1	0.88	t, *J* = 6.8 Hz	C***H₃*** All acyls except linolenyl
2	1.23-1.43	m	$(CH_2)_n$ All acyl chains
3	1.55-1.68	m	C***H₂***CH2COOR All acyl chains
4	2.00	m	C***H₂***CH=CH All unsaturated fatty acids
5	2.2-2.3	m	C***H₂***COOR All acyl chains
6	3.73	q, *J* = 7.0 Hz	CH_3CH_2OH Ethanol
7	4.15 4.29	dd, *J* =12.0, 6.00 Hz dd, *J* =12.0, 6.00 Hz	C***H₂***OCOR Glycerol (triacylglycerols)
8	5.23-5.28	m	C***H***OCOR Glycerol (triacylglycerols)
9	5.30-5.38	m	C***H***=CH All unsaturated fatty acid

Table 4.2 Metabolites identified in the 500 MHz ^{1}H Spectrum of the aqueous phase of Tacle juice at pH 3.41.

Compound	Assignment	^{1}H (ppm)	Multiplicity	^{13}C (ppm)
Amino acids				
Valine	γ-CH_3	0.98	d	
	γ'-CH_3	1.04	d	
Isoleucine	γ-CH_3	0.99		
	δ-CH_3	0.95		
Leucine	γ-CH_3	1.70		
	δ-CH_3	0.95		
Alanine	α-CH	3.79		
	β-CH_3	1.47	d	
Threonine	α-CH	3.96		
	γ-CH_3	1.22	d	
Arginine	β-CH_2	1.65;1.72	m	
	γ-CH_2	1.90	m	
	δ-CH_2	3.23		
GABA (γ-aminobutyric acid)	α-CH_2	2.46	t	
	β-CH_2	1.90	m	
	γ-CH_2	3.03	t	
Glutamine	α-CH	3.79		
	β-CH_2	2.13	m	
	γ-CH_2	2.53	m	
Proline	α-CH	4.13		
	β-CH	2.33	m	
	β'-CH	2.06	m	
	γ-CH_2	1.99	m	
	δ-CH	3.40		
	δ'-CH	3.33		

DMP (dimethylproline)	α-CH	4.07		
	β-CH	2.48	m	
	β'-CH	2.27	m	
	γ-CH_2	2.16	m	
	δ-CH	3.53		
	δ'-CH	3.69		
	N-CH_3	3.09	s	
	N-CH_3′	3.28	s	
Tyrosine	C2,6H ring	7.31	d	
	C3,5H ring	6.91	d	
Carbohydrates				
α-glucose	CH-1	5.22	d	94.83
	CH-2	3.53		73.80
	CH-3	3.70		
	CH-4	3.46		
	CH-5	3.83		
	CH_2-6,6	3.77;3.83		
β-glucose	CH-1	4.64		98.65
	CH-2	3.23	dd	76.93
	CH-3	3.48		78.54
	CH-4	3.38		72.38
	CH-5	3.46		78.62
	CH_2-6,6	3.73; 3.81		63.52
Sucrose	CH-1 (Glc)	5.40	d	94.83
	CH-2	3.57		73.80
	CH-3	3.75		75.55
	CH-4	3.47		71.95
	CH-5	3.85		75.07
	CH_2-6,6	3.80;3.82		62.88
	CH_2-1′	3.67		64.10
	(Fru)			104.2
	CH-2′	4.20		79.18
	CH-3′	4.04		76.93
	CH-4′	3.85		84.05
	CH-5′	3.83		65.73
	CH_2-6′,6′			
α-fructose	CH_2-1,1	3.58		65.70
	CH-3	4.09		78.18
	CH-4	4.09		78.18
	CH-5	3.82		83.36
	CH_2-6,6	3,68; 3.77		65.48
β-fructose	CH-3	3.78		70.34
	CH-4	3.88		72.45
	CH-5	3.99		77.20
	CH_2-6,6	3.69; 4.01		66.67
Organic Acids				
Lactic acid	α-CH	3.71		
	β-CH_3	1.22	d	

Succinic acid	α,β-CH_2	2.64	s	
Malic acid	α-CH	4.46		
	β-CH_2	2.72		
	β'-CH_2	2.86		
Citric acid	αγ-CH	2.78	d	46.6
	α'γ'-CH	2.91	d	46.6
Aspartic acid	α-CH	4.00		
	β-CH_2	2.71	dd	
	β'-CH_2	2.84	dd	
Formic acid	HCOOH	8.32	s	
Other compounds				
Ethanol	CH_3	1.17	t	
	CH	3.67		
Methanol	CH_3	3.32	s	
Phlorin	C4H ring	6.15	t	
	C2,6H ring	6.22	d	

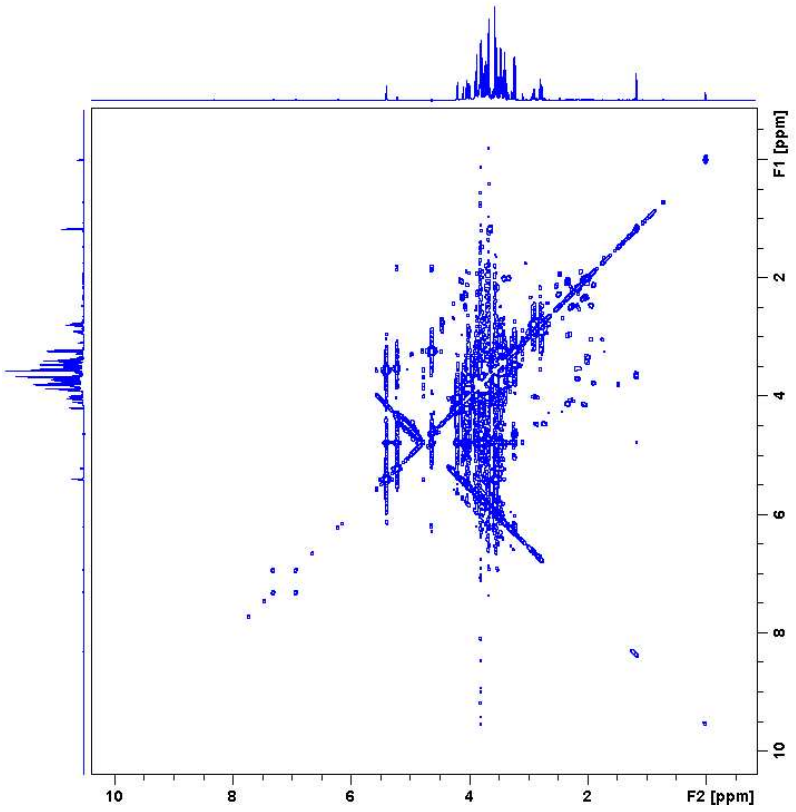

Figure 4.5 2D ^{1}H COSY spectrum (Bruker pulse sequence: *cosygpprqf*) recorded on Tacle juice in D_2O (field strength of 11.74 T).

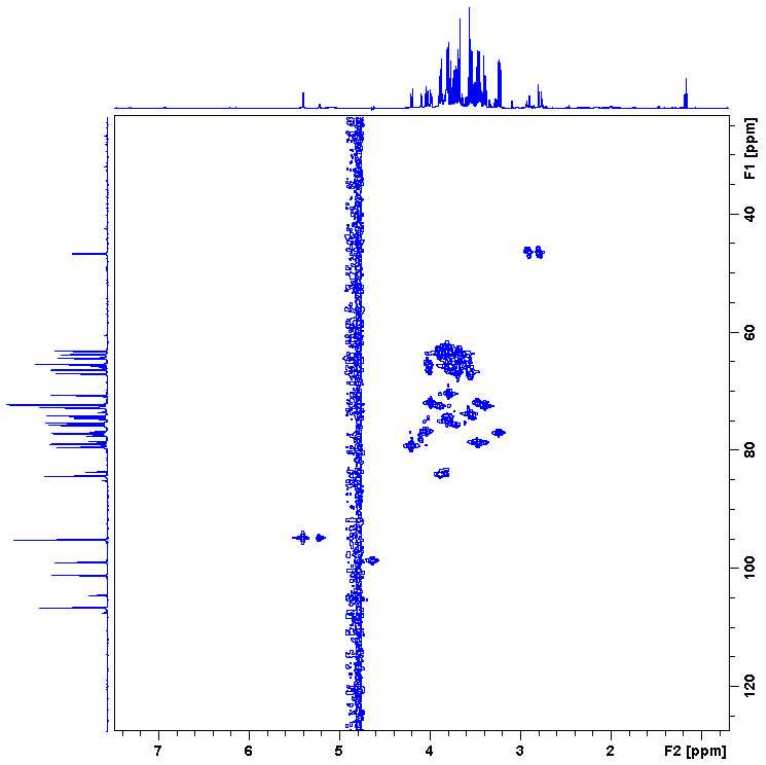

Figure 4.6 2D ^{1}H-^{13}C HMQC spectrum (Bruker pulse sequence: *hmqcgpqf*) recorded on Tacle juice in D_2O (field strength of 11.74 T).

From a purely qualitative point of view, the metabolic profile of tacle juice appears almost identical to that of the parent cultivars (Pappalardo 2022). In the aqueous phase, a total of 11 amino acids were identified together with 6 organic acids, being the citric acid the major among them. The most crowded part of the spectrum (3.0-4.3 ppm) contains the carbinolic protons of the monosaccharide residues, particularly, α- and β-glucose, α- and β-fructose, and sucrose. The remaining down field part the proton spectrum (6-8 ppm) is diagnostic of aromatic signals and it may have some importance for glycosides with an aromatic aglycon. It is the case of phlorin (3,5-dihydroxyphenyl-β-D-glucopyranoside), a long-discussed molecule for the authentication of Citrus juices as a possible marker for fraudulent processing technique (Jungen et al. 2020), whose aromatic protons resonances fall at 6.15 ppm (triplet generated by the para-positioned proton), and at 6.22 ppm (doublet generated by the two magnetically identical, ortho-positioned, aromatic protons). The extraction of the lipid fraction of the tacle juice showed the presence of some very low-intensity signals related to fatty acids, agreeing well with the fact that it is a fruit with very few calories. Fatty acids can be distinguished in the ^{1}H-NMR spectrum only at a class level (saturated, monounsaturated, diunsaturated and polyunsaturated), and it is impossible to distinguish signals of individual fatty chains within the same class. For instance, ^{1}H resonances of long-chain fatty acids such as palmitic and stearic ones are completely overlapped. For this reason,

many assignments reported in the literature, such as in this work, are referred to molecular fragments (methyl, methylenic, allylic methylenic groups, double bonds, etc.) rather than individual compounds (Mannina et al. 2012). Once the original juice (FUF) had been characterized, NMR spectra in the aqueous phase were recorded on the fractions obtained from membrane operations it had undergone. Figure 4.7 shows the NMR spectral profiles related to ultrafiltration samples (RUF and PUF) and diafiltration samples (RDF and PDF). Visually, these fractions appear to have the same metabolomic profile.

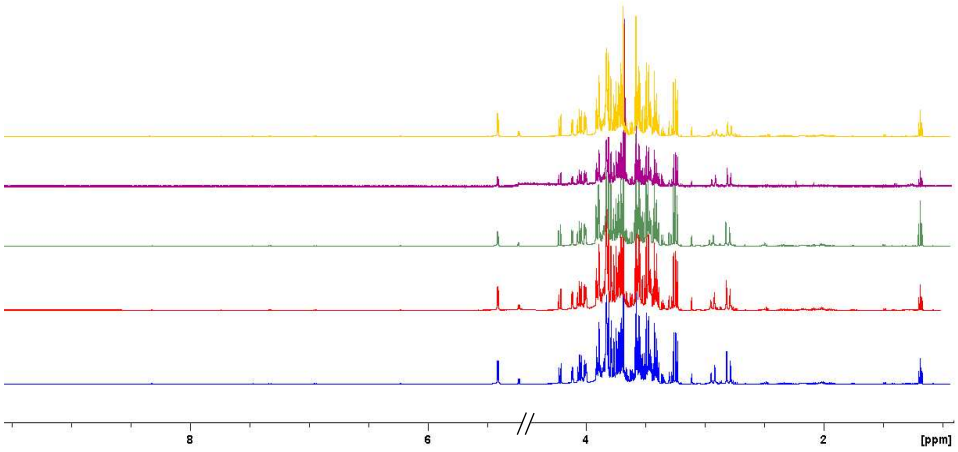

Figure 4.7 Comparison of ^{1}H-NMR spectra of FUF (in blue), RUF (in red) PUF (in green), RDF (in violet), and PDF (in yellow) Tacle samples.

Similarly, the high resolution NMR spectra of the aqueous fraction were recorded for the samples coming from the nanofiltration processes, reported in Figure 4.8.

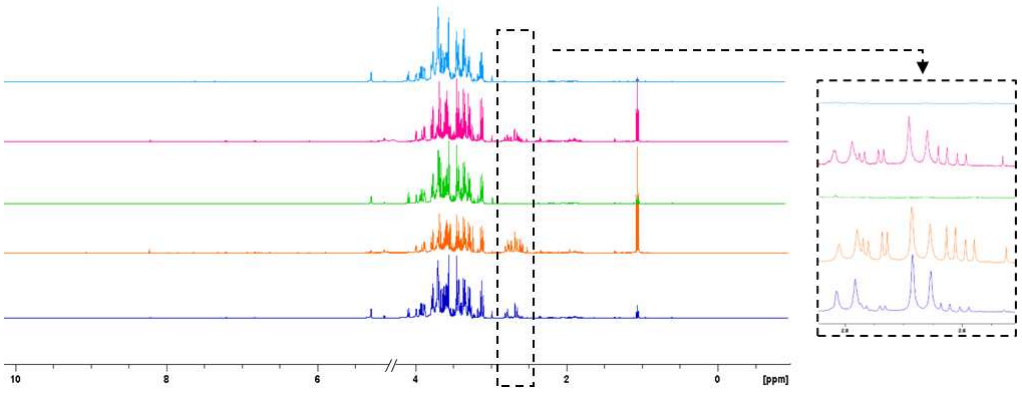

Figure 4.8 Comparison of ^{1}H-NMR spectra of Feed NF (in blue), Permeate NF 1 (in orange) Retentate NF 1 (in green), Permeate NF 2 (in fuchsia), and Retentate NF 2 (in light blue) Tacle samples.

In this case, NMR profiles present differences in some signals and their relative intensities. These differences are especially noticeable in the enlarged region from δ 2.55–2.85 of Figure 4.8, where the citric, aspartic, and malic acid signals fall. In the NF feed, citric acid is present in a higher concentration than the other two acids as NMR is an intrinsically quantitative technique (Malz and Jancke 2005), and with equal number of nuclei, the area of the two generated doublets of citric acid in ^{1}H-NMR spectrum is higher respect to other acid signals. On the other hand, in the NF permeates, the same acids are present but in different proportions: these fractions have a higher aspartic acid content, thus indicating that citric acid is much more retained by NF membranes with respect to aspartic acid. However, in NMR spectra of NF retentates, no relevant signals corresponding to citric acid (in the region δ 2.55–2.85) can be detected. Its signals may fall into the NMR spectra background noise. Furthermore, it should be pointed out that citric acid is a Lewis acid consisting of functional hydroxyl groups which can form complexes with other compounds and hydro-gen bonds with the membrane polymer; thus, it could be partially absorbed on the membrane surface. Moreover, the initial higher concentration of citric acid in the feed solution, its molar mass slightly higher than that of aspartic acid as well as the different pKa values of these organic acid compounds may all contribute to determine a different behavior in terms of NF membrane rejection.

4.4.3.2. Principal Component Analysis applied to NMR and UV-Visible data of UF/DF and NF Samples

To better understand variable correlations, membrane sample similarities/differences, and thus the influence of integrated-membrane processes on the metabolic juice profile, NMR data (block 1) were combined with UV-visible data (block 2) in the Principal Component Analysis (PCA). Combining data from two or more techniques is advantageous if they offer complementary information that, when added together, allows us to overview the process comprehensively and better distinguish samples. For example, if we consider only the NMR variables, there is a cluster separation of UF/DF samples but not as well as when the UV-Vis variables are added. Figure 4.9 shows the PCA score plot obtained from autoscaling and processing data matrix containing NMR data only.

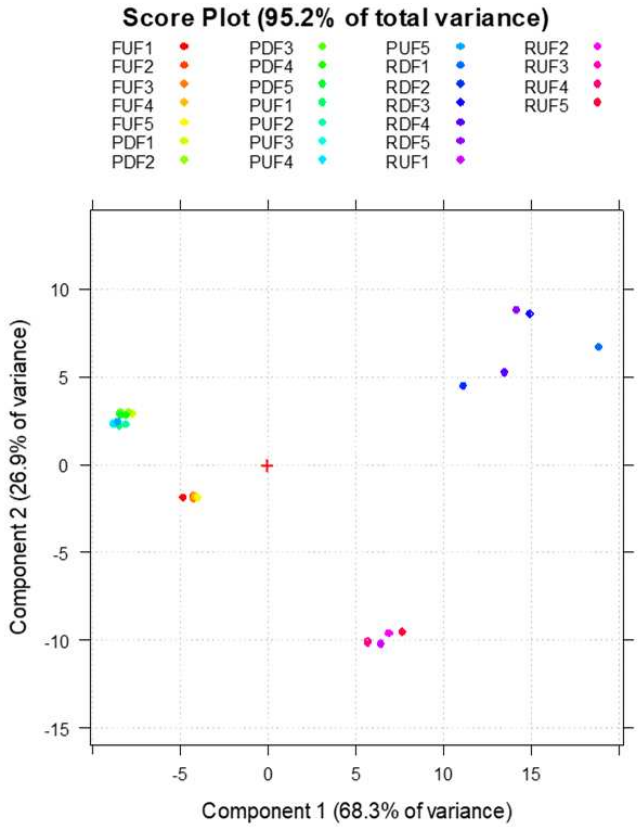

Figure 4.9 Principal component analysis score plot of the studied UF/DF samples using NMR data.

The two principal components in this score plot explain 95.2% of the total variance. We can observe that feed samples differ from the retentate samples (in turn, the retentates from ultrafiltration and diafiltration are separated into two different regions of the diagram). In contrast, the permeate samples separate from the feed and retentate samples but fall into the same region, indicating their similar composition in metabolites identified through NMR. Adding UV-Vis data to the NMR data (Figure 4.10), UF/DF samples were separated into five clusters with no notable outliers: UF permeates and DF permeates are now distinguished very well. Figure 4.10 shows the PCA score plot of fused NMR and UV-Vis data matrix pretreated by block-scaling. PC1 described 59.9% variation of data, while PC2 account for 33.5% of the total subset variance. Therefore, more than 90% of variation can be described only by the first two PCs, and this is why only PC1 and PC2 were taken for further analysis. The evaluation of the PCA score plot indicated that the clustering between FUF, RUF, and PUF samples was along the PC1 variable. These samples all had about the same negative value of PC2, but FUF samples had PC1=0, RUF samples were characterized by PC1>0, while PUF samples hold PC1<0. Thus, PC1 component allowed distinguished samples coming from the ultrafiltration. On the other hand, PC2 component permitted to discriminate ultrafiltration samples from diafiltration samples. In fact, while the first ones were all at

negative value of PC2, the diafiltration samples (RDF and PDF) had positive value of PC2 and were separated among them on the PC1: RDF samples were in the quadrant 1 (upper right), while the PDF samples were in quadrant 2 (upper left). Further details arose from the inspection of the PC loadings of the first two PCs which highlighted the metabolites that contributed to the samples separation. Figure 4.11 reports loadings deriving from NMR and UV-VIS data on different scales indicated with the same color as the corresponding loadings. Block 2 with a lower number of variables, had loadings absolute values high-er than block 1. This didn't mean that variables in block 2 had more importance than variables in block 1, but only that we gave it more significance with the block-scaling pretreatment because this block was made up of a reduced number of variables and, therefore, a reduced variance. Applying block scaling each block has variance 1 and the variables of each block have the same variance.

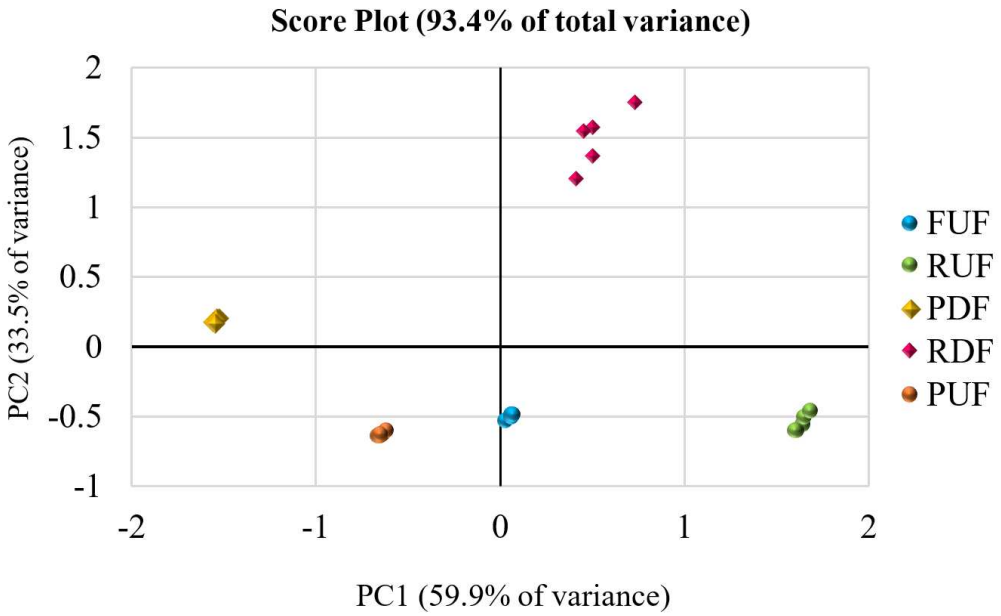

Figure 4.10 Principal component analysis score plot of the studied UF/DF samples using NMR and UV-Vis data

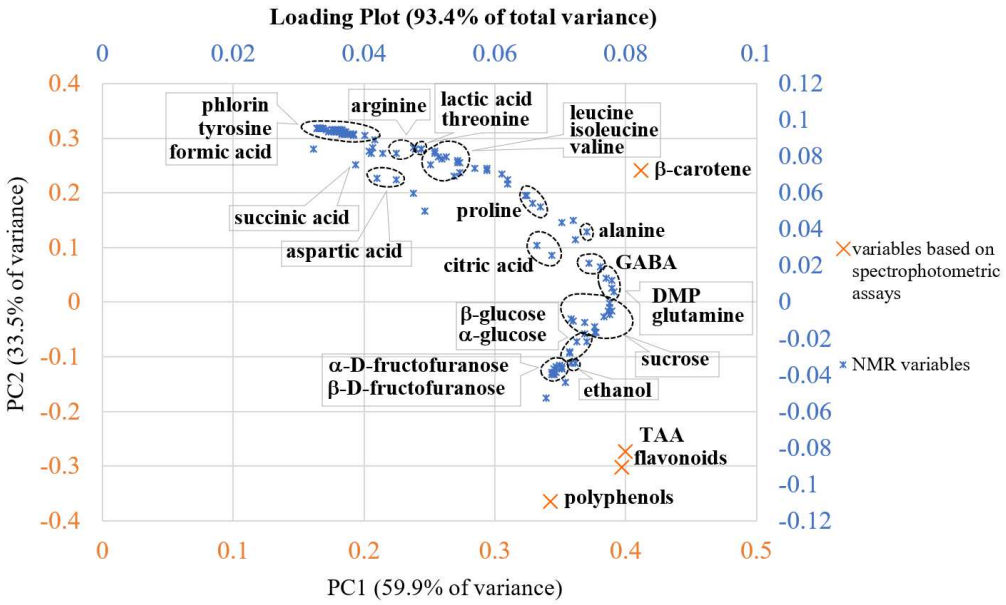

.

Figure 4.11 Principal component analysis loadings plot of the studied UF/DF samples using NMR and UV-Vis data.

Polyphenols, flavonoids and TAA were positively correlated among them. Therefore, as expected, the antioxidant capacity was mainly attributed to polyphenol-type compounds. Comparing the position of samples in the score plot with the loadings position it can be figure out that the samples deriving from UF in batch concentration process have the same metabolic composition, but different concentration of all the metabolites took into account (in order of concentration: RUF>FUF>PUF). Thus, with the investigated membrane in the selected operating conditions, the ultrafiltration process allowed for preserving the original juice composition in terms of antioxidant compounds, sugars, amino acids and organic acids. On the other hand, diafiltration changed the metabolic profile of the permeate and retentate products. The RDF samples were characterized by a higher concentration of β-carotene with respect to the other compounds, being a lipophilic phytochemical slightly soluble in water. Carotenoids are exciting sources in the food field, both for their bioactive potential and colouring properties, making products more attractive to consumers (Sobolev et al. 2015). Observing, in-stead, the PDF samples in the scores plot and looking at the loadings it emerges that they presented a lower content of sugars, polyphenols, flavonoids, and therefore lower TAA, and higher content of amino and organic acids. At the end of each UF/DF process, the PDF and PUF permeates were mixed in the same ratio and nanofiltered. Also for NF samples the total polyphenols, flavonoids and antioxidant activity in vitro were quantified, ^{1}H-NMR spectra were acquired, block-scaling pretreatment was accom-plished,

and PCA was performed on the fused data matrix. Fig. 10 shows the biplot (score and loading plot) obtained.

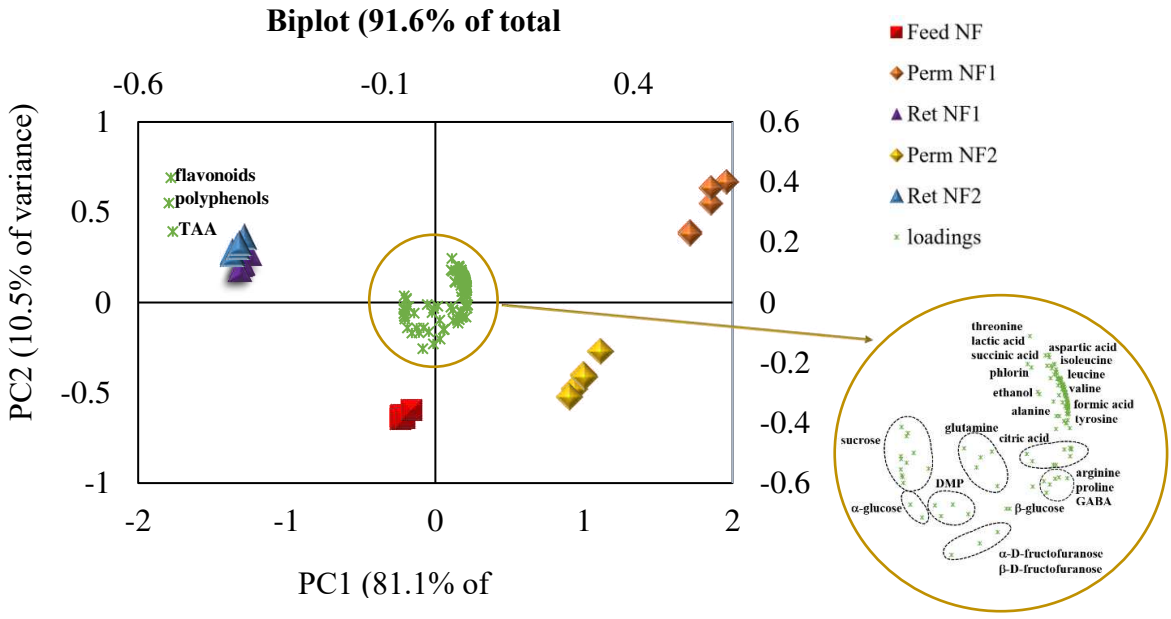

Figure 4.12 Principal component analysis biplot of the studied NF samples. The location of NMR-variables is indicated by the circle of which the zoom and the assignments of the loadings are shown.

91.6% of the total variance was explained by two principal components (PCs), with PC1 accounting for 81.1% of the total variance and PC2 accounting for 10.5%. With the exception of the nanofiltration retentates, the other samples are positioned in different regions of the biplot. NF Feed samples are in the third quadrant (lower left) and present a higher concentration of sugars. Permeates deriving from the nanofiltration with NF2 membrane, cluster in the fourth quadrant (lower right), having a larger amount of GABA, proline, and arginine. NF1 permeates are, instead, in the first quad-rant (upper right) exhibiting a higher concentration of threonine, lactic and succinic acids, aspartic acid, phlorin, isoleucine, leucine, valine. Finally, NF1 and NF2 retentates shared the same second quadrant (upper left), as being characterized by a close metabolite profile, mostly in terms of polyphenols, flavonoids, and TAA. Therefore, under the selected operating conditions, both nanofiltration membranes resulted suit-able for the enrichment of the clarified tacle juice in bioactive compounds.

4.4 Conclusions

High resolution NMR spectroscopy has proven to be a powerful tool for the metabolomic and lipidomic analysis of tacle juice, well recognized for its high content of bioactive compounds. In this work, the characterization of the juice by multinuclear (^{1}H and ^{13}C) 1D and 2D NMR experiments allowed to recognize 25 metabolites in the aqueous phase and identify triglycerides and fatty acid in the extracted organic phase. Moreover, UV-Visible technique was applied to quantify the total content of flavonoids, polyphenols, β-carotene and TAA. In a second step of the work, membrane processes such as ultrafiltration (UF) (also in diafiltration mode) and nanofiltration (NF), were used for producing enriched fractions of bioactive compounds from the raw juice. PCA on NMR and UV-visible fused data provided graphical outputs that were easy to read and interpret, thus turning out to be a very effective procedure to obtain a syn-thetic judgement of how UF/DF and NF membrane processes affect the metabolic profile of the juice. In addition, these techniques confirm the capability of membrane filtration processes with respect to heat treatments in preserving the chemical composition of the original juice without generating new undesirable metabolites. Further studies are underway to evaluate the performance and selectivity of UF and NF membranes in more detail.

4.5 References

Alexandri, E., Ahmed, R., Siddiqui, H., Choudhary, M. I., Tsiafoulis, C. G., & Gerothanassis, I. P. (2017). High resolution NMR spectroscopy as a structural and analytical tool for unsaturated lipids in solution. Molecules, 22(10). https://doi.org/10.3390/molecules22101663

Belmonte-Sánchez, J. R., Romero-González, R., Martínez Vidal, J. L., Arrebola, F. J., & Garrido Frenich, A. (2020). 1H NMR and multi-technique data fusion as metabolomic tool for the classification of golden rums by multivariate statistical analysis. Food Chemistry, 317(January), 126363. https://doi.org/10.1016/j.foodchem.2020.126363

Bera, S. P., Godhaniya, M., & Kothari, C. (2022). Emerging and advanced membrane technology for wastewater treatment: A review. Journal of Basic Microbiology, 62(3–4), 245–259. https://doi.org/10.1002/jobm.202100259

Calò, F., Girelli, C. R., Wang, S. C., & Fanizzi, F. P. (2022). Geographical Origin Assessment of Extra Virgin Olive Oil via NMR and MS Combined with Chemometrics as Analytical Approaches. Foods, 11(1). https://doi.org/10.3390/foods11010113

Casacchia, T., Occhiuzzi, M. A., Grande, F., Rizzuti, B., Granieri, M. C., Rocca, C., et al. (2019). A pilot study on the nutraceutical properties of the Citrus hybrid Tacle® as a dietary source of polyphenols for supplementation in metabolic disorders. Journal of Functional Foods, 52(June 2018), 370–381. https://doi.org/10.1016/j.jff.2018.11.030

Cassano, A., Figoli, A., Tagarelli, A., Sindona, G., & Drioli, E. (2006). Integrated membrane process for the production of highly nutritional kiwifruit juice. Desalination, 189(1-3 SPEC. ISS.), 21–30. https://doi.org/10.1016/j.desal.2005.06.009

Castejón, D., Fricke, P., Cambero, M. I., & Herrera, A. (2016). Automatic 1H-NMR screening of fatty acid composition in edible oils. Nutrients, 8(2). https://doi.org/10.3390/nu8020093

Castillejos-Mijangos, L. A., Acosta-Caudillo, A., Gallardo-Velázquez, T., Osorio-Revilla, G., & Jiménez-Martínez, C. (2022). Uses of FT-MIR Spectroscopy and Multivariate Analysis in Quality Control of Coffee, Cocoa, and Commercially Important Spices. Foods, 11(4). https://doi.org/10.3390/foods11040579

Conidi, C., Castro-Muñoz, R., & Cassano, A. (2020). Membrane-based operations in the fruit juice processing industry: A review. Beverages, 6(1), 1–39. https://doi.org/10.3390/beverages6010018

Davis, W. B. (1947). Determination of Flavanones in Citrus Fruits. Analytical Chemistry, 19(7), 476–478. https://doi.org/10.1021/ac60007a016

Eriksson, L., Byrne, T., Johansson, E., Trygg, J., & Vikström, C. (2006). Multi- and Megavariate Data Analysis Basic Principles and Applications. Umetrics Academy.

Gaglianò, M., Conidi, C., Bartella, L., Salvino, R. A., Di Donna, L., Cassano, A., & De Luca, G. (2021). An Integrated Approach Based on NMR and HPLC–UV-ESI–MS/MS to Characterize Apple Juices and Their Nanofiltration (NF) Bioactive Extracts. Food and Bioprocess Technology, 14(12), 2273–2285. https://doi.org/10.1007/s11947-021-02718-8

Galaverna, G., Di Silvestro, G., Cassano, A., Sforza, S., Dossena, A., Drioli, E., & Marchelli, R. (2008). A new integrated membrane process for the production of concentrated blood orange juice: Effect on bioactive compounds and antioxidant activity. Food Chemistry, 106(3), 1021–1030. https://doi.org/10.1016/j.foodchem.2007.07.018

González-Domfnguez, R., Sayago, A., & Fernández-Recamales, Á. (2020). Fatty acid profiling for the authentication of iberian hams according to the feeding regime. Foods, 9(2), 1–9. https://doi.org/10.3390/foods9020149

Grande, F., Occhiuzzi, M. A., Perri, M. R., Ioele, G., Rizzuti, B., Statti, G., & Garofalo, A. (2021). Polyphenols from citrus tacle® extract endowed with hmgcr inhibitory activity: An antihypercholesterolemia natural remedy. Molecules, 26(18). https://doi.org/10.3390/molecules26185718

Gu, H., Pan, Z., Xi, B., Asiago, V., Musselman, B., & Raftery, D. (2011). Principal component directed partial least squares analysis for combining nuclear magnetic resonance and mass spectrometry data in metabolomics: Application to the detection of breast cancer. Analytica Chimica Acta, 686(1–2), 57–63. https://doi.org/10.1016/j.aca.2010.11.040

Hamulka, J., Jeruszka-bielak, M., Zielinska-pukos, M. A., Magdalena, G., & Drywie, M. E. (2021). Dietary Supplements during COVID-19 Outbreak . Results of Online Studies. Nutrients, 13, 54.

Jungen, M., Schütz, B., & Schweiggert, R. (2020). Influence of species and processing techniques on phlorin in Citrus juices as quantified by 1H-NMR spectroscopy. Lwt, 134(July), 109949. https://doi.org/10.1016/j.lwt.2020.109949

Kechinski, C. P., Guimarães, P. V. R., Noreña, C. P. Z., Tessaro, I. C., & Marczak, L. D. F. (2010). Degradation Kinetics of Anthocyanin in Blueberry Juice during Thermal Treatment. Journal of Food Science, 75(2). https://doi.org/10.1111/j.1750-3841.2009.01479.x

Kumar, D., Ladaniya, M. S., Gurjar, M., Mendke, S., & Kumar, S. (2022). Positive retention of bioactive compounds and biochemical components of Sathgudi sweet orange (Citrus sinensis L. Osbeck) juice concentrate by integrated membrane process. Journal of Food Measurement and Characterization, 16(5), 4161–4170. https://doi.org/10.1007/s11694-022-01499-8

Kumar, R., Bansal, V., Tiwari, A. K., Sharma, M., Puri, S. K., Patel, M. B., & Sarpal, A. S. (2011). Estimation of glycerides and free fatty acid in oils extracted from various seeds from the Indian region by NMR spectroscopy. JAOCS, Journal of the American Oil Chemists' Society, 88(11), 1675–1685. https://doi.org/10.1007/s11746-011-1846-4

Leardi, R.; Melzi, C.; Polotti, G. CAT (Chemometric Agile Tool). Available online: http://gruppochemiometria.it/index.php/

software (accessed on 15 October 2022).

Lime, J., & Griffiths, F. P. (1953). Spectrophotometric Methods for Deter- mining Pigmentation-Beta-Carotene and Lycopene-in Ruby Red Grapefruit, 8(12), 941–944.

Malz, F., & Jancke, H. (2005). Validation of quantitative NMR. Journal of Pharmaceutical and Biomedical Analysis, 38(5 SPEC. ISS.), 813–823. https://doi.org/10.1016/j.jpba.2005.01.043

Mannina, L., Sobolev, A. P., & Viel, S. (2012). Liquid state 1H high field NMR in food analysis. Progress in Nuclear Magnetic Resonance Spectroscopy, 66, 1–39. https://doi.org/10.1016/j.pnmrs.2012.02.001

Mattoli, L., Gianni, M., & Burico, M. (2023). Mass spectrometry-based metabolomic analysis as a tool for quality control of natural complex products. Mass Spectrometry Reviews, 42(4), 1358–1396. https://doi.org/10.1002/mas.21773

Monreal, C., & Hort, C. (2008). Juice Quality of Two New Mandarin-like Hybrids (Citrus clementina Hort . ex Tan x Citrus sinensis L . Osbeck) Containing Anthocyanins, 2074–2078.

Nath, K., Dave, H. K., & Patel, T. M. (2018). Revisiting the recent applications of nanofiltration in food processing industries: Progress and prognosis. Trends in Food Science and Technology, 73(December 2016), 12–24. https://doi.org/10.1016/j.tifs.2018.01.001

Pappalardo, L. (2022). Pomegranate fruit juice adulteration with apple juice: detection by UV–visible spectroscopy combined with multivariate statistical analysis. Scientific Reports, 12(1), 1–7. https://doi.org/10.1038/s41598-022-07979-7

Polidori, J., Dhuique-Mayer, C., & Dornier, M. (2018). Crossflow microfiltration coupled with diafiltration to concentrate and purify carotenoids and flavonoids from citrus juices. Innovative Food Science and Emerging Technologies, 45(August 2017), 320–329. https://doi.org/10.1016/j.ifset.2017.11.015

Rapisarda, P., Fabroni, S., Peterek, S., Russo, G., & Mock, H. P. (2009). Juice of New citrus hybrids (Citrus clementina Hort. ex Tan.×C. sinensis L. Osbeck) as a source of natural antioxidants. Food Chemistry, 117(2), 212–218. https://doi.org/10.1016/j.foodchem.2009.03.101

Rivera-Pérez, A., Romero-González, R., & Garrido Frenich, A. (2022). A metabolomics approach based on 1H NMR fingerprinting and chemometrics for quality control and geographical discrimination of black pepper. Journal of Food Composition and Analysis, 105(August 2021). https://doi.org/10.1016/j.jfca.2021.104235

Ryu, S., Furihata, K., Koda, M., Wei, F., Miyakawa, T., & Tanokura, M. (2016). NMR-based analysis of the chemical composition of Japanese persimmon aqueous extracts. Magnetic Resonance in Chemistry, 54(3), 213–221. https://doi.org/10.1002/mrc.4364

Salvino, R. A., Colella, M. F., & De Luca, G. (2021). NMR-based metabolomics analysis of Calabrian citrus fruit juices and its application to industrial process quality control. Food Control, 121(July 2020), 107619. https://doi.org/10.1016/j.foodcont.2020.107619

Servent, A., Abreu, F. A. P., Dhuique-Mayer, C., Belleville, M. P., & Dornier, M. (2020). Concentration and purification by crossflow microfiltration with diafiltration of carotenoids from a by-product of cashew apple juice processing. Innovative Food Science and Emerging Technologies, 66(July), 102519. https://doi.org/10.1016/j.ifset.2020.102519

Sobolev, A. P., Mannina, L., Proietti, N., Carradori, S., Daglia, M., Giusti, A. M., et al. (2015). Untargeted NMR-based methodology in the study of fruit metabolites. Molecules. https://doi.org/10.3390/molecules20034088

Stämpfli, R., Brühwiler, P., Mourad, S., Verdejo, R., & Shaffer, M. (2007). Development and characterisation of carbon nanotube-reinforced polyurethane foams. EMPA

Activities, 26(2007), 51.

Tristán, A. I., Abreu, A. C., Aguilera-Sáez, L. M., Peña, A., Conesa-Bueno, A., & Fernández, I. (2022). Evaluation of ORAC, IR and NMR metabolomics for predicting ripening stage and variety in melon (Cucumis melo L.). Food Chemistry, 372(June 2021). https://doi.org/10.1016/j.foodchem.2021.131263

Türkyilmaz, M., Tağı, Ş., Dereli, U., & Özkan, M. (2013). Effects of various pressing programs and yields on the antioxidant activity, antimicrobial activity, phenolic content and colour of pomegranate juices. Food Chemistry, 138(2–3), 1810–1818. https://doi.org/10.1016/j.foodchem.2012.11.100

Turrini, F., Zunin, P., & Boggia, R. (2021). Potentialities of rapid analytical strategies for the identification of the botanical species of several ‹‹specialty›› or ‹‹gourmet›› oils. Foods, 10(1). https://doi.org/10.3390/foods10010183

Yao, L. H., Jiang, Y. M., Caffin, N., D'Arcy, B., Datta, N., Liu, X., et al. (2006). Phenolic compounds in tea from Australian supermarkets. Food Chemistry, 96(4), 614–620. https://doi.org/10.1016/j.foodchem.2005.03.009

Yong, C. H., Muhammad, S. A., Aziz, F. A., Nasir, F. I., Mustafa, M. Z., Ibrahim, B., et al. (2022). Detecting adulteration of stingless bee honey using untargeted 1H NMR metabolomics with chemometrics. Food Chemistry, 368(August 2021), 130808. https://doi.org/10.1016/j.foodchem.2021.130808

Zin, M. M., Alsobh, A., Nath, A., Csighy, A., & Bánvölgyi, S. (2022). Concentrations of Beetroot (Beta vulgaris L.) Peel and Flesh Extracts by Reverse Osmosis Membrane. Applied Sciences, 12(13), 6360. https://doi.org/10.3390/app12136360

Chapter 5: NMR Spectroscopy Applied to Metabolic Analysis of Natural Extracts of *Cannabis sativa*

This work was published as: Maria Francesca Colella, Rosachiara Antonia Salvino, Martina Gaglianò, Federica Litrenta, Cesare Oliviero Rossi, Adolfo Le Pera and Giuseppina De Luca, "NMR Spectroscopy Applied to Metabolic Analysis of Natural Extracts of Cannabis sativa" Molecules (2022) 27(11):3509.

The PhD candidate was involved in investigation, acquiring 1D NMR spectra and performing multivariate statistical analyses.

5.1 Introduction

Cannabis sativa is a fast-growing annual dioecious weed, probably native to the Central Asia and the Indian subcontinent (Li 1974; Small 2017), belonging to the *Cannabaceae* family (order Urticales) (ElSohly et al. 2017). Despite his critical taxonomic definition, because of its complex chemical composition and the presence of several spontaneous generations of hybrid species, nowadays, classifying *Cannabis* as a highly polymorphic and hybridized monotypic genus (*Cannabis sativa L.*) is the most accepted definition. Cannabis is one of the oldest and most versatile sources of intoxicant resin, textile fibre and phytocannabinoids, which are extracted from different parts of the plant, especially from the inflorescence and seed oil.

Hemp seed oil, obtained from *Cannabis sativa L.* seeds, is highly appreciated for its nutritional, anti-inflammatory, antioxidant, and immune-stimulating properties (Crescente et al. 2018). It is practically free of cannabinoids (Tura et al. 2022), so it has no psychoactive action but, like other common vegetable oils, it is rich in essential fatty acids (Banskota et al. 2022). As reported in several works, this oil is a rich source of ω-3 and ω-6 polyunsaturated fatty acids (almost 80%), in particular, linoleic acid (LA) and α-linolenic acid (αLA), with a ω-6/ω-3 ratio approximately equal to 3:1 (Spano et al. 2020). Although various factors, such as cultivation area, cultivar, seed origin, agronomic cultivation practices, etc., affect both the chemical composition and the ω-6/ω-3 ratio (Crescente et al. 2018; Spano et al. 2020), this ratio is considered an optimal nutritional value in the prevention of the risk of coronary heart disease (Simopoulos 2008; Teleszko et al. 2022). Due to this characteristic, cannabis seed oils are authorized and widely used in the food

sector ("Ministero della Salute" 2009), such as in the production of functional foods. Despite the growing interest in this product, specific regulations to evaluate its analytical quality parameters are still lacking (Spano et al. 2020). In this context, it would be desirable to find methodologies that could provide useful and rapid information both on the chemical composition and on the important ω-6/ω-3 ratio. The female inflorescences of the Cannabis have been widely used in the traditional medicine of different populations thanks to the pharmacological activity of some phytocannabinoids present in large quantities in these parts of the plant (Mercuri et al. 2002). Phytocannabinoids are a class of terpenophenolic compounds with a 21-carbon backbone: 120 of these molecules, naturally presents in the plant, have been identified and isolated to date (ElSohly et al. 2017; ElSohly and Slade 2005; Radwan et al. 2021). These natural molecules are different from synthetic cannabinoids, generally used as therapeutic agents, and from endocannabinoids, which are endogenous lipid-based retrograde neuro-transmitters capable of interacting with cannabinoid receptors in the human body (Bautista et al. 2021). The renewed and recent interest in Cannabis is due to the identification of these molecules whose different pharmacological activities such as anti-inflammatory effects, cell growth inhibition and tumor regression, seem to be supported by numerous experimental evidence (Baker et al. 2003; Izzo et al. 2009; Odieka et al. 2022). The chemical structures of the most common cannabinoids present in the Cannabis are shown in Figure 5.1. Among them the most representative are the well-known psychotropic agent Δ^9-trans-tetrahydrocannabinol (Δ^9-THC), the cannabidiol (CBD) and its precursor cannabidiolic acid (CBDA). Compared to THC, CBD shows therapeutic benefits without euphoric or dysphoric effects, that is an advantage for clinical applications (Baker et al. 2003; Izzo et al. 2009; Odieka et al. 2022). CBD has become very popular over the years for its health benefits, and nowadays is commercially available as a dietary supplement, lotion, and most importantly as a CBD oil. Indeed, the interest from the scientific community in the therapeutic potential of CBD oil is growing every day (Iftikhar et al. 2021). The reason is simple: it has already been used in various scientific studies, for the treatment of numerous health problems and is now recognized as one of the main elements of the so-called "therapeutic Cannabis" (Kopustinskiene et al. 2022; Russo 2018; Stasiłowicz et al. 2021). Industrial hemp crops, with a low THC content, have always been exploited as food and as a source of textile fibers, but they disappeared in the 1970s due to their association with the type of plants rich in THC (Pisanti and Bifulco 2019). The reintroduction of the cultivation of some hemp cultivars, to produce fibers and seeds, with a THC content lower than 0.2% *w/w*, took place only several years later, i.e., in 2009, by means of an appropriate Regulation published by the European Union ("Regulation (EC) No 1107/2009"). Nowadays, in many

countries, *Cannabis sativa* cultivations and medicines have been legalized under certain conditions due to the immense prospects in various medicinal applications (Brunetti et al. 2020; Schachtsiek et al. 2018). The Italian legislation on *C. sativa* cultivation is somewhat ambiguous about the legal and illegal uses and cultivation of the plant, based on the concentration of psychoactive cannabinoids. "The law 242/2016" about the *Dispositions for the promotion of cultivation and supply chain of agro-industrial hemp* is the most recent regulation in that direction and is the reference text governing industrial hemp production in Italy only for fiber or other industrial uses, different from pharmaceutics, with cultivation based around certified seeds ("Circolare-Camera dei Deputati" 2018). This measure establishes that the THC level must not exceed 0.2 %. However, even more recently, on 4 November 2019, Italian Ministry of Health approved and ratified "Definition of maximum levels of tetrahydrocannabinol (THC) in food" (GU n.11, 15-1-2020) ("Decreto 4 Novembre" 2019). This document fixes the content of THC at a maximum of 2 mg per kilo (0.0002%) in hemp seeds, flour, and derived foods and at a maximum of 5 mg per kilo (0.0005%) in the oil obtained from hemp seeds. It should be noted that now the list of regulated foods provided in the appendix includes only seeds, flours and oil, but it seems that it will be updated based on new scientific evidence. Currently the "Union method for the quantitative determination of the Δ^9-tetrahydrocannabinol content in hemp varieties", described by the annex III of the Commission Delegated Regulation (EU) 2017/1155 (the last update on 15 February 2017), is the only official procedure that member states must use for the quantitative determination of THC by gas chromatography (GC) after extraction with a suitable solvent ("European Union. Annex III" 2017). It describes in detail everything about sampling, including samples dimensions, drying and storage, techniques and reagents for extraction and determination of THC and it provides a tolerance allowed equal to 0.03% in absolute value. However, this official method is quite laborious, and the scientific community is always looking for advanced methodologies that allow to rapidly analyze natural mixtures without requiring manipulations or separations. An effective alternative to classical analytical methodologies could be the use of Nuclear Magnetic Resonance (NMR) spectroscopy. Moreover, as also seen in the previous works of this PhD thesis, the combination of this high-throughput technique with chemometric methods is extremely advantageous to visualize the useful information contained in the experimental NMR data.

The research presented in this work aims to apply NMR methodologies to the study of natural extracts from seeds and inflorescences of different cultivars of *C. sativa*, with a THC/CBD << 1 ratio (Aizpurua-Olaizola et al. 2016; Brighenti, Protti et al. 2021; Ohtsuki et al. 2022; Small 2017).

Specifically, the work aims to: (a) characterize the chemical profile (profiling) of the inflorescences and seeds for different varieties of *C. sativa*, grown in Calabria (South of Italy) via NMR spectroscopy and, in particular, by using 1D (^{1}H NMR, ^{13}C NMR) and 2D (^{1}H COSY, ^{1}H-^{13}C HMQC, ^{1}H J-Res) experiments; (b) evaluate the extraction efficiency of different common solvents as hexane, acetone and ethanol; (c) perform a multivariate statistical analysis (Principal Component Analysis - PCA) based on 1D NMR data, to discriminate samples coming from different extractive process and/or variety by identifying correlations between metabolite that influence each metabolic profile; (d) perform a quantification via NMR of the main cannabinoids (CBD , CBDA and eventually Δ^{9}-THC) using different internal standards.

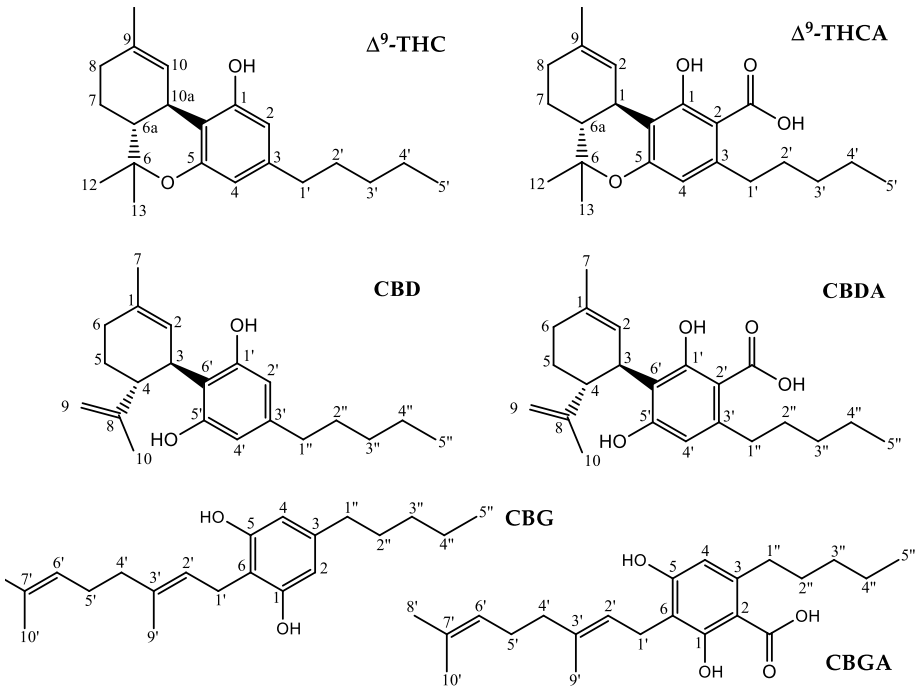

Figure 5.1 Chemical structure and nuclei numbering of molecular fragments in hemp principal cannabinoids.

5.2. Materials and methods

5.2.1. Plant Material and extraction procedure

In this work, two different varieties of hemp were considered − *Tiborszallasi,* and *Kompolti* − both for the metabolic characterization of inflorescences and for the quantitative and statistical analysis. NMR assignments were made on both varieties. Hemp inflorescences from *Tiborszallasi,* and *Kompolti,* grown in Calabria, were harvested in September 2020, i.e., in the ripening period for both cases, selecting a reasonable number of plants for each cultivar located a few meters away in the same crop. All the collected hemp inflorescences

were naturally air-dried, manually separated from twigs and finely chopped. After this procedure, the samples were stored in the dark at 4.0°C until analysis. Moreover, the chemical composition of seed extracts was also investigated via NMR. The seed samples were collected from the *Futura 75* cultivar by selecting, as for the inflorescences, an appropriate number of plants representative of the entire crop. The dry seeds were ground into a powder and stored in the dark at 4.0°C until analysis. All inflorescence and seed samples were provided by "Calabria Maceri e Servizi S.p.A." (Rende, CS, Italy), while the crops were produced by the farm "Le Querce S.r.l" (Montalto Uffugo, CS, Italy). The storage, pre-treatment sampling, and extraction procedures for inflorescences of the *Tiborszallasi*, and *Kompolti* varieties were mostly in accordance with the official "Union method for the quantitative determination of the Δ^9-tetrahydrocannabinol content in hemp varieties" ("European Union. Annex III" 2017). In order to evaluate the efficiency of the extraction and thus highlight any differences between the various extracts, different extraction solvents, commonly available in chemical laboratories and with increasing polarity, were chosen. The solvents used were n-hexane, acetone, and ethanol. For each sample, 1.0 g of dried, chopped, and stored inflorescence was extracted with 45 mL of solvent at room temperature for 20 min using an ultrasonic bath (30 kHz frequency). The obtained extracts were centrifuged for 5 min at 3000 rpm, the solutions were paper filtered, and the residues were extracted once more using the same procedure with another 45 mL of the same solvent. Lastly, the solvents were completely removed under vacuum. Starting from the same dried inflorescence matrix, 24 extractions were carried out for each variety. For the *Tiborszallasi* variety, 9 extractions were performed using ethanol and acetone and 6 using hexane, while for the *Kompolti* variety, 9 extractions were performed using hexane and ethanol and 6 using acetone. For the quantitative analysis, for both varieties, each extraction was carried out in triplicate to calculate an average value for the extraction yield and estimate the relative error. Then, three samples were collected for each solvent for a total of nine extracts for each variety. In addition, a quantitative analysis with gas chromatography (GC) using the flame ionization detector method was conducted on samples of the *Tiborszallasi* variety prepared from the same dried inflorescence matrix as the NMR samples by following the protocol reported in the literature ("European Union. Annex III" 2017). It should be emphasized that, given the chemical complexity of *C. sativa*, the extraction and collection of its various bioactive compounds are not simple and, for this reason, both solvents and different extraction methods are reported in the literature, ranging from microwave-assisted extraction to supercritical fluid extraction (Liu et al. 2022). The extraction procedure for seeds of *Futura 75* was based on dynamic-maceration ultrasound-assisted (ultrasound

assisted extraction (UAE); Hielcher UP 100Hz, 100W pulse, 30 kHz frequency), using ethanol as solvent. Then, 2.00 g of seeds – dried, chopped ad stored– were extracted with 45 mL of ethanol at room temperature for 20 min, under magnetic stirring. The solution was then paper filtered, evaporated under vacuum at 30°C and the residue was extracted with the same procedure one more time with other 45 mL of same solvent (Rezvankhah et al. 2018). The schematic experimental steps are shown in Figure 5.2.

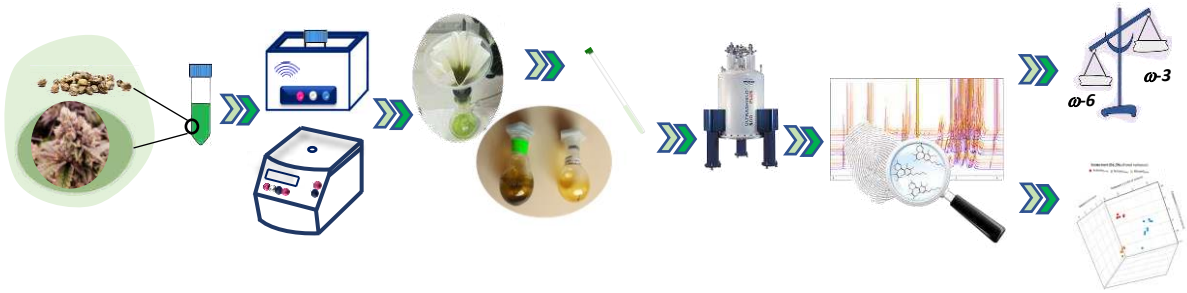

Figure 5.2 Schematic experimental steps involved in the extraction, sample preparation, and NMR characterization of *C. sativa* seeds and inflorescences.

5.2.2 Chemicals and solvents

Pure solvents, ethanol (Absolute, ≥ 99.8% - VWR Chemicals), n-hexane (Laboratory Reagent, ≥ 95% - Sigma Aldrich) and acetone, (ACS Reagent, ≥ 99.5% - Sigma Aldrich) were used for the cannabinoid extractions. Deuterated chloroform ($CDCl_3$ - 99.95 atom % D) as solvent for NMR sample preparation, anthracene, benzoic acid and 3-(trimethylsilyl) propionic-2,2,3,3-d4 acid (TMSP-d4 - 98 atom % D) as internal analytical standards for quantitative NMR analysis were purchased from Sigma-Aldrich (Milan, Italy).

5.2.3 NMR samples preparation, experiment and data processing

To prepare NMR sample, after the evaporation under vacuum, 30.0 mg of seeds extract of *Futura 75* were dissolved in $CDCl_3$ (~ 1 mL) directly in 5 mm *o.d.* NMR tube. On this solution, ^{1}H NMR spectrum (spectral width (SW) of 14.00 ppm, 128 free induction decays (FIDs) and a relaxation delay of 5.0 s and 2D ^{1}H COSY experiment (SW of 14.00 ppm on both dimensions, 2K data points, 40 scans and 256 increments) were recorded. Two other similar extraction procedures were repeated on the same starting matrix of dried seeds. On these extracts 1D ^{1}H NMR spectra were recorded to be used for reproducibility and standard deviation in the calculation of essential fatty acids ratio. ^{1}H NMR spectra were manually phased, baseline corrected and the chemical shifts were reported with respect to the TMS signal used as reference. From the ^{1}H NMR spectra of these extracts the main fatty acids

ratio ω-6/ω-3 can be determined by combining the integrals, obtained after applying the deconvolution procedure, of three different signals: (a) the methyl protons of all the acyl groups (LA), with the exception of those of α-linolenic acid; (b) the methyl protons of ω-3 fatty acid (α-linolenic acid (αLA)) and (c) the methylene protons of linoleic and α-linolenic acyl groups; and using the relations (Siudem et al. 2019):

$$\alpha\text{LA} = \frac{(\text{b})}{(\text{b})+(\text{a})} \tag{5.1}$$

and

$$\text{LA} = \frac{3\cdot(\text{c})-4\cdot(\text{b})}{3\cdot[(\text{b})+(\text{a})]} \tag{5.2}$$

The extracts residue of the two inflorescence varieties were dissolved in 1.20 mL of $CDCl_3$ and 600 µL of this solution was transferred to 5 mm *o.d.* NMR tube. For the quantitative analysis, samples of hemp in $CDCl_3$ were prepared carefully weighing all the components and by adding 0.3 mg of internal standard (anthracene, benzoic acid and TMSP-d4). No additional treatment was necessary for the preparation of NMR samples (Hazekamp et al. 2004; Marchetti et al. 2019). All the NMR experiments were performed on a Bruker Avance 500 MHz spectrometer working at a field strenght of 11.74 T (500 MHz 1H Larmor frequency), equipped with a 5 mm multinuclear probe TBO (Triple resonance Broadband Observe) and a standard variable-temperature control unit BVT-3000. All isotropic spectra were recorded at room temperature in $CDCl_3$ used as field-frequency lock signal.

Spectral assignments of metabolites were based on the one-dimensional (1D) ^{1}H, ^{13}C, ^{13}C-$\{^{1}H\}$ NMR spectra, bi-dimensional (2D) homo and heteronuclear correlation NMR experiments (^{1}H COSY, ^{1}H-^{13}C HMQC) and by comparison with data reports in the literature (Choi et al. 2004; Hazekamp et al. 2004; Marchetti et al. 2019). In addition, J_{ij} couplings between some pair of protons were measured thanks to the homonuclear 2D experiment of ^{1}H J-Resolved spectroscopy (J-Res) (Huang et al. 2015; Ludwig and Viant 2010). For each ^{1}H NMR experiment, 128 FIDs were acquired using a spectral width of 14.00 ppm, a relaxation delay of 5.0 s. The 1D ^{13}C-$\{^{1}H\}$ NMR spectra were recorder with proton broad-band decoupling collecting 8K FIDs, using a SW of 250.00 ppm and a relaxation delay of 5.0 s. For an accurate quantitative analysis of the metabolites present in the complex mixture, it was necessary to calibrate both the 90° pulses on the monitored nuclei (^{1}H and ^{13}C) and the T1 spin-lattice relaxation time. The T1 relaxation time was estimated by using the conventional inversion recovery experiment (10 increments from 0.5 ms to 30.0 s for ^{1}H,

and 24 increments from 0.1 ms to 300.0 s for ^{13}C) (Brighenti, Marchetti et al. 2021). The ^{1}H quantitative NMR (qNMR) spectra were recorded using the same acquisition parameters described before but with a relaxation delay of 20.0 s. Instead, for ^{13}C qNMR quantification experiments (*zgig* Bruker pulse sequence) were performed collecting 4000 FIDs, using a SW of 250.00 ppm, a relaxation delay of 160.0 s, an acquisition time of 10.0 s. The initial relative quantification has been obtained using the equation (3), in which the molar ratio $\frac{M_X}{M_Y}$ between the metabolite to quantify (X) and the internal standard (Y) is reported as function of the ratio between their integral (I_X and I_Y) and the ratio of resonant nuclei that generate the signal considered (N_X and N_Y) (Araneda et al. 2020; Bharti and Roy 2012):

$$\frac{M_X}{M_Y} = \frac{I_X}{I_Y} \cdot \frac{N_Y}{N_X} \tag{5.3}$$

Then, on the basis of the mass of extract used to prepare the NMR sample and the relative extraction yield, the absolute quantification was obtained in terms of percentage on dry weight of hemp flowers.

The ^{1}H COSY experiments were acquired using a SW of 14.00 ppm on both dimensions, 2K data points, 40 scans and 256 increments, the ^{1}H-^{13}C HMQC spectra were recorded using a SW of 14.00 ppm (^{1}H) and 250.00 ppm (^{13}C), 2K datapoints, 512 scans and 40 experiments, while ^{1}H *J*-Res spectra were acquired with a SW of 12.00 ppm, 2K datapoints, 256 scans and 48 experiments. A *sine* and a *qsine* filter were applied on both dimensions, F1 and F2, respectively on COSY and HMQC experiments before Fourier-transformed. Then, 1D NMR spectra were Fourier transformed and manually phased, baseline corrected and aligned using the TMS signal as reference. ^{13}C-{^{1}H} NMR spectra were filtered with 1.0 Hz line broadening before Fourier- transformation. For the multivariate statistical analysis, the ^{1}H NMR spectra were segmented in rectangular bucket of fixed 0.05 ppm. The integration region was defined on the first proton spectra and next it was reported, once saved, on the other spectra bucketed automatically. In particular, variables were manually selected by choosing the regions of NMR spectra with characteristic signals of metabolites and eliminating regions with a poor signal-to-noise ratio. Therefore, regions selected for the subsequent statistical treatment were 0.50-1.15 ppm, 1.3- 2.6 ppm, 3.8-7.0 ppm. Once normalized, the integrals were organized in a data matrix that was mean-centered and scaled. All the data processing steps were carried out using TopSpin 3.6 software (Bruker BioSpin, Rheinstetten, Germany) (“TopSpin” 2018).

5.2.4 Statistical analysis: Principal Component Analysis (PCA)

Multivariate analysis was performed on the 48 1D ^{1}H NMR experiments recorded on the samples prepared from the extracts obtained with different extractive solvents. There were 24 samples for both varieties: *Tiborszallasi,* and *Kompolti*. It should be noted that each sample prepared comes from different extracts, *i.e.*, for example the 9 samples of *Kompolti* in hexane were obtained from 9 extractive procedures of the corresponding inflorescences. Among the possible statistical approach, in this work the principal component analysis (PCA) was used as explorative method. This methodology applied to the data matrix of the bucketing ^{1}H NMR spectra of all extract samples, obtained as described in the previous subsection, allowed to obtain two datasets of 24 samples and 130 variables for each variety that were used as starting point to carry out PCA analysis using R software ("R Core Team." 2019).

5.2.5 Chromatographic experiments

The GC-FID analysis was intended to verify qNMR results for the *Tiborszallasi* variety. It was carried out by using the protocol reported in "European Union. Annex III", 2017, and a gas chromatograph (GC) equipped with: a split/splitless injector and a flame ionization detector (FID) (Dani Master GC1000, Dani instrument, Milan, Italy).

5.3. Results and Discussion

5.3.1 NMR characterization of seeds extracts

Figure 5.3 shows the 1D ^{1}H NMR spectrum of a sample of hemp seed extracts prepared as described in Section 5.2.1.

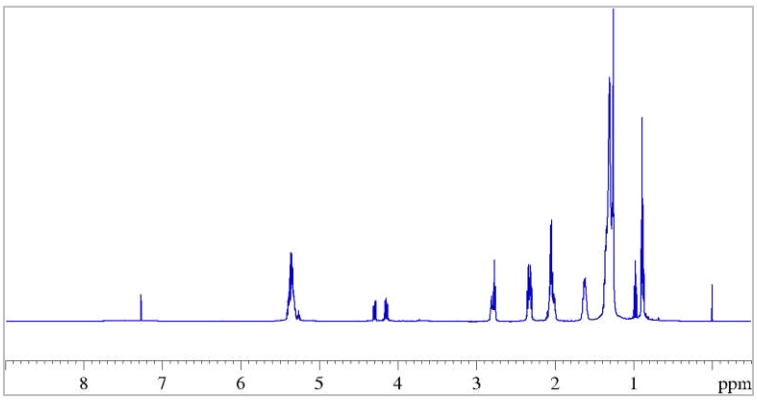

Figure 5.3 ^{1}H NMR spectrum (500 MHz) of hemp seeds oil dissolved in $CDCl_3$ recorder at 298K, obtained with ultrasound assisted extraction (UAE) procedure.

From the proton spectrum it is possible to recognize the classic profile of the esters of polyunsaturated fatty acids (PUFAs) (Popescu et al. 2015; Siudem et al. 2022) and, from the 2D ^{1}H COSY spectrum it is possible to trace all the correlations of the triacylglycerols (TAGs) containing both saturated and unsaturated fatty acids as shown in Figure 5.4.

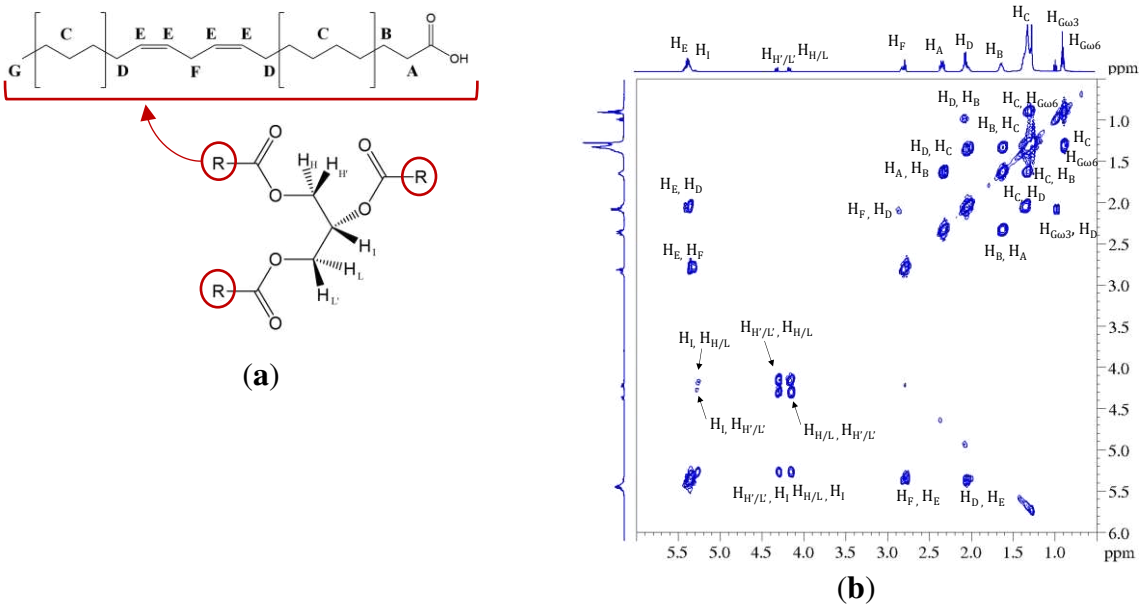

Figure 5.4 (a) General structure and nuclei labelling of molecular fragments in triacylglicerols (TAGs); (b) 2D map ^{1}H COSY of the ethanolic extract with UAE of *C. sativa* seeds. In figure all cross peak corresponding to the homuncular correlations have been highlighted.

Let's consider, for example, the strong signal generated by the α-methylenic protons of all acyl chains (H_A, Figure 5.4) detected between 2.27 ppm and 2.37 ppm. Clearly, the resonance frequency of the group of nuclei (labelling in Figure 5.4) for all fatty acids was not exactly the same and it depends on the nature of chain to which they belong. Consequently, it was not possible to determine a well-resolved multiplicity to the final complex signals appearing in the spectrum due to the overlap of all these signals with a slightly different chemical shift. For this reason, it was indicated as a multiplet (*m*) and the corresponded range of chemical shift is reported in the Table 5.1 in which also the correlations obtained from the COSY spectrum for these protons are also reported. The same reasoning is valid for all the other signals reported as multiplets in Table 5.1, which summarizes all assignments for hemp seeds extracts obtained from the ^{1}H and ^{1}H-^{1}H COSY spectra. In addition to this profiling, the NMR spectroscopy was applied also to evaluate the ω-6/ω-3 essential fatty acids ratio. In fact, since the integrals of the ^{1}H NMR signals were proportional to the number of hydrogen atoms present in each functional group and, overall,

to the number of functional groups present in the sample, from the combination of the integrals of different signals it is possible to calculate the concentration of fatty acids in general, and the ω-6/ω-3 ration in particular. To this end, three different signals in the protonic spectra were considered: (a) the multiplet at 0.88 ppm due to the overlapping triplet signals of the methyl protons of all the acyl groups (LA), with the exception of those of α-linolenic acid; (b) the triplet at 0.97 ppm generated by the methyl protons of ω-3 fatty acid (α-linolenic acid; (αLA)); (c) the multiplet at 2.72-2.86 ppm generated by the diallylic protons of linoleic and α-linolenic acyl groups.

By combining the area of these signals, using the relations (1) and (2) that take into account the number of equivalent nuclei in each group, the concentrations of αLA and LA were calculated, from which the ω-6/ω-3 ratio was obtained (Siudem et al. 2019). Calculations were made considering three different samples for reproducibility and to give a main value and a standard deviation. The value obtained for the ω-6/ω-3 ratio using Equations (5.1) and (5.2) was 2.93 ± 0.07. As can be seen, this value obtained by ^{1}H NMR is very close to the value of 3:1 for ω-6/ω-3 considered optimal for human dietary purposes, since it is able to prevent various diseases such as diabetes, cardiovascular disease, cancer, and other chronic diseases (Crescente et al. 2018; Ohtsuki et al. 2022; Simopoulos 2008; Siudem et al. 2022). On the other hand, the growing interest in hemp seed oil in other fields such as pharmaceuticals and cosmetics (Siudem et al. 2022) has resulted in a constant search for methods that allow fast and systematic quality control: the ω-6/ω-3 ratio is one of these quality parameters (Farinon et al. 2022). Our result is doubly important because, on the one hand, it indicates the quality of the oil extracts from the seeds of the *Futura 75* cultivar grown in Calabria and, on the other hand, it confirms that NMR is a reliable quantitative platform for the fast screening of hemp oil quality. Indeed, the measurement of this ratio is based only on the recording and analysis of the ^{1}H NMR spectra obtained directly from the seed extracts without further derivatization, as is required by the gas chromatography (GC) method, the common and validated method used to determine the composition of oil in terms of fatty acids (Borges et al. 2020). Moreover, our result agrees with that reported in the paper of Siudem et al. 2019, in which the authors analyzed six different samples of hemp seed oils and calculated the ω-6/ω-3 ratio by ^{1}H NMR for each of them using the relationships (5.1) and (5.2). The authors compared these data with those from CG method applied to the same hemp seed oils and found a substantial agreement between them, which proves the effectiveness of the method. It is worth noting that, in a recent paper (Siudem et al. 2022), the ^{1}H NMR methodology—as well as being used in the evaluation of the ω-6/ω-3 ratio—is

successfully combined with chemometric methods in order to observe the differences in several oil samples due to the different time and storage conditions of the oils. Hence, once again, this demonstrates how NMR can be used for the rapid and reliable analysis of hemp seed oil quality as an alternative to the more common classical analytical methods.

Table 5.1 ^{1}H NMR chemical shifts and $^{1}H/^{1}H$ correlations of fatty acids protons in triacylglicerols (TAGs) in $CDCl^{3}$ for hemp seeds extracts.

position	δ_H, multiplicity[a] (*J* in Hz)	COSY
A	2.27-2.37, m	E
B	1.55-1.67, m	C, A
C	1.23-1.39, m	$G_{\omega 6}$ B, D
D	1.98-2.11, m	$G_{\omega 3}$, C, F, E
E	5.28-5.42, m	D, F
F	2.76, t	D, E
$G_{\omega 3}$	0.97, t	D
$G_{\omega 6}$	0.88, t	C
H, L (*Gly*[a])	4.14, dd (11.88, 5.93)	H′, L′, I
I (*Gly*[a])	5.26, m	H, H′, L, L′
H′, L′ (*Gly*[a])	4.29, dd (11.88, 4.31)	H, L, I

[a]Abbreviations: s, singlet; d, doublet; dd, doublet of doublet; t, triplet; m, multiplet; Gly, Glycerol

5.3.2 NMR characterization of flower extracts

Figure 5.5 shows the ^{1}H and ^{13}C NMR spectra of inflorescences ethanolic extract for the *Tiborszallasi* variety. As is evident from the figure, the two spectra exhibit a complex distribution of resonances due to strongly overlapped signals of cannabinoids, having similar molecular structures (Figure 5.1), from which it is very difficult to recognize the single metabolites through the simple inspection.

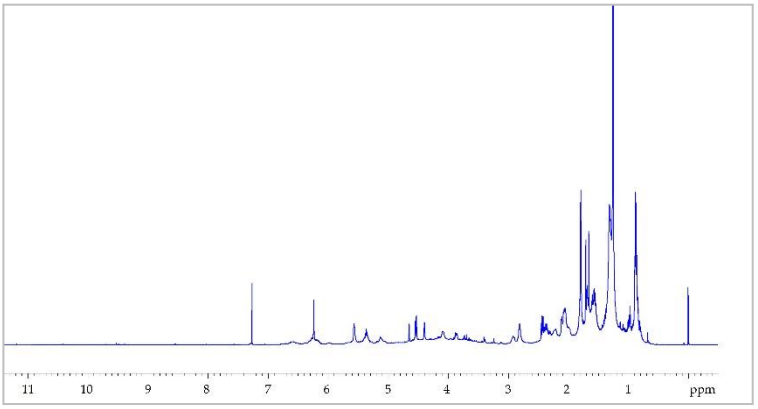

(**a**)

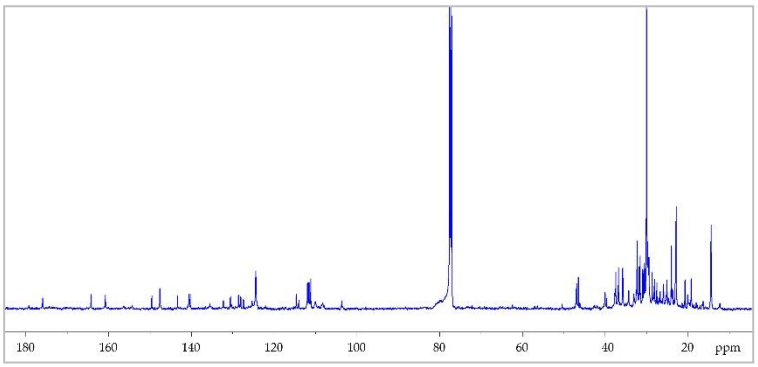

(**b**)

Figure 5.5 NMR spectra (500 MHz) of inflorescence extracts dissolved in $CDCl_3$ recorded at 298K. (**a**) ^{1}H NMR spectrum recorded using *zg30* Bruker standard pulses sequence; for each experiment, 128 FIDs were accumulated using a spectral width of 14.00 ppm and a relaxation delay of 5 s. (**b**) ^{13}C-{^{1}H} NMR spectrum (*zgig* Bruker pulse sequence) performed with proton broad-band decoupling, collecting 8K free induction decays (FIDs) and using a spectral width of 250.00 ppm and a relaxation delay of 5s. One-dimensional NMR FIDs were Fourier-transformed, phased, baseline-corrected, and aligned using the TMS signal as a reference. ^{13}C-{^{1}H} NMR spectra were filtered with 1 Hz line broadening before Fourier transformation.

To overcome these limitations that are characteristic of the 1D spectra of complex mixture, the identification of the various cannabinoids presents in the extracts (CBD, CBDA, CBG, THC), was carried out using the 2D correlation experiments ^{1}H-^{1}H COSY, ^{1}H-^{13}C HMQC, ^{1}H *J*-Res experiments and the data reported in the literature regarding the NMR characterizations of many single isolated cannabinoids (Choi et al. 2004; Ludwig and Viant 2010; Marchetti et al. 2019). It is worth underlining that, even in recent papers (Liu et al. 2022; Mazzara et al. 2022; Ohtsuki et al. 2022) the NMR methodology is mostly used to characterize fractions or single components of *C. sativa* obtained by separation techniques. In Figure 5.6 ^{1}H-^{1}H COSY and ^{1}H-^{13}C HMQC spectra are shown together with the correspondent enlargement on the CBD and CBDA correlations taken as an example of the

metabolic identification procedure adopted. In order to fully characterize the inflorescence extract, the 2D ^{1}H *J*-Res experiments were performed on the same sample (Huang et al. 2015; Ludwig and Viant 2010). In Figure 5.7 is reported the 2D ^{1}H *J*-Res spectrum recorded on the sample of *Tiborszallasi,* and, as an example, the case of H-9$_{cis}$ signal of CBD is reported in the enlargement. The signal of this proton in the 1D ^{1}H NMR spectrum is a multiplet from which it is impossible to extract any useful information. On the contrary, the extrapolation of the column in correspondence of the chemical shift of H-9$_{cis}$ on the F2 dimension of the ^{1}H *J*-Res spectrum gives the 1D profile of the considered signal in which it is possible to measure all the coupling constants. Indeed, as can be seen from the enlargement of Figure 5.7 this signal is a doublet of quadruplet due to the interaction of the proton H-9$_{cis}$ with the proton H-9$_{trans}$ (doublet, $^{2}J_{9cis\text{-}trans}$=2.6 Hz) and with the methyl proton H-10 (quadruplet, $^{4}J_{9cis\text{-}10}$=0.9 Hz).

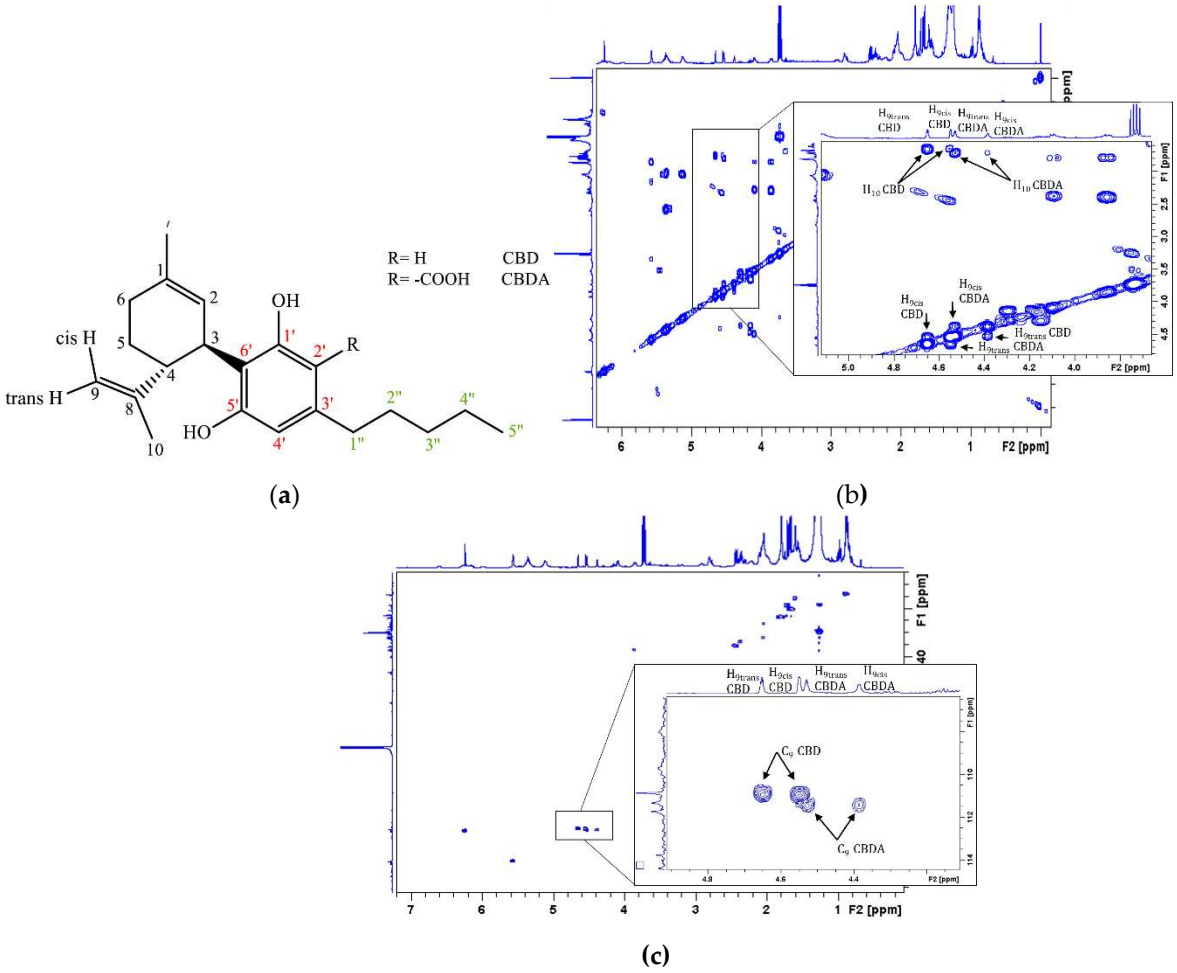

Figure 5.6 (a) Structure of CBD and CBDA are reported together with the atoms numbering adopted; (b) 500 MHz ^{1}H COSY spectrum and (c) ^{1}H -^{13}C HMQC NMR spectrum of inflorescences ethanolic extract sample of *Tiborszallasi*, variety dissolved in $CDCl_3$ recorded at 298K.

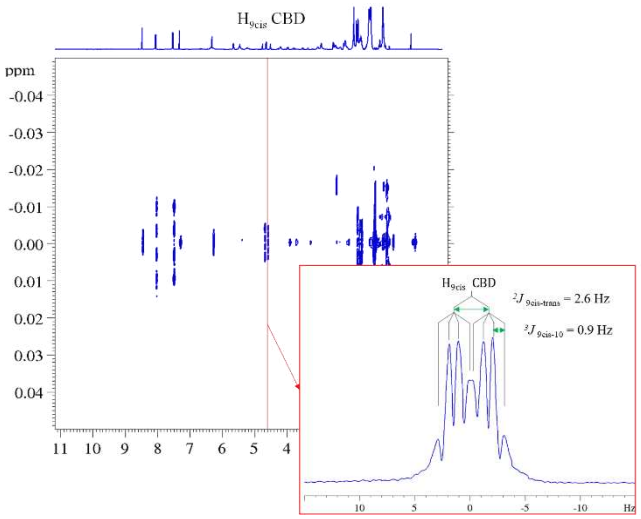

Figure 5.7 ^{1}H J-Res NMR spectrum of inflorescences ethanolic extract sample of *Tiborszallasi*, variety dissolved in $CDCl_3$ recorded at 298K. The projection of H-9_{cis} signal (doublet of quadruplets) of CBD is reported in the enlargement.

The assignments for the various cannabinoids present in the ethanolic extract, CBD, CBDA and CBG, of hemp inflorescences of *Tiborszallasi*, variety and their relative experimental information obtained from the NMR spectra (1D and 2D) are summarized in Table 5.2.

Table 5.2 ^{1}H and ^{13}C chemical shifts of the main cannabinoids in flowers extracts of *Cannabis sativa* (*Tiborszallasi*, variety) in $CDCl_3$.

Compound	δ ^{1}H ppm (multiplicity*, ^{1}H-^{1}H *J*-Coupling - Hz)		δ ^{13}C ppm	
CBD	H_3	3.86 (ddt; J_{H3-H4} =13.00 Hz (d), J_{H3-H2} = 3.51 Hz (d), J_{H3-H5} = 2.51 Hz (t))	C_3	37.01
	H_2	5.57	C_2	124.14
	H_{6a}	2.05 -2.09	C_6	30.36
	H_{6b}	2.22		
	H_5	1.78-1.84 (ddd; J_{H5-H4} = 5.30 Hz (*d*), J_{H5-H6a} =1.30Hz (d), J_{H5-H6b} = 0.60Hz (d))	C_5	28.35
	H_4	2.40 (dd; J_{H4-H3} =13.00Hz (d), J_{H4-H5} = 5.00 Hz (d))	C_4	46.16
	H_7	1.79 (*d* ; $^{3}J_{H7-H2}$ = 0.50 Hz)	C_7	23.69
	H_{9trans}	4.64 (dq ; $J_{9trans-9cis}$ = 2.65 Hz (d), $^{3}J_{9trans-10}$ =1.50 Hz (q))	C_9	110.81
	H_{9cis}	4.53 (dq ; $J_{9cis-9trans}$ = 2.65 Hz (d), $^{3}J_{9cis-10}$ = 0.92 Hz (q))		
	H_{10}	1.66 (dd ; $^{3}J_{10-9cis}$ = 0.92 Hz (d), $^{3}J_{10-9trans}$ =1.50 Hz (d))	C_{10}	20.30
	$H_{2'}$	6.26	$C_{2'}$	109.56
	$H_{4'}$	6.16	$C_{4'}$	107.92

	$H_{1''}$	2.43 (t)	$C_{1''}$	35.46
	$H_{2''}$	1.52-1.61	$C_{2''}$	30.65
	$H_{3''}$, $H_{4''}$	1.27-1.32	$C_{3''}$	31.48
			$C_{4''}$	22.54
	$H_{5''}$	0.86-0.88	$C_{5''}$	14.04
CBDA	H_3	4.08	C_3	35.38
	H_2	5.55	C_2	124.14
	H_{6a}	2.05-2.09	C_6	30.36
	H_{6b}	2.22		
	H_5	1.79 (ddd; $J_{H5\text{-}H4}$ = 5.30 Hz (d), $J_{H5\text{-}H6a}$ = 1.30Hz (d); $J_{H5\text{-}H6b}$ = 0.60Hz (d))	C_5	28.35
	H_4	2.40 (dd; $J_{H4\text{-}H3}$ =13.00Hz (d), $J_{H4\text{-}H5}$ = 5.00 Hz (d))	C_4	46.45
	H_7	1.79 (d ; $^3J_{H7\text{-}H2}$ = 0.50 Hz)	C_7	23.69
	H_{9trans}	4.51 (dq; $^3J_{9cis\text{-}9trans}$ = 3.00 Hz (d) ; $^3J_{9trans\text{-}10}$ =1.76 Hz (q))	C_9	111.21-111.25
	H_{9cis}	4.39 (dm ; $^3J_{9cis\text{-}9trans}$ = 3.00 Hz (d))		
	H_{10}	1.70	C_{10}	18.91
	$H_{4'}$	6.21	$C_{4'}$	111.21-111.25
	$H_{1''a}$	2.81	$C_{1''}$	36.68
	$H_{1''b}$	2.92		
	$H_{2''}$	1.52- 1.61	$C_{2''}$	31.24
	$H_{3''}$, $H_{4''}$	1.27-1.32	$C_{3''}$	31.94
			$C_{4''}$	22.54
	$H_{5''}$	0.86-0.88	$C_{5''}$	14.04
CBG	H_2	6.24	C_2	108.25
	$H_{5'}$, $H_{4'}$	2.04	$C_{4'}$	32.28
			$C_{5'}$	26.51
	$H_{6'}$	5.12	$C_{6'}$	125.08
	$H_{8'}$, $H_{9'}$	1.68	$C_{8'}$	20.51
			$C_{9'}$	23.44

*Abbreviations: d, doublet; t, triplet; q, quadruplet; m, multiplet; dd, doublet of doublet; ddd, doublet of doublet of doublet; ddt, doublet of doublet of triplet; dq, doublet of quadruplet; *d*m, doublet of multiplet.

These results agree with many other literature data (Choi et al. 2004; Hazekamp et al. 2004; Marchetti et al. 2019; Ohtsuki et al. 2022) and demonstrate how the non-separative NMR technique, combining 1D and 2D experiments, can be successfully applied directly to a complex mixture, such as a *Cannabis* extract, for chemical characterization. An interesting result of the present study is the measurement of a large number of $J_{H\text{-}H}$ for the main cannabinoids, carried out again directly on the *Cannabis* extract through the analysis of the

2D J-Res spectra. It must be highlighted that, in the ethanolic extract, the signals related to THC were not detected in the recorded spectra; this means that, in this solvent, the quantity of THC extracted was below the NMR detection limit (Eisenmann et al. 2016). This also occurred for the acetone extracts while the spectra of the hexane extracts showed a small broad peak isolated at 6.40 ppm corresponding to the proton H-10 of Δ^9-THC. This means that hexane, which is also the solvent indicated in the official method for determining the amount of Δ^9-THC in hemp, was the most effective at extracting cannabinoids compared to the other solvents used. Once the assignment of cannabinoids in the *Tiborszallasi* variety was determined, a comparison between the NMR spectra of the samples relating to the *Kompolti* variety was possible. Except for the proton spectrum of the hexane extract of the *Kompolti* variety, in which Δ^9-THC signals were absent (Figure 5.8), no further differences in terms of profile were distinguished in the spectra of any other samples of either variety.

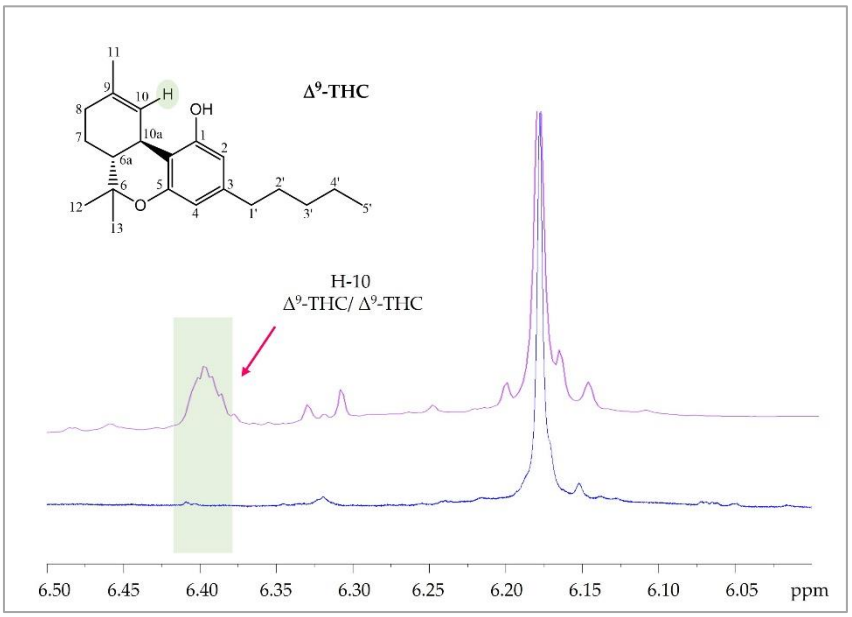

Figure 5.8 Comparison between the enlarged region [6.0 ppm - 6.5ppm] of the ^{1}H NMR spectra from ethanol extract of *Kompolti* (blue) and *Tiborszallasi* (purple) variety. A broad peak isolated at 6.40 ppm corresponding to the proton H-10 of Δ^9-THC appears in the proton spectra of *Tiborszallasi* while this signal was undetectable in the ^{1}H NMR spectrum acquired for *Kompolti*..

The comparison between ^{1}H NMR spectra from both varieties for the different solvents are reported in Figures 5.9 and 5.10.

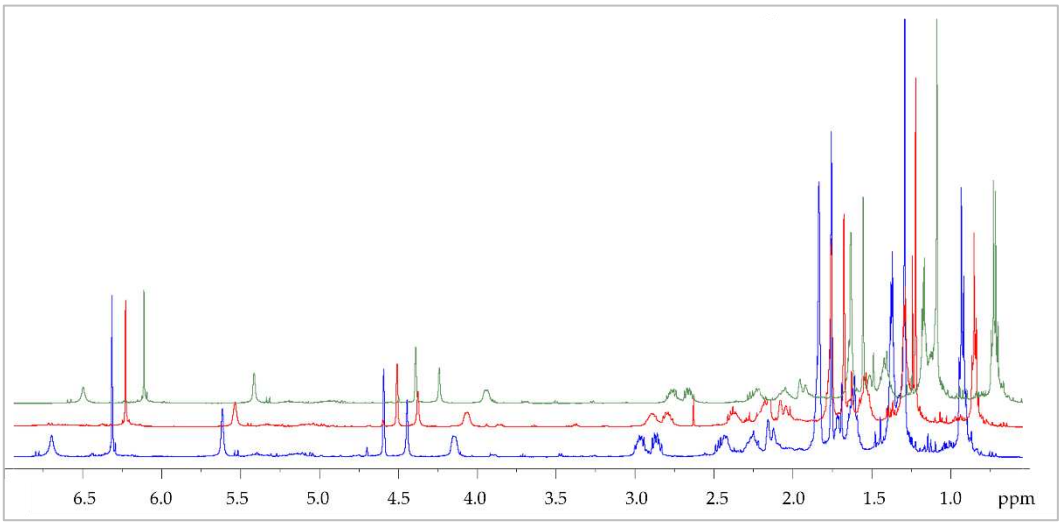

Figure 5.9 Comparison between ^{1}H NMR spectra of ethanol (blue), acetone (red) and hexane (green) extracts for *Tiborszallasi* variety.

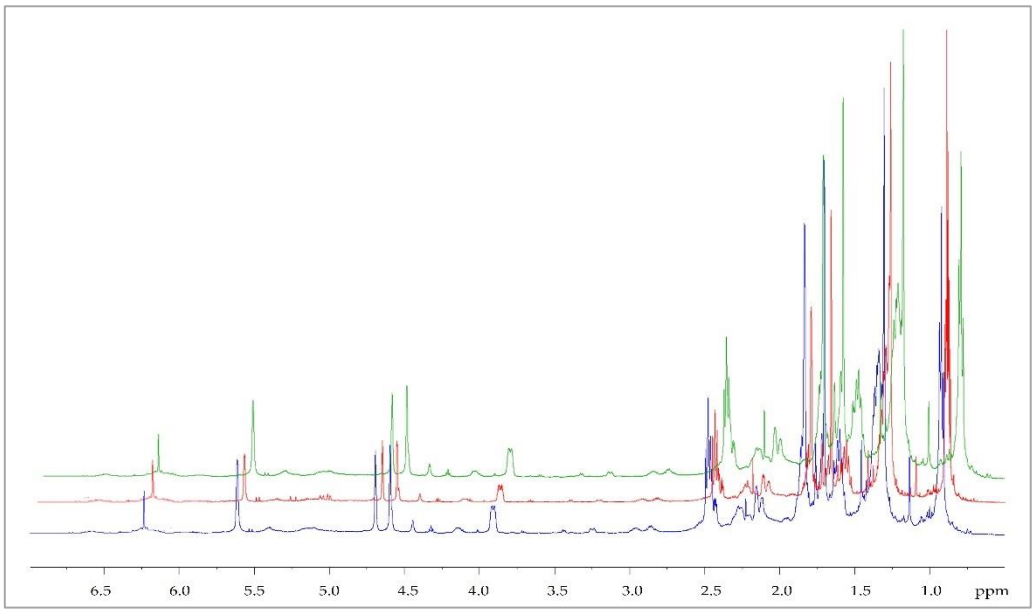

Figure 5.10 Comparison between ^{1}H NMR spectra of ethanol (blue), hexane (red) and acetone (green) extracts for *Kompolti* variety.

In addition to the cannabinoids, by comparison the protonic spectra of hemp seed oil and hemp inflorescence extracts, it was possible to recognize in this last spectrum some signals that referred to the triacylclycerols constituent. In particular, this profile was easily recognizable in

the samples obtained by using ethanol as the extracting solvent. All the signal assignments are reported in the Figure 5.11

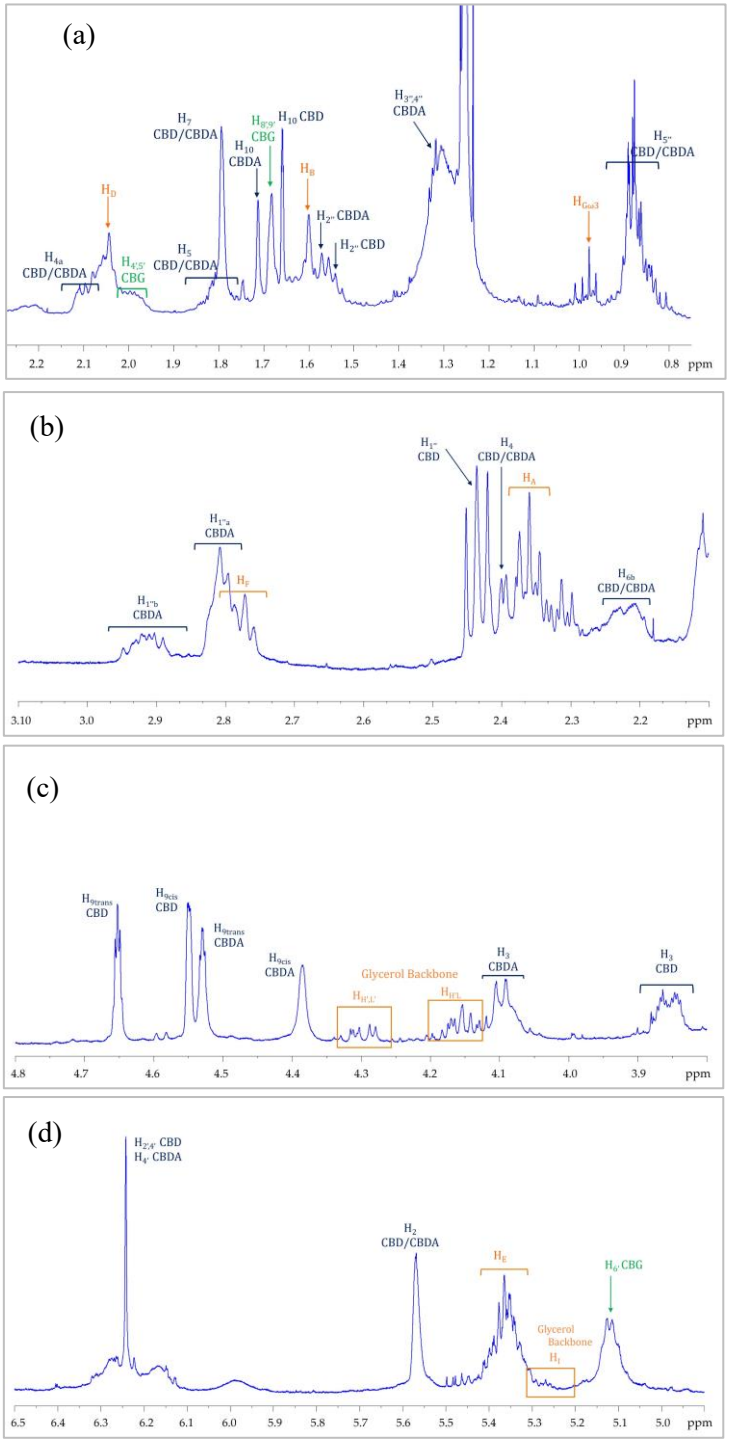

Figure 5.11 [1]H NMR spectrum of an ethanolic extract of *C. sativa* inflorescences (*Tiborszallasi* variety). For the enlarged regions **(a)** [0.8 ppm-2.2ppm], **(b)** [2.2ppm-3.00ppm], **(c)** [3.7ppm-4.8ppm], **(d)** [4.8ppm-6.5ppm] the signal attributions are shown. Signals assignments are reported with different colors: orange for TAGs; grey for the glycerol backbone; blue for CBD/CBDA; green for CBG/CBGA.

5.3.3 Multivariate analysis

Principal Component Analysis (PCA) was applied to discriminate hemp flowers samples based on their ^{1}H NMR spectra (Ren et al. 2015; Webb 2018). The main aim was to observe how the cannabinoids profiles changed for extracts in relation to the nature of solvent extraction and the efficiency of the extraction procedure. PCA was carried out on two different data matrices, one for each hemp variety. For *Tiborszallasi*, the data matrix consists of 24 samples (9 extracts for ethanol and acetone respectively, 6 extracts for hexane) and 130 variables. For *Kompolti* variety the data matrix consists of 24 sample (9 extracts for hexane and ethanol respectively, 6 extracts for acetone) and 130 variables.

Figure 5.12 and Figure 5.13 show the 3D score plot for *Tiborszallasi,* and *Kompolti* variety samples respectively, with a cumulative percentage of explained data variance with the three first PC equal to: (a) 88.1 % (45.5% for PC1, 30.2% for PC2, 12.4% for PC3) for the *Tiborszallasi*, variety and (b) 84.5% (51.8% for PC1, 17.5% for PC2, 15.2% for PC3) for the *Kompolti* variety. This mean that data loss is negligible in both cases. The score plot effectively summarizes the relationship between the samples and highlights what was not discovered by the simple comparison among the protonic spectra: a clear and well-defined separation between samples was observed and every type of extract was clustered into one defined region. Indeed, PC1 allows to discriminate among extracts with non-polar solvent and extracts with higher polarity: hexane extracts had, in fact, positive value of PC1 while the other ones had negative values of PC1. Instead, PC2 seems to best discriminate acetone and ethanol extracts. The same result is obtained for both varieties.

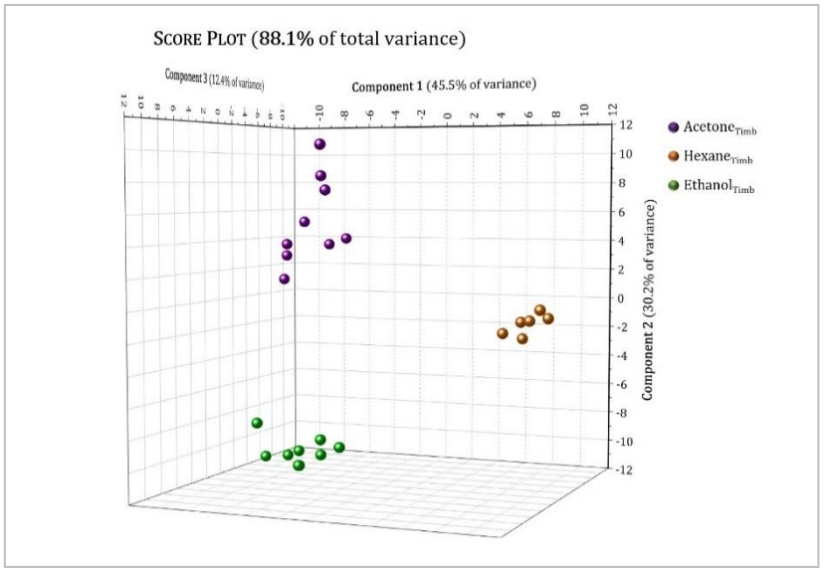

Figure 5.12 Principal Component Analysis (PCA) of hexane (brown dots), acetone (purple dots) and ethanol (green dots) extracts of *Tiborszallasi,* variety of hemp. The scores plot showing the first three PCs (PC1, PC2 and PC3) with their respective variation. R2X(PC1) = 45.5%, R2X(PC2) = 30.2%, R2X(PC3) = 12.4%.

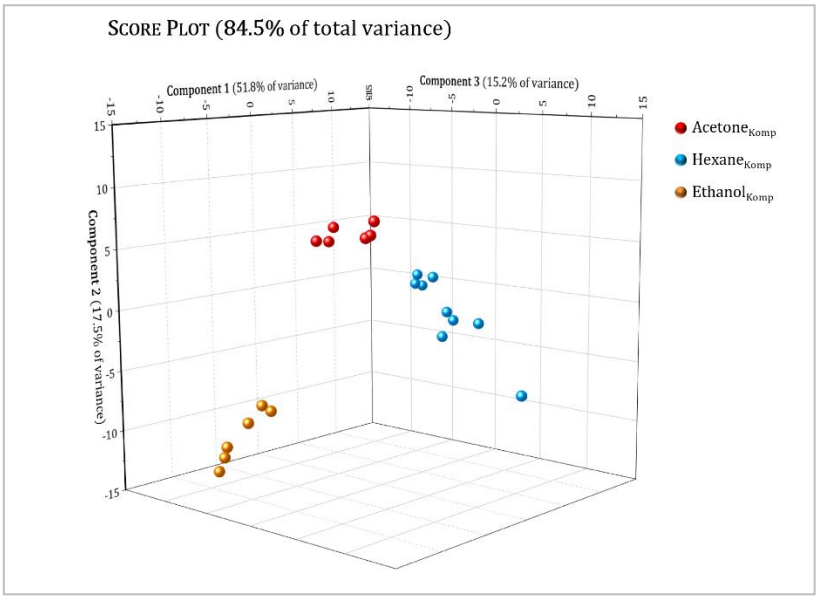

Figure 5.13 Principal Component Analysis (PCA) of hexane (blue dots), acetone (red dots) and ethanol (orange dots) extracts for *Kompolti* variety of hemp. The scores plot showing the first three PCs (PC1, PC2 and PC3) with their respective variation. R2X(PC1) = 51.8%, R2X(PC2) = 17.5%, R2X(PC3) = 15.2%.

However, in order to determine which metabolites, influence better the discrimination and evaluate the quality and efficiency of the extraction procedure, an accurate discussion about loadings is necessary. In Figure 5.14, a 2D biplot of the first two PCs (PC1 and PC2) for the *Tiborszallasi,* variety is reported; this shows the sample differentiation and the changes in the metabolite concentrations from one extract to another and, consequently, the variables responsible for the sample clustering observed in the score diagram.

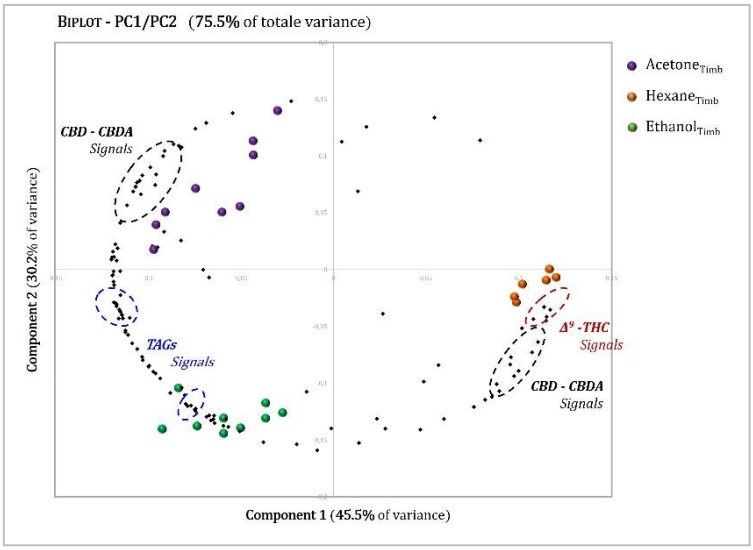

Figure 5.14 Biplot of PCA carried out on NMR spectra of hexane (brown dots), acetone (purple dots) and ethanol (green dots) extracts of *Tiborszallasi*, variety of hemp. The scores plot showing the first two PCs (PC1 and PC2) with their respective variation. R2X(PC1) = 45.5%, R2X(PC2) = 30.2%.

THC is the marker that gives a first clear distinction between hexane and all the other extracts: the THC loadings had positive values of PC1 and negative values of PC2, and these were very close to the scores of the hexane extracts. This means, as also demonstrated by the loadings of CBD and CBDA, that hexane is more efficient in the extraction of Cannabinoids and of THC in particular. Indeed, the latter was below the NMR detection limit in the acetone and ethanol extracts. These results are not surprising since it is well known from the literature (Brighenti, Protti et al. 2021; Valizadehderakhshan et al. 2021) that the polarity of the solvent affects the chemical composition of the cannabinoids present in the extracts.

Focusing on the TAGs previously detected during the signal assignment step, negative values of PC1 were obtained for these loadings. This indicates that extraction with a higher polarity solvent (acetone or ethanol) obtains samples with a lower percentage of cannabinoids but

that are richer in fatty acids than hexane extracts. This peculiarity could be exploited to obtain extracts rich in both bioactive compounds—cannabinoids and TAGs—that could potentially be used in the food and pharmaceutical industries to produce functional foods and supplements.

The same conclusions were also reached for the *Kompolti* variety, whose 2D biplot of the first two PCs is reported in the Figure 5.15.

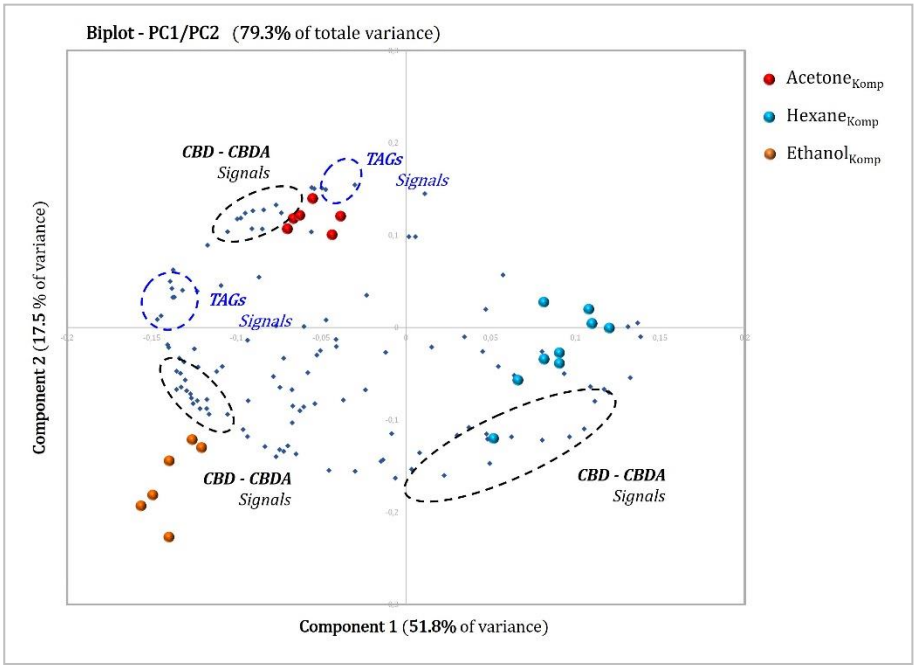

Figure 5.15 Biplot of PCA carried out on NMR spectra of acetone (red dots), hexane (blue dots) and ethanol (orange dots) extracts of *Kompolti* variety of hemp. The scores plot showing the first two PCs (PC1 and PC2) with their respective variation. R2X(PC1) = 51.8%, R2X(PC2) = 17.5%.

The present study has shown that the exploratory PCA method, although simple, is able to differentiate samples coming from different extraction solvents and, in addition, it highlights which cannabinoids form the basis of this differentiation. Chemometrics-aided NMR techniques performed on *C. sativa* components (inflorescences, seed oils, leaves, and other less valuable parts of the plant), or on fractions of them, are widely used to determine different properties of *C. sativa*, as evidenced by the plethora of studies reported in the literature (Brighenti, Protti et al. 2021; Choi et al. 2004; Mudge et al. 2018; Peschel and Politi 2015) and the references reported therein. In many of these works, the combination of ^{1}H-NMR spectra with chemometric tools was used for the metabolomic differentiation of inflorescence extracts from different cultivars and to identify particular markers in order to discriminate different plant chemotypes (Choi et al. 2004; Peschel and Politi 2015). In other

studies (Ingallina et al. 2020; Spano et al. 2021) targeted and non-targeted NMR methodologies were used to identify and quantify compounds of different classes present in the inflorescence extracts of several *C. sativa* cultivars and to monitor their variations in three different harvested stages. The cultivars analyzed in these studies had a THC content always below the legal limit, while the quantities of the other cannabinoids in the extracts were affected by the harvest time and by the solvent.

Although it is not easy to make comparisons given the quantity of factors affecting the composition of cannabinoids, the results obtained in this study substantially agree with the studies described above, and therefore seem to demonstrate the reliability of this method and its possible application in the routine analysis of cannabinoids.

5.3.4 Quantitative analysis of inflorescences

As a support to the results obtained from the PCA analysis and to evaluate if the NMR methodology can be a valid tool in the quantitative determination of the cannabinoids extracted as a function of the solvent used, an NMR quantification was also carried out using ^{1}H and ^{13}C NMR spectra and different internal standards.

Tiborszallasi- and *Kompolti*-type hemp flower samples used for the quantification were obtained, as mentioned before, by ultrasound-assisted extraction using three different common solvents of increasing polarity: hexane, acetone and ethanol. The complete procedure, from extraction to NMR measurement, was performed in triplicate to evaluate repeatability, to calculate an average value for the extraction yield, and to estimate the relative error. The procedure below is described for the *Tiborszallasi*, samples but exactly the same was done for the *Kompolti* variety. The average experimental extraction yields for each procedure were: (a) 17.9 ± 0.3 % for extraction in hexane; (b) 9.9± 0.8 % for extraction with acetone; (c) 19.6 ± 0.9 % for extraction with ethanol. For the quantification of cannabinoids present in the extracts, both 1D ^{1}H NMR and ^{13}C NMR spectra were used. The quantification of cannabinoids by protonic spectra included the use of three different internal standard as anthracene, in accordance with literature (Stasiłowicz et al. 2021), benzoic acid, and 3-(trimethylsilyl)propionic-2,2,3,3-d4 acid (TMSP-d_4). These compounds are highly pure (≥ 99.9%), have low volatility, are chemically inert, and are not similar in the structure to the cannabinoids to be quantified. Indeed, in the case of NMR spectroscopy, it is necessary that they generate well isolated signals in the spectrum, that do not overlap with the peaks assigned to other metabolites in the mixture. In this case, signals of aromatic protons of

anthracene and benzoic acid ranged between 7.4 ppm e 8.5 ppm in the protonic spectrum, and the singlet of the methyl group of TMSP-d_4 was set to 0.00 ppm.

The signals considered for the quantification, using Equation 5.3, were the following: for CBD the H-9_{trans} olefinic proton signal at δ = 4.65 ppm, for CBDA the H-9_{cis} olefinic proton signal was set at δ = 4.38 ppm; and for the Δ^9-THC the H-10 proton signal was set at δ = 6.40 ppm. The results obtained for the three standard used are reported in Table 5.2. For further confirmation of the ^{1}H qNMR results, quantitative ^{13}C NMR spectra were also recorded on the hemp flowers hexane extracts of *Tiborszallasi*, optimizing the acquisition parameters (see section 5.2.3) and the operative conditions (Marchetti et al. 2019). However, in this case, only TMSP-d_4 was used as internal standard for ^{13}C qNMR because aromatic carbons of anthracene and benzoic acid generate signals in the region between 125 ppm - 134 ppm, overlapped with cannabinoids signals. Moreover, given the low sensitivity of the ^{13}C nucleus, the ^{13}C qNMR was useful for the quantitative determination of CBDA, the only cannabinoid whose signals have an acceptable signal-to-noise ratio. The CBDA content (% on dry weight) obtained via ^{13}C qNMR for in *Tiborszallasi,* hexane extract is equal to 6.2 ± 0.9 substantially in agreement with that obtained from protonic spectra using the same internal standard (Table 5.2).

Observing the results reported in Table 5.2, the value obtained for the three cannabinoids CBD, CBDA and Δ^9-THC, for each type of extract, using different internal standard, were fairly reproducible. This means that benzoic acid and TMSP-d_4 seem to be valid alternatives to the anthracene as internal standard for quantification. Indeed, anthracene is the standard that is usually used for the quantification of cannabinoids via NMR, but it has many drawbacks related to its toxicity, its poor solubility in the common solvents and long recording times due to long T1 (Olasehinde and Olaniran 2022). Furthermore, the data show that hexane extracts are richer in cannabinoids than other solvents, as had already emerged in the biplot analysis, and, most interestingly, the quantities obtained for these extracts via NMR matched very well with the experimental data acquired following the official European procedure for the determination of cannabinoid Δ^9-THC as reported in Table 5.3. Indeed, the table shows the comparison, for the same sample of *Tiborszallasi*, inflorescences, between the qNMR data of Δ^9-THC via NMR and those obtained with the official GC-FID technique ("European Union. Annex III" 2017). In the table 5.3, is reported also the GC-FID value concerning the quantity of CBD/CBDA obtained on the same sample. It should be noted that the GC-FID procedure does not allow to discriminate between CBDA and CBD: before extraction, it includes a pretreatment of inflorescences at a high temperature that leads to the

complete decarbossilation of the acidic form of this cannabinoid (CBDA) to the neutral (CBD). So, this unique value should be considered as the sum of the quantities of CBDA and CBD initially present in flowers. As can be seen from the table, also in this case the data via NMR are in perfect agreement with those obtained via GC-FID. It is worth noting that the NMR technique has been proven to be a reliable and powerful tool for the quantification of different natural products and, especially in recent years, has also been successfully applied to the quantification of CBD and other cannabinoids directly on hemp extracts coming from different cultivars using both the ^{1}H and ^{13}C qNMR methodologies (Barthlott et al. 2021; Brighenti, Marchetti et al. 2021; Marchetti et al. 2019; Nagy et al. 2019). Quantitative ^{1}H-NMR is the most widely used method in the quantification of natural extracts and has been shown to have a good level of accuracy and reproducibility. However, its application to hemp extracts presents several drawbacks, due both to the presence of contaminants and to the overlapping of different signals that require the extensive use of deconvolution processes (Risoluti et al. 2020). The use of ^{13}C q-NMR, introduced by Marchetti et al. 2019 partially removes these weaknesses and at the same time offers sufficiently precise and sensitive results. As expected, our results substantially agree with these previous reports on the ^{1}H and ^{13}C qNMR investigations, even if it is necessary to point out that a direct comparison on the quantities of cannabinoids found in the different extracts of the cultivar analyzed is practically impossible given, as we have already highlighted, the large quantity of variables, i.e., cultivar, geographical origin, harvesting period, agronomic practices, extraction methodologies, etc., that affect the composition of cannabinoids. However, the quantitative results of the present study highlight, once again, the remarkable potentialities of the NMR technique which was able to quantify the main metabolites present in the hemp inflorescence extracts we analyzed as they were, without the further treatment or derivatization required by the official technique (Nahar et al. 2020; Sgrò et al. 2021). Moreover, as reported recently by Dadiotis et al. 2022 concerning the quantitative analysis of cannabinoids in hemp extracts using, in a complementary way, the ^{1}H-NMR and ^{1}H-^{1}H COSY NMR spectra, these quantitative data via NMR are comparable with those acquired with other more consolidated techniques applied to the same extracts. This evidence shows good correspondence between the various quantification techniques, as also confirmed by the data we obtained on the *Timborszallase* cultivar given the satisfactory agreement between the NMR and GC-FID data of the hexane solvent. In addition, the quantitative data obtained for the different solvents confirm the purely qualitative indications given by the PCA analysis, which proved to be very informative and fast. These results were obtained for the *Tiborszallasi* variety but, as previously mentioned, the quantification of the main

cannabinoids by ^{1}H and ^{13}C qNMR was also performed for the *Kompolti* variety and the results are reported in Table 5.4.

Table 5.3 ^{1}H NMR data of main cannabinoids in *Timborzallasi* inflorescences compared with GC-FID method.

Compound	qNMR on flowers UAE extracts				GC-FID
	qNMR IS	Hexane	Acetone	Ethanol	
CBDA content*	Anthracene	6.3± 0.8	0.40± 0.1	0.31± 0.04	Validated Laboratory Method
	Benzoic acid	6.5±0.8	0.40± 0.1	0.39± 0.06	
	TMSP-d_4	6.4±0.6	0.41± 0.1	0.41± 0.06	6.9±0.2
CBD content*	Anthracene	0.4±0.1	4.60± 0.8	3.0± 0.1	Referred to **CBD**
	Benzoic acid	0.30±0.06	4.54± 0.6	2.2± 0.1	after decarbossilation
	TMSP-d_4	0.4±0.1	4.59± 0.6	2.9± 0.1	
Δ^9-THC content*	Anthracene	0.11±0.04	< LOD	< LOD	Regulation (EU) N° 639/2014 ("European Union. Annex III" 2017)
	Benzoic acid	0.07±0.02			
	TMSP-d_4	0.10±0.02			0.09±0.01

*% on dry weight

Table 5.4 ^{1}H NMR data of main cannabinoids in *Kompolti* inflorescences.

Compound	qNMR on flowers UAE extracts			
	qNMR IS	Hexane	Acetone	Ethanol
CBDA content*	Anthracene	0.4 ± 0.3	0.4 ± 0.2	0.5 ± 0.2
	Benzoic acid	0.6 ±0.2	0.5 ± 0.1	0.4± 0.1
	TMSP-d_4	0.4 ± 0.3	0.4 ± 0.3	0.5 ± 0.3
CBD content*	Anthracene	5.7 ±0.2	5.4 ± 0.3	5.2 ± 0.2
	Benzoic acid	5.9±0.2	5.2 ± 0.2	5.3 ± 0.1
	TMSP-d_4	5.9±0.2	5.6 ± 0.3	5.3 ± 0.3
Δ^9-THC content*	Anthracene	< LOD	< LOD	< LOD
	Benzoic acid			
	TMSP-d_4			

*% on dry weight

5.4. Conclusions

Cannabis sativa is a fast-growing plant currently grown all over the world that is gaining popularity in various fields of research for its biological and pharmaceutical properties. Actually, *C. sativa* is widely recognized and appreciated for the high nutritional and health-promoting properties of the oil obtained from its seeds, together with the pharmacological activity mainly associated with psychoactive and non-psychoactive cannabinoids and the chemical components mainly extracted from the inflorescences. In this work, NMR spectroscopy was applied to analyze extracts from the seeds and inflorescences of different varieties of *Cannabis sativa* grown in Calabria in order to explore the potentialities of this technique for the qualitative and quantitative analysis of the extracts, and to evaluate the

possibility of using it as an alternative to the most common methods in the quantification of cannabinoids present in inflorescence extracts. The quantitative NMR results obtained from two varieties of hemp inflorescence extracts, using different internal standards and solvents, demonstrated the high potentiality of the proposed technique in this field of application. Indeed, the NMR technique was able to quantify the main cannabinoids present in the extracts, the quantitative data were reproducible, and—most importantly—the data from the hexane solvent were congruent with the data obtained by the GC-FID method. Moreover, while this last methodology is not able to distinguish CBD and CBDA, using the NMR method, it was possible to separate the two contributions and quantify them. This proves, once again, the analytical power of the NMR technique which is not only able to offer the same results obtained from the official method, including the evaluation of THC, but can indicate more informative data without performing particular treatments on the sample. In addition to the characterization and the quantitative study, different extraction procedures were tested and evaluated by NMR spectroscopy with the aim of obtaining inflorescence extracts poor in psychotropic agents and rich in medical cannabinoids and triacylglicerols (TAGs), which have an ω-6/ω-3 ratio that has been found to be excellent from a nutritional point of view. Specifically, extracts of inflorescences obtained by ultrasound-assisted solute–solvent extraction using hexane, acetone and ethanol as solvents were studied. By elaborating the spectral data with a statistical method (PCA) together with the qNMR approach, it was possible to conclude that hexane was more efficient in the extraction of cannabinoids (THC included) than the TAG constituents, while extraction with a higher polarity solvent (acetone or ethanol) obtained samples free from THC (THC content < LOD), rich in TAGs, and with a lower percentage of cannabinoids. This evidence can be exploited to obtain extracts rich in bioactive compounds (both cannabinoids and TAGs) that could potentially be used in the food and pharmaceutical industries, opening new paths for the production of functional foods and supplements.

5.5 References

Aizpurua-Olaizola, O., Soydaner, U., Öztürk, E., Schibano, D., Simsir, Y., Navarro, P., et al. (2016). Evolution of the Cannabinoid and Terpene Content during the Growth of Cannabis sativa Plants from Different Chemotypes. *Journal of Natural Products*, *79*(2), 324–331. https://doi.org/10.1021/acs.jnatprod.5b00949

Araneda, J. F., Chu, T., Leclerc, M. C., Riegel, S. D., & Spingarn, N. (2020). Quantitative analysis of cannabinoids using benchtop NMR instruments. *Analytical Methods*, *12*(40), 4853–4857. https://doi.org/10.1039/d0ay01511c

Baker, D., Pryce, G., Giovannoni, G., & Thompson, A. J. (2003). The therapeutic potential of cannabis. *Lancet Neurology*, *2*(5), 291–298. https://doi.org/10.1016/S1474-4422(03)00381-8

Banskota, A. H., Jones, A., Hui, J. P. M., & Stefanova, R. (2022). Triacylglycerols and Other Lipids Profiling of Hemp By-Products. *Molecules*, *27*(7). https://doi.org/10.3390/molecules27072339

Barthlott, I., Scharinger, A., Golombek, P., Kuballa, T., & Lachenmeier, D. W. (2021). A quantitative1h nmr method for screening cannabinoids in cbd oils. *Toxics*, *9*(6). https://doi.org/10.3390/toxics9060136

Bautista, J. L., Yu, S., & Tian, L. (2021). Flavonoids in Cannabis sativa: Biosynthesis, Bioactivities, and Biotechnology. *ACS Omega*, *6*(8), 5119–5123. https://doi.org/10.1021/acsomega.1c00318

Bharti, S. K., & Roy, R. (2012). Quantitative 1H NMR spectroscopy. *TrAC - Trends in Analytical Chemistry*, *35*, 5–26. https://doi.org/10.1016/j.trac.2012.02.007

Borges, G. R., Birk, L., Scheid, C., Morés, L., Carasek, E., Kitamura, R. O. S., et al. (2020). Simple and straightforward analysis of cannabinoids in medicinal products by fast-GC–FID. *Forensic Toxicology*, *38*(2), 531–535. https://doi.org/10.1007/s11419-020-00522-1

Brighenti, V., Marchetti, L., Anceschi, L., Protti, M., Verri, P., Pollastro, F., et al. (2021). Separation and non-separation methods for the analysis of cannabinoids in Cannabis sativa L. *Journal of Pharmaceutical and Biomedical Analysis*, *206*, 114346. https://doi.org/10.1016/j.jpba.2021.114346

Brighenti, V., Protti, M., Anceschi, L., Zanardi, C., Mercolini, L., & Pellati, F. (2021). Emerging challenges in the extraction, analysis and bioanalysis of cannabidiol and related compounds. *Journal of Pharmaceutical and Biomedical Analysis*, *192*, 113633. https://doi.org/10.1016/j.jpba.2020.113633

Brunetti, P., Pichini, S., Pacifici, R., Busardò, F. P., & del Rio, A. (2020). Herbal preparations of medical cannabis: A vademecum for prescribing doctors. *Medicina (Lithuania)*, *56*(5), 1–15. https://doi.org/10.3390/medicina56050237

Choi, Y. H., Kim, H. K., Hazekamp, A., Erkelens, C., Lefeber, A. W. M., & Verpoorte, R. (2004). Metabolomic differentiation of Cannabis sativa cultivars using 1H NMR spectroscopy and principal component analysis. *Journal of Natural Products*, *67*(6), 953–957. https://doi.org/10.1021/np049919c

Circolare-Camera dei Deputati. (2018). *Circolare—Camera dei Deputati. Circolare 31 Luglio 2018, Prot. 2018/43586. Aspetti Giuridico-Operativi Connessi al Fenomeno della Commercializzazione delle Infiorescenze della Canapa Tessile a Basso Tenore*

di THC e Relazioni con la Normativa Sugli Stupefa.

Crescente, G., Piccolella, S., Esposito, A., Scognamiglio, M., Fiorentino, A., & Pacifico, S. (2018). Chemical composition and nutraceutical properties of hempseed: an ancient food with actual functional value. *Phytochemistry Reviews*, *17*(4), 733–749. https://doi.org/10.1007/s11101-018-9556-2

Dadiotis, E., Mitsis, V., Melliou, E., & Magiatis, P. (2022). Direct Quantitation of Phytocannabinoids by One-Dimensional1 H qNMR and Two-Dimensional1 H-1 H COSY qNMR in Complex Natural Mixtures. *Molecules*, *27*(9). https://doi.org/10.3390/molecules27092965

Decreto 4 Novembre. (2019). *Gazzetta Ufficiale. Decreto 4 Novembre 2019 Definizione di Livelli Massimi di Tetraidrocannabinolo (THC) Negli Alimenti. (20A00016) (GU Serie Generale n.11 del 15-01-2020). Available online: https://www.gazzettaufficiale.it/eli/id/2020/01/15/2 0A00016/sg* .

Eisenmann, P., Ehlers, M., Weinert, C. H., Tzvetkova, P., Silber, M., Rist, M. J., et al. (2016). Untargeted NMR spectroscopic analysis of the metabolic variety of new apple cultivars. *Metabolites*, *6*(3). https://doi.org/10.3390/metabo6030029

ElSohly, M. A., & Slade, D. (2005). Chemical constituents of marijuana: The complex mixture of natural cannabinoids. *Life Sciences*, *78*(5), 539–548. https://doi.org/10.1016/j.lfs.2005.09.011

ElSohly, M., Radwan, M., Gul, W., Chandra, S., & Galal, A. (2017). Phytochemistry of Cannabis sativa L. *Progress in the Chemistry of Organic Natural Products*, *103*, 1–36. https://doi.org/10.1007/978-3-319-45541-9_1

European Union. Annex III. (2017). *Commission Delegated Regulation (EU) 2017/1155 of 15 February 2017 Amending Delegated Regulation (EU) No 639/2014 as Regards the Control Measures Relating to the Cultivation of Hemp, Certain Provisions on the Greening Payment, the Payment for Young Farmers in Control of a Legal Person, the Calculation of the per Unit Amount in the Framework of Voluntary Coupled Support, the Fractions of Payment Entitlements and Certain Notification Requirements Relating to the Single Area Payment Scheme and the Voluntary Coupled Support, and Amending Annex X to Regulation (EU) No 1307/2013 of the European Parliament and of the Council.* Available online: https://eur-lex.europa.eu/eli/reg_del/2017/1155/oj (accessed on 2 April 2022).

Farinon, B., Costantini, L., Molinari, R., Di Matteo, G., Garzoli, S., Ferri, S., et al. (2022). Effect of malting on nutritional and antioxidant properties of the seeds of two industrial hemp (Cannabis sativa L.) cultivars. *Food Chemistry*, *370*(April 2021). https://doi.org/10.1016/j.foodchem.2021.131348

Hazekamp, A., Choi, Y. H., & Verpoorte, R. (2004). Quantitative analysis of cannabinoids from Cannabis sativa using 1H-NMR. *Chemical and Pharmaceutical Bulletin*, *52*(6), 718–721. https://doi.org/10.1248/cpb.52.718

Huang, Y., Zhang, Z., Chen, H., Feng, J., Cai, S., & Chen, Z. (2015). A high-resolution 2D J-resolved NMR detection technique for metabolite analyses of biological samples. *Scientific Reports*, *5*, 1–9. https://doi.org/10.1038/srep08390

Iftikhar, A., Zafar, U., Ahmed, W., Shabbir, M. A., Sameen, A., Sahar, A., et al. (2021). Applications of cannabis sativa L. In food and its therapeutic potential: From a prohibited drug to a nutritional supplement. *Molecules*, *26*(24). https://doi.org/10.3390/molecules26247699

Ingallina, C., Sobolev, A. P., Circi, S., Spano, M., Fraschetti, C., Filippi, A., et al. (2020). Cannabis sativa L. inflorescences from monoecious cultivars grown in central Italy: An untargeted chemical characterization from early flowering to ripening. *Molecules*, *25*(8). https://doi.org/10.3390/molecules25081908

Izzo, A. A. ., Borrelli, F. ., Capasso, R. ., Di Marzo, V. ., & Mechoulam, R. (2009). Non-psychotropic plant cannabinoids: New therapeutic opportunities from an ancient herb. *Trends in Pharmacological Sciences*, *30*, 515–527.

Kopustinskiene, D. M., Masteikova, R., Lazauskas, R., & Bernatoniene, J. (2022). Cannabis sativa L. Bioactive Compounds and Their Protective Role in Oxidative Stress and Inflammation. *Antioxidants*, *11*(4), 1–12. https://doi.org/10.3390/antiox11040660

Li, H. L. (1974). An Archaeological and Historical Account of Cannabis in China Author (s): Hui-Lin Li Published by : Springer on behalf of New York Botanical Garden Press Stable URL : http://www.jstor.org/stable/4253540 Accessed : 15-07-2016 23 : 13 UTC An Archaeologica, *28*(4), 437–448.

Liu, Y., Liu, H. Y., Li, S. H., Ma, W., Wu, D. T., Li, H. Bin, et al. (2022). Cannabis sativa bioactive compounds and their extraction, separation, purification, and identification technologies: An updated review. *TrAC - Trends in Analytical Chemistry*, *149*, 116554. https://doi.org/10.1016/j.trac.2022.116554

Ludwig, C., & Viant, M. R. (2010). Two-dimensional J-resolved NMR spectroscopy: Review of a key methodology in the metabolomics toolbox. *Phytochemical Analysis*, *21*(1), 22–32. https://doi.org/10.1002/pca.1186

Marchetti, L., Brighenti, V., Rossi, M. C., Sperlea, J., Pellati, F., & Bertelli, D. (2019). Use of 13C-qNMR Spectroscopy for the Analysis of Non-Psychoactive Cannabinoids in Fibre-Type Cannabis sativa L. (Hemp). *Molecules*, *24*(6). https://doi.org/10.3390/molecules24061138

Mazzara, E., Torresi, J., Fico, G., Papini, A., Kulbaka, N., Dall'acqua, S., et al. (2022). *A Comprehensive Phytochemical Analysis of Terpenes, Polyphenols and Cannabinoids, and Micromorphological Characterization of 9 Commercial Varieties of Cannabis sativa L. Plants* (Vol. 11). https://doi.org/10.3390/plants11070891

Mercuri, A. M. ., Accorsi, C. A. ., & Bandini Mazzanti, M. (2002). The long history of Cannabis and its cultivation by Romans in central Italy, shown by pollen records from Lago Albano and Lago di Nemi. *Vegetation History and Archaeobotany*, *11*, 263–276. https://doi.org/10.1007/s003340200039

Ministero della Salute. (2009). *Produzione e Commercializzazione di Prodotti a Base di Semi di Canapa Per L'utilizzo nci Settori Dell'alimentazione Umana*.

Mudge, E. M., Murch, S. J., & Brown, P. N. (2018). Chemometric Analysis of Cannabinoids: Chemotaxonomy and Domestication Syndrome. *Scientific Reports*, *8*(1), 1–9. https://doi.org/10.1038/s41598-018-31120-2

Nagy, D. U., Cianfaglione, K., Maggi, F., Sut, S., & Dall'Acqua, S. (2019). Chemical Characterization of Leaves, Male and Female Flowers from Spontaneous Cannabis (Cannabis sativa L.) Growing in Hungary. *Chemistry and Biodiversity*, *16*(3). https://doi.org/10.1002/cbdv.201800562

Nahar, L., Guo, M., & Sarker, S. D. (2020). Gas chromatographic analysis of naturally occurring cannabinoids: A review of literature published during the past decade.

Phytochemical Analysis, *31*(2), 135–146. https://doi.org/10.1002/pca.2886

Odieka, A. E., Obuzor, G. U., Oyedeji, O. O., Gondwe, M., Hosu, Y. S., & Oyedeji, A. O. (2022). The Medicinal Natural Products of Cannabis sativa Linn.: A Review. *Molecules*, *27*(5), 1–23. https://doi.org/10.3390/molecules27051689

Ohtsuki, T., Friesen, J. B., Chen, S. N., McAlpine, J. B., & Pauli, G. F. (2022). Selective Preparation and High Dynamic-Range Analysis of Cannabinoids in "cBD Oil" and Other Cannabis sativa Preparations. *Journal of Natural Products*, *85*(3), 634–646. https://doi.org/10.1021/acs.jnatprod.1c00976

Olasehinde, T. A., & Olaniran, A. O. (2022). Neurotoxicity of anthracene and benz[a]anthracene involves oxidative stress-induced neuronal damage, cholinergic dysfunction and disruption of monoaminergic and purinergic enzymes. *Toxicological Research*, *38*(3), 365–377. https://doi.org/10.1007/s43188-021-00115-z

Peschel, W., & Politi, M. (2015). 1H NMR and HPLC/DAD for Cannabis sativa L. chemotype distinction, extract profiling and specification. *Talanta*, *140*, 150–165. https://doi.org/10.1016/j.talanta.2015.02.040

Pisanti, S., & Bifulco, M. (2019). Medical Cannabis: A plurimillennial history of an evergreen. *Journal of Cellular Physiology*, *234*(6), 8342–8351. https://doi.org/10.1002/jcp.27725

Popescu, R., Costinel, D., Dinca, O. R., Marinescu, A., Stefanescu, I., & Ionete, R. E. (2015). Discrimination of vegetable oils using NMR spectroscopy and chemometrics. *Food Control*, *48*, 84–90. https://doi.org/10.1016/j.foodcont.2014.04.046

R Core Team. (2019). *A Language and Environment for Statistical Computing; R Foundation for Statistical Computing: Vienna, Austria. Available online: https://www.R-project.org/ (accessed on 21 March 2022).*

Radwan, M. M., Chandra, S., Gul, S., & Elsohly, M. A. (2021). Cannabinoids, phenolics, terpenes and alkaloids of cannabis. *Molecules*, *26*(9). https://doi.org/10.3390/molecules26092774

Regulation (EC) No 1107/2009 of the European Parliament and of the Council of 21 October 2009 concerning the placing of plant protection products on the market and repealing Council Directives 79/117/EEC and 91/414/EEC. Off. J. Eur. Union 2009, 309, 1–50. Available online:

https://eur-lex.europa.eu/legalcontent/EN/TXT/?uri=celex%3A32009R1107 (accessed on 14 April 2022).

Ren, S., Hinzman, A. A., Kang, E. L., Szczesniak, R. D., & Lu, L. J. (2015). Computational and statistical analysis of metabolomics data. *Metabolomics*, *11*(6), 1492–1513. https://doi.org/10.1007/s11306-015-0823-6

Rezvankhah, A., Emam-Djomeh, Z., Safari, M., Askari, G., & Salami, M. (2018). Investigation on the extraction yield, quality, and thermal properties of hempseed oil during ultrasound-assisted extraction: A comparative study. *Journal of Food Processing and Preservation*, *42*(10), 1–11. https://doi.org/10.1111/jfpp.13766

Risoluti, R., Gullifa, G., Battistini, A., & Materazzi, S. (2020). Monitoring of cannabinoids in hemp flours by MicroNIR/Chemometrics. *Talanta*, *211*(December 2019), 120672. https://doi.org/10.1016/j.talanta.2019.120672

Russo, E. B. (2018). Cannabis therapeutics and the future of neurology. *Frontiers in*

Integrative Neuroscience, *12*(October), 1–11. https://doi.org/10.3389/fnint.2018.00051

Schachtsiek, J. ., Warzecha, H. ., Kayser, O. ., & Stehle, F. (2018). Current Perspectives on Biotechnological Cannabinoid Production in Plants. *Planta Medica*, *84*, 214–220.

Sgrò, S., Lavezzi, B., Caprari, C., Polito, M., D'Elia, M., Lago, G., et al. (2021). Delta9-THC determination by the EU official method: evaluation of measurement uncertainty and compliance assessment of hemp samples. *Analytical and Bioanalytical Chemistry*, *413*(13), 3399–3410. https://doi.org/10.1007/s00216-021-03283-x

Simopoulos, A. (2008). The importance of the omega-6/omega-3 fatty acid ratio in cardiovascular disease and other chronic diseases. *Experimental biology and medicine (Maywood, N.J.)*, *233*(6), 674–88. https://doi.org/10.3181/0711-MR-311

Siudem, P., Wawer, I., & Paradowska, K. (2019). Rapid evaluation of edible hemp oil quality using NMR and FT-IR spectroscopy. *Journal of Molecular Structure*, *1177*, 204–208. https://doi.org/10.1016/j.molstruc.2018.09.057

Siudem, P., Zielińska, A., Kowalska, V., & Paradowska, K. (2022). 1H NMR and chemometric methods in verification of hemp-seed oil quality. *Journal of Pharmaceutical and Biomedical Analysis*, *212*(November 2021), 2–6. https://doi.org/10.1016/j.jpba.2022.114650

Small, E. (2017). *Classification of Cannabis sativa L.: In relation to agricultural, biotechnological, medical and recreational utilization*. *Cannabis sativa L. - Botany and Biotechnology*. https://doi.org/10.1007/978-3-319-54564-6_1

Spano, M., Di Matteo, G., Ingallina, C., Botta, B., Quaglio, D., Ghirga, F., et al. (2021). A multimethodological characterization of cannabis sativa l. Inflorescences from seven dioecious cultivars grown in Italy: The effect of different harvesting stages. *Molecules*, *26*(10). https://doi.org/10.3390/molecules26102912

Spano, M., Di Matteo, G., Rapa, M., Ciano, S., Ingallina, C., Cesa, S., et al. (2020). Commercial hemp seed oils: A multimethodological characterization. *Applied Sciences (Switzerland)*, *10*(19), 1–15. https://doi.org/10.3390/app10196933

Stasiłowicz, A., Tomala, A., Podolak, I., & Cielecka-Piontek, J. (2021). Cannabis sativa L. As a natural drug meeting the criteria of a multitarget approach to treatment. *International Journal of Molecular Sciences*, *22*(2), 1–31. https://doi.org/10.3390/ijms22020778

Teleszko, M., Zając, A., & Rusak, T. (2022). Hemp Seeds of the Polish 'Bialobrzeskie' and 'Henola' Varieties (Cannabis sativa L. var. sativa) as Prospective Plant Sources for Food Production. *Molecules*, *27*(4). https://doi.org/10.3390/molecules27041448

The law 242/2016. (2016). *Gazzetta Ufficiale. Disposizioni per la Promozione della Coltivazione e della Filiera Agroindustriale della Canapa (16G00258), GU Serie Generale n. 304 del 30-12-2016. Available online: https://www.gazzettaufficiale.it/eli/id/20 16/12/30/16G00258/sg (acce*.

TopSpin. (2018). *Available online: http://www.bruker-biospin.com/topspin.html (accessed on 15 March 2022).*

Tura, M., Ansorena, D., Astiasarán, I., Mandrioli, M., & Toschi, T. G. (2022). Evaluation of Hemp Seed Oils Stability under Accelerated Storage Test. *Antioxidants*, *11*(3). https://doi.org/10.3390/antiox11030490

Valizadehderakhshan, M., Shahbazi, A., Kazem-Rostami, M., Todd, M. S., Bhowmik, & Arnab. (2021). Extraction of Cannabinoids fromCannabis sativaL.(Hemp)—Review. *Agriculture*, *11*(384).

Webb, G. A. (2018). Modern Magnetic Resonance. *Modern Magnetic Resonance*, (June), 1–2293. https://doi.org/10.1007/978-3-319-28388-3

Chapter 6: Evaluation of non-ionic polymeric resins for the recovery of polyphenols from white wine lees

This work involved the followings: Martina Gaglianò, Antonio D. Rodriguez-Lopez, Alfredo Cassano, Giuseppina De Luca, Esperanza M. Garcia-Castello and it is submitted for publication.

In particular, the PhD candidate was involved in planning and performing the experiments, as well as in discussing and interpreting the results and manuscript preparation.

6.1 Introduction

Fermentation is the process by which a grape must transform into wine. During fermentation, yeast converts grape sugars into alcohol. Once the yeast has finished its lifecycle, it settles on the bottom of the vessel used to make the wine, along with the cell membranes of pulp, skin fragments, stem, insoluble salts and macro-molecules. The heavy sediment that results from fermentation is called wine lees and represents the second largest winemaking by-product, accounting for approximately 25% of total winemaking wastes, trailing only grape pomace (60%) and before grape stalks (14%) (De Iseppi et al. 2020; Moro et al. 2021). Other by-products include carbon dioxide from fermentation, exhausted filtration materials, and fining agents. Wine lees are harmful to the environment as they contain phenolic compounds (Jurcevic et al. 2017; Rivas et al. 2021) that change the soil pH if incorporated into lands, thus affecting germination. They can also create unpleasant odours, attract pests, contaminate water, and deplete soil and groundwater oxygen (Mejia et al. 2022). On the other hand, grape water-soluble polyphenols are well-recognized for their beneficial effects on human health, including anti-inflammatory, anticarcinogenic and cardio-protective effects (Buljeta et al. 2023; Toaldo et al. 2014). Such effects have been primarily associated with red wine and explained by its greater content and diversity of polyphenols than white wine (Rosell 2011). Nevertheless, white wines still possess a variety of phenolics, particularly hydroxycinnamic acids and derivatives, and a range of other bioactive products, which could also play a role in the putative positive health effects (Boban et al. 2023). Therefore, recovering these compounds from wine lees and reusing them as a source of antioxidants, nutrient supplements, and food ingredients is considered a smart strategy for valorising these by-products from a circular economy perspective (Messinese et al. 2023). Currently, wine lees are usually used as raw material to produce ethanol and tartaric acid for

application in the food industry according to European Regulations (Niculescu and Ionete 2023) or for animal feed production (Bacic, 2003). However, these applications mainly aim to reduce disposal costs. Therefore, further research is required for an effective recovery of valuable compounds from wine lees, thus increasing the economic sustainability of the global process.

Polyphenol preparation includes two steps: extraction and purification. The easiest and most implemented way to extract compounds from a solid matrix is conventional solid-liquid (S-L) extractions. Pérez-Serradilla and Luque de Castro (2011) recovered bioactive compounds from wine lees using ethanol/water mixtures, while Dimou et al. (2015) used mixtures of acetone/water and methanol/water as solvents. Microwave-assisted extraction (MAE) and ultrasound-assisted extraction (UAE) have been broadly used to improve the extraction of active compounds from many vegetable matrixes (Airouyuwa et al. 2023; Alchera et al. 2022; Boateng 2023; Galvan D'Alessandro et al. 2012; Périno-Issartier et al. 2011; Tabla Ruiz 2020; Tomasi et al. 2023) including wine lees (Barcia et al. 2014; Tao et al. 2014). These extraction methods are non-selective and usually yield a bunch of compounds, including sugars, organic acids, sugar alcohols, amino acids, and proteins.

Membrane technologies have also been investigated along with or as an alternative to traditional extraction methods to enhance eco-friendliness and refine the purification process of biologically active substances (Gaglianò et al. 2022). For instance, Mir-Cerdà et al. (2023) successfully retrieved phenolic acids, flavonoids, and related compounds from lees of an Albariño cultivar wine using a green extraction method that involved only water and a double filtration process with microfiltration and ultrafiltration membranes to clarify the extract. Ultrafiltration and nanofiltration membranes were also tested by Arboleda Meija et al. (2019) in order to fractionate a clarified hydro-alcoholic extract of red wine lees. These membranes did not show a preferential rejection of phenolic compounds over sugars, resulting in suitable bioactive compound concentration but not for separating sugars-polyphenols. Indeed, separating phytochemicals and carbohydrates through membrane filtration is challenging due to their similar molecular weight, as Zagklis and Paraskeva (2015) highlighted in their study on grape marc. Still, this is possible with a further effective separation based on their polarity with adsorption/desorption operations using polymeric resins. These last are spherical synthetic polymers with defined pore structures and high surface areas for efficient and selective removal of organic molecules, primarily in aqueous applications (Caetano et al. 2009). Polymeric adsorbent resins have many advantages, including minimal chemical additives, simple operation, easy recovery, and scalability (Fu

et al. 2007; Zhang et al. 2008). Based on the operation mode, adsorption and desorption with resins can be generally classified as static and dynamic. Static adsorption, also called batch adsorption, occurs in a closed system containing a desired amount of adsorbent contacting with a certain volume of adsorbate solution. In contrast, dynamic adsorption usually occurs in an open system where adsorbate solution continuously passes through a column packed with adsorbent (Xu et al. 2013).

Resin adsorbents are becoming increasingly popular for purifying extracted polyphenols from vegetable products and by-products (Bertin et al. 2011; R. Fu et al. 2016; Ozgen and Sarıoglu 2013; Rico et al. 2022; Wang et al. 2019; Zhao et al. 2023), but on wine lees, this research is still very scarce. In fact, there has only been one research study on red wine lees that quotes the potential use of resins to retrieve polyphenolic bioactive compounds. However, it mainly focuses on recovering tartaric acid through a cation exchange resin (Kontogiannopoulos et al. 2016). Few other works have been conducted to examine macroporous resins for the enrichment of phenolic compounds from grape pomaces (Heravi et al. 2022; Trikas et al. 2017).

This work aims to evaluate the potential of polymeric resins in recovering polyphenols from anhydrous white wine lees while simultaneously purifying them from carbohydrates. For this purpose, two conventional solid-liquid extractions were conducted using a 25% w/w ethanol/water solution and water, respectively. The resulting extracts were then exposed to two Amberlite (XAD 7HP and XAD 16HP) and three Purolite resins (MN 202, PAD 900, PAD 950). The phenolic analysis was performed using spectrophotometric methods, including the Total Phenolic Index (TPI) and Folin-Ciocalteu method (for the determination of Total Phenolic Content (TPC)), while enzymatic methods were used for sugar determination. Static experiments were conducted to evaluate the investigated resins' adsorption and desorption properties. The extract and resin combination that produced the best results in terms of total phenolics (TPs) adsorption/desorption and purification from carbohydrates were subjected to further testing, including assessing adsorption/desorption isotherms and kinetics, regeneration, and dynamic tests for leakage curve analysis.
Therefore, this research contributes to the limited literature on wine lees, assessing a process that could be refined and scaled up for large-scale implementation and leading to the reuse of a valuable waste product, resulting in environmental benefits and economic revenues.

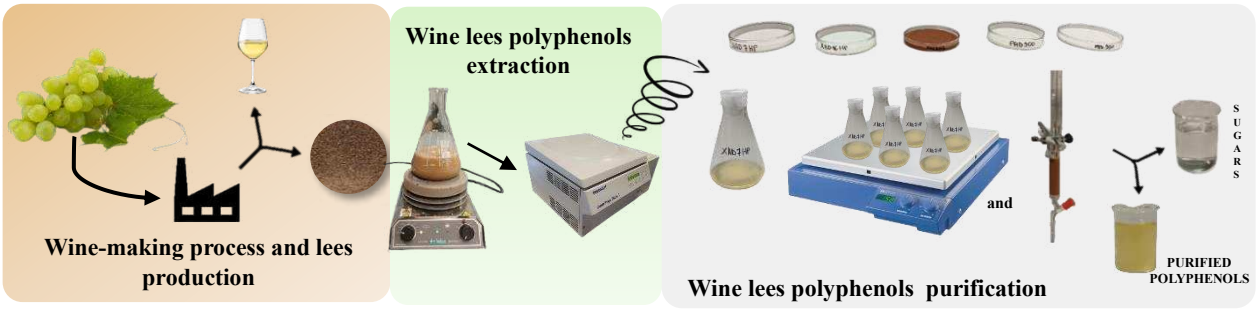

Figure 6.1 Schematic diagram outlining the process for extracting pure polyphenols from white wine lees.

6.2 Material and methods

6.2.1. Preparation of white wine lees extracts

White wine lees were obtained from must of Traminer aromatic (or Gewürztraminer) white grape variety at the end of alcoholic fermentation. They were kindly provided by an Italian wine Company (Masseria Falvo 1727, Saracena, Cosenza, Italy). After collection, the lees were frozen at -20 ºC and defrosted to room temperature before use. After defrosting wine lees were dried in a convective oven at 50 ºC for 48 h. Then, they were milled and sieved with a metallic sieve size of 2 mm. The solid wine lees thus obtained, with a particle size lower than 2 mm, were stored at room temperature until their later use.

The phenolic extraction from the solid fraction of wine lees was performed using two different solid-liquid extractions: the first using an ethanol:water mixture with a weight ratio 25:75 and the second with water as solvent. In both cases, 50 grams of dried and milled lees were weighed and put into a flask. Then, 500 grams of solvent were added (1:10 w/w solid/liquid ratio), and the whole was agitated for 30 minutes at room temperature to preserve the structural integrity of the bioactive compounds. The obtained extract was transferred into falcons and centrifuged at 4500 rpm for 30 minutes (Eppendorf centrifuge 5804R, Germany); the supernatant was removed and re-centrifuged at 10000 rpm for 15 minutes at room temperature to further reduce particles in suspension in order to have a clarified extract.

Hydroalcoholic and aqueous extracts were used to test the performances of resins in retaining polyphenols and releasing sugars. For the other assays, such as isotherms and kinetic studies, aqueous solutions with different TPs concentrations (0.3, 0.5, 0.7, 0.9, 1.1, and 1.4 mg/mL), expressed as TPI, were prepared. These solutions were obtained first by performing a white

wine lees extraction, as described above, but using a 1:2 w/w solid/liquid ratio. The other solutions were obtained from this extract by means of dilutions.

6.2.2. Adsorbents

Specifications of the five resins used in this study, as provided by the manufacturer in the technical data sheet, are summarised in Table 6.1.

Table 6.1 Physical and chemical characteristics of the investigated resins.

Resin	Material	Specific surface area (m^2/g)	Average pore diameter (Å)	Pore volume (mL/g)
Amberlite				
XAD 7HP	Polymethacrylic	520	550	0.95
XAD 16HP	PS/DVB[1]	800	150	0.6
Purolite				
MN 202	PS/DVB[1]	950	220/15[#]	0.3
PAD 900	PDVB[2]	850	220	1.9
PAD 950	Polymethacrylic	450	120	0.6

[1] PS-DVB: polystyrene crosslinked with divinylbenzene.
[2] PDVB: Polydivinylbenzene.
[#] macropores/micropores

Resins are usually stored with NaCl and Na_2CO_3 to prevent bacterial growth. Moreover, they may contain impurities arising from the manufacturing process. To ensure that the experimental results connected with resins use are reliable, it's necessary to remove impurities and salts before starting the experiments using a start-up procedure recommended by manufacturers. For this procedure, five 20 mm diameter × 30 cm height chromatographic columns were prepared and 20 g (wet basis, w.b.) of each resin was charged in each chromatographic column. Then, resins were contacted with the conditioning solutions, as indicated in Table 6.2.

Table 6.2 Resins' pretreatment before experiments.

Start-up procedure	
For **XAD 7HP** and **XAD 16HP** resins	For **MN 202**, **PAD 900**, and **PAD 950** resins
1. 6BV of NaOH 0.2% at the velocity of 2BV/h	1. 6BV of NaOH 2% at the velocity of 2BV/h
2. 6BV of distilled H_2O	2. 6BV of distilled H_2O
3. 3BV of HCl 0.1% at the velocity of 2BV/h	3. 1 BV of HCl 0.1% at the velocity of 2BV/h
4. H_2O until reaching the distilled water pH	4. H_2O until reaching the distilled water pH

BV: Bed volume

After the conditioning step, resins were moved to Petri dishes, dried at room temperature for 48 h and then dried in a vacuum oven (Vaciotem-T, J.P. Selecta, Abrera, Barcelona, Spain) at 60 °C until a constant weight was achieved. Finally, dried resins were stored inside the dryer until their use in further experiments.

6.2.3 Resin screening

First, 0.5 g (dried weight, d.w.) of started-up resins were introduced into an Erlenmeyer flask, put in contact with 25 mL of white wine lees extract and stirred in a reciprocating manner (HS 501 digital, IKA, Staufen, Germany) at 120 rpm and room temperature (20 ± 2 °C) for 24 h to reach equilibrium. After adsorption, the liquid phase, which contains the fraction of non-adsorbed compounds, was separated from the solid matrix. On the liquid fraction, the concentration of total phenolic compounds and sugars was measured. The adsorption progress was determined in terms of two parameters: the adsorption ratio, AR (%), and the adsorption capacity $Q_{t.a}$, calculated according to equations 1-2.

$$AR\ (\%) = \frac{C_0 - C_{t.a}}{C_0} \bullet 100 \tag{6.1}$$

$$Q_{t.a} = \frac{(C_0 - C_{t.a}) \bullet V_0}{W} \tag{6.2}$$

being C_0 the initial (t=0 h) TPs and sugars concentration (mg/mL) and $C_{t.a}$ their concentration (mg/mL) at any time (t=t h) in the feed solution. When t=24 h, $C_{t.a}$ and $Q_{t.a}$ represent the equilibrium concentration and equilibrium adsorption capacity of target compounds, respectively. V_0 is the volume (mL) of the feed solution, and W is the weight of the dry resin (g).

The adsorption with each of the five resins was repeated in duplicate with the aim of testing two desorption approaches. After the adsorption process, resins were separated from the remaining feed solution and, in desorption-approach 1, rinsed with 25 mL of distilled water (first desorption) and waited 4 h of desorption equilibrium time under the same conditions as those for the adsorption process; the aqueous solution was removed from the resin and introduced into a flask with 25 mL of 70% ethanol (second desorption) for 4 h of desorption equilibrium time. In the desorption-approach 2, for each resin separated from the non-adsorbed fraction, 25 mL of 70% ethanol was first used (first desorption) and, after 4 h, removed and resins rinsed with 25 mL of water (second desorption).

The desorption ratio, DR (%), and the desorption capacity, $Q_{t.d}$, were evaluated by using the following equations (Eq. 6.3-6.4).

$$DR(\%) = \frac{C_{t.d} \bullet V_d}{(C_0 - C_{e.a}) \bullet V_0} \cdot 100 \quad (6.3)$$

$$Q_{t.d} = \frac{C_{t.d} \bullet V_d}{W} \quad (6.4)$$

Where $C_{t.d}$ is the concentration (mg/mL) in the desorption solution of target compounds at equilibrium time and V_d is the volume of the desorption solution.

Adsorption and desorption ratios were evaluated for both TPs and sugars of the white wine lees extract and on the basis of carbohydrates and bioactive compounds adsorption-desorption recovery (R(%)), calculated as reported in Eq. 6.5.

$$R\ (\%) = \frac{C_d \bullet V_d}{C_0 \bullet V_0} \bullet 100 \quad (6.5)$$

where, C_d is the concentration (mg/mL) of TPs or sugars in the desorption solution, V_d and V_0 are the volume (mL) of the desorption solution and that of the initial feed solution (mL), respectively.

One extract and one resin were selected and used for studying adsorption isotherms, kinetics of adsorption and desorption and for dynamic test.

6.2.4 Analytical determinations

The total phenolic content (TPC) was determined quantitatively according to the Folin-Ciocalteu colorimetric method. The sample (0.2 mL) was combined with 1 mL of 10% (v/v) Folin-Ciocalteu reagent (Sigma Aldrich) and 0.8 mL of a 7.5% (w/v) sodium carbonate solution. After a 30-minute incubation at room temperature, the extinction was measured at 756 nm wavelength using an Agilent Cary 60 UV-Vis spectrophotometer (Gaglianò et al. 2022). The TPC was determined from extrapolation of calibration curve which was constructed by gallic acid solution. The total phenolic index (TPI) is a faster alternative to this method (Cetó et al. 2012). It is easily determined by diluting the sample and reading the absorbance at 280 nm. The TPI can also be expressed as gallic acid equivalents when used as a standard (Aleixandre-Tudo and Du Toit 2019) as performed in this work.

Sugar analysis was performed by using colorimetric kits Enzytec™ *Liquid* D-Glucose/D-Fructose Cod. E8160 and Enzytec™ *Liquid* Sucrose/D-Glucose Cod. E8180, both from R-Biopharm (Germany), at a wavelength of 340 nm.

6.2.5 Dynamic adsorption and desorption tests

Fixed-bed or column adsorption is the primary option in practical applications. Consequently, once the resin that works best in the static process has been identified, it is interesting to study the dynamic process by determining the critical leakage curve, as it provides the predominant information for designing a column adsorption system. Dynamic adsorption and desorption experiments were carried out on a lab-scale glass columns (2 cm × 30 cm) wet-packed with 5 g d.w. of the selected MN 202 resin. The bed volume (BV) of resin was 15 mL and the packed length of resin bed was 5 cm. Sample solution (white wine lees aqueous extract) flowed through the glass column at the flow rate of 1 mL/min. The eluent from the column was collected at fixed time intervals of 5 min and the concentrations of total phenolics was determined reading absorbance at 280 nm (TPI). By plotting the volume (mL) of effluent liquid (on x-axis) and the concentration (mg/mL) of outlet adsorbate (on y-axis), leakage curve can be obtained (Fu et al. 2007), which is essential for scaling up the results. Once the eluent's absorbance reaches a point that is one-tenth of the loading extract, it is a sign that TPs have leaked out and the resin starts its saturation. This point is referred to as the breakpoint (t_{BP}). After the breakpoint period, the concentration gradually increases until it reaches the exhaustion point time (t_{EP}), at which point the bed becomes ineffective (Heravi et al. 2022). In our experiments, we ceased loading the extract once it reached approximately 97% of the absorbance of the loading extract and then calculated the resin's adsorption capacity and adsorption ratio. Indeed, the area above the leakage curve signifies the mass of TPs in eluted solutions, and it is calculated as Eq. 6.6.

$$mass_{eluted}=\int_{V_{in}}^{V_{EP}} f(V)dV \tag{6.6}$$

where V_{in} and V_{EP} are the initial volume and the volume at the exhaustion point time and $f(V)$ is the 6th degree polynomial function describing the leakage curve. Moreover, knowing the TPs concentration in initial extract and the lees extract volume eluted, it is possible to determine the polyphenols' mass which passed through the resin. The amount of mass retained by the resin, so the amount of bed capacity was determined by subtracting the mass of eluted polyphenols from the mass of incoming polyphenols. After achieved the adsorptive equilibrium, the adsorbate laden column was eluted by ethanol-water (70:30, v/v) solution with a flow rate of 1 mL/min. The concentration of total phenolics in the effluent's fractions (2 mL) were measured always using TPI method; the area under the dynamic leakage curve represents the mass of eluted TP, thus describing the MN 202 desorption capacity.

6.2.6 Adsorption Isotherms

The amount of solute species adsorbed per gram (d.w.) of adsorbent, so the adsorption capacity ($Q_{e.a}$), is a function of temperature, feed solution concentration and pH (Sahoo and Prelot 2020). At a constant temperature and specific solution pH, $Q_{e.a} = f_T(C_{e.a})$ and this is called the *adsorption isotherm function.* To determine the effectiveness of adsorption from a solution, one can measure the decrease in the concentration of the adsorbed species after it is taken up by the solid. This allows the adsorption isotherm to be plotted, displaying the amount of adsorbed species ($Q_{e.a}$) against the equilibrium concentration ($C_{e.a}$). To evaluate the real adsorbed amount of the targeted molecules when equilibrium is reached, it is necessary a previous study of the kinetic of adsorption in order to determine the required time to reach that equilibrium.

Adsorption isotherms, provide information about the potential sorption mechanisms (monolayer/multilayers or homogenous/heterogeneous) by fitting experimental data to mathematical models (such as Langmuir, Freundlich, Sips and Redlich-Peterson) and determining the most appropriate model for representing the measured data.

Langmuir isotherm model assumes monomolecular layer adsorption with a homogeneous distribution of adsorption energies and without mutual interaction between adsorbed molecules. On the other hand, Freundlich isotherm model is used in processes of multilayer adsorption and when non-ideal adsorption on heterogeneous surfaces occurs. Finally, both the Sips and Redlich–Peterson models are combinations of the basic Langmuir and Freundlich ones (Fu et al. 2007; Ray et al. 2020; Rodriguez-Lopez et al. 2021; Sahoo and Prelot 2020). All models are defined by different parameters appearing in their characteristic equations and converted linear forms shown in Table 6.3.

Table 6.3 Adsorption isotherm models.

Isotherm model	General equation	Linearized equation
Langmuir	$Q_{e.a} = \frac{Q_m \cdot K_L \cdot C_{e.a}}{1 + K_L \cdot C_{e.a}}$	$\frac{1}{Q_{e.a}} = \frac{1}{Q_m \cdot K_L \cdot C_{e.a}} + \frac{1}{Q_m}$
Freundlich	$Q_{e.a} = K_F \cdot C_{e.a}^{1/n}$	$\ln(Q_{e.a}) = \ln(Q_{e.a}) + \frac{1}{n} \cdot \ln(C_{e.a})$
Sips	$Q_{e.a} = \frac{Q_S \cdot K_S \cdot C_{e.a}^{\alpha}}{1 + K_S \cdot C_{e.a}^{\alpha}}$	$\frac{1}{Q_{e.a}} = \frac{1}{K_S \cdot Q_S} \cdot \left(\frac{1}{C_{e.a}}\right)^{\alpha} + \frac{1}{Q_S}$
Redlich-Peterson	$Q_{e.a} = \frac{K_{RP} \cdot C_{e.a}}{1 + B_{RP} \cdot C_{e.a}^{\beta}}$	$\ln\left(\frac{K_{RP} \cdot C_{e.a}}{Q_{e.a}} - 1\right) = \ln(B_{RP}) + \beta \cdot \ln(C_{e.a})$

where Q_m (mg/g (d.w.)) is the maximum adsorbed capacity, K_L (mL/mg) is the Langmuir constant which represent the energy of adsorption, K_F and $1/n$ are the Freundlich constants representing the amount sorbed and the intensity of adsorption, respectively. Q_S (mg/g (d.w.)) is the maximum adsorbed capacity K_S (mL/mg) is the Sips adsorption isotherm constant and α is the heterogeneity factor. K_{RP} (mL/mg) and B_{RP} (mL/mg)$^{\beta}$ are the Redlich-Peterson isotherm constants. β is the exponent value in the general Redlich-Peterson equation which lies in between 0 and 1.

In this work, six feed solutions at different TPs concentrations (0.3, 0.5, 0.7, 0.9, 1.1, and 1.4 mg GAE/mL) were prepared as described in Section 2.1. Then, 0.5 g of the selected dried resin (MN 202) was put in contact with 25 mL of each one of the feed solutions. Mixtures were stirred at 120 rpm and at room temperature (20 ± 2 °C) for 24 h. When equilibrium was reached, samples of all mixtures were taken to determine the equilibrium concentration $(C_{e.a})$, and adsorption capacity $(Q_{e.a})$ (Eq. 2). Then, Langmuir, Freundlich, Sips and Redlich-Peterson models were applied, and the SOLVER tool of the MS Excel program was used to carry out the regressions of the experimental data. The goodness of fit of the models to the experimental data was assessed by using the linear regression coefficient (r^2) and the average percentage error (APE), calculated as in Equation 6.7.

$$\text{APE}\,(\%) = \frac{\sum_{I=1}^{N}\left|\frac{Q_{e.a.exp}-Q_{e.a.cal}}{Q_{e.a.exp}}\right|}{N}\cdot 100 \qquad (6.7)$$

where $Q_{e.a.exp}$ and $Q_{e.a.cal}$ are the experimental and calculated adsorption capacities at equilibrium, respectively, and N is the number of measurements.

6.2.7 Adsorption and Desorption Kinetics

Kinetic modeling allows the estimation of sorption rates also leading to suitable rate expressions characteristic of possible reaction mechanisms (Ersali et al. 2013). The kinetic adsorption studies were carried out under the same operating conditions and using the same wine lees solutions with varying concentrations of polyphenols as for the isotherms studies. In each case, 25 ml of the solution was brought into contact with 0.5 g of MN 2O2 resin. Aliquots of the sample solution were taken at particular time intervals (0, 5, 10, 20, 60, and 1440 min) and TPs content was measured to understand when equilibrium was reached. At this point, the not-adsorbed fraction was removed from the resins and ethanol/water 70% v/v solution was used as desorbed solvent. Desorption kinetics studies were carried out under

the same conditions of stirring and temperature as those of adsorption isotherms and kinetics study. During the desorption process, aliquots were taken out (0, 5, 10, 20, 60, and 240 min) and phenolic compounds were measured. To study the adsorption/desorption kinetic, the pseudo-first-order, pseudo-second-order, and intraparticle diffusion kinetic models were used (Rodriguez-Lopez et al. 2021), whose general and integrated equations forms are shown in Table 6.4.

Table 6.4 Equations utilized in analyzing the kinetics of adsorption and desorption.

Kinetic model	General equation	Integrated equation
Pseudo-first-order	$\frac{dQ_{t.i}}{dt} = k_{1.i} \cdot (Q_{e.i} - Q_{t.i})$	$\ln(Q_{e.i} - Q_{t.i}) = \ln(Q_{e.i}) - k_{1.i} \cdot t$
Pseudo-second-order	$\frac{dQ_{t.i}}{dt} = k_{2.i} \cdot (Q_{e.i} - Q_{t.i})^2$	$\frac{t}{Q_{t.i}} = \frac{1}{k_{2.i} \cdot Q_{e.i}^2} + \frac{t}{Q_{e.i}}$
Intraparticle diffusion	$Q_{t.i} = kp_i \cdot t^{\frac{1}{2}} + C_i$	

i = *a* for adsorption ad *d* for desorption.

where $Q_{e.i}$ (mg·g^{-1}) and $Q_{t.i}$ (mg·g^{-1}) are the amount of adsorbed TPs at equilibrium and at time "*t*"; $k_{1.i}$ (min^{-1}), $k_{2.i}$ (g·mg^{-1}·min^{-1}), k (mg·g^{-1}·min$^{-0.5}$) are the pseudo-first-order, pseudo-second-order, and intra-particle diffusion rate constants, respectively; and also C_i is a constant.

6.3 Results and Discussion

Resins XAD 7HP, XAD 16HP, MN 202, PAD 900 and PAD 950 were tested with three different white wine lees extracts: (1) white wine lees extract using 25% w/w ethanol/water as extraction solvent; (2) concentrated extract (extract one after removing the ethanol using the rotavapor) and (3) white wine lees extract using only water as extraction solvent.

6.3.1 Comparison between TPC and TPI

Since as mentioned above, the objective of this work is the obtaining and purification of white wine lees polyphenols, TPs were analyzed both in the three initial extracts and in the fractions coming from resins' use. For this purpose, TPC and TPI methods were used and compared. Figure 6.2 displays this comparison and shows a positive correlation with an r^2

value of 0.9929 between TPC and TPI. The TPI method results in a higher quantity of mg GAE/L of TPs. Thus, the total phenolic content is overestimated, possibly due to other grape component's ability to absorb UV light (Aleixandre-Tudo and Du Toit 2019). However, the ratios between the concentrations in the parameters that define the resin's performance will remain consistent, resulting in similar AR% and DR% values when expressing the polyphenol content as both TPC and TPI. As a result, only the TPI method was used to evaluate polyphenol content for further studies (isotherms, kinetics, and dynamic tests on the best resin) due to its faster and greener nature. In this paragraph, all parameters (AR%, DR%, $Q_{t.a}$, $Q_{t.d}$, R%) shown will be expressed based on the TPI values.

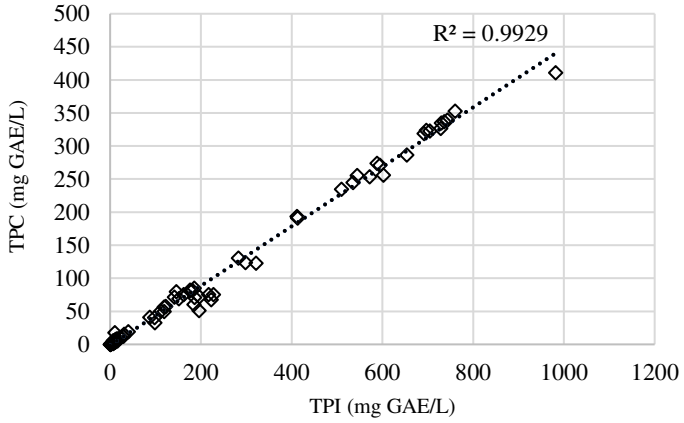

F**igure 6.2** Correlation between Total Phenolic Content (TPC) and Total Phenolic Index (TPI) expressed as gallic acid equivalents.

6.3.2 Selection of proper extract and resin in static

Water/ethanol mixtures are the most popular GRAS (Generally Recognized As Safe) system in green extraction of polyphenols from various natural matrices, including plant by-products. (Gómez-Mejía et al. 2019; Kato-Schwartz et al. 2020; Ramón-Gonçalves et al. 2019). The concentration of ethanol that maximizes extraction can vary depending on the matrix's phenolic compounds (Franco et al. 2018; Vella et al. 2018). Romero-Díez et al. (2018) determined ethanol:water (75:25 v/v) mixture as the optimal solvent for polyphenols extraction in red wine lees. However, in an integrated process made by sequential extraction and resin purification stages, the ethanol concentration in the initial feed is also crucial (Huaman-Castilla et al. 2019); if too high, it is incompatible with the resin adsorption step. Indeed, water or water containing a low percentage of an organic solvent are well suited for the loading step (Tapia-Quirós et al. 2022). For this reason, it was decided to initially extract TPs white wine lees with an ethanol/water mixture that contained just a tiny percentage of

ethanol, set at 25% w/w. Dissolving 50 g (d.b.) of white wine lees in 500 g of ethanol:water (25:75 w/w) mixture, 335 ± 7 mg GAE/L of TPs were extracted, corresponding to approximately 3.4 mg equivalent of gallic acid per gram of dry white wine lees according to the equation 6.8.

$$C = C_1 \times \frac{V}{m} \quad (6.8)$$

where C is TPC (mg GAE/g (d.w.)), C_1 is the concentration of gallic acid equivalents (mg GAE/L) established from the calibration curve, V is the volume of the extract (L), and m is the weight of the dry less (g) (Molole et al. 2022).

As can be seen in Figure 6.3a-e and in Table 6.5, a low recovery of phenolics was measured after testing the Amberlite and Purolite polymeric resins with the hydroalcoholic extract. This is primarily due to the adsorption process (the adsorption ratio for TPs was of about 20% for all the investigated resins). The nature of solvent is one of the factors that influenced the adsorption process. Silva et al. (2007), in their study on optimization of the adsorption of polyphenols from *Inga edulis* leaves, found that the water proportion in the hydroalcoholic feed solution had a strong effect on the adsorption process and concluded that the optimized conditions which maximize the polyphenols adsorptive capacity include the use of an utterly aqueous feed. Therefore, we considered eliminating the ethanol from the 25% w/w ethanol/water extract and retesting all five resins on the concentrated extract with the rotary evaporator. As a result, the polyphenols' adsorption ratio and overall recovery rate increased a little for all the resins (Figure 6.3a-e and Table 6.5), with a particular improvement observed for MN 202 resin. After obtaining these minimal but positive results with extract 2, water was probed as the extraction solvent for TPs from white wine lees. This approach eliminates the need to evaporate the solvent in the next step of adsorption on resin, saving energy and time in industrial production.

Dissolving 50 g (d.w.) of white wine lees in 500 g of distilled water, 323±10 mg GAE/L of TPs were extracted, corresponding to approx. 3.2 mg equivalent of gallic acid, that is about the same amount extracted using the ethanol/water mixture. Furthermore, aqueous extract enhanced the performance of the MN 202 resin in purifying polyphenols, resulting in the highest adsorption rate of 60% for phenolic compounds. This behavior is not reflected also for the other resins, which, on the contrary, continue to show low (XAD 7HP and PAD 950) or zero (XAD 16HP and PAD 900) adsorption. Other studies have also confirmed the impressive performance of MN 202 resin. For instance, De Marco et al. (2010) found that the MN 202 resin could retain up to 99% of the phenolic compounds from olive mill

wastewater. Similarly, Tabla Ruiz (2020) tested different polymeric materials concluding that MN 202 resin represents a good option for polyphenols recovery from waste extracts generated by fruits and vegetables processing.

The adsorption efficiency of a polymeric adsorbent is affected by several factors, including adsorbate type, pH and size, resin physical properties such as pore dimensions, hence the chemical and physical interactions between feed and material (Sandhu and Gu 2013). Compared to the other resins tested in this work, the MN 202 resin is the only one that has two types of pores: micropores (in the range of 10 to 30 Å), which are responsible for the adsorption of small molecules, and macropores which act as "transport channels" that ensure the diffusion of small to large molecules through the resin (Cifuentes-Cabezas et al. 2022). This physical resin characteristic is probably the responsible for MN 202 better adsorption of phenolic compounds identified in wine lees (Jara-Palacios 2019) respect to the other resins. In fact, the macroporous XAD 16HP resin is made of the same material as MN 202, i.e. polystyrene/divinylbenzene, but using the aqueous extract of white wine lees, the adsorption rate with XAD 16HP is almost null. The present findings suggest that the recovery of TPs may be attributed to the bimodal pore size distribution of MN 202 resin, rather than the type of material.

Using the hydroalcoholic extract, the MN 202 resin always worked better but in this case also the XAD 16HP resin (as well as the PAD 900) showed adsorption of around 16%. Based on these results, it may be inferred that using both water and ethanol:water solvents result in two extracts with similar phenolic content. However, the relative composition of phenolic compounds in these extracts may be different (Lim et al. 2019), which leads to varying chemical-physical interactions with resins and ultimately affects their performance. The aqueous extract may boost the extraction of more polar compounds such as phenolic acids and limiting the extraction of less polar compounds and this could explain the almost zero adsorption for XAD 16HP and PAD 900. On the other hand, the ethanol extract may contain a higher percentage of flavonoids with a more hydrophobic character that can better interact with materials such as the XAD 16HP and PAD 900 resins, which are made of PS/DVB or PDVB. However, these assumptions can only be confirmed in light of more specific analytical characterizations of the extracts. Instead, XAD 7HP and PAD 950 resins, being both macroporous resins in polyacrylate showed the same trend: a TPs AD (%) of about 15%-20% in ethanol/water-concentrated extracts and of about 25% when in contact with aqueous extract.

As regards the sugars present in the white wine lees extract, the analysis with enzymatic methods revealed only the presence of glucose and fructose and not sucrose. Other studies (Tagkouli et al. 2022) revealed that wine lees extracts were highly heterogeneous in sugar moieties composition, which may be due to the type of wine lees, which depends on the grape variety and origin and the vinification process, as well as the extraction methodology. In addition, for all the extracts, the adsorption percentage of glucose and fructose was low, and, as a consequence, their recovery in the desorbed fraction with 70% ethanol was not significant (Figure 6.3 and Table 6.5).

Therefore, the resins are effective in not adsorbing carbohydrates and selectively retaining and releasing the polyphenols compounds of interest. However, adsorption is only one step that influences the recovery of polyphenols and the separation from sugars. The second and equally important step for an optimal result is the desorption of the compounds from the resin. In this work, we wanted to test two approaches for desorption: the first, which provided for washing with water and then the actual desorption with 70% v/v ethanol solution and the second, which directly provided for the desorption with EtOH 70% and subsequent washing with H_2O. 70% EtOH solution was chosen as desorbed solvent due to its full compatibility with food, pharmaceutical, and nutraceutical industries and also because it showed high desorbed ratio of TPs. With desorption-step 1, it was possible to obtain more purified polyphenols because washing with water allowed removing the minimum quantity of sugars remaining adsorbed. However, a tiny part (reported in Figure 6.4b) from 3 to a maximum of 16% of desorbed polyphenols compared to the adsorbed amount depending on the resin) of polyphenols was also lost with this washing. On the contrary, by desorption with EtOH 70%, there was no loss of polyphenols, but in some cases, these could not be completely pure. In light of the data reported in Table 6.5, it was clear that the optimal conditions combining a green approach with good adsorption and desorption values are those that provide for the use of the MN 202 resin with the aqueous extract. Since this resin cannot adsorb sugars from this extract, the desorption can be carried out directly with 70% EtOH without washing with water. This approach was followed for simplicity in other studies (isotherms, kinetics and dynamics). Moreover, the best-performing MN 202 resin was further tested in static conditions for regeneration. To reactivate the PS-DVB resin, a chemical cleaning procedure involving 2% NaOH and 0.1% HCl solutions with distilled water washes in between until to reach a neutral pH before use was applied. The aqueous extract of white wine lees was again adsorbed and desorbed with 70% ethanol, and the results

obtained for AR_{TPs}% and DR_{TPs}% were comparable to those obtained with new resin. Therefore, it can be concluded that a complete regeneration (about 99%) was obtained.

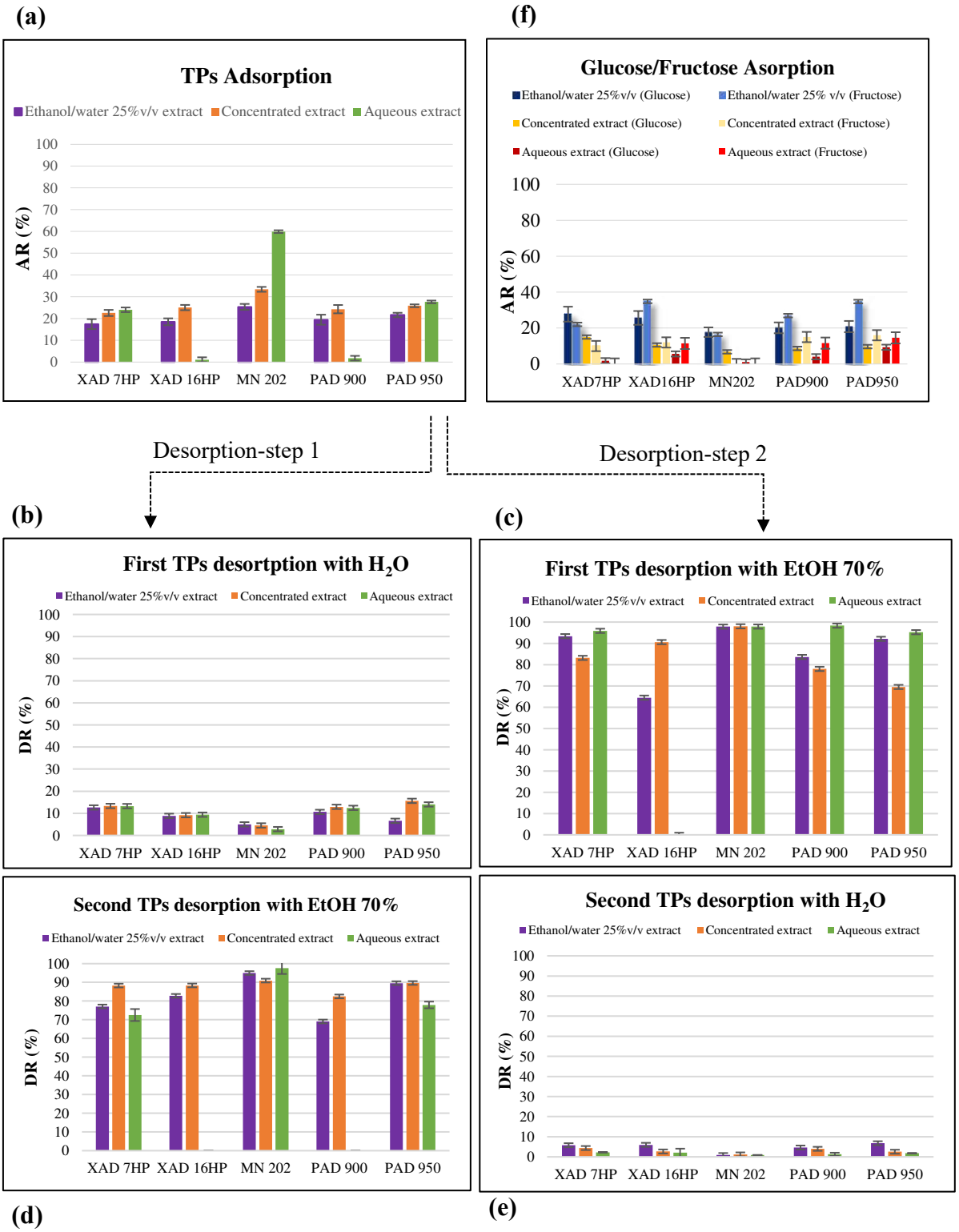

Figure 6.3 Adsorption and desorption ratios of total phenolic compounds (TPs) and adsorption ratios of glucose and fructose for all the extracts and resins investigated.

Table 6.5 Recovery rates of TPs and sugars desorbing with EtOH 70%. Uncertainty was up to ± 15 %.

Desorption-step 1 with EtOH 70%									
	Phenolic compounds			*Glucose*			*Fructose*		
R (%)	Ethanol/water 25% w/w extract	Concentrated extract	Aqueous extract	Ethanol/water 25% w/w extract	Concentrated extract	Aqueous extract	Ethanol/water 25% w/w extract	Concentrated extract	Aqueous extract
XAD 7HP	16.30	18.76	23.02	1.60	zero	zero	3.71	7.28	zero
XAD 16HP	11.92	22.68	1.12	2.20	zero	zero	4.85	4.24	zero
MN 202	24.82	32.74	58.63	5.58	zero	zero	9.00	1.99	zero
PAD 900	16.26	18.95	1.72	2.81	zero	zero	7.53	3.63	zero
PAD 950	19.92	17.96	26.32	1.05	zero	zero	10.28	5.67	zero
Desorption-step 2 with EtOH 70%									
	Phenolic compounds			*Glucose*			*Fructose*		
R (%)	Ethanol/water 25% w/w extract	Concentrated extract	Aqueous extract	Ethanol/water 25% w/w extract	Concentrated extract	Aqueous extract	Ethanol/water 25% w/w extract	Concentrated extract	Aqueous extract
XAD 7HP	13.46	19.92	17.42	6.70	7.28	7.70	2.86	zero	zero
XAD 16HP	15.31	22.12	0.96	5.00	4.24	5.00	1.89	zero	4.00
MN 202	24.09	30.38	58.49	5.03	1.99	2.63	5.00	zero	zero
PAD 900	13.44	20.04	1.59	5.79	3.63	4.61	2.10	zero	1.06
PAD 950	19.27	23.17	21.53	7.09	5.67	8.33	2.82	zero	0.00

6.3.3 Dynamic experiments

Figure 6.4 shows the TPs wine lees leakage curve on MN 202 adsorbent, at an inlet concentration (C_{in}) in the adsorbent bed of 851 ppm (expressed as TPI), at 25°C and a linear velocity of 1mL/min.

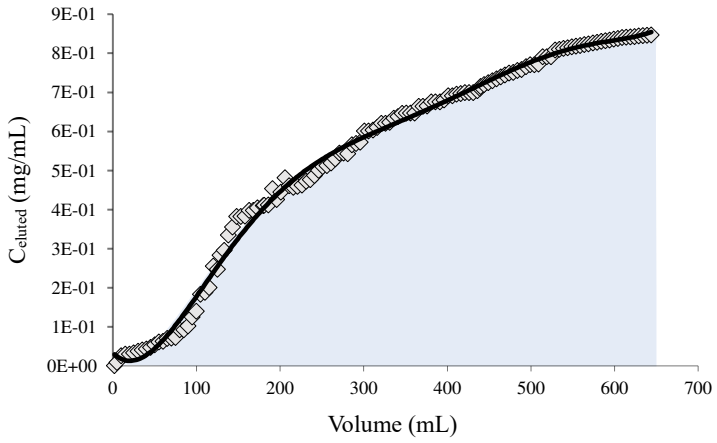

Figure 6.4 Dynamic leakage curve of wine lees TPs on column packed with MN 202 resin.

Total phenolics in solution were almost adsorbed by the resin before 7 BV that is 100 mL, and then the concentrations of TPs in the breakthrough solution increased rapidly until a steady plateau at 33 BV (≈ 500 mL) corresponding to the exhaustion point time (t_{EP}). The total volume of wine lees extract passed through the column was 644 mL, which means 548 mg GAE of TPs loaded in the column (851 mg GAE/mL × 644 mL). Out of the initial 548

mg GAE, a certain amount of TPs has leaked from the column. To determine the exact quantity, the integral was calculated from the initial volume of 0 to the final volume of 644 mL, using the sixth-degree function that fits the leakage curve as shown in the Figure 6.4. The blue highlighted area under the curve represents 345 mg of eluted polyphenols, meaning 203 mg GAE of TPs retained by the resin. Therefore, under the following operating conditions, the TPs AR% was 37% and the $Q_{t.a}$ equal to 40 mg per gram of resin. Thus, for the same MN 202 resin, the amount adsorbed by the dynamic method was smaller than in the batch method. This was probably due to a smaller contact time between fluid and solid phase (Vieira and Beppu 2006).

In the desorption process of TPs from MN 202 resin, the saturated resin was washed with 70% v/v ethanol solution at a flow rate of 1 $mL \cdot min^{-1}$. The dynamic desorption curve obtained for MN 202 resin is reported in Figure 6.5, illustrating that 100 mL (7 BV) of desorption solution were sufficient for completely desorbing TPs from the resin. TPs DR% in dynamic was 85% and $Q_{t.d}$ equals to 2.9 mg per gram of resin.

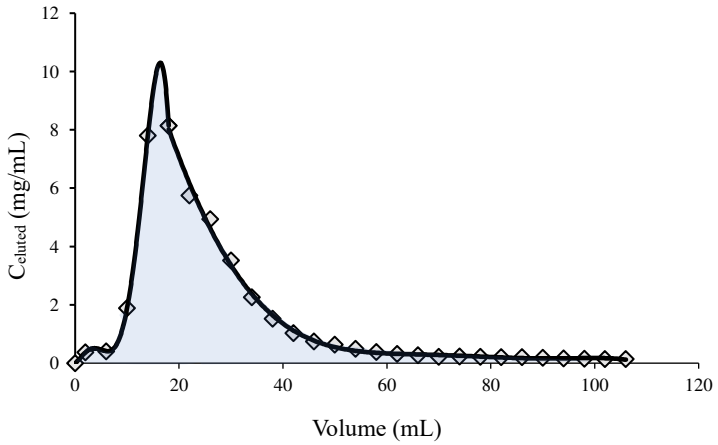

Figure 6.5 Dynamic desorption curves of wine lees TPs on column packed with MN 202 resin.

6.3.4 Adsorption isotherms

In order to understand the mechanism of adsorption of TPs, the correct assignment of the isotherms and kinetics of sorption is of utmost importance. In Table 6.6, we have summarized the parameters and correlation coefficients obtained from fitting data to the Langmuir, Freundlich, Sips, and Redlich-Peterson isotherms.

Table 6.6 Fitting results for wine lees TPs adsorption data with the four proposed models. Experimental conditions: Resin MN202; Temperature=(22 ± 2)°C; t=24h.

Langmuir	Freundlich	Sips	Redlich-Peterson
K_L=1.25 mL/mg	K_F=38.09 (mg/g)(mL/mg)$^{1/n}$	Q_S=75.86 mg/g (d.w.)	K_{RP}=438.00 (mL/mg)(mg/g)
Q_m = 66.84 mg/g (d.w.)	1/n = 0.66	K_S = 1.04 mL/mg	B_{RP} = 10.00 (mL/mg)$^{\beta}$
R_L= 0.36		α = 0.98	β = 0.37
r^2 = 0.967	r^2 = 0.954	r^2 = 0.966	r^2 = 0.930
APE = 6.1 %	APE = 7.4 %	APE = 6.3 %	APE = 7.3 %

Based on the r^2 values, all models fit fairly well the experimental data, with the Langmuir equation being the best and the Redlich-Peterson one being the worst. These results are also confirmed by the APE values: experimental data fit best Langmuir equation, indicating a homogeneous nature of the adsorbent surface. Information on the surface heterogeneity is also consistent with what emerges from the Sips model. When the parameter α in Sips equation is near to 0 it indicates that the adsorbent surface is heterogeneous and follows the Freundlich model, whereas if the value of α is close to 1 (as in this case) it indicates that the surface exhibits homogenous binding sites and the isotherm model is reduced to the Langmuir model.

Moreover, the dimensionless equilibrium parameter, denoted as R_L (equation (6.9)) and related to the Langmuir model allowed to determine that the TPs adsorption was favorable on MN 202 resin (Rodriguez-Lopez et al. 2021).

$$R_L = \frac{1}{1+K_L+C_0'} \tag{6.9}$$

where C_0' is the highest TPs initial concentration. If $0<R_L<1$, adsorption is considered as favorable. It is irreversible for $R_L=0$, unfavorable for $R_L>1$, and linear adsorption when $R_L=1$. In the case of the study, $R_L=0.36$ and thus, the adsorption of phenolic compounds was favorable.

Similarly to R_L, the 1/n parameter in the Freundlich equation and the b parameter in the Redlich-Peterson model indicate favorable TPs adsorption on MN 202, being 1/n less than unity and lying b between 0 and 1 (Cifuentes-Cabezas et al. 2022; Barkakati et al. 2010).

Figure 6.6 compares the predicted values by different models with the experimental data. It can be observed that the Freundlich and Redlich-Peterson models display poor fitting with the observed values. These models fail to show the expected saturation trend, indicating that they are unsuitable for this application.

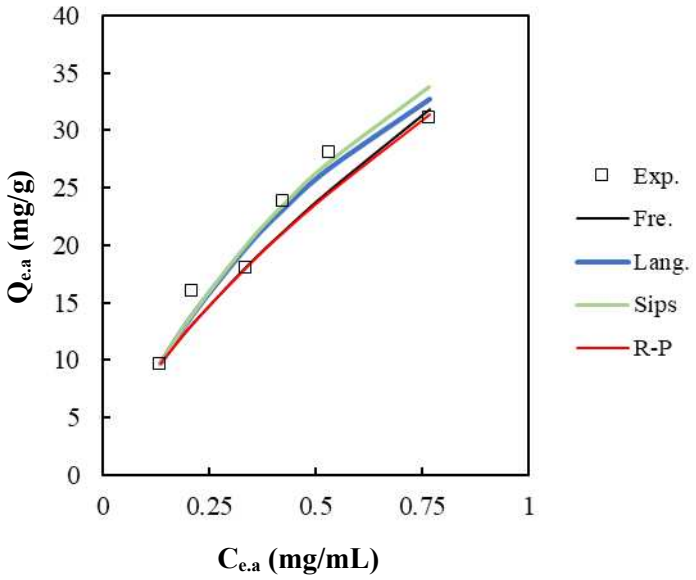

Figure 6.6 Experimental data and predicted model isotherms of TPs wine lees adsorption onto the MN 202 resin.

6.3.5 Adsorption and desorption kinetics

Figure 6.7a illustrates how the concentration of TPs changes over time in various feed solutions during adsorption. Throughout the adsorption process, it was noted that the levels of TPs decreased gradually, irrespective of the concentration of the feed solution. The most significant decline occurred within the initial 20 minutes, with only a slight decrease noted until 60 minutes. Therefore, also adsorption capacity ($Q_{t.a}$) exhibited a rapid increase followed by a leveling-off process (Figure 6.7b). As expected, it was observed that when the concentration of TPs in the feed solution increased, the equilibrium Q_e obtained also increased. Desorption kinetic was also investigate. During the desorption process with a 70% ethanol solution, the asymptotic curves were reached after 20 min of contact time (see Figure 6.8a). Additionally, Figure 6.8b shows that the desorption capacity, $Q_{t.d}$, was proportional to the concentration of TPs.

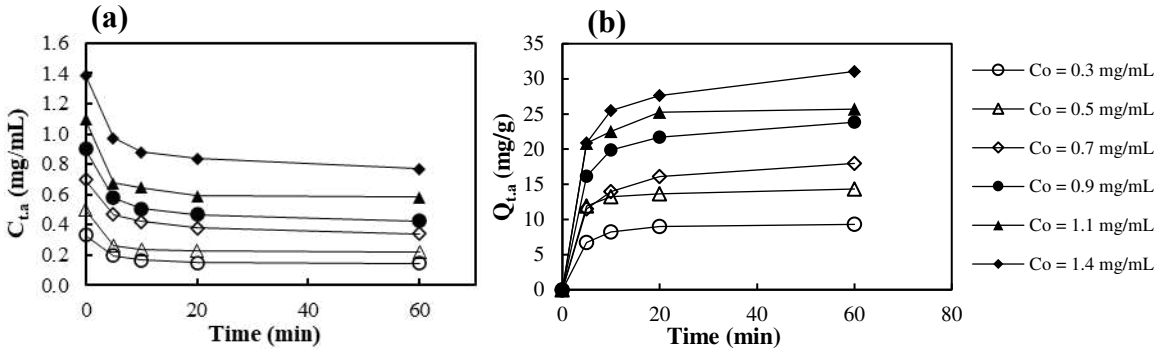

Figure 6.7 Adsorption kinetics for the MN 202 resin: (**a**) TPs concentration course with time; (**b**) Adsorption capacity course with time.

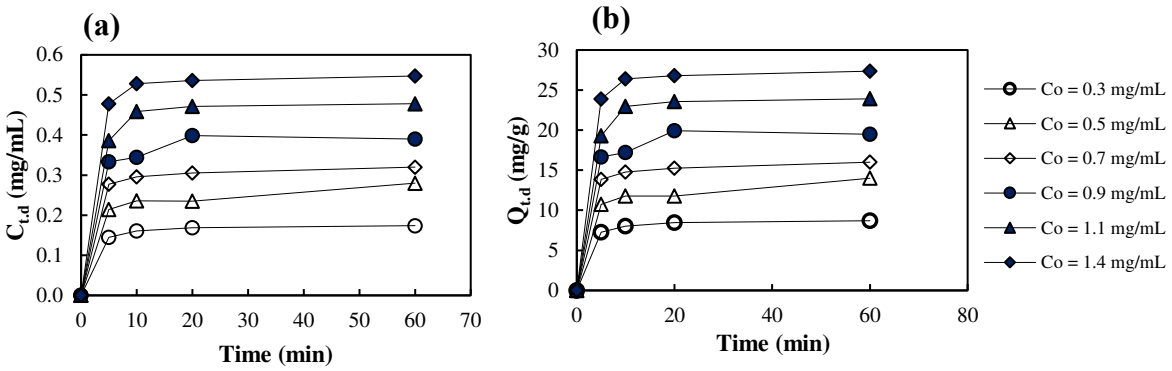

Figure 6.8 Desorption kinetics for the MN 202 resin: (**a**) TPs concentration course with time; (**b**) Desorption capacity course with time.

The adsorption/desorption–time data in Figure 6.7 and 6.8 were treated according to pseudo-first-order, pseudo-second-order, and intraparticle diffusion models. Kinetic models have been used to investigate the mechanism of sorption and possible rate-controlling steps (Marbawi et al. 2019).

To be adsorbed, an adsorbate molecule must find its way to the adsorbent particle by convection, thus: (i) diffuse through the film surrounding the particle (film diffusion); (ii) travel by diffusion along the length of a pore until it finds a vacant adsorption site (intraparticle diffusion); (iii) adsorb onto the solid surface (adsorption onto activate sites).

The overall rate of the adsorption is controlled by the slowest of the above three steps. A combined effect of these steps is also possible. The first step is relatively fast when compared with the second and third ones. Interaction with the surface sites (step 3) can be either by physi- or chemi-sorption (Sahoo and Prelot 2020). The pseudo-first-order model assumes that physisorption limits the adsorption rate of the particles onto the adsorbent, while the pseudo-second-order model considers chemisorption as the rate-limiting mechanism of the process (Sumalinog et al. 2018). Physical adsorption, or physisorption, is caused by Van der Waals or electrostatic forces, while chemisorption involves the formation of strongest

interactions between the adsorbent and the solute. On the other hand, intraparticle diffusion model considers internal diffusion (step 2) as the rate-determining step (Ledesma et al. 2023).

The graphs in Figure 6.9 displays the kinetic plots of linearized forms of the pseudo-first-order (Figures 6.9a and 6.9b) and pseudo-second-order (Figures 6.9c and 6.9d) equations, which are used for adsorption and desorption processes of wine lees on MN 202 resin. In particular, the pseudo-first-order model is used for describing the initial stage of the adsorption/desorption processes, whereas the pseudo-second-order model can appropriately predict the behaviour of the entire adsorption process (Ismail et al. 2020). Additionally, Figures 6.9e and 6.9f depict the kinetic plot of the intra-particle diffusion model for these same processes.

The slope of the pseudo-first-order plot between $\ln(Q_e-Q_t)$ versus time allows us to determine k_1, while the intercept is the predicted Q_e. On the other hand, from the intercept and slope of the pseudo-second-order plot between t/Q_t and time it is possible to calculate k_2 and Q_e. Finally, for the intra-particle diffusion model, the graph plotted between Q_t and $t^{1/2}$ is utilized to calculate the intraparticle diffusion rate constant ($mg.min^{1/2}/g(d.w.)$), k_p, and the intercept constant C. Calculated kinetic parameters are summarized in Table 6.7.

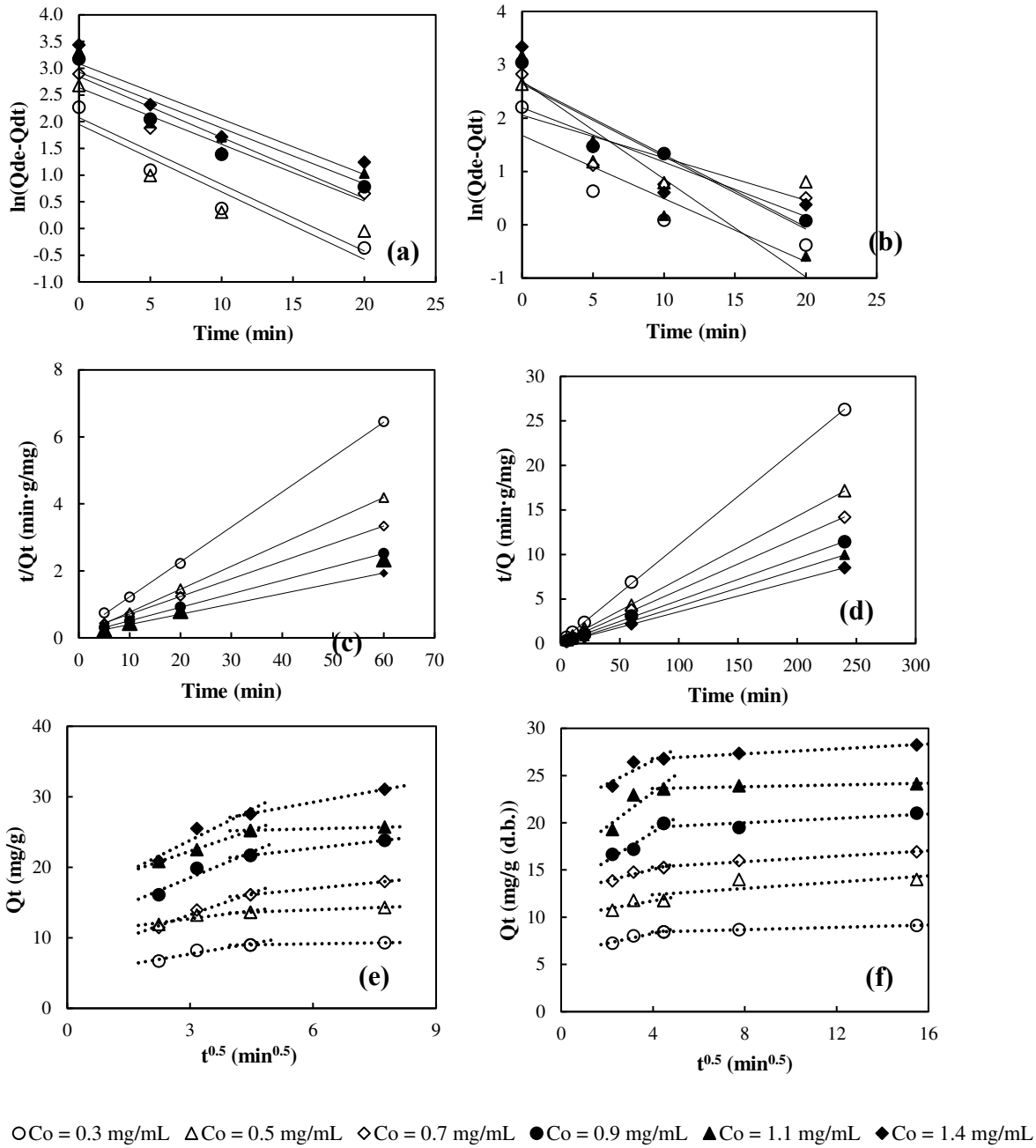

Figure 6.9 Adsorption kinetics models and experimental data: (**a**) Pseudo-first order (**c**) Pseudo-second order (**e**) Intraparticle model. Desorption kinetics models: (**b**) Pseudo-first order and (**d**) Pseudo-second order and (**f**) Intra-particle model.

Table 6.7 Pseudo-first-order, pseudo-second-order, and intraparticle diffusion kinetics equations and related model parameters of TPs on the selected MN 202 resin.

ADSORPTION													
C_0 (mg/mL)	Qe (exp) (mg/g)	Pseudo-First-Order			Pseudo-Second-Order			Intraparticle Diffusion					
								Stage 1			Stage 2		
		K_1 1/min	Qe (cal) (mg/g)	R^2	K_2 mg/(mL·min)	Qe (cal) (mg/g)	R^2	C_1 (mg/g)	K_{p1} (mg/g·min$^{0.5}$)	R_1^2	C_2 (mg/g)	K_{p2} (mg/g·min$^{0.5}$)	R_2^2
0.3	9.6962	0.1263	7.0164	0.9217	0.0604	9.5839	0.9999	4.7146	0.9943	0.9183	8.6015	0.0897	0.9999
0.5	14.5844	0.1249	7.9687	0.7759	0.0579	14.5985	0.9999	10.4582	0.7469	0.8571	12.68	0.2129	0.9999
0.7	18.0413	0.1061	13.9693	0.9367	0.0152	18.9996	0.9999	7.1500	2.0387	0.9802	13.571	0.5683	0.9999
0.9	23.8756	0.1139	17.1998	0.9033	0.0148	24.8911	0.9999	11.2698	2.4183	0.9165	18.777	0.6523	0.9999
1.1	28.0431	0.1045	18.6563	0.8513	0.0291	26.2927	0.9999	16.3650	1.9754	0.9983	24.628	0.1375	0.9999
1.4	31.0614	0.1037	21.8696	0.8717	0.0103	32.5347	0.9999	15.0711	2.9154	0.9066	22.901	1.0527	0.9999
DESORPTION													
C_0 (mg/mL)	Qe (exp) (mg/g)	Pseudo-First-Order			Pseudo-Second-Order			Intraparticle Diffusion					
								Stage 1			Stage 2		
		K_1 1/min	Qe (cal) (mg/g)	R^2	K_2 mg/(mL·min)	Qe (cal) (mg/g)	R^2	C_1 (mg/g)	K_{p1} (mg/g·min$^{0.5}$)	R_1^2	C_2 (mg/g)	K_{p2} (mg/g·min$^{0.5}$)	R_2^2
0.3	9.1304	0.1030	8.8484	0.8036	0.0579	9.1902	0.999	6.1897	0.5226	0.9231	8.1939	0.061	0.9944
0.5	14.0000	0.0267	14.5339	0.6908	0.0342	14.1370	0.999	10.017	0.4282	0.6349	11.713	0.1668	0.5316
0.7	16.9181	0.0551	16.2558	0.7446	0.0281	17.0382	0.999	12.632	0.609	0.9243	14.725	0.1446	0.9722
0.9	21.0102	0.0523	19.8269	0.9045	0.0202	21.1672	0.999	12.957	1.5102	0.9319	19.07	0.1159	0.6976
1.1	24.1368	0.0486	24.2869	0.8912	0.0522	24.2193	0.999	15.292	1.8261	0.7823	23.443	0.0467	0.8954
1.4	28.2480	0.0541	27.6579	0.7446	0.0294	28.3644	0.999	21.635	1.2338	0.7678	26.273	0.1291	0.9892

As shown in Figures 6.9e and 6.9f, each adsorption and desorption process carried out at the various concentrations is divided into two periods based on the two sequential straight lines resulting from successfully fitting adsorption/desorption models to the data. The observation of the two linear diffusional regions can be plausibly ascribed to the bimodal pore size properties of the hyper crosslinked MN 202 polymer adsorbent. Therefore, it is plausible to assign the first linear region of the intraparticle diffusion to the macropores diffusion, whereas the second accounts for micropore diffusion, each with a different gradient as a measure of diffusion rate constant (K_p) (Cheung et al. 2007; Sun et al. 2018).

The rate constants for macropore and micropore diffusion were determined by linear regression (using the intraparticle diffusion equation in Table 6.4) of the two regions, respectively, reported in Table 6.7 (stage 1 and stage 2). The first stage was quicker than the second one. Thus intraparticle diffusion into micropores was the rate-limiting step. However, even though intraparticle diffusion is involved in adsorption and desorption, it is not the only rate-controlling step. This is deducted by considering that the fittings plotted in the first stage for adsorption and desorption concentrations did not pass through the coordinate origin. Thus, other kinetic models may also control the adsorption and desorption rate (Chang et al. 2020).

Regarding pseudo-first-order and pseudo-second-order models, the results shown in Table 6.7 reveal that there is no good correlation between experimental data and pseudo-first-order model for TPs. On the other hand, the pseudo-second-order kinetic model displayed high values of correlation coefficients (R^2= 0.9999) and excellent agreement between the experimental Q_e and the calculated Q_e. These results confirm as the pseudo-second-order kinetic model is the best suited to describe the white wine lees TPs adsorption/desorption onto MN 202 resin.

6.4 Conclusions

In conclusion, this study used five types of food-grade, non-ionic polymer resins to extract and purify polyphenols from sugars extracted from white wine lees through a conventional solid-liquid extraction. The extraction with water as a solvent and the use of MN 202 resin was the perfect combination, which led, in static conditions, to a 58% recovery of polyphenols and complete purification from sugars. A 70% aqueous ethanol solution was used for the desorption of polyphenols from the resin. MN 202 adsorption of TPs from aqueous extract was monomolecular layer as the process was found to conform to Langmuir's isotherm model. The second-order kinetic equation governed the adsorption and desorption processes, also characterized by multilinear intraparticle diffusion. A dynamic test was carried out always using an aqueous extract of wine lees, 5 g of MN 202 resin and a feeding rate of 1 ml/ min. The adsorption ratio in these conditions was lower than in static conditions. Consequentially, further studies should consider optimizing the conditions of the adsorption dynamic process of TPs.

6.5 References

Airouyuwa, J. O., Mostafa, H., Riaz, A., Stathopoulos, C., & Maqsood, S. (2023). Natural Deep Eutectic Solvents and Microwave-Assisted Green Extraction for Efficient Recovery of Bioactive Compounds from By-Products of Date Fruit (Phoenix dactylifera L.) Processing: Modeling, Optimization, and Phenolic Characterization. *Food and Bioprocess Technology*, *16*(4), 824–843. https://doi.org/10.1007/s11947-022-02960-8

Alchera, F., Ginepro, M., & Giacalone, G. (2022). Microwave-Assisted Extraction of Polyphenols from Blackcurrant By-Products and Possible Uses of the Extracts in Active Packaging. *Foods*, *11*(18). https://doi.org/10.3390/foods11182727

Aleixandre-Tudo, J. L., & Du Toit, W. (2019). The Role of UV-Visible Spectroscopy for Phenolic Compounds Quantification in Winemaking. *Frontiers and New Trends in the Science of Fermented Food and Beverages*, 1–21. https://doi.org/10.5772/intechopen.79550

Bacic, T. (2003). Recovery of valuable products from lees and integrated approach to minimise waste and
add value to wine production. University of Melbourne: Final Report to Grape and Wine Research and Development Corporation, (July), 1–43.

Barcia, M. T., Pertuzatti, P. B., Rodrigues, D., Gómez-Alonso, S., Hermosín-Gutiérrez, I., & Godoy, H. T. (2014). Occurrence of low molecular weight phenolics in Vitis vinifera red grape cultivars and their winemaking by-products from São Paulo (Brazil). *Food Research International*, *62*, 500–513. https://doi.org/10.1016/j.foodres.2014.03.051

Barkakati, P., Begum, A., Das, M. L., & Rao, P. G. (2010). Adsorptive separation of Ginsenoside from aqueous solution by polymeric resins: Equilibrium, kinetic and thermodynamic studies. *Chemical Engineering Journal*, *161*(1–2), 34–45. https://doi.org/10.1016/j.cej.2010.04.018

Bertin, L., Ferri, F., Scoma, A., Marchetti, L., & Fava, F. (2011). Recovery of high added value natural polyphenols from actual olive mill wastewater through solid phase extraction. *Chemical Engineering Journal*, *171*(3), 1287–1293. https://doi.org/10.1016/j.cej.2011.05.056

Boateng, I. D. (2023). *Mechanisms, Capabilities, Limitations, and Economic Stability Outlook for Extracting Phenolics from Agro-byproducts Using Emerging Thermal Extraction Technologies and Their Combinative Effects*. *Food and Bioprocess Technology*. Springer US. https://doi.org/10.1007/s11947-023-03171-5

Boban, D., Dželalija, A. M., Gujinović, D., Benzon, B., Ključević, N., Boban, Z., et al. (2023). Differential Effects of White Wine and Ethanol Consumption on Survival of Rats after a Myocardial Infarction. *Applied Sciences (Switzerland)*, *13*(3). https://doi.org/10.3390/app13031450

Buljeta, I., Pichler, A., Šimunović, J., & Kopjar, M. (2023). Beneficial Effects of Red Wine Polyphenols on Human Health: Comprehensive Review. *Current Issues in Molecular Biology*, *45*(2), 782–798. https://doi.org/10.3390/cimb45020052

Caetano, M., Valderrama, C., Farran, A., & Cortina, J. L. (2009). Journal of Colloid and Interface Science Phenol removal from aqueous solution by adsorption and ion exchange mechanisms onto polymeric resins. *Journal of Colloid And Interface Science*,

338(2), 402–409. https://doi.org/10.1016/j.jcis.2009.06.062

Cetó, X., Gutiérrez, J. M., Gutiérrez, M., Céspedes, F., Capdevila, J., Mínguez, S., et al. (2012). Determination of total polyphenol index in wines employing a voltammetric electronic tongue. *Analytica Chimica Acta*, *732*(Jun), 172–179. https://doi.org/10.1016/j.aca.2012.02.026

Chang, J., Shen, Z., Hu, X., Schulman, E., Cui, C., Guo, Q., & Tian, H. (2020). Adsorption of Tetracycline by Shrimp Shell Waste from Aqueous Solutions: Adsorption Isotherm, Kinetics Modeling, and Mechanism. *ACS Omega*, *5*(7), 3467–3477. https://doi.org/10.1021/acsomega.9b03781

Cheung, W. H., Szeto, Y. S., & McKay, G. (2007). Intraparticle diffusion processes during acid dye adsorption onto chitosan. *Bioresource Technology*, *98*(15), 2897–2904. https://doi.org/10.1016/j.biortech.2006.09.045

Cifuentes-Cabezas, M., María Sanchez-Arévalo, C., Antonio Mendoza-Roca, J., Cinta Vincent-Vela, M., & Álvarez-Blanco, S. (2022). Recovery of phenolic compounds from olive oil washing wastewater by adsorption/desorption process. *Separation and Purification Technology*, *298*(June). https://doi.org/10.1016/j.seppur.2022.121562

De Iseppi, A., Lomolino, G., Marangon, M., & Curioni, A. (2020). Current and future strategies for wine yeast lees valorization. *Food Research International*, *137*(April), 109352. https://doi.org/10.1016/j.foodres.2020.109352

Dimou, C., Kopsahelis, N., Papadaki, A., Papanikolaou, S., Kookos, I. K., Mandala, I., & Koutinas, A. A. (2015). Wine lees valorization: Biorefinery development including production of a generic fermentation feedstock employed for poly(3-hydroxybutyrate) synthesis. *Food Research International*, *73*, 81–87. https://doi.org/10.1016/j.foodres.2015.02.020

Ersali, S., Hadadi, V., Moradi, O., & Fakhri, A. (2013). Pseudo-second-order kinetic equations for modeling adsorption systems for removal of ammonium ions using multi-walled carbon nanotube. *Fullerenes, Nanotubes and Carbon Nanostructures*, 150527104639002. https://doi.org/10.1080/1536383x.2013.787610

Franco, D., Rodríguez-Amado, I., Agregán, R., Munekata, P. E. S., Vázquez, J. A., Barba, F. J., & Lorenzo, J. M. (2018). Optimization of antioxidants extraction from peanut skin to prevent oxidative processes during soybean oil storage. *Lwt*, *88*, 1–8. https://doi.org/10.1016/j.lwt.2017.09.027

Fu, R., Wang, Y., Yu, F., Wu, X., Gu, Y., & Chen, W. (2016). Optimization of the macroporous resin-based adsorption of apple polyphenol through response surface methodology, *2248*(March). https://doi.org/10.1080/02772248.2015.1123490

Fu, Y., Zu, Y., Liu, W., Hou, C., Chen, L., Li, S., et al. (2007). Preparative separation of vitexin and isovitexin from pigeonpea extracts with macroporous resins, *1139*, 206–213. https://doi.org/10.1016/j.chroma.2006.11.015

Gaglianò, M., Conidi, C., De Luca, G., & Cassano, A. (2022). Partial Removal of Sugar from Apple Juice by Nanofiltration and Discontinuous Diafiltration. *Membranes*, *12*(7). https://doi.org/10.3390/membranes12070712

Galvan D'Alessandro, L., Kriaa, K., Nikov, I., & Dimitrov, K. (2012). Ultrasound assisted extraction of polyphenols from black chokeberry. *Separation and Purification Technology*, *93*, 42–47. https://doi.org/10.1016/j.seppur.2012.03.024

Gómez-Mejía, E., Rosales-Conrado, N., León-González, M. E., & Madrid, Y. (2019). Citrus peels waste as a source of value-added compounds: Extraction and quantification of bioactive polyphenols. *Food Chemistry*, *295*(May), 289–299. https://doi.org/10.1016/j.foodchem.2019.05.136

Heravi, S., Rahimi, M., Shahriari, M., & Ebrahimi, S. N. (2022). Enrichment of phenolic compounds from grape (Vitis vinifera L .) pomace extract using a macroporous resin and response surface. *Chemical Engineering Research and Design*, *183*, 382–397. https://doi.org/10.1016/j.cherd.2022.05.011

Huaman-Castilla, N. L., Martínez-Cifuentes, M., Camilo, C., Pedreschi, F., Mariotti-Celis, M., & Pérez-Correa, J. R. (2019). The impact of temperature and ethanol concentration on the global recovery of specific polyphenols in an integrated HPLE/RP process on Carménère pomace extracts. *Molecules*, *24*(17), 1–16. https://doi.org/10.3390/molecules24173145

Ismail, B. B., Yusuf, H. L., Pu, Y., Zhao, H., Guo, M., & Liu, D. (2020). Ultrasound-assisted adsorption/desorption for the enrichment and purification of flavonoids from baobab (Adansonia digitata) fruit pulp. *Ultrasonics Sonochemistry*, *65*(January), 104980. https://doi.org/10.1016/j.ultsonch.2020.104980

Jara-Palacios, M. J. (2019). Wine lees as a source of antioxidant compounds. *Antioxidants*, *8*(2), 1–10. https://doi.org/10.3390/antiox8020045

Jurcevic, I. L., Dora, M., Guberovic, I., Petras, M., Brncic, S. R., & Dikic, D. (2017). Polyphenols from wine lees as a novel functional bioactive compound in the protection against oxidative stress and hyperlipidaemia. *Food Technology and Biotechnology*, *55*(1), 109–116. https://doi.org/10.17113/ft b.55.01.17.4894

Kato-Schwartz, C. G., Corrêa, R. C. G., de Souza Lima, D., de Sá-Nakanishi, A. B., de Almeida Gonçalves, G., Seixas, F. A. V., et al. (2020). Potential anti-diabetic properties of Merlot grape pomace extract: An in vitro, in silico and in vivo study of α-amylase and α-glucosidase inhibition. *Food Research International*, *137*(March), 109462. https://doi.org/10.1016/j.foodres.2020.109462

Kontogiannopoulos, K. N., Patsios, S. I., & Karabelas, A. J. (2016). Tartaric acid recovery from winery lees using cation exchange resin : Optimization by Response Surface Methodology. *SEPARATION AND PURIFICATION TECHNOLOGY*, *165*, 32–41. https://doi.org/10.1016/j.seppur.2016.03.040

Ledesma, B., Sabio, E., Mar, C., Rom, S., Fernandez, M. E., Bonelli, P., & Cukierman, A. L. (2023). Batch and Continuous Column Adsorption of p-Nitrophenol onto Activated Carbons with Different Particle Sizes, 1–22.

Lim, K. J. A., Cabajar, A. A., Lobarbio, C. F. Y., Taboada, E. B., & Lacks, D. J. (2019). Extraction of bioactive compounds from mango (Mangifera indica L. var. Carabao) seed kernel with ethanol–water binary solvent systems. *Journal of Food Science and Technology*, *56*(5), 2536–2544. https://doi.org/10.1007/s13197-019-03732-7

Marbawi, H., Ros Saidon Khudri, M. A. M., Othman, A. R., Halmi, M. I. E., Gansau, J. A., & Yasid, N. A. (2019). Kinetic Analysis of the Adsorption of Glyphosate onto Palm Oil Fronds Activated Carbon. *Bioremediation Science and Technology Research*, *7*(1), 29–33. https://doi.org/10.54987/bstr.v7i1.461

Marco, E. De, Savarese, M., & Aldo, B. (2010). ingredienti, (March 2015).

Mejia, J. A. A., Ricci, A., Figueiredo, A. S., Versari, A., Cassano, A., de Pinho, M. N., &

Parpinello, G. P. (2022). Membrane-based Operations for the Fractionation of Polyphenols and Polysaccharides From Winery Sludges. *Food and Bioprocess Technology*, *15*(4), 933–948. https://doi.org/10.1007/s11947-022-02795-3

Messinese, E., Pitirollo, O., Grimaldi, M., Milanese, D., Sciancalepore, C., & Cavazza, A. (2023). By-Products as Sustainable Source of Bioactive Compounds for Potential Application in the Field of Food and New Materials for Packaging Development. *Food and Bioprocess Technology*, (0123456789). https://doi.org/10.1007/s11947-023-03158-2

Mir-Cerdà, A., Carretero, I., Coves, J. R., Pedrouso, A., Castro-Barros, C. M., Alvarino, T., et al. (2023). Recovery of phenolic compounds from wine lees using green processing: Identifying target molecules and assessing membrane ultrafiltration performance. *Science of the Total Environment*, *857*(July 2022), 1–7. https://doi.org/10.1016/j.scitotenv.2022.159623

Molole, G. J., Gure, A., & Abdissa, N. (2022). Determination of total phenolic content and antioxidant activity of Commiphora mollis (Oliv.) Engl. resin. *BMC Chemistry*, *16*(1), 1–11. https://doi.org/10.1186/s13065-022-00841-x

Moro, K. I. B., Bender, A. B. B., da Silva, L. P., & Penna, N. G. (2021). Green Extraction Methods and Microencapsulation Technologies of Phenolic Compounds From Grape Pomace: A Review. *Food and Bioprocess Technology*, *14*(8), 1407–1431. https://doi.org/10.1007/s11947-021-02665-4

Niculescu, V. C., & Ionete, R. E. (2023). An Overview on Management and Valorisation of Winery Wastes. *Applied Sciences (Switzerland)*, *13*(8). https://doi.org/10.3390/app13085063

Ozgen, S., & Sarıoglu, K. (2013). Synthesis and Characterization of Acrylonitrile-co-Divinylbenzene (AN/DVB) Polymeric Resins for the Isolation of Aroma Compounds and Anthocyanins from Strawberry. *Food and Bioprocess Technology*, *6*(10), 2884–2894. https://doi.org/10.1007/s11947-012-0969-4

Pérez-Serradilla, J. A., & Luque de Castro, M. D. (2011). Microwave-assisted extraction of phenolic compounds from wine lees and spray-drying of the extract. *Food Chemistry*, *124*(4), 1652–1659. https://doi.org/10.1016/j.foodchem.2010.07.046

Périno-Issartier, S., Zill-e-Huma, Abert-Vian, M., & Chemat, F. (2011). Solvent Free Microwave-Assisted Extraction of Antioxidants from Sea Buckthorn (Hippophae rhamnoides) Food By-Products. *Food and Bioprocess Technology*, *4*(6), 1020–1028. https://doi.org/10.1007/s11947-010-0438-x

Ramón-Gonçalves, M., Gómez-Mejía, E., Rosales-Conrado, N., León-González, M. E., & Madrid, Y. (2019). Extraction, identification and quantification of polyphenols from spent coffee grounds by chromatographic methods and chemometric analyses. *Waste Management*, *96*, 15–24. https://doi.org/10.1016/j.wasman.2019.07.009

Ray, S. S., Gusain, R., & Kumar, N. (2020). Adsorption equilibrium isotherms, kinetics and thermodynamics. *Carbon Nanomaterial-Based Adsorbents for Water Purification*, 101–118. https://doi.org/10.1016/b978-0-12-821959-1.00005-2

Rico, X., Gullón, B., & Yáñez, R. (2022). A Comparative Assessment on the Recovery of Pectin and Phenolic Fractions from Aqueous and DES Extracts Obtained from Melon Peels. *Food and Bioprocess Technology*, *15*(6), 1406–1421. https://doi.org/10.1007/s11947-022-02823-2

Rivas, M. Á., Casquete, R., Córdoba, M. de G., Ruíz-Moyano, S., Benito, M. J., Pérez-Nevado, F., & Martín, A. (2021). Chemical composition and functional properties of dietary fibre concentrates from winemaking by-products: Skins, stems and lees. *Foods*, *10*(7). https://doi.org/10.3390/foods10071510

Rodriguez-Lopez, A. D., Reig, M., Mayor, L., Ortiz-Climent, M., & Garcia-Castello, E. M. (2021). Characterization of ionic exchange and macroporous resins for their application on the separation and recovery of chlorogenic acid from the wastewater of artichoke blanching. *Sustainability (Switzerland)*, *13*(16). https://doi.org/10.3390/su13168928

Romero-Díez, R., Rodríguez-Rojo, S., Cocero, M. J., Duarte, C. M. M., Matias, A. A., & Bronze, M. R. (2018). Phenolic characterization of aging wine lees: Correlation with antioxidant activities. *Food Chemistry*, *259*(October 2017), 188–195. https://doi.org/10.1016/j.foodchem.2018.03.119

Rosell, C. M. (2011). *The Science of Doughs and Bread Quality*. *Flour and Breads and their Fortification in Health and Disease Prevention*. Elsevier Inc. https://doi.org/10.1016/B978-0-12-380886-8.10001-7

Sahoo, T. R., & Prelot, B. (2020). *Adsorption processes for the removal of contaminants from wastewater: The perspective role of nanomaterials and nanotechnology*. *Nanomaterials for the Detection and Removal of Wastewater Pollutants*. Elsevier Inc. https://doi.org/10.1016/B978-0-12-818489-9.00007-4

Sandhu, A. K., & Gu, L. (2013). Adsorption/desorption characteristics and separation of anthocyanins from muscadine (Vitis rotundifolia) juice pomace by use of macroporous adsorbent resins. *Journal of Agricultural and Food Chemistry*, *61*(7), 1441–1448. https://doi.org/10.1021/jf3036148

Silva, E. M., Pompeu, D. R., Larondelle, Y., & Rogez, H. (2007). Optimisation of the adsorption of polyphenols from Inga edulis leaves on macroporous resins using an experimental design methodology. *Separation and Purification Technology*, *53*(3), 274–280. https://doi.org/10.1016/j.seppur.2006.07.012

Sumalinog, D. A. G., Capareda, S. C., & de Luna, M. D. G. (2018). Evaluation of the effectiveness and mechanisms of acetaminophen and methylene blue dye adsorption on activated biochar derived from municipal solid wastes. *Journal of Environmental Management*, *210*, 255–262. https://doi.org/10.1016/j.jenvman.2018.01.010

Sun, P., Xu, L., Li, J., Zhai, P., Zhang, H., Zhang, Z., & Zhu, W. (2018). Hydrothermal synthesis of mesoporous Mg3Si2O5(OH)4 microspheres as high-performance adsorbents for dye removal. *Chemical Engineering Journal*, *334*(August 2017), 377–388. https://doi.org/10.1016/j.cej.2017.09.120

Tabla Ruiz, N. (2020). *Assessment of polymeric resins for the recovery of polyphenols*. Universitat de Barcelona.

Tagkouli, D., Tsiaka, T., Kritsi, E., Soković, M., Sinanoglou, V. J., Lantzouraki, D. Z., & Zoumpoulakis, P. (2022). Towards the Optimization of Microwave-Assisted Extraction and the Assessment of Chemical Profile, Antioxidant and Antimicrobial Activity of Wine Lees Extracts. *Molecules*, *27*(7). https://doi.org/10.3390/molecules27072189

Tao, Y., Wu, D., Zhang, Q. A., & Sun, D. W. (2014). Ultrasound-assisted extraction of phenolics from wine lees: Modeling, optimization and stability of extracts during storage. *Ultrasonics Sonochemistry*, *21*(2), 706–715. https://doi.org/10.1016/j.ultsonch.2013.09.005

Tapia-Quirós, P., Montenegro-Landívar, M. F., Reig, M., Vecino, X., Cortina, J. L., Saurina, J., & Granados, M. (2022). Recovery of Polyphenols from Agri-Food By-Products: The Olive Oil and Winery Industries Cases. *Foods*, *11*(3), 1–26. https://doi.org/10.3390/foods11030362

Toaldo, I. M., de Gois, J. S., Fogolari, O., Hamann, D., Borges, D. L. G., & Bordignon-Luiz, M. T. (2014). Phytochemical Polyphenol Extraction and Elemental Composition of Vitis labrusca L. Grape Juices Through Optimization of Pectinolytic Activity. *Food and Bioprocess Technology*, *7*(9), 2581–2594. https://doi.org/10.1007/s11947-014-1288-8

Tomasi, I. T., Santos, S. C. R., Boaventura, R. A. R., & Botelho, C. M. S. (2023). Microwave-Assisted Extraction of Polyphenols from Eucalyptus Bark—A First Step for a Green Production of Tannin-Based Coagulants. *Water (Switzerland)*, *15*(2). https://doi.org/10.3390/w15020317

Trikas, E. D., Papi, R. M., Kyriakidis, D. A., & Zachariadis, G. A. (2017). Evaluation of Ion Exchange and Sorbing Materials for Their Adsorption / Desorption Performane towards Anthocyanins , Total Phenolics , and Sugars from a Grape Pomace Extract. https://doi.org/10.3390/separations4010009

Vella, F. M., Laratta, B., La Cara, F., & Morana, A. (2018). Recovery of bioactive molecules from chestnut (Castanea sativa Mill.) by-products through extraction by different solvents. *Natural Product Research*, *32*(9), 1022–1032. https://doi.org/10.1080/14786419.2017.1378199

Vieira, R. S., & Beppu, M. M. (2006). Dynamic and static adsorption and desorption of Hg(II) ions on chitosan membranes and spheres. *Water Research*, *40*(8), 1726–1734. https://doi.org/10.1016/j.watres.2006.02.027

Wang, L., Boussetta, N., Lebovka, N., & Vorobiev, E. (2019). Ultrasonics - Sonochemistry Ultrasound assisted puri fi cation of polyphenols of apple skins by adsorption / desorption procedure. *Ultrasonics - Sonochemistry*, *55*(February), 18–24. https://doi.org/10.1016/j.ultsonch.2019.03.002

Xu, Z., Cai, J. G., & Pan, B. C. (2013). Mathematically modeling fixed-bed adsorption in aqueous systems. *Journal of Zhejiang University: Science A*, *14*(3), 155–176. https://doi.org/10.1631/jzus.A1300029

Zagklis, D. P., & Paraskeva, C. A. (2015). Purification of grape marc phenolic compounds through solvent extraction , membrane filtration and resin adsorption / desorption. *Separation and Purification Technology*, *156*, 328–335. https://doi.org/10.1016/j.seppur.2015.10.019

Zhang, B., Yang, R., Zhao, Y., & Liu, C. (2008). Separation of chlorogenic acid from honeysuckle crude extracts by macroporous resins, *867*, 253–258. https://doi.org/10.1016/j.jchromb.2008.04.016

Zhao, F., Du, L., Wang, J., Liu, H., Zhao, H., Lyu, L., et al. (2023). Function, *156*, 4380–4391. https://doi.org/10.1039/d3fo01211e

General Conclusions

The scope of the work performed during this PhD project was analysing and recovering metabolites, from natural stuff (fruit juices and Cannabis sativa) and by-products (wine lees). Metabolites are small molecules resulting from internal genetic processes and external environmental factors. They can be identified using different techniques including HPLC, NMR, UV-Vis, MS often in association with chemometric methods. A complete understanding of the metabolites composing a matrix is the first step to define the best separation and extraction technique to recover from it, only a particular class of compounds, such as, the bioactive polyphenols. To partially recover phenolic compounds from fruit juices and wine lees, membrane processes as well as adsorption resins, have been found to be highly efficient and advantageous compared to conventional methods. These methods are simple, require minimal equipment, are easy to operate, and consume low amounts of energy. Additionally, they can operate under mild temperature conditions, which helps preserve the biological activity and properties of thermosensitive compounds in the original product.

In the first Chapter of this PhD thesis, theoretical bases of characterization and separation techniques are illustrated, while the following chapters are related to the experimental works carried out during the three years of the doctorate. In Chapter 2, was reporter a study on Calabrian apple juices belonging to four different cultivars, Royal Gala, Pink Lady, Golden Delicious, and Fuji. One of the objectives of this work was the characterization of metabolites present in the food matrix and, at the same time, the possibility of using UF and NF, to obtain from the squeezed apple juice, extracts rich in antioxidants. To improve the overall quality of the study and enhance the coverage of the metabolome two analytical tools were used: NMR and HPLC–UV-ESI–MS/MS. One- and two-dimensional multinuclear NMR spectra combined with chemometric analysis (PCA) were used to identify the metabolic profile of different juice varieties and variations in metabolic composition. On the basis of its higher content of phenolic compounds, the Golden Delicious variety was selected to carry out membrane filtration tests. Specifically, the fresh juice was clarified by UF and then concentrated by NF up to a volume reduction factor (VRF) of 3.3. Permeate and retentate fractions of both processes were analyzed by HPLC–UV and NMR in order to evaluate the membrane selectivity of the selected membranes towards target compounds. The analyses highlighted that the integrated UF-NF process was adequate to collect fractions enriched in bioactive compounds from the initial apple juice. In Chapter 3 a technological challenge was proposed, that is the partial removal of sugars in fruit juices without

compromising their biofunctional properties. The current study was aimed at evaluating the separation of sugars from phenolic compounds in apple juice by using three different spiral-wound nanofiltration (NF) membranes with a molecular weight cut-off (MWCO) in the range of 200–500 Da. A combination of diafiltration and batch concentration processes was investigated to produce apple juice with reduced sugar content and improved health properties thanks to the preservation and concentration of phenolic compounds. For all selected membranes, permeate flux and recovery rate of glucose, fructose, and phenolic compounds, in both diafiltration and concentration processes, were evaluated. The concentration factor of target compounds as a function of the volume reduction factor (VRF) as well as the amount of adsorbed compound on the membrane surface from mass balance analysis were also evaluated. Among the investigated membranes a thin-film composite membrane with an MWCO of 200–300 Da provided the best results in terms of the preservation of phenolic compounds in the selected operating conditions. More than 70% of phenolic compounds were recovered in the retentate stream while the content of sugars was reduced by about 60%. In Chapter 4, the matrix under investigation was Tacle: a citrus variety which recently gained further interest due to its antioxidant and biological properties. This study suggests using Nuclear Magnetic Resonance (NMR) to characterize Tacle juice's metabolic composition as it is intimately linked to its quality. First, polar and apolar solvent systems were used to identify a significant fraction of the Tacle metabolome. Furthermore, the antioxidant capacity and the total content of flavonoids, polyphenols and β-carotene in the juice were investigated with UV-Visible spectroscopy. Tacle juice was clarified and fractionated by ultrafiltration (UF) and nanofiltration (NF) membranes in order to recover and purify its bioactive principles. Finally, the second part of this work sheds light on the spectrophotometric assays and ^{1}H-NMR spectra of fractions coming from membrane operations coupled with a multivariate data analysis technique, PCA, to explore the impact of UF and NF processes on the metabolic profile of the juice. The results of this study demonstrate the efficacy and utility of PCA in providing a comprehensive understanding of the effects of membrane filtration processes on juice composition and confirm the capacity of membrane filtration processes to preserve the chemical composition of the original juice, without generating unwanted metabolites, which is in contrast to the effects of heat treatments. In Chapter 5, NMR technique was used to study *Cannabis sativa*, a herbaceous multiple-use species commonly employed to produce fiber, oil, and medicine. It is now becoming popular for the high nutritional properties of its seed oil and for the pharmacological activity of its cannabinoid fraction in inflorescences. The present study aimed to apply nuclear magnetic resonance (NMR) spectroscopy to provide useful

qualitative and quantitative information on the chemical composition of seed and flower Cannabis extracts obtained by ultra-sound-assisted extraction, and to evaluate NMR as an alternative to the official procedure for the quantification of cannabinoids. The estimation of the optimal ω-6/ω-3 ratio from the ^{1}H NMR spectrum for the seed extracts of the *Futura 75* variety and the quantitative results from the ^{1}H and ^{13}C NMR spectra for the inflorescence extracts of the *Tiborszallasi* and *Kompolti* varieties demonstrate that NMR technology represents a good alternative to classical chromatography, supplying sufficiently precise, sensitive, rapid, and informative data without any sample pre-treatment. In addition, different extraction procedures were tested and evaluated to compare the elaboration of spectral data with the principal component analysis (PCA) statistical method and the quantitative NMR results: the extracts obtained with higher polarity solvents (acetone or ethanol) were poor in psychotropic agents (THC < LOD) but had an appreciable percentage of both cannabinoids and triacylgliceroles (TAGs). These bioactive-rich extracts could be used in the food and pharmaceutical industries, opening new pathways for the production of functional foods and supplements. This PhD thesis continues with the latest experimental work concerning wine lees, that are typical polluting by-products generated by the winemaking industry, well-recognized as a powerful source of bioactive compounds with nutraceutical properties. The current study evaluated a cost-effective and environment-friendly process for extracting and purifying polyphenols from wine lees of the white grape variety, aligning with industry ecology and circular economy principles. The conventional solid-liquid extraction was carried out in the first step of the process by using water and ethanol/water 25% w/w as solvents. Then, five commercial food-grade resins (XAD 7HP, XAD 16HP, MN 202, PAD 900, PAD 950) were screened to purify phenolic compounds from sugars in both extracts. Total phenolics (TPs) were quantified as Total Phenolic Content (TPC) with the Folin-Ciocalteu essay and directly reading the absorbance at 280 nm (Total Phenolic Index (TPI)), while sugars were quantified through an enzymatic method. For all the extract types, particularly with the aqueous extract, the MN 202 resin provided the best performance in static conditions regarding purification from sugars and TPs adsorption and desorption ratio and, thus, of TPs recovery (R% = 58%). Moreover, this resin showed excellent regeneration. The adsorption and desorption behaviour of MN 202 was also studied in dynamic conditions. In static, adsorption isotherms (Langmuir, Freundlich, Sips and Redlich-Peterson isotherms) and kinetics models (pseudo-first-order, pseudo-second-order and intraparticle diffusion) were employed to predict the mechanism of adsorption and desorption of water extracts with this resin. The adsorption process followed Langmuir's adsorption isotherm, which agrees with monomolecular layer adsorption; both

adsorption and desorption processes fitted the kinetic second-order equation and were dominated by multilinear intraparticle diffusion.

To conclude, the work carried out during this thesis project has faced the study of complex natural matrices using HPLC, MS, UV-Vis, and NMR methodologies and the use of cutting-edge techniques for polyphenols' recovery. NMR combined to PCA revealed to be a powerful instrument to solve all the metabolomic problematics dealt with, ranging from sample variety diversification to the membrane processes monitoring. Moreover, both membrane and adsorbent resins operations were found to be effective in the separation, purification and concentration of bioactive compounds from natural matrices and extracts, thus opening the way to new functional products.

Therefore, the obtained outcomes are promising, but there is still room for improvement. For example, among the future perspectives, using ultrafast 2D spectroscopy methods instead of 1D NMR spectra for metabolomics workflow would improve marker identification. Furthermore, for a better separation and purification of nutraceutical compounds, the extraction procedures and the operational conditions for membrane and resin processes could be combined and optimized using the Design of Experiments (DOE), the other branch of chemometrics.

List of publications

Gaglianò, M., Conidi, C., Bartella, L., Salvino, R. A., Di Donna, L., Cassano, A., & De Luca, G. (2021). An Integrated Approach Based on NMR and HPLC–UV-ESI–MS/MS to Characterize Apple Juices and Their Nanofiltration (NF) Bioactive Extracts. *Food and Bioprocess Technology*, 14(12), 2273–2285. https://doi.org/10.1007/s11947-021-02718-8

Gaglianò, M., Conidi, C., De Luca, G., & Cassano, A. (2022). Partial Removal of Sugar from Apple Juice by Nanofiltration and Discontinuous Diafiltration. *Membranes*, 12(7). https://doi.org/10.3390/membranes12070712

Colella, M. F., Salvino, R. A., Gaglianò, M., Litrenta, F., Rossi, C. O., Pera, A. Le, & De Luca, G. (2022). NMR Spectroscopy Applied to the Metabolic Analysis of Natural Extracts of Cannabis sativa. *Molecules,* 27(11). https://doi.org/10.3390/molecules27113509

Gaglianò, M., De Luca, G., Conidi, C., & Cassano, A. (2023). NMR-Based Characterization of Citrus Tacle Juice and Low-Level NMR and UV—Vis Data Fusion for Monitoring Its Fractions from Membrane-Based Operations. *Antioxidants*, 12(1). https://doi.org/10.3390/antiox12010002

List of poster

"An integrated analytical approach based on NMR and HPLC-UV-ESI-MS/MS to characterize Calabrian apple juices and its Nanofiltration (NF) extracts" presented at the "XLIX National Congress on Magnetic Resonance", 08-10 September 2021.

"NMR-based approach to investigate metabolomic profile of Citrus hybrid Tacle before and after pressure-driven membrane operations" presented at the "Italian-French International Conference on Magnetic Resonance", 27-30 September 2022.

"NMR and MS characterization followed by dia-nanofiltration process of apple juice to reduce sugar content and enhance bioactive properties" presented at "EuroMembrane 2022", 20-24 November 2022.

"NMR metabolomic study of a bread-making process: from raw material to bakery goods" presented at the "50th National Congress on Magnetic Resonance", 6-8 September 2023.

List of oral communications

"Nanofiltration of Calabrian apple juice: characterization of bioactive fractions and sugar reduction" held on the "ITM Seminar Day", 20 December 2021.

"NMR and MS as toolset in metabolomics analysis of apple juice and the use of membrane operations for partial removal of sugar" held on "The 8th International Conference on Food Chemistry & Technology (FCT-2022)", 12-14 October 2022.

"Phenolic compounds enhancement and sugar reduction in apple juice by diananofiltration" held on "The 19th Network Young Membrains Meeting (NYM 2022)",17-19 November 2022.

Published Papers

Food and Bioprocess Technology (2021) 14:2273–2285
https://doi.org/10.1007/s11947-021-02718-8

ORIGINAL RESEARCH

An Integrated Approach Based on NMR and HPLC–UV-ESI–MS/MS to Characterize Apple Juices and Their Nanofiltration (NF) Bioactive Extracts

Martina Gaglianò[1] · Carmela Conidi[2] · Lucia Bartella[1,3] · Rosachiara A. Salvino[1] · Leonardo Di Donna[1,3] · Alfredo Cassano[2] · Giuseppina De Luca[1]

Received: 4 August 2021 / Accepted: 30 September 2021 / Published online: 29 October 2021

Abstract

In the present work, Calabrian apple juices belonging to four different cultivars, Royal Gala, Pink Lady, Golden Delicious, and Fuji, were studied. One of the objectives of this work was the characterization of metabolites present in the food matrix and at the same time the possibility of using innovative methodologies based on membrane operations, such as ultrafiltration (UF) and nanofiltration (NF), to obtain from the squeezed apple juice, extracts rich in antioxidants. To improve the overall quality of the study and enhance the coverage of the metabolome two analytical tools were used: NMR and HPLC–UV-ESI–MS/MS. One- and two-dimensional multinuclear NMR spectra combined with chemometric analysis (PCA) were used to identify the metabolic profile of different juice varieties and variations in metabolic composition. On the basis of its higher content of phenolic compounds, the Golden Delicious variety was selected to carry out membrane filtration tests. Specifically, the fresh juice was clarified by UF and then concentrated by NF up to a volume reduction factor (VRF) of 3.3. Permeate and retentate fractions of both processes were analyzed by HPLC–UV and NMR in order to evaluate the membrane selectivity of the selected membranes towards target compounds.

Keywords Apple juice · Ultrafiltration · Nanofiltration · NMR · HPLC–UV-ESI–MS/MS · Bioactive extracts

Introduction

Apple is one of the most commonly consumed fruit in worldwide as well as its juice (Gunathilake & Considine, 2018). Apples and apple juice are appreciated for their nutritional value, aroma, firmness, and health-promoting effects (Harker et al., 2003; Ting et al., 2013). All these quality properties are ultimately based on the metabolic composition (primary and secondary metabolites) of a given fruit (Cuthbertson et al., 2012). In fact, while amino acids, sugars, and organic acids, respectively, determine taste, sweetness, and acidity, the polyphenolic compounds, mostly located in apple skins, are potential disease-preventing agents (Boyer & Liu, 2004; Francini & Sebastiani, 2013; Gerhauser, 2008; Koutsos et al., 2015; Pirlak et al., 2017). Many factors affect the chemical composition of plant-based foods. The metabolome varies with genetic species, environment, cultivation, geographical location, growing season, storage conditions, and industrial treatments (Duda-Chodak et al., 2010; Kumar et al., 2012; Jeong et al., 2015), and even the smallest variation of one of these factors can cause a variation on the concentration of some metabolites or cause the appearance of new ones usually not present (Salvino et al., 2021). Therefore, each fruit cultivar has a unique and specific metabolic profile that can be used as potential marker for quality, origin, and authenticity of fruit and fruit-derived foods (Sobolev et al., 2015). In literature, many analytical methodologies have been applied to determine specific fruits metabolites (Tallapally et al., 2020; Mamat et al., 2020;

✉ Alfredo Cassano
a.cassano@itm.cnr.it

✉ Giuseppina De Luca
giuseppina.deluca@unical.it

[1] Department of Chemistry & Chemical Technologies, University of Calabria, via P. Bucci, 87036 Rende (CS), Italy

[2] Institute on Membrane Technology (ITM), National Research Council (CNR), c/o University of Calabria, via P. Bucci, 17/C, 87036 Rende (Cosenza), Italy

[3] QUASIORA Laboratory, AGRINFRA Research Net, Università Della Calabria, Via P. Bucci Cubo 12/D, 87036 Arcavacata Di Rende (CS), Italy

Lima et al., 2020; Gören et al., 2009; Seger & Sturm, 2007). Nuclear magnetic resonance (NMR) spectroscopy and mass spectrometry (MS), usually hyphenated to chromatographic separation techniques like liquid (LC) or gas (GC) chromatography, are the two most widely used techniques for structural identification of compounds in complex mixtures as they provide complementary data and both are often required for a full characterization (Bingol, 2018; Abreu & Fernández, 2020; Olennikov et al., 2020). NMR is used in metabolomics primarily because it is a highly reproducible, quantitative non-destructive technique, involves a little manipulation of the sample, and allows the detection of metabolites present in relatively high concentrations with a single experiment (Eisenmann et al., 2016; Gathungu et al., 2018). Using NMR, the identification of metabolites can be performed by means of 1D selective experiments, spectral libraries, and 2D experiments that simplify the spectra and disentangle overlapped signals (Sobolev et al., 2015). In addition, the application of chemometric methods can reduce the dimension of the NMR experimental data by identifying possible patterns among samples (Francini et al., 2017; Pereira et al., 2005; Santucci et al., 2015). However, the limitation of this analytical tool is its inherent low sensitivity compared to MS. The limits of detection of MS are comfortably in the femtomole range for analytes with high ionization efficiency (Marshall & Powers, 2017) while NMR is able to determine substances above 5–10 μM (Eisenmann et al., 2016). MS gives molecular weight information and tandem mass spectrometry (MS/MS) provides structural information of compounds based on their fragmentation patterns. On the other hand, the limitation of the MS technique lies in the extraction and derivatization methodologies that must be applied to the sample before being analyzed. For example, LC separation greatly reduces the complexity of samples in MS. Through the retention times and the MS/MS spectral patterns of the analytes of interest, many metabolites, even present in very small quantities, can be identified (Gathungu et al., 2018). However, the characterization of a food product is not only important to determine its quality, origin, or authenticity, but it is also essential to identify the best method for separation and concentration of specific metabolites with bioactive properties. Since apples have pro-health properties, the concentration of their bioactive compounds, especially polyphenols, is of great interest in order to develop natural products suitable for nutraceutical applications. Several technologies have been reported in literature for the separation and enrichment of natural extracts, ranging from the use of organic solvents to greener techniques, but all have some limitations (Azmir et al., 2013). Membrane processes are today well-established technologies in the agro-food production (Brans et al., 2004; Castro-Muñoz et al., 2016; Catarino & Mendes, 2011; Figoli et al., 2006; Galaverna et al., 2008; Uyttebroek et al., 2017) and appear as a promising technology for meeting the recovery of biologically active compounds from foods and their by-products (Castro-Muñoz et al., 2018). Various methods, e.g., high pressures, concentration gradients, and chemical or electrical potential differences, may be adopted as the driving force for membrane separations. Based on the size of the substances to be separated, and the resultant characteristics needed for the membrane, pressure-driven membrane operations are generally classified into microfiltration (MF), ultrafiltration (UF), nanofiltration (NF), and reverse osmosis (RO) (Li & Chase, 2010). These processes have many advantages over conventional methodologies such as high efficiency, simplicity of equipment, easy operation, and low energy consumption (Bhattacharjee et al., 2017). Moreover, they can operate in mild conditions of temperature so preserving the biological activity of thermosensitive compounds and the properties of the original product. They do not require any addition of chemical compounds or preliminary solvent extraction operation, avoiding product contamination and the need for subsequent purification (Conidi & Cassano, 2014). Among these processes, NF is particularly adequate for (i) purification, fractionation, and concentration of several food products and by-products and (ii) the recovery of value added compounds and solvent from food wastes (Nath et al., 2018). NF membranes are at relatively recent development in membrane technology with separation capabilities falling between UF and RO. Their pore size typically ranges from 0.5 to 2 nm, corresponding to a molecular weight cut-off (MWCO) of 200–1000 Da (Paul & Jons, 2016). Polymeric NF membranes contain ionizable groups, such as carboxylic and sulfonic acid groups, which result in charged surfaces in the presence of a feeding solution. As a consequence, the NF separation characteristics are based not only on size exclusion but also on the so-called Donnan exclusion which postulates that ions carrying the same charge as the membrane (so-called co-ions) will be excluded by the membrane (Mohammad et al., 2015). NF membranes can efficiently remove small organic molecules and inorganic salts from the feed solutions offering higher rejection of divalent ions, lower rejection of monovalent ions, and higher flux in comparison to RO membranes. In addition, NF processes are characterized by lower energy consumption and lower applied pressures than RO (in the range 10–40 bar). These features open up many possibilities in the development of specific applications in different fields of the food industry as fruit juice, beverages, dairy, sugar, and vegetable oil processing (Salehi, 2014). To the best of our knowledge, there are still few works regarding the use of this technology in the field of separation and concentration of bioactive compounds from natural matrices (Arend et al., 2019; Cai et al., 2017; Conidi et al., 2011) and especially from apple juices. The present study was undertaken for a twofold purpose: (a) to perform an untargeted NMR-

metabolic analysis of four different varieties of Calabrian apples juices, namely, Golden Delicious, Royal Gala, Pink Lady, and Fuji, grown in the same Calabrian orchard, and harvested in the same period of the year, i.e., February 2020, and (b) to determine the polyphenolic composition, via HPLC–ESI–MS/MS, of a concentrated product obtained from the Golden Delicious variety through the concentration of the clarified juice by NF.

Materials and Methods

Materials

Gioia Succhi Srl (San Ferdinando, Reggio Calabria, Italy) which generally produces juices industrially in large quantities supplied the apple juices used in this work. The fruits used for the preparation of the juices came from the same Calabrian geographical area, i.e., grown in the same Calabrian orchard, and were harvested in the same period of the year, February 2020, therefore with the same degree of ripeness. For our purposes, following the industrial process, five samples were prepared for each apple variety in small quantities, about 500 mL, by combining the material coming from six fruits for each of them. From these initial batches 20 NMR samples, i.e., five NMR samples for each cultivar, were prepared. For the Golden Delicious variety alone, about another 20 L of juice have been prepared, from the same fruits, since these quantities are necessary for the subsequent membrane concentration treatment. Each apple variety, one at a time, was ground entirely (peel, flesh, and seeds) through a small-scale mill. Then, each sample was pasteurized to inhibit the tyrosinase action. Successively, potassium metabisulfite ($K_2S_2O_5$) was added as preservative followed by the addition of a pectolytic enzyme to degrade pectin and to reduce the viscosity of the juice so that it can be handled easily. Finally, the liquid part was separated from the pulp by filtration. Only the liquid part was transferred to aseptic bags and stored in the cold room at −18 °C to be thawed for subsequent processes and analysis. All chemicals and reagents were of commercial origin: 3-(trimethylsilyl) propionic-2,2,3,3-d4 acid sodium salt (98 atom % D), deuterium oxide (99.9 atom % D), and sodium azide were purchased from Sigma-Aldrich as well as chlorogenic, caffeic acids, and the Folin-Ciocalteu reagent. Formic acid, methanol of LC–MS grade (Sigma-Aldrich), and ultrapure water of Milli-Q gradient were used for chromatography.

Concentration of Apple Juice by NF

Apple juice of the Golden Delicious variety was concentrated by NF. In particular, the depectinized juice was previously clarified by UF using a laboratory plant equipped with a 500-kDa polyethersulfone hollow fiber (HF) membrane module (FB-02-FC from Microdyn Nadir, Wiesbaden, Germany) in selected conditions of transmembrane pressure (about 0.40 bar), axial feed flow rate (460 L/h), and temperature (20 ± 2 °C). The clarified juice was then submitted to a NF process performed by using a bench plant manufactured by DeltaE s.r.l. (Cosenza, Italy) and equipped with a stainless steel housing able to accommodate a spiral-wound membrane module featuring an effective membrane area of 0.32 m^2. The equipment consists of a feed tank with a capacity of 5 L, a high-pressure pump, a digital flowmeter, and a control panel. The feed temperature was adjusted by circulating tap water in the two-layered feed tank. Pressure was monitored at the entrance and exit of the membrane module; it was controlled by a back-pressure control valve located after the membrane module and by setting the pump speed on the control panel. The plant was equipped with a NF membrane module in polyamide supplied by GE Osmonics (Desal DK, Minnetonka, MN) with a MWCO of 150–300 Da. Experiments were performed according to a batch concentration configuration in which the permeate is collected separately while the retentate is recycled back to the feed reservoir. The NF process was performed at a temperature of 25 ± 2 °C, a transmembrane pressure of 20 bar, and an axial feed flow rate of 420 L/h up to a volume reduction factor (VRF) of 3.3. VRF is defined as the ratio of feed volume to residual retentate volume according to the following equation (Garcia-Castello et al., 2011):

$$\mathrm{VRF} = \frac{V_f}{V_r} = 1 + \frac{V_p}{V_r} \tag{1}$$

where V_f, V_p, and V_r are the volume of the feed, permeate, and retentate, respectively. The clarified juice with a total soluble solid (TSS) content of about 7° Brix was concentrated up to a final value of 22° Brix. As expected, a decrease in permeate flux was observed throughout the time due to concentration polarization and fouling of the NF membrane. The measured permeate flux was in the range of 0.50–28.12 L/m^2h, while the average permeate flux was equal to 5.72 L/m^2h. After the NF treatment, the membrane module was cleaned according to the manufacturer's instructions. The selectivity of the NF membrane towards bioactive compounds was evaluated at different VRF values. In particular, the analyzed samples through NMR and HPLC–UV were picked up at VRF 2, 2.5, 3, and 3.3, therefore at increased concentration of soluble solids. The observed rejection for a specific compound was calculated according to the following equation:

$$R_i = \left(1 - \frac{C_{ip}}{C_{if}}\right) \cdot 100 \tag{2}$$

where R_i is the observed retention of compound i (%) and C_{ip} and C_{if} are the concentrations of compound i in permeate and feed (mg/L), respectively.

Sample NMR Preparation and Spectral Acquisition

The samples for NMR isotropic analysis were prepared following the procedure reported in literature (Belton et al., 1997; Iaccarino et al., 2019). Apple juices from the four varieties were first thawed at room temperature and a small volume, about 8 mL, of each batch was centrifuged (4000 rpm for 20 min) to remove the suspended substances. To have chemical shifts values comparable to each other and to those reported in the literature, it was necessary to operate at similar pH values. Then, for each centrifuged sample analyzed the pH has been adjusted to a value of 3.25–3.38 by adding microliters of acid solution of 1 M HCl. In addition, an aqueous solution of NaN_3 was added to minimize the alteration in the composition of the juice during the time of sample preparation and acquisition of NMR spectra. Sodium azide acts as a preservative, avoiding the formation and/or degeneration of metabolites by bacteria. TMSP-d_4 (i.e., 3-(trimethylsilyl) propionic-2,2,3,3-d_4 acid sodium salt) was used as internal standard. The samples were then prepared by transferring about 0.5 g of the supernatant at the right pH value in 5-mm o.d. NMR tube together with about 0.03 g of the solution of TMSP-d_4 (100 mM) and NaN_3 (2 mM) in D_2O. A further amount of D_2O was added to this solution and used as the field frequency lock signal. The same preparation was carried out on the samples arising from the membrane processes. All the NMR spectra have been acquired at 298 K on a high-resolution Bruker Avance 500-MHz spectrometer (11.74 T) (Bruker, Fällanden, Switzerland) equipped with a 5-mm TBO probe and a standard variable-temperature unit BVT-3000. The 1D ^{1}H and ^{13}C-{^{1}H} NMR experiments and 2D homo and heteronuclear correlation NMR spectra, ^{1}H-^{1}H COSY and ^{1}H-^{13}C HMQC, were performed on each sample. The latter have been very useful, together with the data present in the literature (Belton et al., 1997; Vermathen et al., 2011, 2012), in assigning the frequencies of the various metabolites. To suppress the residual water signal, the *noesypr1d* sequence has been used for recording the ^{1}H NMR spectra by acquiring, for each spectrum, 256 FID and using a spectral width of 11.26 ppm. Proton broad-band decoupling has been used to record the 1D ^{13}C-{^{1}H} NMR spectra collecting 500 FIDs and using a spectral width of 266.80 ppm and a relaxation delay of 10 s. The COSY experiments were acquired using a SW of 11.26 ppm on both dimensions, 2 K data points, 28 scans, and 512 increments, while the ^{1}H-^{13}C HMQC spectra were recorded using a SW of 11.26 ppm (^{1}H) and 266.80 ppm (^{13}C), 2 K data points, 256 scans, and 32 experiments.

Data Processing and Pre-treatment

The ^{1}H-NMR spectra were phased, baseline-corrected, and the chemical shifts referenced to the TMSP signal. The ^{13}C-{^{1}H} NMR spectra were filtered with 1-Hz line broadening before Fourier-transformed. Each ^{1}H NMR spectrum was segmented into identical intervals ("buckets") of fixed 0.05 ppm in the range from 1.10 to 5.60 ppm. The bucketing procedure was performed defining the integration range on the first spectrum, the integration regions were saved, and the other spectra were bucketed automatically using this saved list. The integrals were normalized and compose the data matrix that exported to an excel file was subjected to statistical analysis. A dataset of 20 samples, 5 for each variety, and 51 variables has been obtained. All the data processing steps were carried out using TopSpin 3.6 software (Bruker BioSpin, Rheinstetten, Germany) (TopSpin, 2018).

Statistical Analysis

In order to discriminate between the different varieties of apples, the spectroscopic data were explored with chemometric techniques, such as unsupervised principal component analysis (PCA). In this study, the PCA has been employed in a descriptive way to simplify and condense the global information provided by the spectra describing the entire chemical composition into a few parametric descriptors. This technique is probably the most commonly used method for unsupervised multivariate data analysis (Ebrahimi et al., 2017). It is able to extract the maximum possible information present in a set of multivariate data by generation of a new set of n uncorrelated variables, the principal components (PCs), by few linear combinations of the original variables and arranged in decreasing order of variance. This means that the first PC accounts for as much of the variability in the data as possible so that each succeeding component accounts decreasing amounts of variance. Hence, the higher PCs can be discarded and keeping only the first PCs (e.g., three or less) the number of variables is reduced without significant loss of information and results in a clearer data visualization. The mathematical calculation produces from the original data matrix two new matrices: the loading matrix and the score matrix, which generate two graphical representations: the loading plot and the score plot. The loading plot allows to analyze the role of each variable in the different components, their direct and inverse correlations, and their importance. The scores express the coordinates for each sample in the new reference system, and the relative plot allows to visualize the behavior of the objects in the different components and their similarities, or to identify groupings of similar objects (clusters), the presence of particular objects (outliers), the occurrence of particular regularities, and distributions. In this work PCA was carried out

by R software (R Core Team, 2019) using both the covariance and correlation methods (Borgognone et al., 2001). In the first method, the data matrix is mean-centered, while in the second (correlation method) the matrix is mean-centered and scaled in order that all column have zero mean and variance of unity. However, since the two methods applied to the samples used do not show appreciable differences in discrimination, the results reported in the "PCA Analysis" section come from the PCA correlation method only. The most common steps usually applied in NMR-based metabolomics are summarized in Fig. 1.

Sample Preparation for LC-UV–ESI–MS/MS and Analysis

HPLC–UV-ESI–MS/MS analysis was carried out on the juice of the Golden Delicious variety only. The juice was initially thawed at room temperature and centrifuged. Then, the supernatant (20 mL) was filtered and passed through C_{18} cartridge (Supelco, USA). The loaded stationary phase was initially washed with water (12 × 20 mL) to remove the sugars and water soluble fraction, and then eluted with 10 mL of methanol. The methanol was evaporated using the rotavapor and sample was redissolved in 3 mL of a solution H_2O:MeOH (50:50 v/v). The purified and concentrated sample was then injected into the HPLC. HPLC–UV analysis was performed using a Fractionlynx instrument (Waters, Milford, MA) equipped with an autosampler/collector Waters 2767 Sample Manager, a 600E pump working in analytical mode, and a 2486-nm UV detector. The HPLC separation was achieved using a 250 × 4.6-mm, 5-µm reversed-phase C_{18} Luna-Phenomenex column at a flow rate of 1 mL/min. The run time was 70 min and the mobile phase was composed by 0.1% formic acid in water (solvent A) and methanol (solvent B). The chromatographic run (70 min) consisted of the following steps: isocratic at 80% A for 7 min, linear gradient from 80 to 40% A in 33 min; isocratic at 40% A for 5 min, linear gradient from 40 to 20% A in 5 min; isocratic at 20% A for 7 min, linear gradient from 20 to 80% A in 5 min; and equilibration of the column for 8 min. The UV detector was set at 280 nm and at 340 nm. Afterward, the different UV fractions were collected at the wavelength of 340 nm. ESI MS and MS/MS spectra were acquired by direct infusion of the UV fractions into a Thermo Scientific TSQ Quantum Vantage triple-stage quadrupole mass spectrometer (Thermo Fisher Scientific, San José, CA). Since polyphenols are easily deprotonable compounds, spectra were acquired in negative ion mode. Tandem mass spectra were acquired using a collision energy (CE) of 15 and 20 eV. The samples deriving from the membrane processes were not purified and concentrated by SPE but were simply centrifuged, and the supernatant was subjected to the HPLC–UV analysis only, in order to verify variations in the chromatographic profiles.

The quantitative analysis was carried out using a different HPLC system (Agilent 1100 series, Agilent Technologies, Waldbronn, Germany) but it was always equipped with a Luna C18 column (250 mm × 4.6 mm, 5 µm, Phenomenex, Torrance) and an UV detector. Peaks were quantified at $\lambda = 340$ nm using also the same mobile phase and the same gradient than that used for the identification.

Results and Discussion

NMR Analysis

Figure 2 shows the ^{1}H NMR spectrum of the Golden Delicious juice obtained with *noesypr1d* sequence. As can be seen from the figure, the spectrum can be divided into three regions: the first which goes from 0 to 3.00 ppm contains the frequencies of aliphatic substances which are mostly amino acids and organic acids; the resonances appeared in the region between 3.00 and 5.60 ppm include the signals of α-glucose, β-glucose, sucrose, and fructose; while the third region, from 5.60 to 10.00 ppm, is the aromatic region relating to phenolic metabolites. As is evident from the spectrum in Fig. 2, the main constituents in apple juice are sugar compounds. Another prominent compound is malic acid with resonances around 2.70 and 4.40 ppm. The signal assignment of the various metabolites was carried out using one-dimensional ^{1}H and ^{13}C-{^{1}H} NMR spectra, 2D correlation experiments ^{1}H-^{1}H COSY and ^{1}H-^{13}C HMQC, and data reported in the literature (Belton et al., 1997; Tomita et al.,

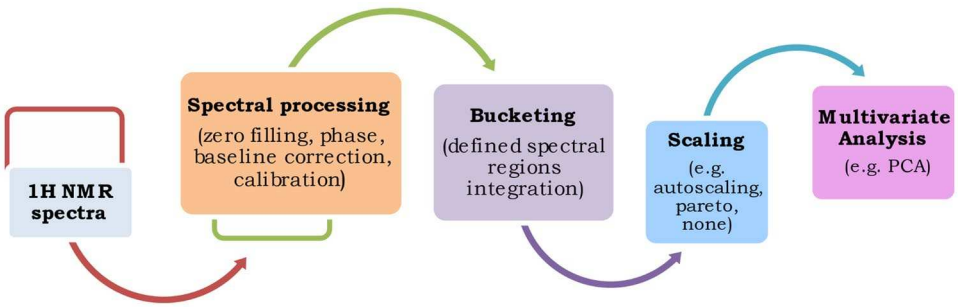

Fig. 1 Schematic steps involved in multivariate analysis starting from ^{1}H NMR spectra

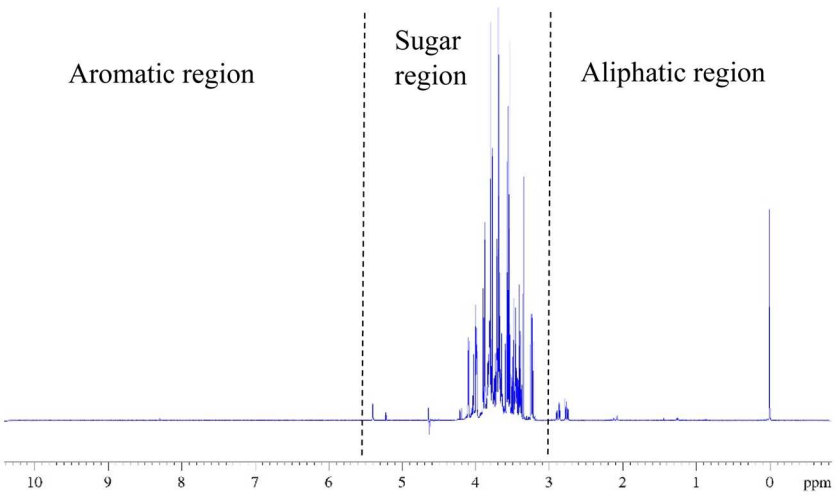

Fig. 2 The 500-MHz ^{1}H NMR spectrum of Golden Delicious apple juice

2015; Vermathen et al., 2011, 2012). In Table 1 are reported the 12 metabolites assigned with all the experimental informations obtained from the NMR spectra relating to Golden Delicious apple juice. Once the metabolic profile for the Golden Delicious was determined, a comparison between the NMR spectra of the samples relating to the other apple varieties was possible. The comparison between proton spectra highlights that the metabolic profile is the same for all the four varieties of apples; in particular, the metabolites recognized for the Golden Delicious variety are recognizable also in the other apple varieties, which show no other signals than those already identified, except different relative intensity of the signals and small variations in chemical shift. In addition, ^{1}H NMR spectra were also recorded on the samples of Golden Delicious juice treated by means of membrane processes. All these spectra are reported in the Supplementary Information, where it is also possible to find the expanded regions of ^{1}H NMR spectra with the relevant chemical shifts associated to the various recognized metabolites, the comparison between ^{1}H NMR spectra from the different varieties, 2D experiments, and the ^{13}C-{^{1}H} NMR spectra.

PCA Analysis

The exploratory analysis PCA has been applied to ^{1}H NMR spectra collected in order to evaluate whether the metabolite spectrum can be used as a criterion to identify and discriminate the samples according to the variety. To perform such analysis, a variable selection is necessary and the NMR region choose by manual selection is the aliphatic region that contains most abundant and characteristic compounds as sugar and organic acids. In particular, in the bucketing process the following chemical shift intervals have been considered: from 1.10 to 1.50 ppm that is the region of the ethanol, L-rhamnitol, and citramalic acid methyl proton signals; from 1.90 to 2.25 ppm that is the region of quinic and chlorogenic acid aliphatic ring signals; from 2.60 to 3.00 ppm which includes the doublets of doublets related to the methylenic and methynic protons of malic acid; and finally from 3.15 to 5.60 ppm which is the sugar region. In the bucketing process some regions have been excluded: the interval from 4.30 to 5.10 ppm, which contains the residual solvent peak, i.e., water signal, and the aromatic region from 5.60 to 10.00 ppm due to the too low S/N (signal to noise) ratio. Hence, region selected for the PCA was 1.10 to 5.60 ppm, and the PCA score plot for this selected region of data summarizes the relationships between the 20 samples and 51 variables. The 3D score plot obtained is reported in Fig. 3, where a cumulative percentage of explained data variance of 81.6% (52.3%, 22.2%, and 7.1% for PC1, PC2, and PC3, respectively) summarizes the relationship between samples. As can be seen from the score plot (Fig. 3), there is a clear separation between the four varieties of apples. Specifically, the Pink Lady variety has negative values of PC2 while Royal Gala, Golden Delicious, and Fuji have positive value of this component. This trend highlights that samples belonging to the Golden Delicious, Fuji, and Royal Gala varieties have a more similar metabolic composition than the juices from the Pink Lady variety. In order to understand how the metabolites contribute to the variety separation, the biplot need to be examined. The biplot is a two-dimensional scattered plot which links the score plot and the loading plot information in a single chart. Due to the low information content of PC3 and since a good separation in varieties is obtained from the first two PCs, the biplot reported in Fig. 4 is a 2D plot where only the PC1 and PC2 are considered. From the biplot emerged that Pink Lady variety is characterized by a major sucrose and malic acid content with respect to other ones, while Golden Delicious and Fuji are richer in α-glucose,

Table 1 The ^{1}H and ^{13}C chemical shifts and multiplicity of compounds in apple juice of Golden Delicious, Pink Lady, Royal Gala, and Fuji varieties

Compound	δ ^{1}H (ppm)	Multiplicity *J* [Hz]	δ ^{13}C (ppm)	Group
Amino acid and organic acid region (0–3 ppm)				
Ethanol	1.17	t [7.09]		CH_3
L-rhamnitol	1.27	d [6.40]		CH_3
Citramalic acid	1.42	S		CH_3
Quinic acid	1.89–2.12			CH_2–CH
Chlorogenic acid	2.01–2.08			CH_2–CH
Malic acid	2.73	dd [16.20, 7.51]		β-CH_2
	2.86	dd [16.20, 4.67]		β-CH_2
	4.47			CH
Sugar region (3–5.6 ppm)				
β-Glucose	3.23	dd [9.99,8.06]	77.18	H–C(2)
	3.40	m	78.78	H–C(5)
	3.46	m	78.85	H–C(3)
	3.46	m	98.87	H–C(5)
	3.46	m		H (6a)–C(6)
	3.73	m		H (6b)–C(6)
	4.63	d		H–C(1)
α-Glucose	3.40	M	74.50	H–C(4)
	3.52	dd [9.80, 3.67]	74.35	H–C(2)
	3.73	m	95.06	H–C(3)
	3.73	m		H (6a)–C(6)
	3.82	m		H–C(5)
	3.82	m		H (6b)–C(6)
	5.22	d [3.10]		H–C(1)
Sucrose	3.46	T	79.40	H–C(4)
	3.55	dd	95.06	H–C(2)
	3.67	s	106.55	H–C′(1)
	3.75	t		H–C(3)
	3.82	m		H–C(6)
	3.86	dd		H–C(5)
	4.20	d		H–C′(3)
	5.40	d [3.82]		H–C(1)
				C′(2)
α-D-fructofuranose	3.54	m	83.58	H (6b)–C(6)
	3.59	m	77.44	H (6a)–C(6)
	3.67	m	78.40	H (1b)–C(1)
	3.80	m	104.44	H (1a)–C(1)
	3.82	m		H–C(2)
	4.10	m		H–C(3)
	4.10	m		H–C(4)
				C(5)
β-D-fructofuranose	3.55	m	66.90	H (6b)–C(6)
	3.69	m	66.90	H (6a)–C(6)
	3.69	m	66.27	H (1b)–C(1)
	3.78	m	70.58	H–C(4)
	3.88	dd	72.18	H–C(3)
	3.98	m	66.27	H–C(2)
	4.01		101.02	H (1a)–C(1)
				C(5)
Aromatic region (5.6–10 ppm)				
Formic acid	8.32	s		H

β-glucose, α-D-fructofuranose, and β-D-fructofuranose. Royal Gala seems to have an intermediate composition between Pink Lady variety and Golden Delicious and Fuji varieties even if it is closer to the last two. Minor compounds such as ethanol, quinic acid, chlorogenic acid, L-rhamitol, and citramalic acid have null values of PC2, i.e., the dimension in which the apple varieties are better separated. This means that these 5 metabolites do not affect the separation and can be neglected as marker of variety separation.

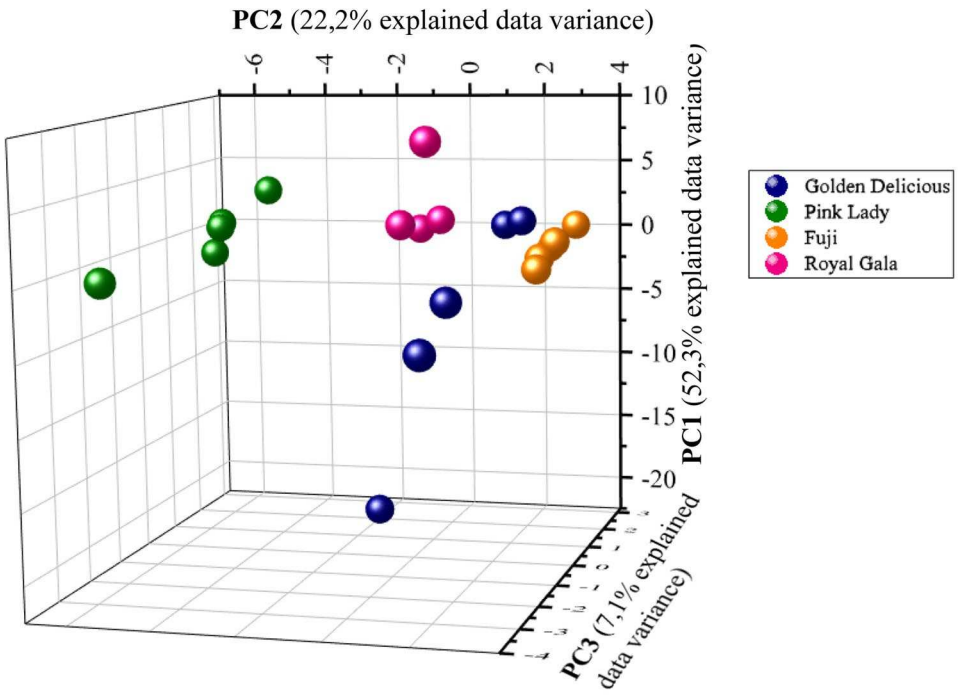

Fig. 3 Principal component analysis (PCA) of Golden Delicious, Pink Lady, Fuji, and Royal Gala juices. The score plot showing the first three PCs: PC1, PC2, and PC3 with their respective variation. $R^2X(PC1) = 52.3\%$, $R^2X(PC2) = 22.2\%$, $R^2X(PC3) = 7.1\%$

HPLC–UV-ESI–MS/MS Results

Due to its low sensitivity, NMR was not able to highlight the phenolic compounds in apple juices; therefore, the HPLC–UV-ESI–MS/MS hyphenated technique was alternatively used. The major polyphenolic groups in apple juice are hydroxycinnamic acids, flavan-3-ols/procyanidins, flavonols, dihydrochalcones, and anthocyanins (Rana & Bhushan, 2016). Figure 5 shows the HPLC–UV chromatogram together with signal attributions of the purified and concentrated supernatant related to Golden Delicious juice after SPE extraction. The collected UV fractions and their infusion into the mass spectrometer together with the use of data reported in literature (Kahle et al., 2005) allowed to identify 10 phenolic compounds reported in Table 2. MS and MS/MS spectra are reported in the Supplementary Information. The HPLC–UV analysis was also performed on the clarified juice (UF permeate) and on permeate and retentate samples from the NF process (Fig. 6).

The quantitative data were performed by external calibration curves with standards. Mean values of three replicates

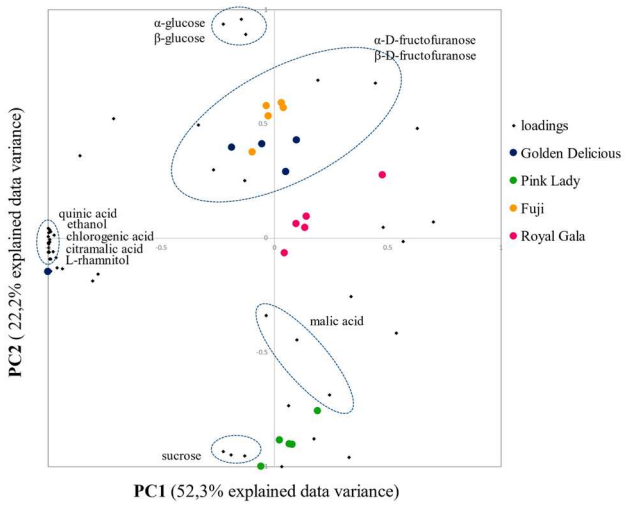

Fig. 4 Biplot of the first two PCs, PC1 and PC2, taking into account the loadings and the scores obtained from the PCA carried out on NMR spectra of the Golden Delicious, Pink Lady, Fuji, and Royal Gala juices

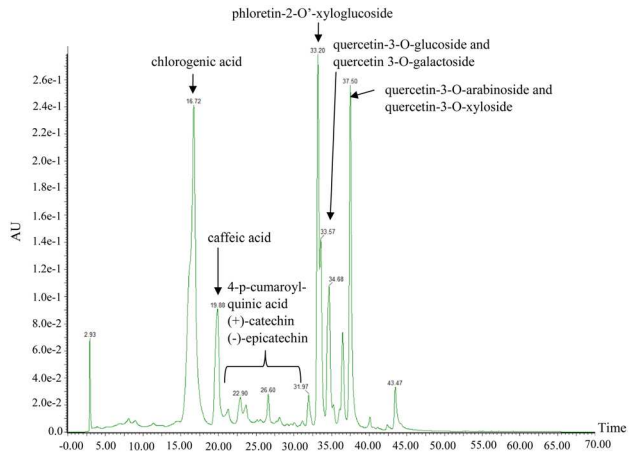

Fig. 5 HPLC–UV chromatogram related to Golden Delicious juice purified and concentrated by means of SPE

Table 2 Polyphenolic compounds in Golden Delicious juice

Group of polyphenols	Compound	$[M-H]^-$ (m/z)	MS^2
Phenolic acids	Chlorogenic acid	353.3	191.1, 179.1
	Caffeic acid	179.0	135.0
	4-p-Cumaroylquinic acid	337.3	191.3, 173.3, 162.9
Flavon-3-ols	(+)-Catechin	289.2	254.3, 205.2, 202.9, 137.0
	(−)-Epicatechin	289.2	254.3, 205.2, 202.9, 137.0
Dihydrochalcones	Phloretin-2′-O-xyloglucoside	567.3	273.2
Flavonols	Quercetin-3-O-glucoside	463.1	299.9, 301.0
	Quercetin-3-O-galactoside	463.1	299.9, 301.0
	Quercetin-3-O-xyloside	433.5	300.0, 301.0
	Quercetin-3-O-arabinoside	433.5	300.0, 301.0

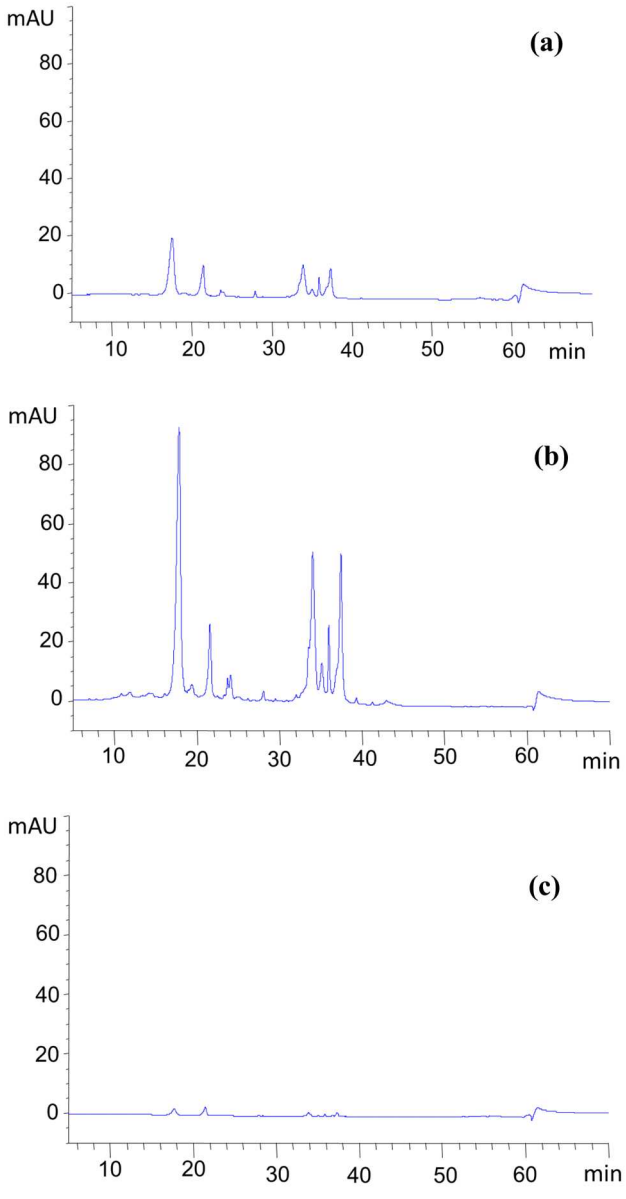

Fig. 6 HPLC–UV chromatograms of (**a**) feed, (**b**) NF permeate, and (**c**) NF retentate of Golden Delicious juice

for each sample together the SD% values are reported in Table 3. According to these data, the rejection index of the NF membrane towards chlorogenic acid and caffeic acid, calculated from Eq. (2), resulted of 94.2% and 69.6%, respectively. These results are in agreement with the MWCO of the NF membrane (150–300 Da) and the molecular weight of target compounds (354.31 g/mol for chlorogenic acid and 180.16 g/mol for caffeic acid). However, several factors, which include the reduction of pore size of the membrane, adsorption of solutes, concentration polarization, and fouling, contribute to the retention of these compounds, other than molecular sieving mechanisms (Nghiem & Hawkes, 2007). Similar results have been reported in literature in the treatment of different agro-food processing wastewater by using the Desal DK membrane. For example, a chlorogenic acid rejection between 88.2% and 96.7% was measured in the treatment of artichoke brines in a range of operating pressures of 4–12 bar (Cassano et al., 2016). Conidi et al. (2019) reported a rejection of about 60% towards caffeic acid in the treatment of clarified licorice wastewaters at an operating pressure of 25 bar; caffeic acid rejections of 75% have been detected in the treatment of microfiltered olive mill wastewaters at 7 bar (Tundis et al., 2020). In Fig. 7 the effect of VRF on the concentration of chlorogenic acid and caffeic acid in the retentate fraction is reported. As expected, the concentration of both compounds increases by increasing the VRF. However, according to the measured rejections, the concentration factor observed for the chlorogenic acid is much higher than that measured for the caffeic acid. An increased concentration of chlorogenic acid and caffeoylquinic acid derivatives by increasing the VRF of the NF treatment of artichoke brine with the Desal DK membrane was also reported by Cassano et al. (2016). Other studies are needed to define and optimize the operating and fluid dynamics conditions and to improve the performance of the NF process in terms of productivity and selectivity towards phenolic compounds with respect to sugars. These preliminary studies confirm the potential of the NF process as a promising technique to obtain enriched fractions of bioactive compounds from apple juices.

Table 3 Phenolic compounds detected in the HPLC analysis of clarified apple juice (feed NF), NF permeate, and NF retentate (VRF = 3.3) (data are mean ± SD, $n = 3$)

Compound	MW (g/mol)	Concentration (mg/L)		
		Clarified juice	NF permeate	NF retentate
Chlorogenic acid	354.31	16.20 ± 0.04	0.94 ± 0.02	60.90 ± 2.70
Caffeic acid	180.16	3.35 ± 0.44	1.02 ± 0.02	7.50 ± 0.46

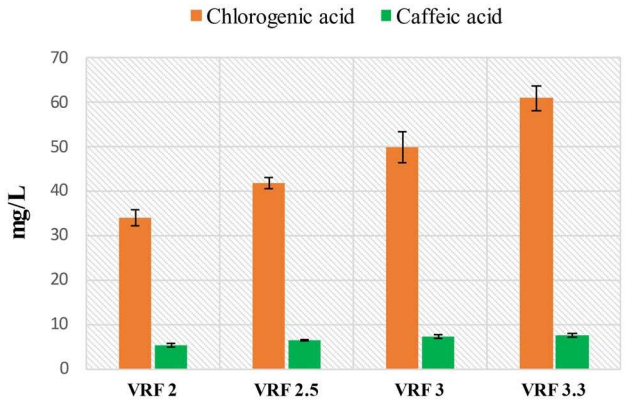

Fig. 7 Histogram showing the increasing in concentration of chlorogenic acid and caffeic acid at the increasing of VRF values

Conclusion

This work was aimed at the metabolic characterization through NMR spectroscopy and HPLC–UV-MS/MS of complex food matrices such as Calabrian apple juices from four different varieties and their bioactive extracts obtained through membrane technologies. By means of high-resolution multinuclear (^{1}H and ^{13}C) 1D and 2D NMR experiments, it was possible to identify 12 metabolites including organic acids and sugars all present in the four varieties. Moreover, the combination of ^{1}H NMR spectra of squeezed juices with multivariate data analysis (PCA) is able to distinguish samples from the four varieties of apples; i.e., each variety is clustered in a defined region. From the PCA score plot it is possible to highlight that Golden Delicious, Fuji, and Royal Gala varieties have a more similar metabolic composition than the juices from the Pink Lady variety. Instead, the PCA biplot shows that the sugars and malic acid contents are responsible of the separation between the four varieties. Since in no variety it has been possible to identify appreciable NMR signals in the aromatic region relating to the polyphenols typically found in apples, HPLC–UV-ESI–MS/MS was alternatively used for this purpose. Due to the higher content of phenolic compounds identified in the Golden Delicious juice, only this variety has been analyzed through mass spectrometry combined with liquid chromatography and 10 polyphenol compounds were identified. The same variety has been subjected to ultrafiltration (UF) and nanofiltration (NF) processes with the aim of producing enriched fractions in phenolic compounds. In addition to characterizing the starting juice, also the UF and the NF permeates as well as the NF retentates at different VRFs were characterized by NMR and by HPLC–UV. The analysis of the ^{1}H NMR spectra of the samples subjected to membrane processes did not show any changes in the metabolic profile of the permeate from the UF compared to the starting juice. The HPLC–UV analysis showed that the chromatographic profile remains the same among the Golden Delicious juice, UF permeate, and sample derived from NF process. This means that the phenolic compounds of interest are both in the permeate and in the retentate of the NF process, but certainly in concentration significantly different. Indeed, NF retentate is much more concentrated in phenolic compounds, even if further studies are needed to understand the separative capacity of the process of NF towards sugars, with respect to the phenolic component. Therefore, up to now, these preliminary results obtained showed that the integrated UF-NF process is able to collect fractions enriched in bioactive compounds from the starting juice of apples.

Supplementary Information The online version contains supplementary material available at https://doi.org/10.1007/s11947-021-02718-8.

Acknowledgements The authors thank Gioia Succhi srl for collecting and supplying samples of Royal Gala, Pink Lady, Golden Delicious, and Fuji apple juices.

Authorship Contribution Martina Gaglianò: investigation, methodology, formal analysis, data curation, writing — original draft. Carmela Conidi: investigation, methodology, formal analysis. Lucia Bartella: investigation, methodology, formal analysis; Rosachiara A. Salvino: investigation, methodology, formal analysis; Leonardo Di Donna: supervision, conceptualization, data curation, investigation, methodology, writing — original draft; Alfredo Cassano: supervision, conceptualization, data curation, investigation, methodology, writing — original draft, writing — review and editing; Giuseppina De Luca: supervision, conceptualization, data curation, investigation, methodology, writing — original draft, writing — review and editing.

Funding This work was supported by the University of Calabria and POR Calabria — FSE/FESR 2014–2020. The authors wish to thank Calabria Regional institution for its financial support through the AgrInfra Calabria POR FESR-FSE Calabria 2014/2020, Action 1.5.1 grant. L.B. thanks Italian Ministry of Education, University and Research for its grant n. AIM1899391–1 in the framework of the project "Azione I.2, Mobilità dei Ricercatori, PON R&I 2014–2020."

Data Availability The datasets generated during and/or analyzed during the current study are available from the corresponding author on reasonable request.

Declarations

Conflict of Interest The authors declare no competing interests.

References

Abreu, A. C., & Fernández, I. (2020). NMR metabolomics applied on the discrimination of variables influencing tomato (*Solanum lycopersicum*). *Molecules, 25*(16), 3738. https://doi.org/10.3390/molecules25163738

Arend, G. D., Rezzadori, K., Soares, L. S., & Petrus, J. C. C. (2019). Performance of nanofiltration process during concentration of strawberry juice. *Journal of Food Science & Technology-Mysore, 56*(4), 2312–2319. https://doi.org/10.1007/s13197-019-03659-z

Azmir, J., Zaidul, I. S. M., Rahman, M. M., Sharif, K. M., Mohamed, A., Sahena, F., Jahurul, M. H. A., Ghafoor, K., Norulain, N. A. N., & Omar, A. K. M. (2013). Techniques for extraction of bioactive compounds from plant materials: A review. *Journal of Food Engineering, 117*(4), 426–436. https://doi.org/10.1016/j.jfoodeng.2013.01.014

Belton, P. S., Delgadillo, I., Gil, A. M., Roma, P., Casuscelli, F., Colquhoun, I. J., et al. (1997). High-field proton studies of apple juices. *Magnetic Resonance in Chemistry, 35,* S52–S60.

Bhattacharjee, C., Saxena, V. K., & Dutta, S. (2017). Fruit juice processing using membrane technology: A review. *Innovative Food Science and Emerging Technologies, 43*, 136–153. https://doi.org/10.1016/j.ifset.2017.08.002

Bingol, K. (2018). Recent advances in targeted and untargeted metabolomics by NMR and MS/NMR methods. *High-Throughput, 7*, 9. https://doi.org/10.3390/ht7020009

Boyer, J., & Liu, R. H. (2004). Apple phytochemicals and their health benefits. *Nutrition Journal, 3*, 1–15. https://doi.org/10.1186/1475-2891-3-5

Borgognone, M. G., Bussi, J., & Hough, G. (2001). Principal component analysis in sensory analysis: Covariance or correlation matrix? *Food Quality and Preference, 12,* 323–326. https://doi.org/10.1016/S0950-3293(01)00017-9.

Brans, G., Schroën, C. G. P. H., Van der Sman, R. G. M., & Boom, R. M. (2004). Membrane fractionation of milk: State of the art and challenges. *Journal of Membrane Science, 243*, 263–272. https://doi.org/10.1016/j.memsci.2004.06.029

Cai, M., Hou, W. Z., Lv, Y. Q., & Sun, P. L. (2017). Behavior and rejection mechanisms of fruit juice phenolic compounds in model solution during nanofiltration. *Journal of Food Engineering, 195*, 97–104. https://doi.org/10.1007/s11947-017-1970-8

Cassano, A., Cabri, W., Mombelli, G., Peterlongo, F., & Giorno, L. (2016). Recovery of bioactive compounds from artichoke brines by nanofiltration. *Food and Bioproducts Processing, 98*, 257–265. https://doi.org/10.1016/j.fbp.2016.02.004

Castro-Muñoz, R., Yáñez-Fernández, J., & Fíla, V. (2016). Phenolic compounds recovered from agro-food by-products using membrane technologies: An overview. *Food Chemistry, 213*, 753–762. https://doi.org/10.1016/j.foodchem.2016.07.030

Castro-Muñoz, R., Conidi, C., & Cassano, A. (2018). Membrane-based technologies for meeting the recovery of biologically active compounds from foods and their by-products. *Critical Reviews in Food Science and Nutrition, 59*(18), 2927–2948. https://doi.org/10.1080/10408398.2018.1478796

Catarino, M., & Mendes, A. (2011). Dealcoholizing wine by membrane separation processes. *Innovative Food Science & Emerging Technologies, 12*(3), 330–337. https://doi.org/10.1016/j.ifset.2011.03.006

Conidi, C., Cassano, A., & Drioli, E. (2011). A membrane-based study for the recovery of polyphenols from bergamot juice. *Journal of Membrane Science, 375*(1–2), 182–190. https://doi.org/10.1016/j.memsci.2011.03.035

Conidi, C., & Cassano, A. (2014). Recovery of phenolic compounds from bergamot juice by nanofiltration membranes. *Desalination and Water Treatment, 56*(13), 3510–3518. https://doi.org/10.1080/19443994.2014.968219

Conidi, C., Fucà, L., Drioli, E., & Cassano, A. (2019). A membrane-based process for the recovery of glycyrrhizin and phenolic compounds from licorice wastewaters. *Molecules, 24*, 2279. https://doi.org/10.3390/molecules24122279

Cuthbertson, D., Andrews, P. K., Reganold, J. P., Davies, N. M., & Lange, B. M. (2012). Utility of metabolomics toward assessing the metabolic basis of quality traits in apple fruit with an emphasis on antioxidants. *Journal of Agricultural and Food Chemistry, 60*(35), 8552–8560. https://doi.org/10.1021/jf3031088

Duda-Chodak, A., Tarko, T., Satora, P., Sroka, P., & Tuszyńsk, T. (2010). The profile of polyphenols and antioxidant properties of selected apple cultivars grown in Poland. *Journal of Fruit and Ornamental Plant Research, 18*(2), 39–50.

Ebrahimi, P., Viereck, N., Bro, R., & Engelsen, S. B. (2017). Chemometric analysis of NMR spectra. In A. G. Webb (Ed.), *Modern Magnetic Resonance* (pp. 1649–1668). Springer.

Eisenmann, P., Ehlers, M., Weinert, C. H., Tzvetkova, P., Silber, M., Rist, M. J., Rist, M. J., Luy, B., & Muhle-Goll, C. (2016). Untargeted NMR spectroscopic analysis of the metabolic variety of new apple cultivars. *Metabolites, 6*(3), 29. https://doi.org/10.3390/metabo6030029

Figoli, A., Tagarelli, A., Mecchia, A., Trotta, A., Cavaliere, B., Lavecchia, R., Sindona, G., & Drioli, E. (2006). Enzyme-assisted pervaporative recovery of concentrated bergamot peel oils. *Desalination, 199*(1–3), 111–112. https://doi.org/10.1016/j.desal.2006.03.025

Francini, A., & Sebastiani, L. (2013). Phenolic compounds in apple (*Malus* × *domestica* Borkh.): Compounds characterization and stability during postharvest and after processing. *Antioxidants, 2*(3), 181–193. https://doi.org/10.3390/antiox2030181

Francini, A., Romeo, S., Cifelli, M., Gori, D., Domenici, V., & Sebastiani, L. (2017). ^{1}H NMR and PCA-based analysis revealed variety dependent changes in phenolic contents of apple fruit after drying. *Food Chemistry, 221*, 1206–1213. https://doi.org/10.1016/j.foodchem.2016.11.038

Galaverna, G., Di Silvestro, G., Cassano, A., Sforza, S., Dossena, A., Drioli, E., & Marchelli, R. (2008). A new integrated membrane process for the production of concentrated blood orange juice: Effect on bioactive compounds and antioxidant activity. *Food Chemistry, 106*(3), 1021–1030. https://doi.org/10.1016/j.foodchem.2007.07.018

Garcia-Castello, E. M., Mayor, L., Chorques, S., Arguelles, A., Vidal-Brotons, D., & Gras, M. L. (2011). Reverse osmosis concentration of press liquor from orange juice solid wastes: Flux decline mechanisms. *Journal of Food Engineering, 106*(3), 199–205. https://doi.org/10.1016/j.jfoodeng.2011.05.005

Gathungu, R. M., Kautz, R., Kristal, B. S., Bird, S. S., & Vouros, P. (2018). The integration of LC-MS and NMR for the analysis of low molecular weight trace analytes in complex matrices. *Mass Spectrometry Reviews, 39*, 35–54. https://doi.org/10.1002/mas.21575

Gerhauser, C. (2008). Cancer chemopreventive potential of apples, apple juice, and apple components. *Planta Medica, 74*(13), 1608–1624. https://doi.org/10.1055/s-0028-1088300

Gören, A. C., Çıkrıkçı, S., Çergel, M., & Bilsel, G. (2009). Rapid quantitation of curcumin in turmeric via NMR and LC–tandem mass spectrometry. *Food Chemistry, 113*(4), 1239–1242. https://doi.org/10.1016/j.foodchem.2008.08.014

Gunathilake, C., & Considine, M. (2018). Flavonoids rich apple for healthy life. *MOJ Food Processing & Technology*, *6*(1), 89–91. https://doi.org/10.15406/mojfpt.2018.06.00149

Harker, F. R., Gunson, F. A., & Jaeger, S. R. (2003). The case for fruit quality: An interpretive review of consumer attitudes, and preferences for apples. *Postharvest Biology and Technology, 28*(3), 333–347. https://doi.org/10.1016/S0925-5214(02)00215-6

Iaccarino, N., Varming, C., Petersen, M. A., Viereck, N., Schütz, B., Toldam-Andersen, T. B., Randazzo, A., & Engelsen, S. B. (2019). Ancient Danish apple cultivars — A comprehensive metabolite and sensory profiling of apple juices. *Metabolites, 9*(7), 139. https://doi.org/10.3390/metabo9070139.

Jeong, S. W., Kim, G.-S., Lee, W. S., Kim, Y.-H., Kang, N. J., Jin, J. S., Lee, G. M., Kim, S. T., El-Aty, A. M. A., Shim, J.-H., & Shin, S. C. (2015). The effects of different night-time temperatures and cultivation durations on the polyphenolic contents of lettuce: Application of principal component analysis. *Journal of Advanced Research, 6*(3), 493–499. https://doi.org/10.1016/j.jare.2015.01.004

Kahle, K., Kraus, M., & Richling, E. (2005). Polyphenol profiles of apple juices. *Molecular Nutrition & Food Research, 49*, 797–806. https://doi.org/10.1002/mnfr.200500064

Koutsos, A., Tuohy, K. M., & Lovegrove, J. A. (2015). Apples and cardiovascular health—Is the gut microbiota a core consideration? *Nutrients, 7*(6), 3959–3998. https://doi.org/10.3390/nu7063959

Kumar, S., Bink, M. C. A. M., Volz, R. K., Bus, V. G. M., & Chagné, D. (2012). Towards genomic selection in apple (*Malus* × *domestica* Borkh) breeding programmes: Prospects challenges and strategies. *Tree Genetics and Genomes, 8*, 1–14. https://doi.org/10.1007/s11295-011-0425-z

Li, J., & Chase, H. A. (2010). Applications of membrane techniques for purification of natural products. *Biotechnology Letters, 32,* 601–608. https://doi.org/10.1007/s10529-009-0199-7

Lima, L. G. B., Montenegro, J., Pimentel de Abreu, J., Barros Santos, M. C., Pimenta do Nascimento, T., Santos, M., Ferreira, A. G., Cameron, L. C., Ferreira, M. S. L., & Teodoro, A. J. (2020). Metabolite profiling by UPLC-MSE, NMR, and antioxidant properties of Amazonian fruits: Mamey apple (*Mammea americana*) Camapu (*Physalis angulata*) and Uxi (*Endopleura uchi*). *Molecules, 25*(2), 342. https://doi.org/10.3390/molecules25020342

Mamat, S. F., Azizan, K. A., Baharum, S. N., Noor, N. M., & Aizat, W. M. (2020). GC-MS and LC-MS analyses reveal the distribution of primary and secondary metabolites in mangosteen (*Garcinia mangostana* Linn) fruit during ripening. *Scientia Horticulturae, 262*, 109004. https://doi.org/10.1016/j.scienta.2019.109004

Marshall, D. D., & Powers, R. (2017). Beyond the paradigm: Combining mass spectrometry and nuclear magnetic resonance for metabolomics. *Progress in Nuclear Magnetic Resonance Spectroscopy, 100*, 1–16. https://doi.org/10.1016/j.pnmrs.2017.01.001

Mohammad, A. W., Teow, Y. H., Ang, W. L., Chung, Y. T., Oatley-Radcliffe, D. L., & Hilal, N. (2015). Nanofiltration membranes review: Recent advances and future prospects. *Desalination, 356*, 226–254. https://doi.org/10.1016/j.desal.2014.10.043

Nath, K., Dave, H. K., & Patel, T. M. (2018). Revisiting the recent applications of nanofiltration in food processing industries: Progress and prognosis. *Trends in Food Science & Technology, 73*, 12–24. https://doi.org/10.1016/B978-0-12-815866-1.00003-0

Nghiem, L. D., & Hawkes, S. (2007). Effects of membrane fouling on the nanofiltration of pharmaceutically active compounds (PhACs): Mechanisms and role of membrane pore size. *Separation and Purification Technology, 57*(1), 176–184. https://doi.org/10.1016/j.seppur.2007.04.002

Olennikov, D. N., Vasilieva, A. G., & Chirikova, N. K. (2020). *Fragaria viridis* fruit metabolites: Variation of LC-MS profile and antioxidant potential during ripening and storage. *Pharmaceuticals, 13*(9), 262. https://doi.org/10.3390/ph13090262

Paul, M., & Jons, S. D. (2016). Chemistry and fabrication of polymeric nanofiltration membranes: A review. *Polymer, 103*, 417–456. https://doi.org/10.1016/j.polymer.2016.07.085

Pereira, G. E., Gaudillere, J.-P., Van Leeuwen, C., Hilbert, G., Maucourt, M., Deborde, C., Moing, A., & Rolin, D. (2005). ^{1}H NMR metabolite fingerprints of grape berry: Comparison of vintage and soil effects in Bordeaux grapevine growing areas. *Analytica Chimica Acta, 563*(1–2), 346–352. https://doi.org/10.1016/j.aca.2005.11.007

Pirlak, L., Ünüvar, G., & Ersoy, N. (2017). Determination of antioxidant activities of some apple cultivars. *Horticultural Science, 44*(3), 120–125. https://doi.org/10.17221/276/2015-HORTSCI

R Core Team. (2019). *R: A language and environment for statistical computing*. Vienna, Austria: R Foundation for Statistical Computing. https://www.R-project.org/

Rana, S., & Bhushan, S. (2016). Apple phenolics as nutraceuticals: Assessment, analysis and application. *Journal of Food Science and Technology, 53*(4), 1727–1738. https://doi.org/10.1007/s13197-015-2093-8

TopSpin. (2018). https://www.bruker.com/en/products-and-solutions/mr/nmr-software/topspin.html

Salehi, F. (2014). Current and future applications for nanofiltration technology in the food processing. *Food and Bioproducts Processing, 92*(C2), 161–177. https://doi.org/10.1016/j.fbp.2013.09.005

Salvino, R., Colella, M., & De Luca, G. (2021). NMR-based metabolomics analysis of Calabrian citrus fruit juices and its application to industrial process quality control. *Food Control, 121*, 107619. https://doi.org/10.1016/j.foodcont.2020.107619

Santucci, C., Brizzolara, S., & Tenori, L. (2015). Comparison of frozen and fresh apple pulp for NMR-based metabolomic analysis. *Food Analytical Method, 8*, 2135–2140. https://doi.org/10.1007/s12161-015-0107-9

Seger, C., & Sturm, S. (2007). Analytical aspects of plant metabolite profiling platforms: Current standings and future aim. *Journal of Proteome Research, 6*(2), 480–497. https://doi.org/10.1021/pr0604716

Sobolev, A. P., Mannina, L., Proietti, N., Carradori, S., Daglia, M., Giusti, A. M., Antiochia, R., & Capitani, D. (2015). Untargeted NMR-based methodology in the study of fruit metabolites. *Molecules, 20*(3), 4088–4108. https://doi.org/10.3390/molecules20034088

Tallapally, M., Sadiq, A. S., Mehtab, V., Chilakala, S., Vemula, M., Chenna, S., & Upadhyayula, V. (2020). GC-MS based targeted metabolomics approach for studying the variations of phenolic metabolites in artificially ripened banana fruits. *LWT - Food Science and Technology, 130*, 109622. https://doi.org/10.1016/j.lwt.2020.109622

Ting, V. J. L., Silcock, P., Bremer, P. J., & Biasioli, F. (2013). X-ray micro-computer tomographic method to visualize the microstructure of different apple cultivars. *Journal of Food Science, 78*(11), E1735–E1742. https://doi.org/10.1111/1750-3841.12290

Tomita, S., Nemoto, T., Matsuo, Y., Shoji, T., Tanaka, F., Nakagawa, H., Ono, H., Kikuchi, J., Ohnishi-Kameyama, M., & Sekiyama, Y. (2015). A NMR-based, non-targeted multistep metabolic profiling revealed L-rhamnitol as a metabolite that characterised apples from different geographic origins. *Food Chemistry, 174*, 163–172. https://doi.org/10.1016/j.foodchem.2014.11.028

Tundis, R., Conidi, C., Loizzo, M. R., Sicari, V., & Cassano, A. (2020). Olive mill wastewater polyphenol-enriched fractions by integrated membrane process: A promising source of antioxidant, hypolipidemic and hypoglycaemic compounds. *Antioxidants, 9*(7), 602. https://doi.org/10.3390/antiox9070602

Uyttebroek, M., Vandezande, P., Van Dael, M., Vloemans, S., Noten, B., Bongers, B., Porto-Carrero, W., Unamunzaga, M. M., Bulut, M., & Lemmens, B. (2017). Concentration of phenolic compounds from apple pomace extracts by nanofiltration at lab and pilot scale with a techno-economic assessment. *Journal of Food Process Engineering, 41*(1), e12629. https://doi.org/10.1111/jfpe.12629

Vermathen, M., Marzorati, M., Baumgartner, D., Good, C., & Vermathen, P. (2011). Investigation of different apple cultivars by high resolution magic angle spinning NMR. A feasibility study. *Journal of Agricultural and Food Chemistry*, *59*(24), 12784–12793. https://doi.org/10.1021/jf203733u

Vermathen, M., Marzoratia, M., & Vermathen, P. (2012). Exploring high-resolution magic angle spinning (HR-MAS) NMR spectroscopy for metabonomic analysis of apples. *CHIMIA International Journal for Chemistry, 66*(10), 747–751. https://doi.org/10.2533/chimia.2012.747

membranes

MDPI

Article

Partial Removal of Sugar from Apple Juice by Nanofiltration and Discontinuous Diafiltration

Martina Gaglianò [1], Carmela Conidi [2], Giuseppina De Luca [1,*] and Alfredo Cassano [2,*]

[1] Department of Chemistry & Chemical Technologies, University of Calabria, Via P. Bucci, 87036 Rende, Italy; martina.gagliano@unical.it
[2] Institute on Membrane Technology, ITM-CNR, Via P. Bucci, 17/C, 87036 Rende, Italy; c.conidi@itm.cnr.it
* Correspondence: giuseppina.deluca@unical.it (G.D.L.); a.cassano@itm.cnr.it (A.C.)

Abstract: Partial removal of sugars in fruit juices without compromising their biofunctional properties represents a significant technological challenge. The current study was aimed at evaluating the separation of sugars from phenolic compounds in apple juice by using three different spiral-wound nanofiltration (NF) membranes with a molecular weight cut-off (MWCO) in the range of 200–500 Da. A combination of diafiltration and batch concentration processes was investigated to produce apple juice with reduced sugar content and improved health properties thanks to the preservation and concentration of phenolic compounds. For all selected membranes, permeate flux and recovery rate of glucose, fructose, and phenolic compounds, in both diafiltration and concentration processes, were evaluated. The concentration factor of target compounds as a function of the volume reduction factor (VRF) as well as the amount of adsorbed compound on the membrane surface from mass balance analysis were also evaluated. Among the investigated membranes a thin-film composite membrane with an MWCO of 200–300 Da provided the best results in terms of the preservation of phenolic compounds in the selected operating conditions. More than 70% of phenolic compounds were recovered in the retentate stream while the content of sugars was reduced by about 60%.

Keywords: apple juice; nanofiltration; diafiltration; total phenolic content (TPC); sugar reduction

Citation: Gaglianò, M.; Conidi, C.; De Luca, G.; Cassano, A. Partial Removal of Sugar from Apple Juice by Nanofiltration and Discontinuous Diafiltration. *Membranes* **2022**, *12*, 712. https://doi.org/10.3390/membranes12070712

Academic Editor: Marek Gryta

Received: 30 June 2022
Accepted: 13 July 2022
Published: 15 July 2022

1. Introduction

Apples are among the most commonly consumed fruits in the world because of their availability throughout the year in a variety of products including fresh fruit, juice, concentrate, and puree [1]. Epidemiological studies have shown that apple consumption as fresh fruit is associated with a reduced risk of chronic pathologies such as cardiovascular disease, specific cancers, and diabetes [2]. These beneficial health effects are mainly attributed to their content of bioactive compounds such as phytochemicals, vitamin C, dietary fibers, and pectin.

Unfortunately, processing steps for producing ready-to-drink apple juices, including juice extraction and clarification, have a negative impact on the health-promoting compounds of apples: typically, the content in polyphenol and vitamin C is reduced following processing and juicing and fibers are almost completely removed in the clarification step [3]. In addition, clear apple juice has been associated with adverse effects, mainly related to its high fructose and low fiber content [4]. Similar to sweetened beverages, apple juice contains, on average, 9.6 g of sugar in 100 g.

New World Health Organization (WHO) guidelines recommend that adults and children reduce their daily intake of free sugars to less than 10% of their total energy intake [5]. A further reduction to less than 5% of their total caloric intake—equivalent to about 25 g of sugar per day for a person with a healthy body weight—provides additional health benefits [6].

In addition, in the last years, consumer food requirements have been changed considerably, with a significant increase in the consumption of foods with beneficial health

properties and a lower consumption of fruit juices enriched in sugar [7]. Therefore, the use of technological methodologies for the partial removal of sugar from apple juice, thus limiting the free sugar intake without compromising its biofunctional properties mainly attributed to phenolic acids and polyphenols [8], appears to be a strategy of great interest for both manufacturers and consumers. The idea is to get a juice with a "large portfolio" of beneficial effects.

Although chromatographic separations continue to attract extensive interest for the target separation of sugars, these processes are difficult to apply on large scale. The alternatives may include biochemical transformations of sugars into corresponding compounds such as ethanol, oligosaccharides, or organic acids, but these would lead to a significant change in the fruit juice, which is not in keeping with the previous goal. A further possibility which, instead, allows for the separation of sugars while maintaining the unchanged metabolic composition of the juice, is represented by membrane filtration. Pressure-driven membrane operations, such as microfiltration (MF), ultrafiltration (UF), nanofiltration (NF), and reverse osmosis (RO) are currently well-established technologies for the clarification, stabilization, fractionation, and concentration steps of fruit juice production [9]. These processes offer several advantages over conventional technologies due to their mild operating conditions of temperature (therefore preserving the functional properties of food products), low operating and maintenance costs, non-use of chemical agents or solvents, and, consequently, the possibility of avoiding product contamination [10].

Their application in the industrial production of fruit and vegetable juices fits well with sustainable food processing, an integral part of the sustainable food supply chain and sustainable development based on the use of low energy and low-impact processing schemes to produce high-quality products with nutritional values close to that of fresh products [11].

In particular, the use of nanofiltration (NF) membranes has been largely investigated for the fractionation and concentration of flavonoids, anthocyanins, carotenoids, sugars, and phenolic compounds from fruit and vegetable matrices including graviola (*Annona muricata* L.) [12], jussara (*Euterpe edulis*) [13], wine lees [14], grape pomace [15], propolis [16], and roselle (*Hibiscus sabdariffa* L.) [17] extracts, as well as elderberry (*Sambucus nigra* L.) [18], pomegranate [19], bergamot [20], and apple [21] juices. Nevertheless, the metabolic composition of apple juice is quite complex and the molecular masses of valuable compounds are close to those of sugars (mono and disaccharides), which results in a membrane insufficient selectivity [22]. In order to increase the level of separation and to achieve a high purity of biomolecules, NF can be operated in diafiltration (DF) mode [23]. Diafiltration involves the addition of water or any other solvent or buffer to the feed solution to enhance the degree of separation of membrane-retained macrosolutes from membrane-permeable microsolutes [24]. It can be performed in a continuous or discontinuous mode [25]. In continuous diafiltration, the solvent is added to the system at the same rate as permeate flux. Discontinuous diafiltration, instead, involves first diluting the sample with water and then, the diluted sample is concentrated back to its original volume by membrane filtration. Each subsequent dilution should remove more of the small molecules [26]. Typical applications have been studied for the recovery of biochemical products from their fermentation broths [27,28], the purification of water-soluble nanoparticles [29], the reduction of alcohol content from alcoholic beverages [30], the purification of phycocyanin from Spirulina (*Arthrospira maxima*) [31], and the separation of sugars from biologically active compounds [23,32], among many others.

The number of publications dealing with sugar reduction in apple juices (or other natural juices) is very limited. Wei et al. [33] investigated the separation of polyphenols and sugars in apple juice by a loose NF membrane (MWCO 1 kDa) obtaining a sugar-reduced juice as a permeate stream. The results showed that at four bar, the sugar recovery in permeate was around 72% and the recovery of polyphenols in retentate was around 43%. Ceramic tubular UF membranes, with an MWCO of 15 kDa, have recently been investigated to produce a concentrate fraction from apple−cranberry cloudy juice with the simultaneous removal of some amount of sugars [34]. Pruksasri et al. [22] proposed a combination of

mechanical pre-fractionation and NF for the reduction of sugar in cloudy apple juice. In the first step, a fruit flesh juice (stream A) with a low content of polyphenols is produced after peeling and coring a certain amount of apple (45% of raw material). In the second step, the flesh juice is treated by NF/diafiltration with the production of a clarified juice (permeate) with low sugar content. The NF permeate is finally mixed with stream B enriched in phenolic compounds produced by milling, pressing, and centrifugation of the rest of the apples together with peels and cores from stream A. Thus, mechanical fractionation was considered as a separation step to reduce the losses of biofunctional compounds.

Bearing in mind that the reduction of sugar in natural fruit juices is a very challenging separation task and its applicability depends on the rejection and selectivity properties of membranes, we investigated an integrated NF/diafiltration approach without peeling apples, thus avoiding any sort of the previous pretreatment. The diafiltration process may contribute to reducing fouling phenomena with a consequent change in selectivity to promote the diffusion of sugars through the membranes. Furthermore, separation characteristics of NF membranes are not only based on size exclusion and this could play in favor of the rejection of polyphenols ahead of sugars during the NF/diafiltration process. In the light of these considerations, the present study evaluated the feasibility of phenolic compounds' separation from sugars in apple juice by using three different spiral-wound commercial membranes with an MWCO in the range of 200–500 Da. The performance of selected membranes was assessed in terms of productivity (permeate fluxes) and selectivity towards target compounds.

2. Materials and Methods

2.1. Chemicals

Folin−Ciocalteu phenol reagent, gallic acid, and sodium hydroxide were purchased from Sigma Aldrich (Milan, Italy), while sodium carbonate anhydrous was purchased from Carlo Erba (Milan, Italy). "Yellow line" enzymatic kits were supplied by Roche Diagnostics (Darmstadt, Germany).

2.2. Feed Solution

Apple juice was supplied by Gioia Succhi S.r.l. (San Ferdinando, Reggio Calabria, Italy) and processed according to the procedure reported by Gaglianò et al. [21]. The juice was clarified by using a laboratory plant equipped with hollow-fiber UF membranes made of polyethersulfone with an MWCO of 500 kDa (FB-02-FC from Microdyn Nadir, Wiesbaden, Germany). Then, the clarified juice was submitted to a discontinuous diafiltration, followed by an NF process in batch concentration mode. The clarified apple juice composition is reported in Table 1.

Table 1. Composition of clarified apple juice subjected to a diafiltration−nanofiltration process.

Parameter	Value
Glucose (g/L)	17.2 ± 1.3
Fructose (g/L)	43.7 ± 2.4
Total phenolic content (mgGAE/L)	241.5 ± 8.1
Total soluble solids (°Brix)	7.0 ± 0.1
pH	3.78 ± 0.02

2.3. Diafiltration−Nanofiltration Process: Experimental Set-Up and Procedure

NF-based diafiltration experiments were performed by using a bench plant (DeltaE S.r.l., Cosenza, Italy) equipped with a stainless steel housing able to accommodate a spiral-wound element with a dimension of 1.8" × 1.2" (membrane area of about 0.23 m^2). The experimental setup consists of a high-pressure pump (Cat Pumps, Milano, Italy, Model 3CP1221), a 5 L stainless steel feed tank, a digital flowmeter (SM6000, ifm electronic gmbh, Essen, Germany), two pressure gauges (Wika Instrument, Lawrenceville, GA, USA), and a control panel. The feed temperature was adjusted by circulating tap water in

the two-layered feed tank. The pressure was monitored at the entrance and exit of the membrane module through a frequency inverter and a needle valve located after the membrane module. NF experiments were performed by using three selected spiral-wound membrane modules supplied by Microdyn-Nadir (Wiesbaden, Germany). Their properties are summarized in Table 2.

Table 2. Characteristics of selected membranes according to manufacturers unless otherwise stated.

Membrane Type	**TS40**	**XN45**	**NP030**
Membrane material	TFC	TFC	PES
Configuration	spiral-wound	spiral-wound	spiral-wound
Max. operating pressure (bar)	41	41	35
Max. operating temperature (°C)	50	50	70
pH	1–12	1–12	0–14
Membrane surface area (m^2)	0.23	0.23	0.23
Nominal MWCO (Da)	200–300	300–500	300–400
Contact angle (°)	30 [a]	57 [b]	80 [c]
Water permeability at 25 °C (kg/m^2hbar)	4.48 [d]	6.12 [d]	2.99 [d]

TFC, thin-film composite, PES, polyethersulphone; [a] data from Zdarta et al. [35]; [b] data from Peiris et al. [36]; [c] data from Boussu et al. [37]; [d] own measurements.

The diafiltration volume (ratio of the solvent volume added per volume of feed solution) was calculated as follows [38]:

$$DV = \frac{V_p}{V_0} = \frac{V_w}{V_0} \quad (1)$$

where V_p and V_0 are the volumes of permeate and feed solution, respectively, and V_w is the volume of water added during the diafiltration process.

The NF process was operated at a transmembrane pressure (TMP) of 25 bar, an axial feed flowrate (Qf) of 7 L/min, and a temperature (T) of 25 ± 1 °C during the diafiltration step. Then, the juice was concentrated according to a batch concentration configuration in the same operating conditions up to a volume reduction factor (VRF) of 4. VRF is defined as the ratio of feed volume to residual retentate volume according to the following equation:

$$VRF = \frac{V_f}{V_r} = 1 + \frac{V_p}{V_r} \quad (2)$$

where V_f, V_p, and V_r are the volume of the feed, permeate, and retentate, respectively.

During both diafiltration and batch concentration steps, the permeate flux was gravimetrically measured at different time intervals.

The flow chart of the experimental set-up is shown in Figure 1.

The fouled membranes were cleaned with an enzymatic solution (Ultrasil 53, 1.0%, 40 °C, 60 min) followed by an alkaline cleaning (Ultraclean WA, 0.2%, 40 °C, 60 min) and final rinsing with tap water. The cleaning efficiency was evaluated by the flux recovery method [39] measuring the water permeability before and after the enzymatic/chemical cleaning.

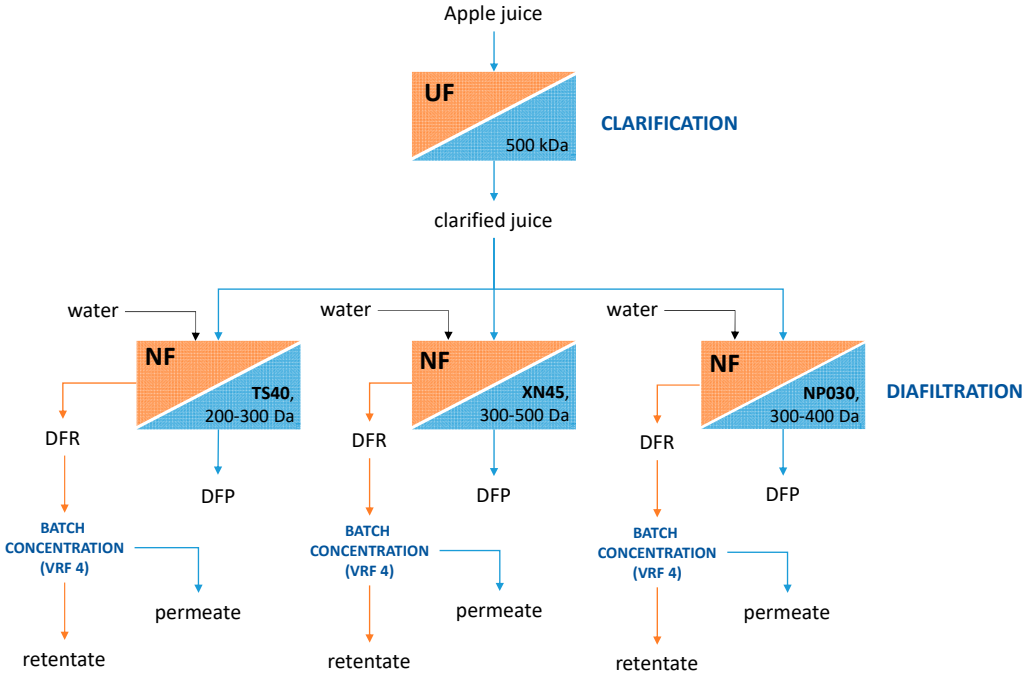

Figure 1. Flow chart of the experimental set-up (UF, ultrafiltration; NF, nanofiltration; DFR, diafiltrated retentate; DFP, diafiltrated permeate).

2.4. Performance Parameters

The membrane performance was measured in terms of permeate flux, J_p, concentration factor, $CF_{i(R,P)}$, and recovery rate, $R_{i(R,P)}$ (%), of a certain species.

The volumetric flux of permeate (L/m^{2}h) was calculated according to the following equation:

$$J_p = \frac{V_P}{A \cdot t} \tag{3}$$

where V_p is the volume of collected permeate (L), t is the time (h), and A the membrane permeation area (m^2).

The recovery rate (%) of a species i is obtained by its total mass in either permeate or retentate divided by its total mass in feed solution [33,40]:

$$R_{i(R,P)} = \frac{C_{i(R,P)} \cdot V_{i(R,P)}}{C_{i(F)} \cdot V_{i(F)}} \tag{4}$$

where $C_{i(R,P)}$ and $V_{i(R,P)}$ are the concentration and the volume of species i in either permeate or retentate solution, while $C_{i(F)}$ and $V_{i(F)}$ are the concentration and the volume of species i in the feed.

The volume V_{iI} of species i in retentate solution and the volume of species i in the feed $V_{i(F)}$ are equal when samples are collected at different DV values during diafiltration. This implies that volumes can be simplified in Equation (4) and the yield values for specific components throughout the diafiltration process can be calculated as a fraction of the original solute concentration remaining in the feed [23]:

$$R_{i(R)} = \frac{C_{i(R)}}{C_{i(F)}} \tag{5}$$

The concentration factor is the concentration of species *i* in either permeate or retentate solution $C_{i(R,P)}$ divided by its concentration in the feed solution $C_{i(F)}$ [33]:

$$CF_{i(R,P)} = \frac{C_{i(R,P)}}{C_{i(F)}} \quad (6)$$

The adsorbed phenolics and amount of sugar Q_{ADS} (mg/m^2) on the membrane surface at different VRF values was determined as follows [41]:

$$Q_{ADS} = \frac{C_F V_F - (C_R V_R + C_P V_P)}{A} \quad (7)$$

where V_F, V_R, and V_P are the feed, retentate, and permeate volumes, respectively; C_R and C_P are the concentration of phenolics or sugars in the retentate and permeate streams, respectively, and A is the the membrane surface area.

2.5. Analytical Measurements

The collected samples include: NF feed, NF retentates at different DV values, NF retentate, and NF permeate at different VRF values. Total soluble solids (TSS), total phenolic content (TPC), D-glucose, and D-fructose were measured. The results of the analytical measurements were expressed as the mean ± standard deviation (SD) of three independent determinations.

2.5.1. Total Soluble Solids

Total soluble solids (TSS) measurements were carried out by using a hand refractometer (Atago Co., Ltd., Tokyo, Japan) with a scale range of 0–32 °Brix.

2.5.2. Total Phenolic Content

The total phenolic content (TPC) was determined by the Folin−Ciocalteu method [42]. The sample (0.2 mL) was mixed with 1 mL of 10% (*w*/*v*) Folin−Ciocalteu reagent and 0.8 mL of a 7.5% (*w*/*v*) sodium carbonate solution. After 30 min of incubation at room temperature, the absorbance of the resulting solution was measured at 765 nm against a blank.

Spectrophotometric measurements were performed with the Shimadzu UV-160A UV-visible spectroscopy system. The TPC was calculated on the basis of the calibration curve of gallic acid and expressed as mg of gallic acid equivalents per liter (mg GAE/L).

2.5.3. D-Glucose and D-Fructose Quantification

D-glucose and D-fructose were determined enzymatically in a specific way. A multiparametric automatic analyzer (iMagic-M9, Darmstadt, Germany) was used to independently perform all the manual analytical procedures required for enzymatic tests. The system automatically collects and dispenses reagents and samples and calculates the analytical data. Detailed procedures used for sample preparation, enzymes, and reactions involved in the determinations of the sugars of interest are reported by R-Biopharm AG [43,44].

3. Results and Discussion

3.1. Permeate Flux Evaluation

Permeate fluxes and permeate quality are the most important aspects for the selection of a proper membrane [45]. Figure 2 shows the permeate flux (J_p) as a function of diafiltration volumes for all the investigated membranes in the selected operating conditions. For each membrane, the permeate flux increased by increasing the diafiltration volume. The addition of water during the process reduced the viscosity of the feed solution [46] and limited the formation of the concentration polarization layer on the membrane's surface. Therefore, the clogging of membrane pores was reduced and the transport of microsolutes through the membrane was facilitated [47]. The XN45 membrane exhibited the highest

permeate flux with values higher than 60 kg/m^{2}h at a DV of 5.5. On the other hand, the NP030 membrane showed much lower fluxes in comparison with TS40 and XN45 membranes, whose greater hydrophilicity played an important role in water solution transport through the membrane [48,49].

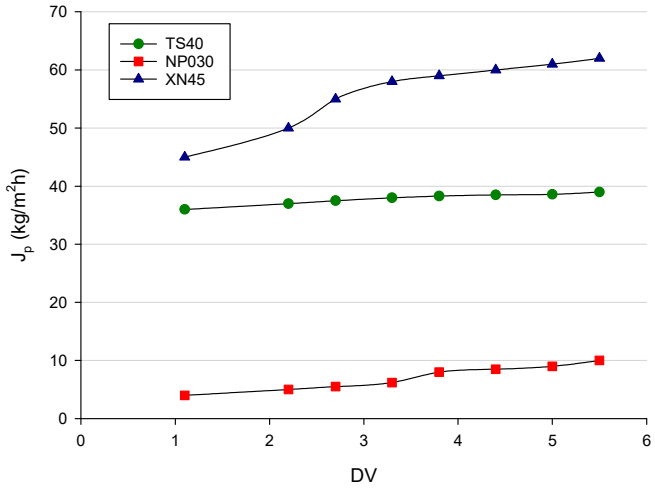

Figure 2. Diafiltration of clarified apple juice with selected membranes. Permeate flux as a function of diafiltration volume (Operating conditions: TMP, 25 bar; Qf, 7 L/min; T, 25 ± 1 °C).

Figure 3 shows the permeate flux (J_p) as a function of VRF during the NF process of the diafiltered juice with selected membranes according to the batch concentration configuration and in the same operating conditions of the diafiltration process. For XN45 and TS40 membranes, the build-up of solutes at the upstream interface (concentration polarization) determined a rapid permeate flux decay, followed by a long and gradual decline towards a steady-state limit value. Fouling mechanisms, such as the adsorption of particles on the membrane pore walls and pore plugging, are additional phenomena [50]. In the selected operating conditions, steady-state values for XN45 and TS40 membranes were in the order of 48 kg/m^{2}h and 8 kg/m^{2}h, respectively. For the NP030 membrane, the initial permeate flux was about 10 kg/m^{2}h, much lower than those observed for the other two investigated membranes. In addition, for this membrane, the permeate flux reduction at VRF 4 was only about 20% in relation to the initial value.

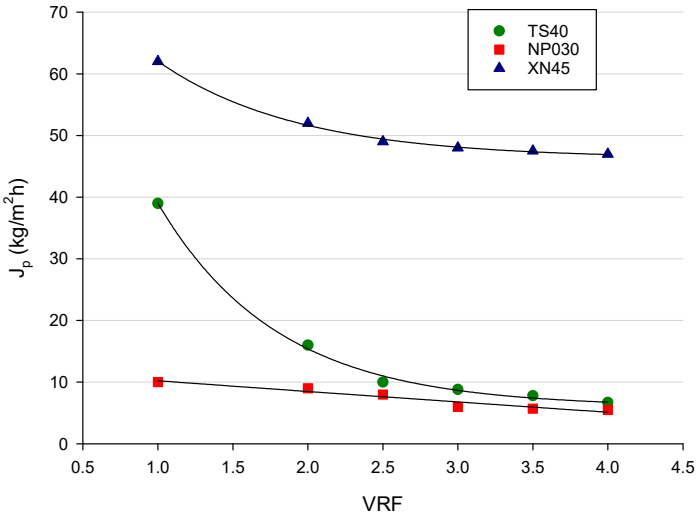

Figure 3. Nanofiltration in batch concentration mode of diafiltered apple juice with selected membranes. Permeate flux as a function of volume reduction factor (Operating conditions: TMP, 25 bar; Q_f, 7 L/min; T, 25 ± 1 °C).

For all selected membranes, the cleaning efficiency after the cleaning protocol was higher than 90%.

3.2. Recovery Rate of D-Glucose, D-Fructose, and TPC during Discontinuous Diafiltration

The recovery rate of both phenolic compounds and carbohydrates in the retentate stream was plotted as a function of the diafiltration volume, as shown in Figure 4. The selected membranes showed a similar behaviour: in particular, the recovery rate of both sugars and TPC decreased in the retentate by increasing the diafiltration volume indicating that the addition of distilled water as washing solvent during the diafiltration process caused the removal of these compounds in the clarified extract. Nevertheless, carbohydrates and TPC were removed at varying degrees for different membranes. Regardless of the diafiltration volume, the separation factor between TPC and sugars remained almost unchanged during the process: in fact, the more the number of diavolumes increased, the more the sugars passed into the permeate in the same ratio at which the polyphenols also passed. This has both negative and positive aspects. The negative aspect is linked to the fact that the separation between the compounds in the selected operating conditions cannot be improved with the addition of water, but this also represents an advantage from an economic point of view because the separation reached at DV 5.5 is almost the same as that obtained at DV 1.1. This implies a lower consumption of fresh water is needed to achieve the same result.

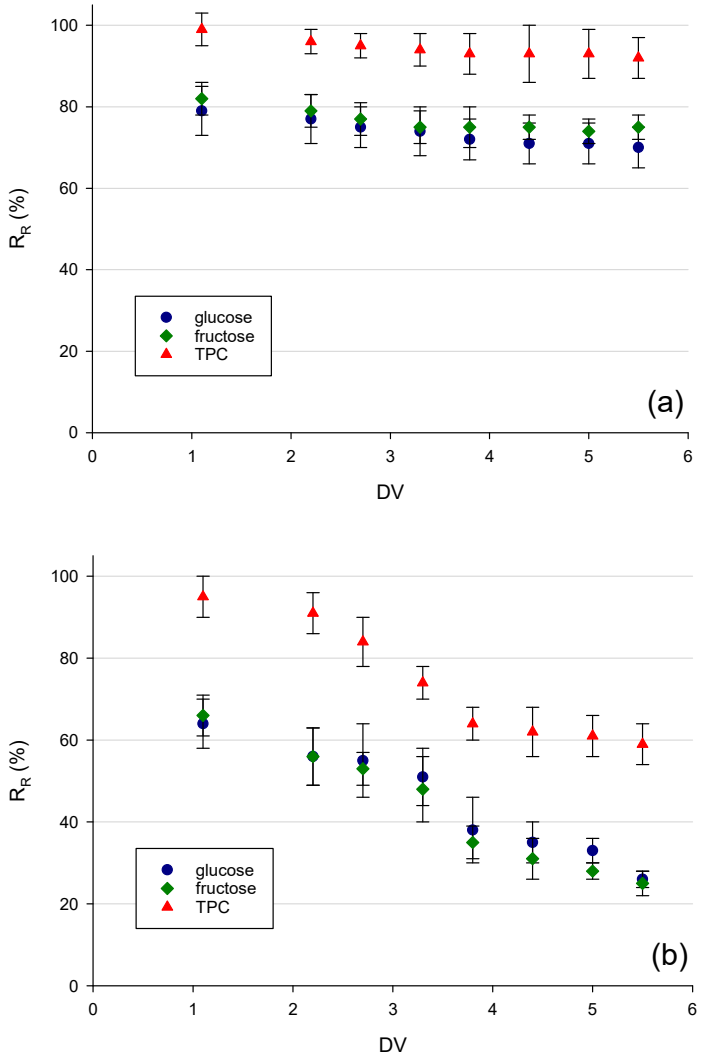

Figure 4. *Cont.*

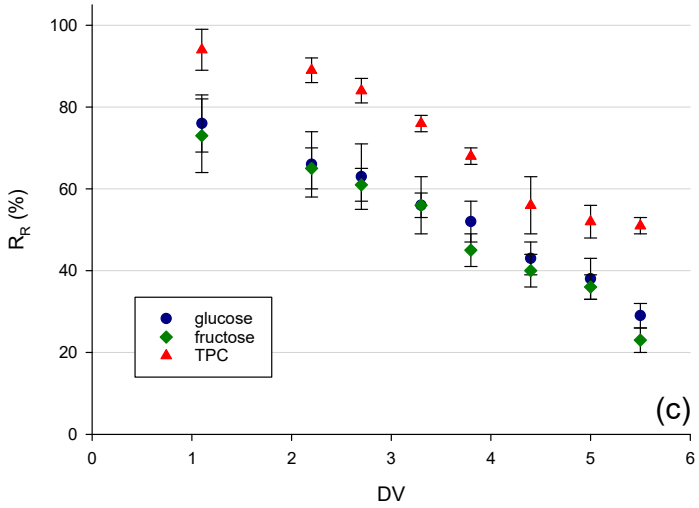

Figure 4. Recovery rate of total phenolic compounds, glucose, and fructose in the retentate stream during diafiltration with (**a**) TS40 (**b**) NP030 and (**c**) XN45 membranes.

Although the NP030 membrane was characterized by lower permeate fluxes, it allowed for the achievement of a greater separation factor between TPC and carbohydrates. At DV of 1.1, nearly 36% of D-glucose and 34% of D-fructose were removed, while 95% of TPC remained in the retentate juice. According to Pruksasri et al. [22], a degree of sugar reduction of about 30–40% could be an appropriate target. Therefore, a single diananofiltration process accomplished with an appropriate membrane and proper selected operating conditions may be applicable to remove a sufficient amount of sugar and efficiently recover phenolic compounds without losing their activity. In this way, a diafiltered retentate as the high-added value product can be obtained with significant advantages from both nutritional and economical points of view.

3.3. Concentration Factor of D-Glucose, D-Fructose, and TPC during Nanofiltration in Batch Concentration Mode

After diafiltration, the clarified juice was concentrated up to VRF 4 with each one of the investigated membranes. In this way, it was possible to evaluate the behaviour of each membrane in retaining and separating the compounds of interest in concentration mode. It is known that rejection is controlled by molecular size and interaction force between the membrane and the solute [51]. Among the investigated membranes, the TS40 had a higher rejection of sugars and polyphenols due to its lower MWCO of 200–300: in fact, the concentration factor at VRF 4 was 3.5 for TPC and 2.6 for sugars, respectively (Figure 5a). Therefore, only about 12.5% of the polyphenols were lost during the batch concentration process, while about 35% of sugars were further removed. The XN45 membrane showed the same trend: a higher concentration factor for polyphenols was observed in comparison to glucose and fructose. However, this membrane exhibited the worst separation gap between carbohydrates and TPC and a major removal in the retentate sample for all compounds. The concentration factor at VRF 4 was 2.3 for TPC, 2.0 for fructose, and 1.6 for glucose, respectively (Figure 5c). On the contrary, for the NP030 membrane, the concentration factor was higher for glucose and fructose than polyphenols, independently of the VRF value.

For all selected membranes, the retention level was relatively high when compared with the molecular weight of glucose (180.1559 g/mol) and fructose (180.16 g/mol). These results can be explained assuming that other phenomena, in addition to the steric hindrance, affect the retention coefficients including interactions between the solute and membrane material, as well as the association of sugars with phenolic compounds [52].

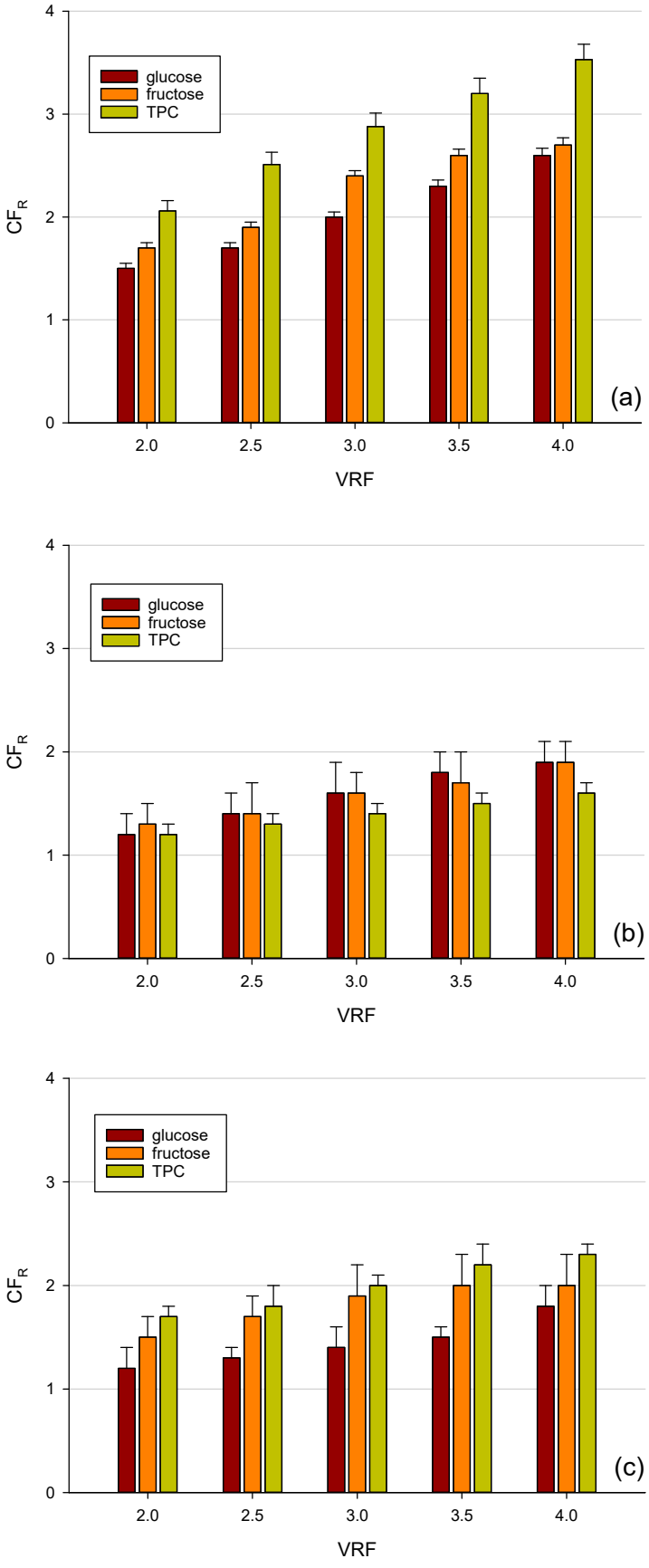

Figure 5. Concentration factor of total phenolic compounds, glucose, and fructose in the retentate stream during the concentration with (**a**) TS40 (**b**) NP030 and (**c**) XN45 membranes.

In addition, for all selected membranes, a significant increase in phenolic compounds was observed by increasing the VRF of the process. An increased concentration of phenolic compounds as a function of the VRF of the process was also observed in the treatment of mate bark aqueous extracts [53] and artichoke brine [54], with spiral-wound NF membranes characterized by an approximate MWCO of 150–300 Da (Desal HL and Desal DG from GE Osmonics, respectively). Different factors, including the surface morphology, pore size distribution, and adhesion in the membrane may contribute to this phenomenon [55].

In Figure 6, the recovery rate of TPC, glucose, and fructose in the retentate stream as a function of VRF for all selected membranes is shown. At VRF 4, more than 70% of phenolic compounds were recovered in the retentate of the TS40 membrane; at the same time, the removal efficiency of glucose and fructose was 59% and 56%, respectively (corresponding to a recovery factor in the retentate of 41% and 44%, respectively).

For membranes NP030 and XN45, the recovery factors of both phenolic compounds and sugars in the retentate stream were significantly lower than those observed for the TS40 membrane. Indeed, for the NP030 membranes, the recovery factors of sugars and phenolic compounds were about 10% and 20%, respectively. Similar values were observed for the recovery of sugar compounds in the retentate of the XN45 membrane while for phenolic compounds, the recovery factor at VRF 4 was 26%. Therefore, the global result indicated the TS40 membrane was the best one to preserve phenolic compounds of apple juice through a combination of diafiltration and batch concentration processes while reducing the content of sugars by an order of 60%.

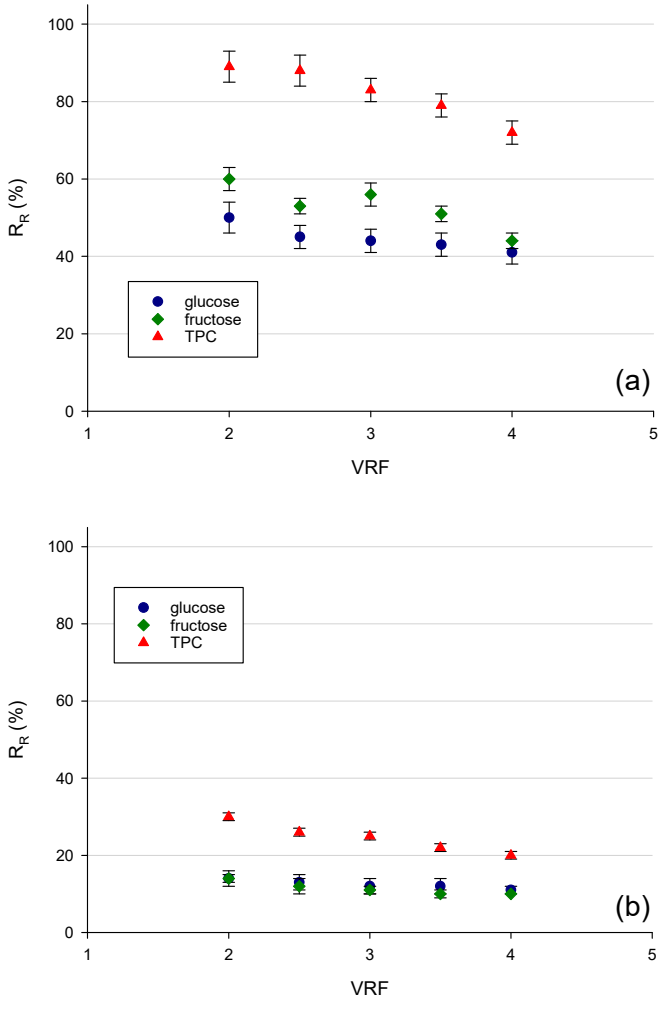

Figure 6. *Cont.*

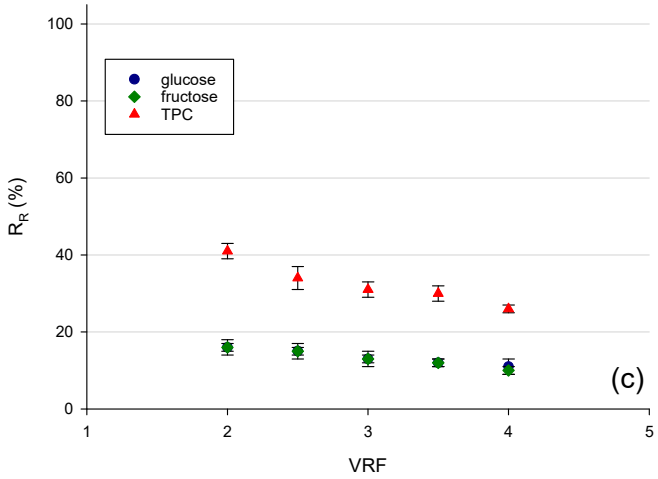

Figure 6. Recovery rate of total phenolic compounds, glucose, and fructose in the retentate stream during the batch concentration process with (**a**) TS40 (**b**) NP030 and (**c**) XN45 membranes.

3.4. Mass Balance and Adsorption of Sugars and TPC

The mass balance of the whole filtration process, which includes the initial feed solution, the diafiltrated solution, the permeate stream, and the remaining retentate can give an insight into deposit formation on the membrane surface and eventual pore blocking. Table 3 shows the mass balance related to sugars and TPC in both diafiltration and concentration processes for the selected membranes. As it can be seen, the batch concentration configuration is characterized by a substantial deviation from the mass balance in comparison to diafiltration. These results can be attributed to pore blocking phenomena due to the adsorption of monosaccharides and low molecular weight phenolic compounds on both the outer and inner membrane surface.

Table 3. Mass balance (%) of glucose, fructose, and TPC in diafiltration and batch concentration processes for selected membrane.

Membrane Type	Process	Component		
		Glucose	Fructose	TPC
TS40	Diafiltration	94.62	93.56	97.49
	Batch concentration	68.81	68.19	81.51
NP030	Diafiltration	95.83	99.99	90.98
	Batch concentration	59.07	59.63	54.33
XN45	Diafiltration	100.00	99.99	99.99
	Batch concentration	63.13	72.45	58.00

The TS40 membrane showed the lowest deviation from the mass balance of TPC during nanofiltration in concentration mode. This might be due to the smallest MWCO of this membrane which tends to prevent the inner pore blocking of polyphenols. On the other hand, the mass balance of both sugars and TPC in the diafiltration process was higher than 91% for all selected membranes. Diafiltration ensures more favorable hydrodynamic conditions in the membrane boundary layer, thus controlling the thickness of the concentration polarization layer and pore-clogging. These conditions reduce the amount of sugar adsorbed on the membrane, improving their diffusion. Similar results have been reported recently by Tonova et al. [56] who evaluated the performance of the NP030 membrane in flat-sheet configuration in the separation of saccharides from phenolics from an aquatic weed hydrolysate.

In Figure 7 the adsorbed amount of sugar and TPC on the selected membranes evaluated at the end of the batch concentration process is reported. The amount of adsorbed fructose for the TS40 membrane, about 217 g/m^2, was much higher in comparison to the

other NF membranes. The adsorbed amount of glucose for this membrane (82.39 g/m^2) was also higher than the other two membranes (30.13 and 31.73 g/m^2 for NP030 and XN45 membranes, respectively). On the other hand, the adsorbed amount of phenolic compound for all selected membranes was much lower than that of sugars in relation to the predominant content of sugars in the original juice. Among the selected membranes, the NP030 exhibited the highest amount of adsorbed phenolics (1.16 g/m^2 against 0.74 and 0.33 g/m^2 for TS40 and XN45 membranes, respectively). Saleh et al. [57] reported up to 4.3 g of polyphenolics adsorbed per m^2 of the membrane in the treatment of apple juice with a SelRO® spiral-wound membrane of 1 kDa MWCO (MPS-36 from Koch Membrane Systems).

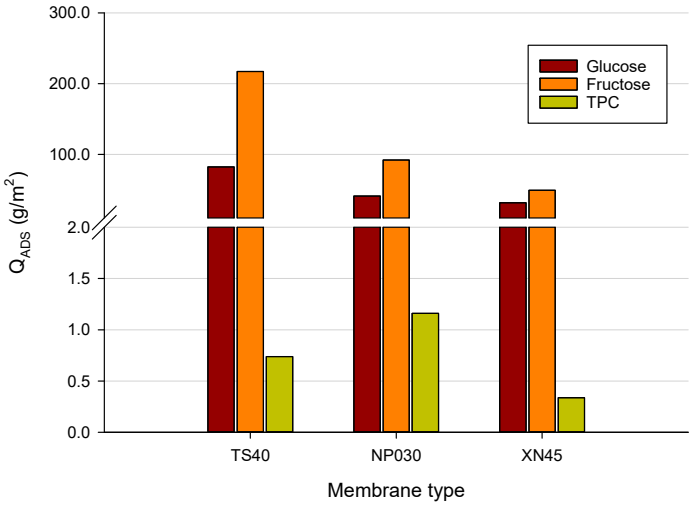

Figure 7. Amount of adsorbed glucose, fructose, and TPC for selected membranes.

The more hydrophobic character of the NP030 membrane, with a top layer in PES material, enhances the adsorption of phenolic compounds on the membrane surface and the formation of a hydrophobic layer onto the membrane surface which could modify the physicochemical properties of the membrane [58], leading to lower permeate fluxes and modification of the rejection performance. Susanto et al. [59] supported the existence of benzene ring−benzene ring interactions to justify the adsorption of phenolic compounds on PES membranes. Moreover, the formation of multiple hydrogen bonds between polyphenols and the additive poly(vinyl)pyrrolidone (PVP) usually used in the manufacturing process in PES membranes is considered an additional contribution to the adsorption phenomena of phenolic compounds [60].

Cai et al. [61] found that for phenolic compounds, a cake/gel layer as a reversible fouling was the main fouling resistance, while the adsorption played a significant role in the irreversible fouling resistance of polyamide and polypiperazine amide NF membranes with MWCOs of 240 and 150 Da, respectively.

4. Conclusions

Nanofiltration membranes with an MWCO in the range of 200–600 Da were tested to reduce the sugar content in apple juice through a combination of diafiltration and batch concentration processes. For all selected membranes, the recovery rate of both sugars and phenolic compounds decreased in the retentate by increasing the diafiltration volume; however, the separation factor between phenolic compounds and sugars remained almost unchanged during the diafiltration process.

Among the investigated membranes, the TS40 membrane, a thin-film composite membrane with the lowest MWCO (200–300 Da), showed the highest retention of sugars and phenolic compounds in the selected operating conditions of both diafiltration and concentration processes. More than 70% of phenolic compounds were recovered in the

retentate stream of this membrane at a volume reduction factor of 4, while recoveries of glucose and fructose were 41 and 44%, respectively. On the other hand, the other investigated membranes allowed for the recovery of a much lower amount of phenolic compound in the retentate stream despite a greater removal of sugars on the permeate side. Therefore, the global results indicate that the combination of diafiltration and batch concentration with the TS40 membrane is a good compromise to remove up to 60% of sugars from apple juice with minimal losses of phenolic compounds.

Author Contributions: Investigation, methodology, formal analysis, data curation, writing—original draft, M.G.; investigation, methodology, formal analysis, C.C.; supervision, conceptualization, data curation, investigation, methodology, writing—original draft, writing—review and editing, A.C.; supervision, conceptualization, data curation, investigation, methodology, writing—original draft, writing—review and editing, G.D.L. All authors have read and agreed to the published version of the manuscript.

Funding: This work was supported by the University of Calabria and Calabria region within the framework POR Calabria—FSE/FESR 2014–2020.

Institutional Review Board Statement: Not applicable.

Informed Consent Statement: Not applicable.

Data Availability Statement: The data presented in this study are available upon request from the corresponding author.

Acknowledgments: The authors thank Gioia Succhi S.R.L. (San Ferdinando, Italy) for collecting and supplying samples of Golden Delicious apple juice.

Conflicts of Interest: The authors declare no conflict of interest.

References

1. Wojdylo, A.; Oszmianski, J.; Laskowski, P. Polyphenolic compounds and antioxidant activity of new and old apple varieties. *J. Agric. Food Chem.* **2008**, *56*, 6520–6530. [CrossRef] [PubMed]
2. Koutsos, A.; Tuohy, K.M.; Lovegrove, J.A. Apples and cardiovascular health—Is the gut microbiota a core consideration? *Nutrients* **2015**, *7*, 3959–3998. [CrossRef] [PubMed]
3. Vallée Marcotte, B.; Verheyde, M.; Pomerleau, S.; Doyen, A.; Couillard, C. Health benefits of apple juice consumption: A review of interventional trials on humans. *Nutrients* **2022**, *14*, 821. [CrossRef] [PubMed]
4. Samborska, K.; Kamińska, P.; Jedlińska, A.; Matwijczuk, A.; Kamińska-Dwórznicka, A. Membrane processing in the sustainable production of low-sugar apple-cranberry cloudy juice. *App. Sci.* **2018**, *8*, 1082. [CrossRef]
5. World Health Organization. Guideline: Sugars Intake for Adults and Children, Geneva. 2015. Available online: https://www.who.int/publications/i/item/9789241549028 (accessed on 28 June 2022).
6. World Health Organization. A Healthy Diet Sustainably Produced. 2018. Available online: https://apps.who.int/iris/bitstream/handle/10665/278948/WHO-NMH-NHD-18.12-eng.pdf (accessed on 28 June 2022).
7. Bigliardi, B.; Galati, F. Innovation trends in the food industry: The case of functional foods. *Trends Food Sci. Technol.* **2013**, *31*, 118–129.
8. Brglez Mojzer, E.; Knez Hrnčič, M.; Škerget, M.; Knez, Ž.; Bren, U. Polyphenols: Extraction methods, antioxidative action, bioavailability and anticarcinogenic effects. *Molecules* **2016**, *21*, 901. [CrossRef]
9. Conidi, C.; Castro-Muñoz, R.; Cassano, A. Membrane-based operations in the fruit juice processing industry: A review. *Beverages* **2020**, *6*, 18. [CrossRef]
10. Charcosset, C. Classical and recent applications of membrane processes in the food industry. *Food Eng. Rev.* **2021**, *13*, 322–343. [CrossRef]
11. Lazarides, H.N. Food processing technology in a sustainable food supply chain. *Procedia Food Sci.* **2011**, *1*, 1918–1923. [CrossRef]
12. de Moraes, I.V.M.; Rabelo, R.S.; Pereira, J.A.D.; Hubinger, M.D.; Schmidt, F.L. Concentration of hydroalcoholic extracts of graviola (*Annona muricata* L.) pruning waste by ultra and nanofiltration: Recovery of bioactive compounds and prediction of energy consumption. *J. Clean. Prod.* **2018**, *174*, 1412–1421. [CrossRef]
13. Vieira, G.S.; Moreira, F.K.V.; Matsumoto, R.L.S.; Michelon, M.; Filho, F.M.; Hubinger, M.D. Influence of nanofiltration membrane features on enrichment of jussara ethanolic extract (*Euterpe edulis*) in anthocyanins. *J. Food Eng.* **2018**, *226*, 31–41. [CrossRef]
14. Arboleda Meija, J.A.; Parpinello, G.P.; Versari, A.; Conidi, C.; Cassano, A. Microwave-assisted extraction and membrane-based separation of biophenols from red wine lees. *Food Bioprod. Process.* **2019**, *117*, 74–83. [CrossRef]

15. Arboleda Meija, J.A.; Ricci, A.; Figueiredo, A.S.; Versari, A.; Cassano, A.; de Pinho, M.N.; Parpinello, G.P. Membrane-based operations for the fractionation of polyphenols and polysaccharides from winery sludges. *Food Bioprocess. Technol.* **2022**, *15*, 933–948.
16. Tylkowski, B.; Trusheva, B.; Bankova, V.; Giamberini, M.; Peev, G.; Nikolova, A. Extraction of biologically active compounds from propolis and concentration of extract by nanofiltration. *J. Membr. Sci.* **2010**, *348*, 124–130. [CrossRef]
17. Cissé, M.; Vaillant, F.; Pallet, D.; Dornier, M. Selecting ultrafiltration and nanofiltration membranes to concentrate anthocyanins from roselle extract (*Hibiscus sabdariffa* L.). *Food Res. Int.* **2011**, *44*, 2607–2614. [CrossRef]
18. Tundis, R.; Loizzo, M.R.; Bonesi, M.; Sicari, V.; Ursino, C.; Manfredi, I.; Conidi, C.; Figoli, A.; Cassano, A. Concentration of bioactive compounds from elderberry (*Sambucus nigra* L.) juice by nanofiltration membranes. *Plant Food Hum. Nutr.* **2018**, *73*, 336–343. [CrossRef]
19. Conidi, C.; Cassano, A.; Caiazzo, F.; Drioli, E. Separation and purification of phenolic compounds from pomegranate juice by ultrafiltration and nanofiltration membranes. *J. Food Eng.* **2017**, *195*, 1–13. [CrossRef]
20. Conidi, C.; Cassano, A.; Drioli, E. A membrane-based study for the recovery of polyphenols from bergamot juice. *J. Membr. Sci.* **2011**, *375*, 182–190. [CrossRef]
21. Gaglianò, M.; Conidi, C.; Bartella, L.; Salvino, R.A.; di Donna, L.; Cassano, A.; de Luca, G. An integrated approach based on NMR and HPLC–UV-ESI–MS/MS to characterize apple juices and their nanofiltration (NF) bioactive extracts. *Food Bioprocess Technol.* **2021**, *14*, 2273–2285. [CrossRef]
22. Pruksasri, S.; Lanner, B.; Novalin, S. Nanofiltration as a potential process for the reduction of sugar in apple juices on an industrial scale. *LWT* **2020**, *133*, 110118. [CrossRef]
23. Conidi, C.; Cassano, A.; Drioli, E. Membrane diafiltration for enhanced purification of biologically active compounds from goji berries extracts. *Sep. Purif. Technol.* **2022**, *282*, 119991. [CrossRef]
24. Doran, P.M. Unit Operations. In *Bioprocess Engineering Principles*; Doran, P.M., Ed.; Elsevier: Amsterdam, The Netherlands, 2013; pp. 445–595.
25. Loewe, D.; Dieken, H.; Grein, T.A.; Salzig, D.; Czermak, P. A combined ultrafiltration/diafiltration process for the purification of oncolytic measles virus. *Membranes* **2022**, *12*, 105. [CrossRef] [PubMed]
26. Schwartz, L. *Diafiltration: A Fast, Efficient Method for Desalting or Buffer Exchange of Biological Samples. Pall Scientific & Technical Report*; Pall Life Sciences: Ann Arbor, MI, USA, 2003.
27. Khunnonkwao, P.; Jantama, K.; Kanchanatawee, S.; Galier, S.; Roux-de Balmann, H. A two steps membrane process for the recovery of succinic acid from fermentation broth. *Sep. Purif. Technol.* **2018**, *207*, 451–460. [CrossRef]
28. Zhou, H.; Ni, J.; Huang, W.; Zhang, J. Separation of hyaluronic acid from fermentation broth by tangential flow microfiltration and ultrafiltration. *Sep. Purif. Technol.* **2006**, *52*, 29–38. [CrossRef]
29. Sweeney, S.F.; Woehrle, G.H.; Hutchison, J.E. Rapid purification and size separation of gold nanoparticles via diafiltration. *J. Am. Chem. Soc.* **2006**, *128*, 3190–3197. [CrossRef]
30. Ambrosi, A.; Motke, M.B.; Souza-Silva, É.A.; Zini, C.A.; McCutcheon, J.R.; Cardozo, N.; Tessaro, I.C. Beer dealcoholization by forward osmosis diafiltration. *Innov. Food Sci. Emerg. Technol.* **2020**, *63*, 102371. [CrossRef]
31. Nisticò, D.M.; Piro, A.; Oliva, D.; Osso, V.; Mazzuca, S.; Fagà, F.A.; Morelli, R.; Conidi, C.; Figoli, A.; Cassano, A. A combination of aqueous extraction and ultrafiltration for the purification of phycocyanin from *Arthrospira maxima*. *Microorganisms* **2022**, *10*, 308. [CrossRef]
32. Almanasrah, M.; Brazinha, C.; Kallioinen, M.; Duarte, L.C.; Roseiro, L.B.; Bogel-Lukasik, R.; Carvalheiro, F.; Manttari, M.; Crespo, J.G. Nanofiltration and reverse osmosis as a platform for production of natural botanic extracts: The case study of carob by-products. *Sep. Purif. Technol.* **2015**, *149*, 389–397. [CrossRef]
33. Wei, D.S.; Hossain, M.; Saleh, Z.S. Separation of polyphenolics and sugar by ultrafiltration: Effects of operating conditions on fouling and diafiltration. *Int. J. Nutr. Food Eng.* **2007**, *1*, 115–122.
34. Barańska, A.; Kot, A.; Samborska, K. Ultrafiltration as a method to obtain sugar reduced cloudy juices—A research on juice's properties. *Zeszyty Problemowe Postępów Nauk Rolniczych* **2020**, *600*, 3–11. [CrossRef]
35. Zdarta, J.; Thygesen, A.; Holm, M.S.; Meyer, A.S.; Pinelo, M. Direct separation of acetate and furfural from xylose by nanofiltration of birch pretreated liquor: Effect of process conditions and separation mechanism. *Sep. Purif. Technol.* **2020**, *239*, 116546. [CrossRef]
36. Peiris, R.H.; Hallé, C.; Budman, H.; Moresoli, C.; Peldszus, S.; Huck, P.M.; Legge, R.L. Identifying fouling events in a membrane-based drinking water treatment process using principal component analysis of fluorescence excitation-emission matrices. *Water Res.* **2010**, *44*, 185–194. [CrossRef] [PubMed]
37. Boussu, K.; Vandecasteele, C.; van der Bruggen, B. Relation between membrane characteristics and performance in nanofiltration. *J. Membr. Sci.* **2008**, *310*, 51–65. [CrossRef]
38. Mittal, R.; Lamdande, A.G.; Sharma, R.; Raghavarao, K.S.M.S. Membrane processing for purification of R-Phycoerythrin from marine macro-alga, *Gelidium pusillum* and process integration. *Sep. Purif. Technol.* **2020**, *252*, 117470. [CrossRef]
39. Chen, V.; Li, H.; Li, D.; Tan, S.; Petrus, H.B. Cleaning strategies for membrane fouled with protein mixtures. *Desalination* **2006**, *200*, 198–200. [CrossRef]
40. Sun, X.; Lu, H.; Wang, J. Recovery of citric acid from fermented liquid by bipolar membrane electrodialysis. *J. Clean. Prod.* **2017**, *143*, 250–256. [CrossRef]

41. Conidi, C.; Cassano, A.; Garcia-Castello, E. Valorization of artichoke wastewaters by integrated membrane process. *Water Res.* **2014**, *48*, 363–374. [CrossRef]
42. Singleton, V.L.; Orthofer, R.; Lamuela-Raventós, R.M. Analysis of total phenols and other oxidation substrates and antioxidants by means of Folin-Ciocalteu reagent. *Methods Enzimol.* **1999**, *299*, 152–178.
43. Enzytec Liquid D-Glucose. 2017. Available online: https://food.r-biopharm.com/wp-content/uploads/2017/05/E-Liquid_IFU_E8140_Glucose_EN.pdf (accessed on 28 June 2022).
44. Enzytec Liquid D-Glucose/D-Fructose. 2017. Available online: https://food.r-biopharm.com/wp-content/uploads/2017/07/e-liquid_ifu_e8160_glucose-fructose_en.pdf (accessed on 28 June 2022).
45. Laorko, A.; Li, Z.; Tongchitpakdee, S.; Chantachum, S.; Youravong, W. Effect of membrane property and operating conditions on phytochemical properties and permeate flux during clarification of pineapple juice. *J. Food Eng.* **2010**, *100*, 514–521. [CrossRef]
46. Servent, A.; Abreu, F.A.P.; Dhuique-Mayer, C.; Belleville, M.P.; Dornier, M. Concentration and purification by crossflow microfiltration with diafiltration of carotenoids from a by-product of cashew apple juice processing. *Innov. Food Sci. Emerg. Technol.* **2020**, *66*, 102519. [CrossRef]
47. Nguyen, D.T.N.N.; Lameloise, M.L.; Guiga, W.; Lewandowski, R.; Bouix, M.; Fargues, C. Optimization and modeling of diananofiltration process for the detoxification of ligno-cellulosic hydrolysates—Study at pre-industrial scale. *J. Membr. Sci.* **2016**, *512*, 111–121. [CrossRef]
48. Lyu, H.; Fang, Y.; Ren, S.; Chen, K.; Luo, G.; Zhang, S.; Chen, J. Monophenols separation from monosaccharides and acids by two-stage nanofiltration and reverse osmosis in hydrothermal liquefaction hydrolysates. *J. Membr. Sci.* **2016**, *504*, 141–152. [CrossRef]
49. Nicolini, J.V.; Borges, C.P.; Ferraz, H.C. Selective rejection of ions and correlation with surface properties of nanofiltration membranes. *Sep. Purif. Technol.* **2016**, *171*, 238–247. [CrossRef]
50. De Oliveira, R.C.; de Barros, S.T.D. Beer clarification with polysulfone membrane and study on fouling mechanism. *Braz. Arch. Biol. Technol.* **2011**, *54*, 1335–1342. [CrossRef]
51. Suhalim, N.S.; Kasim, N.; Mahmoudi, E.; Shamsudin, I.J.; Mohammad, A.W.; Zuki, F.M.; Jamari, N.L.A. Rejection mechanism of ionic solute removal by nanofiltration membranes: An overview. *Nanomaterials* **2022**, *12*, 437. [CrossRef]
52. Muñoz, P.; Pérez, K.; Cassano, A.; Ruby-Figueroa, R. Recovery of anthocyanins and monosaccharides from grape marc extract by nanofiltration membranes. *Molecules* **2021**, *26*, 2003. [CrossRef]
53. Prudêncio, A.P.A.; Prudêncio, E.S.; Amboni, R.D.M.C.; Murakami, A.N.N.; Maraschin, M.; Petrus, J.C.C.; Ogliari, P.J.; Leite, R.S. Phenolic composition and antioxidant activity of the aqueous extract of bark from residues from mate tree (*Ilex paraguariensis* St. Hil.) bark harvesting concentrated by nanofiltration. *Food Bioprod. Process.* **2012**, *90*, 399–405. [CrossRef]
54. Cassano, A.; Cabri, W.; Mombelli, G.; Peterlongo, F.; Giorno, L. Recovery of bioactive compounds from artichoke brines by nanofiltration. *Food Bioprod. Process.* **2016**, *98*, 257–265. [CrossRef]
55. Tsuru, T.; Sudoh, T.; Yoshioka, T.; Asaeda, M. Nanofiltration in non-aqueous solutions by porous silica-zirconia membranes. *J. Membr. Sci.* **2001**, *185*, 253–261. [CrossRef]
56. Tonova, K.; Lazarova, M.; Dencheva-Zarkova, M.; Genova, J. Nanofiltration of aquatic weed hydrolysate: Diafiltration versus concentration mode for separating saccharides from phenolics. *Chem. Eng. Res. Des.* **2022**, *182*, 360–370. [CrossRef]
57. Saleh, Z.S.; Stanley, R.; Wibisono, R. Separation and concentration of health compounds by membrane filtration. *Int. J. Food Eng.* **2006**, *2*, 4. [CrossRef]
58. Sotto, A.; Arsuaga, J.M.; van der Bruggen, B. Sorption of phenolic compounds on NF/RO membrane surfaces: Influence on membrane performance. *Desalination* **2013**, *309*, 64–73. [CrossRef]
59. Susanto, H.; Feng, Y.; Ulbricht, M. Fouling behavior of aqueous solutions of polyphenolic compounds during ultrafiltration. *J. Food Eng.* **2009**, *91*, 333–340. [CrossRef]
60. Cassano, A.; de Luca, G.; Conidi, C.; Drioli, E. Effect of polyphenols-membrane interactions on the performance of membrane-based processes. A review. *Coord. Chem. Rev.* **2017**, *351*, 45–75. [CrossRef]
61. Cai, M.; Hou, W.; Li, Z.; Lv, Y.; Sun, P. Understanding nanofiltration fouling of phenolic compounds in model juice solution with two membranes. *Food Bioprocess. Technol.* **2017**, *10*, 2123–2131. [CrossRef]

antioxidants

MDPI

Article

NMR-Based Characterization of Citrus Tacle Juice and Low-Level NMR and UV—Vis Data Fusion for Monitoring Its Fractions from Membrane-Based Operations

Martina Gaglianò [1,2], Giuseppina De Luca [1,*], Carmela Conidi [2] and Alfredo Cassano [2,*]

[1] Department of Chemistry & Chemical Technologies, University of Calabria, Via P. Bucci, 87036 Rende, Italy
[2] Institute on Membrane Technology, ITM-CNR, 87036 Rende, Italy
* Correspondence: giuseppina.deluca@unical.it (G.D.L.); a.cassano@itm.cnr.it (A.C.); Tel.: +39-0984-493323 (G.D.L.); +39-0984-492067 (A.C.)

Abstract: Tacle is a citrus variety which recently gained further interest due to its antioxidant and biological properties. This study suggests using Nuclear Magnetic Resonance (NMR) imaging to characterize Tacle juice's metabolic composition as it is intimately linked to its quality. First, polar and apolar solvent systems were used to identify a significant fraction of the Tacle metabolome. Furthermore, the antioxidant capacity and the total content of flavonoids, polyphenols and β-carotene in the juice were investigated with UV—Visible spectroscopy. Tacle juice was clarified and fractionated by ultrafiltration (UF) and nanofiltration (NF) membranes in order to recover and purify its bioactive principles. Finally, the second part of this work sheds light on the spectrophotometric assays and ^{1}H-NMR spectra of fractions coming from membrane operations coupled with a multivariate data analysis technique, PCA, to explore the impact of UF and NF processes on the metabolic profile of the juice.

Keywords: Tacle juice; NMR; UV—Visible; ultrafiltration/diafiltration; nanofiltration

Citation: Gaglianò, M.; De Luca, G.; Conidi, C.; Cassano, A. NMR-Based Characterization of Citrus Tacle Juice and Low-Level NMR and UV—Vis Data Fusion for Monitoring Its Fractions from Membrane-Based Operations. *Antioxidants* **2023**, *12*, 2. https://doi.org/10.3390/antiox12010002

Academic Editor: David Arráez-Román

Received: 24 November 2022
Revised: 7 December 2022
Accepted: 16 December 2022
Published: 20 December 2022

1. Introduction

Tacle is a new triploid citrus hybrid developed in Sicily using traditional, strictly non-GMO techniques. Both its name and flavour recall the two parents' cultivars: the Tarocco orange (*C. sinensis* L. Osbeck) and the Monreal Clementine (*C. clementina* Hort. ex Tan.) [1]. This innovative fruit was mainly studied for its high antioxidant activity [2], which confers the citrus extracts' health-promoting effects of lowering risks for chronic heart and vascular diseases and treating metabolic disorders such as obesity and diabetes [3,4]. The outbreak of the COVID-19 pandemic has increased the already-high consumer demand for immune-boosting, natural and organic products [5]. The high nutraceutical profile of Tacle responds perfectly to this need. Still, the main bottleneck may lie in the juice's production process, which must allow for the obtaining of processed food very close to the raw material. Hence, apart from the sensory attributes, one should minimize the loss of colour, texture and significantly bioactive compounds. Traditionally, fruit processing techniques include clarification with filter aids and fining agents, as well as thermal processes such as pasteurization, sterilization and concentration aimed at improving the shelf life of the juice by preventing enzymes, spoilage and pathogenic microorganisms. Unfortunately, these processes lead to a dramatic change in the phenolic and carotenoid compounds, vitamins, taste and color of juices, as well as to the formation of undesirable substances such as furfural, 5-hydroxymethylfurfural, furan and acrylamide [6]. Consequently, the fruit juice's quality is compromised in terms of its nutritional, functional, physicochemical and sensorial properties. Pressure-driven membrane operations have emerged in the past as non-thermal technological alternatives to traditional methods given their ability to minimize the degradation of

functional molecules and promote the development of high-quality products with considerable shelf stability [7–9]. Among them, microfiltration (MF) and ultrafiltration (UF) provide cost-effective alternatives to traditional fining and clarification methodologies for separating the raw juice into a fibrous concentrated pulp (retentate) and a clarified fraction free of spoilage microorganisms (permeate), which are suspended solids and colloids such as proteins [10]. The combination of these processes with diafiltration (DF) increases the purity of the obtained fractions. For instance, carotenoid extracts from solid by-products of cashew apple (*Anacardium occidentale* L.) juice processing, as well as from orange juice, have been obtained through a combination of crossflow MF and DF [11,12]. Clarified juices can be further fractionated or concentrated by using nanofiltration (NF) and reverse osmosis (RO) operations [13,14]. The environmental friendliness, economics and ease of use are further advantages encouraging the application of these technologies [15]. The evaluation of membrane processes in retaining metabolites which exhibit high nutritional value, shape organoleptic characteristics and thus formulate the fundamental quality properties of the product can be detected by means of several analytical methodologies [16–19]. NMR spectroscopy is emerging as a leading technique in metabolomic studies, as it is a fast, robust and reliable technique which allows the detection of a wide range of structurally diverse metabolites simultaneously. Because the richness of information often results in high spectral complexity, it calls for using multivariate analysis to study large numbers of spectra and extract meaningful information. Among the multivariate statistical analysis techniques, principal component analysis (PCA) is widely used and is recognized as one of the primary unsupervised compression techniques for exploratory data analysis. Recently, NMR-based metabolomics coupled with chemometric analysis has been applied to obtain metabolic profiles of various kinds of food, including honey, olive oil, apple and pomegranate juice, thus establishing adulteration, variety, geographical origin, quality and authenticity [20–23]. PCA has also been applied very successfully to study the industrial processing of citrus fruit juices to evaluate for reliable process control, to assess the quality of orange juice and to identify potentially mislabeled samples [24]. Furthermore, even though it is still a scientific challenge, NMR measurements can be combined with metabolomic and statistical data from other techniques. For example, Tristán et al. [25] probed the feasibility of using FTIR and NMR data to achieve, through the models developed, a fast and accessible tool for evaluating the ripe state of the melon fruits. Additionally, fusion of ^{1}H-NMR and chromatographic techniques (gas and liquid chromatography) data coupled with mass spectrometry was applied to provide more an accurate knowledge about the classification of golden rums [26]. The combined use of multi-technique data in chemometric analysis produced the best results compared to the individual techniques in classifying and distinguishing samples [27].

In this work, NMR has been applied to the analysis of Tacle juice with multiple aims. A preliminary chemical characterization of the juice was performed by using deuterium oxide (D_2O) and deuterated chloroform ($CDCl_3$) as solvents in order to capture both polar and non-polar metabolites from the original sample, thus improving the coverage of its metabolome. The juice was treated by UF to obtain a clarified fraction free of suspended solids and with a phenolic composition similar to that of the raw juice. The combination with DF was also studied in order to improve the purity of the retentate fraction. A final NF step was performed in order to measure the fraction of concentrated bioactive compounds from the clarified juice. NMR experiments and colourimetric assays were carried out on UF/DF and NF fractions to investigate and monitor how membrane processes affected the metabolic profile of the juice. Antioxidant activity and total content of flavonoids, polyphenols and β-carotene were the variables determined by means of UV—Visible spectroscopy, and were evaluated in combination with NMR measurements for the principal statistical analysis (PCA).

2. Materials and Methods

2.1. Tacle Juice and Juice Processing

Tacle juice was supplied by Società Agricola Terzeria S.r.l located in Francavilla Marittima (CS), Calabria. The juice was ultrafiltered by using a laboratory plant equipped with a hollow fiber membrane module supplied by Microdyn-Nadir (Wiesbaden, Germany). It featured polyethersulfone hollow fiber membranes with an inner diameter of 0.8 mm and a molecular cut-off weight (MWCO) of 500 kDa. The UF process was performed in selected operating conditions according to the batch concentration configuration in order to clarify the juice to a volume reduction factor (VRF, defined as the ratio between the initial feed volume and the volume of the resulting retentate) of 4.08. At the end of the UF process, two different streams were produced from the original juice (feed UF, abbreviated as FUF): a clarified juice (indicated as PUF) and a retentate juice (indicated as RUF). Then, the retentate was diafiltered in a continuous mode by adding water to the feed tank at the same rate as the permeate flux, so as to keep the feed volume constant during the process. Two fractions were collected at the end of the diafiltration process: a retentate stream (named as RDF) and a permeate stream (named as PDF). Both permeates resulting from ultrafiltration and diafiltration operations were then merged in the same ratio. The mixed product was then subjected to a nanofiltration process by using a laboratory plant equipped with a stainless-steel housing able to accommodate a spiral-wound membrane module with an effective membrane area of 0.38 m^2. NF experiments were performed in selected operating conditions by using two different membrane modules, both in thin-film composites supplied by Microdyn-Nadir: a membrane module with a MWCO of 200–300 Da (NF1) and a membrane module with a MWCO of 300–500 Da (NF2). The NF processes were performed up to a VRF of 3.5. A schematic layout of the investigated process is depicted in Figure 1. UF/DF and NF processes were repeated five times on five batches of Tacle juice. Each batch, previously frozen at a temperature of −18 °C, was thawed after approximately two weeks to be subjected to membrane processes, and the resulting fractions were then frozen again to be re-thawed for the analysis of chemical characteristics. All samples collected from juice processing, for a total of 50 samples, were spectroscopically and spectrophotometrically analyzed and statistically processed by PCA.

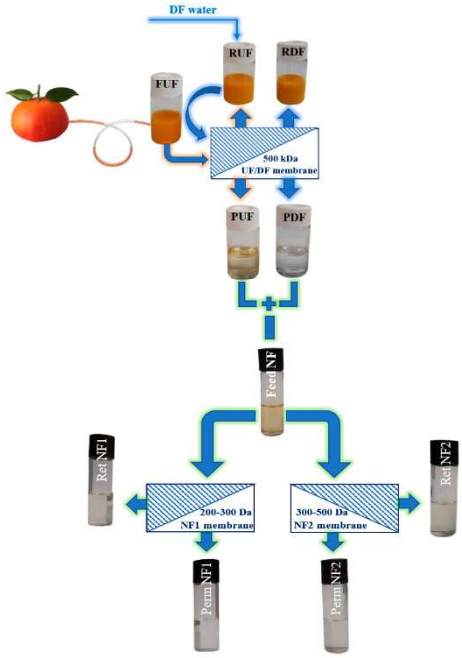

Figure 1. Schematic layout of the investigated process (UF, ultrafiltration; DF, diafiltration; NF, nanofiltration; F, feed; R, retentate; P, permeate).

2.2. NMR Sample Preparation

The chemical composition of polar compounds in Tacle juice was evaluated on a sample prepared as follows: Tacle juice (FUF) was thawed at room temperature, diluted at a 1:1 ratio with distilled water and centrifuged (6000 rpm × 5 min) to separate the supernatant from the pulp. In addition, the pH of the supernatant was measured since it is crucial for this parameter to be known before the signal's attribution phase to the various metabolites, whose resonance frequency is strongly dependent on the pH. In this specific case, the pH value of the sample was measured as 3.41. Subsequently, a volume of 500 µL of supernatant was transferred into a 5 mm NMR tube, to which 100 µL of D_2O and 20 µL of a 100 mM solution of TMSP-d_4 (sodium deuterated 3-trimethylsilylpropionate) and 20 mM of NaN_3 in D_2O were added. Deuterated water was used for locking the signal, 3-(trimethylsilyl)propionic-2,2,3,3-d4 acid sodium salt (TMSP-d_4) was used for referencing chemical shift, and sodium azide (NaN_3) was used to prevent the onset of bacteria capable of destroying juice metabolites during the recording of uni- and bi-dimensional multinuclear NMR experiments. The preparation of the NMR samples used for multivariate statistical analysis did not require uae of the internal standard nor the sodium azide, given the much shorter times for recording a single proton spectrum. NMR sample preparation for RUF and RDF were exactly the same as for FUF. These samples were diluted and centrifuged, and then 500 µL of supernatant was added to 100 µL of D_2O in an NMR tube. PUF and PDF samples were diluted as well but they did not need to be centrifuged, as they lack suspended solids which might interfere with the homogeneity of the magnetic field. Instead, all NF samples were neither diluted nor centrifuged, but weredirectly transferred in the NMR tube with D_2O, always at a 5:1 ratio. Before transferring the supernatants or samples directly into the NMR tube, the pH value was evaluated for each sample type. Utilizing NaOH or HCl solutions, the pH value of UF samples were adjusted to be the same, just as for NF samples. Equivalent pH values imply the same position in the chemical shift of the signals relating to the metabolites present, which is essential for the steps before and after PCA. A synthetic scheme of the NMR sample preparation in aqueous phase is shown in Figure 2.

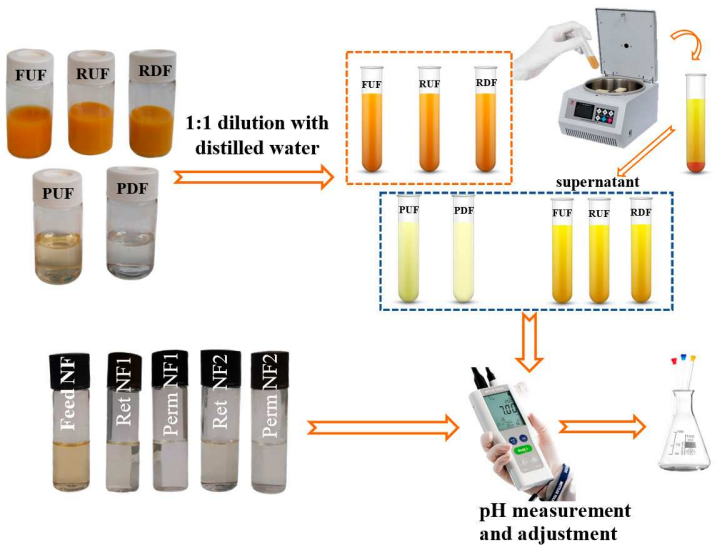

Figure 2. Polar phase sample preparation.

On the other hand, to characterize the apolar fraction of Tacle juice metabolome, a simple, efficient and low-solvent-consuming, ultrasound-assisted extraction (UAE) method was investigated utilizing the deuterated solvent $CDCl_3$. Then, 1 mL of Tacle juice (FUF) was combined with 1 mL of $CDCl_3$ containing 0.01% TMS, and placed in an Ultrasonic Bath (UAE; Hielcher UP 100 Hz, 100 W pulse, 30 kHz frequency) for 15 min. After the extraction, two separate phases were observed: the aqueous phase above, which was removed, and

the organic phase below, which was transferred into a 5 mm NMR glass tube. A synthetic scheme of the NMR sample preparation in organic phase is shown in Figure 3.

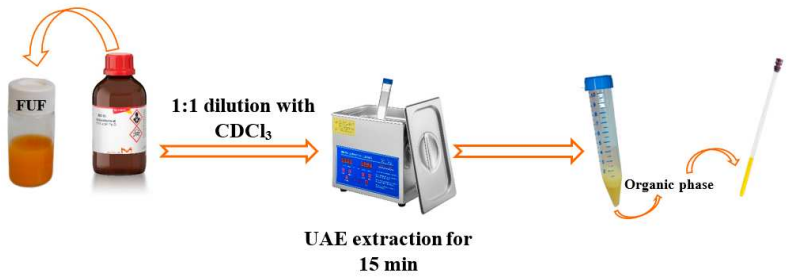

Figure 3. Organic phase sample preparation.

2.3. NMR Data Acquisition and Processing

All spectra were acquired on a Bruker Avance 500 spectrometer operating at 500.13 MHz, 298 K and a magnetic field of 11.7 tesla. To suppress the residual water signal through selective irradiation at the water frequency during the mixing and recycle delays, ^{1}H NMR spectra of polar extracts were acquired using a NOESY pre-saturation pulse sequence (Bruker sequence denoted as *noesypr1d*). For each experiment, 512 FIDs were acquired using a spectral width of 11.25 ppm and a relaxation delay of 3 s. For lipophilic extracts, ^{1}H NMR spectra were obtained using the Bruker pulse sequence *zg*. The acquisition conditions for $CDCl_3$ extracts were as follows: number of scans (NS) = 512; spectral width (SW) = 11.25 ppm; size of FID (TD) = 65,536; relaxation delay (D1) = 3 s. All ^{1}H-NMR spectra were phased and then baseline-corrected using the software TopSpin 3.6.2. (Bruker Corporation, Billerica, MA, USA). The obtained spectra were calibrated according to the internal standard. Additionally, the ^{1}H^{1}H correlation spectroscopy (COSY) and ^{1}H-^{13}C heteronuclear multiple-quantum coherence (HMQC) spectra were recorded in the aqueous and organic phases to verify metabolites' chemical shift assignments using the Bruker sequences *cosygpprqf* and *hmqcgpqf*. A sine filter and a qsine filter were applied on both dimensions, F1 and F2, respectively, on the COSY and HMQC experiments before they were Fourier-transformed.

2.4. UV—Visible Analysis of Total Polyphenols, Flavonoids, In Vitro Total Antioxidant Activity and β-Carotene

Total polyphenols were measured colourimetrically via the Folin—Ciocalteau method, as reported elsewhere [28]. Gallic acid was used as a calibration standard, and results were expressed as mg gallic acid equivalent (GAE) per liter of sample (mg GAE/L). The total flavonoid content was determined according to the Davis method [29]. Quantification was done on the basis of the standard curve of naringin (r^2 = 0.990), with the results expressed as mg naringin equivalents (NE)/L. The total antioxidant activity (TAA) was assessed via the 2,2-azino-bis (ethylbenzothiazoline-6-sulfonic acid) (ABTS) assay by monitoring the reduction of the radical cation as the percentage inhibition of absorbance at 734 nm [30]. Results of TAA were expressed in terms of mM of 6-hydroxy-2,5,7,8-tetramethylchroman-2-carboxylic acid (Trolox) equivalent. The concentration of β-carotene was determined using the spectrophotometric method reported by Lime et al. [31] and results were expressed as μg β-carotene/mL. Total content of β-carotene was quantified only in UF/DF samples because as a large and lipophilic compound, we expected to find it mostly in the starting juice and in the UF retentate fractions. Since the subsequent steps of the membrane processes (NF) concerned the use and treatment of the clarified juice, focus was placed on monitoring low molecular weight compounds, which is why β-carotene was not quantified for NF samples. Total phenolics and total flavonoids, having lower molecular weights and TAA, were instead determined for all UF/DF and NF samples. Each analysis on each sample was replicated three times, and the mean values obtained were inserted into the matrix containing the NMR data and considered as variables for the PCA statistical analysis.

2.5. Chemometric Analysis and Procedure

NMR aqueous phase spectra recorded on membrane samples were aligned, divided into uniform spectral bins (so-called buckets) of 0.05 ppm-width and the signal area was integrated for each bucket. The water region from δ 4.2–5.1 was excluded from the spectra along with the region from δ 5.5–5.9 which does not contain any significant signal. For the residual regions (δ 0.6–8.4 for UF/DF samples and δ 0.4–9.1 for NF samples), binning was performed. The buckets were normalized to the whole spectral area and exported in an Excel file. A dataset of 25 samples and 127 NMR variables had been obtained for UF/DF processes, while 25 samples and 144 NMR variables were considered for NF processes. On the 50 samples of UF/DF and NF processes, the content of total phenolics, flavonoids and antioxidant activity were quantified. For the 25 samples of UF/DF the total β-carotene was also determined. Adding these variables obtained with the UV—Visible technique, the data matrices used for the chemometric analysis were formed as follows: 25 samples and 131 variables (127 NMR + 4 UV—Vis variables) for UF/DF, 25 samples and 147 variables (144 NMR + 3 UV—Vis variables) for NF. In this way, a large block of variables (NMR variables) dominated over a smaller block of variables (UV—Visible variable) for purely numeric reasons. To address this problem and give each block the same importance, a block-scaling procedure was employed in the pre-processing phase of multivariate data [32]. This corresponds to down-weighting blocks of variables in relation to a selected basis-scaling procedure. The basis-scaling method generally entails scaling to unit variance, mainly when variables differ noticeably in nature and numerical range [33]. In this work, block-scaling treatment was carried out previously and then PCA was performed on the fused matrices, which combined NMR and UV—Vis data. Multivariate statistical analysis was performed with the Chemometric Agile Tool (CAT), an R-based chemometric software developed by the Chemistry Group of the Italian Chemical Society [34].

3. Results and Discussion

3.1. Tacle Juice Metabolic Profiling by NMR

The characterization of the metabolic profile of Tacle juice through NMR spectroscopy was performed in both aqueous and lipophilic citrus extracts to obtain as much compositional information as possible about major compounds in the tested samples. Figure 4a–c shows three ^{1}H-NMR spectral expansions of an aqueous extract of Tacle evidencing the assigned metabolites. Most of them belong to sugars, amino acids and organic acids. As mentioned before, all assignments were based on the analysis of 1D and 2D NMR experiments (reported in the supplementary material in Figures S1 and S2) and on the use of HMDB database and literature data [35,36]. Additionally, Figure 4d provides a typical ^{1}H-NMR spectrum of an organic extract where the main families of metabolites identified were fatty acids and triacylglycerols (TAGs). A numeric nomenclature is used to identify each signal, following a descending field order. The assignment of the different signals was based on previous reports on the ^{1}H-NMR analysis of fats [37–40] and is summarized in Table 1.

Table 1. ^{1}H-NMR peak assignment of a typical lipid extract from Tacle juice. Peak labels (1 to 9) agree with those given in Figure 4d.

Peak	δ ppm	Multiplicity, *J* (Hz)	Assignment
1	0.88	t, *J* = 6.8 Hz	CH_3 All acyls except linolenyl
2	1.23–1.43	m	$(CH_2)_n$ All acyl chains
3	1.55–1.68	m	CH_2CH2COOR All acyl chains
4	2.00	m	CH_2CH=CH All unsaturated fatty acids
5	2.2–2.3	m	CH_2COOR All acyl chains
6	3.73	q, *J* = 7.0 Hz	CH_3CH_2OH Ethanol
7	4.15 4.29	dd, *J* =12.0, 6.00 Hz dd, *J* =12.0, 6.00 Hz	CH_2OCOR Glycerol (triacylglycerols)
8	5.23–5.28	m	CHOCOR Glycerol (triacylglycerols)
9	5.30–5.38	m	CH=CH All unsaturated fatty acid

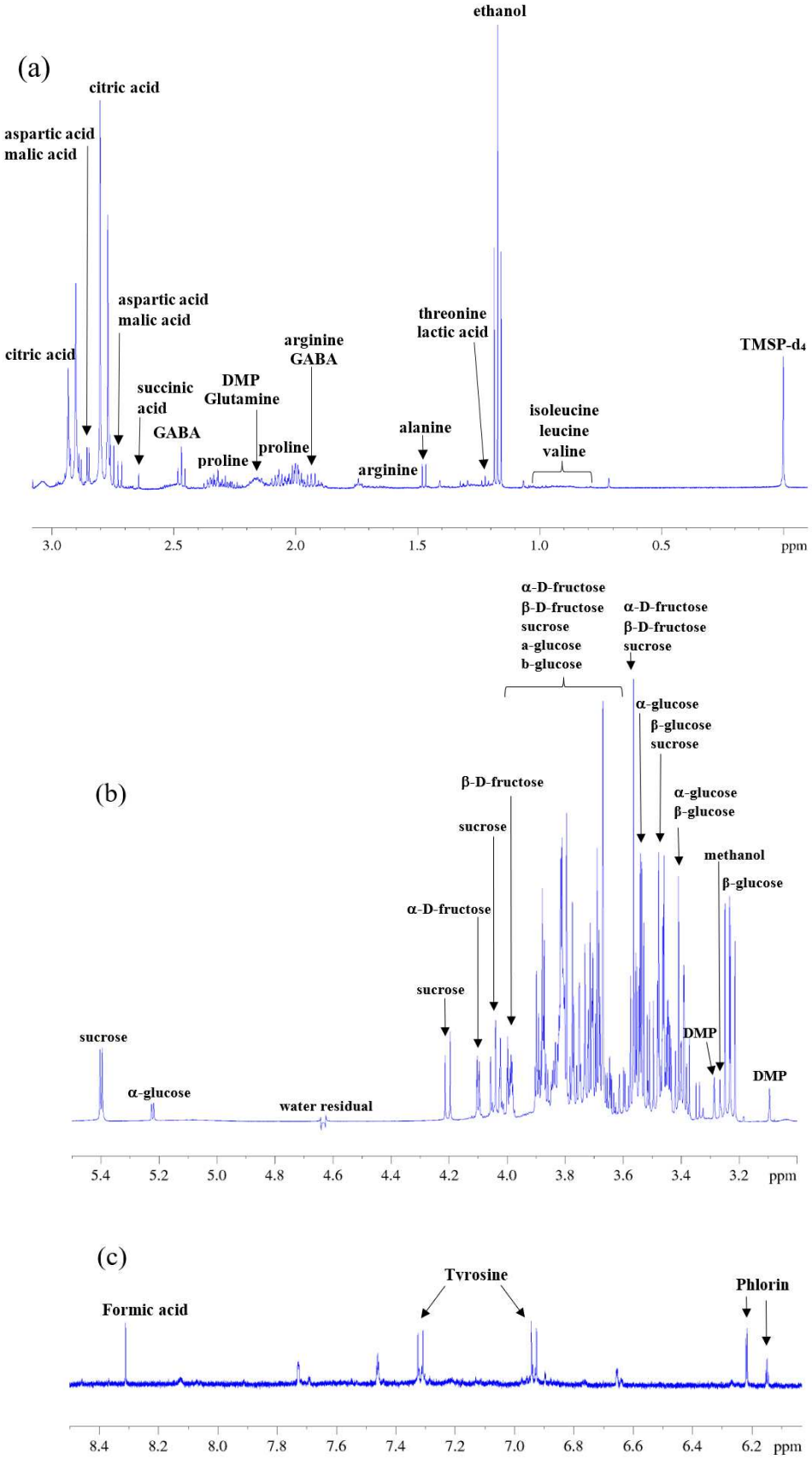

Figure 4. *Cont*.

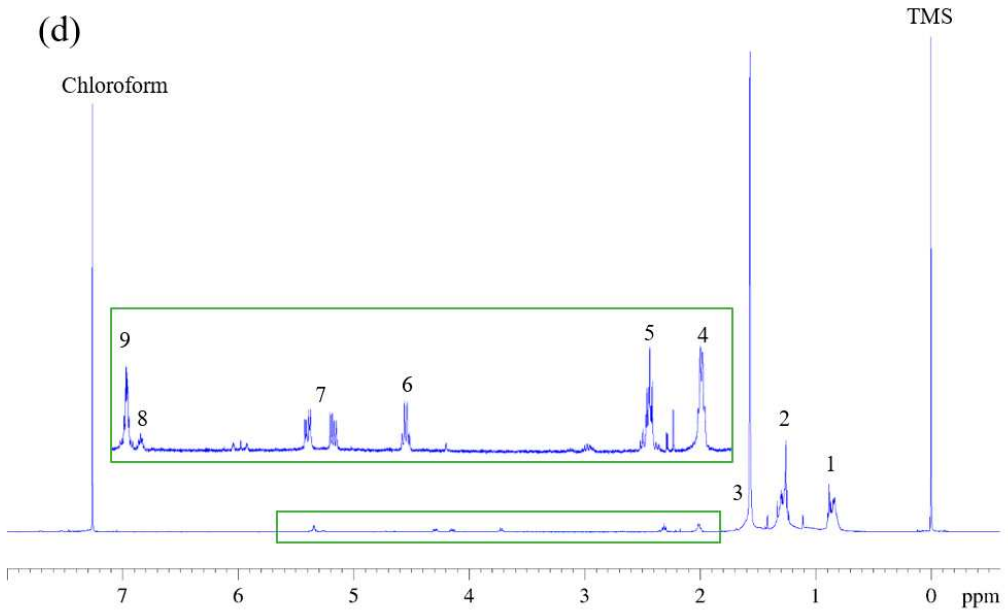

Figure 4. ^{1}H-NMR spectra obtained at 500 MHz of (**a**–**c**) the aqueous phase of Tacle juice divided into three regions (see Supplementary Material, Table S1 for assignment) and (**d**) lipophilic Tacle extract.

From a purely qualitative point of view, the metabolic profile of Tacle juice appears to be almost identical to those of the parent cultivars [20]. In the aqueous phase, a total of 11 amino acids were identified together with 6 organic acids, citric acid being the most major among them. The most crowded part of the spectrum (3.0–4.3 ppm) contains the carbinolic protons of the monosaccharide residues, particularly α- and β-glucose, α- and β-fructose, and sucrose. The remaining down-field part the proton spectrum (6–8 ppm) is diagnostic of aromatic signals and it may have some importance for glycosides with an aromatic aglycon. Such is the case for phlorin (3,5-dihydroxyphenyl-β-D-glucopyranoside), a long-discussed molecule for the authentication of citrus juices as a possible marker for fraudulent processing techniques [41], whose aromatic protons resonances fall at 6.15 ppm (triplet generated by the para-positioned proton) and at 6.22 ppm (doublet generated by the two magnetically identical, ortho-positioned aromatic protons). The extraction of the lipid fraction of the Tacle juice showed the presence of some very low-intensity signals related to fatty acids, agreeing well with the fact that it is a fruit with very few calories. Fatty acids can be distinguished in the ^{1}H-NMR spectrum only at a class level (saturated, monounsaturated, diunsaturated and polyunsaturated), and it is impossible to distinguish between signals of individual fatty chains within the same class. For instance, ^{1}H resonances of long-chain fatty acids such as palmitic and stearic acids are completely overlapped. For this reason, many assignments reported in the literature, such as in this work, are referred to as molecular fragments (methyl, methylenic, allylic methylenic groups, double bonds, etc.) rather than individual compounds [42]. Once the original juice (FUF) had been characterized, NMR spectra in the aqueous phase were recorded on the fractions obtained from membrane operations it had undergone. Figure 5 shows the NMR spectral profiles related to ultrafiltration samples (RUF and PUF) and diafiltration samples (RDF and PDF). Visually, these fractions appear to have the same metabolomic profile.

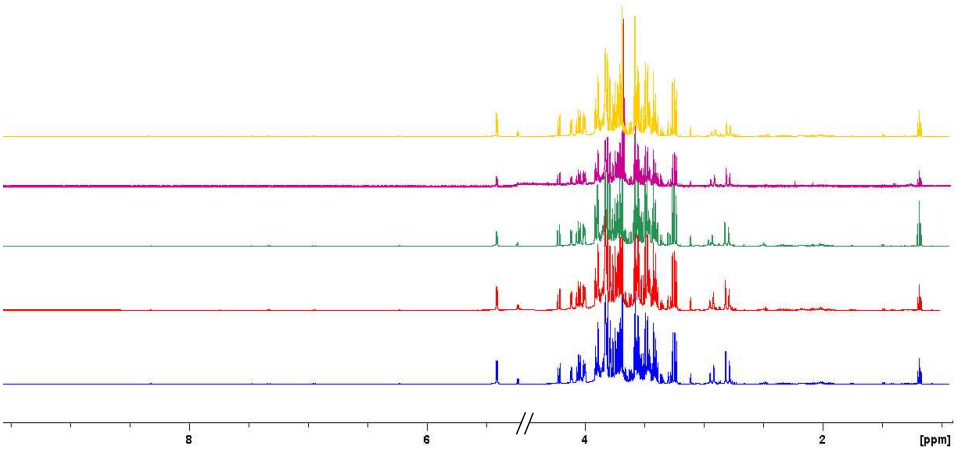

Figure 5. Comparison of ^{1}H-NMR spectra of FUF (in blue), RUF (in red) PUF (in green), RDF (in violet), and PDF (in yellow) Tacle samples.

Similarly, the high-resolution NMR spectra of the aqueous fraction were recorded for the samples coming from the nanofiltration processes, reported in Figure 6.

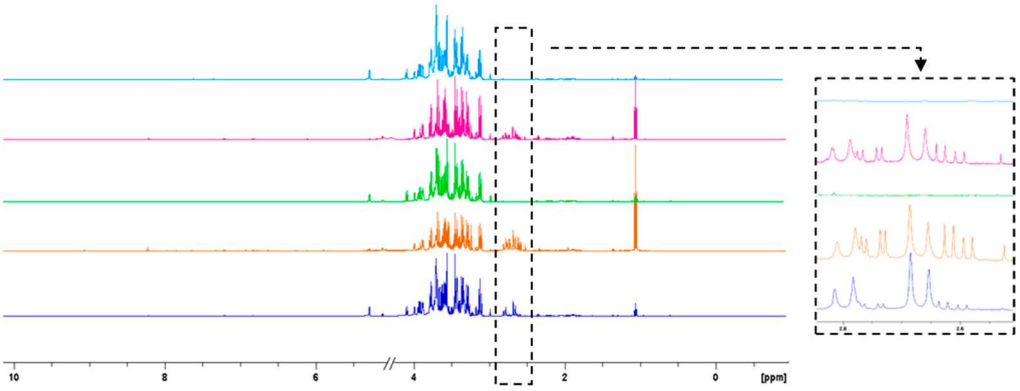

Figure 6. Comparison of ^{1}H-NMR spectra of Feed NF (in blue), Permeate NF 1 (in orange) Retentate NF 1 (in green), Permeate NF 2 (in fuchsia) and Retentate NF 2 (in light blue) Tacle samples.

In this case, NMR profiles present differences in some signals and their relative intensities. These differences are especially noticeable in the enlarged region from δ 2.55–2.85 of Figure 6, where the citric, aspartic and malic acid signals fall. In the NF feed, citric acid is present at a higher concentration than the other two acids, as NMR is an intrinsically quantitative technique [43], and with an equal number of nuclei, the area of the two generated doublets of citric acid in the ^{1}H-NMR spectrum is higher with respect to other acid signals. On the other hand, in the NF permeates, the same acids are present, but in different proportions: these fractions have a higher aspartic acid content, thus indicating that citric acid is retained much more by NF membranes with than by aspartic acid. However, in NMR spectra of NF retentates, no relevant signals corresponding to citric acid (in the region δ 2.55–2.85) can be detected. Its signals may fall into the NMR spectra background noise. Furthermore, it should be pointed out that citric acid is a Lewis acid consisting of functional hydroxyl groups, which can form complexes with other compounds and hydrogen bonds with the membrane polymer; thus, it could be partially absorbed on the membrane surface. Moreover, with the initially higher concentration of citric acid in the feed solution, its molar mass slightly higher than that of aspartic acid as well as the different pK_a values of these organic acid compounds may all contribute to determine a different behavior in terms of NF membrane rejection.

3.2. Principal Component Analysis Applied to NMR and UV—Visible Data of UF/DF and NF Samples

To better understand variable correlations, membrane sample similarities/differences, and thus the influence of integrated-membrane processes on the metabolic juice profile, NMR data (block 1) were combined with UV—visible data (block 2) in the principal component analysis (PCA). Combining data from two or more techniques is advantageous if they offer complementary information that, when added together, allows us to interpret the process comprehensively and better distinguish between the samples. For example, if we consider only the NMR variables, there is a cluster separation of UF/DF samples, but not when the UV—Vis variables are added. Figure 7 shows the PCA score plot obtained from autoscaling and processing the data matrix containing NMR data only.

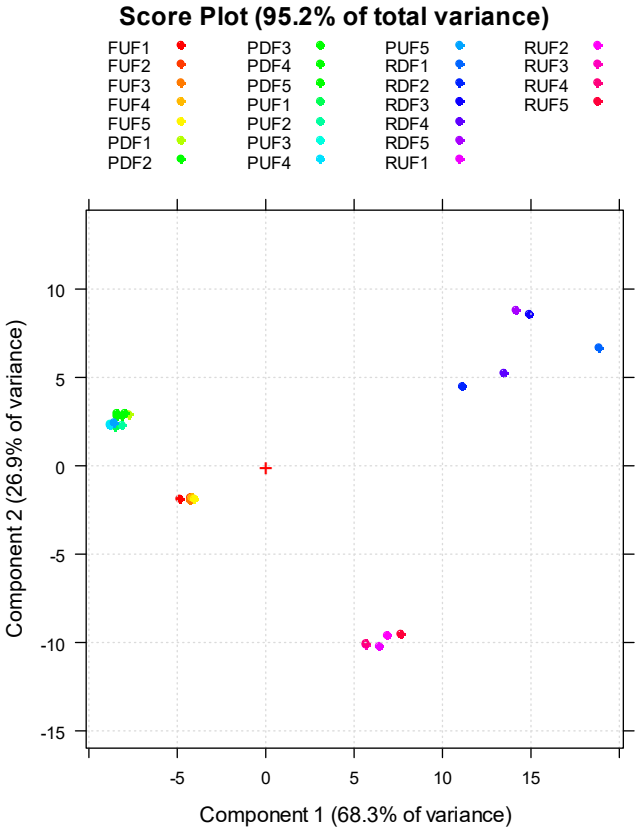

Figure 7. Principal component analysis score plot of the studied UF/DF samples using NMR data.

The two principal components in this score plot explain 95.2% of the total variance. We can observe that feed samples differ from the retentate samples (in turn, the retentates from ultrafiltration and diafiltration are separated into two different regions of the diagram). In contrast, the permeate samples separate from the feed and retentate samples but fall into the same region, indicating their similar composition in metabolites identified through NMR. Adding UV—Vis data to the NMR data (Figure 8), UF/DF samples were separated into five clusters with no notable outliers; UF permeates and DF permeates are now distinguished very well. Figure 8 shows the PCA score plot of fused NMR and UV—Vis data matrix pretreated by block-scaling. PC1 described 59.9% variation of data, while PC2 accounted for 33.5% of the total subset variance. Therefore, more than 90% of variation can be described only by the first two PCs, and this is why only PC1 and PC2 were selected for further analysis. The evaluation of the PCA score plot indicated that the clustering between FUF, RUF and PUF samples was along the PC1 variable. These samples all had approximately the same negative value of PC2, but FUF samples had PC1 = 0 and RUF samples were characterized by PC1 > 0, while PUF samples hold PC1 < 0. Thus, the PC1 component allowed for distinguished samples coming from the ultrafiltration. On the other hand,

the PC2 component permitted us to discriminate ultrafiltration samples from diafiltration samples. In fact, while the first ones were all at a negative value of PC2, the diafiltration samples (RDF and PDF) had a positive value of PC2 and were separated among them on the PC1; RDF samples were in quadrant 1 (upper right), while the PDF samples were in quadrant 2 (upper left). Further details arose from the inspection of the PC loadings of the first two PCs, which highlighted the metabolites that contributed to the samples separation. Figure 9 reports loadings deriving from NMR and UV—VIS data on different scales indicated with the same color as the corresponding loadings. Block 2, with a lower number of variables, had loadings of absolute values higher than block 1. This did not mean that variables in block 2 had more importance than variables in block 1, but only that we awarded it more significance with the block-scaling pretreatment because this block consisted of a reduced number of variables and, therefore, a reduced variance. Applying block-scaling, each block has a variance of 1 and the variables of each block have the same variance.

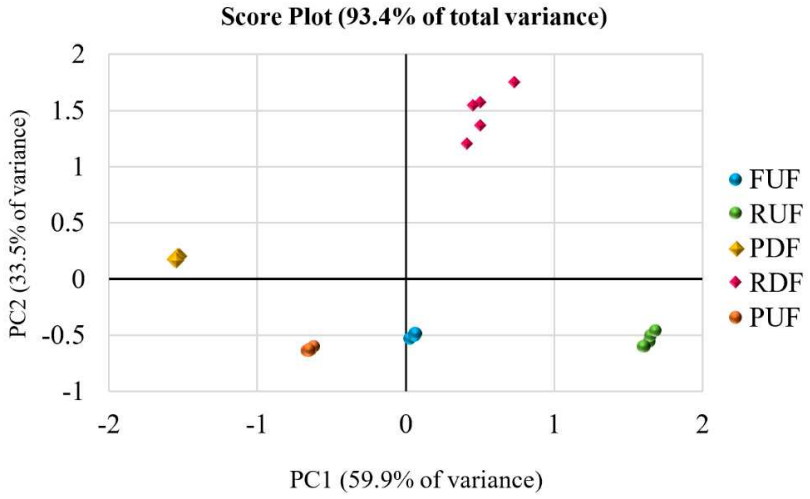

Figure 8. Principal component analysis score plot of the studied UF/DF samples using NMR and UV—Vis data.

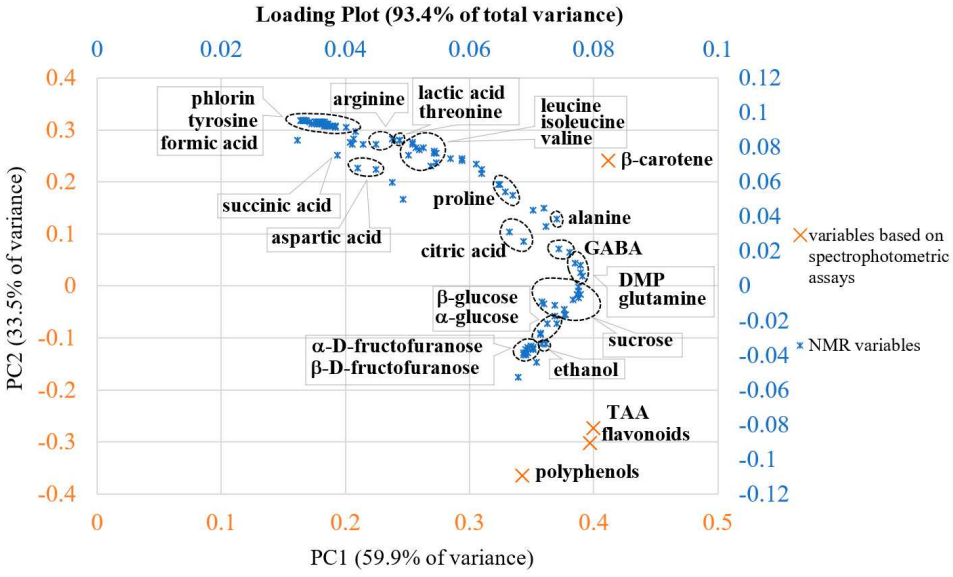

Figure 9. Principal component analysis loadings plot of the studied UF/DF samples using NMR and UV—Vis data.

Polyphenols, flavonoids and TAA were positively correlated with each other. Therefore, as expected, the antioxidant capacity was mainly attributed to polyphenol-type compounds. Comparing the position of samples in the score plot with the loadings position, it can be deduced that the samples derived from UF in the batch concentration process have the same metabolic composition, but different concentrations of all the metabolites were taken into account (in order of concentration: RUF > FUF > PUF). Thus, with the investigated membrane in the selected operating conditions, the ultrafiltration process allowed for preserving of the original juice composition in terms of antioxidant compounds, sugars, amino acids and organic acids. On the other hand, diafiltration changed the metabolic profile of the permeate and retentate products. The RDF samples were characterized by a higher concentration of β-carotene with respect to the other compounds, as it is a lipophilic phytochemical slightly soluble in water. Carotenoids are exciting sources in the food industry, for both their bioactive potential and colouring properties which make products more attractive to consumers [35]. When instead observing the PDF samples in the scores plot and looking at the loadings, it appears that they presented a lower content of sugars, polyphenols and flavonoids, and therefore a lower TAA, along with a higher content of amino and organic acids. At the end of each UF/DF process, the PDF and PUF permeates were mixed in the same ratio and nanofiltered. Additionally, for NF samples, the total polyphenols, flavonoids and antioxidant activity in vitro were quantified, ^{1}H-NMR spectra were acquired, block-scaling pretreatment was accomplished, and PCA was performed on the fused data matrix. Figure 10 shows the biplot (score and loading plot) obtained.

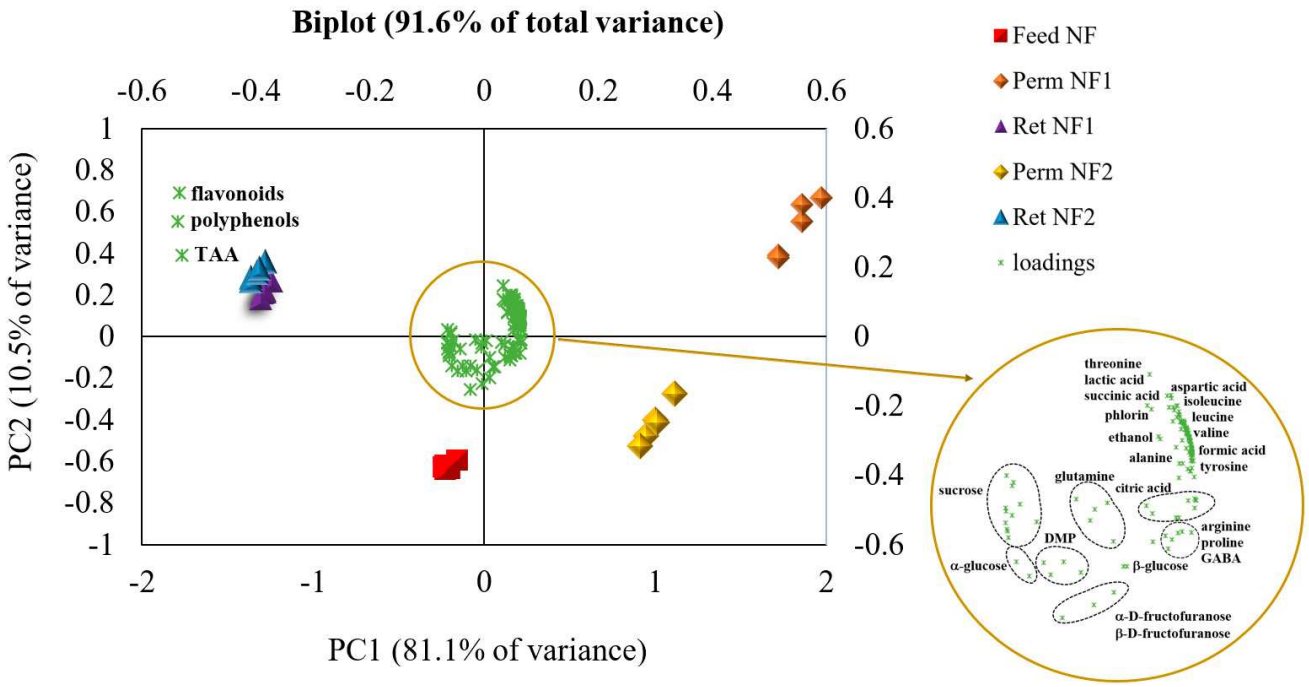

Figure 10. Principal component analysis biplot of the studied NF samples. The location of NMR-variables is indicated by the circle in which the assignments of the loadings are shown.

It was found that 91.6% of the total variance was explained by two principal components (PCs), with PC1 accounting for 81.1% of the total variance and PC2 accounting for 10.5%. With the exception of the nanofiltration retentates, the other samples are positioned in different regions of the biplot. NF Feed samples are in the third quadrant (lower left) and present a higher concentration of sugars. Permeates deriving from the nanofiltration with NF2 membrane cluster in the fourth quadrant (lower right), having a larger amount of GABA, proline and arginine. NF1 permeates are in the first quadrant (upper right), exhibiting a higher concentration of threonine, lactic and succinic acids, aspartic acid,

phlorin, isoleucine, leucine and valine. Finally, NF1 and NF2 retentates shared the second quadrant (upper left), being characterized by a close metabolite profile, mostly in terms of polyphenols, flavonoids and TAA. Therefore, under the selected operating conditions, both nanofiltration membranes were found to be suitable for the enrichment of the clarified Tacle juice in bioactive compounds.

4. Conclusions

High-resolution NMR spectroscopy has proven to be a powerful tool for the metabolomic and lipidomic analysis of Tacle juice, well recognized for its high content of bioactive compounds. In this work, the characterization of the juice by multinuclear (^{1}H and ^{13}C) 1D and 2D NMR experiments allowed us to recognize 25 metabolites in the aqueous phase and to identify triglycerides and fatty acid in the extracted organic phase. Moreover, the UV—Visible technique was applied to quantify the total content of flavonoids, polyphenols, β-carotene and TAA. In a second step of this work, membrane processes such as ultrafiltration (UF) (also in diafiltration mode) and nanofiltration (NF) were used for producing enriched fractions of bioactive compounds from the raw juice. PCA on NMR and UV—visible fused data provided graphical outputs that were easy to read and interpret, demonstrating a very effective procedure for obtaining a synthetic judgement of how UF/DF and NF membrane processes affect the metabolic profile of the juice. In addition, these techniques confirm the capability of membrane filtration processes with respect to heat treatments in preserving the chemical composition of the original juice without generating new undesirable metabolites. Further studies are underway to evaluate the performance and selectivity of UF and NF membranes in more detail.

Supplementary Materials: The following supporting information can be downloaded at: https://www.mdpi.com/article/10.3390/antiox12010002/s1, Table S1: Metabolites identified in the 500 MHz ^{1}H Spectrum of the aqueous phase of Tacle juice at pH 3.41. Figure S1: 2D ^{1}H COSY spectrum (Bruker pulse sequence: *cosygpprqf*) recorded on Tacle juice in D_2O (field strength of 11.74 T). Figure S2: 2D ^{1}H-^{13}C HMQC spectrum (Bruker pulse sequence: *hmqcgpqf*) recorded on Tacle juice in D_2O (field strength of 11.74 T).

Author Contributions: Conceptualization, M.G., G.D.L., C.C. and A.C.; investigation, M.G., G.D.L., C.C. and A.C.; supervision, G.D.L. and A.C.; methodology, M.G., G.D.L., C.C. and A.C.; formal analysis, M.G., G.D.L., C.C. and A.C.; data curation, M.G., G.D.L. and A.C.; writing—original draft, M.G., G.D.L. and A.C.; software, M.G.; writing—review and editing, G.D.L. and A.C. All authors have read and agreed to the published version of the manuscript.

Funding: This work was supported by the University of Calabria and POR Calabria—FSE/FESR 2014–2020.

Institutional Review Board Statement: Not applicable.

Informed Consent Statement: Not applicable.

Data Availability Statement: Data are contained within the article and supplementary materials.

Acknowledgments: The authors warmly thank Benito Scazziota from Società Agricola Terzeria srl soc. Benefit—Francavilla Marittima (CS) for providing the Tacle juice samples; moreover, the student Serena Oliveto is kindly acknowledged for her work on the project during her third-year internship under the supervision of G. De Luca at the University of Calabria.

Conflicts of Interest: The authors declare no conflict of interest.

References

1. Rapisarda, P.; Bellomo, S.E.; Fabroni, S.; Russo, G. Juice Quality of Two New Mandarin-like Hybrids (*Citrus clementina* Hort. Ex Tan × *Citrus sinensis* L. Osbeck) Containing Anthocyanins. *J. Agric. Food Chem.* **2008**, *56*, 2074–2078. [CrossRef] [PubMed]
2. Rapisarda, P.; Fabroni, S.; Peterek, S.; Russo, G.; Mock, H.P. Juice of New Citrus Hybrids (*Citrus clementina* Hort. Ex Tan. × *C. Sinensis* L. Osbeck) as a Source of Natural Antioxidants. *Food Chem.* **2009**, *117*, 212–218. [CrossRef]

3. Casacchia, T.; Occhiuzzi, M.A.; Grande, F.; Rizzuti, B.; Granieri, M.C.; Rocca, C.; Gattuso, A.; Garofalo, A.; Angelone, T.; Statti, G. A Pilot Study on the Nutraceutical Properties of the Citrus Hybrid Tacle® as a Dietary Source of Polyphenols for Supplementation in Metabolic Disorders. *J. Funct. Foods* **2019**, *52*, 370–381. [CrossRef]
4. Grande, F.; Occhiuzzi, M.A.; Perri, M.R.; Ioele, G.; Rizzuti, B.; Statti, G.; Garofalo, A. Polyphenols from Citrus Tacle® Extract Endowed with Hmgcr Inhibitory Activity: An Antihypercholesterolemia Natural Remedy. *Molecules* **2021**, *26*, 5718. [CrossRef]
5. Hamulka, J.; Jeruszka-Bielak, M.; Górnicka, M.; Drywień, M.E.; Zielinska-Pukos, M.A. Dietary Supplements during COVID-19 Outbreak. Results of Google Trends Analysis Supported by PLifeCOVID-19 Online Studies. *Nutrients* **2021**, *13*, 54. [CrossRef] [PubMed]
6. Kechinski, C.P.; Guimarães, P.V.R.; Noreña, C.P.Z.; Tessaro, I.C.; Marczak, L.D. Degradation kinetics of anthocyanin in blueberry juice during thermal treatment. *J. Food Sci.* **2010**, *75*, 173–176. [CrossRef]
7. Galaverna, G.; Di Silvestro, G.; Cassano, A.; Sforza, S.; Dossena, A.; Drioli, E.; Marchelli, R. A New Integrated Membrane Process for the Production of Concentrated Blood Orange Juice: Effect on Bioactive Compounds and Antioxidant Activity. *Food Chem.* **2008**, *106*, 1021–1030. [CrossRef]
8. Cassano, A.; Figoli, A.; Tagarelli, A.; Sindona, G.; Drioli, E. Integrated Membrane Process for the Production of Highly Nutritional Kiwifruit Juice. *Desalination* **2006**, *189*, 21–30. [CrossRef]
9. Conidi, C.; Castro-Muñoz, R.; Cassano, A. Membrane-Based Operations in the Fruit Juice Processing Industry: A Review. *Beverages* **2020**, *6*, 18. [CrossRef]
10. Kumar, D.; Manju, M.S.L.; Sachin, G.; Sunil, M. Positive Retention of Bioactive Compounds and Biochemical Components of Sathgudi Sweet Orange (*Citrus sinensis* L. Osbeck) Juice Concentrate by Integrated Membrane Process. *J. Food Meas. Charact.* **2022**, *16*, 4161–4170. [CrossRef]
11. Servent, A.; Abreu, F.A.P.; Dhuique-Mayer, C.; Belleville, M.P.; Dornier, M. Concentration and purification by crossflow microfiltration with diafiltration of carotenoids from a by-product of cashew apple juice processing. *Innov. Food Sci. Emerg. Technol.* **2020**, *66*, 102519. [CrossRef]
12. Polidori, J.; Dhuique-Mayer, C.; Dornier, M. Crossflow microfiltration coupled with diafiltration to concentrate and purify carotenoids and flavonoids from citrus juices. *Inn. Food Sci. Emerg. Technol.* **2018**, *45*, 320–329. [CrossRef]
13. Nath, K.; Dave, H.K.; Patel, T.M. Revisiting the Recent Applications of Nanofiltration in Food Processing Industries: Progress and Prognosis. *Trends Food Sci. Technol.* **2018**, *73*, 12–24. [CrossRef]
14. Zin, M.M.; Alsobh, A.; Nath, A.; Csighy, A.; Bánvölgyi, S. Concentrations of Beetroot (*Beta vulgaris* L.) Peel and Flesh Extracts by Reverse Osmosis Membrane. *Appl. Sci.* **2022**, *12*, 6360. [CrossRef]
15. Bera, S.P.; Godhaniya, M.; Kothari, C. Emerging and Advanced Membrane Technology for Wastewater Treatment: A Review. *J. Basic Microbiol.* **2022**, *62*, 245–259. [CrossRef]
16. Yao, L.H.; Jiang, Y.M.; Caffin, N.; D'Arcy, B.; Datta, N.; Liu, X.; Singanusong, R.; Xu, Y. Phenolic Compounds in Tea from Australian Supermarkets. *Food Chem.* **2006**, *96*, 614–620. [CrossRef]
17. Castillejos-Mijangos, L.A.; Acosta-Caudillo, A.; Gallardo-Velázquez, T.; Osorio-Revilla, G.; Jiménez-Martínez, C. Uses of FT-MIR Spectroscopy and Multivariate Analysis in Quality Control of Coffee, Cocoa, and Commercially Important Spices. *Foods* **2022**, *11*, 579. [CrossRef]
18. Rivera-Pérez, A.; Romero-González, R.; Garrido Frenich, A. A Metabolomics Approach Based on 1H NMR Fingerprinting and Chemometrics for Quality Control and Geographical Discrimination of Black Pepper. J. *Food Compos. Anal.* **2022**, *150*, 110722. [CrossRef]
19. Mattoli, L.; Gianni, M.; Burico, M. Mass Spectrometry-Based Metabolomic Analysis as a Tool for Quality Control of Natural Complex Products. *Mass Spectrom. Rev.* **2022**, e21773. [CrossRef]
20. Pappalardo, L. Pomegranate Fruit Juice Adulteration with Apple Juice: Detection by UV–Visible Spectroscopy Combined with Multivariate Statistical Analysis. *Sci. Rep.* **2022**, *12*, 5151. [CrossRef]
21. Calò, F.; Girelli, C.R.; Wang, S.C.; Fanizzi, F.P. Geographical Origin Assessment of Extra Virgin Olive Oil via NMR and MS Combined with Chemometrics as Analytical Approaches. *Foods* **2022**, *11*, 113. [CrossRef] [PubMed]
22. Yong, C.H.; Muhammad, S.A.; Aziz, F.A.; Nasir, F.I.; Mustafa, M.Z.; Ibrahim, B.; Kelly, S.D.; Cannavan, A.; Seow, E.K. Detecting Adulteration of Stingless Bee Honey Using Untargeted 1H NMR Metabolomics with Chemometrics. *Food Chem.* **2022**, *368*, 130808. [CrossRef] [PubMed]
23. Gaglianò, M.; Conidi, C.; Bartella, L.; Salvino, R.A.; Di Donna, L.; Cassano, A.; De Luca, G. An Integrated Approach Based on NMR and HPLC–UV-ESI–MS/MS to Characterize Apple Juices and Their Nanofiltration (NF) Bioactive Extracts. *Food Bioprocess Technol.* **2021**, *14*, 2273–2285. [CrossRef]
24. Salvino, R.A.; Colella, M.F.; De Luca, G. NMR-Based Metabolomics Analysis of Calabrian Citrus Fruit Juices and Its Application to Industrial Process Quality Control. *Food Control* **2021**, *121*, 107619. [CrossRef]
25. Tristán, A.I.; Abreu, A.C.; Aguilera-Sáez, L.M.; Peña, A.; Conesa-Bueno, A.; Fernández, I. Evaluation of ORAC, IR and NMR Metabolomics for Predicting Ripening Stage and Variety in Melon (*Cucumis melo* L.). *Food Chem.* **2022**, *372*, 131263. [CrossRef] [PubMed]
26. Belmonte-Sánchez, J.R.; Romero-González, R.; Martínez Vidal, J.L.; Arrebola, F.J.; Garrido Frenich, A. 1H NMR and Multi-Technique Data Fusion as Metabolomic Tool for the Classification of Golden Rums by Multivariate Statistical Analysis. *Food Chem.* **2020**, *317*, 126363. [CrossRef] [PubMed]
27. Gu, H.; Pan, Z.; Xi, B.; Asiago, V.; Musselman, B.; Raftery, D. Principal Component Directed Partial Least Squares Analysis for Combining Nuclear Magnetic Resonance and Mass Spectrometry Data in Metabolomics: Application to the Detection of Breast Cancer. *Anal. Chim. Acta* **2011**, *686*, 57–63. [CrossRef]

28. Türkyilmaz, M.; Tagı, S.; Dereli, U.; Ozkan, M. Effects of various pressing programs and yields on the antioxidant activity, antimicrobial activity, phenolic content and color of pomegranate juices. *Food Chem.* **2013**, *138*, 1810–1818. [CrossRef]
29. Davis, W.B. Determination of flavanones in citrus fruits. *Anal. Chem.* **1947**, *19*, 476–477. [CrossRef]
30. Re, R.; Pellegrini, N.; Proteggente, A.; Pannala, A.; Yang, M.; Rice-Evans, C.A. Antioxidant activity applying and improved ABTS radical cation decolorization assay. *Free Radic. Biol. Med.* **1999**, *26*, 1231–1237. [CrossRef]
31. Lime, B.J.; Griths, F.P.; O'Connor, R.T.; Heinzelman, D.C.; McCall, E.R. Spectrophotometric methods for determining pigmentation—Beta-carotene and lycopene—In ruby red grapefruit. *J. Agric. Food Chem.* **1957**, *5*, 941–944. [CrossRef]
32. Turrini, F.; Zunin, P.; Boggia, R. Potentialities of Rapid Analytical Strategies for the Identification of the Botanical Species of Several "specialty" or "gourmet" Oils. *Foods* **2021**, *10*, 183. [CrossRef] [PubMed]
33. Eriksson, L.; Byrne, T.; Johansson, E.; Trygg, J.; Vikström, C. *Multi- and Megavariate Data Analysis: Basic Principles and Applications*; MKS Umetrics AB: Malmö, Sweden, 2013; Volume 1, ISBN 9789197373050.
34. Leardi, R.; Melzi, C.; Polotti, G. CAT (Chemometric Agile Tool). Available online: http://gruppochemiometria.it/index.php/software (accessed on 15 October 2022).
35. Sobolev, A.P.; Mannina, L.; Proietti, N.; Carradori, S.; Daglia, M.; Giusti, A.M.; Antiochia, R.; Capitani, D. Untargeted NMR-Based Methodology in the Study of Fruit Metabolites. *Molecules* **2015**, *20*, 4088–4108. [CrossRef] [PubMed]
36. Ryu, S.; Furihata, K.; Koda, M.; Wei, F.; Miyakawa, T.; Tanokura, M. NMR-Based Analysis of the Chemical Composition of Japanese Persimmon Aqueous Extracts. *Magn Reson Chem.* **2016**, *54*, 213–221. [CrossRef]
37. González-Domfnguez, R.; Sayago, A.; Fernández-Recamales, Á. Fatty Acid Profiling for the Authentication of Iberian Hams According to the Feeding Regime. *Foods* **2020**, *9*, 149. [CrossRef]
38. Kumar, R.; Bansal, V.; Tiwari, A.K.; Sharma, M.; Puri, S.K.; Patel, M.B.; Sarpal, A.S. Estimation of Glycerides and Free Fatty Acid in Oils Extracted from Various Seeds from the Indian Region by NMR Spectroscopy. *J. Am. Oil Chem. Soc.* **2011**, *88*, 1675–1685. [CrossRef]
39. Alexandri, E.; Ahmed, R.; Siddiqui, H.; Choudhary, M.I.; Tsiafoulis, C.G.; Gerothanassis, I.P. High Resolution NMR Spectroscopy as a Structural and Analytical Tool for Unsaturated Lipids in Solution. *Molecules* **2017**, *22*, 1663. [CrossRef]
40. Castejón, D.; Fricke, P.; Cambero, M.I.; Herrera, A. Automatic 1H-NMR Screening of Fatty Acid Composition in Edible Oils. *Nutrients* **2016**, *8*, 93. [CrossRef]
41. Jungen, M.; Schütz, B.; Schweiggert, R. Influence of Species and Processing Techniques on Phlorin in Citrus Juices as Quantified by 1H-NMR Spectroscopy. *LWT* **2020**, *134*, 109949. [CrossRef]
42. Mannina, L.; Sobolev, A.P.; Viel, S. Liquid State 1H High Field NMR in Food Analysis. *Prog. Nucl. Magn. Reson. Spectrosc.* **2012**, *66*, 1–39. [CrossRef]
43. Malz, F.; Jancke, H. Validation of Quantitative NMR. *J. Pharm. Biomed. Anal.* **2005**, *38*, 813–823. [CrossRef] [PubMed]

molecules

MDPI

Article

NMR Spectroscopy Applied to the Metabolic Analysis of Natural Extracts of *Cannabis sativa*

Maria Francesca Colella [1], Rosachiara Antonia Salvino [1], Martina Gaglianò [1], Federica Litrenta [2], Cesare Oliviero Rossi [1], Adolfo Le Pera [3] and Giuseppina De Luca [1,*]

[1] Department of Chemistry and Chemical Technologies (CTC), University of Calabria—UNICAL, Via P. Bucci 14C, 87036 Arcavacata di Rende, Italy; mariafrancesca.colella@unical.it (M.F.C.); rosachiara.salvino@unical.it (R.A.S.); martina.gagliano@unical.it (M.G.); cesare.oliviero@unical.it (C.O.R.)
[2] Department of Biomedical, Dental and Morphological and Functional Imaging Sciences (Biomorf), University of Messina, Polo Universitario dell'Annunziata, 98168 Messina, Italy; federica.litrenta@unime.it
[3] Calabra Maceri e Servizi s.p.a., Via M. Polo 54, 87036 Rende, Italy; laboratorio@calabramaceri.it
* Correspondence: giuseppina.deluca@unical.it

Abstract: *Cannabis sativa* is a herbaceous multiple-use species commonly employed to produce fiber, oil, and medicine. It is now becoming popular for the high nutritional properties of its seed oil and for the pharmacological activity of its cannabinoid fraction in inflorescences. The present study aims to apply nuclear magnetic resonance (NMR) spectroscopy to provide useful qualitative and quantitative information on the chemical composition of seed and flower *Cannabis* extracts obtained by ultra-sound-assisted extraction, and to evaluate NMR as an alternative to the official procedure for the quantification of cannabinoids. The estimation of the optimal ω-6/ω-3 ratio from the ^{1}H NMR spectrum for the seed extracts of the *Futura 75* variety and the quantitative results from the ^{1}H and ^{13}C NMR spectra for the inflorescence extracts of the *Tiborszallasi* and *Kompolti* varieties demonstrate that NMR technology represents a good alternative to classical chromatography, supplying sufficiently precise, sensitive, rapid, and informative data without any sample pre-treatment. In addition, different extraction procedures were tested and evaluated to compare the elaboration of spectral data with the principal component analysis (PCA) statistical method and the quantitative NMR results: the extracts obtained with higher polarity solvents (acetone or ethanol) were poor in psychotropic agents (THC < LOD) but had an appreciable percentage of both cannabinoids and triacylgliceroles (TAGs). These bioactive-rich extracts could be used in the food and pharmaceutical industries, opening new pathways for the production of functional foods and supplements.

Keywords: *Cannabis sativa* L.; cannabinoid extraction; NMR spectroscopy; qNMR; metabolic profile; principal component analysis

Citation: Colella, M.F.; Salvino, R.A.; Gaglianò, M.; Litrenta, F.; Oliviero Rossi, C.; Le Pera, A.; De Luca, G. NMR Spectroscopy Applied to the Metabolic Analysis of Natural Extracts of *Cannabis sativa*. *Molecules* **2022**, *27*, 3509. https://doi.org/10.3390/molecules27113509

Academic Editor: Akihito Yokosuka

Received: 22 April 2022
Accepted: 26 May 2022
Published: 30 May 2022

1. Introduction

Cannabis sativa is a fast-growing annual dioecious weed, probably native to Central Asia and the Indian subcontinent [1,2], belonging to the *Cannabaceae* family (order *Urticales*) [3]. Despite its critical taxonomic definition, because of its complex chemical composition and the presence of several spontaneous generations of hybrid species, nowadays, classifying *Cannabis* as a highly polymorphic and hybridized monotypic genus (*Cannabis sativa* L.) is the most accepted definition. Cannabis is one of the oldest and most versatile sources of intoxicating resin, textile fiber, and phytocannabinoids, which are extracted from different parts of the plant, especially from the inflorescence and for seed oil. Hemp seed oil, obtained from *Cannabis sativa L.* seeds, is highly appreciated for its nutritional, anti-inflammatory, antioxidant, and immune-stimulating properties [4]. It is practically free of cannabinoids [5], so it has no psychoactive action but, like other common vegetable oils, it is rich in essential fatty acids [6]. As reported in several works, this oil is a rich source of ω-3 and ω-6 polyunsaturated fatty acids (almost 80%), in particular, linoleic acid

(LA) and α-linolenic acid (αLA), with a ω-6/ω-3 ratio approximately equal to 3:1 [7]. Although various factors, such as cultivation area, cultivar, seed origin, agronomic cultivation practices, etc., affect both the chemical composition and the ω-6/ω-3 ratio [4,7], this ratio is considered an optimal nutritional value in the prevention of the risk of coronary heart disease [8,9]. Due to this characteristic, cannabis seed oils are authorized and widely used in the food sector [10], such as in the production of functional foods. Despite the growing interest in this product, specific regulations to evaluate its analytical quality parameters are still lacking [7]. In this context, it would be desirable to find methodologies that can provide useful and rapid information both on the chemical composition and on the important ω-6/ω-3 ratio.

The female inflorescences of the *Cannabis* plant have been widely used in the traditional medicine of different populations thanks to the pharmacological activity of some phytocannabinoids present in large quantities in these parts of the plant [11]. Phytocannabinoids are a class of terpenophenolic compounds with a 21-carbon backbone: 120 of these molecules naturally present in the plant have been identified and isolated to date [3,12,13]. These natural molecules are different from synthetic cannabinoids, generally used as therapeutic agents, and from endocannabinoids, which are endogenous lipid-based retrograde neurotransmitters capable of interacting with cannabinoid receptors in the human body [14]. The renewed and recent interest in cannabis is due to the identification of these molecules, whose different pharmacological activities such as anti-inflammatory action, cell growth inhibition, and tumor regression seem to be supported by numerous experimental evidence [15–17]. The chemical structures of the most common cannabinoids present in the cannabis plant are shown in Figure 1. Among them, the most representative are the well-known psychotropic agent Δ^9-trans-tetrahydrocannabinol (Δ^9-THC), cannabidiol (CBD), and its precursor cannabidiolic acid (CBDA). Compared to THC, CBD shows therapeutic benefits without euphoric or dysphoric effects, which is an advantage for clinical applications [15–17]. CBD has become very popular over the years for its health benefits, and nowadays is commercially available as a dietary supplement, a lotion, and most importantly, as a CBD oil. Indeed, the interest from the scientific community in the therapeutic potential of CBD oil is growing every day [18]. The reason is simple: it has already been used in various scientific studies for the treatment of numerous health problems, and is now recognized as one of the main elements of the so-called "therapeutic *Cannabis*" [19–21]. Industrial hemp crops, with a low THC content, have always been exploited as food and as a source of textile fibers, but they disappeared in the 1970s due to their association with the type of plants rich in THC [22]. The reintroduction of the cultivation of some hemp cultivars to produce fibers and seeds with a THC content lower than 0.2% *w*/*w* took place only several years later, i.e., in 2009, by means of an appropriate regulation published by the European Union [23]. Nowadays, in many countries, *Cannabis sativa* cultivations and medicines have been legalized under certain conditions due to their immense prospects in various medicinal applications [24,25]. The Italian legislation on *C. sativa* cultivation is somewhat ambiguous regarding the legal and illegal uses and cultivation of the plant, and differs based on the concentration of psychoactive cannabinoids. The law 242/2016 "Dispositions for the promotion of cultivation and supply chain of agro-industrial hemp" [26] is the most recent regulation in that direction, and is the reference text governing industrial hemp production in Italy for fiber or other industrial uses different from pharmaceutics, with cultivation based around certified seeds [27]. This measure establishes that the THC level must not exceed 0.2 %. However, even more recently, on 4 November 2019, the Italian Ministry of Health approved and ratified the "Definition of maximum levels of tetrahydrocannabinol (THC) in food" (GU n.11, 15-1-2020) [28]. This document fixes the content of THC at a maximum of 2 mg per kilo (0.0002%) in hemp seeds, flour, and derived foods and at a maximum of 5 mg per kilo (0.0005%) for the oil obtained from hemp seeds. It should be noted that the list of regulated foods provided in the appendix includes only seeds, flours and oil, but it seems that it will soon be updated based on new scientific evidence. Currently, the "Union method for the quantitative determination of the

Δ9-tetrahydrocannabinol content in hemp varieties", described by the annex III of the Commission Delegated Regulation (EU) 2017/1155 (last updated on 15 February 2017), is the only official procedure that member states must use for the quantitative determination of THC by gas chromatography (GC) after extraction with a suitable solvent [29]. It describes in detail everything about sampling, including sample dimensions, drying and storage, and techniques and reagents for the extraction and determination of THC, and it provides an allowed tolerance equal to 0.03% in absolute value. However, this official method is quite laborious, and the scientific community is always looking for advanced methodologies that will allow us to rapidly analyze natural mixtures without requiring manipulations or separations. An effective alternative to classical analytical methodologies could be the use of nuclear magnetic resonance (NMR) spectroscopy. NMR spectroscopy is a powerful and versatile technique that has progressively become a well-established tool in different areas of scientific research such as medicine, biology, and chemistry. The importance of NMR in the structural investigation of chemical compounds in liquid or solid phases is widely known, and its applicative power in addition to mass spectrometry (MS) has brought satisfactory results, particularly in the metabolic characterization of complex mixtures such as foods or natural extracts [30]. Despite it yielding relatively low-sensitivity measurements compared to MS (10 to 100 times better) with lower limits of detection (LOD), typically with an order of magnitude around micromolar [31], high-resolution NMR is becoming increasingly popular for fingerprinting as well as profiling. In particular, compared to MS, NMR spectroscopy is non-destructive, non-biased, non-invasive, does not damage analytes, and allows the use of samples such as tissues obtained, e.g., from biopsies, for further experiments [30]. Moreover, this technique is often fast and with low operating costs, it is easily quantifiable, and requires little or no chromatographic separation, sample treatment, or chemical derivatization. NMR is also a multinuclear technique that permits the routine and contemporaneous identification of a wide range of metabolites (such as sugars, organic acids, alcohols, polyols, and other highly polar compounds) in a highly quantitative and reproducible way thanks to 1D and 2D experiments. In addition, the combination of this high-throughput technique with chemometric methods is extremely advantageous because it gives the possibility to visualize, maximize, and therefore analyze the useful information contained in the experimental NMR data. The research presented in this work is placed in this scenario and aims to apply NMR methodologies to the study of natural extracts from the seeds and inflorescences of different cultivars of *C. sativa* with a THC/CBD << 1 ratio [32–35].

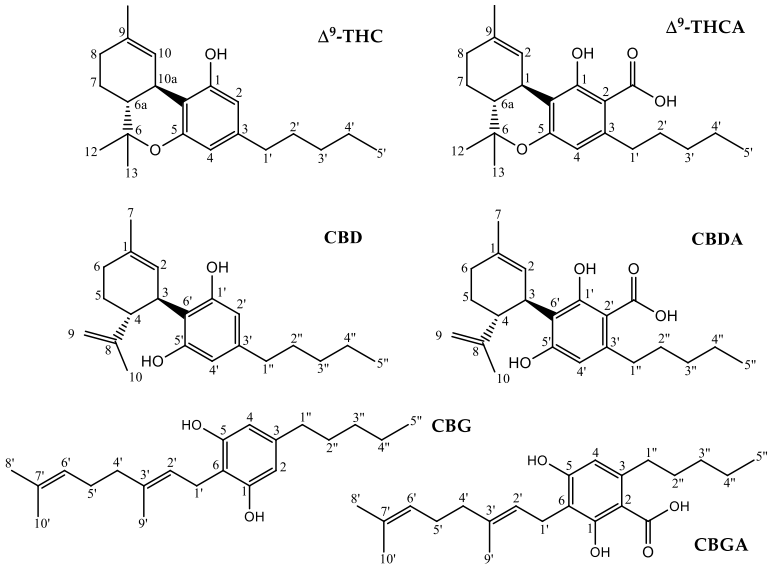

Figure 1. Chemical structure and nuclei numbering of molecular fragments in hemp principal cannabinoids.

Specifically, the work aims to: (a) characterize the chemical profiles of the inflorescences and seeds for different varieties of *C. sativa* grown in Calabria (South of Italy) via NMR spectroscopy and, in particular, by using 1D (^{1}H NMR, ^{13}C NMR) and 2D (^{1}H COSY, ^{1}H-^{13}C HMQC, ^{1}H *J*-Res) experiments; (b) evaluate the extraction efficiency of different common solvents such as hexane, acetone and ethanol; (c) perform a multivariate statistical analysis (principal component analysis—PCA) based on 1D NMR data to discriminate samples coming from different extractive processes and/or varieties by identifying correlations between the metabolites that influence each metabolic profile; (d) and perform a quantification via NMR of the main cannabinoids (CBD, CBDA, and eventually Δ^9-THC) using different internal standards.

2. Materials and Methods

2.1. Plant Material and Extraction Procedure

In this work, two different varieties of hemp were considered—*Tiborszallasi* and *Kompolti*—for both the metabolic characterization of inflorescences and for the quantitative and statistical analyses. NMR assignments were made on both varieties. Hemp inflorescences from *Tiborszallasi* and *Kompolti* grown in Calabria were harvested in September 2020, i.e., in the ripening period for both cases, selecting a reasonable number of plants for each cultivar located a few meters away in the same crop. All the collected hemp inflorescences were naturally air-dried, manually separated from twigs, and finely chopped. After this procedure, the samples were stored in the dark at 4.0 °C until analysis. Moreover, the chemical composition of the seed extracts was also investigated via NMR. The seed samples were collected from the *Futura 75* cultivar by selecting, as for the inflorescences, an appropriate number of plants representative of the entire crop. The dry seeds were ground into a powder and stored in the dark at 4.0 °C until analysis.

All inflorescence and seed samples were provided by "Calabria Maceri e Servizi S.p.A." (Rende, CS, Italy), while the crops were produced by the farm "Le Querce S.r.l" (Montalto Uffugo, CS, Italy).

The storage, pre-treatment sampling, and extraction procedures for the inflorescences of the *Tiborszallasi* and *Kompolti* varieties were mostly in accordance with the official "Union method for the quantitative determination of the Δ^9-tetrahydrocannabinol content in hemp varieties" (Annex III of the Commission Delegated Regulation (EU) No. 639/2014, 11 March 2014) [29]. In order to evaluate the efficiency of the extraction and thus highlight any differences between the various extracts, different extraction solvents commonly available in chemical laboratories and with increasing polarity were chosen. The solvents used were n-hexane, acetone, and ethanol. For each sample, 1.0 g of dried, chopped, and stored inflorescence was extracted with 45 mL of solvent at room temperature for 20 min using an ultrasonic bath (30 kHz frequency). The obtained extracts were centrifuged for 5 min at 3000 rpm, the solutions were paper filtered, and the residues were extracted once more using the same procedure with another 45 mL of the same solvent. Lastly, the solvents were completely removed under vacuum. Starting from the same dried inflorescence matrix, 24 extractions were carried out for each variety. For the *Tiborszallasi* variety, 9 extractions were performed using ethanol and acetone and 6 using hexane, while for the *Kompolti* variety, 9 extractions were performed using hexane and ethanol and 6 using acetone. For the quantitative analysis, for both varieties, each extraction was carried out in triplicate to calculate an average value for the extraction yield and estimate the relative error. Then, three samples were collected for each solvent for a total of nine extracts for each variety. In addition, a quantitative analysis with gas chromatography (GC) using the flame ionization detector (FID) method was conducted on samples of the *Tiborszallasi* variety prepared from the same dried inflorescence matrix as the NMR samples by following the protocol reported in the literature [29]. It should be emphasized that, given the chemical complexity of *C. sativa*, the extraction and collection of its various bioactive compounds are not simple and, for this reason, both solvents and different extraction methods are reported in the literature, ranging from microwave-assisted extraction to supercritical fluid extraction [36].

The extraction procedure for seeds of *Futura 75* were based on dynamic-maceration ultrasound-assisted extraction (UAE; Hielcher UP 100Hz, 100 W pulse, 30 kHz frequency), using ethanol as the solvent. Then, 2.00 g of seeds—dried, chopped and stored—were extracted with 45 mL of ethanol at room temperature for 20 min under magnetic stirring. The solution was then paper filtered, evaporated under vacuum at 30 °C, and the residue was extracted with the same procedure one more time with another 45 mL of same solvent [37]. The schematic experimental steps are shown in Figure 2.

Figure 2. Schematic experimental steps involved in the extraction, sample preparation, and NMR characterization of *C. sativa* seeds and inflorescences.

2.2. Chemicals and Solvents

Pure solvents, ethanol (Absolute, ≥99.8%—VWR Chemicals, Briare, France), n-hexane (Laboratory Reagent, ≥95%—Sigma Aldrich, Darmstadt, Germany) and acetone, (ACS Reagent, ≥99.5%—Sigma Aldrich, Darmstadt, Germany) were used for the cannabinoid extractions. Deuterated chloroform ($CDCl_3$—99.95 atom % D) as the solvent for NMR sample preparation, and anthracene, benzoic acid and 3-(trimethylsilyl) propionic-2,2,3,3-d_4 acid (TMSP-d_4—98 atom % D) as internal analytical standards for the quantitative NMR analysis were purchased from Sigma-Aldrich (Milan, Italy).

2.3. NMR Sample Preparation, Experimentation, and Data Processing

To prepare the NMR sample, after the evaporation under vacuum, 30.0 mg of seed extract of *Futura 75* was dissolved in $CDCl_3$ (~1 mL) directly in a 5 mm *o.d.* NMR tube. In this solution, the ^{1}H NMR spectrum (spectral width (SW) of 14.00 ppm, 128 free induction decays (FIDs) and a relaxation delay of 5.0 s) and the 2D ^{1}H COSY experiment (SW of 14.00 ppm on both dimensions, 2K data points, 40 scans, and 256 increments) were recorded. Two other similar extraction procedures were repeated on the same starting matrix of the dried seeds. From these extracts, 1D ^{1}H NMR spectra were recorded to be used for reproducibility and standard deviation in the calculation of the essential fatty acids ratio. ^{1}H NMR spectra were manually phased, baseline-corrected, and the chemical shifts were reported with respect to the TMS signal used as reference. From the ^{1}H NMR spectra of these extracts, the main fatty acids ω-6/ω-3 ratio can be determined by combining the integrals, obtained after applying the deconvolution procedure, of three different signals: (a) the methyl protons of all the acyl groups (LA), with the exception of those of α-linolenic acid; (b) the methyl protons of ω-3 fatty acid (α-linolenic acid (αLA)); (c) the methylene protons of the linoleic and α-linolenic acyl groups; and using the relations [38]:

$$\alpha\text{LA} = \frac{(\text{b})}{(\text{b}) + (\text{a})} \quad (1)$$

$$\text{LA} = \frac{3{\cdot}(\text{c}) - 4{\cdot}(\text{b})}{3{\cdot}[(\text{b}) + (\text{a})]} \quad (2)$$

The extract residues of the two inflorescence varieties were dissolved in 1.20 mL of $CDCl_3$ and 600 µL of this solution was transferred into a 5 mm *o.d.* NMR tube. For the quantitative analysis, samples of hemp in $CDCl_3$ were prepared by carefully weighing all the components and by adding 0.3 mg of internal standard (anthracene, benzoic acid

and TMSP-d_4). No additional treatment was necessary for the preparation of the NMR samples [39,40].

All the NMR experiments were performed on a Bruker Avance 500 MHz spectrometer (Bruker, Fällanden, Switzerland) working at a field strength of 11.74 T (500 MHz ^{1}H Larmor frequency), equipped with a 5 mm multinuclear probe TBO (triple-resonance broadband observe) and a standard variable-temperature control unit BVT-3000 (Bruker, Fällanden, Switzerland). All isotropic spectra were recorded at room temperature with $CDCl_3$ used as a field-frequency lock signal.

Spectral assignments of metabolites were based on the one-dimensional (1D) ^{1}H, ^{13}C, and ^{13}C-{^{1}H} NMR spectra, the bi-dimensional (2D) homo- and heteronuclear correlation NMR experiments (^{1}H COSY, ^{1}H-^{13}C HMQC) and by comparison with the data reports in the literature [39–41]. In addition, J_{ij} couplings between some pairs of protons were measured thanks to the homonuclear 2D experiment of ^{1}H *J*-Resolved spectroscopy (*J*-Res) [42,43]. For each ^{1}H NMR experiment, 128 FIDs were acquired using a spectral width of 14.00 ppm and a relaxation delay of 5.0 s. The 1D ^{13}C-{^{1}H} NMR spectra were recorded with proton broad-band decoupling, collecting 8K FIDs using a SW of 250.00 ppm and a relaxation delay of 5.0 s. For an accurate quantitative analysis of the metabolites present in the complex mixture, it was necessary to calibrate both the 90° pulses on the monitored nuclei (^{1}H and ^{13}C) and the T1 spin-lattice relaxation time. The T1 relaxation time was estimated by using the conventional inversion recovery experiment (10 increments from 0.5 ms to 30.0 s for ^{1}H, and 24 increments from 0.1 ms to 300.0 s for ^{13}C) [44]. The ^{1}H quantitative NMR (qNMR) spectra were recorded using the same acquisition parameters described before but with a relaxation delay of 20.0 s. Instead, for ^{13}C qNMR, quantification experiments (*zgig* Bruker pulse sequence) were performed, collecting 4000 FIDs using a SW of 250.00 ppm, a relaxation delay of 160.0 s, and an acquisition time of 10.0 s.

The initial relative quantification was obtained using Equation (3), in which the molar ratio $\frac{M_X}{M_Y}$ between the metabolites to quantify (X) and the internal standard (Y) is reported as a function of the ratio between their integral (I_X and I_Y) and the ratio of resonant nuclei that generates the considered signal (N_X and N_Y) [45,46].

$$\frac{M_X}{M_Y} = \frac{I_X}{I_Y} \cdot \frac{N_Y}{N_X} \tag{3}$$

Then, on the basis of the mass of extract used to prepare the NMR sample and the relative extraction yield, the absolute quantification was obtained in terms of the percentage of the dry weight of the hemp flowers.

The ^{1}H COSY experiments were acquired using a SW of 14.00 ppm in both dimensions, 2K data points, 40 scans, and 256 increments; the ^{1}H-^{13}C HMQC spectra were recorded using SWs of 14.00 ppm (^{1}H) and 250.00 ppm (^{13}C), 2K datapoints, 512 scans, and 40 experiments, and ^{1}H *J*-Res spectra were acquired with a SW of 12.00 ppm, 2K datapoints, 256 scans, and 48 experiments. A *sine* and a *qsine* filter were applied in both dimensions, F1 and F2, for the COSY and HMQC experiments, respectively, before being Fourier-transformed. Then, 1D NMR spectra were Fourier-transformed and manually phased, baseline-corrected, and aligned using the TMS signal as a reference. ^{13}C-{^{1}H} NMR spectra were filtered with 1.0 Hz line broadening before Fourier transformation. For the multivariate statistical analysis, the ^{1}H NMR spectra were segmented in a rectangular bucket fixed at 0.05 ppm. The integration region was defined in the first proton spectra and next it was reported, once saved, in the other spectra bucketed automatically. In particular, variables were manually selected by choosing the regions of NMR spectra with characteristic signals of metabolites and eliminating regions with a poor signal-to-noise ratio. Therefore, regions selected for the subsequent statistical treatment were 0.50–1.15 ppm, 1.3–2.6 ppm, and 3.8–7.0 ppm. Once normalized, the integrals were organized in a data matrix that was mean-centered and scaled. All the data processing steps were carried out using TopSpin 3.6 software (Bruker BioSpin, Rheinstetten, Germany) (TopSpin, 2018) [47].

2.4. Statistical Analysis: Principal Component Analysis (PCA)

Multivariate analysis was performed on the 48 1D ^{1}H NMR experiments recorded from the samples prepared from the extracts obtained with different extractive solvents. There were 24 samples for both varieties: *Tiborszallasi* and *Kompolti*. It should be noted that each sample prepared came from a different extract, i.e., for example, the 9 samples of *Kompolti* in hexane were obtained from 9 extractive procedures of the corresponding inflorescences. Among the possible statistical approaches, in this work, principal component analysis (PCA) was used as an explorative method. PCA is a technique able to reduce the dimensionality of a multivariate problem without losing information. This mathematical treatment allows us to clearly visualize samples in a two- or three-dimensional space and reveals trends in the data or groupings of samples (clusters) based on their similarity [48–50]. This methodology, applied to the data matrix of the bucketing ^{1}H NMR spectra of all extract samples, obtained as described in the previous subsection, allowed us to obtain two datasets of 24 samples and 130 variables for each variety that were used as starting points to carry out PCA analysis using R software (R software (R Core Team, 2019)) (Vienna, Austria) [51].

2.5. Chromatographic Experiments

GC-FID analysis was intended to verify the qNMR results for the *Tiborszallasi* variety. It was carried out by using the protocol reported in [29] and a gas chromatograph (GC) equipped with a split/splitless injector and a flame ionization detector (FID) (Dani Master GC1000, Dani instrument, Milan, Italy).

3. Results and Discussion

3.1. NMR Characterization of Seeds Extracts

Figure 3 shows the 1D ^{1}H NMR spectrum of a sample of hemp seed extracts prepared as described in Section 2.1.

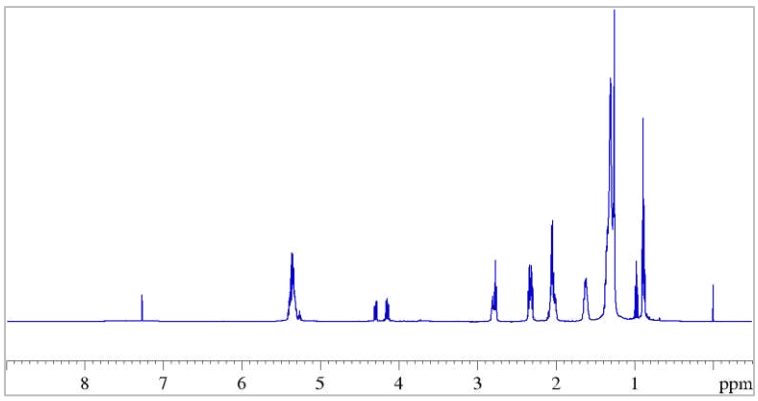

Figure 3. ^{1}H NMR spectrum (500 MHz) of hemp seed oil dissolved in $CDCl_3$ recorder at 298K, obtained with ultrasound-assisted extraction (UAE) procedure.

From the proton spectrum, it is possible to recognize the classic profile of the esters of polyunsaturated fatty acids (PUFAs) [52,53] and, from the 2D ^{1}H COSY spectrum, it is possible to trace all the correlations of the triacylglycerols (TAGs) containing both saturated and unsaturated fatty acids, as shown in Figure 4.

Let us consider, for example, the strong signal generated by the α-methylenic protons of all acyl chains (H_A, Figure 4) detected between 2.27 ppm and 2.37 ppm. Clearly, the resonance frequency of the group of nuclei (labelled in Figure 4) for all fatty acids was not exactly the same, and it depended on the nature of the chain to which they belonged. Consequently, it was not possible to determine a well-resolved multiplicity to the final complex signals appearing in the spectrum due to the overlap of all these signals with slightly different chemical shifts. For this reason, it was indicated as a multiplet (*m*) and the corresponding range of chemical shift is reported in Table 1, in which the correlations

obtained from the COSY spectrum for these protons are also reported. The same reasoning is valid for all the other signals reported as multiplets in Table 1, which summarizes all assignments for hemp seed extracts obtained from the ^{1}H and ^{1}H COSY spectra.

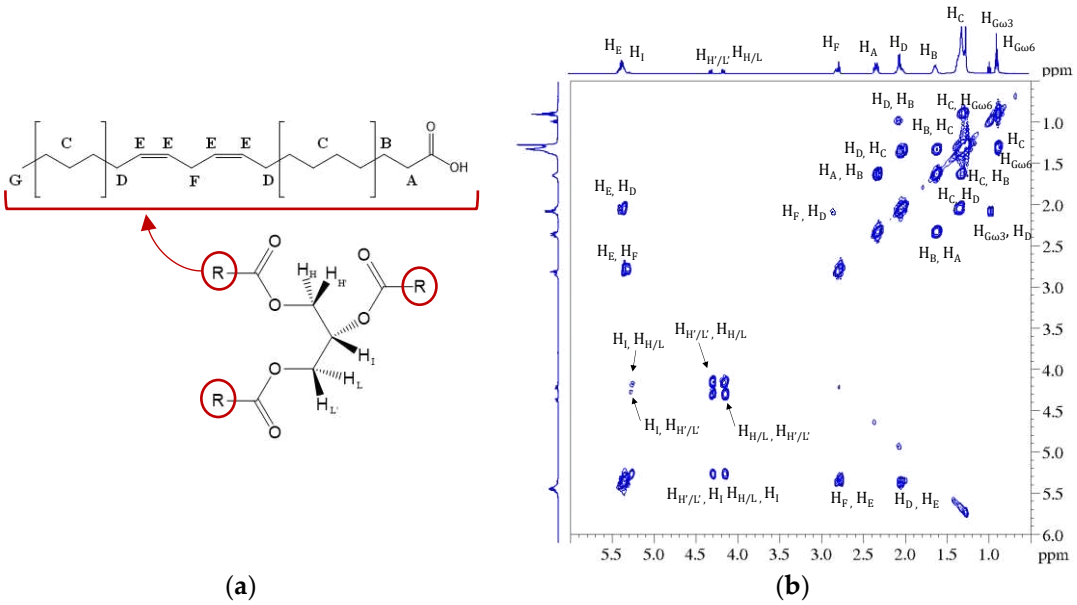

Figure 4. (**a**) General structure and nuclei labelling of molecular fragments in triacylglicerols (TAGs); (**b**) 2D map ^{1}H COSY of the ethanolic extract with the UAE of *C. sativa* seeds. In the figure, all cross peaks corresponding to the homuncular correlations have been highlighted.

Since the integrals of the ^{1}H NMR signals were proportional to the number of hydrogen atoms present in each functional group and, overall, to the number of functional groups present in the sample, from the combination of the integrals of different signals it is possible to calculate the concentration of fatty acids in general, and the ω-6/ω-3 ratio in particular. To this end, three different signals in the protonic spectra were considered: (a) the multiplet at 0.88 ppm due to the overlapping triplet signals of the methyl protons of all the acyl groups (LA), with the exception of those of α-linolenic acid; (b) the triplet at 0.97 ppm generated by the methyl protons of ω-3 fatty acid (α-linolenic acid; (αLA)); (c) the multiplet at 2.72–2.86 ppm generated by the diallylic protons of the linoleic and α-linolenic acyl groups. By combining the area of these signals, using the relations (1) and (2) that take into account the number of equivalent nuclei in each group, the concentrations of αLA and LA were calculated, from which the ω-6/ω-3 ratio was obtained [38].

Calculations were made considering three different samples for reproducibility and to give a main value and a standard deviation. The value obtained for the ω-6/ω-3 ratio using Equations (1) and (2) was 2.93 ± 0.07. As can be seen, this value obtained by ^{1}H NMR is very close to the value of 3:1 for ω-6/ω-3 considered optimal for human dietary purposes, since it is able to prevent various diseases such as diabetes, cardiovascular disease, cancer, and other chronic diseases [4,9,53,54]. On the other hand, the growing interest in hemp seed oil in other fields such as pharmaceuticals and cosmetics [53] has resulted in a constant search for methods that allow fast and systematic quality control: the ω-6/ω-3 ratio is one of these quality parameters [55]. Our result is doubly important because, on the one hand, it indicates the quality of the oil extracts from the seeds of the *Futura 75* cultivar grown in Calabria and, on the other hand, it confirms that NMR is a reliable quantitative platform for the fast screening of hemp oil quality. Indeed, the measurement of this ratio is based only on the recording and analysis of the ^{1}H NMR spectra obtained directly from the seed extracts without further derivatization, as is required by the gas chromatography (GC) method, the common and validated method used to determine the composition of oil in terms of fatty acids [56]. Moreover, our result agrees with that reported in the paper

of Siudem et al. [38] in which the authors analyzed six different samples of hemp seed oils and calculated the ω-6/ω-3 ratio by ^{1}H NMR for each of them using the relationships (1) and (2). The authors compared these data with those from CG method applied to the same hemp seed oils and found a substantial agreement between them, which proves the effectiveness of the method. It is worth noting that, in a recent paper [53], the ^{1}H NMR methodology—as well as being used in the evaluation of the ω-6/ω-3 ratio—is successfully combined with chemometric methods in order to observe the differences in several oil samples due to the different time and storage conditions of the oils. Hence, once again, this demonstrates how NMR can be used for the rapid and reliable analysis of hemp seed oil quality as an alternative to the more common classical analytical methods.

Table 1. ^{1}H NMR chemical shifts and ^{1}H/^{1}H correlations of fatty acid protons in triacylglicerols (TAGs) in $CDCl_3$ for hemp seed extracts.

Position	δ_H, Multiplicity [a] (*J* in Hz)	COSY
A	2.27–2.37, m	E
B	1.55–1.67, m	C, A
C	1.23–1.39, m	$G_{\omega6}$ B, D
D	1.98–2.11, m	$G_{\omega3}$, C, F, E
E	5.28–5.42, m	D, F
F	2.72–2.86, m	D, E
$G_{\omega3}$	0.97, t	D
$G_{\omega6}$	0.88, m	C
H, L (*Gly* [a])	4.14, dd (11.88, 5.93)	H′, L′, I
I (*Gly* [a])	5.26, m	H, H′, L, L′
H′, L′ (*Gly* [a])	4.29, dd (11.88, 4.31)	H, L, I

[a] Abbreviations: *d*—doublet; *dd*—doublet of doublet; *t*—triplet; *m*—multiplet; *Gly*—Glycerol.

3.2. NMR Characterization of Flower Extracts

Figure 5 shows the ^{1}H and ^{13}C NMR spectra of inflorescence ethanolic extracts for the *Tiborszallasi* variety. As is evident from the figure, the two spectra exhibit a complex distribution of resonances due to strongly overlapped signals of cannabinoids with similar molecular structures (Figure 1), from which it is very difficult to recognize single metabolites through simple inspection.

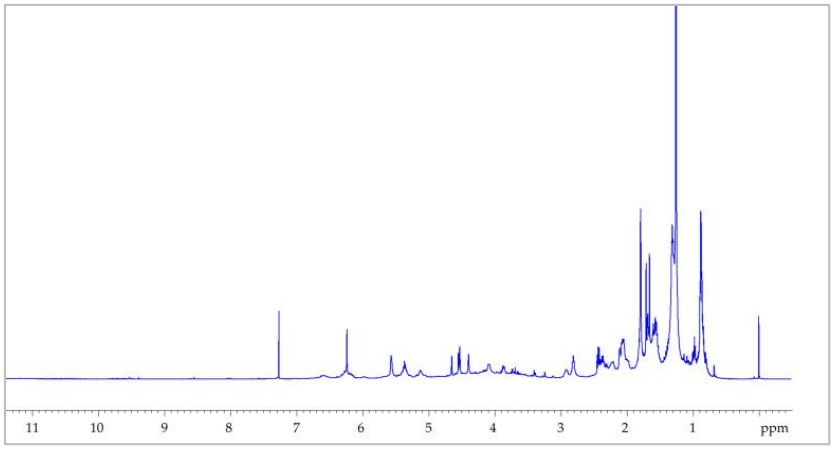

(**a**)

Figure 5. *Cont.*

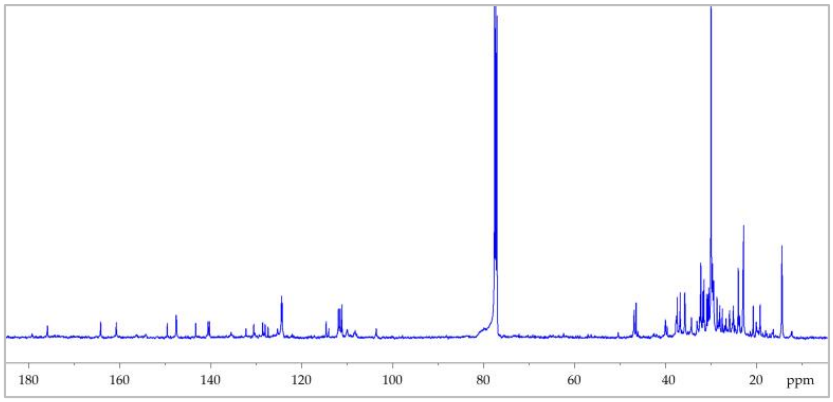

(**b**)

Figure 5. NMR spectra (500 MHz) of inflorescence extracts dissolved in CDCl3 recorded at 298K. (**a**) ^{1}H NMR spectrum recorded using *zg30* Bruker standard pulses sequence; for each experiment, 128 FIDs were accumulated using a spectral width of 14.00 ppm and a relaxation delay of 5 s. (**b**) ^{13}C-{^{1}H} NMR spectrum (*zgig* Bruker pulse sequence) performed with proton broad-band decoupling, collecting 8K free induction decays (FIDs) and using a spectral width of 250.00 ppm and a relaxation delay of 5s. One-dimensional NMR FIDs were Fourier-transformed, phased, baseline-corrected, and aligned using the TMS signal as a reference. ^{13}C-{^{1}H} NMR spectra were filtered with 1 Hz line broadening before Fourier transformation.

To overcome these limitations that are characteristic of the 1D spectra of complex mixtures, the identification of the various cannabinoids present in the extracts (CBD, CBDA, CBG, THC) was carried out using the 2D correlation experiments ^{1}H COSY, ^{1}H-^{13}C HMQC, and ^{1}H *J*-Res and the data reported in the literature regarding the NMR characterizations of many single isolated cannabinoids [40–42]. It is worth underlining that, even in recent papers [35,36,57], the NMR methodology is mostly used to characterize fractions or single components of *C. sativa* obtained by separation techniques. In Figure 6, ^{1}H COSY and ^{1}H-^{13}C HMQC spectra are shown together with the corresponding enlargement on the CBD and CBDA correlations taken as an example of the metabolic identification procedure adopted. In order to fully characterize the inflorescence extract, the 2D ^{1}H *J*-Res experiments were performed on the same sample [42,43]. This type of experiment is capable of separating coupling and chemical shift information into two orthogonal dimensions, allowing for multiplet analysis. The one-dimensional spectrum (^{1}H or ^{13}C) is shown in the F2 dimension, while the couplings related to each chemical shift can be read in the indirect dimension, F1, at the chemical shift value of the multiplet signal to be studied. In Figure 7, the 2D ^{1}H *J*-Res spectrum recorded on the sample of *Tiborszallasi* is reported, and, as an example, the case of H-9$_{cis}$ signal of CBD is reported in the enlargement. The signal of this proton in the 1D ^{1}H NMR spectrum is a multiplet from which it is impossible to extract any useful information. On the contrary, the extrapolation of the column in correspondence to the chemical shift of H-9$_{cis}$ in the F2 dimension of the ^{1}H *J*-Res spectrum gives the 1D profile of the considered signal in which it is possible to measure all the coupling constants. Indeed, as can be seen from the enlargement of Figure 7, this signal is a doublet of a quadruplet due to the interaction of the proton H-9$_{cis}$ with the proton H-9$_{trans}$ (doublet: $^{2}J_{9cis\text{-}trans}$ = 2.6 Hz) and with the methyl proton H-10 (quadruplet: $^{4}J_{9cis\text{-}10}$ = 0.9 Hz).

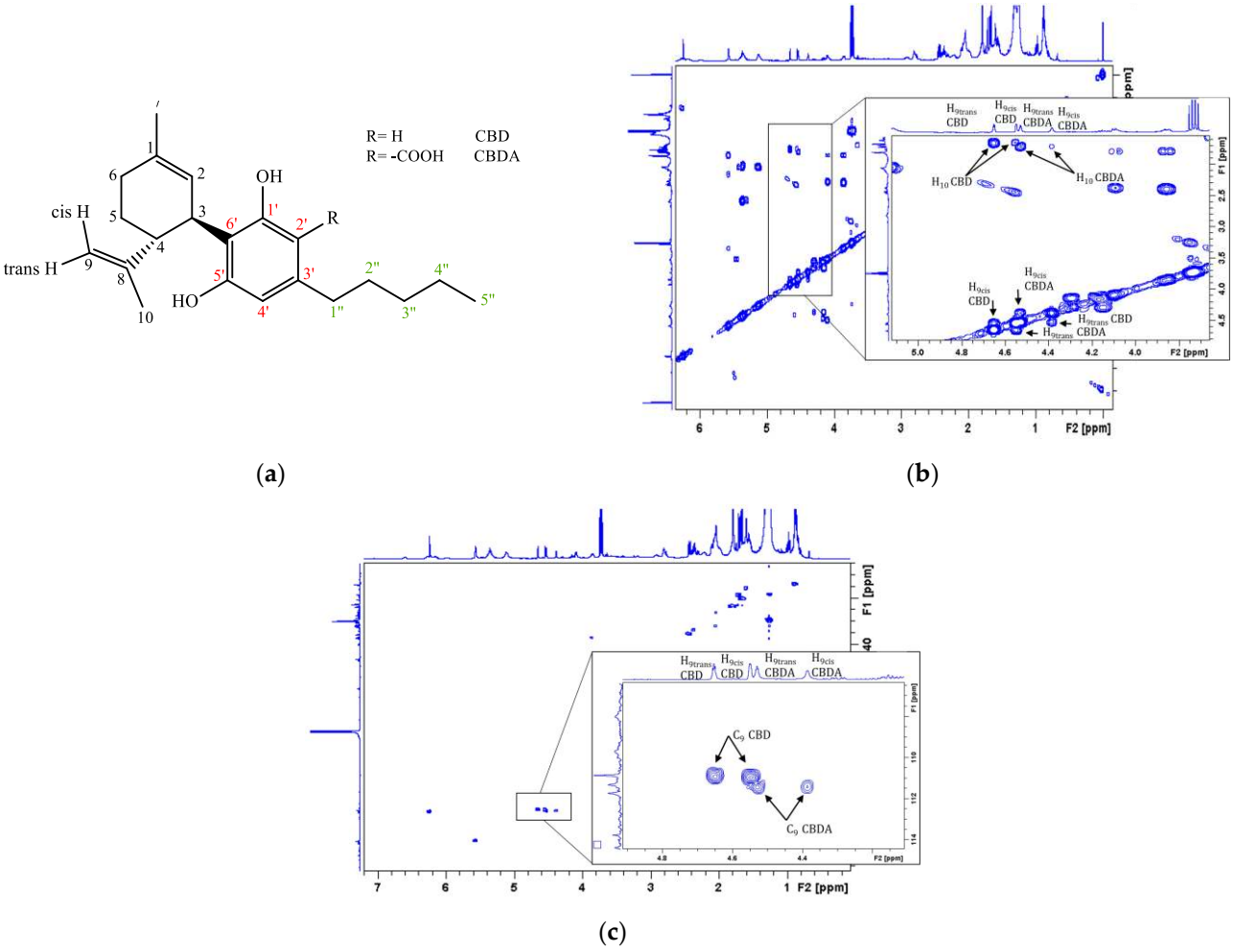

Figure 6. (**a**) Structure of CBD and CBDA reported together with atom numbering adopted; (**b**) 500 MHz ^{1}H COSY spectrum; and (**c**) ^{1}H-^{13}C HMQC NMR spectrum of inflorescence ethanolic extract sample of *Tiborszallasi*, a variety dissolved in $CDCl_3$ and recorded at 298K.

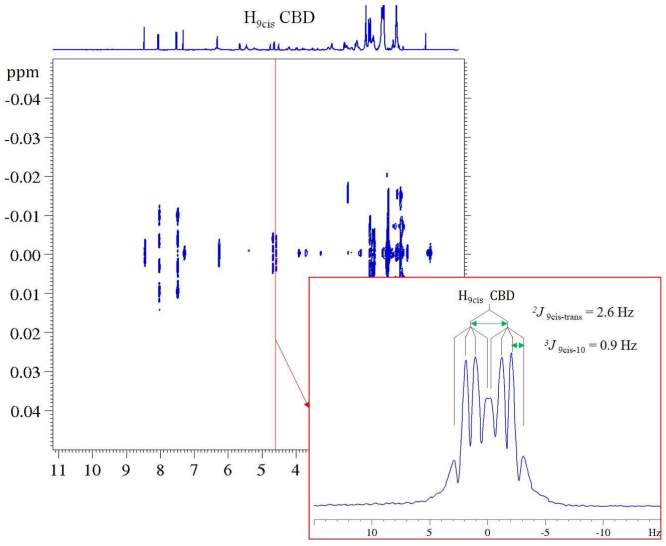

Figure 7. ^{1}H *J*-Res NMR spectrum of inflorescence ethanolic extract samples of *Tiborszallasi* dissolved in $CDCl_3$ and recorded at 298K. The projection of the H-9_{cis} signal (doublet of quadruplets) of CBD is reported in the enlargement.

The assignments for the various cannabinoids present in the ethanolic extract, CBD, CBDA, and CBG of the hemp inflorescences of the *Tiborszallasi* variety and their relative experimental information obtained from the NMR spectra (1D and 2D) are summarized in Table 2. These results agree with many other literature data [35,39–41] and demonstrate how the non-separative NMR technique, combining 1D and 2D experiments, can be successfully applied directly to a complex mixture, such as a *Cannabis* extract, for chemical characterization. An interesting result of the present study is the measurement of a large number of $J_{H\text{-}H}$ for the main cannabinoids, carried out again directly on the *Cannabis* extract through the analysis of the 2D J-Res spectra. It must be highlighted that, in the ethanolic extract, the signals related to THC were not detected in the recorded spectra; this means that, in this solvent, the quantity of THC extracted was below the NMR detection limit [31]. This also occurred for the acetone extracts while the spectra of the hexane extracts showed a small broad peak isolated at 6.40 ppm corresponding to the proton H-10 of Δ^9-THC. This means that hexane, which is also the solvent indicated in the official method for determining the amount of Δ^9-THC in hemp, was the most effective at extracting cannabinoids compared to the other solvents used. Once the assignment of cannabinoids in the *Tiborszallasi* variety was determined, a comparison between the NMR spectra of the samples relating to the *Kompolti* variety was possible. Except for the proton spectrum of the hexane extract of the *Kompolti* variety, in which Δ^9-THC signals were absent, no further differences in terms of profile were distinguished in the spectra of any other samples of either variety. All these spectra are reported in the Supplementary Materials, where it is also possible to find the comparison between ^{1}H NMR spectra from both varieties for the different solvents.

Table 2. ^{1}H and ^{13}C chemical shifts of the main cannabinoids in the flower extracts of *Cannabis sativa* (*Tiborszallasi* variety) in $CDCl_3$.

Compound		δ ^{1}H ppm (Multiplicity *, ^{1}H-^{1}H *J*-Coupling—Hz)	δ ^{13}C ppm	
CBD	H_3	3.86 (ddt; $J_{H3\text{-}H4}$ = 13.00 Hz (d), $J_{H3\text{-}H2}$ = 3.51 Hz (d), $J_{H3\text{-}H5}$ = 2.51 Hz (t))	C_3	37.01
	H_2	5.57	C_2	124.14
	H_{6a}	2.05–2.09	C_6	30.36
	H_{6b}	2.22		
	H_5	1.78–1.84 (ddd; $J_{H5\text{-}H4}$ = 5.30 Hz (*d*), $J_{H5\text{-}H6a}$ = 1.30 Hz (d), $J_{H5\text{-}H6b}$ = 0.60 Hz (d))	C_5	28.35
	H_4	2.40 (dd; $J_{H4\text{-}H3}$ = 13.00 Hz (d), $J_{H4\text{-}H5}$ = 5.00 Hz (d))	C_4	46.16
	H_7	1.79 (d;$^3J_{H7\text{-}H2}$ = 0.50 Hz)	C_7	23.69
	H_{9trans}	4.64 (dq; $J_{9trans\text{-}9cis}$ = 2.65 Hz (d), $^3J_{9trans\text{-}10}$ = 1.50 Hz (q))	C_9	110.81
	H_{9cis}	4.53 (dq; $J_{9cis\text{-}9trans}$ = 2.65 Hz (d), $^3J_{9cis\text{-}10}$ = 0.92 Hz (q))		
	H_{10}	1.66 (dd; $^3J_{10\text{-}9cis}$ = 0.92 Hz (d), $^3J_{10\text{-}9trans}$ = 1.50 Hz (d))	C_{10}	20.30
	$H_{2'}$	6.26	$C_{2'}$	109.56
	$H_{4'}$	6.16	$C_{4'}$	107.92
	$H_{1''}$	2.43 (t)	$C_{1''}$	35.46
	$H_{2''}$	1.52–1.61	$C_{2''}$	30.65
	$H_{3''}$, $H_{4''}$	1.27–1.32	$C_{3''}$	31.48
			$C_{4''}$	22.54
	$H_{5''}$	0.86–0.88	$C_{5''}$	14.04
CBDA	H_3	4.08	C_3	35.38
	H_2	5.55	C_2	124.14
	H_{6a}	2.05–2.09	C_6	30.36
	H_{6b}	2.22		

Table 2. *Cont.*

Compound	δ ^{1}H ppm (Multiplicity *, ^{1}H-^{1}H *J*-Coupling—Hz)		δ ^{13}C ppm	
CBDA	H_5	1.79 (ddd; $J_{H5\text{-}H4}$ = 5.30 Hz (*d*), $J_{H5\text{-}H6a}$ = 1.30 Hz (d), $J_{H5\text{-}H6b}$ = 0.60 Hz (d))	C_5	28.35
	H_4	2.40 (dd; $J_{H4\text{-}H3}$ = 13.00 Hz (d), $J_{H4\text{-}H5}$ = 5.00 Hz (d))	C_4	46.45
	H_7	1.79 (d; $^{3}J_{H7\text{-}H2}$ = 0.50 Hz)	C_7	23.69
	H_{9trans}	4.51 (dq; $^{3}J_{9cis\text{-}9trans}$ = 3.00 Hz (d); $^{3}J_{9trans\text{-}10}$ = 1.76 Hz (q))	C_9	111.21–111.25
	H_{9cis}	4.39 (dm; $^{3}J_{9cis\text{-}9trans}$ = 3.00 Hz (d))		
	H_{10}	1.70	C_{10}	18.91
	$H_{4'}$	6.21	$C_{4'}$	111.21–111.25
	$H_{1''a}$	2.81	$C_{1''}$	36.68
	$H_{1''b}$	2.92		
	$H_{2''}$	1.52–1.61	$C_{2''}$	31.24
	$H_{3''}$, $H_{4''}$	1.27–1.32	$C_{3''}$	31.94
			$C_{4''}$	22.54
	$H_{5''}$	0.86–0.88	$C_{5''}$	14.04
CBG	H_2	6.24	C_2	108.25
	$H_{5'}$, $H_{4'}$	2.04	$C_{4'}$	32.28
			$C_{5''}$	26.51
	$H_{6'}$	5.12	$C_{6'}$	125.08
	$H_{8'}$, $H_{10'}$	1.68	$C_{8'}$	20.51
			$C_{10''}$	23.44

* Abbreviations: d—doublet; t—triplet; q—quadruplet; m—multiplet; dd—doublet of doublet; ddd—doublet of doublet of doublet; ddt—doublet of doublet of triplet; dq—doublet of quadruplet; dm—doublet of multiplet.

In addition to the cannabinoids, by comparison of the protonic spectra of the hemp seed oil and hemp inflorescence extracts, it was possible to recognize in this last spectrum some signals that referred to the triacylclycerols constituent. In particular, this profile was easily recognizable in the samples obtained by using ethanol as the extracting solvent. All the signal assignments are reported in Figure 8. Regarding the solvents, it must be underlined that many are used for cannabinoid extraction but, to date, there is no specific protocol. However, it is not surprising that we were able to better recognize the fatty acid profiles in the ethanol extracts since, from the literature data [58], it seems that ethanol has a greater extraction power than acetone and hexane. On the other hand, hexane, while showing the worst performance in terms of total yield, leads to cleaner extracts with fewer contaminants and extracts richer in cannabinoids [59]. For this reason, hexane is used for the selective analysis of cannabinoids in the official method established by the European Commission [29]. It should be noted that this was also evident in our spectra recorded on the hexane extracts. Indeed, these extracts have a cleaner profile than the other two solvents and allowed us, for the Tiborszallasi variety, to quantify the THC content together with the other cannabinoids.

3.3. Multivariate Analysis

Principal component analysis (PCA) was applied to discriminate hemp flowers samples based on their ^{1}H NMR spectra [48–50]. The main aim was to observe how the cannabinoid profiles changed for extracts in relation to the nature of solvent extraction and the efficiency of the extraction procedure. PCA was carried out on two different data matrices, one for each hemp variety. For *Tiborszallasi*, the data matrix consisted of 24 samples (9 extracts for ethanol and acetone, respectively, 6 extracts for hexane) and 130 variables. For the *Kompolti* variety, the data matrix consisted of 24 sample (9 extracts for hexane and ethanol, respectively, 6 extracts for acetone) and 130 variables.

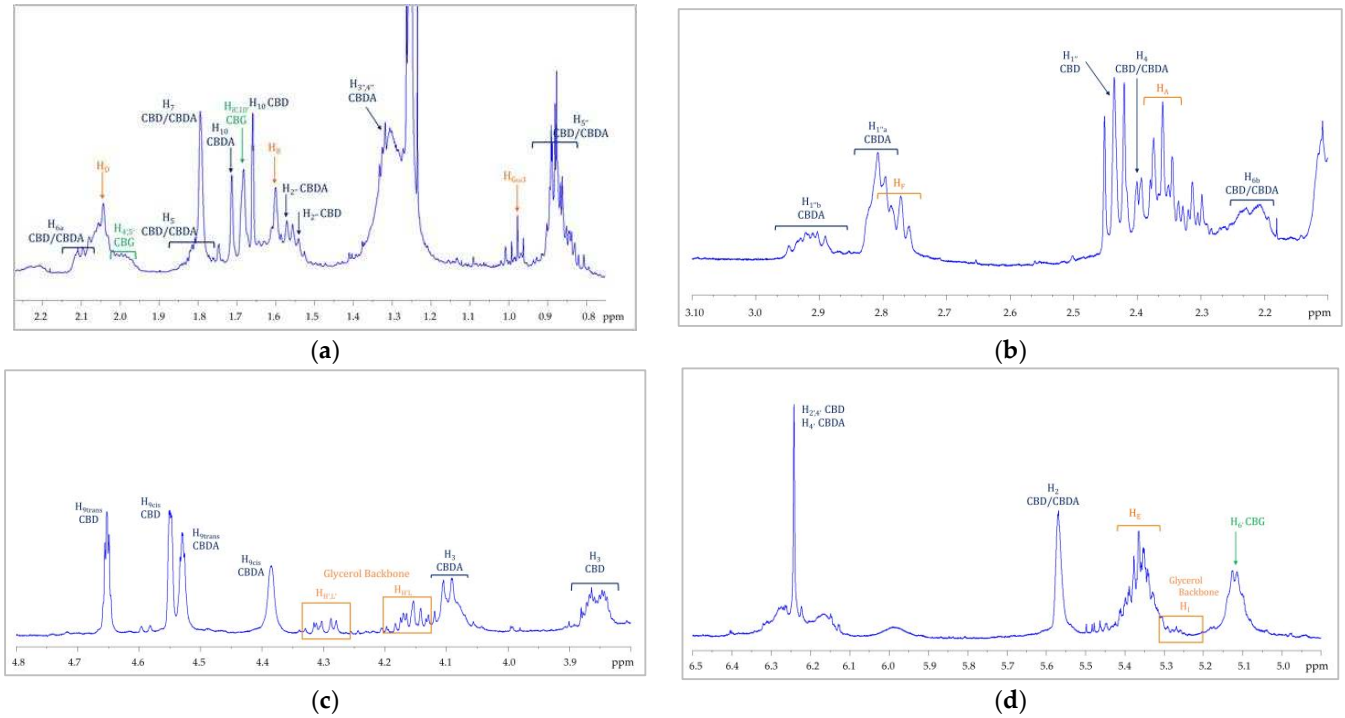

Figure 8. ^{1}H NMR spectrum of an ethanolic extract of *C. sativa* inflorescences (*Tiborszallasi* variety). For the enlarged regions of (**a**) [0.8 ppm–2.2 ppm], (**b**) [2.2 ppm–3.00 ppm], (**c**) [3.7 ppm–4.8 ppm], and (**d**) [4.8 ppm–6.5 ppm] the signal attributions are shown. Signal assignments are reported with different colors: orange for TAGs; grey for the glycerol backbone; blue for CBD/CBDA; green for CBG/CBGA.

Figures 9 and 10 show the 3D score plot for the *Tiborszallasi* and *Kompolti* variety samples, respectively, with a cumulative percentage of explained data variance for the three first PCs equal to: (a) 88.1 % (45.5% for PC1, 30.2% for PC2, 12.4% for PC3) for the *Tiborszallasi* variety and (b) 84.5% (51.8% for PC1, 17.5% for PC2, 15.2% for PC3) for the *Kompolti* variety. This means that data loss was negligible in both cases. The score plot effectively summarizes the relationship between the samples and highlights what was not discovered by the simple comparison among the protonic spectra: clear and well-defined separation between samples was observed and every type of extract was clustered into one defined region. Indeed, PC1 allows us to discriminate among extracts with non-polar solvent and extracts with higher polarity: hexane extracts had, in fact, positive values of PC1, while the other ones had negative values of PC1. Instead, PC2 seems to best discriminate between the acetone and ethanol extracts. The same result was obtained for both varieties.

However, in order to determine which metabolites have greater influence on the discrimination and evaluation of the quality and efficiency of the extraction procedure, an accurate discussion about loadings is necessary.

In Figure 11, a 2D biplot of the first two PCs (PC1 and PC2) for the *Tiborszallasi* variety is reported; this shows the sample differentiation and the changes in the metabolite concentrations from one extract to another and, consequently, the variables responsible for the sample clustering can be observed in the score diagram.

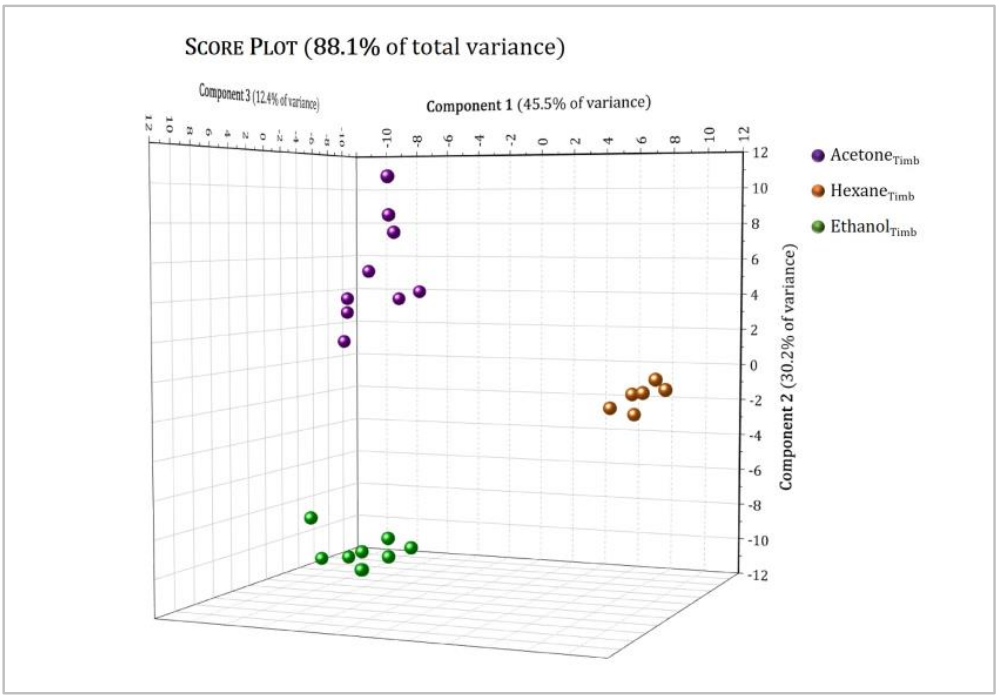

Figure 9. Principal component analysis (PCA) of hexane (brown dots), acetone (purple dots) and ethanol (green dots) extracts of the *Tiborszallasi* variety of hemp. The score plot shows the first three PCs (PC1, PC2 and PC3) with their respective variations. R2X(PC1) = 45.5%, R2X(PC2) = 30.2%, R2X(PC3) = 12.4%.

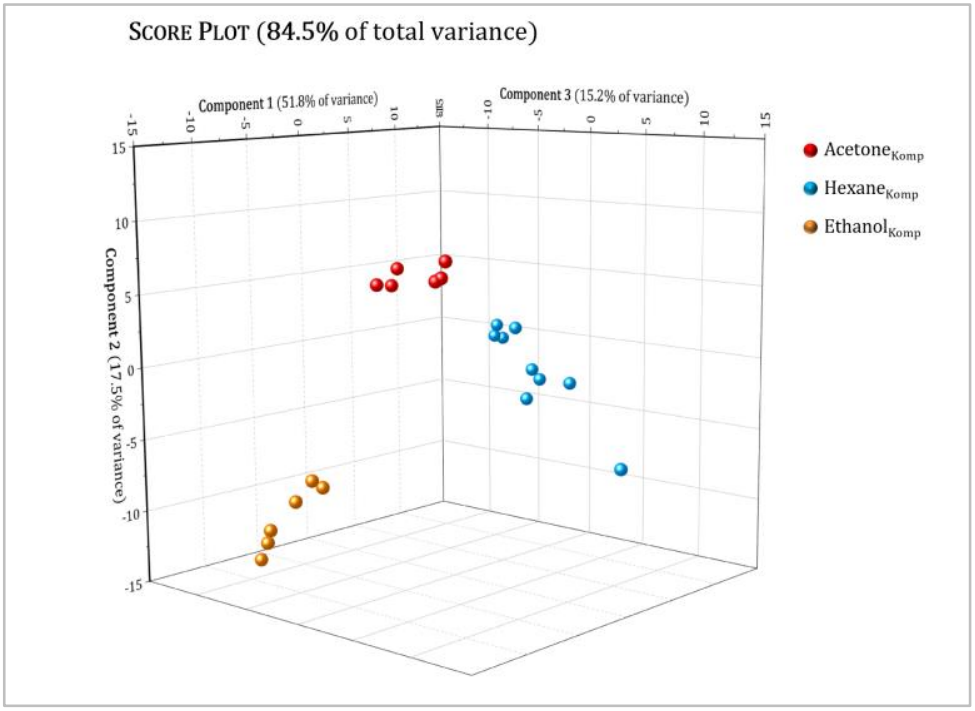

Figure 10. Principal component analysis (PCA) of hexane (blue dots), acetone (red dots), and ethanol (orange dots) extracts for the *Kompolti* variety of hemp. The score plot shows the first three PCs (PC1, PC2 and PC3) with their respective variation. R2X(PC1) = 51.8%, R2X(PC2) = 17.5%, R2X(PC3) = 15.2%.

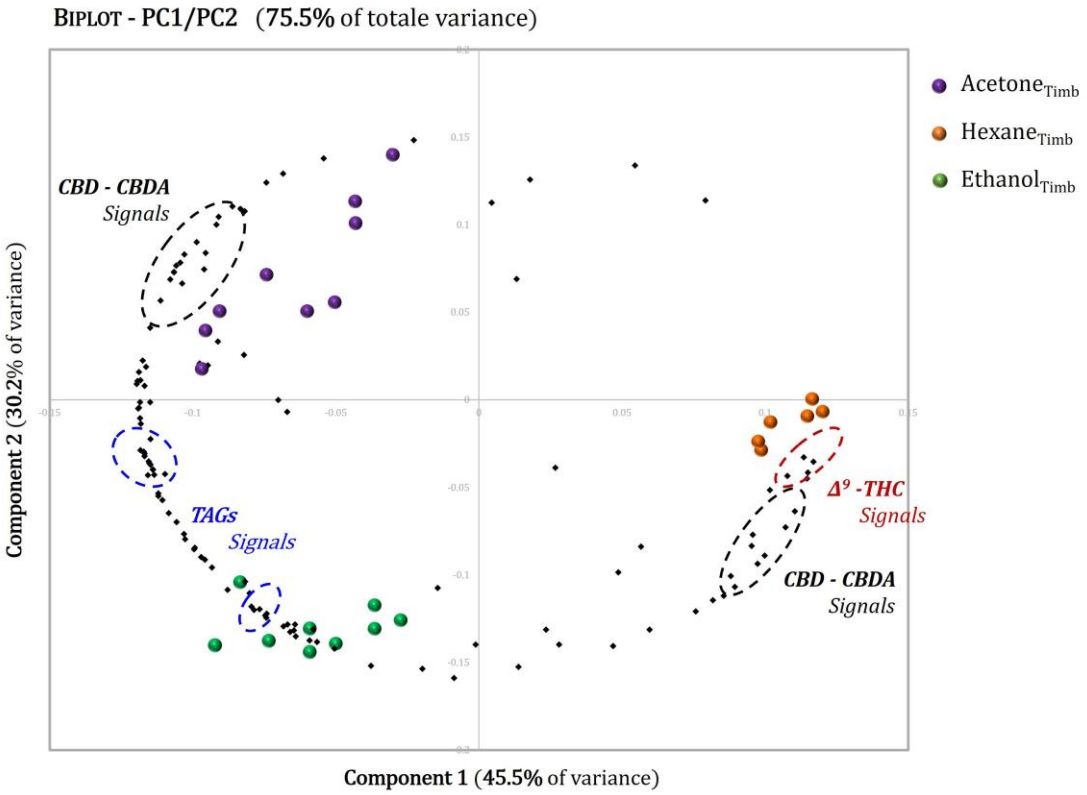

Figure 11. Biplot of PCA carried out on NMR spectra of hexane (brown dots), acetone (purple dots) and ethanol (green dots) extracts of the *Tiborszallasi* variety of hemp. The score plot shows the first two PCs (PC1 and PC2) with their respective variations. R2X(PC1) = 45.5%, R2X(PC2) = 30.2%.

THC is the marker that gives the first clear distinction between hexane and all the other extracts: the THC loadings had positive values of PC1 and negative values of PC2, and these were very close to the scores of the hexane extracts. This means, as also demonstrated by the loadings of CBD and CBDA, that hexane is more efficient in the extraction of cannabinoids and of THC in particular. Indeed, the latter was below the NMR detection limit in the acetone and ethanol extracts. These results are not surprising since it is well known from the literature [34,60] that the polarity of the solvent affects the chemical composition of the cannabinoids present in the extracts.

Focusing on the TAGs previously detected during the signal assignment step, negative values of PC1 were obtained for these loadings. This indicates that extraction with a higher polarity solvent (acetone or ethanol) obtains samples with a lower percentage of cannabinoids but that are richer in fatty acids than hexane extracts. This peculiarity could be exploited to obtain extracts rich in both bioactive compounds—cannabinoids and TAGs—that could potentially be used in the food and pharmaceutical industries to produce functional foods and supplements.

The same conclusions were also reached for the *Kompolti* variety, whose 2D biplot of the first two PCs is reported in the Supplementary Materials.

The present study has shown that the exploratory PCA method, although simple, is able to differentiate samples coming from different extraction solvents and, in addition, it highlights which cannabinoids form the basis of this differentiation. Chemometrics-aided NMR techniques performed on *C. sativa* components (inflorescences, seed oils, leaves, and other less valuable parts of the plant), or on fractions of them, are widely used to determine different properties of *C. sativa*, as evidenced by the plethora of studies reported in the literature [34,41,61–65] and the references reported therein. In many of these works, the combination of ^{1}H-NMR spectra with chemometric tools was used for the metabolomic differentiation of inflorescence extracts from different cultivars and to identify particular

markers in order to discriminate different plant chemotypes [41,61]. In other studies [62,66], targeted and non-targeted NMR methodologies were used to identify and quantify compounds of different classes present in the inflorescence extracts of several *C. sativa* cultivars and to monitor their variations in three different harvested stages. The cultivars analyzed in these studies had a THC content always below the legal limit, while the quantities of the other cannabinoids in the extracts were affected by the harvest time and by the solvent. Although it is not easy to make comparisons given the quantity of factors affecting the composition of cannabinoids, the results obtained in this study substantially agree with the studies described above, and therefore seem to demonstrate the reliability of this method and its possible application in the routine analysis of cannabinoids.

3.4. Quantitative Analysis of Inflorescences

As a support to the results obtained from the PCA analysis and to evaluate if the NMR methodology could be a valid tool in the quantitative determination of the cannabinoids extracted as a function of the solvent used, an NMR quantification was also carried out using ^{1}H and ^{13}C NMR spectra and different internal standards.

Tiborszallasi- and *Kompolti*-type hemp flower samples used for the quantification were obtained, as mentioned before, by ultrasound-assisted extraction using three different common solvents of increasing polarity: hexane, acetone and ethanol. The complete procedure, from extraction to NMR measurement, was performed in triplicate to evaluate repeatability, to calculate an average value for the extraction yield, and to estimate the relative error. The procedure below is described for the *Tiborszallasi* samples, but exactly the same was performed for the *Kompolti* variety.

The average experimental extraction yields for each procedure were: (a) 17.9 $\pm$ 0.3% for extraction with hexane; (b) 9.9 $\pm$ 0.8% for extraction with acetone; (c) 19.6 $\pm$ 0.9% for extraction with ethanol.

For the quantification of the cannabinoids present in the extracts, both 1D ^{1}H NMR and ^{13}C NMR spectra were used. The quantification of cannabinoids by protonic spectra included the use of three different internal standards: anthracene, in accordance with literature [20], benzoic acid, and 3-(trimethylsilyl)propionic-2,2,3,3-d_4 acid (TMSP-d_4). These compounds are highly pure ($\geq$ 99.9%), have low volatility, are chemically inert, and are not similar in structure to the cannabinoids to be quantified. Indeed, in the case of NMR spectroscopy, it is necessary that they generate well-isolated signals in the spectrum that do not overlap with the peaks assigned to other metabolites in the mixture. In this case, signals of aromatic protons of anthracene and benzoic acid ranged between 7.4 ppm and 8.5 ppm in the protonic spectrum, and the singlet of the methyl group of TMSP-d_4 was set to 0.00 ppm.

The signals considered for the quantification, using Equation (3), were the following: for CBD, the H-9_{trans} olefinic proton signal was set at δ = 4.65 ppm; for CBDA, the H-9_{cis} olefinic proton signal was set at δ = 4.38 ppm; and for Δ^9-THC, the H-10 proton signal was set at δ = 6.40 ppm. The results obtained for the three standards used are reported in Table 2. For further confirmation of the ^{1}H qNMR results, quantitative ^{13}C NMR spectra were also recorded on the hemp flower hexane extracts of *Tiborszallasi*, optimizing the acquisition parameters (see Section 2.3) and the operative conditions [40]. However, in this case, only TMSP-d_4 was used as an internal standard for ^{13}C qNMR because the aromatic carbons of anthracene and benzoic acid generated signals in the region between 125 ppm and 134 ppm, thereby overlapping with the cannabinoid signals. Moreover, given the low sensitivity of the ^{13}C nucleus, the ^{13}C qNMR was useful for the quantitative determination of CBDA, the only cannabinoid whose signals had an acceptable signal-to-noise ratio. The CBDA content (% on dry weight) obtained via ^{13}C qNMR for *Tiborszallasi* in hexane extract was equal to 6.2 $\pm$ 0.9, which was substantially in agreement with that obtained from protonic spectra using the same internal standard (Table 2).

Observing the results reported in Table 2, the value obtained for the three cannabinoids CBD, CBD and Δ^9-THC, for each type of extract using different internal standards,

were fairly reproducible. This means that benzoic acid and TMSP-d_4 seem to be valid alternatives to anthracene as internal standards for quantification. Indeed, anthracene is the standard that is usually used for the quantification of cannabinoids via NMR, but it has many drawbacks related to its toxicity, its poor solubility in common solvents, and long recording times due to long T1 [67]. Furthermore, the data show that hexane extracts are richer in cannabinoids than other solvents, as had already emerged in the biplot analysis, and, most interestingly, the quantities obtained for these extracts via NMR matched very well with the experimental data acquired following the official European procedure for the determination of cannabinoid Δ^9-THC, as reported in Table 3. Indeed, the table shows the comparison, for the same sample of *Tiborszallasi* inflorescences, between the qNMR data of Δ^9-THC via NMR and those obtained with the official GC-FID technique [29]. In the table, the GC-FID value concerning the quantity of CBD/CBDA obtained from the same sample is also reported. It should be noted that the GC-FID procedure does not allow discrimination between CBDA and CBD: before extraction, it includes a pretreatment of inflorescences at a high temperature that leads to the complete decarbossilation of the acidic form of this cannabinoid (CBDA) to the neutral (CBD). So, this unique value should be considered as the sum of the quantities of CBDA and CBD initially present in flowers. As can be seen from the table, also in this case, the data via NMR are in perfect agreement with those obtained via GC-FID. It is worth noting that the NMR technique has been proven to be a reliable and powerful tool for the quantification of different natural products and, especially in recent years, has also been successfully applied to the quantification of CBD and other cannabinoids directly on hemp extracts coming from different cultivars using both the ^{1}H and ^{13}C qNMR methodologies. [40,44,68–71]. Quantitative ^{1}H-NMR is the most widely used method in the quantification of natural extracts and has been shown to have a good level of accuracy and reproducibility. However, its application to hemp extracts presents several drawbacks, due both to the presence of contaminants and to the overlapping of different signals that require the extensive use of deconvolution processes [72]. The use of ^{13}C q-NMR, introduced by Marchetti et al. [40], partially removes these weaknesses and at the same time offers sufficiently precise and sensitive results. As expected, our results substantially agree with these previous reports on the ^{1}H and ^{13}C qNMR investigations, even if it is necessary to point out that a direct comparison on the quantities of cannabinoids found in the different extracts of the cultivar analyzed is practically impossible given, as we have already highlighted, the large quantity of variables, i.e., cultivar, geographical origin, harvesting period, agronomic practices, extraction methodologies, etc., that affect the composition of cannabinoids. However, the quantitative results of the present study highlight, once again, the remarkable potentialities of the NMR technique which was able to quantify the main metabolites present in the hemp inflorescence extracts we analyzed as they were, without the further treatment or derivatization required by the official technique [73,74]. Moreover, as reported recently by Dadiotis et al. [75] concerning the quantitative analysis of cannabinoids in hemp extracts using, in a complementary way, the ^{1}H-NMR and ^{1}H-^{1}H COSY NMR spectra, these quantitative data via NMR are comparable with those acquired with other more consolidated techniques applied to the same extracts. This evidence shows good correspondence between the various quantification techniques, as also confirmed by the data we obtained on the *Timborszallase* cultivar given the satisfactory agreement between the NMR and GC-FID data of the hexane solvent.

In addition, the quantitative data obtained for the different solvents confirm the purely qualitative indications given by the PCA analysis, which proved to be very informative and fast.

These results were obtained for the *Tiborszallasi* variety but, as previously mentioned, the quantification of the main cannabinoids by ^{1}H and ^{13}C qNMR was also performed for the *Kompolti* variety and the results are reported in the Supplementary Materials.

Table 3. ^{1}H NMR data of the main cannabinoids in *Timborzallasi* inflorescences compared with the GC-FID method.

Compound	qNMR on Flowers UAE Extracts				GC-FID
	qNMR IS	Hexane	Acetone	Ethanol	
CBDA content *	Anthracene	6.3 ± 0.8	0.40 ± 0.1	0.31 ± 0.04	Validated Laboratory Method 6.9 ± 0.2 Referred to **CBD** after decarbossilation
	Benzoic acid	6.5 ± 0.8	0.40 ± 0.1	0.39 ± 0.06	
	TMSP-d_4	6.4 ± 0.6	0.41 ± 0.1	0.41 ± 0.06	
CBD content *	Anthracene	0.4 ± 0.1	4.60 ± 0.8	0.30 ± 0.1	
	Benzoic acid	0.30 ± 0.06	4.54 ± 0.6	2.2 ± 0.1	
	TMSP-d_4	0.4 ± 0.1	4.59 ± 0.6	2.9 ± 0.1	
Δ^9-THC content *	Anthracene	0.11 ± 0.44	<LOD	<LOD	Regulation (EU) N° 639/2014 [15] 0.09 ± 0.01
	Benzoic acid	0.07 ± 0.02			
	TMSP-d_4	0.10 ± 0.02			

* % of dry weight.

4. Conclusions

Cannabis sativa is a fast-growing plant currently grown all over the world that is gaining popularity in various fields of research for its biological and pharmaceutical properties. Actually, *C. sativa* is widely recognized and appreciated for the high nutritional and health-promoting properties of the oil obtained from its seeds, together with the pharmacological activity mainly associated with psychoactive and non-psychoactive cannabinoids and the chemical components mainly extracted from the inflorescences. In this work, NMR spectroscopy was applied to analyze extracts from the seeds and inflorescences of different varieties of *Cannabis sativa* grown in Calabria in order to explore the potentialities of this technique for the qualitative and quantitative analysis of the extracts, and to evaluate the possibility of using it as an alternative to the most common methods in the quantification of cannabinoids present in inflorescence extracts. The quantitative NMR results obtained from two varieties of hemp inflorescence extracts, using different internal standards and solvents, demonstrated the high potentiality of the proposed technique in this field of application. Indeed, the NMR technique was able to quantify the main cannabinoids present in the extracts, the quantitative data were reproducible, and—most importantly—the data from the hexane solvent were congruent with the data obtained by the GC-FID method. Moreover, while this last methodology is not able to distinguish CBD and CBDA, using the NMR method, it was possible to separate the two contributions and quantify them. This proves, once again, the analytical power of the NMR technique which is not only able to offer the same results obtained from the official method, including the evaluation of THC, but can indicate more informative data without performing particular treatments on the sample.

In addition to the characterization and the quantitative study, different extraction procedures were tested and evaluated by NMR spectroscopy with the aim of obtaining inflorescence extracts poor in psychotropic agents and rich in medical cannabinoids and triacylglicerols (TAGs), which have an ω-6/ω-3 ratio that has been found to be excellent from a nutritional point of view. Specifically, extracts of inflorescences obtained by ultrasound-assisted solute–solvent extraction using hexane, acetone and ethanol as solvents were studied. By elaborating the spectral data with a statistical method (PCA) together with the qNMR approach, it was possible to conclude that hexane was more efficient in the extraction of cannabinoids (THC included) than the TAG constituents, while extraction with a higher polarity solvent (acetone or ethanol) obtained samples free from THC (THC content < LOD), rich in TAGs, and with a lower percentage of cannabinoids. This evidence can be exploited to obtain extracts rich in bioactive compounds (both cannabinoids and TAGs) that could potentially be used in the food and pharmaceutical industries, opening new paths for the production of functional foods and supplements.

Supplementary Materials: The following supporting information can be downloaded at: https://www.mdpi.com/article/10.3390/molecules27113509/s1, Figure S1: Comparison between ^{1}H NMR spectra ethanol (blue), acetone (red) and hexane (green) extracts for the Tiborszallasi variety; Figure S2: Comparison between ^{1}H NMR spectra of ethanol (blue), hexane (red) and acetone (green) extracts for the Kompolti variety; Figure S3: Comparison between the enlarged region [6.25 ppm–6.5ppm] of the ^{1}H NMR spectra from the hexane extract of the Tiborszallasi (blue) and Kompolti (purple) varieties. A broad peak isolated at 6.40 ppm corresponding to the proton H-10 of Δ9-THC appears in the proton spectra of Tiborszallasi, while this signal is undetectable in the ^{1}H NMR spectrum acquired for Kompolti; Figure S4: Biplot of PCA carried out on NMR spectra of acetone (red dots), hexane (blue dots) and ethanol (orange dots) extracts of the Kompolti variety of hemp. The score plot shows the first two PCs (PC1 and PC2) with their respective variations. R2X(PC1) = 51.8%, R2X(PC2) = 17.5%; Table S1: The ^{1}H NMR data of main cannabinoids in Kompolti inflorescences.

Author Contributions: Conceptualization, M.F.C. and G.D.L.; methodology, G.D.L.; validation, C.O.R., A.L.P.; formal analysis, M.G.; investigation, M.F.C., R.A.S., F.L.; data curation, M.F.C. and R.A.S.; writing—original draft preparation, M.F.C., R.A.S., G.D.L.; writing—review and editing, G.D.L. and C.O.R.; supervision, G.D.L. and C.O.R.; All authors have read and agreed to the published version of the manuscript.

Funding: This work was supported by the University of Calabria and POR Calabria—FSE/FESR 2014–2020.

Institutional Review Board Statement: Not applicable.

Informed Consent Statement: Not applicable.

Data Availability Statement: All data generated or analyzed during this study are included in this published article.

Conflicts of Interest: The authors declare no conflict of interest.

Sample Availability: Samples of the compounds are not available from the authors.

References

1. Small, E. Classification of *Cannabis sativa* L. In *Relation to Agricultural, Biotechnological, Medical and Recreational Utilization. In Cannabis sativa L.—Botany and Biotechnology*, 1st ed.; Chandra, S., Hemant, L., ElSohly, M.A., Eds.; Springer International Publishing: Cham, Switzerland, 2017; pp. 1–62.
2. Li, H.L. An archaeological and historical account of *Cannabis* in China. *Econ. Bot.* **1974**, *28*, 437–447. [CrossRef]
3. ElSolhy, M.A.; Tadwan, M.M.; Gul, W.; Chandra, S.; Galal, A. Phytochemistry of *Cannabis sativa* L. *Prog. Chem. Org. Nat. Prod.* **2017**, *103*, 1–36.
4. Crescente, G.; Piccolella, S.; Esposito, A.; Scognamiglio, M.; Fiorentino, A.; Pacifico, S. Chemical composition and nutraceutical properties of *hemp* seeds: An ancient food with actual functional value. *Phytochem. Rev.* **2018**, *17*, 733–749. [CrossRef]
5. Tura, M.; Ansorena, D.; Astiasarán, I.; Mandrioli, M.; Toschi, T.G. Evaluation of *Hemp* Seed Oils Stability under Accelerated Storage Test. *Antioxidants* **2022**, *11*, 490. [CrossRef]
6. Banskota, A.H.; Jones, A.; Hui, J.P.M.; Stefanova, R. Triacylglycerols and Other Lipids Profiling of *Hemp* By-Products. *Molecules* **2022**, *27*, 2339. [CrossRef]
7. Spano, M.; Di Matteo, G.; Rapa, M.; Ciano, S.; Ingallina, C.; Cesa, S.; Menghini, L.; Carradori, S.; Giusti, A.M.; Di Sotto, A.; et al. Commercial *Hemp* Seed Oils: A Multimethodological Characterization. *Appl. Sci.* **2020**, *10*, 6933. [CrossRef]
8. Teleszko, M.; Zając, A.; Rusak, T. *Hemp* Seeds of the Polish 'Bialobrzeskie' and 'Henola' Varieties (*Cannabis sativa* L. var. sativa) as Prospective Plant Sources for Food Production. *Molecules* **2022**, *27*, 1448. [CrossRef]
9. Simopoulos, A.P. The importance of the omega-6/omega-3 fatty acid ratio in cardiovascular disease and other chronic disease. *Exp. Biol. Med.* **2008**, *233*, 674–688. [CrossRef]
10. Ministero della Salute. *Produzione e Commercializzazione di Prodotti a Base di Semi di Canapa Per L'utilizzo nci Settori Dell'alimentazione Umana*; Ministero della Salute: Roma, Italy, 2009; pp. 1–4.
11. Mercuri, A.M.; Accorsi, C.A.; Bandini Mazzanti, M. The long history of *Cannabis* and its cultivation by Romans in central Italy, shown by pollen records from Lago Albano and Lago di Nemi. *Veget. Hist. Archaeobot.* **2002**, *11*, 263–276. [CrossRef]
12. ElSolhy, M.A.; Slade, D. Chemical Constituents of marijuana: The complex mixture of natural cannabinoids. *Life Sci.* **2005**, *78*, 539–548. [CrossRef]
13. Radwan, M.M.; Chandra, S.; Gul, S.; Elsohly, M.A. Cannabinoids, phenolics, terpenes and alkaloids of cannabis. *Molecules* **2021**, *26*, 2774. [CrossRef] [PubMed]

14. Bautista, J.L.; Yu, S.; Tian, L. Flavonoids in *Cannabis sativa*: Biosynthesis, bioactivities, and biotechnology. *ACS Omega* **2021**, *6*, 5119–5123. [CrossRef] [PubMed]
15. Baker, D.; Pryce, G.; Giovannoni, G.; Thompson, A.J. The therapeutic potential of *Cannabis*. *Lancet. Neurol.* **2003**, *2*, 191–298. [CrossRef]
16. Izzo, A.A.; Borrelli, F.; Capasso, R.; Di Marzo, V.; Mechoulam, R. Non-psychotropic plant cannabinoids: New therapeutic opportunities from an ancient herb. *Trends Pharmacol. Sci.* **2009**, *30*, 515–527. [CrossRef] [PubMed]
17. Odieka, A.E.; Obuzor, G.U.; Oyedeji, O.O.; Gondwe, M.; Hosu, Y.S.; Oyedeji, A.O. The Medicinal Natural Products of *Cannabis sativa* Linn.: A Review. *Molecules* **2022**, *27*, 1689. [CrossRef]
18. Iftikhar, A.; Zafar, U.; Ahmed, W.; Shabbir, M.A.; Sameen, A.; Sahar, A.; Bhat, Z.F.; Kowalczewski, P.Ł.; Jarzębski, M.; Aadil, R.M. Applications of *Cannabis sativa* L. in Food and Its Therapeutic Potential: From a Prohibited Drug to a Nutritional Supplement. *Molecules* **2021**, *26*, 7699. [CrossRef]
19. Russo, E.B. *Cannabis* Therapeutics and the Future of Neurology. *Front. Integr. Neurosci.* **2018**, *12*, 51. [CrossRef] [PubMed]
20. Stasiłowicz, A.; Tomala, A.; Podolak, I.; Cielecka-Piontek, J. *Cannabis sativa* L. as a Natural Drug Meeting the Criteria of a Multitarget Approach to Treatment. *Int. J. Mol. Sci.* **2021**, *22*, 778. [CrossRef]
21. Kopustinskiene, D.M.; Masteikova, R.; Lazauskas, R.; Bernatoniene, J. *Cannabis sativa* L. Bioactive Compounds and Their Protective Role in Oxidative Stress and Inflammation. *Antioxidants* **2022**, *11*, 660. [CrossRef]
22. Pisanti, S.; Bifulco, M. Medical *Cannabis*: A plurimillennial history of an evergreen. *J. Cell. Physiol.* **2019**, *234*, 8342–8351. [CrossRef]
23. European Commission. Regulation (EC) No 1107/2009 of the European Parliament and of the Council of 21 October 2009 concerning the placing of plant protection products on the market and repealing Council Directives 79/117/EEC and 91/414/EEC. *Off. J. Eur. Union* **2009**, *309*, 1–50. Available online: https://eur-lex.europa.eu/legal-content/EN/TXT/?uri=celex%3A32009R1107 (accessed on 14 April 2022).
24. Schachtsiek, J.; Warzecha, H.; Kayser, O.; Stehle, F. Current Perspectives on Biotechnological Cannabinoid Production in Plants. *Planta Med.* **2018**, *84*, 214–220. [CrossRef] [PubMed]
25. Brunetti, P.; Pichini, S.; Pacifici, R.; Busardò, F.P.; del Rio, A. Herbal preparations of medical *cannabis*: A vademecum for prescribing doctors. *Medicina* **2020**, *56*, 237. [CrossRef]
26. Gazzetta Ufficiale. Legge 2 Dicembre 2016, n.242. Disposizioni per la Promozione della Coltivazione e della Filiera Agroindustriale della Canapa (16G00258), GU Serie Generale n. 304 del 30-12-2016. Available online: https://www.gazzettaufficiale.it/eli/id/2016/12/30/16G00258/sg (accessed on 20 April 2022).
27. Circolare—Camera dei Deputati. Circolare 31 Luglio 2018, Prot. 2018/43586. Aspetti Giuridico-Operativi Connessi al Fenomeno della Commercializzazione delle Infiorescenze della Canapa Tessile a Basso Tenore di THC e Relazioni con la Normativa Sugli Stupefacenti. Available online: https://www.camera.it/temiap/2018/12/14/OCD177-3851.pdf (accessed on 2 April 2022).
28. Gazzetta Ufficiale. Decreto 4 Novembre 2019 Definizione di Livelli Massimi di Tetraidrocannabinolo (THC) Negli Alimenti. (20A00016) (GU Serie Generale n.11 del 15-01-2020). Available online: https://www.gazzettaufficiale.it/eli/id/2020/01/15/20A00016/sg (accessed on 20 April 2022).
29. European Union. Annex III, Commission Delegated Regulation (EU) 2017/1155 of 15 February 2017 Amending Delegated Regulation (EU) No 639/2014 as Regards the Control Measures Relating to the Cultivation of Hemp, Certain Provisions on the Greening Payment, the Payment for Young Farmers in Control of a Legal Person, the Calculation of the per Unit Amount in the Framework of Voluntary Coupled Support, the Fractions of Payment Entitlements and Certain Notification Requirements Relating to the Single Area Payment Scheme and the Voluntary Coupled Support, and Amending Annex X to Regulation (EU) No 1307/2013 of the European Parliament and of the Council. Available online: https://eur-lex.europa.eu/eli/reg_del/2017/1155/oj (accessed on 2 April 2022).
30. Vignoli, A.; Ghini, V.; Meoni, G.; Licari, C.; Takis, P.G.; Tenori, L.; Turano, P.; Luchinat, C. High-Throughput Metabolomics by 1D NMR. *Angew. Chem. Int.* **2019**, *58*, 968–994. [CrossRef] [PubMed]
31. Eisenmann, P.; Ehlers, M.; Weinert, C.H.; Tzvetkova, P.; Silber, M.; Rist, M.J.; Luy, B.; Muhle-Goll, C. Untargeted NMR Spectroscopic Analysis of the Metabolic Variety of New Apple Cultivars. *Metabolites* **2016**, *6*, 29. [CrossRef] [PubMed]
32. Chandra, S.; Lata, H.; Khan, I.A.; ElSohly, M.A. Cannabis sativa L.—Botany and Horticulture. In *Cannabis sativa L.—Botany and Biotechnology*, 1st ed.; Chandra, S., Hemant, L., ElSohly, M.A., Eds.; Springer International Publishing: Cham, Switzerland, 2017; pp. 79–100.
33. Aizpurua-Olaizola, O.; Soydaner, U.; Öztürk, E.; Schibano, D.; Simsir, Y.; Navarro, P.; Etxebarria, N.; Usobiaga, A. Evolution of the Cannabinoid and Terpene Content during the Growth of *Cannabis sativa* Plants from Different Chemotypes. *J. Nat. Prod.* **2016**, *79*, 324–331. [CrossRef]
34. Brighenti, V.; Protti, M.; Anceschi, L.; Zanardi, C.; Mercolini, L.; Pellati, F. Emerging challenges in the extraction, analysis and bioanalysis of cannabidiol and related compounds. *J. Pharm. Biomed. Anal.* **2021**, *192*, 113633. [CrossRef]
35. Ohtsuki, T.; Friesen, J.B.; Chen, S.N.; McAlpine, J.B.; Pauli, G.F. Selective Preparation and High Dynamic-Range Analysis of Cannabinoids in "CBD Oil" and Other *Cannabis sativa* Preparations. *J. Nat. Prod.* **2022**, *85*, 634–646. [CrossRef]
36. Liu, Y.; Liu, H.-Y.; Li, S.-H.; Ma, W.; Wu, D.-T.; Li, H.-B.; Xiao, A.-P.; Liu, L.-L.; Zhu, F.; Gan, R.-Y. *Cannabis sativa* bioactive compounds and their extraction, separation, purification, and identification technologies: An updated review. *TrAC* **2022**, *149*, 116554. [CrossRef]

37. Rezvankhah, A.; Emam-Djomeh, Z.; Safari, M.; Askari, G.; Salami, M. Investigation on the extraction yield, quality, and thermal properties of *hemp* seed oil during ultrasound-assisted extraction: A comparative study. *J. Food Process. Preserv.* **2018**, *42*, e13766. [CrossRef]
38. Siudem, P.; Wawer, I.; Paradowska, K. Rapid evaluation of edible *hemp* oil quality using NMR and FT-IR spectroscopy. *J. Mol. Struct.* **2019**, *1177*, 204–208. [CrossRef]
39. Hazekamp, A.; Choi, Y.H.; Verpoorte, R. Quantitative Analysis of Cannabinoids from *Cannabis sativa* using ^{1}H-NMR. *Chem. Pharm. Bull.* **2004**, *52*, 718–721. [CrossRef] [PubMed]
40. Marchetti, L.; Brighenti, V.; Rossi, M.C.; Sperlea, J.; Pellati, F.; Bertelli, D. Use of 13C-qNMR Spectroscopy for the Analysis of Non-Psychoactive Cannabinoids in Fibre-Type *Cannabis sativa* L. (*Hemp*). *Molecules* **2019**, *24*, 1138. [CrossRef]
41. Choi, Y.H.; Kim, H.K.; Hazekamp, A.; Erkelens, C.; Lefeber, A.W.M.; Verpoorte, R. Metabolomic differentiation of *Cannabis sativa* cultivars using ^{1}H NMR spectroscopy and principal component analysis. *J. Nat. Prod.* **2004**, *67*, 953–957. [CrossRef] [PubMed]
42. Ludwig, C.; Viant, M.R. Two-dimensional J-resolved NMR spectroscopy: Review of a key methodology in the metabolomics toolbox. *Phytochem. Anal.* **2010**, *21*, 22–32. [CrossRef] [PubMed]
43. Huang, Y.; Zhang, Z.; Chen, H.; Feng, J.; Cai, S.; Chen, Z. A high-resolution 2D *J*-resolved NMR detection technique for metabolite analyses of biological samples. *Sci. Rep.* **2015**, *5*, 8390. [CrossRef]
44. Brighenti, V.; Marchetti, L.; Anceschi, L.; Protti, M.; Verri, P.; Pollastro, F.; Mercolini, L.; Bertelli, D.; Zanardi, C.; Pellati, F. Separation and non-separation methods for the analysis of cannabinoids in *Cannabis sativa* L. *J. Pharm. Biomed.* **2021**, *206*, 114346. [CrossRef]
45. Kumar Bharti, S.; Roy, R. Quantitative 1H NMR Spectroscopy. *TrAC* **2012**, *35*, 5–26.
46. Araneda, J.F.; Chu, T.; Leclerc, M.C.; Riegel, S.D.; Spingarn, N. Quantitative analysis of cannabinoids using benchtop NMR instruments. *Anal. Methods* **2020**, *12*, 4853–4857. [CrossRef]
47. TopSpin. 2018. Available online: http://www.bruker-biospin.com/topspin.html (accessed on 15 March 2022).
48. Varmuz, K.; Filzmoser, P. *Introduction to Multivariate Statistical Analysis in Chemometrics*, 1st ed.; CRC Press Taylor & Francis Group: Boca Raton, FL, USA, 2009; pp. 59–101.
49. Ebrahimi, P.; Viereck, N.; Bro, R.; Engelsen, S.B. Chemometric Analysis of NMR Spectra. In *Modern Magnetic Resonance*, 2nd ed.; Webb, A.G., Ed.; Springer International Publishing: Cham, Switzerland, 2018; pp. 1649–1668.
50. Ren, S.; Hinzman, A.A.; Kang, E.L.; Szczesniak, R.; Lu, L.J. Computational and Statistical Analysis of Metabolomics Data. *Metabolomics* **2015**, *11*, 1492–1513. [CrossRef]
51. R Core Team. *R: A Language and Environment for Statistical Computing*; R Foundation for Statistical Computing: Vienna, Austria, 2019; Available online: https://www.R-project.org/ (accessed on 21 March 2022).
52. Popescu, R.; Costinel, D.; Dinca, O.R.; Marinescu, A.; Stefanescu, I.; Ionete, R.E. Discrimination of vegetable oils using NMR spectroscopy and chemometrics. *Food Control* **2015**, *48*, 84–90. [CrossRef]
53. Siudem, P.; Wawer, I.; Kowalska, V.; Paradowska, K. Rapid ^{1}H NMR and chemometric methods in verification of *hemp*-seed oil quality. *J. Pharm. Biomed.* **2022**, *212*, 114650. [CrossRef] [PubMed]
54. Mikulcová, V.; Kašpárková, V.; Humpolíček, P.; Bunková, L. Formulation, Characterization and Properties of *Hemp* Seed Oil and Its Emulsions. *Molecules* **2017**, *22*, 700. [CrossRef] [PubMed]
55. Farinon, B.; Costantini, L.; Molinari, R.; Di Matteo, G.; Garzoli, S.; Ferri, S.; Ceccantoni, B.; Mannina, L.; Merendino, N. Effect of malting on nutritional and antioxidant properties of the seeds of two industrial *hemp* (*Cannabis sativa L.*) cultivars. *Food Chem.* **2022**, *370*, 131348. [CrossRef]
56. Borges, G.R.; Birk, L.; Scheid, C.; Morés, L.; Carasek, E.; Kitamura, R.O.S.; Roveri, F.; Eller, S.; de Oliveira Merib, J.; de Oliveria, T.F. Simple and straightforward analysis of cannabinoids in medicinal products by fast-GC–FID. *Forensic Toxicol.* **2020**, *38*, 531–535. [CrossRef]
57. Mazzara, E.; Torresi, J.; Fico, G.; Papini, A.; Kulbaka, N.; Dall'Acqua, S.; Sut, S.; Garzoli, S.; Mustafa, A.M.; Cappellacci, L.; et al. A Comprehensive Phytochemical Analysis of Terpenes, Polyphenols and Cannabinoids, and Micromorphological Characterization of 9 Commercial Varieties of *Cannabis sativa* L. *Plants* **2022**, *11*, 891. [CrossRef]
58. Brighenti, V.; Pellati, F.; Steinbach, M.; Maran, D.; Benvenuti, S. Development of a new extraction technique and HPLC method for the analysis of non-psychoactive cannabinoids in *Cannabis sativa* L. fibosa (*hemp*). *J. Pharm. Biomed. Anal.* **2017**, *143*, 228–236. [CrossRef]
59. Pellati, F.; Brighenti, V.; Sperlea, J.; Marchetti, L.; Bertelli, D.; Benvenuti, S. New methods for the comprehensive analysis of bioactive compounds in *Cannabis sativa* L. (*hemp*). *Molecules* **2018**, *23*, 2639. [CrossRef]
60. Valizadehderakhshan, M.; Shahbazi, A.; Kazem-Rostami, M.; Todd, M.S.; Bhowmik, A.; Wang, L. Extraction of Cannabinoids from *Cannabis sativa* L. (*Hemp*)—Review. *Agriculture* **2021**, *11*, 384. [CrossRef]
61. Peschel, W.; Politi, M. ^{1}H NMR and HPLC/DAD for *Cannabis sativa* L. Chemotype distinction, extract profiling and specification. *Talanta* **2015**, *140*, 150–165. [CrossRef]
62. Spano, M.; Di Matteo, G.; Ingallina, C.; Botta, B.; Quaglio, D.; Ghirga, F.; Balducci, S.; Cammarone, S.; Campiglia, E.; Giusti, A.M.; et al. Emerging challenges in the extraction, analysis and bioanalysis of cannabidiol and related compounds. *Molecules* **2021**, *26*, 2912. [CrossRef] [PubMed]

63. Monti, M.C.; Frei, P.; Weber, S.; Scheurer, E.; · Mercer-Chalmers-Bender, K. Beyond Δ9-tetrahydrocannabinol and cannabidiol: Chemical differentiation of cannabis varieties applying targeted and untargeted analysis. *Anal. Bioanal. Chem.* **2022**, *414*, 3847–3862. [CrossRef] [PubMed]
64. Palmieri, S.; Mascini, M.; Ricci, A.; Fanti, F.; Ottaviani, C.; Lo Sterzo, C.; Sergi, M. Identification of *Cannabis sativa* L. (*hemp*) Retailers by Means of Multivariate Analysis of Cannabinoids. *Molecules* **2019**, *24*, 3602. [CrossRef] [PubMed]
65. Mudge, E.M.; Murch, S.J.; Brown, P.N. Chemometric Analysis of Cannabinoids: Chemotaxonomy and Domestication Syndrome. *Sci. Rep.* **2018**, *8*, 13090. [CrossRef] [PubMed]
66. Ingallina, C.; Sobolev, A.P.; Circi, S.; Spano, M.; Fraschetti, C.; Filippi, A.; Di Sotto, A.; Di Giacomo, S.; Mazzoccanti, G.; Gasparrini, F.; et al. *Cannabis sativa* L. Inflorescences from Monoecious Cultivars Grown in Central Italy: An Untargeted Chemical Characterization from Early Flowering to Ripening. *Molecules* **2020**, *25*, 1908. [CrossRef] [PubMed]
67. Olasehinde, T.A.; Olaniran, A.O. Neurotoxicity of anthracene and benz[a]anthracene involves oxidative stress-induced neuronal damage, cholinergic dysfunction and disruption of monoaminergic and purinergic enzymes. *Toxicol. Res.* **2022**, *80*, 105312. [CrossRef]
68. Nagy, D.U.; Cianfaglione, K.; Maggi, F.; Sut, S.; Dall'Acqua, S. Chemical Characterization of Leaves, Male and Female Flowers from Spontaneous *Cannabis* (*Cannabis sativa* L.) Growing in Hungary. *Chem. Biodivers.* **2019**, *16*, e1800562. [CrossRef]
69. Kostas Ioannidis, K.; Dadiotis, E.; Mitsis, V.; Melliou, E.; Magiatis, P. Biotechnological Approaches on Two High CBD and CBG *Cannabis sativa* L. (Cannabaceae) Varieties: In Vitro Regeneration and Phytochemical Consistency Evaluation of Micropropagated Plants Using Quantitative ^{1}H-NMR. *Molecules* **2020**, *25*, 5928. [CrossRef]
70. Siciliano, C.; Bartella, L.; Mazzotti, F.; Aiello, D.; Napoli, A.; De Luca, P.; Temperini, A. 1H NMR quantification of cannabidiol (CBD) in industrial products derived from *Cannabis sativa* L. (*hemp*) seeds. *IOP Conf. Ser. Mater. Sci. Eng.* **2019**, *572*, 012010. [CrossRef]
71. Barthlott, I.; Scharinger, A.; Golombek, P.; Kuballa, T.; Lachenmeier, D.W. A Quantitative 1H NMR Method for Screening Cannabinoids in CBD Oils. *Toxics* **2021**, *9*, 136. [CrossRef]
72. Risoluti, R.; Gullifa, G.; Battistini, A.; Materazzi, S. Monitoring of cannabinoids in *hemp* flours by MicroNIR/Chemometrics. *Talanta* **2020**, *211*, 120672. [CrossRef] [PubMed]
73. Sgrò, S.; Lavezzi, B.; Caprari, C.; Polito, M.; D'Elia, M.; Lago, G.; Furlan, G.; Girotti, S.; Ferri, E.N. Delta9-THC determination by the EU official method: Evaluation of measurement uncertainty and compliance assessment of *hemp* samples. *Anal. Bioanal. Chem.* **2021**, *413*, 3399–3410. [CrossRef] [PubMed]
74. Nahar, L.; Guo, M.; Sarker, S.D. Gas chromatographic analysis of naturally occurring cannabinoids: A review of literature published during the past decade. *Phytochem. Anal.* **2020**, *31*, 135–146. [CrossRef] [PubMed]
75. Dadiotis, E.; Mitsis, V.; Melliou, E.; Magiatis, P. Direct Quantitation of Phytocannabinoids by One-Dimensional 1H qNMR and Two-Dimensional 1H-1H COSY qNMR in Complex Natural Mixtures. *Molecules* **2022**, *27*, 2965. [CrossRef] [PubMed]